4-octyl Itaconate and Itaconate in the Regulation of Type I Interferon in Macrophages



Thesis submitted to

Trinity College Dublin, the University of Dublin

for the degree of

Doctor of Philosophy

by

Shane Myles O'Carroll

Under supervision of

Prof. Luke A. J. O'Neill

Inflammation Research Group

School of Biochemistry and Immunology

2025

Declaration

This thesis is submitted by the undersigned to the University of Dublin for the examination of Doctor of Philosophy. I declare that this thesis has not been submitted as an exercise for a degree at this or any other university and is entirely my own work with the exception of the following figures:

Figure 4.1.7 a

This work was performed by Alexander Hooftman.

Figure 4.1.7 b

This work was performed by Sara Charki.

Figure 4.1.8

This work was performed by Anne McGettrick.

Figure 4.1.10

This work was performed by Alexander Hooftman.

Figure 4.1.18

This work was carried out in collaboration with Christian Peace.

Figure 4.1.20

This work was carried out in collaboration with Christian Peace.

Figure 4.1.26

This work was carried out in collaboration with Christian Peace.

Figure 4.1.33

This work was carried out in collaboration with Juliana Escher-Toller.

I agree to deposit this thesis in the University's open access institutional repository or allow the library to do so on my behalf, subject to Irish Copyright Legislation and Trinity College Library conditions of use and acknowledgement.

Shane O'Carroll

Shane O'Carroll

Acknowledgements

First, I would like to thank you, Luke, for your leadership, guidance, and unwavering support, which have been instrumental in my professional development over these past four years. Your insightful feedback and encouragement have been invaluable. When projects seem to be in trouble, you always find the silver lining and set a clear target for us to aim for. We always leave a one-on-one crisis meeting optimistic and ready to go.

You are commended for fostering an enjoyable, fun, and energetic lab environment. I have had many adventures during my time in the lab, such as you taking us on the infamous Luke O'Neill history tour of the Trinity campus, where you become a tour guide in the Book of Kells, followed by a gaggle of lab members and other tourists who think you're a legitimate tour guide.

We had great lab trips, such as the infamous trip to Torun, Poland, the home of Copernicus and pierogi dumplings, a highlight of my time in the lab. Many laughs were had, and tears were shed. A fond memory from Torun was the lab meeting, which began seriously but soon descended into jovial heckling and, finally, a journal club of a paper investigating how lobsters get high. The trip to Galway for the FH Nature paper was also great fun as the boyband gave each other COVID in the steam room. The countless dinners, leaving parties, Christmas parties, *vivas*, and publications were always an event and generously funded by yourself.

Our COVID time has often been recounted as unique and special. Looking over a dark, void Dublin skyline as others worked from home was a delightful break from isolation during lockdown as we worked on COVID research in the lab. Don't forget the lockdown Christmas party where half of the lab was home sick with COVID, and the boyband and I, acting as Santa Clause, spent 3 hours driving around Dublin delivering gifts to those in quarantine like yourself. Following strict COVID guidelines, you gave us all big hugs to thank us. What fun we have. When the experiments fail, at least we're having fun doing it. Thank you for being a mentor and leader. I am proud to have the privilege of working under your guidance.

To the LONers, who make the lab such a special place. Without you, the lifers, Cait and Kathy, the lab would abruptly stop. Thank you, Cait, for keeping things running smoothly in the background. I never knew you liked Karaoke so much! To **Kathy**, thank you for keeping the lab running and especially getting legs from abroad. You're an asset to the lab, which is evident when other labs run to you for help. To **Eva**, an old bench mate and Lilly adventurer. Thanks for all the fun chats and advice in the lab; so much fun that I didn't move the centrifuge back to separate us. Our trip to Lilly, especially the airport Philly cheese steaks. Make sure to go back and see your neighbour from Sweden soon. To **Anne,** thank you for the great times, chats, and all you've done for me and helped me with over the last few years. Hopefully I can now source you some IRFU tickets soon! To the girl band **Marah, Alessia, Maureen,** and **Ciana,** what fun we had over the years; playing pranks in the lab, football in Irishtown, watching Italy beat England in the Euros, the fun nights out it's been such a fun four years. To **Emily**, thank you for everything you've helped me with over the years: in-vivos, career advice, and being great fun on a night out. Seeing you becoming a PI gives inspiration and hope. To **Juliana**, a fellow gym go-er and neutrophil extraordinaire, you have made the lab a friendly and warm place. I'm looking forward to working together in the future.

To the **boyband**. It's been a pleasure to meet such a fun group of lads. Go-karting, football, scooter adventures in Torun, getting COVID in the Galway saunas, gossiping and chatting science and career tactics over a pint, and **Tristram** panic buying 200 euro worth of wine in Bordeaux, we had the best time and long may it continue. In order of seniority, **Alex,** the karting king. Thank you for taking me under your wing when I first joined. Unlike **Tristram**, you taught me to do a western blot. To **Tristram,** often seen equipped with an umbrella, Canada goose jacket and sunglasses, thanks for ruining my Christmas by giving me COVID; I appreciate it. We had a fun time in the lab together. You've always been genuinely supportive and interested in my work and development. To **Hauke,** who probably isn't listening because he's listening to a podcast at his bench. A lover of a good deal and an integral boyband member. To **Karl**, although you departed early, you're not forgotten. AMDG brotha'. Finally, Christian is an elusive man whose whereabouts we can never tell at any moment. You've played a significant part in my time here in the lab, especially over the last two years since the others rudely decided to graduate. From a career perspective, I'm glad we both joined forces on the SDH project. It's a brilliant example of the synergy of collaborating in science. Without your expertise,

this project would never have gotten to this stage in my four years. Most importantly, our gym sessions, tennis sessions, and coffee trips made it all the more fun.
To the not-so-newbies **Orlaith** and **Yukun**. You've been a great and fun addition to the lab, and I look forward to seeing you both advance in your careers.
To **Sam**, the honorary lab member, you enjoy entering the lab, messing with dry ice, getting no work done, and then leaving. That sounds like the perfect LON lab member to me.
To the newbies, **Jaiya** and **Victoria**: You guys are such a great addition to the next generation of the LON lab, and I'm sure you'll do great things.

Thank you to my family for encouraging and supporting me to this point and beyond.

I have saved the most important for last—a special thank you to my amazing Sara, my number one supporter from the beginning and to whom this thesis is dedicated. You always supported me when work wasn't going according to plan. When things went well, you were the first to celebrate my achievements even when I didn't. It was also great to have you join the lab which you contributed greatly and added your medical twist to lab meetings.
Thank you, my love and my best friend.

I dedicate this thesis to my wife Sara.

Table of Contents

Declaration ***2***

Acknowledgements ***4***

Abbreviations ***13***

Abstract ***17***

Chapter 1. Introduction ***19***

1.1 General introduction **20**

1.2 Innate immunity **21**

1.2.1 Macrophages 21

1.2.2 M1 macrophages 22

1.2.3 M2 macrophages 22

1.2.4 Innate immune receptors 23

1.2.5 Toll-like receptor 4 signalling 24

1.3 Type I interferons **27**

1.3.1 Type I interferons in disease 30

1.3.2 Type I interferons in viral infection 30

1.3.3 Type I interferons in bacterial infection 30

1.3.4 IL1β / IFNβ co-regulation 31

1.3.5 Type I interferons in inflammation 31

1.4 Mitochondria **32**

1.4.1 Mitochondria in disease 33

1.4.2 The TCA cycle and cancer 33

1.4.3 Mitochondrial nucleic acid release mechanisms 34

1.4.4 Mitochondrial nucleic acids activate PRRs 35

1.4.5 Cytosolic Mt-dsRNA sensors 35

1.5 Immunometabolism **36**

1.5.1 M1 metabolic reprogramming 36

1.5.2 M2 metabolic reprogramming 38

1.6 Fumarate hydratase regulates mitochondrial nucleic acid release **38**

1.7 Itaconate: a potent immunometabolic regulator **40**

1.7.1 History of itaconate 40

1.7.2 Itaconate in mammalian cells 40
1.7.3 Properties of itaconate 44
1.7.4 Anti-microbial roles of itaconate 44
1.7.5 Antiviral roles of itaconate 45
1.7.6 Itaconate is an enzyme inhibitor 49
1.7.7 Itaconate inhibits SDH 49
1.7.8 Itaconate inhibits TET2 49
1.7.9 Itaconate inhibits its synthesis via enzyme inhibition 50
1.7.10 Itaconate acts via receptor signalling 50
1.7.11 Itaconate: a cysteine modifier 51
1.7.12 Itaconate and NRF2 51
1.7.13 Itaconate and NLRP3 52
1.7.14 Structurally similar compounds and itaconate derivatives 52
1.7.15 Itaconate catabolism 52
1.7.16 Mesaconate and citraconate 53
1.7.17 Itaconate in disease 54
1.7.18 Itaconate ameliorates a model of EAE 54
1.7.19 Itaconate is pro-tumour 55
1.7.20 Synthesised derivatives 56

1.8 Metabolic regulation of type I interferon responses 60

1.8.1 Itaconate and 4-OI differentially regulate IFNβ 60

1.9 Aims 63

Chapter 2 Materials and Methods 64

2.1 Materials 65

2.1.1Buffers 65
2.1.2 Reagents 65
2.1.3 Cell culture reagents 67
2.1.4 Cell lines and primary cells 67
2.1.5 Stimulants and metabolites 67
2.1.6 Antibodies 67
2.1.7 Western blotting reagents 68
2.1.8 RT-qPCR reagents and primers 68
2.1.9 Primer list 69
2.1.10 ELISA Reagents 70

2.2 Methods 71

2.2.1 Derivation of bone marrow-derived macrophages 71

2.2.2 Cell lines 72
2.2.3 Ethidium Bromide Treatment 72
2.2.4 siRNA knockdown in BMDMs 72
2.2.5 siRNA knockdown in PBMCs 73
2.2.6 Organelle/cytosolic separation 74
2.2.7 Seahorse XF Complex II Assay 74
2.2.8 Western blot 75
2.2.9 RT-qPCR 76
2.2.10 RNA sequencing 77
2.2.11 Immune Response Enrichment Analysis (IREA) 79
2.2.12 Mitochondrial membrane potential assay 80
2.2.13 Generation of human macrophages 80
2.2.14 Ethics 80
2.2.15 ELISA 81
2.2.16 Immunofluorescence imaging 81
2.2.17 Quantification and statistical analyses 82
2.2.18 MTT assay (SDH activity) 82
2.2.19 SDH-deficient tumours 82

Chapter 3. 4-Octyl itaconate blocks PRR-induced type I interferon via NRF2 84

3.1.1. 4-OI blocks LPS-induced IFNβ 85
3.1.2. 4-OI blocks LPS-induced ISGs 85
3.1.3. 4-OI blocks poly(I:C)-induced IFNβ 85
3.1.4. 4-OI blocks poly(I:C)-induced ISGs 85
3.1.5. 4-OI blocks R848-induced IFNβ and ISGs 85
3.1.6. 4-OI blocks 2'-3'-cGAMP-induced IFNβ and ISGs 85
3.1.7 4-OI blocks CpG ODN-induced IFNβ and ISGs 92
3.1.8 4-OI blocks LPS-induced *Ifnb1* independent of IFNAR signalling 92
3.1.9 NRF2 activators 4-OI, DMF, and DEM block LPS-induced *Ifnb1* 92
3.1.10 KEAP1 knockdown blocks LPS-induced *Ifnb1* 96
3.1.11 Nrf2 knockdown partially rescues the suppressive effect of 4OI on LPS-induced *Ifnb1* 96

3.2 Discussion 100

3.2.1 4-OI blocks PRR-induced type I interferons 100
3.2.2 4-OI blocks type I interferon partially mediated by NRF2 regulation 100

Chapter 4. Itaconate drives mtRNA-induced Type I interferon production via inhibition of succinate dehydrogenase 102

4.1 Results ***103***

4.1.1 IFNβ is an important cytokines in the itaconate-mediated transcriptional response . 103

4.1.2 Itaconate boosts LPS-induced IFNβ ... 103

4.1.3 Itaconate boosts R848-induced IFNβ and ISGs ... 103

4.1.4 Itaconate boosts poly(I:C)-induced IFNβ but not ISGs ... 108

4.1.5 Itaconate boosts CpG-ODN-induced IFNβ and ISGs ... 108

4.1.6 Itaconate boosts *Ifnb1* and NRF2-dependent gene *Hmox1 in-vivo* ... 108

4.1.7 ACOD1 is necessary for a robust LPS-induced type I interferon response in BMDMs. 108

4.1.8 *IRG1* is necessary for a robust IFNβ production in activated PBMCs ... 113

4.1.9 ACOD1 is necessary for a robust LPS-induced IFNβ response in THP1s ... 113

4.1.10 Itaconate inhibits succinate dehydrogenase activity. ... 116

4.1.11 SDH inhibition boosts LPS-induced IFNβ and ISGs in macrophages ... 118

4.1.12 RNA-seq analysis of itaconate and TTFA-treated BMDMs ... 118

4.1.13 Gene Set Enrichment Analysis of itaconate treated BMDMs ... 121

4.1.14 Loss of SDHA boosts LPS-induced IFNβ in macrophages ... 121

4.1.15 Loss of SDHB boosts LPS-induced IFNβ in macrophages ... 121

4.1.16 SDH-deficient tumours have increased IFNB production ... 125

4.1.17 SDH inhibition boosts LPS-induced IFNβ via RIG-I / MDA5-dependent signalling ... 125

4.1. 18 Successful knockdown of Mb21d1, Ddx58, Tlr9, and Ifih1 ... 128

4.1.19 Mb21d1, Ifih1, and Ddx58 knockdown is specific to their agonists ... 128

4.1.20 SDH inhibition boosts LPS-induced IFNβ via RIG-I/MDA5-dependent signalling ... 128

4.1.21 Itaconate boosts LPS-induced IFNβ via MDA5-dependent signalling ... 132

4.1. 23 SDH-induced *Ifnb1* expression is STING-independent ... 135

4.1.24 Itaconate boosts LPS-induced IFNβ in a TLR9-dependent manner ... 135

4.1.25 Mitochondrial nucleic acids regulate SDH-induced IFNβ ... 138

4.1.26 Mitochondrial transcriptional inhibition blocks itaconate-induced Ifnb1 ... 138

4.1. 27 LPS induces mitochondrial encoded gene expression ... 138

4.1.28 SDH inhibition drives cytosolic mtRNA release ... 142

4.1.29 Inhibition of SDH boosts LPS-induced *Ifnb1* independent of Bax and Bak ... 142

4.1.31 VDAC1 oligomerisation regulates SDH-induced IFNβ ... 146

4.1.32 VDAC1 inhibition blocks itaconate-induced mitochondrial nucleic acid release ... 146

4.1.33 SDH inhibition increases mitochondrial membrane potential ... 149

4.1.34 LPS-induced cytosolic mtRNA release is dependent on IRG1 ... 149

4.2 Discussion ***152***

4.5.1 Rationale **153**

4.5.2 Itaconate boosts type I interferon production **153**

4.5.3 Itaconate blocks SDH 154

4.5.4 SDH inhibition boosts type I interferon responses 155

4.5.5 SDH-inhibition by itaconate leads to mtRNA release 157

4.5.6 SDH inhibition leads to mitochondrial dysfunction 158

4.5.7 SDH-induced mtRNA release is VDAC dependant 159

4.6 Conclusion 160

Chapter 5 Overall discussion and future perspectives 162

5.1 Itaconate versus 4-OI 162

5.2 Future perspectives 167

5.2.1 Therapeutic potential 167

6 References 169

Publications 194

Abbreviations

2OGDDs	2-Oxoglutarate-dependent dioxygenases
5hmC	5-hydroxymethylcytosine
5mC	5-methylcytosine
AA5	Atpenin A5
ACOD1	Aconitate decarboxylase
AIM2	Absent in melanoma 2
ALDOA	Aldolase A
ARE	Antioxidant response element
BMDMs	Bone marrow derived macrophages
CAPS	Cryopyrin-associated periodic syndrome
CD14	Cluster of differentiation 14
cGAS	Cyclic GMP-AMP synthase
CMPK2	Cytidine/uridine monophosphate kinase 2
DAMP	Danger associated molecular patterns
DAMPs	Damage associated molecular patterns
DDX58	DExD/H-box helicase 58
DMF	Dimethyl fumarate
EtBr	Ethidium Bromide
FEN1	flap-structure-specific endonuclease 1
FH	Fumarate Hydratase
GAPDH	Glyceraldehyde-3-phosphate dehydrogenase
GSEA	Gene Set Enrichment Analysis
HSV	Herpes Simplex Virus

IAV	Influenza A virus
ICL	Isocitrate lyase
IDH	Isocitrate dehydrogenase
IFIH1	Interferon Induced With Helicase C Domain 1
IFNα	Interferon alpha
IFNAR	IFNα/β receptor
IFNɣ	Interferon gamma
IFNβ	Interferon beta
IMM	Inner mitochondrial membrane
IRAK1	Interleukin-1 receptor-associated kinase 1
IREA	Immune Response Enrichment Analysis
IRF1	Interferon response factor 1
IRG1	Immune-responsive gene 1
ISG15	Interferon Stimulated Gene 15
ISRE	Interferon-Stimulated Response Element
JAK	Janus kinase
K_m	Michaelis constant
LBP	LPS-binding protein
LDH	Lactate dehydrogenase
LPS	Lipopolysaccharide
MAVS	Mitochondrial antiviral-signaling protein
MD2	Myeloid differentiation protein 2
MDA5	Melanoma differentiation-associated protein 5
MDSCs	Myeloid-derived suppressor cells

MDVS	Mitochondrial-derived Vesicles
MMP	Mitochondrial membrane potential
MHC	Major histocompatibility complex
MPTP	Mitochondrial permeability transition pore
MS	Multiple sclerosis
mt-NA	Mitochondrial Nucleic Acid
MTB	*Mycobacterium tuberculosis*
MTT	3-(4, 5-dimethylthiazol-2-yl)-2,5-diphenyltetrazolium
MYD88	Myeloid differentiation primary response 88
NK	Natural killer
NLRP3	Nod-Like Receptor Protein 3
NRF2	Nuclear factor erythroid 2-related factor 2
OXGR1	Oxoglutarate receptor 1
OXPHOS	Oxidative phosphorylation
PAMP	Pathogen-associated molecular patterns
PCA	Principle component analysis
POLG	Mitochondrial Polymerase ɣ
PRR	Pattern recognition receptor
RET	Reverse electron transport
RIG-I	Retinoic-acid-inducible gene I
ROS	Reactive oxygen species
SDH	Succinate dehydrogenase
SLE	Systemic lupus erythematosus (SLE)
SQR	Succinate-Ubiquinone Reductase

STAT	Signal transducers and activators of transcription
STING	Stimulator of interferon genes
TAM	Tumour associated macrophages
TCA	Tricarboxylic acid
TET2	Ten eleven translocation 2
TFAM	Transcription factor A, mitochondrial
TLR4	Toll-like receptor 4
TMEM173	Transmembrane protein 173
TRAM	TRIF-Related Adaptor Molecule
TRIF	TIR-domain-containing adapter-inducing interferon-β
TRIF	TIR-domain-containing adapter-inducing interferon-β
TTFA	2-thenoyltrifluoroacetone
TYK2	Tyrosine kinase 2
VDAC1	Voltage-dependent anion channel 1
VSV	Vesicular stomatitis Indiana virus
WNV	West Nile Virus
ZIKV	Zika Virus

Abstract

Itaconate is an endogenous immunomodulatory metabolite produced by the enzyme aconitate decarboxylase 1 (ACOD1), a product of the gene *immune-responsive gene 1* (*Irg1)*. Itaconate is the most highly upregulated metabolite after stimulation with the gram-negative bacterial product lipopolysaccharide (LPS) in inflammatory macrophages.

Itaconate is anti-inflammatory, antiviral, and antimicrobial and has been investigated in many inflammatory disease models. Its immunomodulatory potential has gathered significant interest, which aims to use itaconate derivatives and ACOD1 modulators as therapies for inflammatory diseases.

Itaconate partially mediates its immunomodulatory properties by covalently modifying cysteine residues on target proteins, affecting protein function. Itaconate, particularly its cell-permeable derivative 4-octyl itaconate (4-OI), has been shown to alkylate NLRP3, inhibiting NLRP3-NEK7 binding and subsequent inflammasome activation. 4-OI also activates NRF2, which translocates to the nucleus and acts as a transcription factor to drive many antioxidant and cytoprotective genes. Furthermore, itaconate mediates its effects via enzyme inhibition, particularly mitochondrial complex II, also known as succinate dehydrogenase (SDH) and ten eleven translocation 2 (TET2) inhibition. Itaconate's inhibition of SDH creates a breakpoint in the tricarboxylic acid (TCA) cycle, a central feature of macrophage metabolic reprogramming, which inhibits IL1β production.

Importantly, itaconate has been shown to boost LPS-induced type I interferons, while *Irg1*$^{-/-}$ BMDMs produce less type I interferons. However, the itaconate derivative and tool compound, 4-OI, blocks LPS-induced type I interferons and interferon-stimulated genes (ISGs). It is curious, therefore, how itaconate and its proposed tool compound, 4-OI, have opposing effects in this regard. In this thesis, I have investigated how IFNβ is regulated by itaconate and its derivative, 4-OI.

I have found that 4-OI blocked IFN-β and ISGs upon macrophage challenge with LPS and ligands for TLR3,7/8,9, and Stimulator of Interferon genes (STING).

Mechanistically, the suppression of LPS-induced IFN-β by 4-OI was shown to be partially NRF2-dependent.

Opposite to 4-OI, I have confirmed that itaconate boosts LPS-induced IFNβ. Furthermore, I have demonstrated that SDH inhibition is responsible for this response by utilising SDH inhibitors and SDH-deficient cells, including human SDH-deficient tumours. I have shown that SDH inhibition by itaconate mediates mitochondrial double-stranded RNA (mtdsRNA) release. Mechanistically, mtRNA release depended on the mitochondrial transporter Voltage-dependent anion channel (VDAC). Following this, the mtdsRNA sensors melanoma differentiation-associated protein 5 (MDA5) and retinoic-acid-inducible gene I (RIG-I) are required for IFNβ production in response to SDH inhibition by itaconate. This was linked to a disease model involving SDH-inhibition, SDH-deficient paraganglioma, where I demonstrated that *IFNB* is upregulated. Inhibition of SDH by itaconate links TCA cycle modulation to type I interferon production via mtRNA.

These results show a clear difference between itaconate and its derivative, 4-OI, on innate immune responses of murine macrophages.

Together, these results further our understanding of the immunoregulatory role of itaconate. I have shown that 4-OI blocks type I interferon via NRF2 and that itaconate boosts LPS-induced type I interferons through SDH inhibition and mtdsRNA release. This thesis further emphasises the role of the TCA cycle in inflammation, demonstrates the complexity of itaconate biology, and highlights the importance of understanding the immunomodulatory mechanisms of itaconate for generating new therapeutics based on itaconate for immunological diseases.

Chapter 1. Introduction

1.1 General introduction

The recent advancement of tools for metabolomic analysis has led to the emergence of the field of immunometabolism, whereby immunologists can now study the metabolic perturbations in immune cells and how these changes regulate immune cell function in health and disease. With this, it is well-established that metabolites have roles independent of metabolism and can moonlight as immunological signalling molecules, similar to cytokines(1). In particular, the tricarboxylic acid (TCA) cycle is more than just a metabolic hub; its intermediates control many immunological responses. Notable examples include succinate, which has been linked to activation of HIF1α and subsequent regulation of IL1β(2), and fumarate, whose accumulation has been linked to type I IFN induction (3, 4).

Itaconate has emerged as a key regulator of macrophage biology. It is potently induced by inflammatory stimuli such as lipopolysaccharide (LPS) and has a range of targets, with the net effect being anti-inflammatory. Itaconate and a cell-permeable derivative, 4-OI, have been shown to regulate type I IFNs. They are the subject of this thesis, whereby the inhibitory effect of 4-OI on type I IFNs has been explored. Conversely, the stimulatory effect of itaconate on type I IFNs has been elucidated and shown to involve inhibition of succinate dehydrogenase (SDH), leading to mitochondrial double-stranded RNA (dsRNA) release, which acts on RIG-I and MDA5 to trigger this response.

In my thesis, I have therefore found a clear difference between itaconate and 4-OI in their regulation of type I IFNs in macrophages, a key cell type in this thesis.

These results show a clear difference between itaconate and its derivative 4-OI in their regulation of type I interferons. Furthermore, these results expand our understanding of itaconate biology and its regulation of macrophage innate immunity and emphasise the importance of the TCA cycle in inflammation.

1.2 Innate immunity

The immune response is the body's self-defence mechanism against invading pathogens. This system can be separated into two responses: the innate and adaptive immune responses. The innate immune response is the body's first immunological response to danger. It comprises physical barriers such as the skin and the mucosa and immune cells such as macrophages, dendritic cells, and neutrophils (5).

These immune cells act quickly to sense and sound the alarm to any form of danger in the body, whether self-made or foreign. They are essential in mediating the adaptive immune response, which is more specific and ultimately eliminates the invader. They also mediate long-lasting immunity should such an invader reappear (6).

1.2.1 Macrophages

Macrophages are vital immune cells that connect the innate and adaptive immune systems. are the most versatile cells of the haematopoietic system are located in various organs of the body. Macrophages are crucial in human biology, playing key roles in development, homeostasis, and immunity. They derive from circulating monocytes, which originate from the haematopoietic stem cells in the bone marrow. Tissue-resident macrophages develop from the yolk sac, the first site of mammalian haematopoiesis (7). Tissue-resident macrophages comprise Kupffer cells located in the liver, alveolar macrophages found in the lungs, and microglia present in the brain. These macrophages play vital roles in the immune response, which includes immunomodulation, antigen presentation, phagocytosis, and the production of cytokines. (8).

The term "macrophage" is derived from the Greek words "makro, meaning 'big,' and "phage," meaning 'to eat.' This terminology accurately reflects one of the primary functions of macrophages as phagocytes, which are specialized cells with an extraordinary ability to consume pathogens, eliminate debris, and dispose of dead cells (9). Phagocytosed pathogens are processed inside macrophages, and their antigens are displayed on the cell surface through major histocompatibility complex (MHC) class II molecules. These antigens are recognised by T helper cells, which play a vital role in commencing the adaptive immune response (10). Activated macrophages also secrete

cytokines and chemokines, which contribute to inflammation, the recruitment of other immune cells, and the regulation of the adaptive immune response. The fate of macrophage function is influenced by innate immune signals such as Pathogen-Associated Molecular Patterns (PAMPs), Damage-Associated Molecular Patterns (DAMPs), cytokines produced by T cells or T cell-macrophage direct interactions, epigenetic regulation and external stimuli such as pharmacological compounds, and tissue environments such as hypoxic conditions. These states can be loosely separated into two polarisation states, generally known as "M1" or "M2" (11).

1.2.2 M1 macrophages

Classically activated macrophages are a well-documented phenotype in macrophage biology and the immune response to bacterial infection, such as *Mycobacterium tuberculosis* (MTB) or human immunodeficiency virus (HIV) infection. M1 macrophages are activated by the bacterial product lipopolysaccharide (LPS) and interferon-gamma (IFNɣ). *In-vivo* IFN-ɣ is derived from T helper (T_H1), $CD8^+$ T cells and NK cells (12). T_H1-derived IFN-ɣ binds the interferon-gamma receptor (IFNGR), which leads to JAK/ STAT signalling.

Surface markers such as CD80, CD86, CD64, CD16, and CD32 are typically associated with classically activated macrophages (13). These macrophages also secrete key pro-inflammatory cytokines, including IL-1β, TNF, and IL-18. Additionally, classically activated macrophages produce reactive oxygen species (ROS) and nitric oxide (NO), which contribute to their microbicidal activity. This results in a phenotype that is immune-stimulatory, pro-inflammatory, anti-bacterial, and anti-tumour. Furthermore, they release chemokines such as CCL2, CCL3, and CXCL10, which help recruit other immune cells to the site of infection or inflammation (14).

1.2.3 M2 macrophages

Alternatively activated macrophages, are, *in-vivo,* activated by T helper 2 (T_H2) cytokines such as IL13, IL4, IL-10 and TGFβ during allergy, cellular and humoral responses to parasites, and extracellular pathogens (15). M2 macrophages are associated with surface markers, including CD163, CD206, CD209, FIZZ1, and YM1/2. This alternative activation leads to an anti-inflammatory response characterised by the

production of IL10 and TGFβ. M2 macrophages produce the chemokines CCL17, CCL18, IL-10, TGFβ, and CCL22, which aid tissue repair. This response is pro-wound healing, pro-homeostatic and immunosuppressive (15).

1.2.4 Innate immune receptors

While the adaptive immune response is responsible for antigen-specific immune responses, the innate immune response also offers a degree of specificity. Innate immune sensors, known as germline-encoded pattern recognition receptors (PRRs), are localised to cell membranes and the cytosol. These receptors detect molecular patterns derived from pathogen-associated molecular patterns (PAMPs), which are structures found in pathogens that are essential for their survival are often conserved across species. Additionally, PRRs can recognise damage-associated molecular patterns (DAMPs) released from damaged or dying cells.

Activation of PRRs triggers a cascade of signalling pathways that converge on the activation of transcription factors, which enter the nucleus and promote the transcription of various cytokines and chemokines. These molecules mediate immune responses by promoting inflammation, recruiting immune cells, and facilitating communication with the adaptive immune system. In the case of viral infections, PRR activation induces type I interferon responses, which help limit viral replication.

This innate immune response is rapid, occurring within minutes to hours after sensing a danger signal. The specificity of the response is determined by the type of PRR activated, allowing the immune system to mount a response tailored to the particular threat. After the danger has been eliminated, resolution occurs, involving the cessation of inflammatory signalling and the production of anti-inflammatory factors to restore homeostasis.

However, dysregulated PRR activity can lead to immune-related diseases, including immunodeficiency, inflammatory disorders, and autoimmune conditions (16).

The types of PRRs include toll-like receptors (TLRs), NOD-like receptors (NLRs), c-type lectin receptors (CLRs), and Rig-I-like receptors (5). This thesis focuses on TLR4 signalling and nucleic acid sensing pathways.

1.2.5 Toll-like receptor 4 signalling

TLRs are a subcategory of PRRs located on the cell surface and on endosomes. Humans and mice have 10 and 12, respectively. TLRs detect a broad range of PAMPS and DAMPS, including LPS, flagellin, and viral and mitochondrial RNA. TLR activation leads to TIR domain activation and a signalling cascade, leading to changes in cellular activities, such as transcriptional, translational and metabolic changes. In particular, TLR4 senses LPS derived from gram-negative bacteria. Specifically, serum LPS-binding protein (LBP) sequesters LPS aggregates termed micelles. Cluster of differentiation 14 (CD14) then isolates an LPS monomer from the micelle and passes it to the TLR4/ Myeloid differentiation protein 2 (MD-2) complex localised on the outer cell membrane (17). Upon activation, cell-membrane-bound TLR4 activates the Myeloid differentiation primary response 88 (MYD88)-dependent pathway. Specifically, TLR4 binds to MYD88-adapter like (MAL) (18), which binds MYD88 and subsequently Interleukin-1 receptor-associated kinase 1 (IRAK1). IRAK1 activation leads to Myddosome formation consisting of IRAK1, IRAK2, and IRAK4 (19). The active Myddosome then recruits the ubiquitin ligase TRAF6, which leads to TAK1 activation and activation of the IKK complex consisting of IKKα, IKKβ, and IKKɣ. This leads to NFκB transcription factor activation, translocation into the nucleus and transcription of canonical pro-inflammatory cytokines such as IL1β, TNF and IL6. This MYD88-dependent pathway is often referred as the early phase which occurs within minutes and responds faster than the TRIF-dependent pathway.

Activated TLR4 can also be endocytosed (20), whereby signalling occurs via the TIR-domain-containing adapter-inducing interferon-β (TRIF)-dependent, MYD88-independent pathway, leading to interferon response factor 3 (IRF3) transcription factor activation and subsequent induction of Type I Interferon responses and an antiviral response. This is referred to as the late phase and occurs within hours. Specifically, TLR4 binds to the TRIF-Related Adaptor Molecule (TRAM) in the endosome. TRAM then bridges the connection between TLR4 and TRIF. TRIF forms a complex with TRAF3 and TBKI. TBK1 phosphorylation phosphorylates IRF3, which enters the nucleus and binds to the Interferon-Stimulated Response Element (ISRE) to mediate the transcription of IFNα/β (21, 22) **(**Figure 1**).**

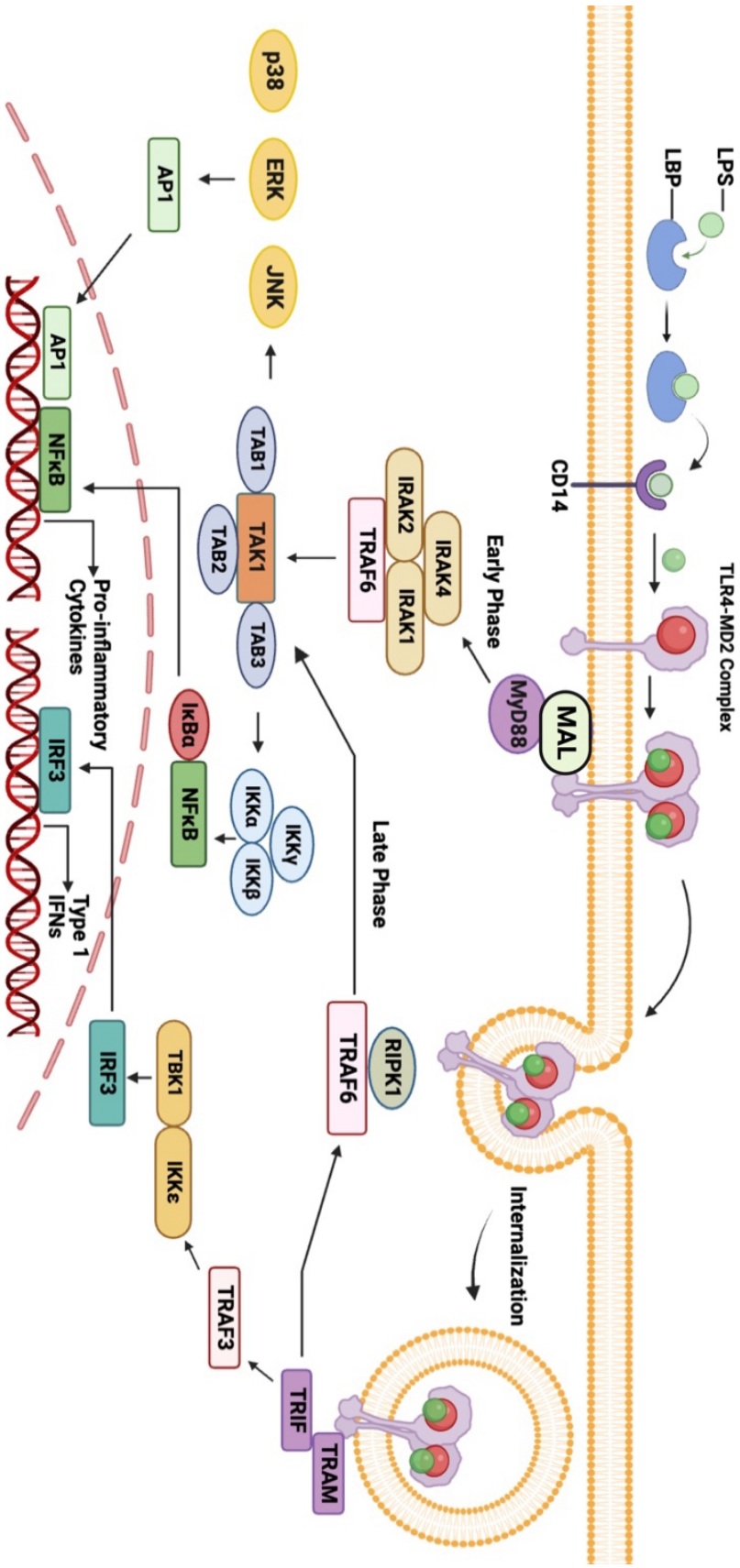


Figure 1. Toll-Like Receptor 4 signalling pathway

Figure 1. Toll-Like Receptor 4 signalling pathway

TLR4 senses LPS derived from gram-negative bacteria. Specifically, serum LBP sequesters LPS aggregates or micelles. CD14 then isolates an LPS monomer from the micelle and passes it to the TLR4/ MD-2 complex localised on the outer cell membrane (17). Upon activation, cell-membrane-bound TLR4 activates the MYD88-dependent pathway. Specifically, TLR4 binds to MAL (18) which binds MYD88 and subsequently IRAK1. IRAK1 activation leads to Myddosome formation consisting of IRAK1, IRAK2, and IRAK4 (19). The active Myddosome then recruits the ubiquitin ligase TRAF6, which leads to TAK1 activation and activation of the IKK complex consisting of IKKα, IKKβ, and IKKɣ. This leads to NFκB transcription factor activation and transcription of canonical pro-inflammatory cytokines such as IL1β, TNF and IL6. Activated TLR4 can also be endocytosed (20), whereby signalling occurs via the TRIF-dependent, MYD88-independent pathway, leading to interferon response factor 3 (IRF3) transcription factor activation and subsequent induction of Type I Interferon responses and an antiviral response. Specifically, in the endosome, TLR4 binds to TRAM. TRAM then bridges the connection between TLR4 and TRIF. TRIF forms a complex with TRAF3 and TBKI. TBK1 phosphorylation phosphorylates IRF3, which enters the nucleus and binds to the ISRE to mediate the transcription of IFNα/β (21, 22). Image created with Biorender.com

1.3 Type I interferons

Interferons are cytokines that interfere with viral replication in infected cells (23). They are produced by innate immune cells, such as macrophages and dendritic cells, and non-immune cells, such as fibroblasts and epithelial cells (24). Type I interferons consist of IFNα, IFNβ IFNε, IFNκ, and IFNω (25). There are 13 IFNα subtypes in humans, located on chromosome 9 and located on chromosome 4 in mice (26, 27).

A robust type I interferon response depends on PRR-induced recognition of viral or bacterial components such as nucleic acids like genomic RNA and DNA. These sensors include the endosomal viral dsRNA sensor TLR3, TLR4, the ssRNA sensors TLR7, the ssRNA sensors TLR8, and TLR9, which sense unmethylated CpG DNA. These sensors also include the cytosolic sensors RIG-I and MDA5, which sense dsRNA (28, 29). After viral recognition, this leads to intracellular signalling events, which converge on the induction of type I interferons. Viral dsRNA or the tool compound high molecular weight poly(I: C) can be sensed by TLR3, leading to downstream signalling via TRIF, TRAF and TBK1, which activates transcription factors IRF3 and IRF7 and type I interferons. RIG-I sensed di and tri-phosphate dsRNA, and MDA5 senses long dsRNA. Their activation leads to MAVS activation on the mitochondria and subsequent TBK1 and IRF3 activation. cGAS senses dsDNA and leads to the production of 2'-3'-cGAMP, which activates STING, TBK1, and IRF3-mediateed type I interferons. TLR7/8 and TLR9 sense ssRNA and dsDNA, respectively. Their activation leads to MYD88, IRAK1/4, TRAF3/6, and IRF7-induced type I interferons (30) **(see Figure 2**).

Subsequently, IFNα/β binds to the heterodimeric transmembrane receptor IFNα/β receptor (IFNAR) composed of IFNAR1 and IFNAR2 in an autocrine or paracrine manner. IFNAR binding activates Janus kinase (JAK1) and tyrosine kinase 2 (TYK2), which leads to STAT1/STAT2 activation and forms a complex with IRF9, termed ISGF3, which binds to the interferon-stimulated response elements (ISRE) and transcribes hundreds of antiviral, antiproliferative and immunomodulatory interferon-stimulated genes (ISGs) (30-32) **(see Figure 2).**

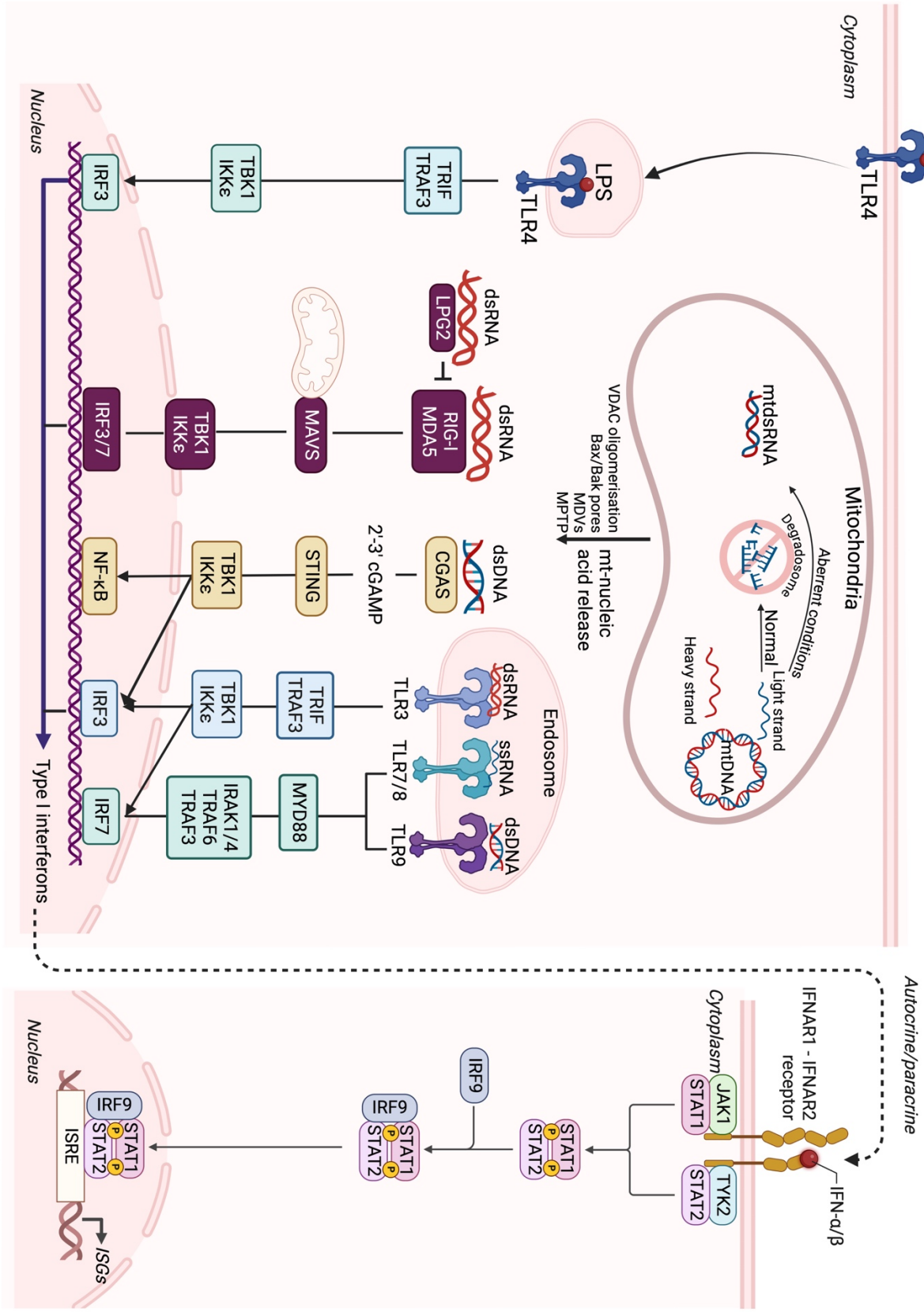


Figure 2. Mitochondrial nucleic acid release and PRR-induced type I interferon signalling

Figure 2. Mitochondrial nucleic acid release and PRR-induced type I interferon signalling

Mitochondria undergo bidirectional transcription, resulting in the generation of both light and heavy-strand-encoded RNA. Under normal conditions, the degradosome degrades the light strand encoded RNA, preventing the formation of immunogenic dsRNA. Mitochondrial nucleic acid release can occur during apoptosis, inflammatory diseases, mtDNA stress via TFAM deficiency, inflammasome activation, and infection (39). These nucleic acids are released via Bax/Bak pores, VDAC oligomerisation, mPTP pores and MDVs. Due to the proteobacterial origin of mitochondria, the release of their nucleic acids is immunogenic and sensed by PRRs. These sensors include the endosomal viral dsRNA sensors TLR3, the ssRNA sensors TLR7, the ssRNA sensors TLR8, and TLR9, which senses unmethylated CpG DNA. These sensors also include the cytosolic sensors RIG-I and MDA5, which sense dsRNA (28). After viral recognition, this leads to intracellular signalling events, which converge on the induction of type I interferons. Viral or mitochondrial dsRNA or poly(I:C) can be sensed by TLR3, leading to downstream signalling via TRIF, TRAF and TBK1, which activates transcription factors IRF3 and IRF7 to and subsequently, type I interferons. RIG-I sensed di and tri-phosphate dsRNA, and MDA5 senses long dsRNA. Their activation leads to MAVS activation on the mitochondria and TBK1 and IRF3 activation. cGAS senses dsDNA and leads to the production of 2'-3'-cGAMP which activates STING, TBK1, and IRF3-mediateed type I interferons. TLR7/8 and TLR9 sense ssRNA and dsDNA, respectively. Their activation leads to MYD88, IRAK1/4, TRAF3/6, and IRF7-induced type I interferons. Subsequently, IFNα/β binds to the heterodimeric transmembrane receptor IFNα/β receptor (IFNAR) composed of IFNAR1 and IFNAR2. IFNAR binding activates Janus kinase (JAK1) and tyrosine kinase 2 (TYK2), which leads to STAT1/STAT2 activation and forms a complex with IRF9, termed ISGF3, which binds to the interferon-stimulated response elements (ISRE) and transcribes hundreds of antiviral, antiproliferative and immunomodulatory interferon-stimulated genes (ISGs) (31) Image created with Biorender.com referencing Peace et al., (33).

1.3.1 Type I interferons in disease

Nearly all cells express the receptors for type I interferons, demonstrating their important role in orchestrating the immune response to various circumstances, such as viral, bacterial, and parasitic infections. The importance of type I interferon responses is demonstrated during diseases where type I interferons are dysregulated, including chronic viral infection, bacterial infection, autoimmunity, and cancer (31).

1.3.2 Type I interferons in viral infection

In response to viral infections, macrophages produce type I IFNs α/β and subsequent induction of ISGs, which halt viral replication in infected and nearby cells. Furthermore, type I IFNs act on other immune cells. For example, type I IFNs boost antigen presentation in antigen-presenting cells and promote differentiation into dendritic cells. Furthermore, during active viral infection, type I IFNs boost the anti-viral responses of adaptive immune cells such as natural killer (NK) cells, T cells, myeloid cells, and B cells. Type I IFNs induce a T_H1, IFNɣ producing phenotype in humans. They also improve the cytotoxic effect and IFNɣ production in NK cell responses (31).

However, type I interferons can also be detrimental to viral infection and contribute to chronic viral infection. During chronic infection, however, type I interferons can be immunosuppressive and thus prevent timely viral clearance. This can occur by increasing the production of the immunosuppressive cytokine IL10 and increasing the expression of PDL1 on antigen-presenting cells, which causes the inhibition and death of T cells, preventing viral clearance (31).

1.3.3 Type I interferons in bacterial infection

Classically, interferons are antiviral cytokines. However, type I interferons also determine the outcome of bacterial infection based on the type and site of bacterial infection, how the bacteria replicate and their associated virulence factors. In some cases, type I IFNs are protective for the host. Type-I interferon signalling also mediates bacterial killing. As previously mentioned, TLR4 induces type I interferon production in response

to gram-negative bacteria (21). Type I interferons also contribute to immunity against invading bacteria (34). Mechanistically, type I interferons mediate the production of IFNɣ in response to bacterial infection which aids in macrophage microbicidal activity.

Furthermore, bacterial-induced type I interferon responses in macrophages contribute to reactive oxygen species and nitric oxide synthesis to kill bacteria (35, 36). Type I interferons also induce the expression of the ISG indoleamine-2,3-dioxygenase, which regulates amino acid catabolism and reduces tryptophan availability for cytosolic bacteria such as *Chlamydia psittaci* (37). Type I interferons also prevent the entero-invasion of invasive bacteria such as *Shigella flexneri* across the intestinal endothelial layer (38). Type I interferons also cause maturation and activation of immature DC, leading to the production of IL12 and the subsequent STAT4 signalling and immune cell recruitment and activation of NK cells and T_H1 cells to produce IFNɣ (39).

1.3.4 IL1β / IFNβ co-regulation

IL1β is the infamous pro-inflammatory cytokine central to immune cell inflammatory responses. IL1β signalling dysregulation can be seen in diseases where IL1β is chronically upregulated, such as Cryopyrin-Associated Autoinflammatory Syndromes (CAPS). Individuals with CAPS present with the characteristic inflammatory phenotype of high fever, rash, and malaise. IFNβ is known to be a negative regulator of IL1β. This was seen in the 1990s when IFNβ could both block IL1β and induce the expression of Interleukin 1-receptor antagonist (IL1RA) in human PBMCs (40-42). Furthermore, $IFN\beta^{-/-}$ mice express elevated IL1β after *Salmonella typhimurium* infection (43).

However, elevated IFNβ can be deleterious in some bacterial infections, such as MTB. Elevated IL1β boosts eicosanoids to block IFNβ, which is linked to bacterial containment. Furthermore, MTB-infected patients with low IL1β, dysregulated eicosanoids, and elevated IFNβ is associated with increased disease severity (44).

1.3.5 Type I interferons in inflammation

The term interferonopathies is assigned to a group of genetic Mendelian disorders which is characterised by dysregulated interferon production. This can be via overproduction,

oversensitivity, or the inability to negatively regulate the interferon response. Examples include systemic lupus erythematosus (SLE) (45), Aicardi–Goutieres syndrome (46), and STING-associated vasculopathy (47, 48). In SLE patients, anti-mtRNA and mtDNA IgG and IgM autoantibodies are clinical markers of disease in murine models and patients (49).

During a viral infection, an appropriate host innate immune response relies on a timely type I interferon response, which inhibits the viral replication cycle. Viral clearance is followed by a return to homeostasis, characterized by a reduction in viral PAMPs, decreased activation of PRRs, and lower levels of inflammatory cytokines (50). Anti-inflammatory cytokines, such as IL-10 and TGF-β, are produced to limit the inflammatory response. Additionally, regulatory T cells and myeloid-derived suppressor cells contribute to driving an anti-inflammatory response. Macrophages clear debris caused by the viral infection and inflammation through phagocytosis. This process helps prevent excessive type I interferon responses, as seen in certain autoimmune diseases (51). Understanding how type I interferons regulate disease in different contexts is important for future therapeutic developments.

1.4 Mitochondria

Eukaryotic cells arose 2 billion years ago after the endosymbiotic relationship with an α-proteobacterium, which evolved into the modern-day mitochondrion. Mitochondria are double-membraned organelles with their own circular chromosome of 16.5 kb in mammals. The mitochondrial genome encodes 37 genes; 2 rRNA-encoding genes, 22 tRNA-encoding genes, and 13 genes which encode proteins involved in oxidative phosphorylation (OXPHOS) involved in the generation of the proton gradient and generates approximately 60 kg of ATP per person per day (52, 53). The remaining 99% of mitochondrial proteins needed for mitochondrial function are transcribed in the nucleus, translated in the cytosol and are imported into the mitochondria via mitochondrial localisation sequences (54).

1.4.1 Mitochondria in disease

Mitochondrial diseases are a result of errors of metabolism and emphasise the importance of mitochondria in health and disease. They are characterised by a group of metabolic diseases determined by mutations in the nuclear or mitochondrial genome that affect mitochondrial function, most of all, the OXPHOS system (55). These groups of disorders are complex, can present at different ages in humans, and affect multiple organs. Their complexity is demonstrated by mutations in different sites of the same protein complex which can result in vastly different clinical presentations (56). Leigh syndrome is one of the most common mitochondrial disorder, affecting 1 in 40,000 people worldwide. Symptoms commonly present in early childhood and include neurological abnormalities and heart, vision, and breathing complications (57). There are approximately 75 genes associated with Leigh syndrome, 80% are nuclear-encoded and involve the generation of cellular ATP including SDHA, the catalytic domain of succinate dehydrogenase (58).

1.4.2 The TCA cycle and cancer

Paragangliomas are rare neuroendocrine neoplasms that develop from abnormal growth of chromaffin cells. They are found in adrenal glands as pheochromocytomas or throughout the body as paragangliomas. They can be benign or malignant, producing excessive catecholamines, such as adrenaline, leading to symptoms of high blood pressure, tachycardia, and sweating and can be lethal if untreated. Treatment involves tumour excision or more extreme interventions (59). They are often triggered by pathogenic mutation of tricarboxylic acid (TCA) cycle enzymes such as SDH subunits, fumarate hydratase, malate dehydrogenase and Isocitrate dehydrogenase 1. These mutations often lead to protein dysfunction and can lead to the accumulation of oncometabolites succinate, fumarate, L2HG, and D2HG. These metabolites can outcompete α-KG for 2-oxoglutarate-dependent dioxygenases (2-OGDD), leading to tumorigenesis (60). SDH is a heterotetrametric protein complex encoded by the nuclear genome. Mutations in SDH can lead to several mitochondrial disorders, including neoplasms such as paragangliomas and gastrointestinal stromal tumours, neurodegenerative disorders such as Leigh syndrome, and other disorders such as cardiomyopathy and Cowden syndromes (61).

The incidence of paraganglioma in the general population is relatively low but increases in those who have germline mutations in SDHB, SDHC, and SDHD. This leads to excessive succinate accumulation and subsequent oncogenesis via DNA hypermethylation, succinate receptor 1 (SUCNR1) signalling and HIF1α stabilisation. Furthermore, in the tumour microenvironment (TME), succinate can be immunosuppressive and promote an M2-like macrophage polarisation, inhibiting $CD8^+$ T-cell proliferation and activation (62).

1.4.3 Mitochondrial nucleic acid release mechanisms

Mitochondrial DNA undergoes bidirectional transcription, which leads to the generation of light and heavy-strand-encoded RNA. These overlapping transcripts can form dsRNA structures. Under normal conditions, the degradosome rapidly degrades the light strand to prevent mtdsRNA formation (63). Initially, it was thought that these immunogenic mitochondrial nucleic acids were only released during times of cell death or apoptosis, but it is now appreciated that mitochondrial nucleic acid release has been shown to occur in numerous contexts, including inflammatory diseases, mtDNA stress via mitochondrial transcription factor A (TFAM) deficiency, inflammasome activation, and infection (64). Furthermore, mitochondrial nucleic acid release is a feature of autoimmune diseases such as SLE (65).

Bax/Bak are known to release mtDNA during apoptosis (66). However, mt nucleic acids have now been shown to be released in non-apoptotic macrophages via VDAC, mitochondrial permeability transition pore (mPTP) opening, and mitochondrial-derived vesicles (MDVs).

VDAC is located on the outer mitochondrial membrane. VDAC1, the monomer, undergoes oligomerisation to create a mitochondrial outer membrane pore. This oligomerisation occurs under times of mitochondrial stress such as in response to mitochondrial reactive oxygen species (mtROS) production. Oxidised mtDNA is then either repaired or cleaved by the endonuclease flap-structure-specific endonuclease 1 (FEN1) into 500-650 base pair segments. This cleavage step is necessary for oxidised mtDNA to cross the inner mitochondrial membrane (IMM) via the mitochondrial permeability transition pore (MPTP) and finally leave VDAC oligomers (67).

Mitochondrial DNA damage is associated with SLE and its associated damage and disease duration (68). PBMCs from SLE patients also have increased VDAC oligomerisation. VBIT4, a VDAC oligomerisation inhibitor, has been shown to block serum mtDNA, interferons and disease severity in a mouse model of MRL/MpJ-*Fas*^{lpr} lupus-prone mice (69).

1.4.4 Mitochondrial nucleic acids activate PRRs

PRRs can also sense these mitochondrial nucleic acids. These receptors include mtDNA sensors TLR9 (which senses hypomethylated CpG motifs on mtDNA), cGAS, which senses mtdsDNA > 18 bp, absent in melanoma 2 (AIM2), which senses mtdsDNA, and Nod-Like Receptor Protein 3 (NLRP3), which senses oxidised mtdsDNA (70). MtRNA sensors include RIG-I and MDA5, TLR7/8, which senses ssRNA, and TLR3, which senses mtdsRNA. The release of mitochondrial nucleic acids is known to be pathological. There are many contexts in which mitochondrial nucleic acids are released to drive immunopathology. In the context of alcohol-induced hepatitis, mtdsRNAs derived from hepatocytes stimulate TLR3 in Kupfer cells to drive IL17 and alcohol-associated liver disease (71). In a model of acute kidney injury, nephrotoxic agents cause immunopathogenic mtDNA release, which drives cGAS signalling and leads to renal tubule inflammation (72). Furthermore, mtdsRNA release has been implicated in Huntington's Disease. Specifically, Huntington's disease patients elicit greater mtdsRNA cytosolic release in neurons, which leads to inflammatory responses and neuronal cell death implicated in the disease (73). Moreover, mtdsRNA levels are elevated in the synovial fluid and damaged cartilage of individuals with osteoarthritis. In an osteoarthritis mouse model, mitochondrial damage in chondrocytes causes mtdsRNA release, which is sensed by TLR3 to elicit a type I interferon response and inflammatory response. This process was shown to be rescued via autophagy-induced sequestration of mtdsRNA (74). These studies show a clear association with mitochondrial nucleic acids and disease pathology.

1.4.5 Cytosolic Mt-dsRNA sensors

Mt-dsRNA is sensed by cytosolic sensors RIG-I (75), encoded by Ddx58, and MDA5 (76), encoded by Ifih1. MDA5 senses longer dsRNA (>1000 bp) via the RNA phosphate

backbone and the 2'hydroxyl group. This leads to the sequence-independent recognition of dsRNA.

RIG-I senses shorter dsRNA featuring 5' di and tri-phosphate groups. Shorter mtdsRNA are known to be generated during mtDNA double-stranded breaks (DSBs) in times of replication errors or cellular stressors such as chemotherapeutic agents or ionizing radiation (77). mrdsRNA from DSBs is known to drive a RIG-I-mediated type I interferon responses and is a immune surveillance mechanism (78).

Therefore, mitochondria can produce ligands for both RIG-I and MDA5 signalling. Upon activation of RIG-I or MDA5, RIG-I undergoes tetramerization, while MDA5 undergoes oligomerisation, both via their respective CARD domains. Their activation promotes MAVS aggregation at the outer mitochondrial membrane (79). MAVS activates TBK1 and IKK leading to IRF3 and NFκB transcription factor activation. This leads to the subsequent type I interferon and inflammatory cytokine responses **(see Figure 2).**

1.5 Immunometabolism

Over the last decade, with the advancements of metabolic analysis tools, immunologists have focused on how immune cell metabolism can dictate their effector functions. This has led to the emergence of the new, exciting field of immunometabolism, which can be defined as the intricate relationship between immune cell metabolism and how it regulates immune cell effector function. Immunometabolism has therapeutic potential whereby regulating immune cell metabolism may control immunological responses in autoimmunity, cancer, and infection (1, 80).

An important metabolic pathway that regulates immune cell function is the TCA cycle, also known as the citric acid cycle or Krebs cycle. It has been demonstrated that TCA cycle intermediates act as signalling molecules to regulate immune cell function, separate from their well-established metabolic roles (81).

1.5.1 M1 metabolic reprogramming

Resting macrophages respire utilising an uninterrupted TCA cycle. However, LPS stimulation of resting macrophages leads to an M1-like phenotype. Metabolically, M1 macrophages have suppressed OXPHOS and cause TCA cycle reprogramming. This

reprogramming is due to breakpoints occurring at IDH and SDH, leading to the accumulation of TCA cycle-derived metabolites citrate, itaconate, and succinate. Citrate is a prime example of a metabolite which also has immunological functions. Citrate accumulates, exits the mitochondria, and is converted into acetyl-CoA in the cytosol, which is involved in the acetylation of histones and the transcription of the anti-inflammatory cytokine IL-10. It can also be further converted into malonyl-CoA, which is used to produce prostaglandins via phospholipid synthesis (80). Furthermore, malonyl-CoA can malonylate lysine residues on target proteins such as glyceraldehyde-3-phosphate dehydrogenase (GAPDH), which is an inflammatory signal in macrophages (82). Citrate accumulation can, via cis-aconitate and the enzyme ACOD1, lead to itaconate accumulation. Itaconate accumulation causes the second breakpoint in the TCA cycle during metabolic reprogramming via SDH inhibition, leading to succinate accumulation (80).

Succinate accumulation is a key feature of inflammatory macrophages and has multiple mechanisms of action. Succinate directly inhibits prolyl hydroxylases (PHDs), causing HIF1α stabilisation and activation, which then drives mitochondrial ROS (mtROS), nitric oxide and the expression of core glycolytic genes involved in glucose import and glycolysis including those encoding GLUT1, PKM2, LDHA and PFKFB3. An increase in glycolysis also increases the production of inflammatory mediators associated with M1-like macrophages (1, 83).

Succinate can also be oxidised by SDH, leading to reverse electron transport (RET) at mitochondrial complex I and subsequent PHD inhibition and HIF activation. Succinate can also directly bind to G protein-coupled receptor 91 (GPR91), increasing cell chemotaxis, and promoting an anti-inflammatory cytokine signature. Succinate is also involved in succinylation of lysine residues on target proteins such as PKM2, which can regulate macrophage function (80). These changes contribute, in part, to their improved microbial killing and anti-tumour capacity. However, a dysregulated inflammatory response can contribute to immunopathology and chronic inflammatory disease including neurodegeneration (84), autoimmunity (85), and cancer (86).

1.5.2 M2 metabolic reprogramming

On the opposite end of the spectrum, M2-like macrophages, such as seen with IL-4 stimulation, are important in wound repair, tissue remodelling, and the resolution of inflammation and the return to homeostatic norms. Metabolically, M2-macrophages utilise OXPHOS and fatty acid oxidation, and produce less ROS compared to M1 macrophages. IL-4-stimulated macrophages increase glutamine metabolism, which forms glutamate and enters into the TCA cycle as αKG, which exits the mitochondria and acts as a co-factor with Jumonji domain-containing protein-3 (JMJD3), a histone demethylase, which mediates the transcription of anti-inflammatory cytokines (80, 87). Dysregulated M2 polarisation can be pro-fibrotic or pro-tumour as M2-like tumour-associated macrophages (TAMs) are immunosuppressive and contribute to immune evasion and tumour progression. Due to their heterogeneity, macrophage polarisation states are less polarised, but more of a spectrum.

1.6 Fumarate hydratase regulates mitochondrial nucleic acid release

It has been previously documented that the TCA cycle enzyme fumarate hydratase (FH) is required for an appropriate cytokine response in macrophages. This is evident as FH inhibition boosts IFNβ in macrophages. Mechanistically, genetic ablation or pharmacological inhibition of FH increases mitochondrial membrane potential (MMP), causing mtRNA release, which is sensed by TLR7, RIG-I, and MDA5 to induce IFNβ. Furthermore, Hooftman *et al*., demonstrate that this process occurs endogenously, as prolonged LPS stimulation of BMDMs leads to decreased FH expression, which leads to increased mtRNA release (3). Furthermore, cells from patients with SLE, which have increased IFNβ and increased mtRNA, have decreased FH expression.

A complementary study by Zecchini et al., demonstrated a similar phenotype in kidney cells. They show that chronic loss of FH in their model leads to mtDNA release. Mechanistically, the mtDNA is released, it is sensed by cGAS and leads to STING, TBK1, and subsequent IRF3 activation and induction of IFNβ and the innate immune response (4). Furthermore, they show that FH inhibition and mtDNA release are evident in hereditary leiomyomatosis and renal cell cancer and suggest a link between

mitochondrial dysfunction, mtDNA, chronic inflammation, and tumorigenesis seen in this disease. Interestingly, both of these studies demonstrate that MAVS, important in RIG-I, MDA5, and cGAS signalling, was dispensable for this response (4).

These results emphasise a role for mitochondria and, importantly, a TCA cycle enzyme in regulating innate immunity. It is interesting, therefore, whether other TCA cycle enzymes, such as SDH, may regulate similar mechanisms.

From a therapeutic perspective, it is important to uncover regulatory mechanisms of macrophage activation to discover better and more effective therapeutics for inflammatory diseases (88). Therefore, it is becoming increasingly evident that the TCA cycle is an immunometabolic hub, and controlling how TCA cycle intermediates regulate immune cell function has the potential to treat inflammatory diseases (1). One such metabolite, central to this thesis, is itaconate, which will now be discussed in more detail.

1.7 Itaconate: a potent immunometabolic regulator

1.7.1 History of itaconate

Itaconic acid, also termed methylenesuccinic acid, was first discovered by the Swiss chemist Samuel Baup, in 1837, as an unknown byproduct of the thermal decomposition of citric acid described it as "a new citric acid" (89). Three years later, the German scientist Gustav Crasso attributed the name itaconate to this unknown compound as an anagram of aconitate (90). In 1931 itaconate was discovered to be synthesised endogenously in the fungus *Aspergillus itaconicus* (91). The importance of itaconate in mammalian metabolism was not appreciated at this time. In 1949, itaconate was first demonstrated to inhibit SDH (92). Since the 1960s, the biotechnology industry used itaconate, derived from *Aspergillus terreus,* in polymer synthesis due to the double bond on its methylene group (93).

1.7.2 Itaconate in mammalian cells

In the year 1995, *Irg1* was demonstrated to be inducible by LPS in RAW 264.7 macrophages, linking it to the inflammatory response (94). Furthermore, in 2011, Strelko *et al*., discovered that itaconate was produced in LPS and IFN-γ -stimulated macrophages and further showed it is synthesised by cis-aconitate decarboxylase (ACOD1) in immune cells and hypothesised itaconate's role in the immune response (95). In 2013, Michelucci *et al.,* discovered that the gene *Irg1* encodes the protein ACOD1, which is responsible for itaconate synthesis formed by the decarboxylation of cis-aconitate (96). The carbon structures needed for itaconate synthesis are sourced from both the oxidative TCA cycle and the reductive carboxylation of α-ketoglutarate via isocitrate dehydrogenase (IDH) (**see Figure 3**) (97). Its structure consists of an organic α,β unsaturated dicarboxylic acid ($C_5H_6O_4$) containing two carboxyl groups and a double bond, which gives it thiol reactivity (98, 99). Upon LPS stimulation of macrophages, itaconate is produced via the decarboxylation of cis-aconitate by ACOD1. Itaconate accumulates intracellularly and can exit the cell via ATP-binding cassette transporter G2 (ABCG2) in an ATPase-dependent manner (100). Extracellular underivatised itaconate can indeed enter cells. Chen *et al.,* demonstrate that extracellular itaconate can enter hepatocytes via SLC13A3

in-vitro and *in-vivo* and improves antibacterial innate immunity in hepatocytes (101). It's yet unknown whether this is the itaconate importer in other cells.

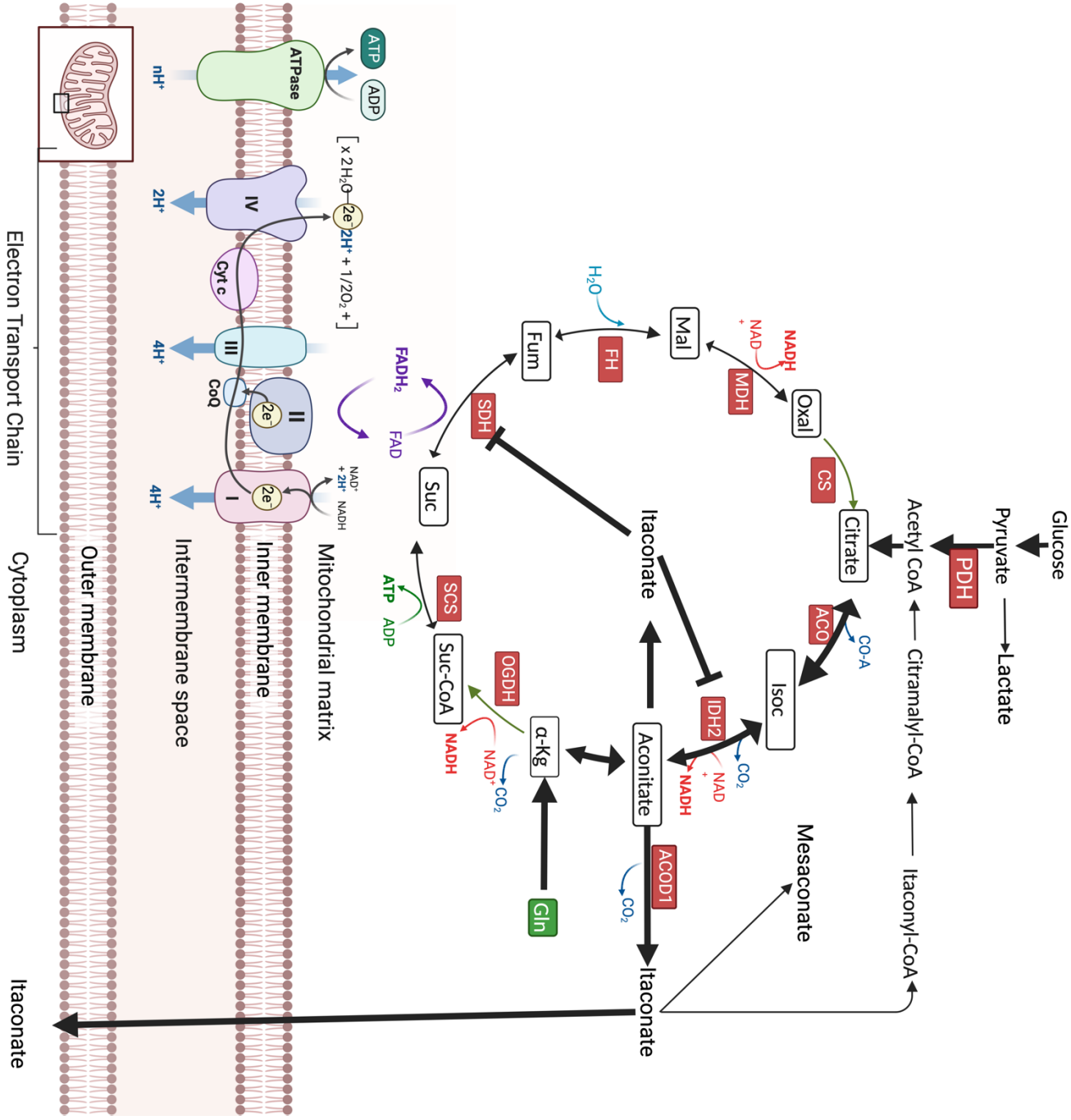


Figure 3. OXPHOS, the ETC, itaconate synthesis, and metabolism

Figure 3. Itaconate synthesis and metabolism

The carbon structures needed for itaconate synthesis are sourced from both the oxidative TCA cycle and the reductive carboxylation of α-ketoglutarate via isocitrate dehydrogenase (IDH) (97). It's structure consists of an organic α,β unsaturated dicarboxylic acid ($C_5H_6O_4$) containing two carboxyl groups and a double bond, which gives it thiol reactivity (98, 99). Upon LPS-stimulation of macrophages, itaconate is produced via the decarboxylation of cis-aconitate by ACOD1. After itaconate synthesis, itaconate can be further metabolised, by succinyl-CoA synthetase, into itaconyl-CoA. Itaconyl-CoA can then be hydrated by Citrate lyase subunit beta-like (CLYBL) protein into (s)-citramalyl-CoA which feeds into the formation of acetyl-CoA and pyruvate (102-104). SDH inhibition by itaconate is essential to macrophage metabolic reprogramming and is important in many of the immunomodulatory and antiviral mechanisms demonstrated by itaconate (2, 105). Itaconate inhibits SDH via competitive inhibition of the active site SDHA. SDH inhibition causes succinate accumulation, which leads to PHD inhibition and HIF1α stabilisation, SUCNR1 binding, RET, and succination (2, 105). Itaconate inhibits its own synthesis via inhibition of IDH2, likely by altering NADP+/NADPH ratios and inhibiting SDH (97).Pyruvate dehydrogenase (PDH). Aconitase 2 (ACO). Isocitrate dehydrogenase (IDH). oxoglutarate dehydrogenase complex (OGDH). succinyl-CoA synthetase (SCS). Succinate dehydrogenase (SDH). Fumarate hydratase (FH). Malate dehydrogenase (MDH). Citrate synthase (CS). Nicotinamide adenine dinucleotide (NAD). Flavin adenine dinucleotide (FAD). Image created with Biorender.com

1.7.3 Properties of itaconate

Research regarding itaconate biology in immunity is constantly expanding, and new mechanisms of how itaconate functions are frequently uncovered. These mechanisms include cysteine reactivity, enzyme inhibition, antibacterial and antiviral properties, receptor signalling, and epigenetic regulation. Furthermore, itaconate has been implicated in many disease models. Itaconate is anti-microbial (106-108). Itaconate is antiviral in zika virus-infected murine neurons (109). Itaconate ameliorates a pharmacologically induced EAE model *in vivo* (110). Itaconate is antifibrotic in a murine model of idiopathic pulmonary fibrosis (111). Itaconate also ameliorated type II collagen-induced arthritis in rats *in-vivo* (112). Itaconate also ameliorates a murine model of renal (113), cerebral (114) ischemia-reperfusion injury and systemic inflammation.

1.7.4 Anti-microbial roles of itaconate

Itaconate has multiple anti-microbial mechanisms. It was first shown to be anti-microbial by inhibiting bacterial Isocitrate lyase (ICL), a key enzyme in the glyoxylate shunt pathway needed for bacterial growth, in *Mycobacterium tuberculosis*, *Salmonella enterica,* and *Pseudomonas Indigofera* (106, 107, 115). Moreover, the itaconate derivative, itaconyl-CoA is also anti-microbial. When itaconate is converted into itaconyl-CoA, it blocks methylmalonyl-CoA mutase (MCM) in MTB, which inhibits propionyl-CoA–dependent MTB growth (116). Furthermore, itaconate is also anti-microbial during Salmonella infection. Macrophages directly shuttle itaconate into Salmonella containing vacuoles in a mechanism by which Rab32, a Rab family Guanine triphosphate, along with its co-factor Bloc3, interacts with ACOD1 and localises it to vacuoles, which directs itaconate synthesis directly into Salmonella-containing vacuoles to kill Salmonella (117). This process was shown to be regulated by the microbial-induced activation of the lysosomal biogenesis factor transcription factor EB (TFEB) (118) (**Figure 4**).

Some bacteria have evolved to utilise itaconate to their advantage, emphasising its importance as an anti-microbial metabolite. For example, some bacteria metabolise itaconate into fuel or develop ways to regulate itaconate for their benefit. *Yersinia pestis* and *Pseudomonas aeruginosa* express genes such as itaconate coenzyme A transferase,

itaconyl-CoA hydratase, and (S)-citramalyl-CoA lyase, which metabolises itaconate into carbon sources, such as acetyl-coA and pyruvate which allow their survival in macrophages (108). Moreover, *Staphylococcus aureus* causes persistent lung infections in humans. *S. aureus* has been shown to drive host itaconate production, which inhibits *S. aureus* glycolysis via inhibiting Aldolase A and thus leads to excessive extracellular polysaccharides which further stimulates itaconate production in a feed-forward loop. These extracellular polysaccharides can be used for biofilm formation and act as a selection pressure for strains that use itaconate for biofilm formation. This leads to bacterial survival and subsequent chronic airway infection (119) (**Figure 4**).

Neutrophils are the primary immune cells which combat *S. aureus* infection via NADPH oxidase-induced oxidative burst. Neutrophils are now understood to produce itaconate in response to *S. aureus* infection. *S. aureus* evades neutrophil bacterial killing by inducing itaconate production, which blocks neutrophil glycolysis and NADPH oxidase-dependent oxidative burst (120). Discovering that different bacteria have demonstrated convergent evolution to either utilise or evade itaconate, further supports these anti-microbial claims (**Figure 4).**

1.7.5 Antiviral roles of itaconate

Itaconate has been shown to have antiviral properties in the context of Zika virus (ZIKV), West Nile Virus (WNV), and Influenza A virus (IAV) infection (121). Daniels *et al.,* demonstrate that ZIKV-infected murine neurons induced itaconate production via ZBP1, RIPK1/3, and IRF1 induction, leading to SDH inhibition and the accumulation of succinate. Furthermore, *Irg1*$^{-/-}$ mice had increased ZIKV and WNV titers and increased mortality compared to *Irg1*$^{+/+}$ mice *in-vivo* after this intracranial infection model. The antiviral response of itaconate, in this study, was attributed to SDH inhibition by itaconate. Furthermore, a well-established SDH inhibitor, dimethyl malonate (DMM), was also anti-viral in this model of neuronal ZIKV and WNV intracranial infection *in-vivo* (109). This antiviral effect was attributed to the antiviral immune response of murine neurons rather than the direct antiviral effects of itaconate (**Figure 4).**

Itaconate was also shown to have anti-influenza properties. Sohail *et al.,* demonstrated that IAV primarily targets monocytes and drives ACOD1 in monocytes and

macrophages. In a murine model of IAV infection, ACOD1 competent mice had reduced inflammatory markers and maintained a normal body weight compared to ACOD1 knockout mice. Furthermore, exogenous itaconate and derivatives, although they all drove a separate and unique cytokine profile, all three compounds commonly reduced the expression of pro-inflammatory cytokines and chemokines CXCL10 (IP-10) and CCL2 (MCP-1) in IAV-infected dTHP1 cell lines. Furthermore, itaconate blocked interferon responses, including inhibition of phosphor-STAT1 in IAV-infected dTHP1 cell lines. Moreover, human lung tissue from patients with emphysema and pulmonary arterial hypertension was treated with 10 mM itaconate followed by IAV infection and showed a significant reduction in CXCL10, ISG15, and *IP10* with no effect on IAV viral titre. However, in A549 cells, both itaconate and, to a greater extent, 4-OI could inhibit IAV viral titres. Finally, itaconate had no effect on *IFNB* expression in IAV-infected PBMCs (122).

Figure 4. Antiviral and antibacterial properties of itaconate

Figure 4. Antiviral and antibacterial properties of itaconate

Upon exposure to pathogens, macrophages upregulate the gene *Irg1,* which encodes for the protein ACOD1, causing itaconate synthesis. **1**, During bacterial infection, such as with Mtb and *S. typhimurium*, macrophage-derived itaconate inhibits isocitrate lyase (ICL), which inhibits the glyoxylate shunt required for their growth and pathogenicity (106, 107). **2**, Itaconate is further metabolised into itaconyl-CoA, which inhibits methylmalonyl-CoA mutase (MCM) and prevents propionyl-CoA–dependent bacterial growth in Mtb (116). **3**, In murine neuronal cells, zika virus infection is sensed by ZBP1 and leads to RIPK1/3 activation and IRF1-induced induction of *Irg1* and subsequent ACOD1-induced itaconate production. Itaconate-dependent SDH inhibition blocks zika virus replication and leads to an antiviral state (109). **4**, Salmonella-infected macrophages induce TFEB-induced ACOD1 expression and subsequent itaconate production. ACOD1 localises with RAB32 GTPase and the co-factor BLOC3 which directs itaconate synthesis directly into Salmonella-containing vacuoles (117, 118). Bacteria, such as *S. aureus* and *P. aeruginosa* can also use itaconate as fuel for their own survival. Itaconate causes membrane stress in *S. aureus* and *P. aeruginosa* and inhibits aldolase A (ALDOA) and, thus, bacterial glycolysis. This leads to extracellular polysaccharide accumulation, which induces ACOD1, leading to further itaconate production and a positive feed-forward loop of extracellular polysaccharides that bacteria can use for biofilm formation. This selects for bacterial strains that produce biofilms, leading to bacterial survival and pathogenesis (119). ***5****, P. aeruginosa* infected murine lungs stimulate local macrophage-induced itaconate production which binds to OXGR1 GPCR in ciliated cells, leading to Ca^{2+} signalling and increased cilia-induced mucin clearance and improved bacterial clearance and survival (123). **6**, *S. aureus* evades bacterial killing by inducing TFEB-induced itaconate in neutrophils which inhibits neutrophil glycolysis and NADPH oxidase-induced oxidative burst (120). Image created with Biorender.com

1.7.6 Itaconate is an enzyme inhibitor

Itaconate causes enzyme inhibition in host cells, and bacteria to modulate inflammatory responses and bacterial clearance. This occurs either by alkylation of cysteines, competitive inhibition, or metabolic regulation. Itaconate has been shown to inhibit glycolytic enzymes. LPS-stimulated macrophages are known to upregulate aerobic glycolysis as part of their metabolic reprogramming to quickly source ATP needed for their inflammatory response and M1 polarisation (124). Qin *et al.,* demonstrated, using a thiol-reactive probe to uncover the cysteine reactivity of itaconate, that itaconate causes the cysteine modification of several glycolytic genes, including GAPDH, lactate dehydrogenase (LDH), and ALDOA. Itaconate modified Cys73 and Cys339 on ALDOA and Cys84 of LDHA, which inhibited their enzyme activity in LPS-stimulated Raw264.7 macrophages. This suggests that itaconate blocks glycolysis via ALDOA enzyme inhibition and is an important mechanism in the anti-inflammatory function of itaconate (125).

1.7.7 Itaconate inhibits SDH

SDH inhibition by itaconate is essential to macrophage metabolic reprogramming and is important in many of the immunomodulatory and antiviral mechanisms demonstrated by itaconate (2, 105). Itaconate inhibits SDH via competitive inhibition of the active site SDHA. As the Michaelis constant (K_m) for succinate is 0.29 mM, the dissociation constant (Ki) for itaconate is 0.22 mM (126), and physiological intracellular succinate levels are approximately 1 mM, that would infer that itaconate IC50 and IC100 are approximately 1 mM and 10 mM, respectively. These are itaconate concentrations which have been demonstrated after LPS stimulation by other groups (127, 128). SDH inhibition causes succinate accumulation, which leads to PHD inhibition and HIF1α stabilization, SUCNR1 binding, RET, and succination as described above (2, 105).

1.7.8 Itaconate inhibits TET2

2OGDDs are a group of enzymes that play an important role in cellular metabolism, epigenetic regulation of gene transcription, hypoxia-inducible factor regulation, and are cancer biology. Ten eleven translocation 2 (TET2) is one such enzyme. TET2 enzymes

convert 5-methylcytosine (5mC) to 5-hydroxymethylcytosine (5hmC) with the aid of Fe^{2+} and α-ketoglutarate as co-factors and generate succinate and CO_2 as byproducts. This occurs at DNA sites, facilitating DNA demethylation and gene transcription (129). Itaconate has been shown to outcompete α-ketoglutarate for its co-substrate site, inhibiting TET2 catalytic activity, preventing DNA demethylation and inhibiting transcription factor accessibility and subsequent gene transcription. Tet2 inhibition by itaconate blocked NFκB and STAT signalling in RAW 246.7 macrophages leading to suppression of secondary inflammatory cytokine signalling (130). They also demonstrated, using 4-OI-treated versus *Tet2*-KO RAW 264.7 cells, that 4-OI and *Tet2*-KO cells had a large proportion of commonly regulated LPS-induced gene transcription. They also showed that underivatised itaconate blocks LPS-induced *Nfkbiz*, *Il1b, Cxcl9, Cxcl10,* and *Cxcl11* in a TET2-dependent manner. They also demonstrated that ACOD1-deficient mice were more susceptible to sepsis, which was dependent on TET2. These results suggest that underivatised itaconate inhibits TET2, which may significantly impact the LPS-induced transcriptional response in macrophages. However, the extent to which itaconate, rather than 4-OI used here, regulates gene transcription via TET2-inhibition is still to be demonstrated (130).

1.7.9 Itaconate inhibits its synthesis via enzyme inhibition

Itaconate production in murine macrophages depends on the oxidative TCA cycle and the reductive carboxylation of α-ketoglutarate via isocitrate dehydrogenase (IDH). Itaconate inhibits its synthesis via inhibition of IDH2, likely by altering NADP+/NADPH ratios and inhibiting SDH (97).

1.7.10 Itaconate acts via receptor signalling

Itaconate has recently been shown to act via receptor signalling. Itaconate can exit macrophages via ABCG2 (100) and binds GPR99, also termed oxoglutarate receptor 1 (OXGR1) of respiratory epithelial cells in a mouse model of pulmonary infection of *Pseudomonas aeruginosa.* OXGR1 receptor binding by itaconate leads to its activation, endocytosis and Ca^{2+} signalling, which leads to ERK signalling, increased cilia motility, and increased bacterial clearance (123). According to the Human Protein Atlas (131), OXGR1 expression is localised to cells such as extravillous trophoblasts and epithelial

cells with low expression in macrophages and other immune cells. It is unclear how itaconate signalling via OXGR1 regulates inflammatory macrophage function.

1.7.11 Itaconate: a cysteine modifier

Cysteines are relatively less abundant than other amino acids but are essential to protein function. Cysteine residues on proteins are highly nucleophilic due to the low dissociation energy of its sulfhydryl group (132). Over the past decade, there has been increasing evidence for the role of electrophilic compounds in inflammation (133). The unsaturated double bond of itaconate makes it a nucleophile and permits nucleophilic attack of cysteine residues, undergoing a covalent Michael addition termed 2'3-dicarboxypropylation. Cysteine modifications by itaconate and derivatives have shaped the field of itaconate biology.

1.7.12 Itaconate and NRF2

NRF2 is an anti-inflammatory transcription factor that regulates approximately 250 genes involved in the anti-inflammatory, cytoprotective and anti-oxidant response in macrophages (134, 135). This antioxidant response suppresses cellular ROS and HIF1α-induced inflammation (136). Furthermore, free NRF2 binds to the proximity and prevents RNA pol II binds to the promoter regions of *Il1b* and *Il6,* preventing transcription factor binding and their subsequent transcription (134). Nrf2 is protective in many disease models, including sepsis (137). Due to its regulatory importance, NRF2 is tightly controlled by KEAP1 and targets NRF2 for proteasomal degradation.

Bambouskova *et al.,* demonstrated that underivatised itaconate activated the KEAP1-NRF2 response. They showed that LPS-stimulated *Irg1*$^{+/+}$ BMDMs had higher NRF2 protein expression (138). Furthermore, Cifani *et al*., demonstrated, utilising differential tandem mass spectrometry on purified recombinant KEAP1 treated with 0 mM, 5 mM, or 50 mM itaconate, that 5 mM itaconate alkylated KEAP1 shown by a mass shift of 130.03 Da at Cys489, a NRF2-binding domain (139). Moreover, the itaconate derivatives DI and 4-OI have been shown to also activate NRF2 (138, 140). 4-OI have been shown to alkylate KEAP1 at Cys-151, preventing KEAP1-induced degradation of NRF2 and allows free NRF2 to promote an anti-inflammatory response (140).

1.7.13 Itaconate and NLRP3

The NLRP3 inflammasome is a central hub in the inflammatory response. Inflammasome activation requires two signals. Signal one leads to the transcriptional upregulation of IL1β and IL18 and can be mediated by LPS, while signal two is mediated by cellular stress such as ROS or ATP (141). Lampropoulou et al., demonstrated that, in an inflammasome assay of LPS +ATP treatment, *Irg1*$^{+/+}$ BMDMs produced less IL1β and IL18 compared to wild-type (WT) (126). However, this did not conclude whether this was a result of itaconate regulating signal one, or signal two such as inflammasome assembly. This is also confounded as itaconate can activate NRF2 which blocks *Il1b* transcription (134). Subsequently the same group showed that underivatised itaconate does not affect *Il1b* transcription, which would suggest that itaconate regulates inflammasome activation.

Hooftman *et al*., demonstrated that *Irg1*$^{-/-}$ BMDMs had increased inflammasome activation when compared to WT. Furthermore, 4-OI blocked LDH release, ASC speck formation, gasdermin d and IL1β processing. This suggested that 4OI affects inflammasome activation, rather than the priming stage. Indeed, 4-OI was shown to modify Cys-548 on NLRP3, preventing NLRP3-NEK7 interaction and subsequent inflammasome activation and IL1β release (142). *In-vivo* results demonstrated that 4-OI ameliorated urate-induced peritonitis while 4-OI blocked IL1β in CAPS patients.

1.7.14 Structurally similar compounds and itaconate derivatives

Given the importance of cysteines in protein structure, their modification is an important regulatory feature of itaconate. Derivatives were therefore created to improve, exploit or manipulate the characteristics of itaconate. Such derivatives include 4-OI, dimethyl itaconate (DI), and 4-ethyl itaconate (4-EI).

1.7.15 Itaconate catabolism

Itaconate can be further metabolised into itaconyl-CoA by the enzyme succinyl-CoA synthetase. Itaconyl-CoA can then be hydrated by Citrate lyase subunit beta-like

(CLYBL) protein into (s)-citramalyl-CoA which feeds into the formation of acetyl-CoA and pyruvate (102-104) (See **Figure 3**).

Itaconyl-CoA can react with lysine residues on target proteins. The amount of lysine modifications on the proteome seems to be significantly smaller than cysteine modification by itaconate, therefore the implications of itaconyl-CoA modifications are yet to be fully elucidated. As previously mentioned, itaconyl-CoA blocks methylmalonyl-CoA mutase (MCM) in Mtb, which inhibits. propionyl-CoA–dependent bacterial growth (116). Interestingly, 4-OI cannot form itaconyl-CoA due to the lack of a carboxylate group, which is present in itaconate. This could explain more differences between itaconate and its derivative 4-OI (143).

1.7.16 Mesaconate and citraconate

ACOD1 is, at least indirectly, responsible for mesaconate synthesis. He *et al*., demonstrated that mesaconate was absent in ACOD1 KO cells after LPS stimulation. He *et al*., demonstrated that both mesaconate and itaconate inhibit glycolysis to a similar extent. Furthermore, both itaconate and mesaconate inhibited LPS-induced *IL1b, Il6, and Il10* gene expression, and IL6 and IL10 production in RAW264.7 cells. Furthermore, in BMDMs, mesaconate did not affect inflammasome activation. Interestingly, mesaconate increased the LPS-induced ISG CXCL10 but could not measure IFNβ in their assay (144).

Mesaconate did not have the same effect on TCA cycle activity and cellular respiration as itaconate. By metabolomic analysis, he et al. showed that mesaconate did not cause succinate accumulation in human monocyte-derived macrophages whereas itaconate could. Furthermore, He et al., demonstrated, utilising ^{13}C-isotope tracing in RAW264.7 cells to compare the ratio of M4 fumarate and succinate, that itaconate inhibited SDH activity while mesaconate had minimal effect in whole cells and no effect on isolated mitochondria. They concluded, along with mesaconate not causing succinate accumulation, that mesaconate does not inhibit SDH, an important feature of itaconate. Chen *et al.* demonstrated, utilising succinate/fumarate ratios as a readout for SDH activity, that mesaconate is a weak SDH inhibitor at high super physiological levels with an inhibitory capacity of approximately 2% of that demonstrated by itaconate. Chen et

al., demonstrate that citraconate is derived from an itaconate-independent metabolism and did not block SDH in an *in-vitro* enzyme assay, nor did citraconate supplementation to dTHP1 or A549 cells lead to succinate accumulation, a product of SDH inhibition. Interestingly, Chen *et al.,* demonstrated that citraconate is an endogenous ACOD1 inhibitor via substrate inhibition (144, 145). Furthermore, Chen *et al*., demonstrated that, in IAV-infected dTHP1 cells, IAV increased mtROS positive cells which could be reduced by itaconate, citraconate, but not mesaconate.

The relative electrophilicity of itaconate and these derivatives was investigated and mesaconate was determined to be the least electrophilic, while citraconate was the most electrophilic and the most potent NRF2 activator. Furthermore, ACOD1 was shown not to be responsible for mesaconate or citraconate synthesis, nor was there spontaneous interconversion between any of the three compounds (145).

1.7.17 Itaconate in disease

1.7.18 Itaconate ameliorates a model of EAE

Aso *et al*., demonstrate that itaconate is protective in a murine model of Experimental autoimmune encephalomyelitis (EAE). Underivatised itaconate-treated mice had improved clinical and inflammatory score, and lost less body weight. Furthermore, they hypothesised that itaconate would suppress pathogenic Th17 cells and demonstrated that adoptive transfer of itaconate-treated Th17 cells improved the above markers. Mechanistically, itaconate blocks Th17 differentiation and promotes Treg polarisation via inhibition of glycolysis and OXPHOS. This occurs by reducing the S-adenosyl-L-methionine/S-adenosylhomocysteine ratio in Th17 cells and 2-hydroxyglutarate levels in Tregs. These changes alter chromatin accessibility for transcription factors such as RORɣT, preventing the induction of IL17a which prevents Th17 differentiation (110). Another study showed that 4-OI was protective in EAE by preventing microglia polarisation and driving the NRF2-anti-inflammatory pathway (146).

1.7.19 Itaconate is pro-tumour

Studies on itaconate have primarily focused on immune cells. However, itaconate has been demonstrated to have roles in cancer. Many studies have converged on the same theory that itaconate is pro-tumour by causing the accumulation of the oncometabolite succinate, suppressing $CD8^+$ T cell anti-tumour function and the inhibition of TET2 2-OGDDs. The mechanism of TET2 inhibition by itaconate has been mentioned in the enzyme inhibition section above. TET2 inhibition or loss of function-causing mutations is known to cause genome instability, leading to malignancies such as leukaemia in mice (147-149)

Zhao *et al.,* 2022 were the first to theorise itaconate as an immune checkpoint metabolite. They demonstrated that itaconate was secreted by myeloid-derived suppressor cells (MDSCs), which was taken up by $CD8^+$ T cells and blocked its serine and aspartate synthesis which impeded their proliferation and antitumoral function (150).

Chen *et al.,* subsequently published similar works which demonstrated that ACOD1 expression was elevated in several human cancers, including breast invasive carcinoma, head and neck squamous cell carcinoma, and stomach adenocarcinoma and that TAMs upregulated ACOD1 as an immunosuppressive immune escape mechanism. They showed that *Irg1*$^{-/-}$ mice injected with B16-F10 melanoma cell line, MC38 colorectal tumour cell line, or E0771 breast tumour cell line had increased overall survival and reduced tumour volume and weight. They also showed that ACOD1 was expressed via NFκB activation in both murine and human tumour-associated macrophages (TAMs). Itaconate was shown to block TET2, resulting in reduced inflammatory cytokines production and reduced intratumorally infiltrating $CD8^+$ T-cells and responded better to immunotherapies such as ant-PDL1. This impeded tumour killing and led to tumour progression (151).

Gu *et al*, demonstrated similar findings in the liver. They showed that itaconate was pro-tumour in a model of hepatocellular carcinoma in mice. They demonstrated that *Irg1*$^{-/-}$ mice had decreased $PD1^+$ and $TIM3^+$ $CD8^+$ T cells. They showed that itaconate upregulated $PD1^+$ and $TIM3^+$ by succinate-dependent tri-methylation of histone H3 on lysine 4 (H3K4me3), of the *Eomes* promoter and caused $CD8^+$-T cell exhaustion. They

clearly showed, by $CD8^+$ T cell deletion or adoptive transfer, that itaconate was pro-tumour via $CD8^+$ T cell exhaustion, seen by reduced proliferation, cytotoxic function and inflammatory cytokine production. They then performed a correlative analysis and showed that high macrophage ACOD1 expression was a poor prognostic marker in clinical hepatocellular carcinoma patients. This group showed that 20 mg/kg ibuprofen inhibited IRG1/itaconate axis and was antitumour in Hepa 1-6 cell-induced orthotopic HCC model, which was reversed by 4-OI addition (152). Recently another group claimed that this pro-tumour effect of itaconate was dependent on ACOD1-induced production of inhibitory peptides and independent of extracellular itaconate (153). Nevertheless, these data suggest the significant role ACOD1 plays in tumorigenesis and warrants the development of ACOD1 inhibitors, such as citraconate, in anticancer therapeutics (154).

1.7.20 Synthesised derivatives

It was previously presumed that itaconate was unable to cross cell membranes. Itaconate derivatives such as dimethyl itaconate (DI) and 4-OI were synthesised, mimicking the properties of itaconate and improving membrane permeability. 4-OI has an octyl group on the fourth carbon and increases membrane permeability by increasing hydrophobicity. However, it is important to note that studies now show that un-derivatised itaconate can enter cells and is a valid method for experimentation (155). Hooftman *et al.,* demonstrated that 4-OI can be converted into itaconate and is a convenient method for delivering itaconate into the cell. This was performed by treating human macrophages with $^{13}C_5$-labelled 4-OI which resulted in the detection of $^{13}C_5$-labelled itaconate as early as 30 minutes after treatment. It's important to note that $^{13}C_5$-labelled 4-OI was still detectable alongside $^{13}C_5$-labelled itaconate (142). Furthermore, 4-OI acts like a prodrug, whereby the octyl group is cleaved by esterases to form intracellular itaconate, particularly in organs with high esterase content such as the liver (156). DI, on the other hand, cannot be converted to itaconate and is therefore considered a worse itaconate tool compound. However, Swain *et al*., demonstrated that itaconate treated-BMDMs caused succinate accumulation, indicative of SDH inhibition, while 4-OI and DI-treated BMDMs did not (155). This suggests that a significant difference between itaconate and derivatives may be their ability to inhibit SDH as mentioned above. Furthermore, Swain *et al*., demonstrated that itaconate derivatives DMI and 4-OI depleted glutathione levels

while itaconate could not, indicating that the derivatives are much more electrophilic than un-derivatised itaconate (155).

Itaconate modifies proteins by undergoing a Michael addition reaction, where the nucleophilic thiol group of a cysteine group on a protein attacks the electrophilic β carbon on the α,β -unsaturated carbonyl system, forming a covalent bond. Many screens have been performed to uncover novel cysteine modifications by itaconate. These include tandem mass spectrometry of itaconate or 4-OI-treated BMDMs with LPS to find direct modifications (140). Other screens use cysteine reactive probes to modify all available cysteines to indirectly show potential cysteine modifications. Results with these cysteine-reactive probes have been promising as these probes modified proteins found to be modified by 4-OI, such as KEAP1, ALDOA, and LDHA (157). Others combined both mechanisms where itaconate-treated cells and non-treated cells are then both treated with a cysteine probe and the cysteine modified in the control group but not the itaconate-treated group are deemed "protected" or modified by itaconate. Bourner *et al*., stimulated THP1 ACOD1$^{+/+}$ and ACOD1$^{-/-}$ cells with LPS + IFNɣ to cause itaconate accumulation in ACOD1$^{+/+}$ cells only. They treated both samples with a cysteine reactive probe and then performed a LC-MS/MS to create a competition ratio and determine cysteine reactivity by itaconate. Bourner *et al.,* demonstrated that Cys-13 on IRAK4 was modified by endogenous itaconate in human cells. They also showed that ACOD1 KO THP1 cells and human macrophages had elevated TNFα, IL6, IL1β, CXCL10, but reduced IFNβ. Indicating that itaconate is a negative regulator of inflammatory signalling but boosts LPS-induced IFNβ in human macrophage cell lines (158).

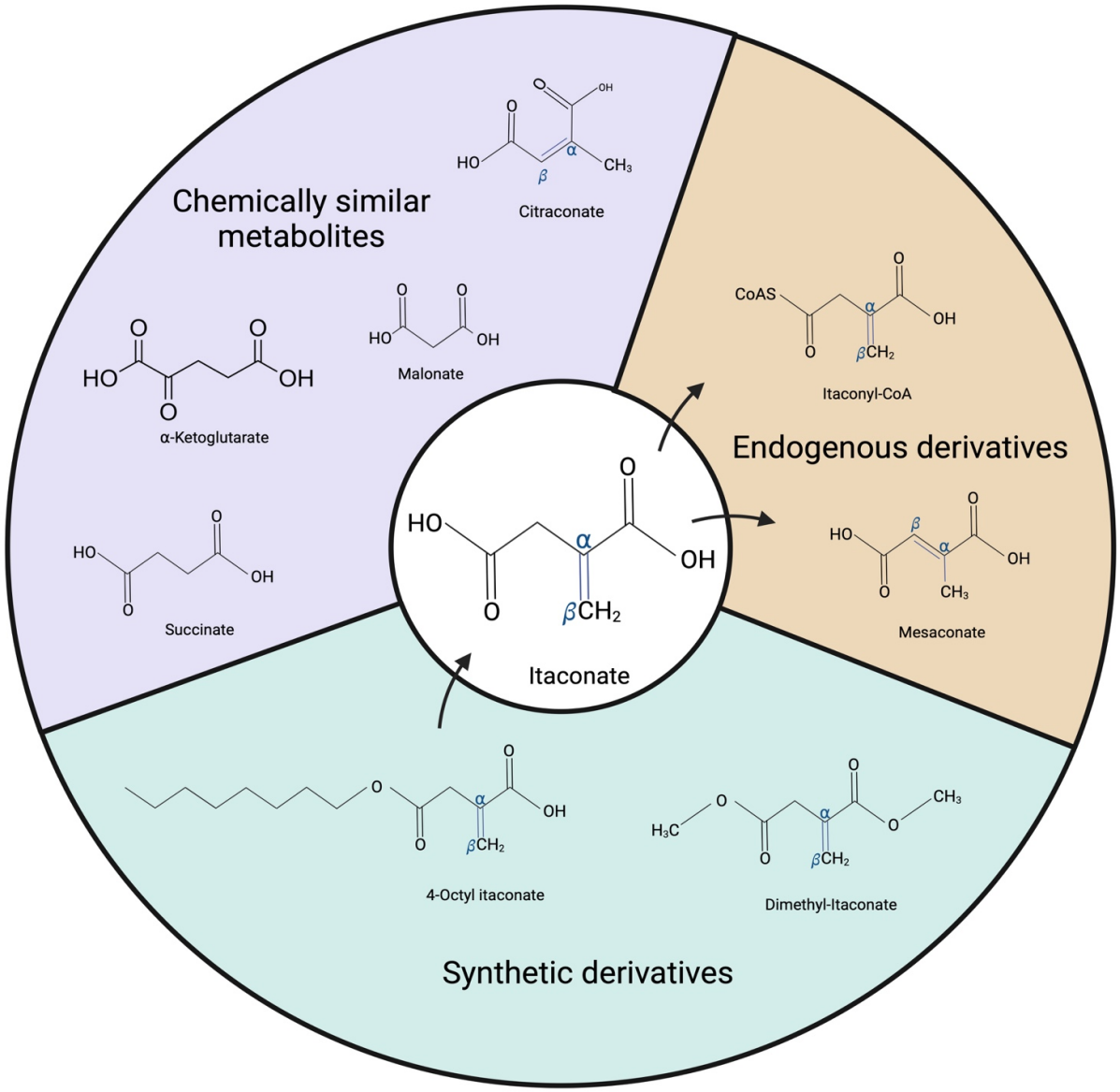


Figure 5. Schematic of itaconate, its derivatives and chemically similar metabolites 4-OI is a more electrophilic, cell-permeable derivative that can be converted into itaconate and leads to increased intracellular itaconate (142). DI is a more cysteine reactive derivative than itaconate and is not converted into itaconate. Itaconate can be metabolised into itaconyl-CoA and re-enter the TCA cycle. Itaconate can also be metabolised into mesaconate. Itaconate is structurally similar to succinate, leading to SDH inhibition. Citraconate is a structurally similar metabolite derived via an itaconate-independent pathway and is an ACOD1 inhibitor, inhibiting itaconate synthesis. Malonate is also a structurally similar compound, whereby dimethyl malonate is an SDH inhibitor and a tool compound to investigate the effects of itaconate mediated by SDH inhibition. Image created with Biorender.com

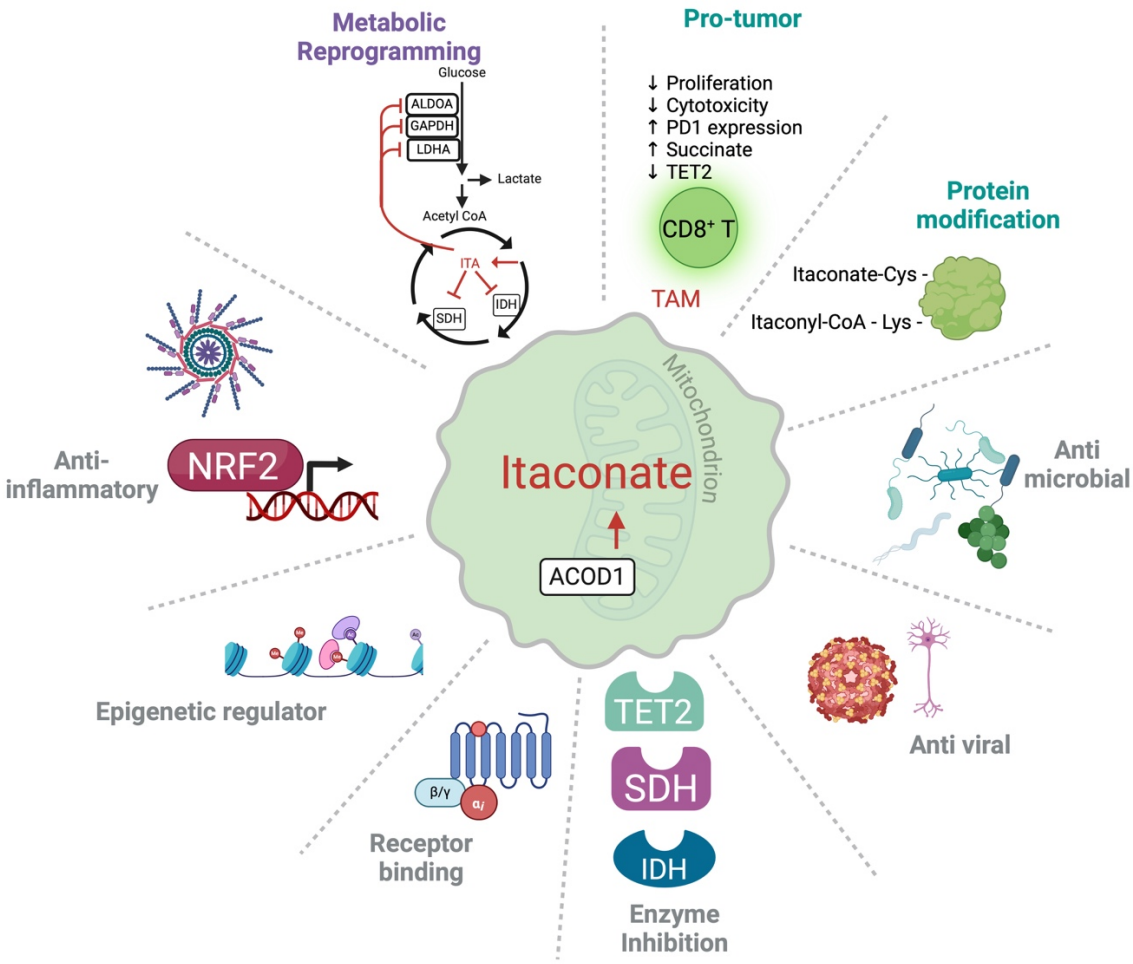


Figure 6. Itaconate biology at a glance

Itaconate mediates macrophage metabolic reprogramming by causing breakpoints in the TCA cycle at SDH and IDH. Itaconate is pro-tumour by causing accumulation of the oncometabolite succinate, by inhibiting TET2 2-OGDDs, and by inhibiting $CD8^+$ T cells. Itaconate causes modification of cysteine residues which alters protein function. Itaconate is also metabolised into itaconate co-A, which can modify lysine-residues and is less common and less understood. Itaconte is anti-microbial against bacterial infection such as Mtb and antiviral in some contexts against Zika virus and IAV. Itaconate is anti-apoptotic via modification of gasdermin-d. Itaconate causes the modification of enzymes via competitive inhibition of regulating metabolism. Itaconate can bind to GPCR OXGR1. Itaconate inhibits TET2, leading to epigenetic regulation by preventing the demethylation of DNA and inhibiting transcription factor accessibility and subsequent gene transcription. Itaconate is anti-inflammatory by activating NRF2 and inhibiting inflammasome activation. Image created with Biorender.com

1.8 Metabolic regulation of type I interferon responses

It has been well documented that viral infection leads to host cell metabolic changes, which can provide intermediates for viral replication or aid in host antiviral immunity. However, less is known about how metabolic changes can regulate type I interferon responses.

Viral infection causes macrophage metabolic reprogramming and aerobic glycolysis (159), contributing to the antiviral response such as IAV infection. Increased glycolysis includes the increase in the hexosamine biosynthesis pathway and pentose phosphate pathway, which leads to the synthesis of O-GlcNAc transferase (OGT), an enzyme involved in protein O-GlcNAcylation. OGT is induced and modifies IRF5, which leads to subsequent IFNβ induction and the antiviral response (160). Furthermore, macrophage infection with vesicular stomatitis viruses (VSVs) causes O-GlcNAcylation of MAVS on serine 366, necessary for ubiquitination and its activation, which leads to MAVs activation and increased type I interferon signalling (161). These authors theorise that glucose metabolism leads to modification of target proteins leading to their activation and subsequent induction of interferon, leading to antiviral immunity.

Another link between glycolysis and antiviral innate immunity was made by Zhang *et al*. They show that glucose metabolism is downregulated after stimulation with TL3 activation via poly(I:C). Furthermore, they show that this inhibition of glycolysis after poly(I:C) promotes interferon production. They further demonstrate that lactate dehydrogenase inhibition regulates interferon production and that lactate is sensed by MAVS and inhibits its interferon induction. This was repeated *in-vivo* where mice were fasted and infected with VSV had exacerbated type I interferon production, which could be suppressed with lactate treatment (162, 163). Taken together, there is evidence that cellular metabolism can regulate type I interferon responses.

1.8.1 Itaconate and 4-OI differentially regulate IFNβ

Itaconate and its derivative 4-OI were presumed to have identical immunoregulatory functions. Swain *et al*., demonstrated, along with others, that 4-OI blocked LPS-induced IFNβ. (140, 155). Ryan *et al., 2023* further demonstrated that 4-OI blocks interferon-dependent tissue factor and subsequent thromboinflammation and lethality in an LPS, *E. coli*, and *S. aureus*-induced sepsis model *in-vivo* (164). Since 2020, significant research

has been done regarding the mechanism of this phenotype. Ryan *et al*., demonstrated that the suppressive effect of 4-OI on LPS-induced type I interferons was NRF2 dependent (165). This NRF2 dependency was also shown in poly(I:C)-induced type I interferon in BMDMS (166). While the suppressive effect of type I interferon by DI was shown to be NRF2-independent (138). Furthermore, 4-OI also blocked STING expression in an NRF2-dependent manner in human monocyte-derived macrophages (167). However, the inhibitory mechanism is unlikely to be entirely dependent on NRF2 due to the high thiol reactivity of 4-OI. Olagnier *et al.,* demonstrated that 4-OI blocked the inflammatory response in Sars-CoV-2-infected cell lines and human PBMCs including *IFNB1* expression. Mechanistically, Olagnier *et al.,* showed that 4-OI blocked *IFNB1* expression in an NRF2 manner by blocking IRF3 phosphorylation and dimerisation. However, 4-OI was antiviral against SARS-CoV-2, HSV1, HSV2, VACV, and ZIKV in an interferon-independent mechanism (168). Waqas *et al*., demonstrated that 4-OI is antiviral by inhibiting IAV replication cycle (169). Specifically, 4-OI alkylated chromosomal maintenance 1 protein, a nuclear export protein which prevented IAV from exiting the nucleus, a step necessary for IAV and other CRM1-dependent viruses from replicating. Moreover, 4-OI alkylated STING on Cys-65, Cys-71, Cys-88, and Cys-147 which inhibited STING phosphorylation and subsequent interferon signalling and also blocked STING expression (167). 4-OI is, therefore, interesting in the context of bacterial and viral infection, whereby it has anti-viral and anti-inflammatory properties, limiting immunopathology (168)

Unlike 4-OI, there remains some ambiguity regarding the itaconate-induced regulation of interferon, in particular, the mechanism by which this occurs. Initially, research suggested that itaconate blocks type I interferon responses. However, this was demonstrated with the derivative 4-OI (140). Swain *et al*., then demonstrated that exogenous treatment of underivatised itaconate for 3 and 12 hours led to intracellular itaconate accumulation, demonstrating that itaconate can get into BMDMs. Swain *et al*., demonstrated that, in BMDMs, itaconate and 4-OI could differentially regulate type I interferon responses. They showed that *Irg1*$^{-/-}$ BMDMs produced less IFNβ and a reduced type I interferon signature in response to LPS which was then rescued by administration of underivatised itaconate in *Irg1*$^{-/-}$ BMDMs, demonstrating that itaconate boosts LPS-induced type I interferon responses in BMDMs (155).

However, Li *et al.,* demonstrated that the STING agonist DXAA could upregulate itaconate production. As mentioned above, 4-OI alkylated STING and subsequent interferon signalling. Furthermore, Li *et al.,* show that underivatised itaconate blocked DXAA-induced *Ifnb1* expression. They demonstrated that 3 mM underivatised itaconate treatment blocked STING agonist, DMXAA, induced STING phosphorylation in RAW264.7 macrophage cell line. This was also shown with endogenous itaconate as DXMAA-treated *Irg1*$^{-/-}$ BMDMs had elevated STING phosphorylation and *Ifnb1* expression compared to *Irg1*$^{+/+}$ BMDMs, while itaconate supplementation of *Irg1*$^{-/-}$ BMDMs reversed this phenotype (170). Mechanistically, itaconate blocks STAT1 phosphorylation in infected dTHP1 cell lines (122), and JAK1 phosphorylation in IL-4-treated BMDMs (171).

There therefore remains a convoluted relationship between interferons and itaconate **(Table 1).**

	Itaconate	**4-OI**
Type I IFNs	↑↓ (122, 155)	↓↓↓ (140)
NRF2	↑	↑↑↑ (140)
NLRP3	Inhibits IL1β release (142)	Inhibits activation (142)
JAK1	Inhibits	Inhibits (171)
Electrophilicity	↑	↑↑↑ (155)
SDH inhibition	↑↑ (155)	-
IAV titres	↓	↓↓↓ (122)
OXGR1	Activates (123)	Unknown

Table 1. Effect of 4-OI and itaconate on cellular responses

1.9 Aims

Research up to the commencement of this PhD in September 2020 demonstrated that 4-OI could block type I interferon responses, but minimal mechanistic insight into this phenotype had been discovered. This project began with the aim of investigating how, mechanistically, itaconate and its derivative, 4-OI, differentially regulate type I interferon responses. I hypothesised that 4-OI may block type I interferons via NRF2 activation. I also hypothesised that itaconate may boost type I interferons via SDH inhibition. To test these hypotheses, I used the following aims.

- To determine whether 4-OI can inhibit type I interferon responses and, using genetic and pharmacological approaches, whether this inhibition is NRF2-dependent.

- To determine whether itaconate can boost type I interferon responses and, using genetic and pharmacological approaches, whether this inhibition is SDH-dependent.

Chapter 2 Materials and Methods

2.1 Materials

2.1.1Buffers

Name	Composition
Stacking Gel Buffer Tris HCL pH 6.8	60.5g TRIS, 500ml H_2O. pH to 6.8
Resolving Gel Buffer Tris HCL pH 8.8	181.71g/LdH_2O, pH to 8.8.
PBS (10X)	NaCl (1.45 M), NaH2PO4 (39 mM), NaH2PO4 (22.7 M)
Sample Loading Buffer (5X)	Tris pH 6.8 [0.125M], glycerol [10%], SDS [0.02%], DTT [5%]
SDS-PAGE Running Buffer (10X)	Tris [25mM], glycine [192mM], SDS [0.1%]
SDS PAGE transfer buffer (10X)	Tris [0.25M], glycine [1.9M], SDS [35mM]
ELISA Wash Buffer	0.05% TWEEN in PBS
Tris-buffered saline tween (TBST) (10X)	Tris (12.11g), NaCl (87.6g), tween 20 (10ml), distilled H_2O to 1L

Table 2. Name and composition of buffers

2.1.2 Reagents

Reagent	Provider	Catalogue number
DMEM, high glucose, GlutaMax™	Thermo Sientific	10566016
Red cell lysis buffer	Sigma Aldrich	R7767
LPS (*Escherichia coli,* serotype EH100)	Enzo Life Sciences	ALX-581-010-L001
High molecular weight poly(I:C)	Invivogen	(tlrl-pic)
DMSO	Sigma Aldrich	D8418
ODN-2088	Miltenyi Biiotec	130-105-815
2'-3' cGAMP	Invivogen	tlrl-nacga23
Diethyl maleate	Sigma Aldrich	D97703 -100G

Itaconic acid	Sigma Aldrich	I29204-100G
4-octyl itaconate	Sigma Aldrich	SML2338-25MG
2'-3'-cGAMP	Invivogen	tlrl-nacga23-02
Dimethyl Fumarate	MedChemExpress	HY-17363
rhIFNgamma	Immunotools	11343536
Phorbol 12-myristate 13-acetate	Merck	19-144
Atpenin A5	Fisher Scientific Ltd	15907305
TTFA	Medchem express	HY-D0190
G3-YSD	Invivogen	tlrl-ydna
G3-YSD control	Invivogen	tlrl-ydnac
5'PPP-dsRNA	Invivogen	tlrl-3prna
5'PPP-dsRNA control	Invivogen	tlrl-3prnac
Ethidium Bromide	Merck-Sigma	E7637-5G
IMT1	MedChemexpress	HY-134539
Dimethyl Malonate	Sigma	136441-250g
VBIT4	Medchem express	HY-129122
RPMI	Biosciences (GIBCO)	61870-010

Table 3. List of reagents

2.1.3 Cell culture reagents

DMEM, RPMI, T175 flasks and 10cm cell culture dishes were purchased from Thermo Fisher Scientific (Waltham, USA). FCS was purchased from Biosera (Nuaille, France). Penicillin- streptomycin, and red cell lysis buffer were purchased from Sigma Aldrich (St Louis, USA). L929 supernatant was obtained by removing the supernatant from L929 cells at 60-70% confluency.

2.1.4 Cell lines and primary cells

L929 cell line was purchased from Sigma Aldrich. BMDMs were taken from hind quarters of 6-10-week-old C57BL/6 mice, acquired from Harlan Laboratories (Bicester, UK). THP1 ACOD1$^{-/-}$ and ACOD1$^{+/+}$ cells were donated from Frank Charles Dorsey at Eli Lilly. Experiments carried out all have prior ethical approval from Trinity College Dublin Animal Research Ethics Committee under the relevant project and individual authorisations, granted by the Health Products Regulatory Authority (HPRA).

2.1.5 Stimulants and metabolites

LPS from Escherichia coli, serotype EH100, was purchased from Enzo Life Sciences (Farmingdale, USA). Poly (I:C) (#tlr-pic), CpG-ODN (tlrl-1668), R848 (tlrl-r848), and 2'-3' cGAMP (tlrl-nacga23) were all purchased from Invivogen (San Diego, USA). Dimethyl itaconate (DMI), dimethyl sulfoxide (DMSO), diethyl maleate (DEM), itaconic acid and 4-octyl itaconate (4-OI) were purchased from Sigma Aldrich.

2.1.6 Antibodies

Anti-Nrf2 (D1Z9C) was purchased from cell signalling. Anti-mouse -actin antibody was purchased from Sigma Aldrich. Anti-IRG1 antibody (AB222411) was purchased from ABCAM. Anti- alpha-tubulin antibody (2144S) was purchased from CST/Brennan. Anti-Lamin B1 antibody (12586S) was purchased from CST/Brennan.

2.1.7 Western blotting reagents

The gel running system was purchased from BioRad (Berkeley, USA). HEPES, triton X-100, aprotinin, sodium orthovanadate, PMSF, benzonase nuclease, sodium dodecyl sulphate (SDS), N,N,N′,N′-Tetramethylethylenediamine (TEMED), ammonium persulphate (APS), tris base, hydrochloric acid and acrylamide were all purchased from Sigma Aldrich. StrataClean Resin was purchased from Agilent Technologies (Santa Clara, USA). Spectra BR protein ladder and disuccinimidyl suberate (DSS) were purchased from Thermo Fisher Scientific. PVDF transfer membrane was purchased from Merck Millipore (Burlington, USA). Marvel powdered milk was purchased from Tesco. WesternBright ECL spray was purchased from Advansta (San Jose, USA). The system used for protein visualisation was a ChemiDocTM MP Imaging System from BioRad.

2.1.8 RT-qPCR reagents and primers

Primers were designed and then purchased from Eurofins Genomics (Ebersberg, Germany). Primer sequences are provided in a table below. RNA extraction kit, reverse transcription kit, 8-strip PCR tubes, caps, plate seals, SYBR green master mix, and 96-well qPCR plates were all purchased from Applied Biosystems (Foster City, USA). Amplification grade DNAse I was purchased from Thermo Fisher Scientific. cDNA synthesis was performed on a Veriti 96-well fast thermal cycler from Applied Biosystems, and qPCR was performed on a 7500 fast real-time PCR system, also from Applied Biosystems.

2.1.9 Primer list

Gene	**Forward primer**	**Reverse primer**
D-loop	AATCTACCATCCTCCGTGAAACC	TCAGTTTAGCTACCCCCAAGTTTAA
Ddx58	CTGACATTCGAGTGGTTGAGA	TGGTTTAGGGTGTGGCTTAC
Ifih1	CGGGAAGGTTATCGTTCTTGT	GCTGGGTATCGCCACTTAAT
Ifnb1	ATGGTGGTCCGAGCAGAGAT	CCACCACTCATTCTGAGGCA
ND4	TAATCGCACATGGCCTCACA	CATTTGAAGTCCTCGGGCCA
ND5	CAGCACAATTTGGCCTCCAC	TAGTCGTGAGGGGGTGGAAT
ND6	CCCGCAAACAAAGATCACCC	TCTTGATGGTTTGGGAGATTGGT
RPS13	CGAAAGCATCTTGAGAGGAACA	TCGAGCCAAACGGTGAATC
Rps18	GCGAGTACTCAACACCAACA	CCTCAACACCACATGAGCATA
CGas	GAGGAAATCCGCTGAGTCATT	TCCTTCTCCACACTGACATCTA
ACOD1	AGAAGCCCTGCCAAGGAGTCCAAA	CCAGAGCTTCTCGGCACTTTGTCG
Snx9	ATGGATGACGGCGTGAAGGAGC	TGGAGCTGAACACTGCCGCTAA
Tlr9	AGTGTCACTTCCTCAATTCTCTG	CATGTTGGGAGATGGAGGATT
IFNB	ATGACCAACAAGTGTCTCCTCC	GCTCATGGAAAGAGCTGTAGTG
Sdhb	AAGAAGGATGAGTCCCAGGAG	CTTGTCTCCGTTCCACCAGTA
Il1b	GAGGACATGAGCACCTTCTTT	GCCTGTAGTGCAGTTGTCTAA
Tmem173	TGGCCTTCTGGTCCTCTATAA	CCGTGGGCAACATTTAACTTC
Bak	CTGGAACCCAACAGCATCTT	GTCGTAGCGCCGGTTAATATC
Bax	GGAGATGAACTGGACAGCAATA	GAAGTTGCCATCAGCAAACAT
Vdac1	TGGACTGAAGCTCACCTTTG	TCCCTCTTGTACCCTGTCTT
Hmox1	CCTCACAGATGGCGT	GCTGATCTGGGGTTT
Atf3	GAGGCGGCGAGAAAGAAATA	CAGCTCAGCATTCACACTCT

Isg15	GCCAGAAGCAGACTCCTTAAT	ACACCAGGAAATCGTTACCC
Usp18	TCAGTGCCTGCAGAAATACA	TCCGTGATCTGGTCCTTAGT
Caspase11	GGTGGTGAAAGAGGAGCTTAC	CCAGGAATGTGCTGTCTGAT

Table 4. List of Primers

2.1.10 ELISA Reagents

Murine IFNβ duoset ELISA kits were purchased from R&D Systems (Minneapolis, USA). TMB substrate reagent set was purchased from BD Biosciences. NuncTM 96-well ELISA plates were purchased from Thermo Fisher Scientific. Plates were read on a FLUOstar OPTIMA from BMG Labtech (Ortenberg, Germany).

2.2 Methods

2.2.1 Derivation of bone marrow-derived macrophages

All mice were on a C57BL/6JOlaHsd background unless stated below. Wild-type (WT) mice were bred in-house. Irg1$^{-/-}$ mice (named C57BL/6N-Acod1$^{em1(IMPC)J}$/J) were generated by CRISPR-targeted deletion of exon 4 of Acod1, and were purchased from The Jackson Laboratory. Mice were euthanised by CO_2 gas chamber and confirmed by cervical dislocation. Mice fur was sprayed thoroughly with 70% ethanol. Legs, including Hip, femur and tibia were removed as a whole and stored in steralines containing DMEM. A scissors was used to remove muscle from bone and to expose the bone marrow. Using a 25 gauge needle and 20ml syringe containing DMEM, high glucose, Glutamax™, the bone marrow was flushed into a 50ml Falcon tube. The bone marrow was centrifugated for 5 min at 453 x g. The supernatant was discarded. The pellet was resuspended in 3 mL Red Cell Lysis Buffer and allowed to incubate at room temperature for 3-5 min. 7 ml DMEM, high glucose, GlutaMax™, was added and the centrifugation step was repeated. 24ml DMEM, high glucose, GlutaMax™ containing 10% FCS, 1% Penicillin/Streptomycin was added to new 50 ml falcon tubes. After the centrifugation step, the supernatant was discarded and the pellet was resuspended in 6 ml L929 conditioned media. A 70µm nylon cell strainer (Fischer, Cat; 22363548) was placed atop a Falcon tube and cells resuspended in 6mL L929 were passed through the filter. Cells were added to non-tissue culture-coated petri dishes (10 ml per dish) and incubated for 6 days at 37°C, 5% CO_2. After 6 days, the cell media was aspirated. 10ml PBS was added to each plate and scraped to remove the cell monolayer, using a cell scraper, into suspension. The cell suspension was added into a 50 ml Falcon tube and centrifuged at 453xg for 5 min. Supernatants were removed and the pellet was resuspended in 10ml DMEM containing 10% FCS, 1% Penicillin/Streptomycin. Cells were counted with a hematocytometer or cell counter. Cells were seeded at 0.5 * 10^6 cells/well using DMEM, high glucose, GlutaMax™ containing 10% FCS, 1% Pen/Strep, 10% L929. Cells were checked to be stuck to the well bottom before experiments commenced (~4 hours).

2.2.2 Cell lines

SDHA$^{-/-}$ RAW 264.7 cell lines were donated from Marina Simarro, Department of Cell Biology, Histology and Pharmacology, Faculty of Medicine, University of Valladolid, 47005 Valladolid, Spain and described in (172).

2.2.3 Ethidium Bromide Treatment

Bone marrow-derived macrophages (BMDMs) were cultured with or without ultrapure ethidium bromide (100 ng/mL) and incubated for six days prior to treatment. The depletion of mitochondrial RNA (mtRNA) was assessed by RT-qPCR, targeting mtDNA-encoded genes (mt-ND4, mt-ND5, mt-ND6).

2.2.4 siRNA knockdown in BMDMs

BMDMs were prepared as described and seeded at $0.5x10^6$ cells per well. Master mix for RNAimax was made containing 250 ul serum-free DMEM media, 5 ul RNAimax per sample as per the table below. Master mix was made for siRNA (one tube for control siRNA, one for gene of interest siRNA), 250 ul serum-free media per sample and 1 ul RNAimax per sample at a final concentration of 50nM siRNA. Supernatants were replaced with 500µl serum-free media. The RNAimax master mix was mixed with the siRNA master mix and pipette gently 10 times with a 1ml pipette. This mix was allowed to rest for 25 minutes on a roller. 500µl of this master mix was gently added to the corresponding wells. Cells were then incubated for 8 hours at 37ºC, 5% CO_2 for 8 hours. Media was aspirated and replaced with DMEM, high glucose, GlutaMax™ containing 10% FCS, 1% Penicillin/Streptomycin and 10% L929. Cells were allowed to rest for 18 hours before experiments.

Reagent	**Volume per well (µl) (12 well plate)**
Serum-free media	250
RNAiMax	5

Table 5. RNAi Max Master Mix

Reagent	Volume per well (µl) (12 well plate)
Serum-free media	250
siRNA	1

Table 6. siRNA Master Mix

Silencer Select siRNA

siRNA	Provider	Catalogue number
Nfe2l2	Bioscience	4390815, assay ID s70522
Negative control	Bioscience	4390844
Ifih1	Bioscience	4390771, assay ID s89787
Ddx58	Bioscience	4390771, assay ID s106376
Tlr9	Bioscience	4390771, assay ID s96269
Mb21d1	Bioscience	4390771, assay ID s103167
Bax	Bioscience	4390771 assay ID s62874
Bak1	Bioscience	4390771 assay ID s62861
Vdac1	Bioscience	4390771, assay ID s75920
Snx9	Bioscience	4390771, assay ID s83576
Tmem173	Bioscience	4390771, assay ID s91058

Table 7. Silencer Select siRNA

2.2.5 siRNA knockdown in PBMCs

Anonymised untransfused blood samples were obtained from the Irish Blood Transfusion Board. All procedures involving human samples were approved by the School of Biochemistry and Immunology Research Ethics Committee (TCD) and were conducted in accordance with TCD's guidelines for good research practice. A 30 mL whole blood sample was layered on 20 mL of Lymphoprep (Axis-Shield) and centrifuged for 20 minutes at 400 x g without using the brake. The upper plasma layer was then removed and discarded. The mononuclear cell layer at the plasma-density gradient medium interface was retained and mixed with 20 mL of PBS. The cells were centrifuged again for 8 minutes at 300 x g, and the supernatant was discarded. The remaining mononuclear

cell pellet was resuspended, counted, and 1 × 10^6 cells per point were used for siRNA transfection. The cells were resuspended in nucleofector buffer along with five pmol siRNA (IRG1 (s60727)) and pulsed using the Y-010 program on the AMAXA nucleofector machine. Finally, the cells were plated in 1 mL of RPMI supplemented with 10% FCS and incubated in a CO2 incubator for 48 hours.

2.2.6 Organelle/cytosolic separation

Bone marrow-derived macrophages (BMDMs) were plated at a density of 0.5×10^6 cells per well and treated as required. After treatment, the cells were washed once with room temperature PBS, then scraped on ice into ice-cold PBS and pelleted by centrifugation at 500g for 5 minutes at 4°C. The supernatant was removed and discarded, and the pellet was resuspended in 400 µL of extraction buffer (150 mM NaCl, 50 mM HEPES pH 7.4, and 25 µg/mL digitonin). The samples were placed on a rotating mixer at 4°C for 10 minutes, followed by centrifugation at 2,000g at 4°C for 5 minutes. The resulting supernatant, representing the cytosolic fraction, was used for RNA and DNA isolation with the AllPrep DNA/RNA Mini kit (Qiagen) or concentrated using Strataclean resin (Agilent) for western blot analysis. The pellet, containing membrane-bound organelles, was lysed in RNA lysis buffer for RNA isolation or in western blot lysis buffer for western blot analysis as per western blot protocol 2.2.8. To detect the presence of mtRNA and mtDNA in the cytosol, qPCR was performed using primers specific for the mitochondrial D-loop on cDNA (from RNA isolated from the cytosolic fraction for mtRNA) and on DNA isolated from the cytosolic fraction (for mtDNA).

2.2.7 Seahorse XF Complex II Assay

Cells were plated at a density of 100,000 cells per well in 100 µL and allowed to adhere overnight. The assay was conducted as previously described. Briefly, cells were treated as required, followed by replacement of the medium with a mitochondrial assay solution (MAS) containing a plasma membrane permeabilizer (Agilent). The cells were then incubated in a CO2-free environment for 40 minutes. The plate was subsequently transferred to the Seahorse XFe/XF96 Analyzer, where the experiment was initiated. Data analysis was performed using Seahorse Wave software (Agilent), and the results shown represent experiments with at least three pooled biological replicates.

2.2.8 Western blot

$0.5*10^6$ cells were lysed in 30-100ul of Sample Loading Buffer (5X), scrape using pipette tip for 20 s of constant scraping. Lysates were extracted into Eppendorf. Samples were heated to heat block 95ºC, 5 min. Use immediately or freeze -20ºC 15µl aliquots. If frozen re-add samples to heat block 95ºC, 5min before use.

SDS polyacrylamide gel was performed using the Bio-Rad system using a 5% stacking gel. The percentage resolving gel was protein size dependant. `Running buffer was added up to the 4 gel mark regardless of the number of gels used. The system was first run at 80V until the molecular weight had passed through the stacking gel. After this, the gel was run at 100-120V for ~40mins.

Reagent	**8% Resolving Gel**	**10% Resolving Gel**	**12% Resolving Gel**	**Stacking Gel**
dH_2O	3.5ml	3ml	2.5ml	2ml
30% Acrylamide Mix	2ml	2.5ml	3ml	0.5ml
Tris-HCL pH 6.8 (1M)				375µl
Tris-HCL pH 8.8 (1.5M)	1.9ml	1.9ml	1.9ml	-
10% SDS	75µl	75µl	75µl	30µl
10% APS	75µl	75µl	75µl	30µl
TEMED	3µl	3µl	3µl	3µl

Table 8. Polyacrylamide master mix

Electrophoresis transfer

The BioRad wet transfer system was used for this procedure. To assemble a gel and membrane sandwich, open the cassette. Soak the sponge and 2 filter papers in transfer buffer. Place the soaked sponge on the cathode side of the cassette, then add 2 soaked

filter papers to the sponge. Lay the gel on top of the filter paper and lay an activated PVDF membrane on top. Remove any bubbles with a roller. Add two soaked filter papers and roll again to remove any bubbles. Add a sponge on top and close the cassette. The chamber was closed and the transfer was run at 200mA per box for 2 hours, or at 60mA overnight.

Antibody probing and imaging

After transfer, the PVDF membrane was removed from the transfer cell and washed once in TBST for 5 minutes in a 50ml falcon. The membrane was then incubated in skimmed milk powder (5% in TBST) for 1 hour. The membrane was then incubated in primary antibody (diluted in 5% milk powder) rolling overnight at 4^{o}C The membrane was washed three times in TBST for five minutes per wash. The membrane was then incubation with secondary antibody (diluted in 5% milk powder) for one hour rolling at room temperature. The membrane was then washed three times for five minutes each in TBST on a roller. Prior to visualisation, the membrane was immersed in WesternBright ECL Spray. Protein visualisation took place on a ChemiDoc MPTM Imaging System, and both chemiluminescent and white light images were taken.

2.2.9 RT-qPCR

RNA extraction

After cell treatment, supernatants were removed and cells were lysed in 350µl RNA lysis buffer. RNA extraction from cells was performed using a PureLink RNA Mini Kit (Invitrogen) according to the manufacturer's instructions. Isolated RNA was quantified using a NanoDrop 2000 spectrophotometer, and RNA concentration was normalised with RNAse-free water. If necessary, samples were DNAse treated using DNAse 1 (D4263-5VL) from SIGMA.

Reverse transcription

Samples were converted into cDNA using the High Capacity cDNA Reverse Transcription Kit (4368813) from Biosciences/Applied Biosystems. 10µl of RNA was added to 10µl of reverse transcription master mix as per manufacturers instructions. The reaction was performed in PCR tubes by a thermal cycler using the following steps: 25^{o}C

for 5 minutes, 42°C for 30 minutes, 85°C for 5 minutes. The resulting cDNA was diluted a final volume of 100-200 µl in RNAse-free water and stored at -20°C until further use.

Reagent	Volume per sample
10X RT buffer	2
10X Random primers	2
25X Deoxyribonucleotide triphosphates (dNTPs)	1
Multiscribe reverse transcriptase enzyme	1
dH2O	4

Table 9. Reverse transcription master mix

qPCR

4µl of cDNA was added to 6µl of qPCR master mix containing gene primers listed in the primer list,. The reaction was performed in a 96-well qPCR plate by a 7500 Fast Real-Time PCR machine. Relative expression was calculated from the CT values for each sample and gene of interest.

Reagent	Volume (µl) per sample
SYBR green master mix	5
Primer	0.3
dH_2O	0.7

Table 10. qPCR master mix

2.2.10 RNA sequencing

$0.5*10^6$ cells were pre-treated with 10 mM itaconic acid (pH 7.4) or TTFA (0.5 mM) for three hours followed by 100ng LPS for 4 hours. RNA was isolated, as described in 2.2.9, and shipped to Novogene Co. for analysis.

Library Construction, Quality Control and Sequencing

The following was adapted from the methods section sent along with results.

mRNA was isolated from total RNA using poly-T oligo-attached magnetic beads. After fragmentation, the first strand cDNA was synthesized using random hexamer primers, followed by the second strand cDNA synthesis using either dUTP for directional library or dTTP for non-directional library. For the non-directional library, it was ready after end

repair, A-tailing, adapter ligation, size selection, amplification, and purification. For the directional library, it was ready after end repair, A-tailing, adapter ligation, size selection, USER enzyme digestion, amplification, and purification

Bioinformatics Analysis Pipeline

Data Quality Control

Raw data (raw reads) in FASTQ format were initially processed using in-house Perl scripts. During this step, clean data (clean reads) were generated by removing reads containing adapters, reads with poly-N sequences, and low-quality reads from the raw data. Additionally, Q20, Q30, and GC content were calculated. All subsequent analyses were conducted using the high-quality clean data.

Mapping Reads to the Reference Genome

The reference genome and gene model annotation files were downloaded directly from the genome website. The index for the reference genome was constructed using Hisat2 v2.0.5, and paired-end clean reads were aligned to the reference genome with the same version of Hisat2. Hisat2 was selected as the mapping tool because it generates a splice junction database from the gene model annotation file, which provides more accurate mapping compared to non-splice mapping tools.

Quantification of Gene Expression Levels

FeatureCounts v1.5.0-p3 was utilized to count the number of reads mapped to each gene. The FPKM (Fragments Per Kilobase of transcript sequence per Million base pairs sequenced) of each gene was then calculated based on gene length and read counts. FPKM accounts for both sequencing depth and gene length, and it is a commonly used method for estimating gene expression levels.

Differential Expression Analysis

For DESeq2 with Biological Replicates: Differential expression analysis between two conditions/groups (with two biological replicates per condition) was performed using the DESeq2 R package (1.20.0). DESeq2 applies statistical routines based on a negative binomial distribution model for determining differential expression in digital gene

expression data. The resulting P-values were adjusted using the Benjamini and Hochberg approach to control the false discovery rate. Genes with an adjusted P-value ≤ 0.05 were considered differentially expressed.

GO and KEGG Enrichment Analysis of Differentially Expressed Genes

Gene Ontology (GO) enrichment analysis of differentially expressed genes was conducted using the clusterProfiler R package, which corrects for gene length bias. GO terms with a corrected P-value less than 0.05 were considered significantly enriched. KEGG, a database for understanding high-level biological functions from molecular-level data, was used for pathway analysis. The statistical enrichment of differentially expressed genes in KEGG pathways was tested with the clusterProfiler R package.

Gene Set Enrichment Analysis

Gene Set Enrichment Analysis (GSEA) is a computational method used to determine if a pre-defined Gene Set shows a significant consistent difference between two biological states. Genes were ranked based on the degree of differential expression between samples, and predefined Gene Sets were tested for enrichment at the extremes of the ranking list. The local version of the GSEA analysis tool was used, with GO and KEGG datasets applied independently.

2.2.11 Immune Response Enrichment Analysis (IREA)

The Immune Response Enrichment Analysis is an online tool developed by Cui et al. (173). It leverages the Immune Dictionary, which is derived from single-cell transcriptomic profiles of over 17 immune cell types in response to 86 cytokines, encompassing more than 1,400 cytokine–cell type combinations in mouse lymph nodes in vivo. This tool compares user gene expression data with the Immune Dictionary reference data to predict the cytokines most active in the user's dataset. The analysis operates similarly to GO pathway enrichment analysis but is more specifically tailored for studying immune processes. User data can come from a variety of contexts, including disease, treatment, vaccination, or any immune-related process.

2.2.12 Mitochondrial membrane potential assay

Immunofluorescence imaging BMDMs were plated in 35 mm dishes at $0.5x10^6$ (cells ml-1 481) in 2 ml DMEM. After treatments, TMRM (25 nm, Thermo, M20036) and HOESCHT blue (0.5 μg ml-1, Invitrogen, H3570) were added to the culture media for 30 minutes at 37 oC. Cells were then washed 3x with warm PBS and fresh DMEM (10% FCS) containing TMRM (1.25 nM) was added. Dishes were imaged using a Leica SP8x scanning confocal microscope with a ×100.0 objective. Images were analysed using the LAS X Life Science Microscope Software Platform (Leica). The same microscope instrument settings were used for all samples, and all images were analysed using the same settings

2.2.13 Generation of human macrophages

Human blood samples from healthy donors were collected and processed at the School of Biochemistry and Immunology at the Trinity Biomedical Sciences Institute (TCD). Blood samples were obtained anonymously, and written informed consent for the use of blood for research purposes was obtained from the donors.

2.2.14 Ethics

All the procedures involving experiments on human samples were approved by the School of Biochemistry and Immunology Research Ethics Committee (TCD). Experiments were conducted according to the TCD guide on good research practice, which follows the guidelines detailed in the National Institutes of Health Belmont Report (1978) and the Declaration of Helsinki. Whole blood (30 ml) was layered on 20 ml Lymphoprep (Axis-Shield), followed by centrifugation for 20 min at 400*g* with the brake off, after which the upper plasma layer was removed and discarded. The layer of mononuclear cells at the plasma-density gradient medium interface was retained, and 20 ml PBS was added. Cells were centrifuged for 8 min at 300*g* and the resulting supernatant was removed and discarded. The remaining pellet of mononuclear cells was resuspended, counted and plated at 1×10^6 cells per ml in RPMI supplemented with FCS (10%) and penicillin–streptomycin (1%).

PBMCs were obtained, and CD14+ monocytes were isolated using a MagniSort Human CD14 Positive Selection kit (Thermo Fisher) according to the manufacturer's protocol. CD14 monocytes were then differentiated in T-175 flasks in RPMI containing FCS (10%), penicillin–streptomycin (1%) and recombinant human M-CSF (1:1,000). After 6 days, the supernatant was discarded, cells were scraped and counted, and human monocyte-derived macrophages) were plated in 12-well plates at 1 × 106 cells per ml in RPMI containing FCS (10%) and penicillin–streptomycin (1%).

2.2.15 ELISA

DuoSet ELISA kits for IFN-β were purchased from R&D Systems and used according to the manufacturer's instructions. Appropriately diluted cell supernatants were added to each plate in duplicate or triplicate. IFN-β levels were measured using DuoSet ELISA kits from R&D Systems or Abcam (ab252363). To determine IFN-β concentrations in serum samples and human cells, the Quantikine ELISA kit for IFN-β (R&D Systems) was used, also following the manufacturer's instructions. Absorbance at 450 nm was measured using a FLUOstar Optima plate reader. Corrected absorbance values were calculated by subtracting background absorbance, and cytokine concentrations were determined by extrapolating from a standard curve plotted using GraphPad Prism 9.2.0.

2.2.16 Immunofluorescence imaging

BMDMs were plated in 35 mm dishes at 0.5x106 (cells ml-1 481) in 2 ml DMEM. After treatments, TMRM (25 nm, Thermo, M20036) and HOESCHT blue (0.5 μg ml-1, Invitrogen, H3570) were added to the culture media for 30 minutes at 37oC. Cells were then washed 3x with warm PBS and fresh DMEM (10% FCS) containing TMRM (1.25 nM) was added. Dishes were imaged using a Leica SP8x scanning confocal microscope with a ×100.0 objective. Images were analysed using the LAS X Life Science Microscope Software Platform (Leica). The same microscope instrument settings were used for all samples, and all images were analysed using the same settings

2.2.17 Quantification and statistical analyses

Details of all statistical analyses are provided in the figure legends. Data are expressed as mean ± S.E.M., unless otherwise noted. Representative western blots are shown. Statistical significance was determined using one-way analysis of variance (ANOVA), with multiple comparisons corrected using the Tukey test, and a significance threshold of P-adjusted < 0.05. For omics data analysis, the Bioconductor package *limma* was utilized through an R-based online tool. Data visualization was done using a heatmap with autoscaled gene features. Significant changes were assessed via overrepresentation analysis using Enrichr and GSEA 4.3.2. GraphPad Prism v.9.2.0 was employed to perform statistical calculations for bar plots, applying appropriate tests such as one-way ANOVA and two-tailed unpaired t-tests, with adjusted P-values evaluated using methods like Tukey and Sidak tests. Sample sizes were based on previous experiments using similar methodologies. Unless specified otherwise, all data points represent biological replicates from distinct samples. Each figure includes data from at least three independent experiments with multiple biological replicates, unless otherwise indicated.

2.2.18 MTT assay (SDH activity)

MTT Assay

MTT was obtained from Sigma and prepared in PBS at a concentration of 1 mg/ml. Cells were plated in 96-well plates and treated accordingly. In each plate, three wells contained only medium, serving as a blank. At the conclusion of the experiment, remove the medium and wash the cells once with 100 µl PBS. Add 100 µl of MTT (1mg/mL) solution per well. Incubate at 37°C for 2 hours or overnight, covered in tin foil. MTT solution was discarded and DMSO (100 µL) was added and incubated at 37°C for 20 minutes in the dark to form crystals. Measure absorbance on a spectrophotometer at λ=595 nm.

2.2.19 SDH-deficient tumours

Whole tissue from SDH-deficient (n=5) and sex, age, and anatomical site-matched SDH-competent (n=5) tumours were taken. Genetic testing of loss of SDH and whole tissue RNA extraction was performed in the Departments of Histopathology and Paediatrics, Trinity College Dublin, Ireland. SDHB immunohistochemistry was performed on the

diagnostic tissue and prompted confirmatory germline genetic testing and review by the clinical geneticist, where the tumour immunoreactivity for SDHB was lost. Loss of SDH was also confirmed by RT-qPCR. In several cases a familial predisposition was already apparent. Ethical approval was granted in accordance with Children's Health Ireland Research Ethics Committee guidelines. Material Transfer Agreement approval was granted in accordance with Trinity College Dublin Material transfer agreement guidelines.

Chapter 3. 4-Octyl itaconate blocks PRR-induced type I interferon via NRF2

3.1.1. 4-OI blocks LPS-induced IFNβ

It was previously reported that 4-OI could inhibit LPS-induced type I interferon responses (140, 155). These findings were repeated, showing that the pre-treatment of BMDMs with 4-OI followed by LPS stimulation suppressed LPS-induced IFNβ protein (**Figure 3.1. 1 a**) and *Ifnb1* mRNA **(Figure 3.1. 1 b)** in a concentration-dependent manner in BMDMs.

3.1.2. 4-OI blocks LPS-induced ISGs

As IFNβ production leads to the induction of ISGs, I tested whether 4-OI could also inhibit ISGs, including *Isg15* (**Figure 3.1. 2 a)**, *Usp18* (**Figure 3.1. 2 b)**, and *Caspase-11* (**Figure** Error! Reference source not found. **c)**. Indeed, pretreatment of BMDMs with 4-OI could block LPS-induced induction of ISGs.

3.1.3. 4-OI blocks poly(I:C)-induced IFNβ

The investigation then investigated how 4-OI regulated type I interferon responses in response to different PRR agonists. 4-OI pre-treatment suppressed poly(I:C)-induced IFNβ protein **(Figure 3.1. 3 a)** and *Ifnb1* mRNA (**Figure 3.1. 3 b)** in murine macrophages.

3.1.4. 4-OI blocks poly(I:C)-induced ISGs

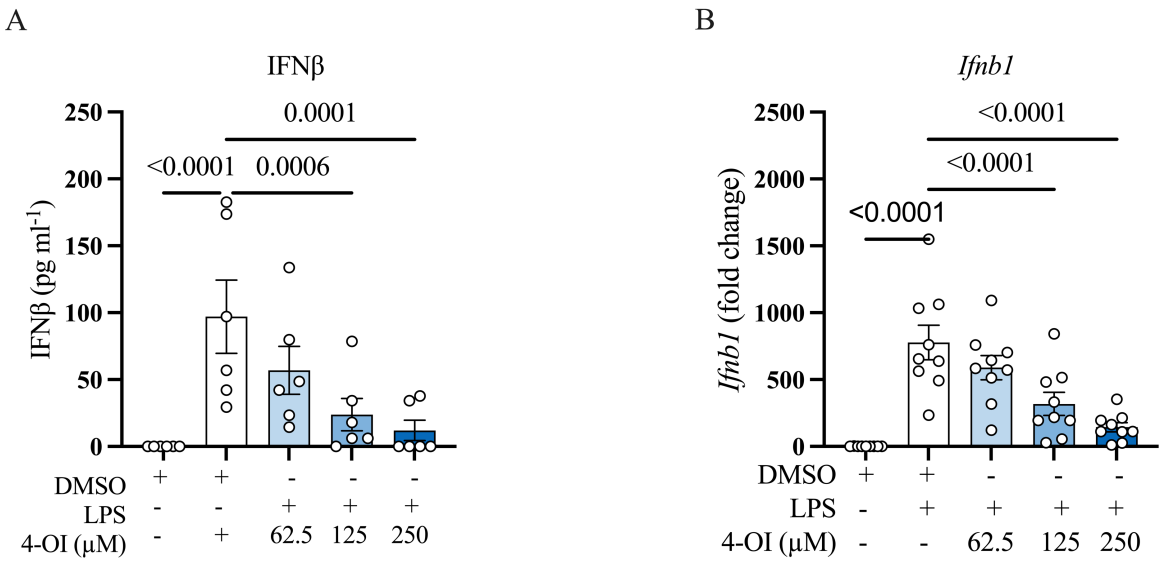
Next, results showed that 4-OI blocked poly(I:C)ISGs *Isg15* **(Figure 3.1. 4 a)**, *Usp18* **(Figure 3.1. 4 b)**, and *Caspase-11* **(Figure 3.1. 4 c)**.

3.1.5. 4-OI blocks R848-induced IFNβ and ISGs

It was next demonstrated that 4-OI could block R848-induced IFNβ protein (**Figure 3.1. 5 a)**, *Ifnb1* mRNA (**Figure 3.1. 5 b)** and ISGs; *Isg15* (**Figure 3.1. 5 c)**, *Caspase-11* (**Figure 3.1. 5 d)**, and *Usp18* (**Figure 3.1. 5 e).**

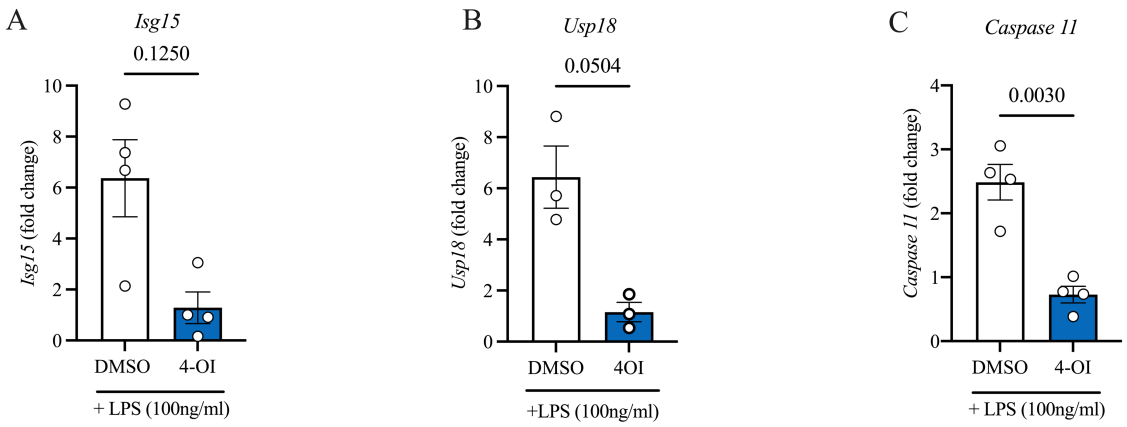
3.1.6. 4-OI blocks 2'-3'-cGAMP-induced IFNβ and ISGs

It was next demonstrated that 4-OI could block STING-induced IFNβ protein (**Figure 3.1. 6 a)**, *Ifnb1* mRNA (**Figure 3.1. 6 b)**, and ISGs *Isg15* (**Figure 3.1. 6 c)**, *Caspase-11* (**Figure 3.1. 6 d)**, and *Usp18* (**Figure 3.1. 6 e)**



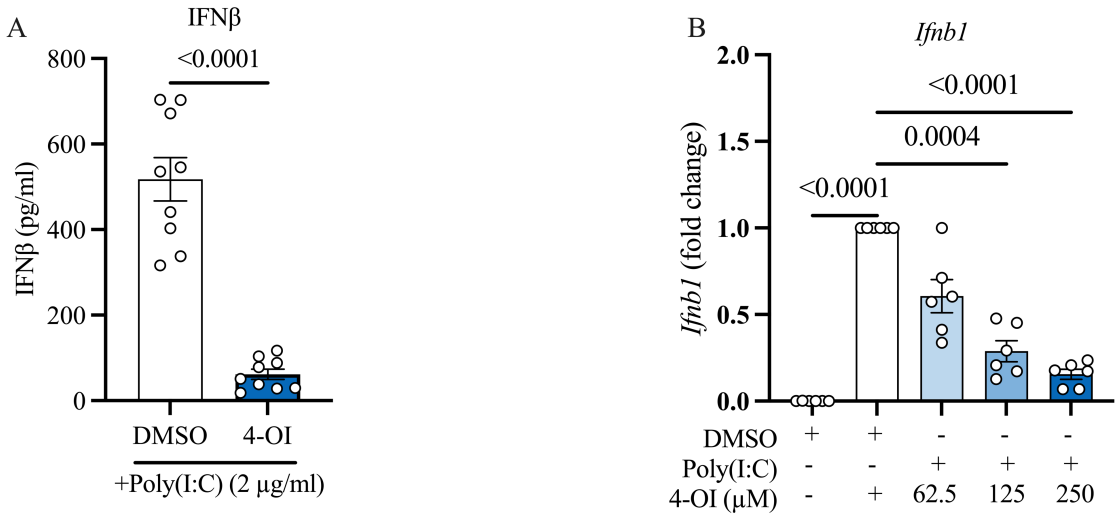
3.1. 1 4-OI blocks LPS-induced IFNβ

BMDMs (0.5x10^6 cells) were pre-treated with 4-OI or DMSO for 3 hours followed by LPS (100 ng/ml) for 4 h. Supernatants were analysed for IFNβ by ELISA **(a)**. Cell lysates were harvested and analysed by RT-qPCR for the expression of *Ifnb1* relative to *Rps18* **(b)**. Data are mean ± SEM for n=6 (a) and n=9 (b) from 3 independent experiments. P value is calculated by RM one-way ANOVA with Šídák's multiple comparisons test.



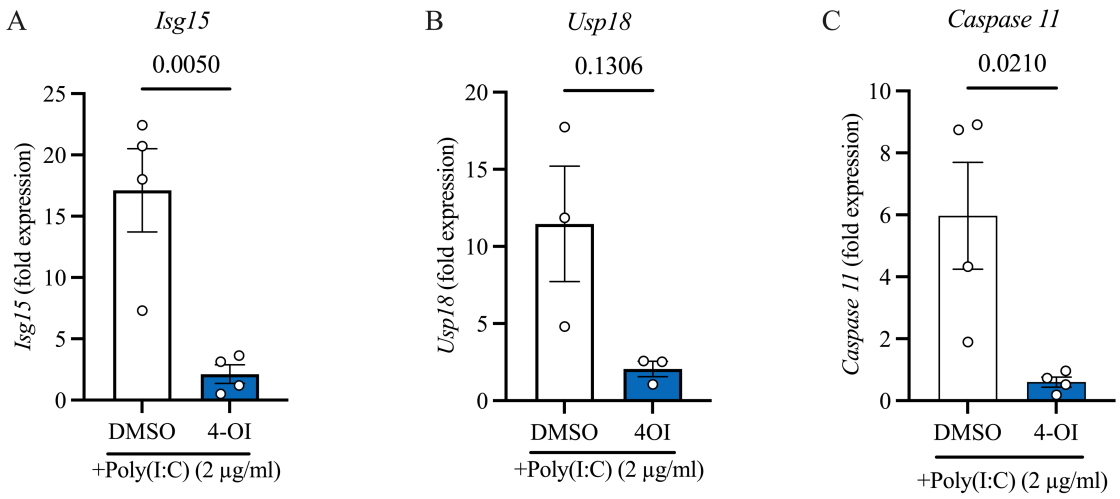
3.1. 2 4-OI blocks LPS-induced ISGs

BMDMs ($0.5x10^6$ cells) were pre-treated with 4-OI (250 µM) or DMSO for 3 hours followed by LPS (100 ng/ml, 18 h). Cell lysates were harvested and analysed by RT-qPCR for the expression of ISGs; *Isg15* **(a)**, *Usp18* **(b)**, and *Caspase-11* relative to *Rps18* **(c)**. Data are mean ± SEM. For n = 4 from 4 independent experiments (a), n = 3 from 3 independent experiments (b), n = 4 from 4 independent experiments (c). P value is calculated by paired t-test.



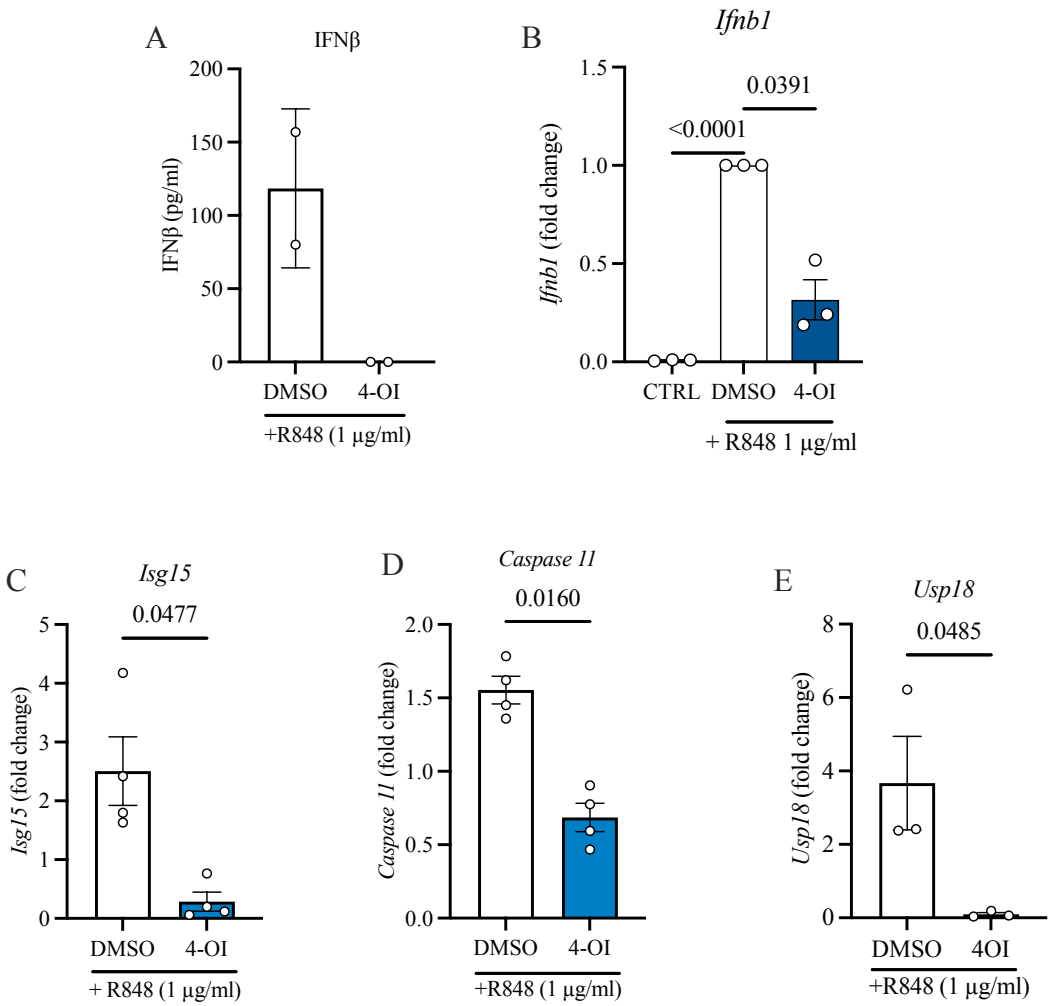
3.1. 3 4-OI blocks poly(I:C)-induced IFNβ

BMDMs (0.5x10^6 cells) were pre-treated with 4-OI (250 µM) or DMSO for 3 hours followed by poly(I:C) (2 µg/ml) for 18 h. Supernatants were analysed for IFNβ by ELISA **(a)**. BMDMs (0.5x10^6 cells) were pre-treated with 4-OI or DMSO for 3 hours followed by poly(I:C) (2 µg/ml) for 4 h. Cell lysates were harvested and analysed by RT-qPCR for the expression of *Ifnb1* relative to *Rps18* **(b)**. Data are mean ± SEM for n=9 (a), and n=6 (b) from 3 independent experiments. P value as calculated by paired *t*-test and one-way ANOVA with Šídák's multiple comparisons test respectively.



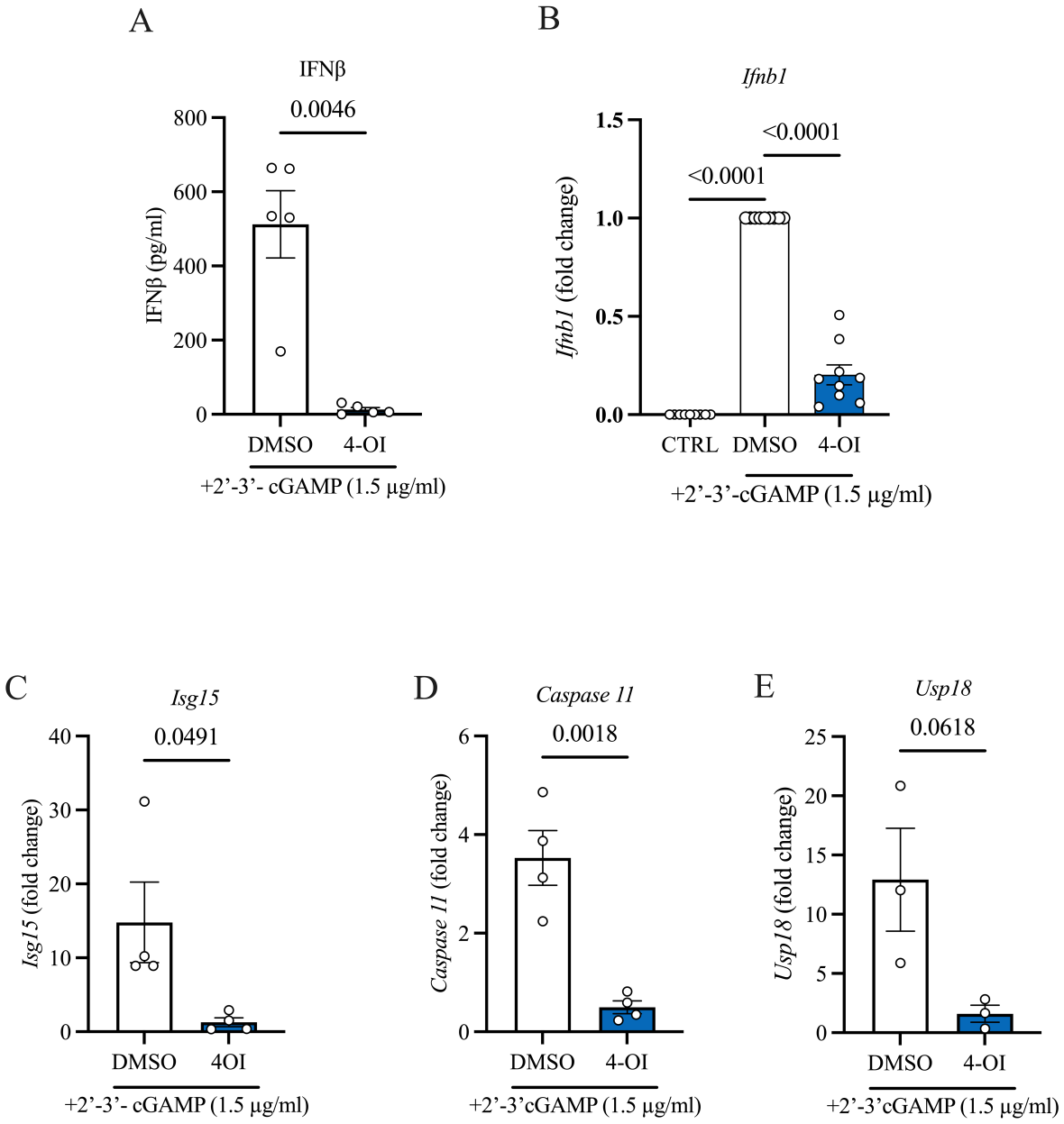
3.1. 4 4-OI blocks poly(I:C)-induced ISGs

BMDMs (0.5x10^{6} cells) were pre-treated with 4-OI (250 µM) or DMSO for 3 hours followed by poly(I:C) (2 µg/ml) for 18 h. Cell lysates were harvested and analysed by RT-qPCR for the expression of ISGs; *Isg15* **(a)**, *Usp18* **(b)**, and *Caspase-11* **(c)**, Data are mean ± SEM. for n=4 from 4 independent experiments (a), n=3 from 3 independent experiments (b), and n=4 from 4 independent experiments (c). P value as calculated by paired *t*-test.



3.1. 5 4-OI blocks R848-induced IFNβ and ISGs

BMDMs (0.5x10^6 cells) were pre-treated with 4-OI (250µM) or DMSO for 3 hours followed by R848 (1 µg/ml) for 18 h. Supernatants were analysed for IFNβ by ELISA **(a)**. Cell lysates were harvested and analysed by RT-qPCR for the expression of *Ifnb1* **(b)**, *Isg15* **(c)**, *Caspase-11* **(d),** and *Usp18* relative to *Rps18*. Data are mean ± SD. for n=2 from 2 independent experiments (a), mean ± SEM. for n=3 from 3 independent experiments (b), n=4 from 4 independent experiments, n=3 from 3 independent experiments (d,e) P-value is calculated by paired t-test.



3.1. 6 4-OI blocks 2'-3'-cGAMP-induced IFNβ and ISGs

BMDMs (0.5x10^6 cells) were pre-treated with 4-OI (250µM) or DMSO for 3 hours followed by 2'-3'-cGAMP (1.5 µg/ml) for 18 h. Supernatants were analysed for IFNβ by ELISA **(a)**. Cell lysates were harvested and analysed by RT-qPCR for the expression of *Ifnb1* **(b)**, *Isg15* **(c)**, *Caspase-11* **(d),** and *Usp18*. Data are mean ± SEM. for n=5 from 3 independent experiments (a), n=9 from 3 independent experiments (b), n=4 from 4 independent experiments (c,d), and n=3 from 3 independent experiments (e). P-value is calculated by paired *t*-test.

3.1.7 4-OI blocks CpG ODN-induced IFNβ and ISGs

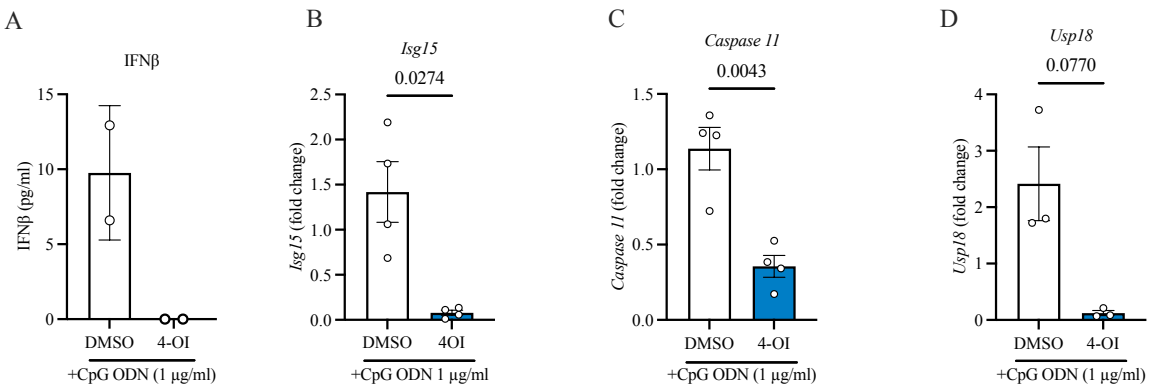
It was next demonstrated that 4-OI could block CpG-ODN-induced IFNβ protein (**Figure 3.1. 7 a**), mRNA (**Figure 3.1. 7 b**) and ISGs *Isg15* (**Figure 3.1. 7 c**)*, Caspase-11* (**Figure 3.1. 7 d**)*,* and *Usp18* (**Figure 3.1. 7 e**)

3.1.8 4-OI blocks LPS-induced *Ifnb1* independent of IFNAR signalling

Previous literature demonstrates that 4-OI modifies JAK1 to block JAK/STAT signalling (171). As JAK/STAT is important in the production of *Ifnb1* in murine macrophages (174), It was hypothesised that 4-OI blocks *Ifnb1* via inhibition of JAK/STAT signalling in BMDMs. To investigate this, I pre-treated IFNAR$^{-/-}$ BMDMs with 4-OI followed by LPS. If 4-OI inhibited *Ifnb1* via JAK1 inhibition only, then 4-OI would have no effect in IFNAR$^{-/-}$ BMDMs. Results demonstrated that 4-OI pre-treatment can block LPS-induced *Ifnb1* in IFNAR$^{-/-}$ BMDMs, suggesting that 4-OI blocks *Ifnb1* expression upstream of IFNAR signalling. **(Figure 3.1.8 a).** As a control, *Isg15* expression was significantly reduced in IFNAR$^{-/-}$ BMDMs **(Figure 3.1.8 b)**. Furthermore, *Hmox1* expression was significantly increased in 4-OI-treated IFNAR$^{-/-}$ BMDMs **(Figure 3.1.8 c).**

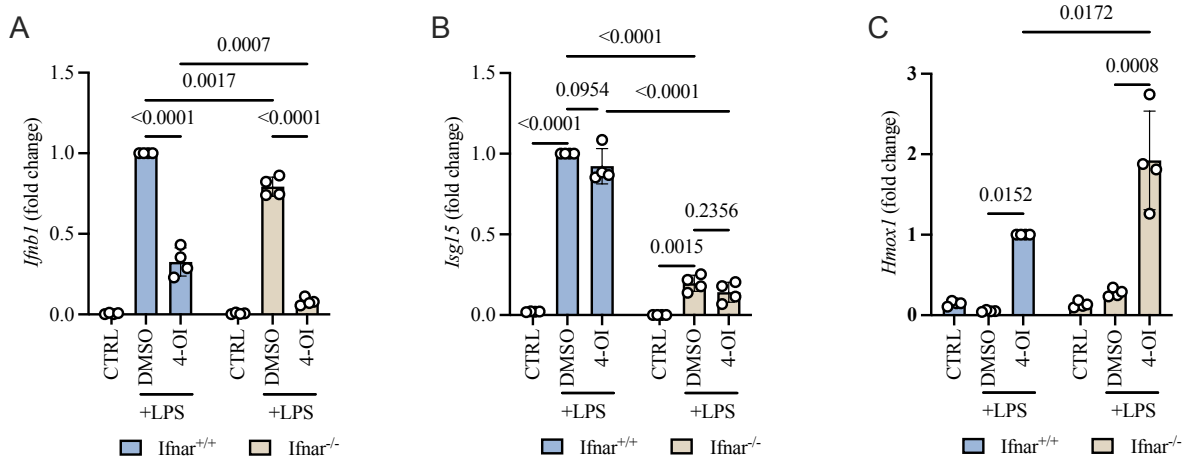
3.1.9 NRF2 activators 4-OI, DMF, and DEM block LPS-induced *Ifnb1*

As 4-OI is a known NRF2 activator via alkylation of KEAP1 (140), it was hypothesised that 4-OI blocks the induction of type I interferon via KEAP1-induced liberation of NRF2. Pre-treating BMDMs with NRF2 activators 4-OI, dimethyl fumarate (DMF), and diethyl maleate (DEM) blocked LPS-induced *Ifnb1* **(Figure 3.1.9 a).** NRF2 activators in this context could induce the expression of the NRF2-dependent gene *Hmox1* **(Figure 3.1.9 b).**



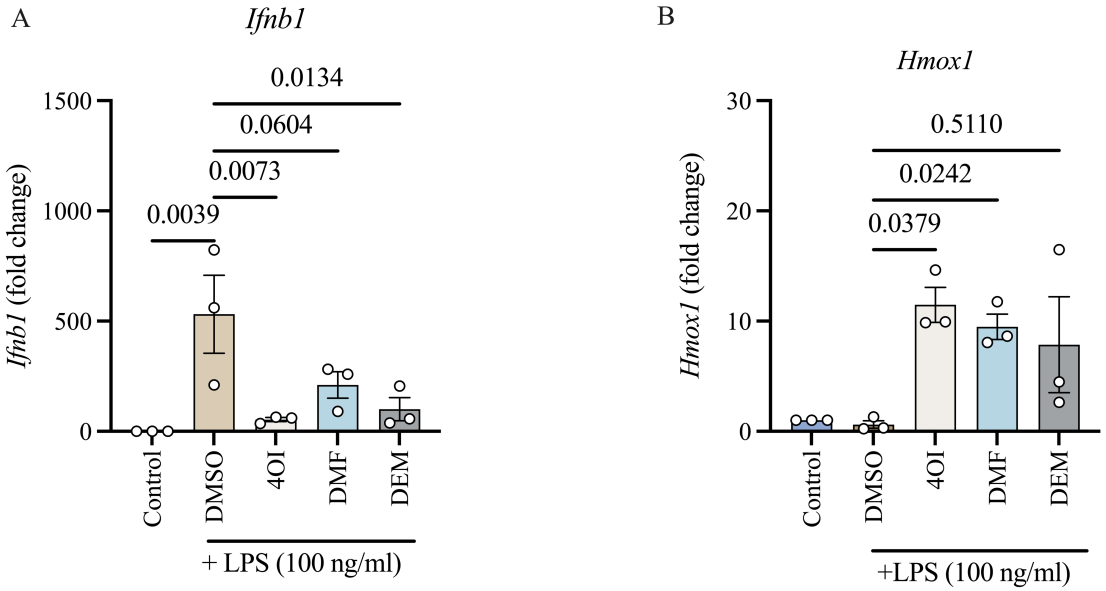
3.1. 7 4-OI blocks CpG ODN-induced IFNβ and ISGs

BMDMs (0.5x10^6 cells) were pre-treated with 4-OI (250µM) or DMSO for 3 hours followed by CpG ODN (1 µg/ml) for 18 h. Supernatants were analysed for IFNβ by ELISA **(a)**. Cell lysates were harvested and analysed by RT-qPCR for the expression of *Isg15* **(b)**, *Caspase 11* **(c)**, and *Usp18* **(d)** relative to *Rps18*. Data are mean ± SD for n=2 from 2 independent experiments (a), mean ± SEM. n=4 from 4 independent experiments (b,c), and n=3 from 3 independent experiments (d). P-value is calculated by paired t-test.



3.1. 8 4-OI blocks LPS-induced *Ifnb1* independent of IFNAR signalling

BMDMs ($0.5x10^6$ cells) of $Ifnar^{+/+}$ and $Ifnar^{-/-}$ were pre-treated with 4-OI (250 µM) for 3 hours followed by LPS (100 ng/mL) for 4 hours. Cell lysates were harvested and analysed by RT-qPCR for the expression of *Ifnb1* **(a)**, *Isg15* **(c)**, and *Hmox1* **(c)** relative to *Rps18*. Data are mean ± SD. for n=4 from 2 independent experiments. P-value is calculated two-way ANOVA with Tukey's multiple comparisons.



3.1. 9 NRF2 activators 4-OI, DMF, and DEM block LPS-induced *Ifnb1*

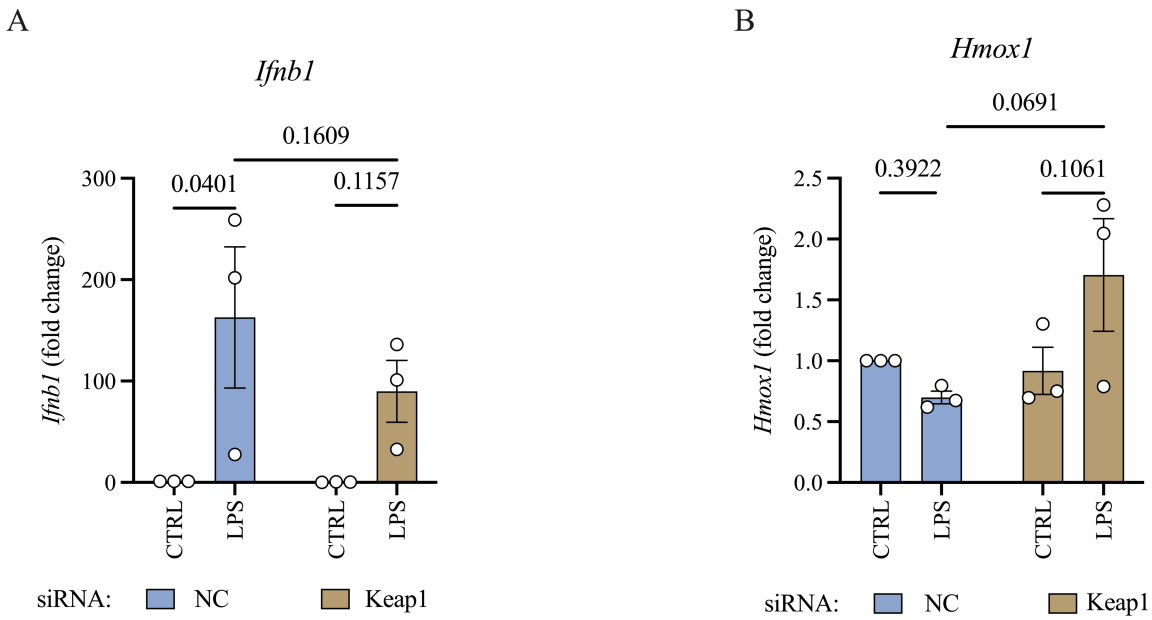
BMDMs ($0.5x10^6$ cells) were pre-treated with 4-OI (250 μM), DMF (12.5 μM), and DEM (100 μM) for 3 hours followed by 4-hour stimulation with LPS (100 ng/ml), after which supernatants and cell lysates were collected. Lysates were analysed by RT-qPCR for *Ifnb1* (**a**), and the NRF2-dependant gene *Hmox1* (**b**) relative to *Rps18*. Data are represented as mean ± SEM. for n=3 from 3 independent experiments. P-value is calculated using RM one-way ANOVA followed by Sidak's multiple comparisons test.

3.1.10 KEAP1 knockdown blocks LPS-induced *Ifnb1*

I next hypothesised that Keap1 knockdown would mimic the suppressive effect of 4-OI. Results demonstrated that, after KEAP1 knockdown, LPS produced less *Ifnb1* than in the control group **(Figure 3.1.10 a).** Keap1 knockdown boosted the expression of *Nrf2*-dependent gene *Hmox1* **(Figure 3.1.10 b).**

3.1.11 Nrf2 knockdown partially rescues the suppressive effect of 4OI on LPS-induced *Ifnb1*

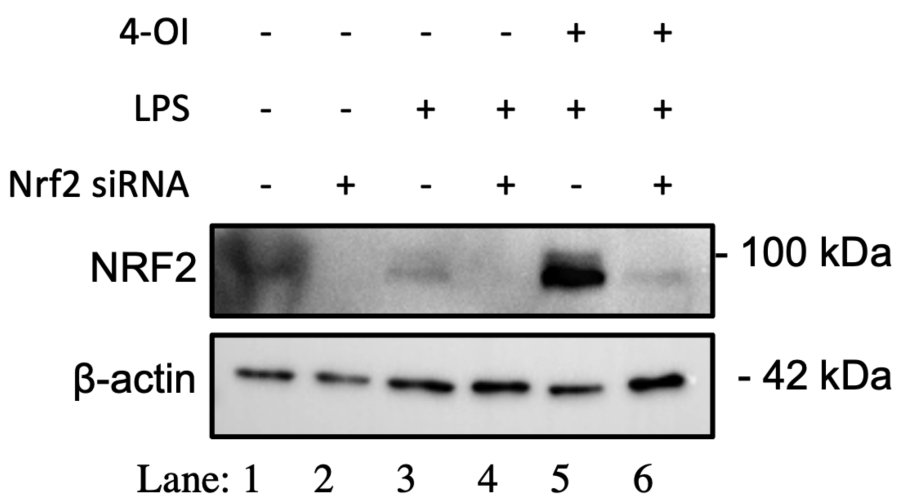
My hypothesis that 4-OI blocked LPS-induced type I interferon via liberation of NRF2 was supported with the previous results. It was next hypothesised that loss of NRF2 would impede the suppressive effect of 4-OI on IFNβ. To investigate this, siRNA knockdown of NRF2 was implemented **(Figure 3.1.11 compare lane 5 and 6).** Results showed that 4-OI stimulated BMDMs have more *Ifnb1* mRNA levels after NRF2 knockdown when compared to control knockdown indicating a partial role for NRF2 in the inhibitory effect of 4-OI **(Figure 3.1.12 a).** The NRF2-dependent gene *Hmox1* was also significantly suppressed after *Nrf2* knockdown in 4-OI-treated BMDMs **(Figure 3.1.12 b).**



3.1. 10 Keap1 knockdown blocks LPS-induced *Ifnb1*

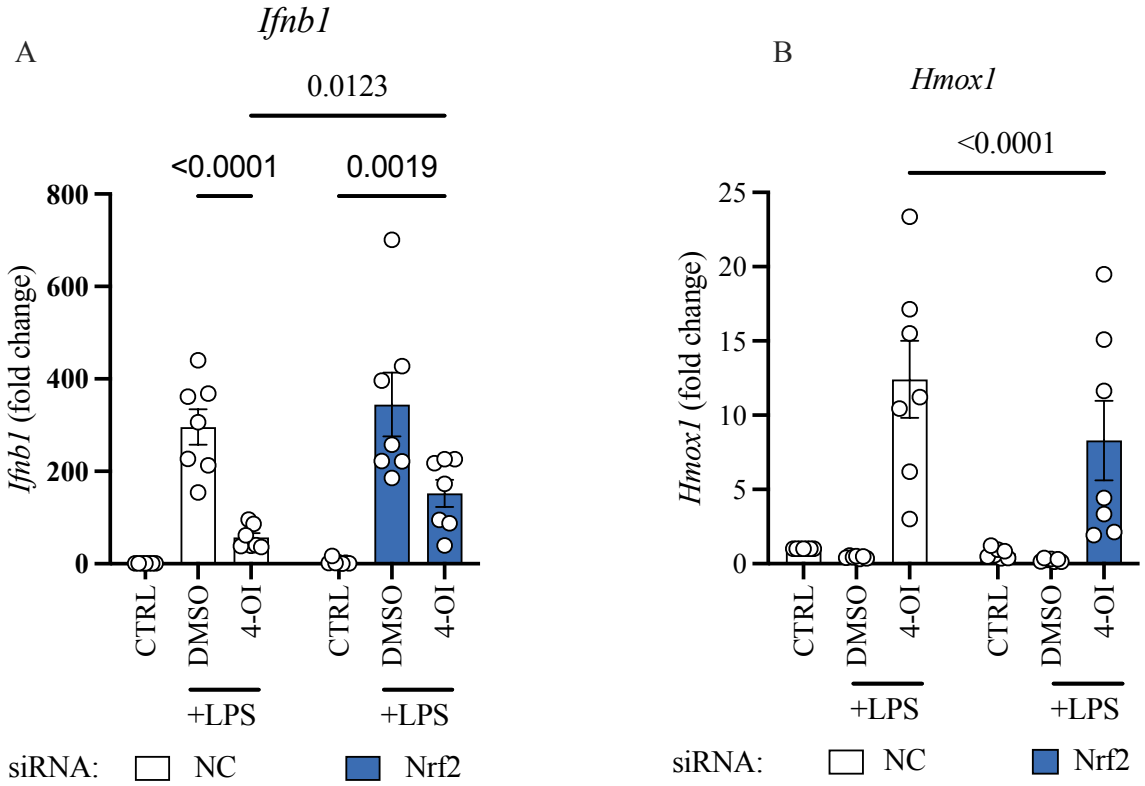
BMDMs ($0.5x10^6$ cells) were incubated with 50 nM control siRNA or Keap1 siRNA for 8 hours after which cells are replaced with media and rested for 18 h. Cells were then treated with LPS (100 ng/ml) for 4h. Lysates were analysed for *Ifnb1* **(a)** and the NRF2-dependant gene, *Hmox1* **(b)** as indirect evidence of *Keap1* knockdown. Data are mean ± SD. for n=3 from 1 independent experiment. p-values are calculated by RM two-way ANOVA with multiple comparison.

A



3.1. 11 Nrf2 knockdown partially rescues the suppressive effect of 4OI on LPS-induced *Ifnb1*

BMDMs ($0.5x10^6$ cells) were incubated with 50nM control siRNA or Nrf2 siRNA for 8 hours, after which cells were replaced with media and rested for 18 h. These cells were then pre-treated with 4OI (250 μM) or DMSO for 3 hours, followed by 4 h treatment with LPS (100 ng/ml). Cell lysates were harvested to measure NRF2 and successful knockdown (comparing lane 5 and 6) by western blot (a). The blot is representative of two independent experiments.



3.1. 12 Nrf2 knockdown partially rescues the suppressive effect of 4OI on LPS-induced *Ifnb1*

BMDMs (0.5x10^6 cells) were incubated with 50nM control siRNA or Nrf2 siRNA for 8 hours after which cells are replaced with media and rested for 18 h. These cells are then pre-treated with 4OI (250 μM) or DMSO for 3 hours, followed by 4 h treatment with LPS (100 ng/ml). Lysates were analysed for *Ifnb1* **(b)** the Nrf2 dependant gene, *Hmox1* relative to *Rps18* **(c)** as another marker of successful *Nrf2* knockdown by RT-qPCR. Data are mean ± SEM for n = 7 from 4 independent experiment. P-values was calculated using RM two-way ANOVA followed by Sidak's multiple comparisons test.

3.2 Discussion

3.2.1 4-OI blocks PRR-induced type I interferons

Research shows that 4-OI blocks LPS-induced IFNβ and ISGs in BMDMs (140, 155). I proposed to uncover a mechanism for this inhibition. Cysteine modification is an essential mechanism of action of 4-OI and is more cysteine reactive than itaconate. With this in mind, it was hypothesised that 4-OI caused an intracellular modification of a TLR signalling protein to regulate type I interferon production. In an attempt to narrow down the potential signalling pathways involved in IFNβ, which could be modified by 4-OI, multiple pattern recognition receptor (PRR) agonists were utilised to induce a robust interferon response. Using this approach, I hypothesised that 4-OI may suppress interferons in some contexts and not others, which would narrow down signalling pathways regulated by 4-OI. It was demonstrated that 4-OI could block the induction of IFNβ and ISGs upon stimulation of TLR 3 (using poly(I:C)), TLR 4 (using LPS), TLR 7/8 (using R848), TLR 9 (using CpG ODN), and STING (using 2'-3'cGAMP). These results suggested that 4-OI suppressed IFNβ via a mechanism common among these signalling pathways. Subsequently, research demonstrated that 4-OI alkylated JAK1, which inhibits JAK1 phosphorylation (171). JAK1 signalling is known to be important in the induction of ISGs. However, it is also important in the robust induction of IFNβ in LPS challenged BMDMs as $IFNAR^{-/-}$ BMDMs produce less LPS-induced IFNβ via regulation of IRF7 (174). It was hypothesised that the JAK1 alkylation by 4-OI perturbed the IFNAR signalling pathway and thus the IFNβ response. Results demonstrated that $IFNAR^{-/-}$ BMDMs expressed reduced *ISG15* and *Ifnb1* expression. However, 4-OI was equally able to block *Ifnb1* in $IFNAR^{-/-}$ versus $IFNAR^{+/+}$ BMDMs. This suggested that the inhibition of IFNβ was independent of JAK/STAT inhibition and may be upstream of IFNAR signalling pathways.

3.2.2 4-OI blocks type I interferon partially mediated by NRF2 regulation

Next, as NRF2 liberation by KEAP1 alkylation is a well-documented modification by 4-OI, it was proposed that this inhibition of type I interferon responses was via the liberation of NRF2 from KEAP1. Moreover, while itaconate boosts NRF2-dependent

genes, suggesting NRF2 activation, 4-OI is a much more potent activator of NRF2. Research previously demonstrated that NRF2 suppressed type I interferon responses basally in BMDMs (175). Furthermore, research also showed that 4-OI could block STING-induced type I interferon and the phosphorylation and dimerisation of IRF3 in THP1s, a human monocyte cancer cell line (167). However, whether the effect of 4-OI on IFNβ was NRF2-dependent was not linked in macrophages at this point. I demonstrated that NRF2 activators 4-OI, DMF, and DEM boosted the NRF2-dependent gene expression and also blocked *Ifnb1*, supporting the previous research suggesting that NRF2 activators suppress type I interferon. It was then demonstrated that 4-OI was less able to suppress *Ifnb1* expression after Nrf2 knockdown. As Nrf2 knockdown did not fully rescue the suppressive effect of 4-OI on *Ifnb1*, two hypotheses could be proposed for this effect. It could be that the knockdown was not a complete knockdown of NRF2, allowing for the remaining NRF2 to be liberated by KEAP1 alkylation by 4-OI, or that NRF2 is only partially responsible for the suppression of type I interferon responses by 4-OI. It would be imperative to use NRF2 knockout macrophages to fully understand this nuance. In parallel, a knockdown of Keap1 was performed with the aim to mimic the function of 4-OI which would increase levels of free NRF2. Indeed, Keap1 knockdown slightly blocked *Ifnb1* and boosted *Hmox1,* suggesting that NRF2 was partially responsible for the suppression of type I interferon responses.

Overall therefore, in this chapter, I have demonstrated that 4-OI is a global inhibitor of type I IFN production, blocking multiple stimuli. NRF2 activation plays a role in this effect possibly via inhibition of IRF3. In the next results chapter, I describe my findings on how underivatised itaconate boosts LPS-induced type I IFN production.

Chapter 4. Itaconate drives mtRNA-induced Type I interferon production via inhibition of succinate dehydrogenase

4.1 Results

4.1.1 IFNβ is an important cytokines in the itaconate-mediated transcriptional response

A recent publication in *Nature* developed an online software called Immune Response Enrichment analysis (IREA) which is a GSEA platform that is more specific for immune cells (173). This tool compares user gene expression data with the Immune Dictionary reference data from Ciu et al., to predict the cytokines most active in the user's dataset. I set out to see what were the most active cytokines in the transcriptional change mediated by itaconate-treated BMDMs. To investigate this, the total number of significantly upregulated and downregulated DEGs among itaconate-treated BMDMs was input into the database and the immune cell term "macrophage" was selected. The program revealed an enrichment score and p value of important cytokines in the transcriptional response to itaconate. Of note, type I interferons IFNα/β were revealed to be among the most significantly active in the itaconate-induced transcriptional response **(Figure 4.1.1).**

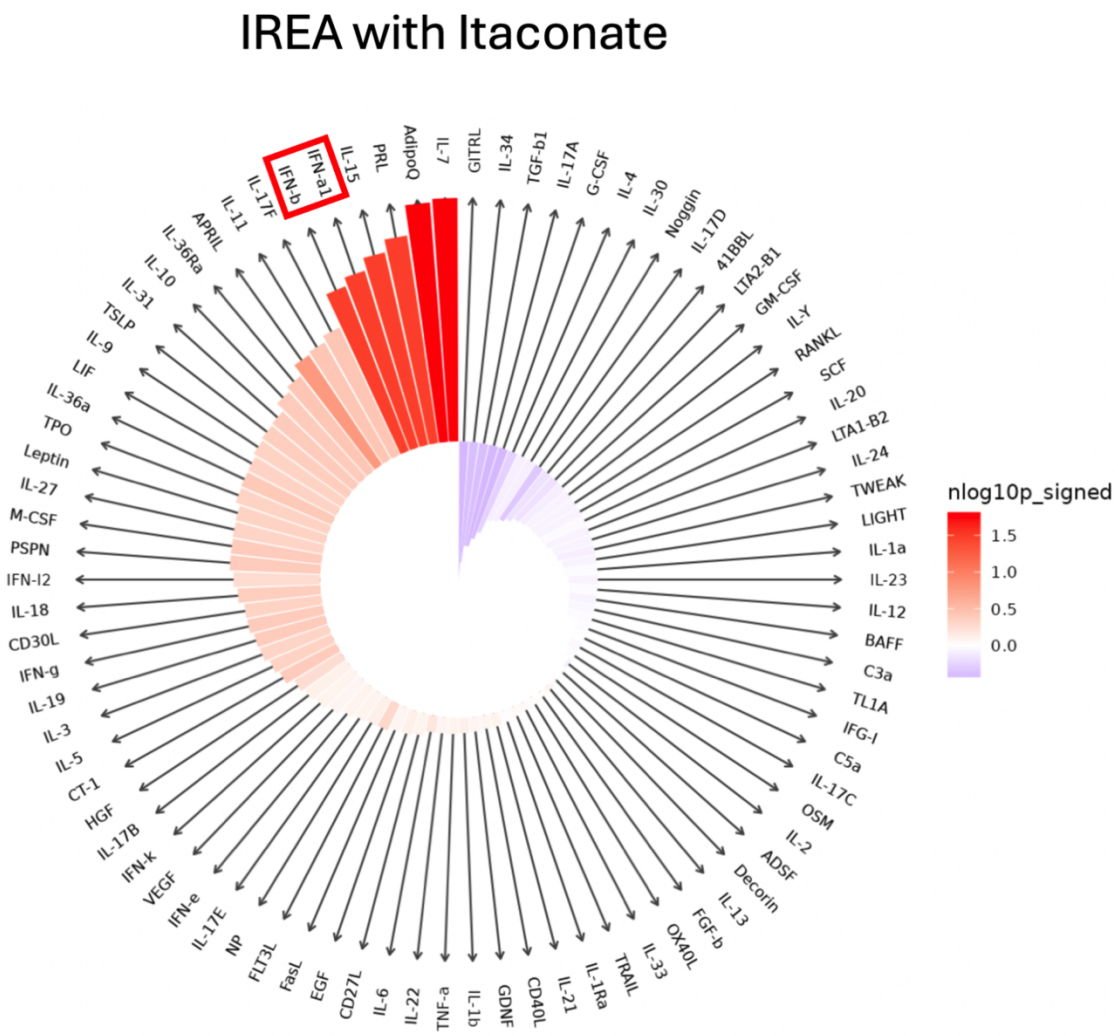
4.1.2 Itaconate boosts LPS-induced IFNβ

I first investigated whether itaconate regulated type I IFN production following the work of Swain *et al.,* who demonstrated that itaconate boosted LPS-induced type I IFN production (155). BMDMs were pre-treated with 10 mM itaconate for three hours followed by LPS for four hours. The results demonstrated that itaconate alone fails to induce IFNβ, however, itaconate increased LPS-induced IFNβ **(Figure 4.1.2 a).** This was also seen at mRNA level (**Figure 4.1.2 b).** Furthermore, itaconate boosted LPS-induced *IFNB* mRNA in human macrophages (**Figure** Error! Reference source not found. **c).** These results show that exogenous un-derivatised itaconate boosts LPS-induced IFNβ in murine and human macrophages.

4.1.3 Itaconate boosts R848-induced IFNβ and ISGs

Next, I decided to investigate how itaconate pre-treatment regulated type I interferons mediated by other PRR agonists. R848, a TLR7/8 agonist was used as an inducer of type I interferons. BMDMs were pre-treated with itaconate for 6 hours and the stimulated with R848 for 18 hours. Itaconate boosted R848-induced IFNβ **(Figure 4.1.3 a).** Furthermore,

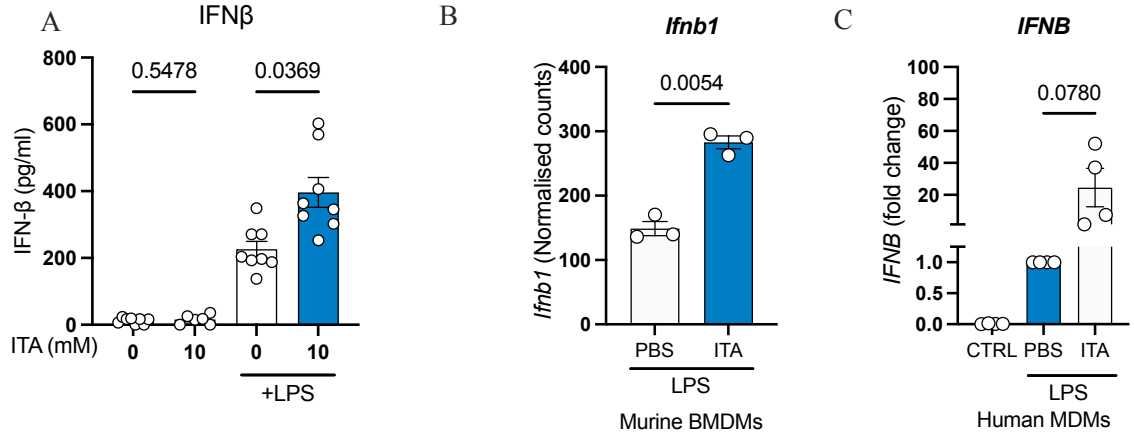
itaconate also boosted R848-induced ISGs such as *Caspase-11* **(Figure 4.1.3 b)**, *Usp18* **(Figure 4.1.3 c)**, and *Isg15* **(Figure 4.1.3 d).**



Cytokine	Enrichment Score	pval	padj
IL7	11127.7005	0.0004	0.0154
Adiponectin	10970.7251	0.0002	0.0154
Prolactin	9595.0087	0.0020	0.0333
IL15	9021.5171	0.0023	0.0333
IFNa1	8439.3600	0.0018	0.0333
IFNb	8048.0145	0.0022	0.0333

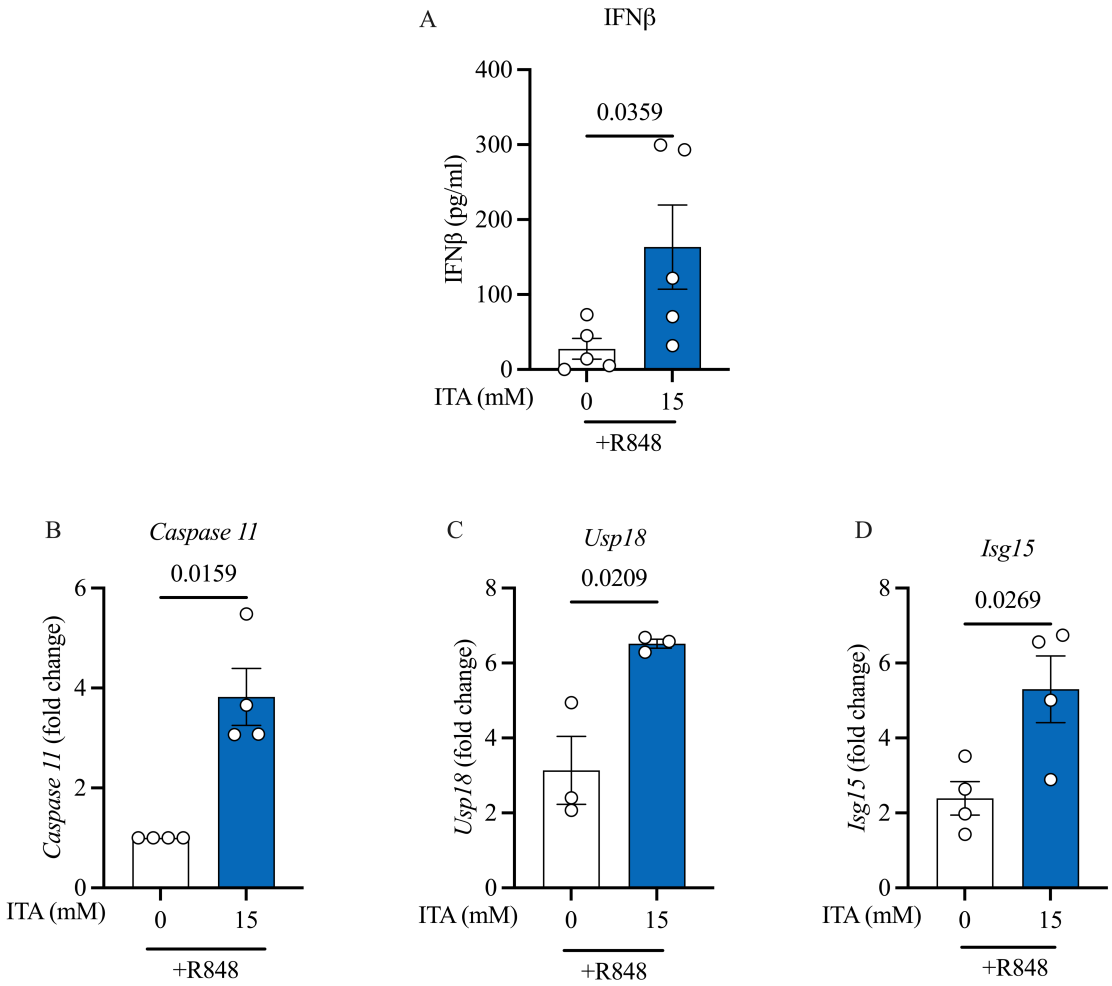
4.1.1 IFNβ is an important cytokine in itaconate-induced transcriptional response

Immune response enrichment analysis (IREA) plot from RNA-seq data of significantly (padj < 0.05) differentially expressed genes in BMDMs ($0.5x10^6$ cells) pre-treated with 10 mM itaconate for three hours, followed by four hours of LPS (100 ng/ml) stimulation. Total differentially expressed genes names were used as input data for the IREA program.



4.1.2 Exogenous itaconate boosts LPS-induced IFNβ

IFNβ release from BMDMs (0.5x10^6 cells) pre-treated with itaconate (10 mM) or PBS for 3 hours followed by LPS (100 ng/mL) for 4 hours **(a).** *Ifnb1* normalised counts from BMDMs pre-treated with itaconate (10 mM) or PBS for 3 hours followed by LPS (100 ng/mL) for 4 hours (**b**). RT-qPCR of *IFNB* expression relative to *Rps13* in Human MDMs pretreated with ITA (10 mM) for 3 hours followed by LPS (100 ng/mL) for 4 hours**.** Data are mean ± SEM. for n=8 from 3 independent experiments (a), mean ± SD for n=3 from one experiment (b), n=4 from 2 independent experiments (c). P values calculated using two-tailed Student's *t*-test for paired comparison and two-way ANOVA for multiple comparisons.



4.1.3 Itaconate boosts R848-induced IFNβ and ISGs

BMDMs ($0.5x10^6$ cells) were pre-treated with itaconate (15 mM) for 6 hours followed by R848 (1 µg/mL) for 18 hours. Supernatants were analysed for IFNβ (**a**). Lysates were analysed by RT-qPCR for ISGs *Caspase 11* (**b**), *Usp18* (**c**), and *Isg15* (**d**) relative to *Rps18*. Data are mean ± SEM. for n=5 from 5 independent experiments (a), for n=4 from 4 independent experiments (b,d), for n=3 from 3 independent experiments (c). P values calculated using two-tailed Student's t-test for paired comparison.

4.1.4 Itaconate boosts poly(I:C)-induced IFNβ but not ISGs

Utilising high molecular weight poly(I:C) as a TLR3 ligand in BMDMs, I demonstrated that itaconate boosted poly(I:C)-induced IFNβ **(Figure 4.1.4 a).** However, itaconate failed to boost poly(I:C)-induced ISGs *Caspase-11, Usp18,* and *Isg15* **(Figure 4.1.4 B-D).**

4.1.5 Itaconate boosts CpG-ODN-induced IFNβ and ISGs

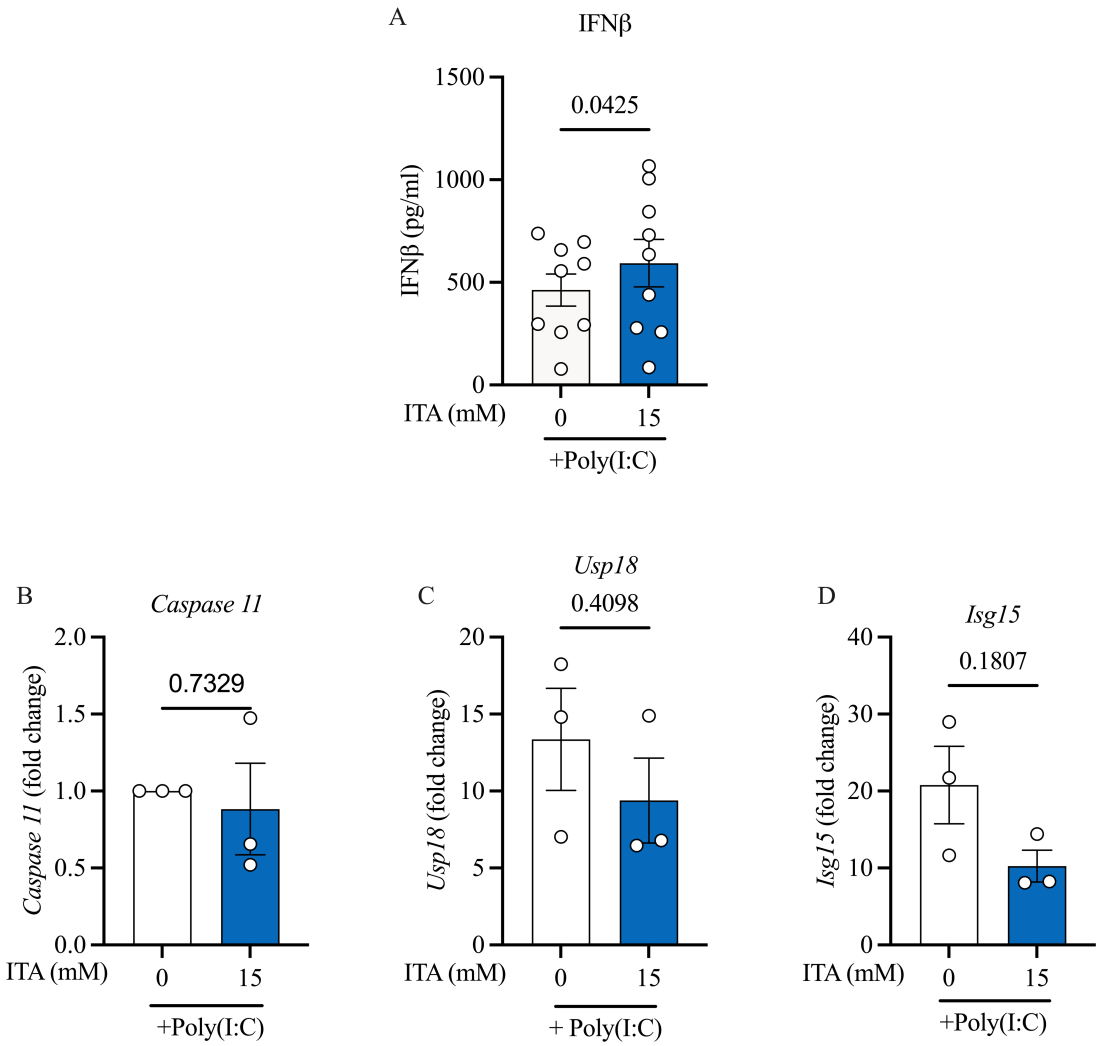
I next pre-treated BMDMs with itaconate for 6 hours followed by the TLR9 agonist CpG-ODN for 18 h. These results demonstrated that itaconate boosted TLR9-induced IFNβ release **(Figure 4.1.5 a)** and the expression of ISGs *Caspase 11, ISG15,* and *Usp18* **(Figure 4.1.5 B-D).**

4.1.6 Itaconate boosts *Ifnb1* and NRF2-dependent gene *Hmox1 in-vivo*

It was next decided to investigate whether itaconate could regulate IFNβ *in-vivo*. An intraperitoneal injection of 50 mg/kg or 100 mg/kg of itaconate for six hours was performed in mice. Peritoneal exudate cells was isolated which consists of mainly myeloid cells. It was determined that itaconate boosted *Ifnb1* (P = 0.1552) **(Figure 4.1.6 a)**, and the NRF2-dependent gene *Hmox1* **(Figure 4.1.6 b).**

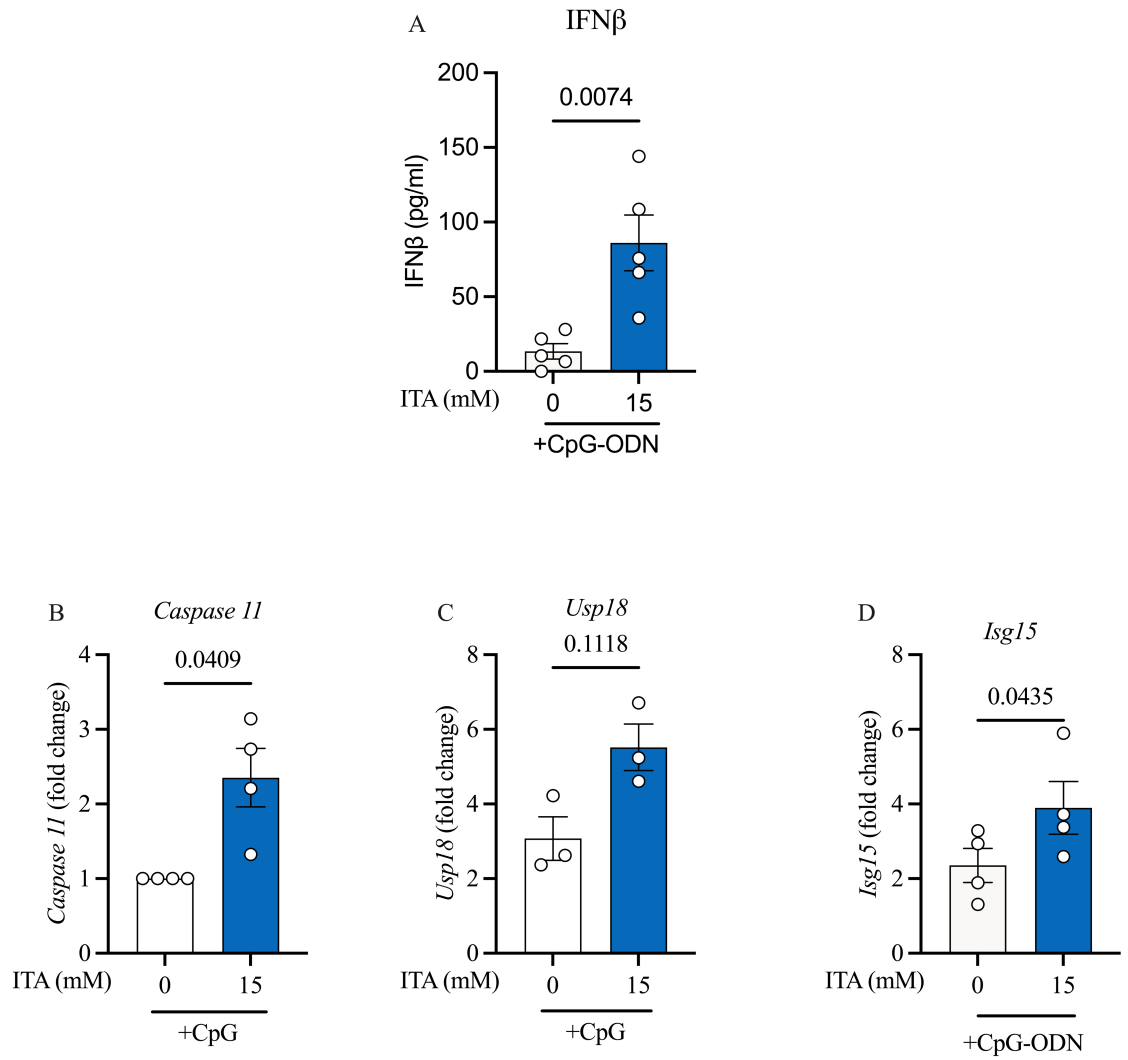
4.1.7 ACOD1 is necessary for a robust LPS-induced type I interferon response in BMDMs

It was discovered that itaconate supplementation of BMDMs and human macrophages boosted LPS-induced type I interferon production, I then decided, using a genetic knockout model of loss of ACOD1, to investigate if endogenous itaconate boosts LPS-induced type I interferon. Results showed that LPS-challenged $Irg1^{+/+}$ BMDMs produced significantly higher levels of IFNβ when compared to $Irg1^{-/-}$ BMDMs (**Figure 4.1.7 a**). Furthermore, lysates were also analysed for gene expression and showed a significant reduction in *Isg15* expression over eight hours (**Figure 4.1.7 c**).



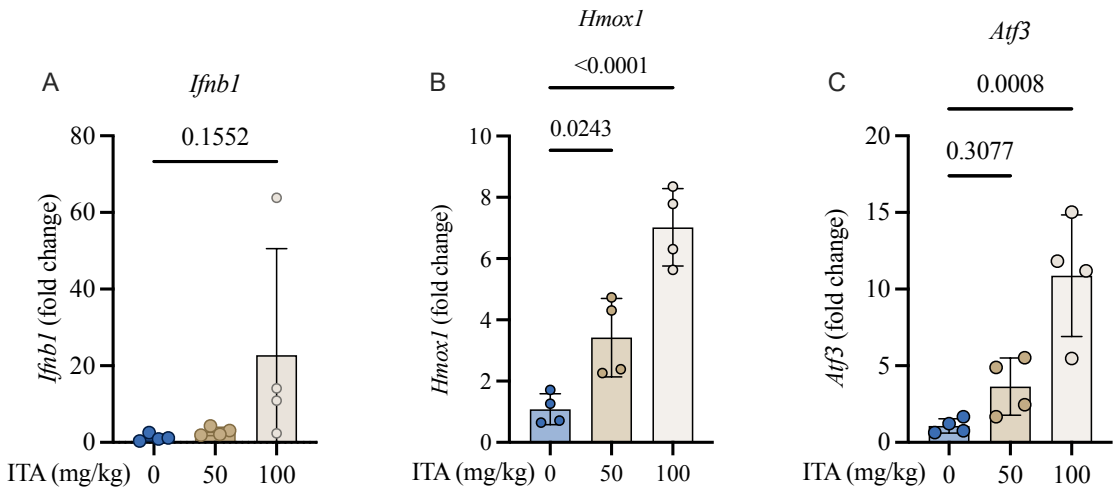
4.1.4 Itaconate boosts poly(I:C)-induced IFNβ but not ISGs

BMDMs (0.5x10^6 cells) were pre-treated with itaconate or PBS (15 mM) for 6 hours followed by poly(I:C) (1 µg/mL) for 18 h hours. Supernatants were analysed for IFNβ release (**a**). Lysates were analysed by RT-qPCR for ISGs *Caspase 11* (**b**), *Usp18* (**c**), and *Isg15* (**d**) relative to *Rps18*. Data are mean ± SEM. for n=9 from 6 independent experiments (a) and n=3 from 3 independent experiments (b-d). P values calculated using two-tailed Student's *t*-test for paired comparison.



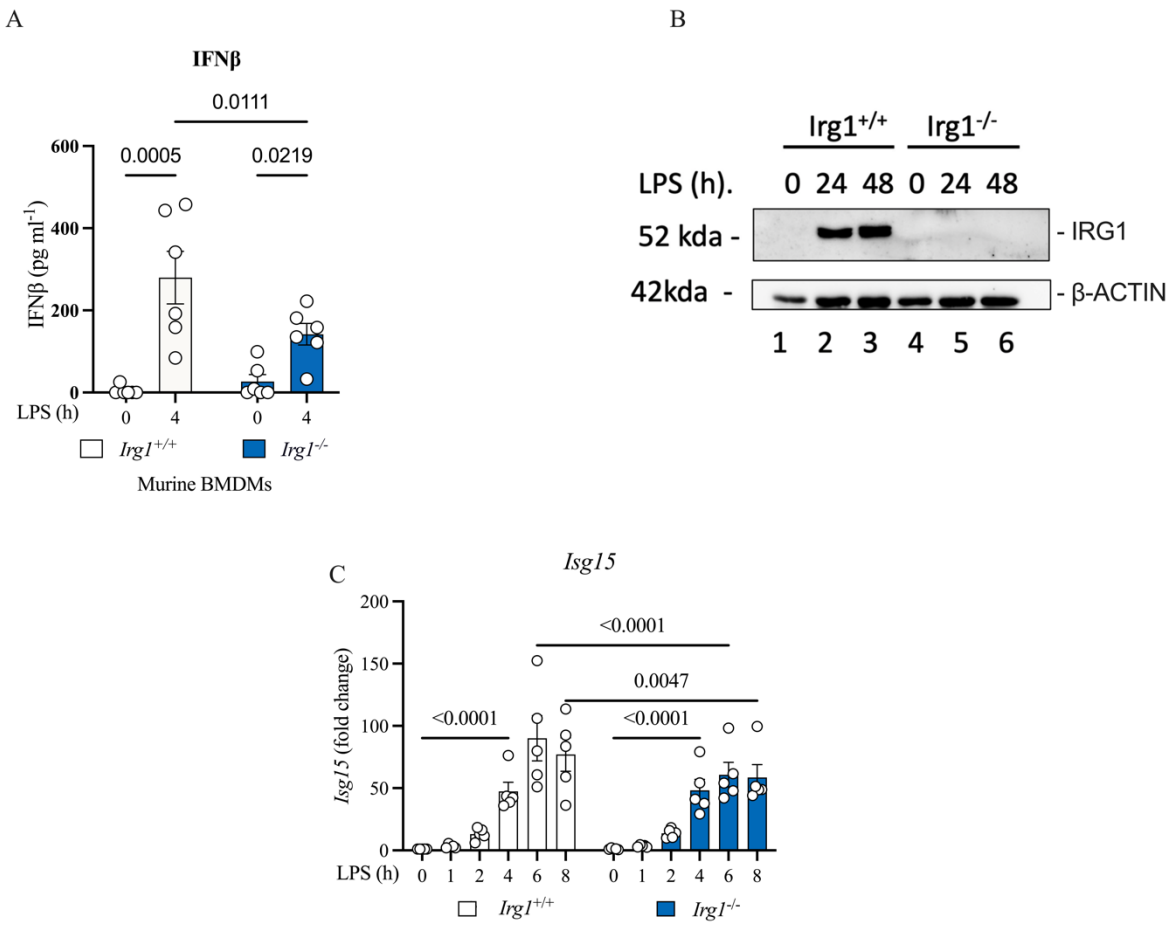
4.1.5 Itaconate boosts CpG-ODN-induced IFNβ and ISGs

BMDMs (0.5x10^6 cells) were pre-treated with itaconate (15 mM) or PBS for 6 hours followed by CpG-ODN (1 µg/mL) for 18 hours. Supernatants were analysed for IFNβ release (**a**). Lysates were analysed by RT-qPCR for ISGs *Caspase 11* (**b**), *Usp18* (**c**), and *Isg15* (**d**) relative to *Rps18*. Data are mean ± SEM. for n=5 from 5 independent experiments (a), n=4 from 4 independent experiments (b,d), and n=3 from 3 independent experiments (c). P values calculated using two-tailed Student's *t*-test for paired comparison.



4.1.6 Itaconate boosts *Ifnb1* and NRF2-dependent gene Hmox1 *in-vivo*

RT-qPCR data for *Ifnb1* **(a)**, *Hmox1* **(b)**, and *Atf3* **(c)** relative to *Rps18* from peritoneal exudate cells after intraperitoneal injection of control (PBS) or itaconic acid (50 mg/kg and 100 mg/kg) for 6 hours. Data are mean ± SD. for n=4 from one experiment. P values were calculated using Ordinary one-way ANOVA with multiple comparisons.



4.1.7 ACOD1 is necessary for a robust LPS-induced type I interferon production in BMDMs

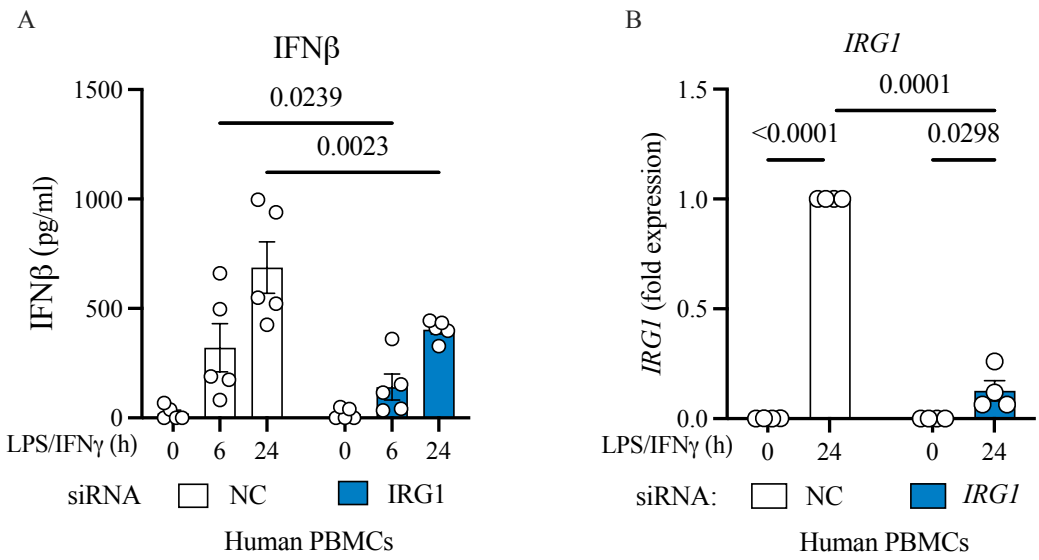
IFNβ release from *Irg1*$^{+/+}$ and *Irg1*$^{-/-}$ BMDMs stimulated with LPS (100 ng/mL) for 4 hours **(a)**. Western blot of IRG1 expression from *Irg1*$^{+/+}$ and *Irg1*$^{-/-}$ BMDMs **(b)**. *Isg15* expression by RT-qPCR from *Irg1*$^{+/+}$ and *Irg1*$^{-/-}$ BMDMs relative to *Rps18* (**c**). Data are mean ± SEM. for n=6 from 3 independent experiments (a), western blot is a representative blot (b), and n = 5 from 5 independent experiments (c). P values were calculated using a two-tailed Student's *t*-test for paired comparison and RM two-way ANOVA with multiple comparisons.

4.1.8 *IRG1* is necessary for a robust IFNβ production in activated PBMCs

I next investigated whether endogenous itaconate could also regulate IFNβ in human cells. To investigate this, human PBMCs were generated from blood donors. The resulting PBMCs underwent genetic silencing for *IRG1* **(Figure 4.1.8 b)**, and were then stimulated with LPS and IFNɣ for six and 24 hours. The results showed that *IRG1* silencing produced significantly less IFNβ in human PBMCs **(Figure 4.1.8 a).**

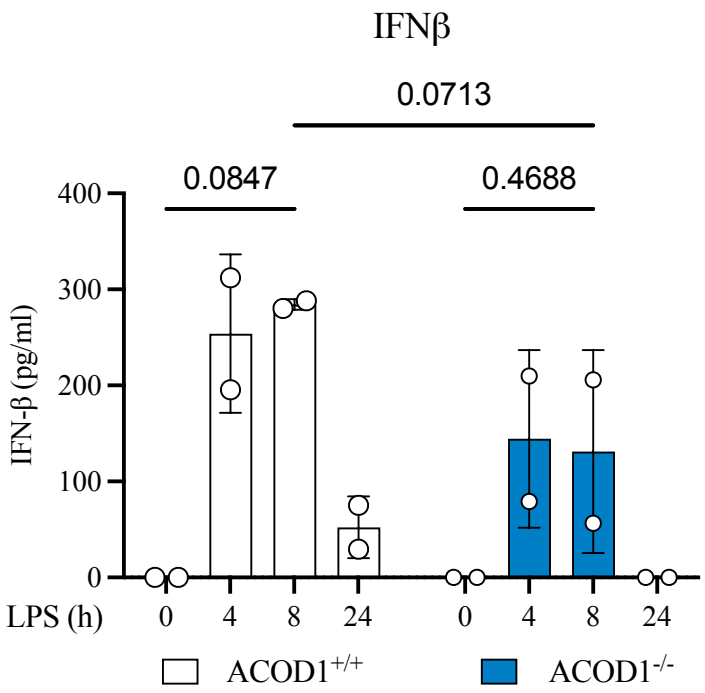
4.1.9 ACOD1 is necessary for a robust LPS-induced IFNβ response in THP1s

As *IRG1* silencing reduced IFNβ release in human PBMCs, I confirmed that itaconate boosts LPS-induced IFNβ human monocyte cell lines in which ACOD1 has been deleted. Results showed that LPS-challenged ACOD1$^{+/+}$ THP1 macrophages produced higher levels of IFNβ than ACOD1-deleted THP1s.



4.1.8 *IRG1* is necessary for a robust IFNβ production in activated PBMCs

Human PBMCs ($0.5x10^6$ cells) underwent *IRG1* silencing and subsequent stimulation with LPS + IFNɣ (100 ng/mL) for 24 hours. Supernatants were analysed for IFNβ release by ELISA **(a)** and *IRG1* expression by RT-qPCR **(b)** relative to *RPS13*. Data are mean ± SEM. for n=5 from 3 independent experiments P values calculated using two-way ANOVA with multiple comparisons.



4.1.9 ACOD1 is necessary for a robust LPS-induced IFNβ response in THP1s

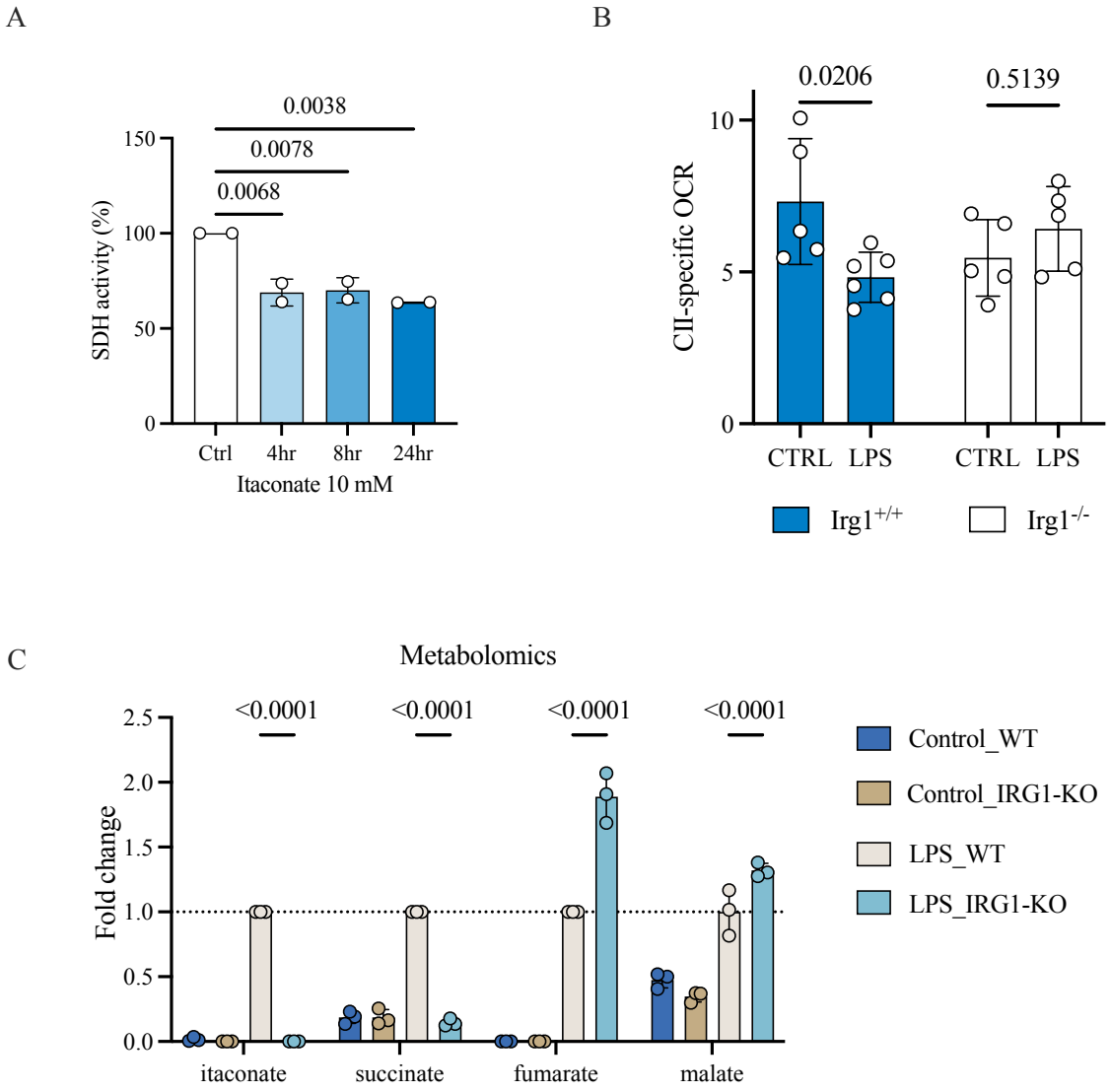
IFNβ release in THP1 human ACOD1$^{+/+}$ and IRG1$^{-/-}$ macrophage cell line after PMA (100 ng/mL) for 72 hours followed by LPS (100ng/ml). Data are mean ± SD. for n=2 from 2 independent experiments. P values calculated using RM two-way ANOVA.

4.1.10 Itaconate inhibits succinate dehydrogenase activity.

As FH inhibition boosted type I IFN production in response to LPS (3, 4, 176), I next explored the role of inhibition of SDH by itaconate here. I therefore examined whether itaconate could inhibit SDH. Results demonstrate that itaconate inhibited SDH activity in an SDH enzyme (MTT) assay (**Figure 4.1.10 a).**

To verify that endogenously produced itaconate also inhibited SDH, a complex II-specific seahorse was performed on LPS-stimulated *Irg1*$^{+/+}$ and *Irg1*$^{-/-}$ BMDMs. Results showed that *Irg1*$^{+/+}$ BMDMs had lower SDH activity in response to LPS whereas LPS did not lower SDH activity in *Irg1*$^{-/-}$ BMDMs (**Figure 4.1.10 b**). This indicates that both exogenous and endogenously produced itaconate can inhibit SDH in our model.

SDH inhibition in macrophages results in the accumulation of its substrate succinate (3). Raw metabolomic data sourced from Hooftman et al.,2023, deposited online was reanalysed and showed that *Irg1*$^{+/+}$ BMDMs accumulate succinate and itaconate and a reduction in fumarate and malate when compared to *Irg1*$^{-/-}$ BMDMs after 24-hour LPS stimulation **(Figure 4.1.10 c).**



4.1. 10 Itaconate inhibits succinate dehydrogenase activity

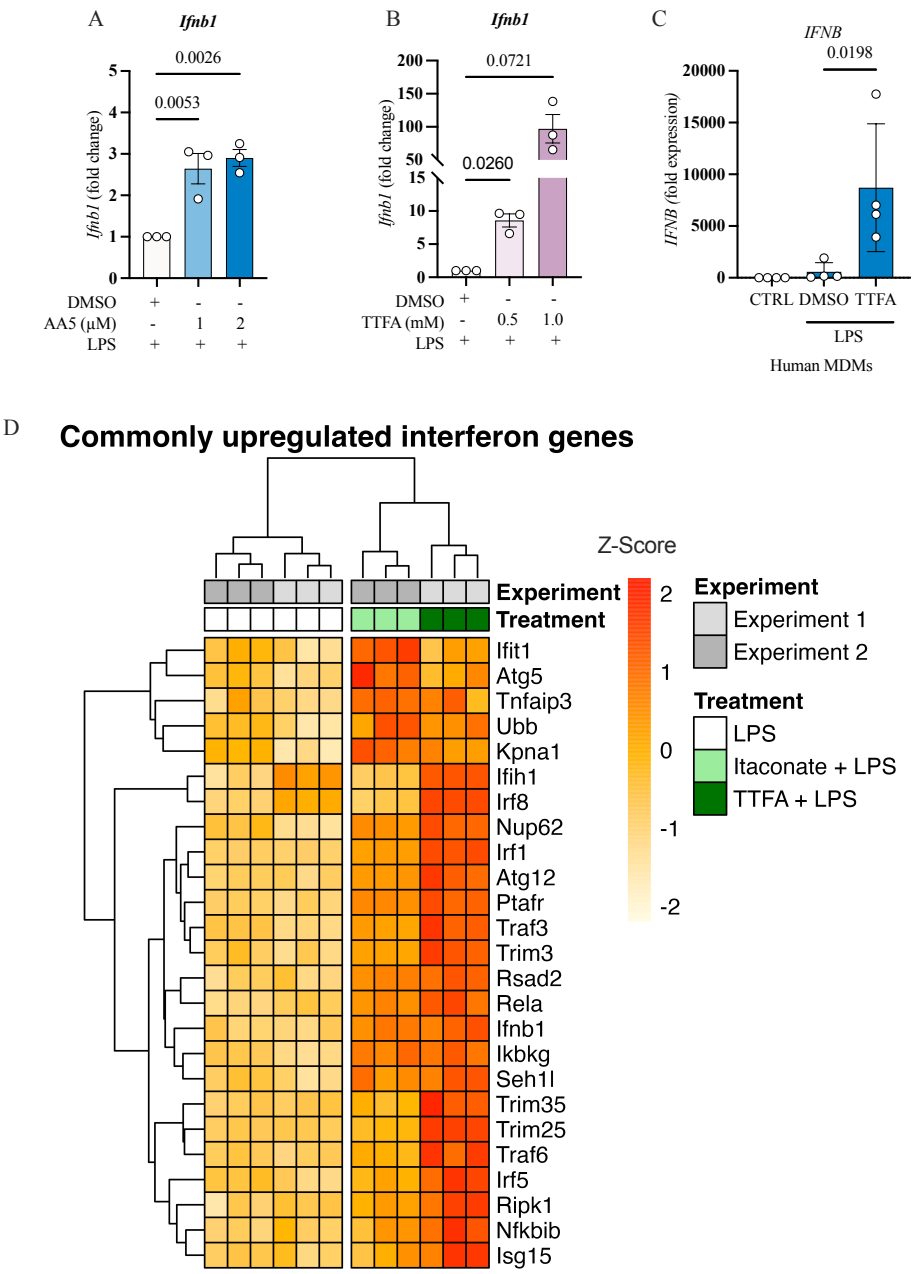
SDH activity (MTT) assay on BMDMs treated with 10 mM itaconate for 4,8, and 24 hours (**a**). Complex II-specific seahorse with *Irg1*$^{+/+}$ and *Irg1*$^{-/-}$ BMDMs treated with LPS for 24 h (n=5) **(b)**. Metabolomics data from *Irg1*$^{+/+}$ and *Irg1*$^{-/-}$ BMDMs treated with LPS for 24 h from publicly available data from Hooftman et al **(c)**. Data are mean ± SD. for n=2 from one experiment (a), for n=5 from one independent experiments (b). P values were calculated using Ordinary One-Way ANOVA (a) and two-way ANOVA with multiple comparisons (b,c)

4.1.11 SDH inhibition boosts LPS-induced IFNβ and ISGs in macrophages

Having demonstrated SDH inhibition by itaconate, I next tested the specific and well-characterised SDH inhibitors atpenin A5 (AA5) and 2-thenoyltrifluoroacetone (TTFA) (177, 178). Results showed that AA5 and TTFA significantly boosted LPS-induced *Ifnb1* expression in BMDMs **(Figure 4.1.11 a and b).** Furthermore, this results was repeated in human monocyte-derived macrophages **(Figure 4.1.11 c).** To further investigate how SDH inhibition boosts LPS-induced type I interferons, RNA-seq was performed on itaconate or TTFA pre-treated BMDMs followed by LPS challenge. 25 ISGs were significantly upregulated (p-adjusted value < 0.05) among both itaconate and TTFA pre-treated BMDMs including *Isg15, Ifnb1, Irf1, Ifih1, Rsad2,* and *Ifit1* **(Figure 4.1.11 d).** These results indicate that SDH inhibition boosts LPS-induced type I interferon in murine and human macrophages.

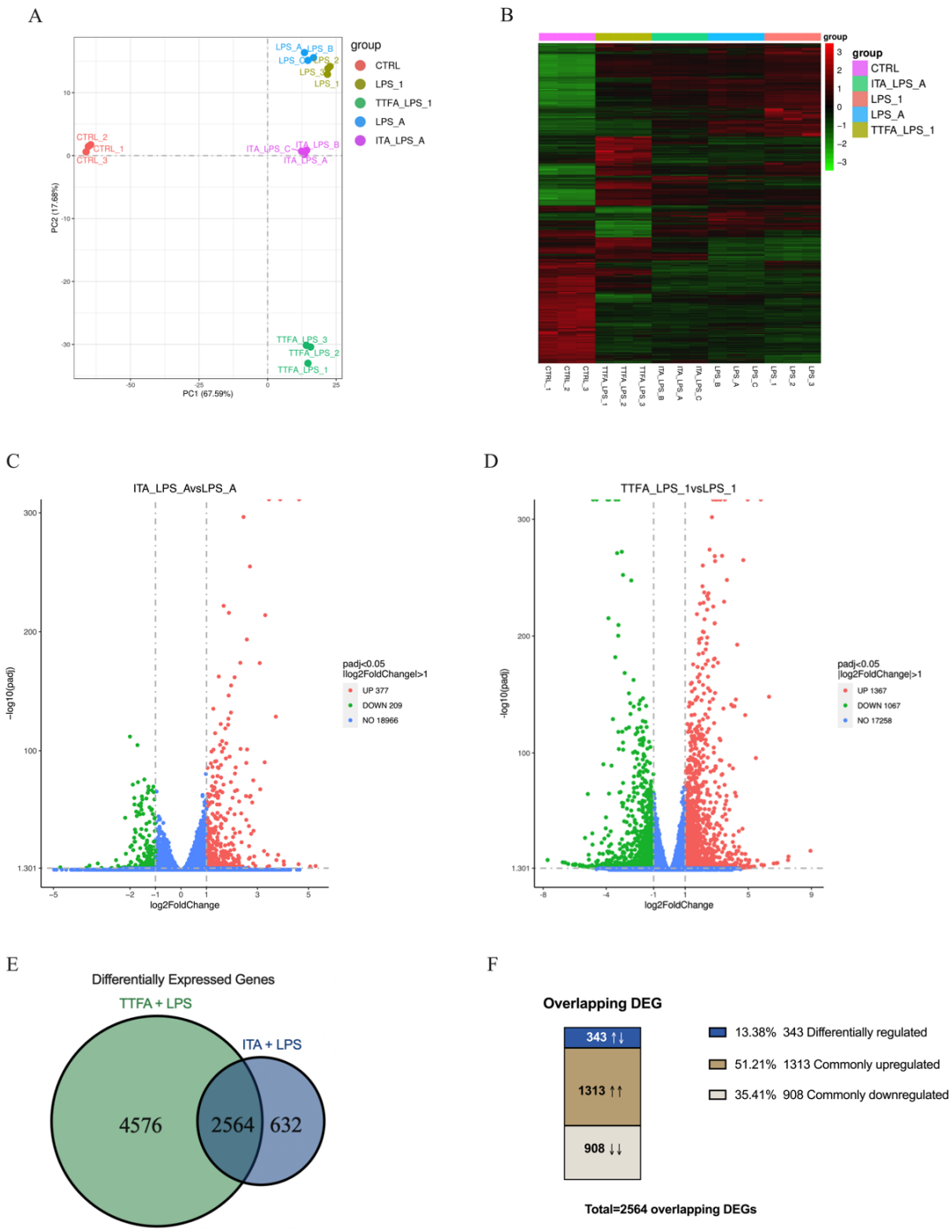
4.1.12 RNA-seq analysis of itaconate and TTFA-treated BMDMs

To fully understand the role of itaconate on macrophage function, an RNA-seq experiment was performed using BMDMs pre-treated with either itaconate or TTFA followed by LPS in biological triplicate. Principle component analysis (PCA) plot illustrates that samples separated into clear groups indicating that different conditions induce unique transcriptional responses **(Figure 4.1.12 a)** as can be seen in the heatmap with hierarchical clustering of z-scores from total gene normalised counts (**Figure 4.1.12 b).** The upregulated and downregulated genes of itaconate or TTFA-treated BMDMs can be seen in **Figure 4.1.12 c and d.** TTFA-treated BMDMs had a larger transcriptional response with 7,140 DEGs (p-val < 0.05) while itaconate-treated BMDMs had a smaller response (3,196 DEGs). Among the total number of significantly differentially expressed genes between itaconate and TTFA-treated BMDMs, 2564 genes were commonly differentially expressed between the two conditions (**Figure 4.1.12 e).** Among the 2564 overlapping DEGs among the two conditions, 51.21 % or 1313 genes were commonly upregulated and 35.41 % or 908 were commonly downregulated with just 13.38 % or 343 DEGs were differentially regulated (**Figure 4.1.12 f).**



4.1. 11 SDH inhibition boosts LPS-induced IFNβ and ISGs in macrophages

BMDMs (0.5x10^6 cells) were pre-treated with either control (DMSO), or SDH inhibitors AA5 **(a),** or TTFA (**b**) for 3 hours before LPS (100 ng/mL) stimulation for 4 hours and analysed, by RT-qPCR, *Ifnb1* expression relative to *Rps18*. *IFNB* expression relative to *Rps13* by RT-qPCR in Human MDMs pretreated with TTFA (0.5 mM) for 3 hours followed by LPS (100 ng/mL) for 4 hours (**c**). Heatmap shows (z-score) from normalised counts of ISGs commonly upregulated with TTFA and itaconate-treated BMDMs (padj < 0.05). Data are mean ± SEM. for n=3 from 3 independent experiments (a,b), mean ± SEM for n=4 donors from 1 experiments (c). P values calculated using one-way ANOVA for multiple comparisons.



4.1. 12 RNA-seq analysis of itaconate and TTFA-treated BMDMs

BMDMs (0.5x10^6 cells) were treated with either itaconate (10 mM), PBS, TTFA (0.5 mM), or DMSO, followed by LPS (100 ng/mL) for 4 hours. PCA plot of analysed samples **(a)**. Heatmap with heirarchichal clustering of z-score from total normalised counts **(b)**. Volcano plot of differentially expressed genes of itaconate **(c)** or TTFA **(d)** pre-treated BMDMs followed by 4 hour LPS (100 ng/mL) challenge. Illustration of overlapping differentially expressed genes **(E)**. Parts of a whole graph illustrating the distribution of overlapping differentially expressed genes among itaconate and TTFA-treated BMDMs **(f).**

4.1.13 Gene Set Enrichment Analysis of itaconate treated BMDMs

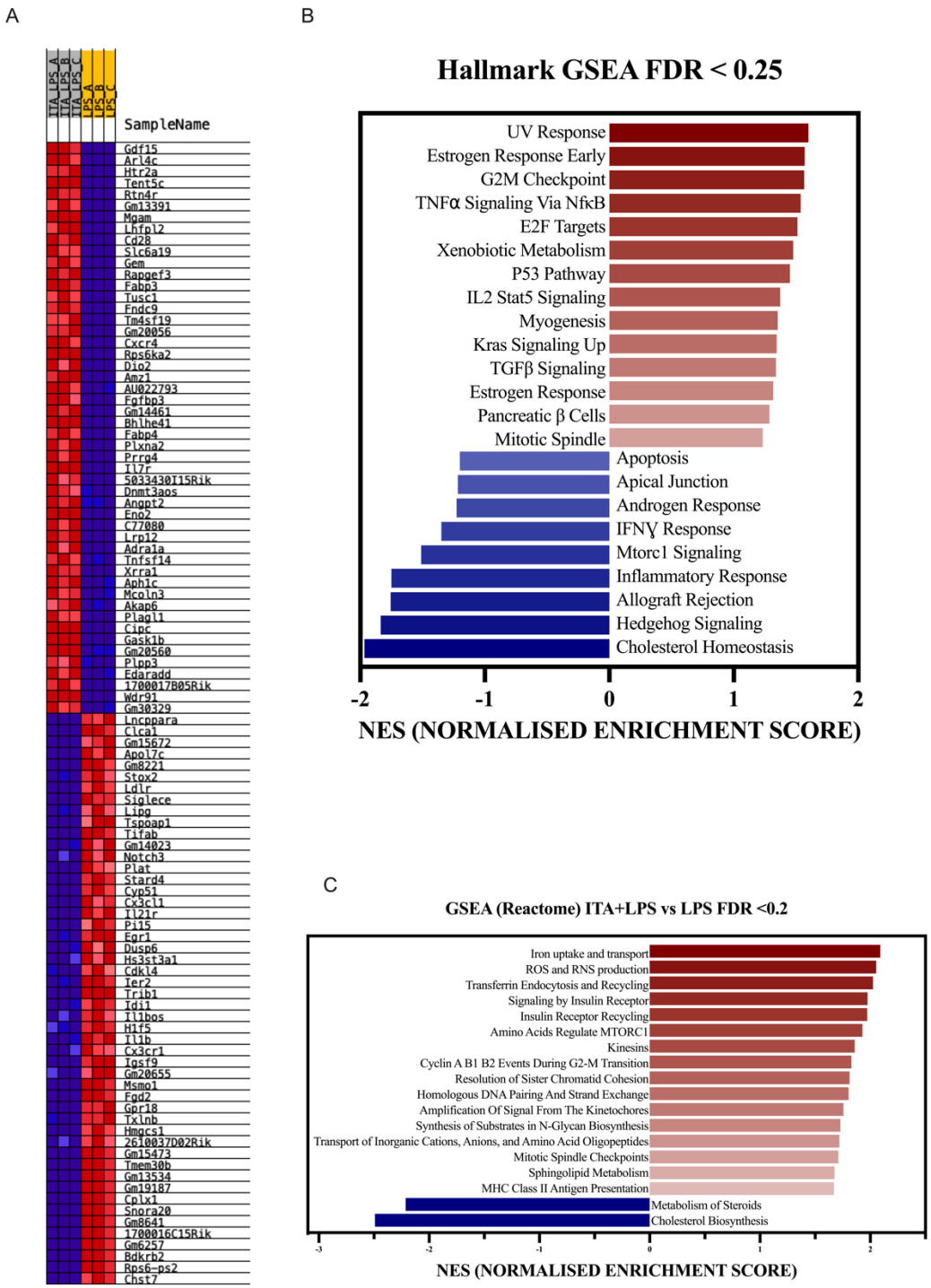
I then investigated the differentially expressed genes in itaconate treated BMDMs. Figure **Error! Reference source not found.**a shows the most significant DEGs of which *Gdf15* is the most upregulated. A Gene Set Enrichment Analysis (GSEA) was then performed using Hallmark and Reactome gene set databases which resulted in the upregulation of pathways such as *P53 pathway, TNFA signalling, Iron uptake, ROS generation*, and the downregulation of pathways such as *the inflammatory response, apoptosis, cholesterol homeostasis and biosynthesis* **(Figure 4.1.13 B and C).**

4.1.14 Loss of SDHA boosts LPS-induced IFNβ in macrophages

To confirm the role for SDH in IFN production, I next tested $SDHA^{-/-}$ RAW.264 murine macrophage cell lines. Results showed that LPS-stimulated $SDHA^{-/-}$ RAW.264 murine macrophages produced more IFNβ over the time course than SDHA-competent cells **(Figure 4.1.14)**.

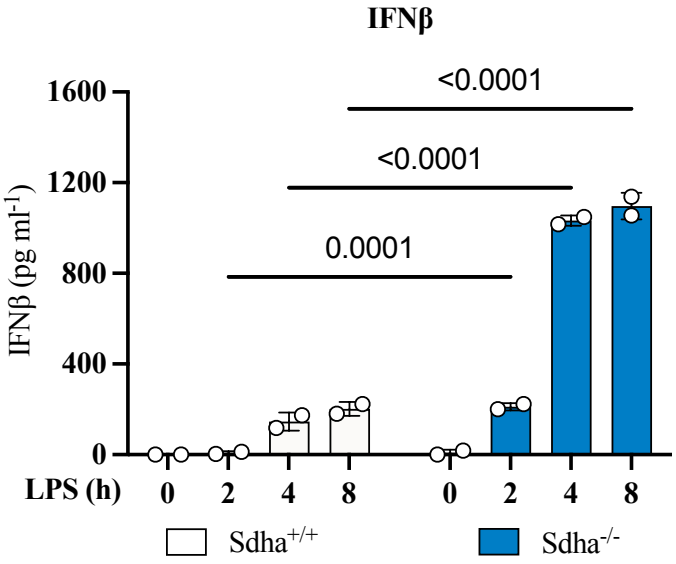
4.1.15 Loss of SDHB boosts LPS-induced IFNβ in macrophages

I next tested inducible SDHB-deficient BMDMs, using $SDHB^{Cre\text{-}ERT2}$ mice generated in collaboration with Stanford University. $SDHB^{Cre\text{-}ERT}$ macrophages were isolated and stimulated with Tamoxifen to induce the loss of SDHB. Tamoxifen treatment significantly reduced *sdhb* expression **(Figure 4.1.15 a).** $SDHB^{fl/fl}$ BMDMs produced significantly less *Il1b* in response to LPS **(Figure 4.1.15 b).** Furthermore, $SDHB^{fl/fl}$ BMDMs produced significantly more IFNβ message and protein compared to $SDHB^{+/+}$ BMDMs **(Figure 4.1.15 c and d)**. These data show that SDH ablation, by pharmacological and genetic approach, boosts LPS-induced type I IFNs.



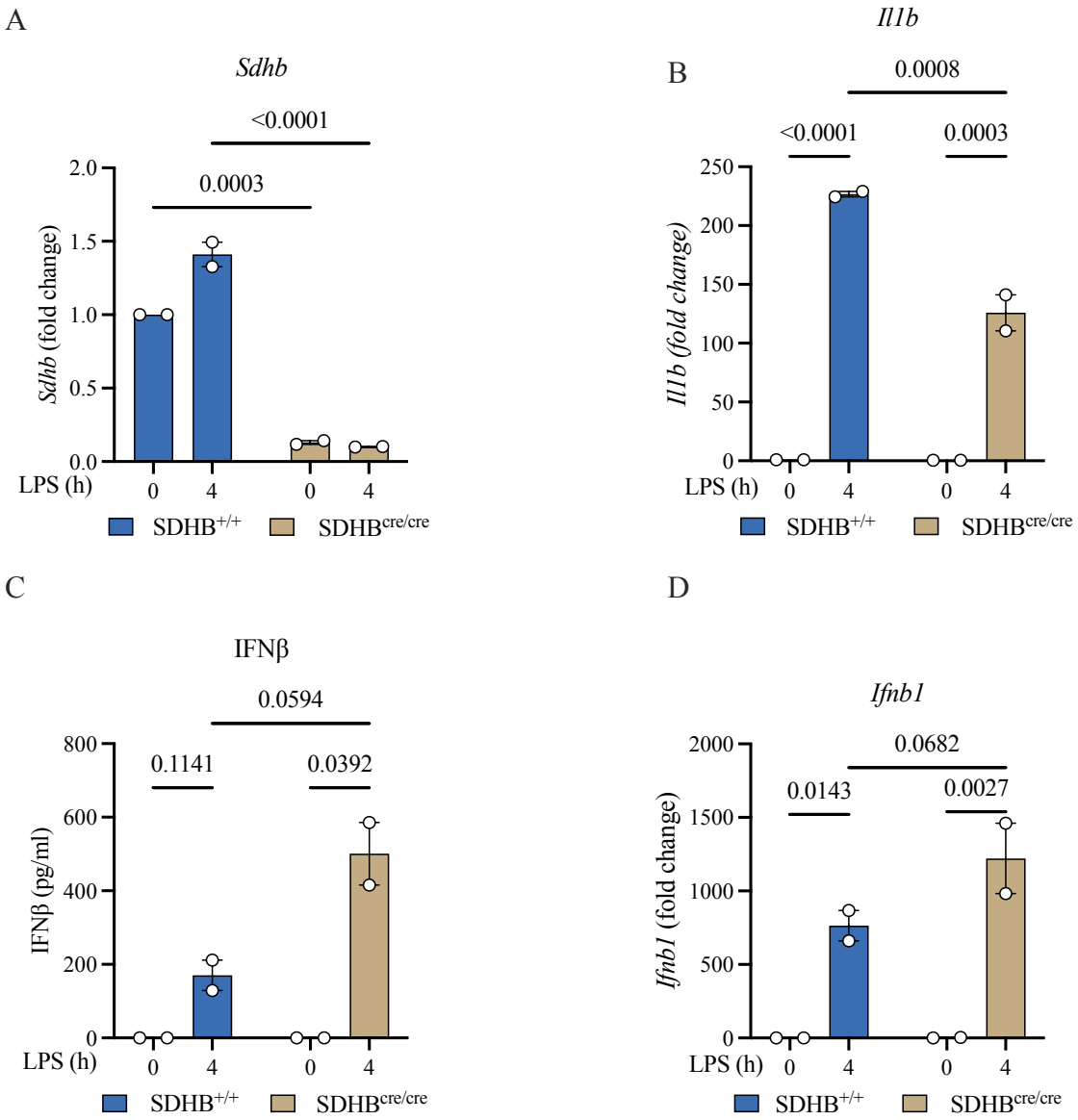
4.1. 13 Gene Set Enrichment Analysis of itaconate-treated BMDMs

BMDMs ($0.5x10^6$ cells) were pre-treated with itaconate (10 mM) for 3 hours followed by LPS (100 ng/mL) for 4 hours. GSEA was performed from RNA-seq analysis. Top differentially expressed genes of itaconate -treated BMDMs (**a**). Gene set enrichment analysis (Hallmark, FDR < 0.25) of BMDMs with itaconate pre-treatment followed by LPS (**b**). Gene set enrichment analysis (Reactome, FDR < 0.2) of BMDMs with itaconate pre-treatment followed by LPS (**c**).



4.1 14 Loss of SDHA boosts LPS-induced IFNβ in macrophages

Sdha$^{+/+}$ and Sdha$^{-/-}$ RAW.264 macrophages (0.5x10^{6} cells) were stimulated with LPS (100 ng/mL) for 2,4, and 8 hours. IFNβ release was measured by ELISA. Data are ± SD. for n=2 from 2 independent experiments. P values are calculated by two-way ANOVA with multiple comparisons.



4.1. 15 Loss of SDHB boosts LPS-induced IFNβ in macrophages

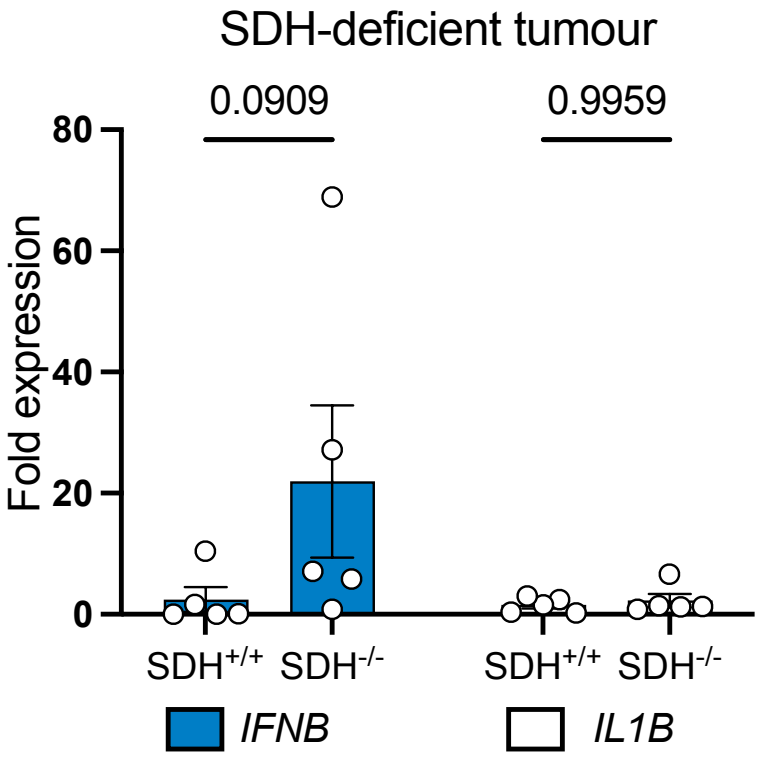
SDHB$^{Cre\text{-}ert2}$ BMDMs (0.5x10^6 cells) treated with ethanol as control or tamoxifen for 72 h to induce loss of SDHB. BMDMs were then stimulated with LPS for 4 hours. RT-qPCR data shows *Sdhb* (**a**), *Il1b* (**b**), and *Ifnb1* (**d**), relative to *Rps18* and IFNβ release (**c**). Data are mean ± SD. for n=2 from one experiment. P values were calculated using RM-two way ANOVA for multiple caparisons.

4.1.16 SDH-deficient tumours have increased IFNB production

As a final approach to replicate SDH loss, I next investigated SDHB-deficient paraganglioma tumour samples for the expression of *IFNB* and *IL1B*. Results from n=5 SDH-deficient paraganglioma showed increased *IFNB* expression ($p = 0.0909$) compared to SDHB competent tumours. Furthermore, results from the same experiment showed no difference in *IL1B* expression. These data suggest that SDH ablation boosts LPS-induced type I IFN.

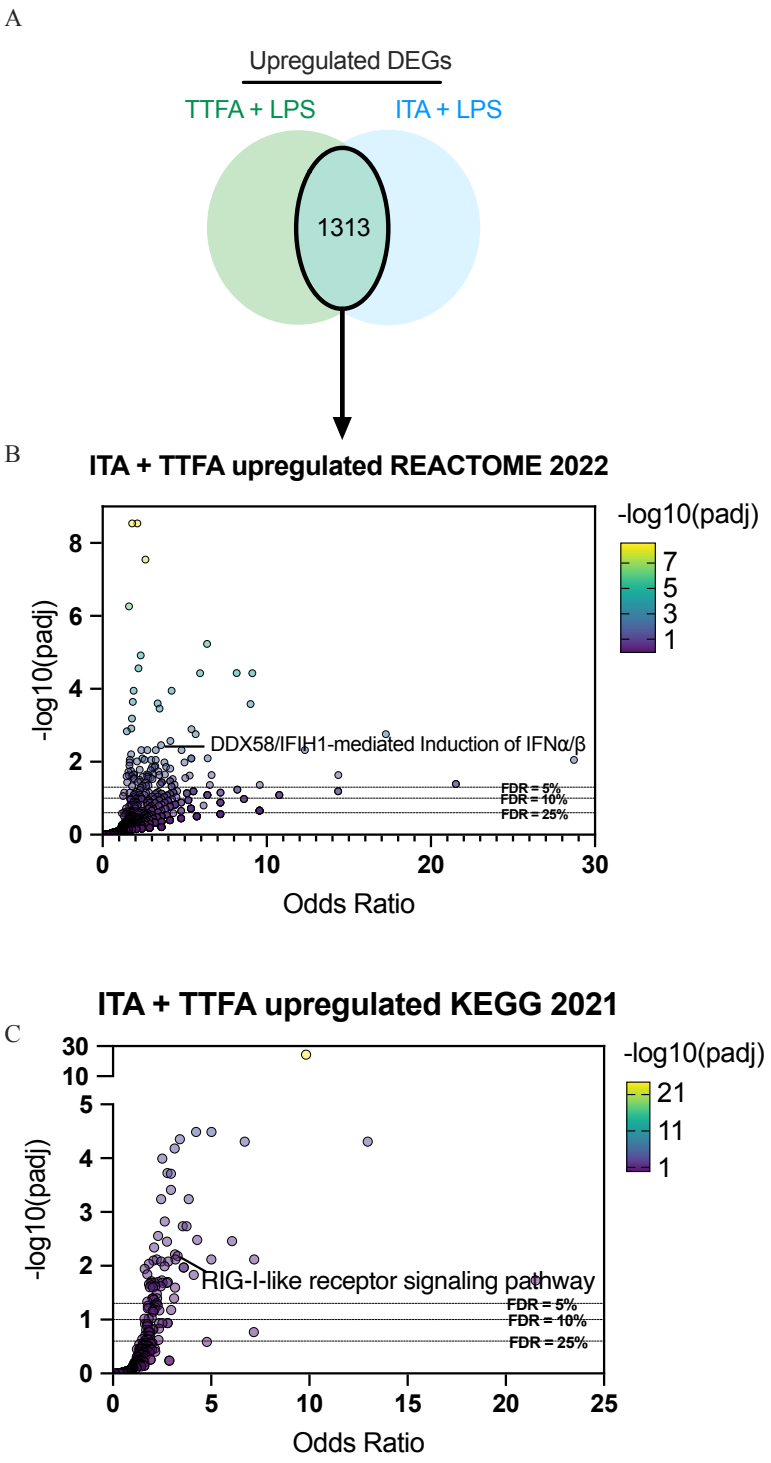
4.1.17 SDH inhibition boosts LPS-induced IFNβ via RIG-I / MDA5-dependent signalling

I next investigated how SDH inhibition, by itaconate, increases type I IFN production. RNA-seq data from itaconate or TTFA pre-treated BMDMs followed by LPS treatment was used. I performed pathway enrichment analysis using commonly significantly upregulated DEGs ($padj < 0.05$, $Log_2FC > 0$) among both itaconate and TTFA-treated macrophages **(Figure 4.1.17 a).** Within the REACTOME analysis, *DDX58/IFIH1-induced Induction of IFN-α/β* stood out as an interferon-related pathway that may be responsible for the induction of type I interferon **(Figure 4.1.17 b).** Furthermore, the KEGG pathway analysis revealed a significant upregulation of *RIG-I-like receptor signalling pathway* **(Figure 4.1.17 c).** These results suggest a role for RIG-I and MDA5 in itaconate-induced induction of type I interferon via SDH inhibition.



4.1. 16 SDH-deficient tumours produce increased IFNB production

SDH-deficient tumours versus anatomical site, age, and sex-matched controls were excised and genotyped to confirm SDH loss. Whole tissue underwent RNA extraction and RT-qPCR for *IFNB* and *IL1B* expression Data are mean ± SD. for n=5 from one experiment. P values were calculated using one -way ANOVA.



4.1. 17 SDH inhibition boosts LPS-induced RIG-I / MDA5-dependent signalling

Venn diagram of overlapping upregulated DEGs from RNA-seq analysis of BMDMs (n = 3) stimulated with TTFA (0.5 mM) and itaconate (10 mM) for 3 hours , followed by LPS for 4 hours, padj < 0.05) **(a)**. REACTOME Pathway enrichment analysis **(b)** and KEGG pathway enrichment analysis **(c)** of commonly upregulated of BMDMs (n = 3) stimulated with TTFA (0.5 mM) and itaconate (10 mM) for 3 hours , followed by LPS for 4 hours, padj < 0.05).

4.1. 18 Successful knockdown of Mb21d1, Ddx58, Tlr9, and Ifih1

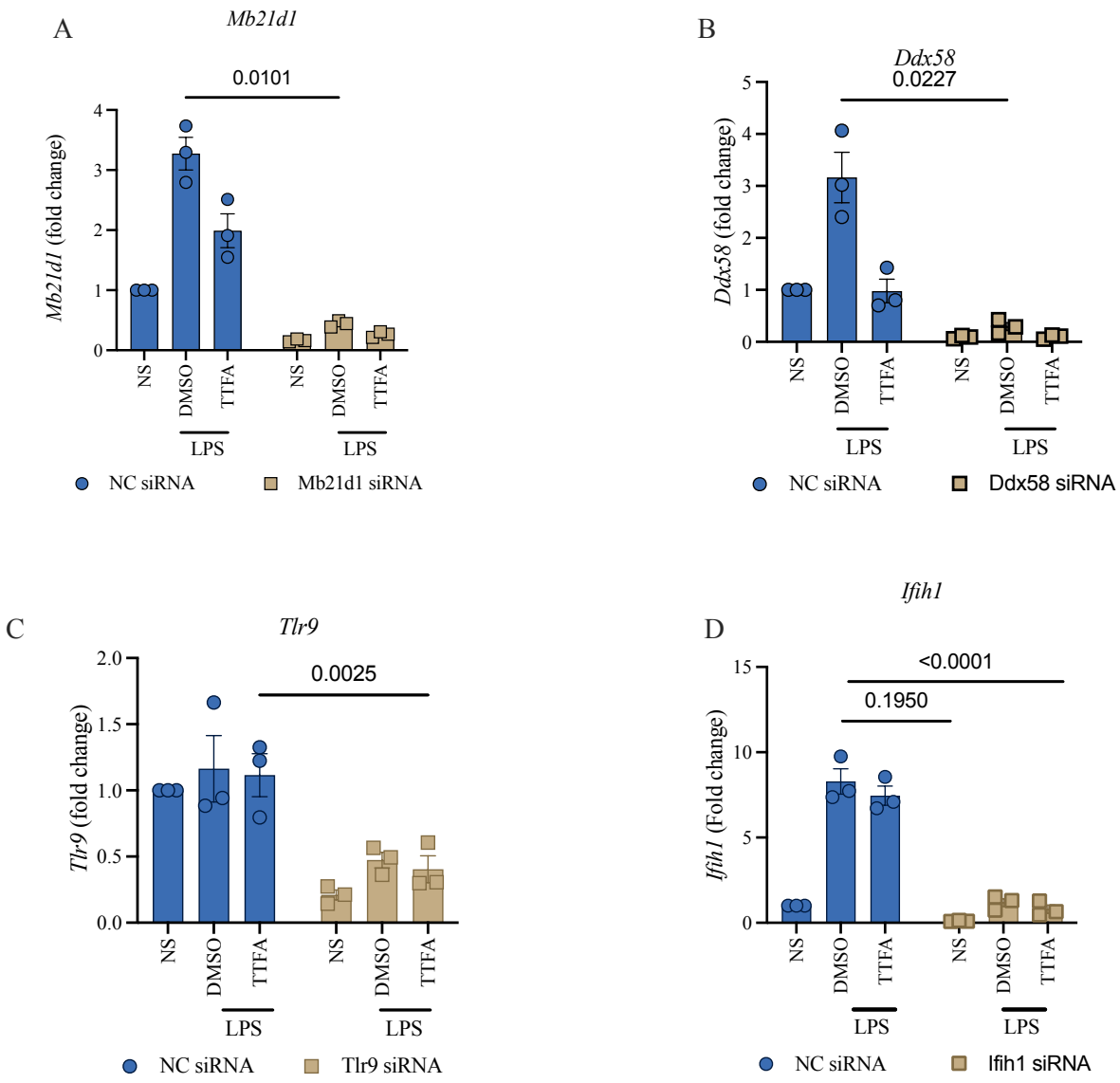
Previous work from our lab and others demonstrated that pharmacological inhibition of the TCA cycle enzyme fumarate hydratase (FH) led to mitochondrial DNA and RNA release into the cytosol which acts as a DAMP to mediate type I interferon responses (3, 4). I therefore hypothesised that SDH inhibition would mediate mitochondrial nucleic acid release. To investigate this, BMDMs underwent siRNA silencing of nucleic acid sensors cGas, RIG-I, and TLR9. These BMDMs were then pre-treated with TTFA followed by LPS. Lysates were analysed for the expression of cGas (encoded by Mb21d1) after Mb21d1 knockdown **(Figure 4.1.18 a).** Results showed that Md21d1 expression was significantly reduced after Mb21d1 knockdown. Ddx58 expression, encoding RIG-I, was significantly reduced after RIG-I knockdown **(Figure 4.1.18 b).** Tlr9 expression was significantly reduced after Tlr9 knockdown **(Figure 4.1.18 c).** Ifih1 expression was reduced after Ifih1 knockdown **(Figure 4.1.18 d).**

4.1.19 Mb21d1, Ifih1, and Ddx58 knockdown is specific to their agonists

I next confirmed that RIG-I, MDA5, and cGAS knockdowns were specific for their respective sensors. For this I utilised the cGAS-specific agonist G3-YSD (179) **(Figure 4.1.19 a)**, the MDA5 agonist transfected high molecular weight poly (I:C) **Figure 4.1.19 b)**, and the cGAS agonist 5'-PPP-dsRNA (**Figure 4.1.19 c)**. I showed that each of these agonists boosted IFNβ in a concentration-dependent manner. Knockdown of the respective nucleic acid sensors blocked this IFNβ induction confirming specificity of the knockdown.

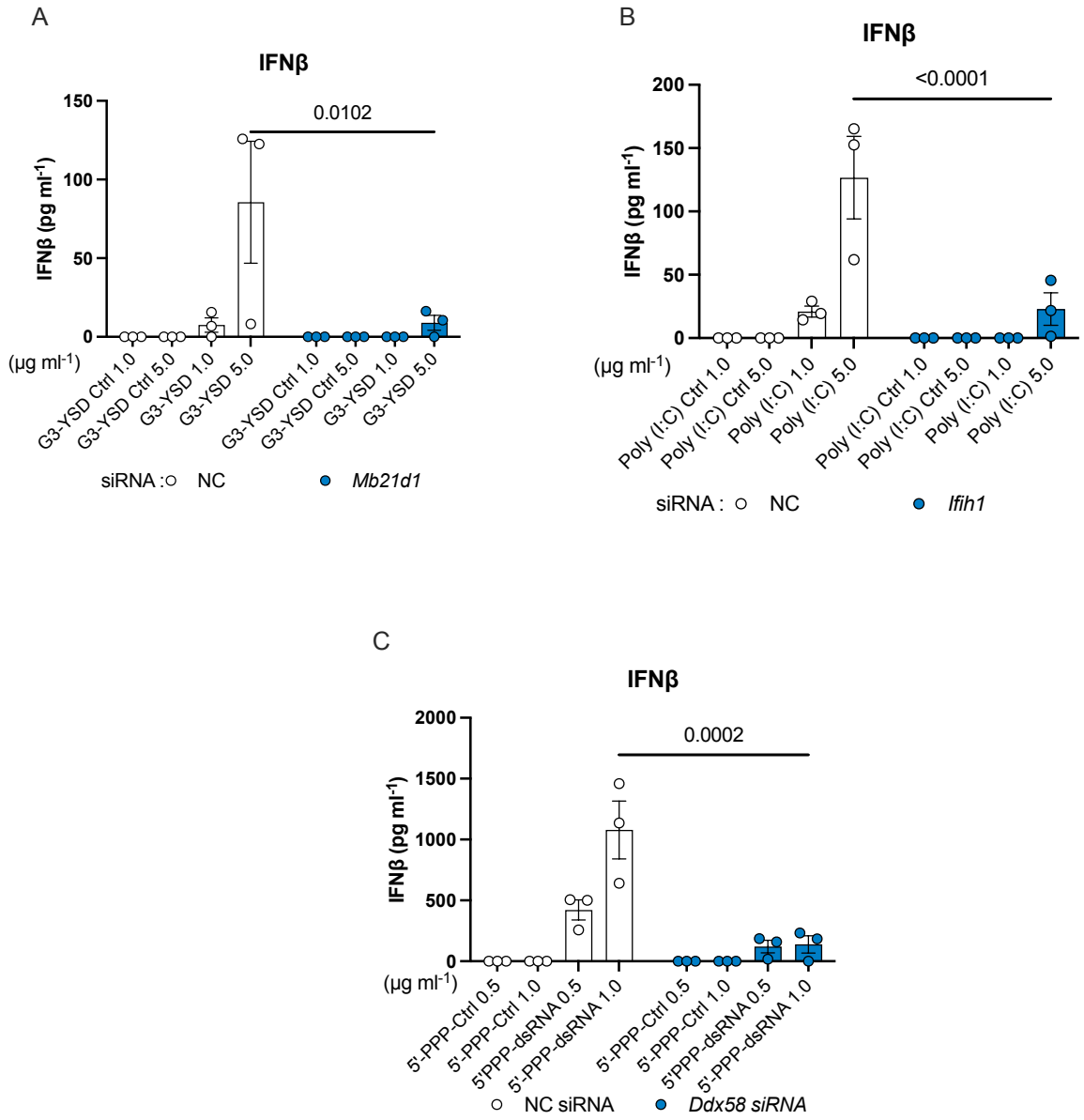
4.1.20 SDH inhibition boosts LPS-induced IFNβ via RIG-I/MDA5-dependent signalling

I next investigated if these nucleic acid sensors contributed to the induction of LPS-induced IFNβ production. Results showed that cGAS and TLR9 knockdown had no effect on *Ifnb1* expression **(Figure 4.1.20 a).** However, RIG-I and Ifih1 knockdown ablated the TTFA-induced IFNβ production, suggesting a role for RNA sensors RIG-I and MDA5 in the induction of type I interferon seen with SDH inhibition.



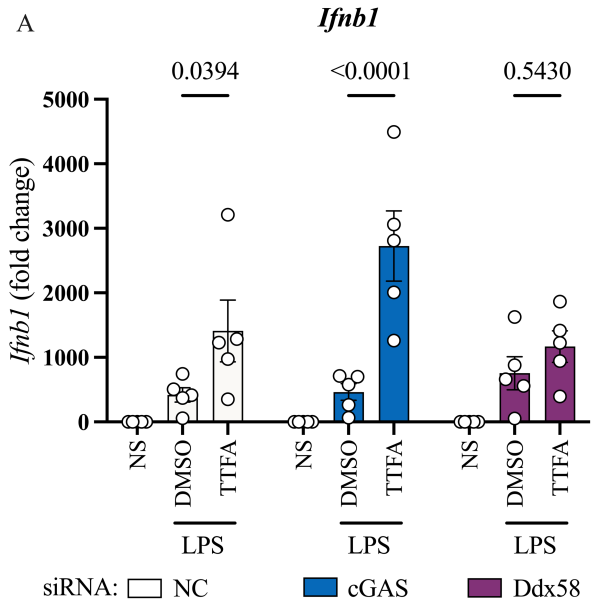
4.1. 18 Successful knockdown of Mb21d1, Ddx58, Tlr9, and Ifih1

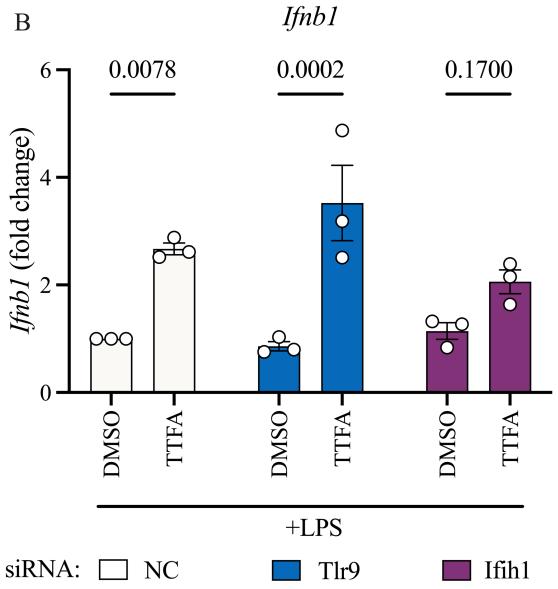
BMDMs (0.5x10^6 cells/mL) underwent siRNA knockdown of Mb21d1, Ddx58, Tlr9, and Ifih1. After siRNA knockdown, cells were pre-treated with TTFA (0.5 mM) for 3 hours and LPS (100 ng/mL) for 4 hours. Lysates underwent RT-qPCR for expression of *Mb21d1* **(a)**, *Ddx58* **(b)**, *Tlr9* **(c)**, and *Ifih1* **(c)** relative to *Rps18*. Data are presented as mean ± SEM. for n=3 from 3 independent experiments. P value is calculated using RM two-way ANOVA followed by Tukey's multiple comparisons test.



4.1. 19 Mb21d1, Ifih1, and Ddx58 knockdown is specific to their agonists

BMDMs (0.5 x 10^6 cells) underwent siRNA knockdown for *Mb21d1, Ifih1,* and *Ddx58.* IFNβ release in BMDMs transfected with G3-YSD (**a**), HMW Poly(I:C) (**b**), or 5'PPP-dsRNA (**c**). Data are mean ± SEM. For n=3 from 3 independent experiments. P values are calculated using one-way ANOVA for multiple comparisons.





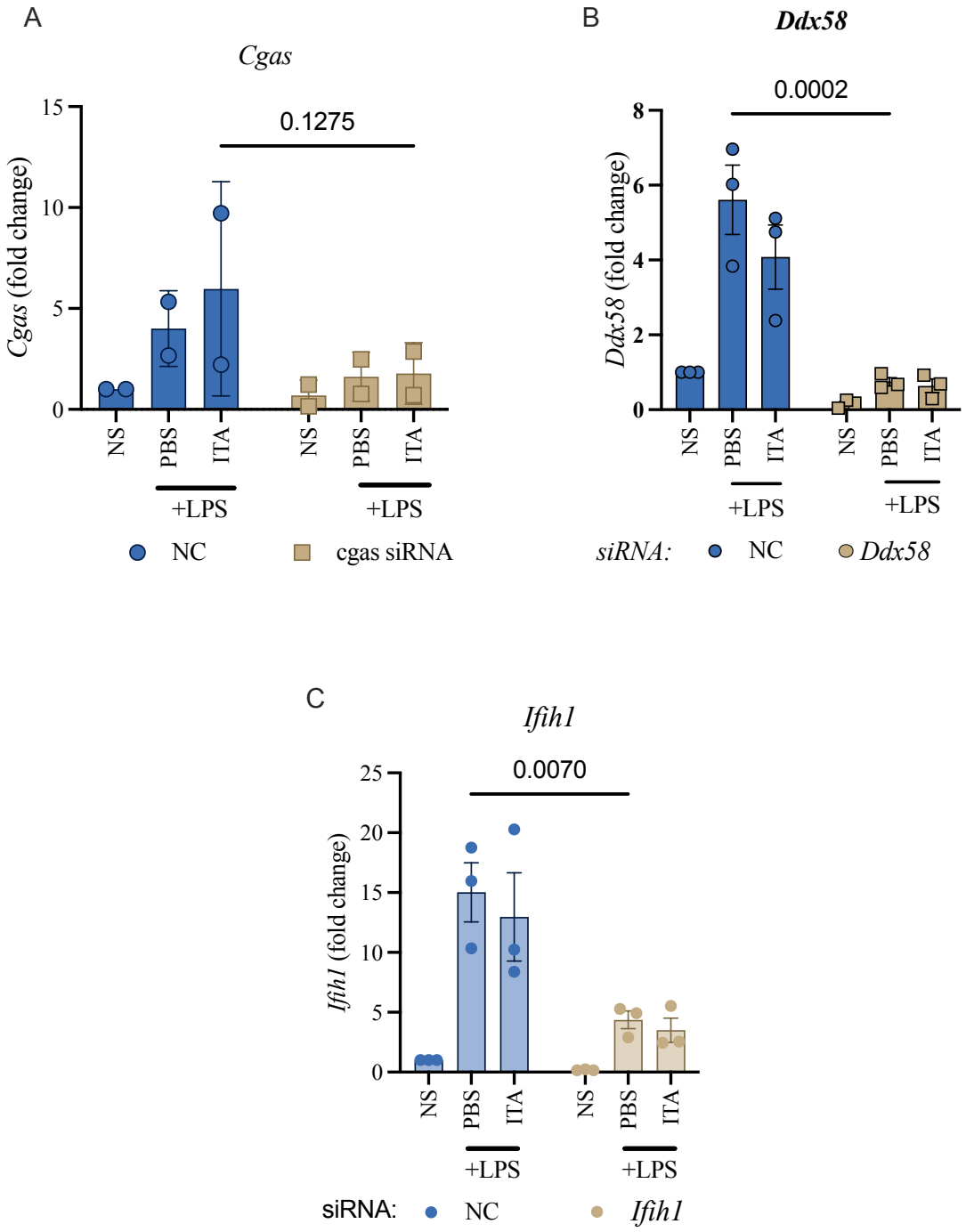
4.1. 20 SDH inhibition boosts LPS-induced IFNβ via RIG-I/MDA5-dependent signalling

BMDMs (0.5x10^6 cells) underwent siRNA knockdown for cGAS, Ddx58, Tlr9, and Ifih1. After knockdown, cells were pre-treated with TTFA (0.5 mM) for 3 hours followed by LPS (100 ng/mL) for 4 hours. Lysates underwent RT-qPCR for *Ifnb1* expression in BMDMs after *cGas, Ddx58* (**a**) *(*n=5; LPS 4h), and *Tlr9,* and *Ifih1* (LPS 4h) knockdown (**b**). Data are mean ± SEM. for n=5 from two independent experiments (a), for n=3 from 3 independent experiments. P values were calculated using two-way ANOVA for multiple comparisons.

4.1.21 Itaconate boosts LPS-induced IFNβ via MDA5-dependent signalling

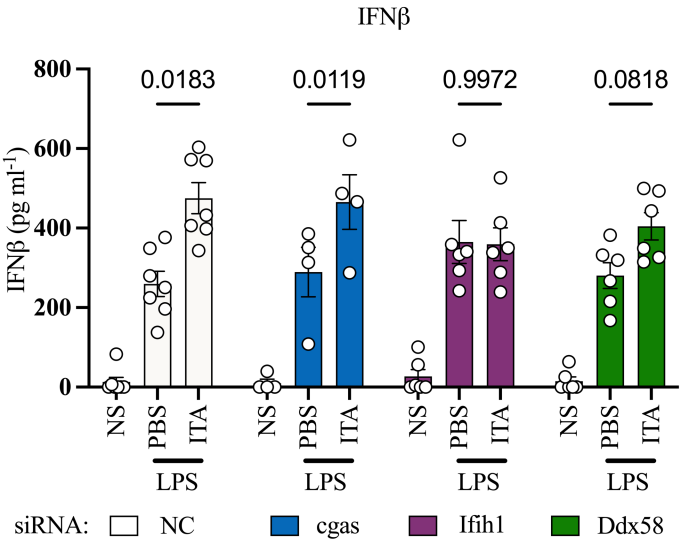
BMDMs underwent siRNA silencing of nucleic acid sensors cGas, MDA5 or RIG-I. These BMDMs were then pre-treated with itaconate followed by LPS. Lysates were analysed for the expression of *cGas* (encoded by *Mb21d1*) after *Mb21d1* knockdown **(Figure 4.1.21 a).** Results showed that *Md21d1* expression was significantly reduced after *Mb21d1* knockdown. *Ddx58* expression, encoding RIG-I, was significantly reduced after RIG-I knockdown **(Figure 4.1.21 b).** *Ifih1* expression was reduced after Ifih1 knockdown **(Figure 4.1.21 c).**

I next tested the effect of itaconate on these knockdowns. These results indicate that itaconate-dependent induction of IFNβ was independent of cGAS and RIG-I but dependent on MDA5 (**Figure 4.1.22**).



4.1. 21 Itaconate boosts LPS-induced IFNβ via MDA5-dependent signalling

BMDMs underwent siRNA knockdown for CGAS, DDX58, and IFIH1. After knockdown, BMDMs were pre-treated with itaconate (10 mM) for 3 hours followed by LPS (100 ng/mL) for 4 hours. Lysates were analysed by RT-qPCR for *Ifnb1* expression relative to *Rps18* in BMDMs after *Cgas* (**a**), *Ifih1* **(b),** and *Ddx58* (**c**) Data are mean ± SD. for n=2 from 2 independent experiments (a), and mean ± SEM n=3 from 3 independent experiments. P values calculated using two-way ANOVA for multiple comparisons.



4.1. 22 Itaconate boosts LPS-induced IFNβ via RIG-I / MDA5-dependent signalling

BMDMs ($0.5x10^6$ cells) underwent siRNA knockdown of cGas, Ifih1, and Ddx58. After, cells were pre-treated with itaconate (10 mM) for 3 hours followed by LPS (100 ng/mL) for 4 hours.

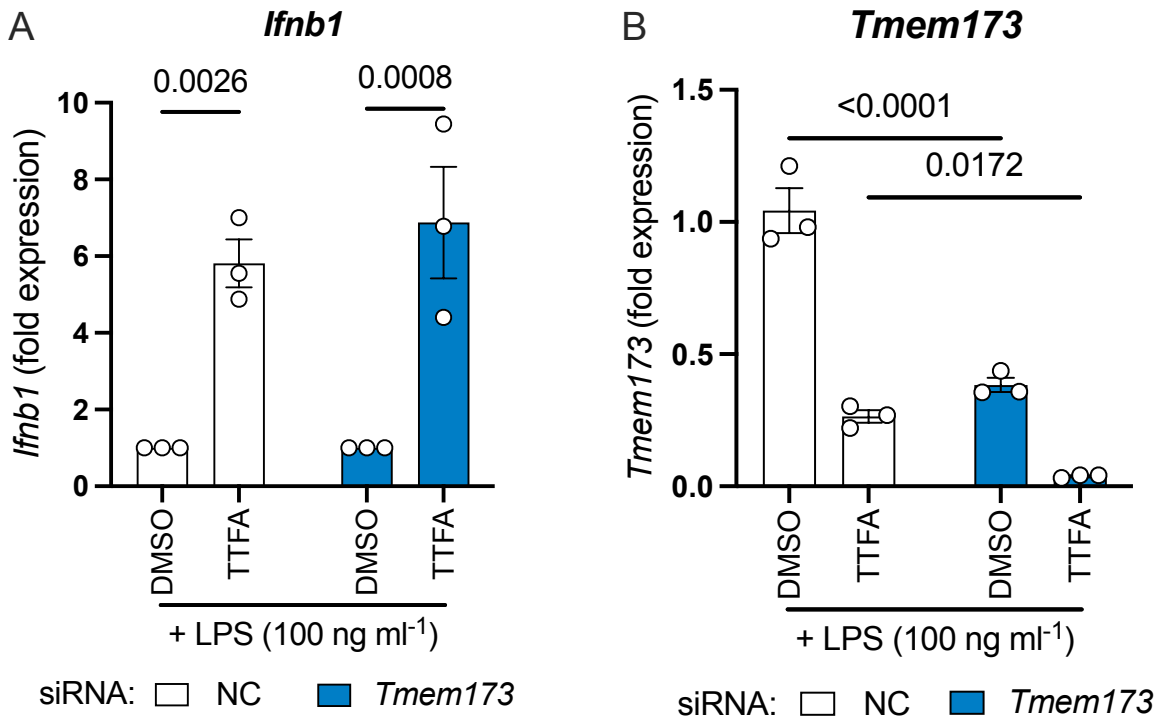
IFNβ release in was measured after *cGas*, *Ifih1,* and *Ddx58* knockdown Data are presented as ± SEM. for n= 6 from 3 independent experiments. P values calculated using two-way ANOVA with Tukey's multiple comparisons.

4.1. 23 SDH-induced *Ifnb1* expression is STING-independent

To verify that CGAS signalling is not involved in the induction of type I interferons mediated by SDH inhibition, STING (encoded by *Tmem173)* was knocked down in BMDMs and subsequently pre-treated with TTFA and then treated with LPS for 4 h. Results showed that STING knockdown had no effect on TTFA-induced *Ifnb1* **(Figure 4.1.23).**

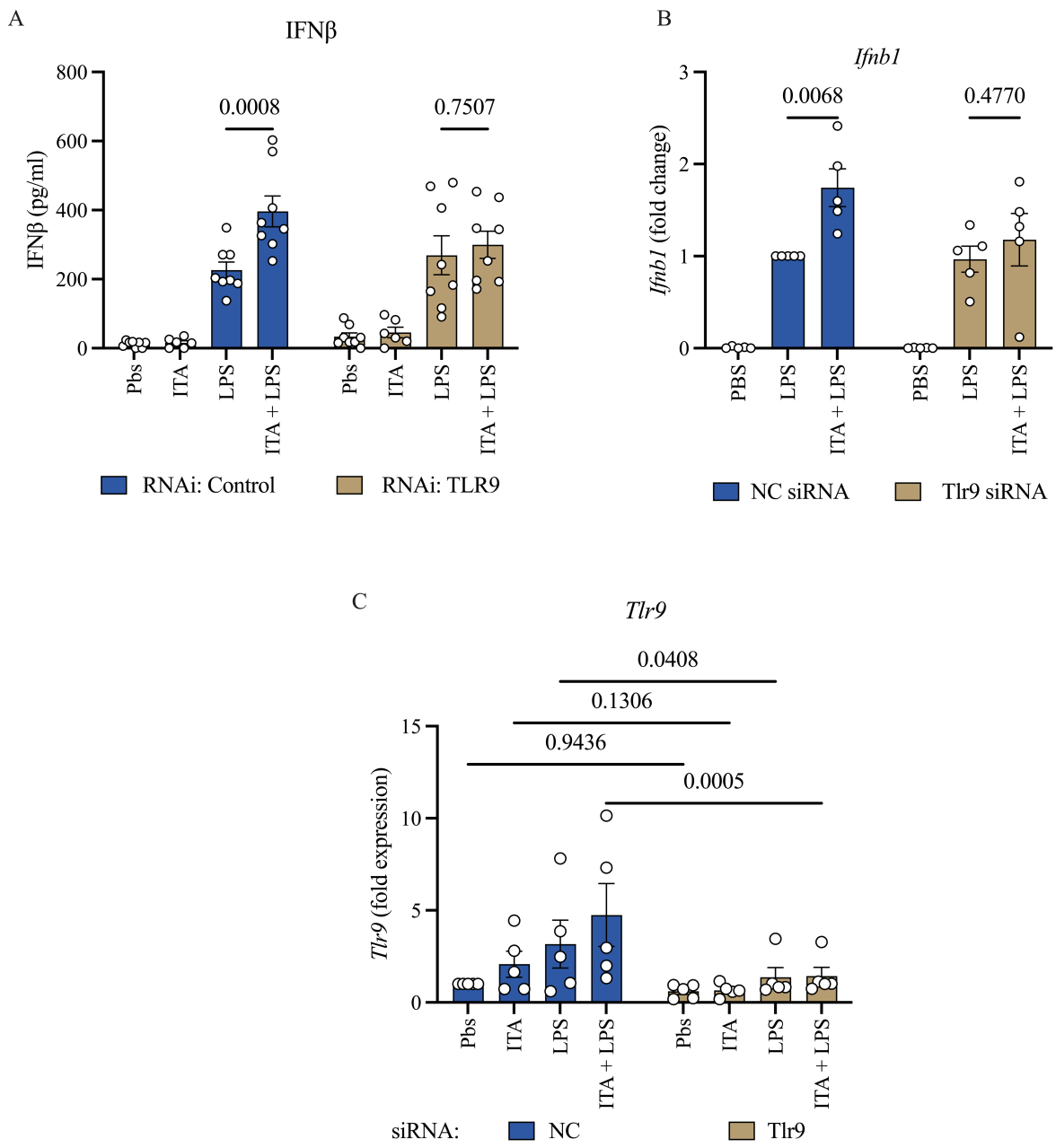
4.1.24 Itaconate boosts LPS-induced IFNβ in a TLR9-dependent manner

It has been shown that nucleic acid sensors RIG-I and MDA5 were responsible for the induction of IFNβ after SDH inhibition. It was hypothesised that other PRRs might be involved in this regulation of IFNβ. To investigate this, BMDMs underwent siRNA knockdown of the PRR TLR9. Results shows that TLR9 knockdown significantly blocks TLR9 expression **(Figure 4.1.24 c).** Itaconate fails to boost LPS-induced IFNβ protein and *Ifnb1* expression **(Figure** Error! Reference source not found. **a and b).** This suggests that TLR9, a DNA sensor may have a role for the induction of itaconate-induced type I interferon.



4.1. 23 SDH-induced *Ifnb1* expression is STING-independent

Ifnb1 (**a**) and Tmem173 (**b**) expression relative to *Rps18* in BMDMs (0.5 x106 cells) after Tmem173 siRNA and pre-treated with DMSO or TTFA (0.5 mM) for 3 hours followed by LPS (100 ng/mL) for 4 hours. Data are mean ± SEM. for n=3 from 3 independent experiments. P values were calculated using two-way ANOVA for multiple comparisons.



4.1. 24 Itaconate boosts LPS-induced IFNβ in a TLR9-dependent manner

BMDMs (0.5x10^6 cells) underwent Tlr9 knockdown and were pre-treated with itaconate (10 mM) for 3 hours followed by LPS (100 ng/ml) for 4 hours. IFNβ release was measured by ELSIA (**a**). *Ifnb1* (**c**) and *Tlr9* (**b**) expression was measured by RT-qPCR relative to *Rps18*. Data are mean ± SEM. for n=8 from 4 independent experiments. P values are calculated using two-way ANOVA with Sidak's multiple comparisons.

4.1.25 Mitochondrial nucleic acids regulate SDH-induced IFNβ

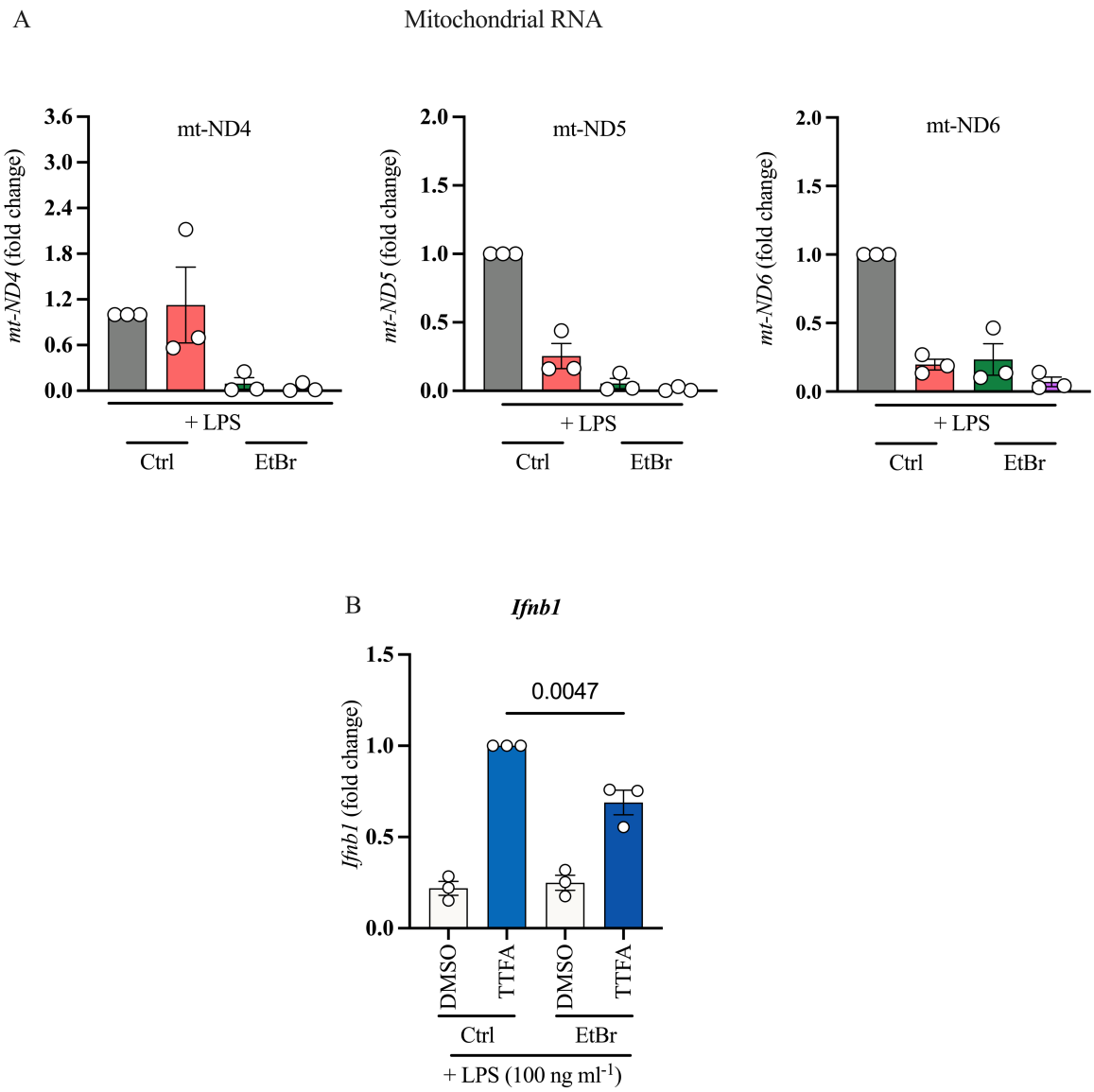
Ethidium bromide (EtBr) accumulates preferentially in mitochondria over the nucleus and intercalates mtDNA to block mitochondrial transcription and production of mtRNA (180). To investigate whether nucleic acids are important in IFNβ production due to SDH inhibition, BMDMs were pre-treated with EtBr to deplete mitochondrial nucleic acids. These BMDMs were then pre-treated with TTFA and analysed for the expression of mitochondrial genes *mt-Nd4, mt-ND5*, and *mt-Nd6*. Results showed that EtBr treatment blocked *mt-Nd4, mt-ND5*, and *mt-Nd6* expression **(Figure 4.1.25).** Furthermore, EtBr treatment blunted TTFA-induced *Ifnb1* expression **(Figure 4.1.25),** suggesting nucleic acids are important in the induction of IFNβ mediated by SDH inhibition.

4.1.26 Mitochondrial transcriptional inhibition blocks itaconate-induced Ifnb1

Mitochondrial transcription is required for the generation of mtRNA and the subsequent induction of mt-RNA-induced IFNβ (74). IMT1 is a mitochondrial RNA polymerase (POLRMT) inhibitor. Pre-treating BMDMs with IMT1 and itaconate followed by LPS inhibits itaconate-induced *Ifnb1*.These data suggest that mitochondrial transcription is needed for itaconate-induced *Ifnb1* **(Figure 4.1.26)**.

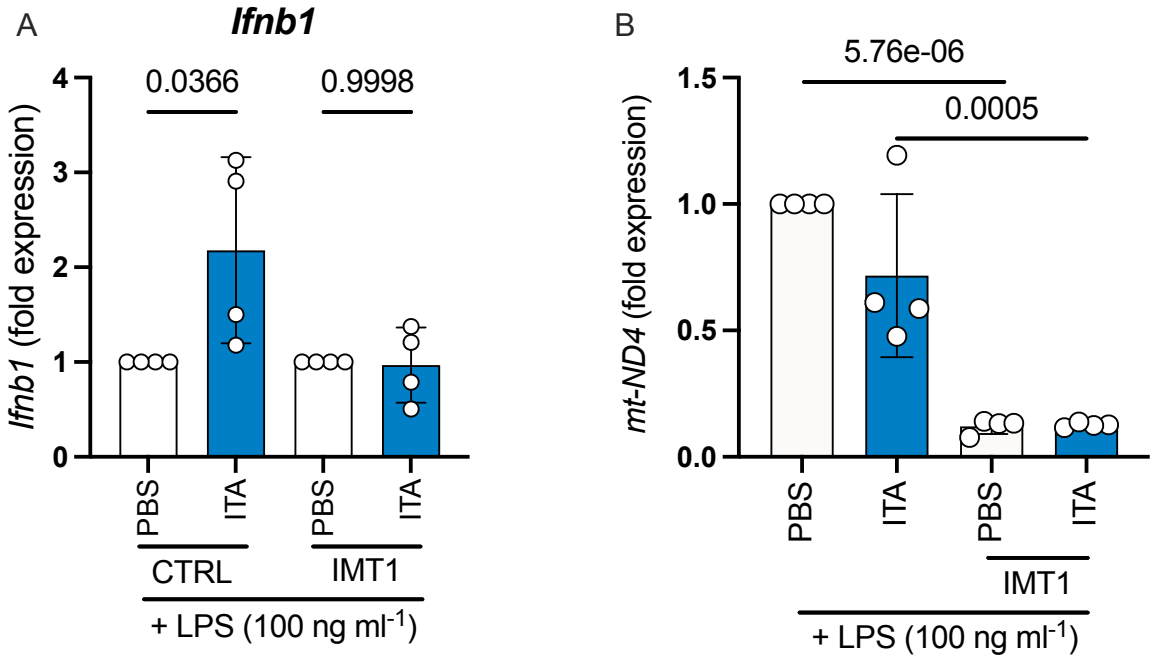
4.1. 27 LPS induces mitochondrial encoded gene expression

I investigated the gene expression data of LPS-stimulated BMDMs and found that LPS-stimulated BMDMs significantly upregulated the expression of a large proportion of mitochondrial-encoded genes including *mt-nd1, mt-nd2, mt-nd4, mt-nd5,* and *mt-nd6* **(Figure 4.1.27).**



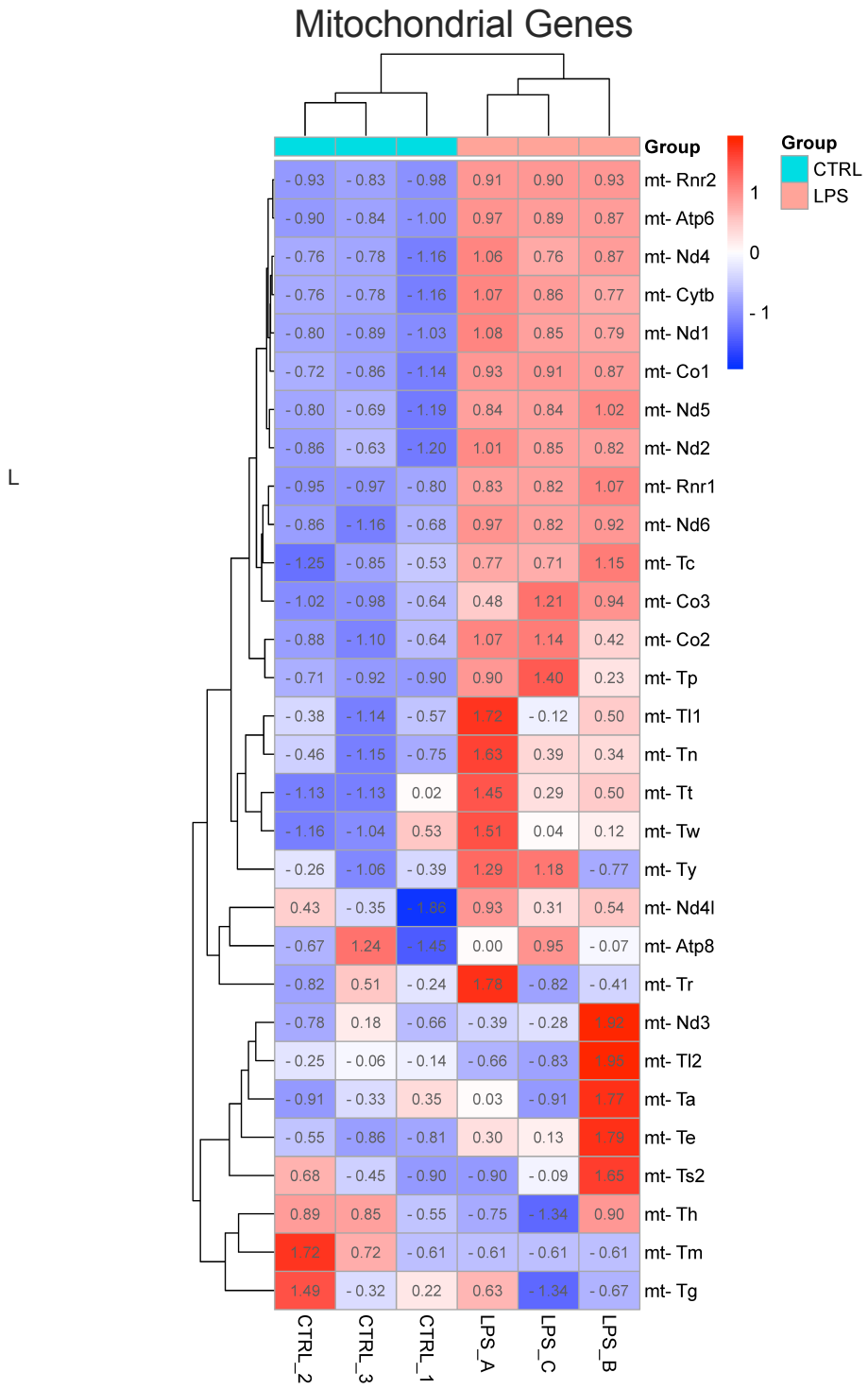
4.1 25 Mitochondrial nucleic acids regulate SDH-induced IFNβ

RT-qPCR of mitochondrial DNA-encoded genes relative to *Rps18* in BMDMs ($0.5x10^6$ cells) after mtDNA depletion with EtBr (100 ng / mL) (6 days) followed by TTFA pre-treatment (0.5 mM) for 3 hours and LPS (100 ng/mL) stimulation for 4 hours **(a).** RT-qPCR data of *Ifnb1* expression relative to *Rps18* of BMDMs in ctrl or EtBr-containing media which were pre-treated with DMSO or TTFA (0.5 mM) for 3 hours before LPS (100 ng/mL) stimulation for 4 hours **(b)**. Data are mean ± SEM. for n=3 from 3 independent experiments. P value is calculated by one-way ANOVA with Šídák's multiple comparisons.



4.1. 26 Mitochondrial transcription inhibition blocks itaconate-induced *Ifnb1*

Ifnb1 (**a**) and *mt-Nd4* (**b**) expression relative to *Rps18* in BMDMs ($0.5x10^6$ cells) pre-treated with DMSO, IMT1 (10 µM), PBS, or ITA (10 mM) for 3 hours followed by LPS (100 ng/mL) for 4 hours. Data are mean ± SD. for n=4 from 2 independent experiments. P values were calculated using one-way and two-way ANOVA for multiple comparisons.



4.1. 27 LPS induces mitochondrial encoded gene expression

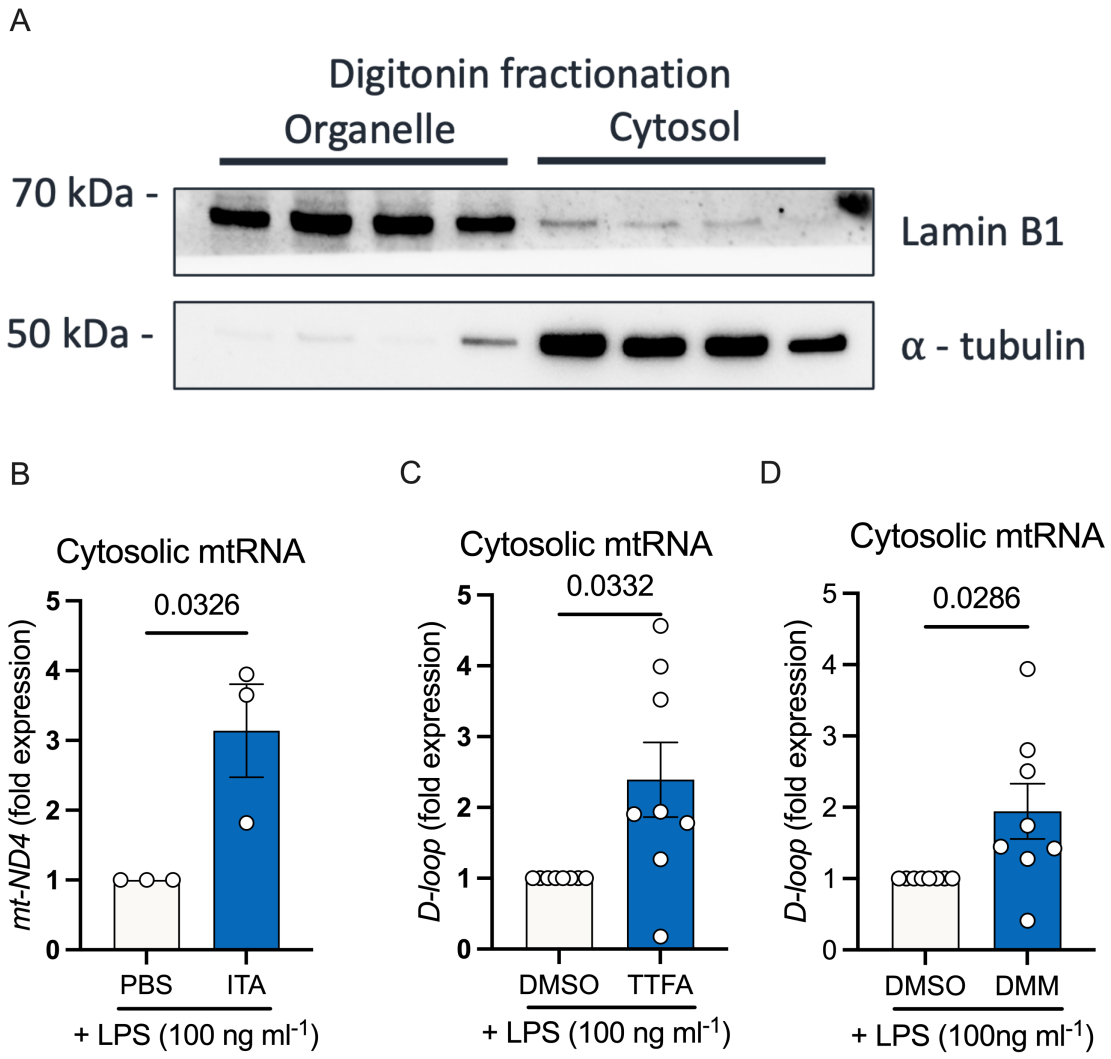
BMDMs ($0.5x10^6$ cells) were treated with LPS (100ng/mL) for 4 hours and underwent RNA-seq analysis. Differentially expressed genes analysis was performed and a heatmap (z-score from normalised counts) was created of total mitochondrial encoded genes.

4.1.28 SDH inhibition drives cytosolic mtRNA release

I next directly examined the release of mtRNA in the cytosol as a result of SDH inhibition. After treatment with SDH inhibitors TTFA, itaconate, or DMM, BMDMs underwent a digitonin fractionation step to isolate the cytosolic fraction. This can be seen from western blot analysis where Lamin B1, normally found in nuclear membranes, acts as a control for the organelle fraction. α-Tubulin acts as a control for the cytosolic fraction. Results by western blot showed a clear separation of Lamin B1 in the organelle fraction and α-tublin in the cytosolic fraction, indicating successful isolation of the cytosol **(Figure 4.1.28 a)**. RNA extraction and RT-qPCR were performed on the cytosolic fraction for the expression of mitochondrial gene *D-loop*. Results showed that TTFA, itaconate, and DMM boosted LPS-induced cytosolic mtRNA *D-loop* **(Figure 4.1.28 b-d)**. This suggests that SDH-inhibition boosts mitochondrial RNA release into the cytosol.

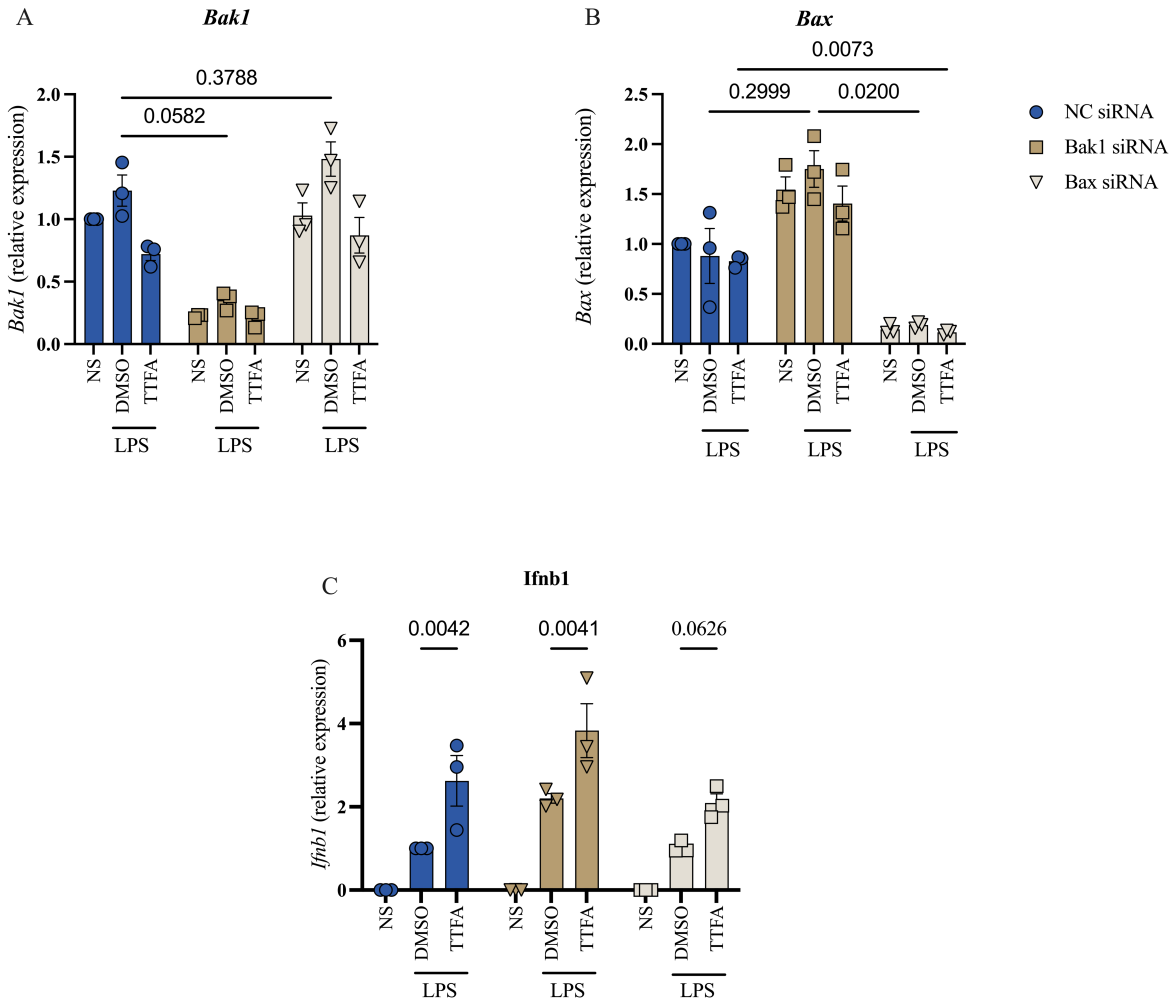
4.1.29 Inhibition of SDH boosts LPS-induced *Ifnb1* independent of Bax and Bak

It was next decided to investigate what mitochondrial nucleic acid transporters were responsible for the induction of IFNβ. To investigate this, BMDMs underwent siRNA knockdown of known mitochondrial nucleic acid transporters Bax, Bak1 Snx9, and Vdac1. *Bak1* and *Bax* expression was significantly reduced after their respective siRNA knockdown **(Figure 4.1.29 a and b).** Lysates were analysed for the expression of *Ifnb1*. Results showed that Bak1 and Bax knockdown did not affect TTFA-induced *Ifnb1* expression **(Figure 4.1.29 c)**. Furthermore, Snx9 knockdown **(Figure 4.1.30 a)** had no effect on TTFA-induced *Ifnb1* expression **(Figure 4.1.30 c)**. However, Vdac1 knockdown **(Figure 4.1.30 b)** suppressed TTFA-induced *Ifnb1* expression **(Figure 4.1.30 c)**. This suggests that mitochondrial RNA may be released through VDAC1 to stimulate RIG-I and MDA5 to boost IFNβ production.



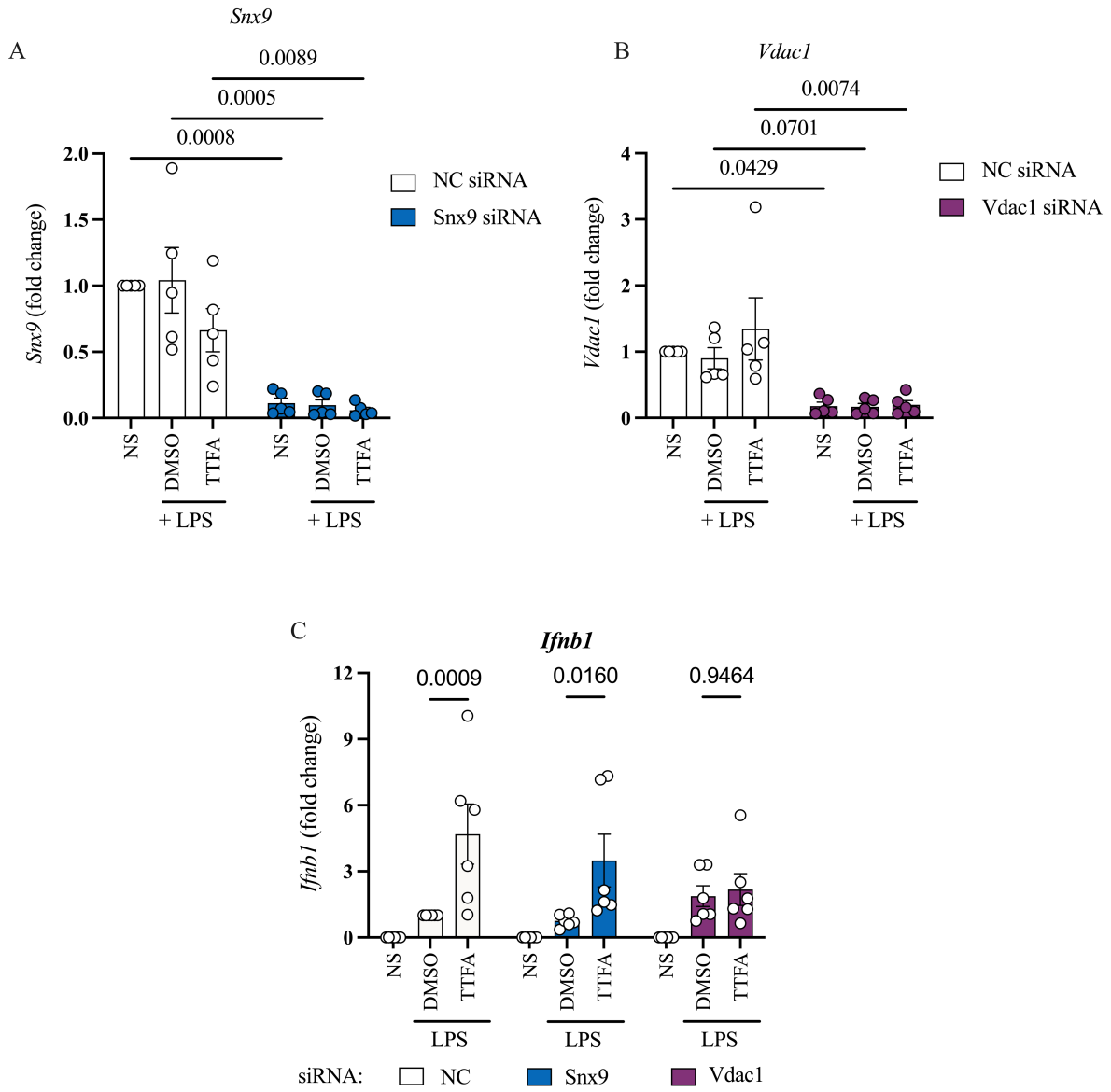
4.1.28 SDH inhibition drives cytosolic mtRNA release

Western blot of organellar fraction (Lamin B1) and cytosolic fractions (α-Tubulin) of BMDMs after subcellular digitonin fractionation and is representative of 2 independent experiments **(a)**. *mt-ND4* expression relative to *Rps18* in the isolated cytosolic fraction of BMDMs pre-treated with PBS or itaconate (10 mM) for 3 hours **(b)**. *D-loop* expression relative to *Rps18* in the isolated cytosolic fraction of BMDMs pre-treated with DMSO **(c),** TTFA (0.5 mM), or **(d),** DMM followed by LPS (100 ng/mL) for 4 hours. Data are mean ± SEM. for =3 from 3 independent experiments (b), for =8 from 4 independent experiments (c,d). P value is calculated by paired *t*-test.



4.1.29 Inhibition of SDH boosts LPS-induced *Ifnb1* independent of Bax and Bak

BMDMs ($0.5x10^6$ cells) underwent siRNA knockdown of *Bak1* and *Bax* followed by TTFA (0.5 mM) for 3 hours pre-treatment and LPS (100 ng/mL) treatment for 4 hours. Lysates were analysed by RT-qPCR for *Bak1* **(a),** *Bax* (**b**), and *Ifnb1* (**c**) relative to *Rps18*. Data are mean ± SEM. for n=3 from 3 independent experiments. P values are calculated using two-way ANOVA with multiple comparisons.



4.1.30 SDH-induced Ifnb1 is dependent on Vdac1, not Snx9

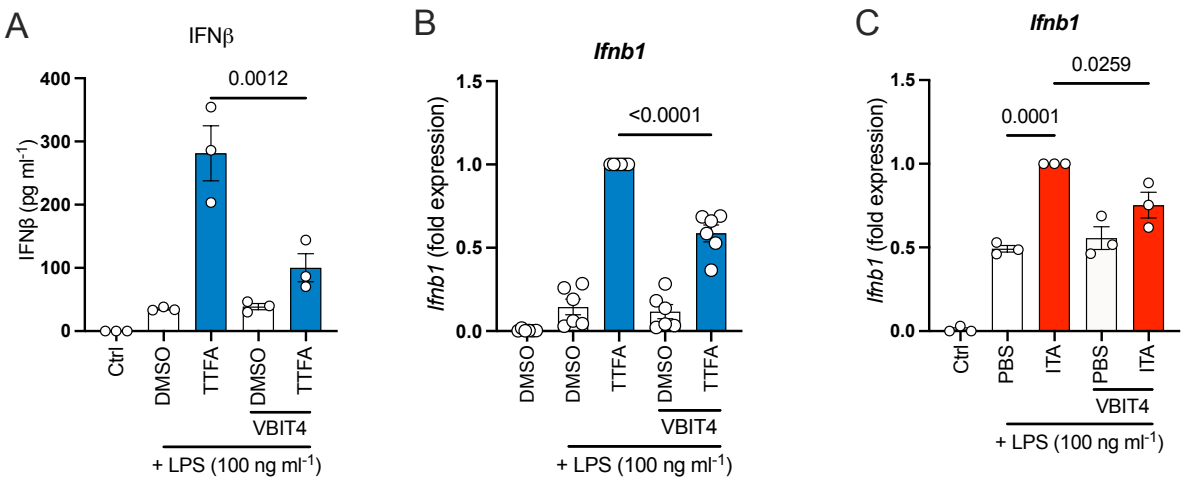
RT-qPCR data of BMDMs ($0.5x10^6$ cells) in the presence of control, Snx9 or Vdac1 siRNA followed by DMSO or TTFA pre-treatment (0.5 mM) for 3 hours followed by LPS (100 ng/mL) stimulation for 4 hours, n=6). RT-qPCR on genes *Snx9* **(a)**, *Vdac1* **(b)**, and *Ifnb1* **(c)** relative to *Rps18* were analysed. Data are mean ± SEM. for n=6 from 3 independent experiments. P values calculated using two-way ANOVA with Tukey's multiple comparisons.

4.1.31 VDAC1 oligomerisation regulates SDH-induced IFNβ

VDAC1 is known to transport mitochondrial DNA into the cytosol. It was shown that VDAC1 knockdown blocks TTFA-induced *Ifnb1* expression. To provide additional evidence for this, a pharmacological inhibitor of VDAC1 oligomerisation, VBIT4, was used to see if VDAC1 inhibition would suppress the boost in IFNβ mediated by SDH inhibition (69). Results showed that VBIT4 blocked the boost in IFNβ and *Ifnb1* seen with TTFA **(Figure 4.1.31 a)** and itaconate **(Figure 4.1.31b).** These results suggest that VDAC1, regulates the induction of IFNβ mediated via SDH inhibition.

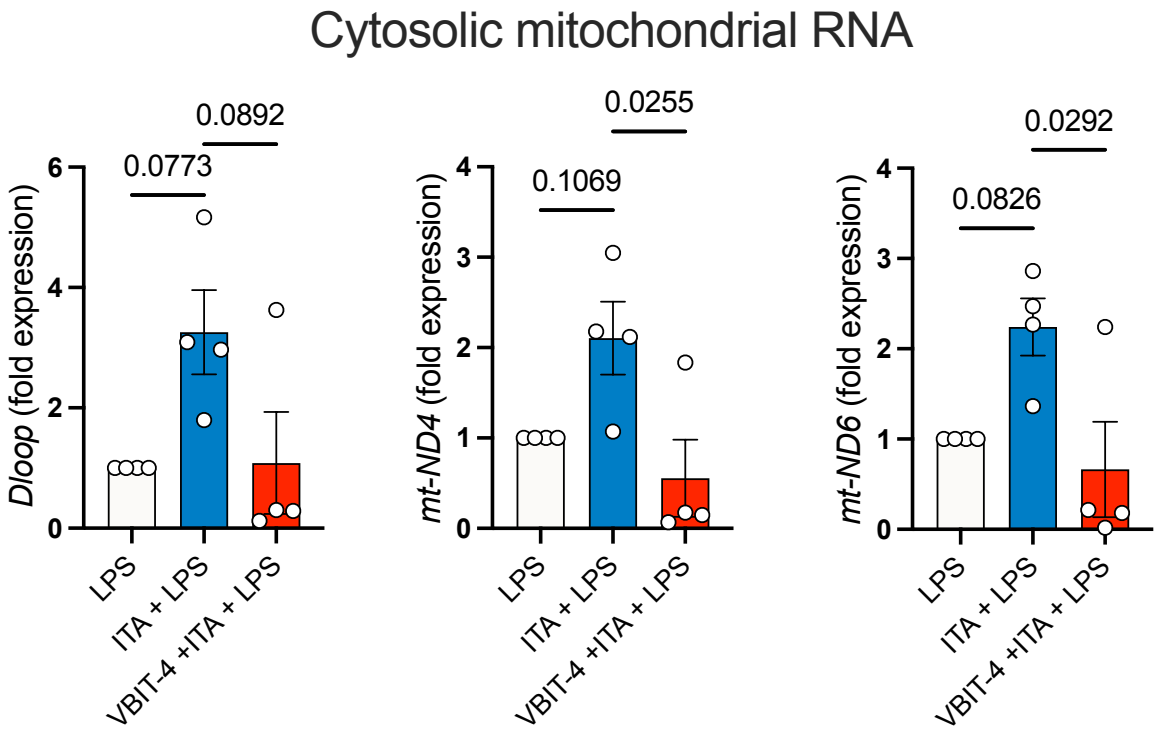
4.1.32 VDAC1 inhibition blocks itaconate-induced mitochondrial nucleic acid release

I next tested whether VDAC1 regulates the cytosolic release of mtdsRNA to drive IFNβ. mtRNA release via SDH-inhibition to drive IFNβ. Results showed that pharmacological VDAC inhibition by VBIT4 reduced expression of cytosolic mtRNA genes *Dloop, mt-Nd4,* and *mt-Nd6* induced after itaconate treatment. This indicates that VDAC is responsible for itaconate-induced cytosolic mtRNA release.



4.1. 31 VDAC1 oligomerisation regulates SDH-induced IFNβ

IFNβ release (**a**) and *Ifnb1* expression (**b**) in BMDMs ($0.5x10^6$ cells) pre-treated with VBIT-4 (10 µM) for 16 hours, DMSO or TTFA (0.5 mM) for 3 hours followed by LPS (100 ng/mL) for 4 hours. *Ifnb1* expression relative to *Rps18* in BMDMs ($0.5x10^6$ cells) pre-treated with DMSO or VBIT-4 (10 µM) for 16 hours followed by PBS or Itaconate (10 mM) for 3 hours followed by LPS (100 ng/mL) for 4 hours. Data are mean ± SEM. for n=3 from 3 independent experiments (a,c), n=3 from 3 independent experiments, and n=6 from 3 independent experiments. P value is calculated by one-way and two-way ANOVA.



4.1. 32 VDAC1 inhibition blocks itaconate-induced mitochondrial nucleic acid release

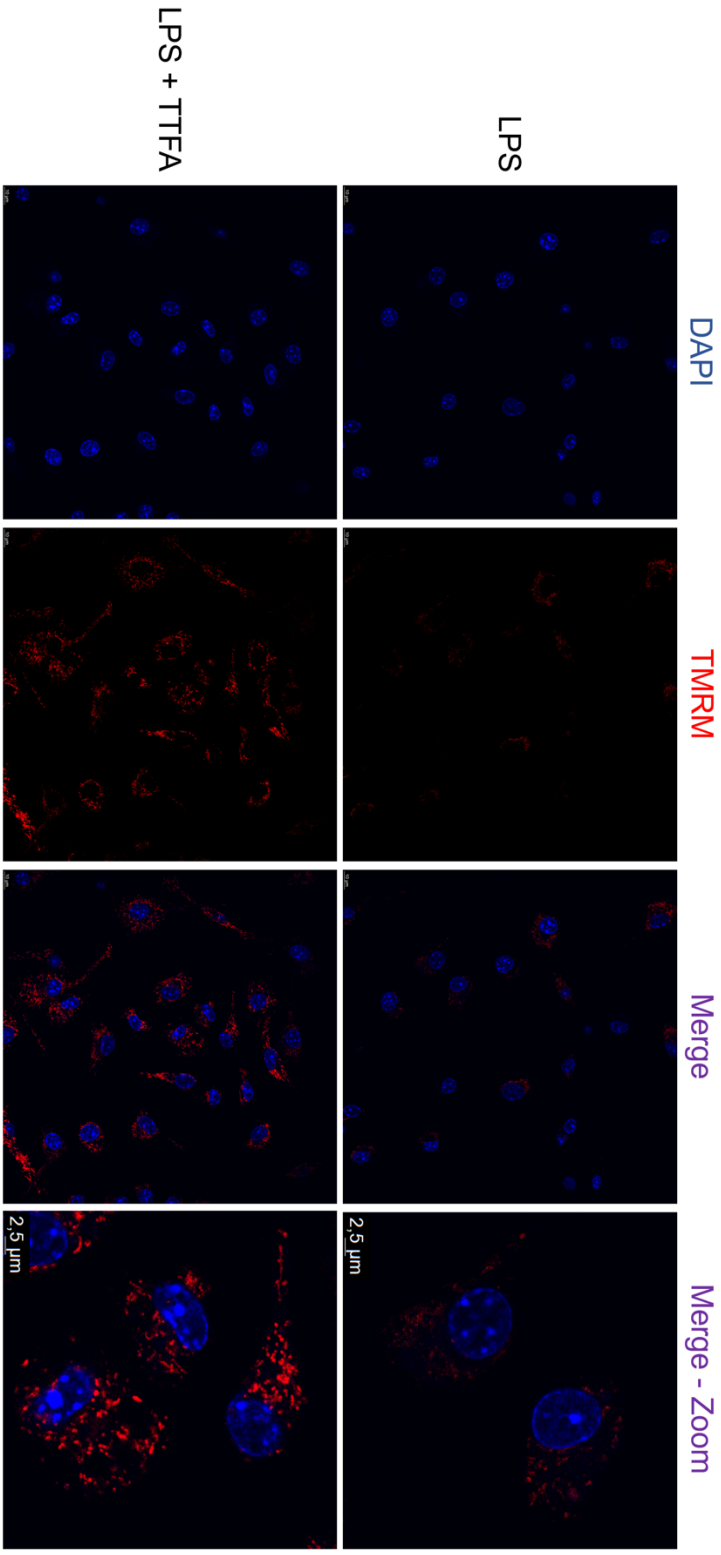
RT-qPCR of mitochondrial *D-loop, mt-ND4,* and *mt-ND6* gene expression relative to *Rps18* on the isolated cytosolic fraction of BMDMs ($0.5x10^6$ cells) pre-treated with DMSO or VBIT-4 (10 µM) for 16 hours followed by PBS or Itaconate (10 mM) for 3 hour pre-treatment followed by LPS (100 ng/mL) for 4 hours. Data are mean ± SEM. for n=4 from 3 independent experiments. P values were calculated using one-way ANOVA for multiple comparisons.

4.1.33 SDH inhibition increases mitochondrial membrane potential

I next tested whether SDH inhibition causes a change in MMP which might lead to nucleic acid release via VDAC1. The results were visualised by immunofluorescence and illustrate that the Merge-Zoom panel on the right side of the illustration showed that TTFA increased the presence of red TMRM staining, indicative of increased MMP. This shows that SDH- inhibition boosts MMP which might lead to mtdsRNA release (**Figure 4.1.33)**.

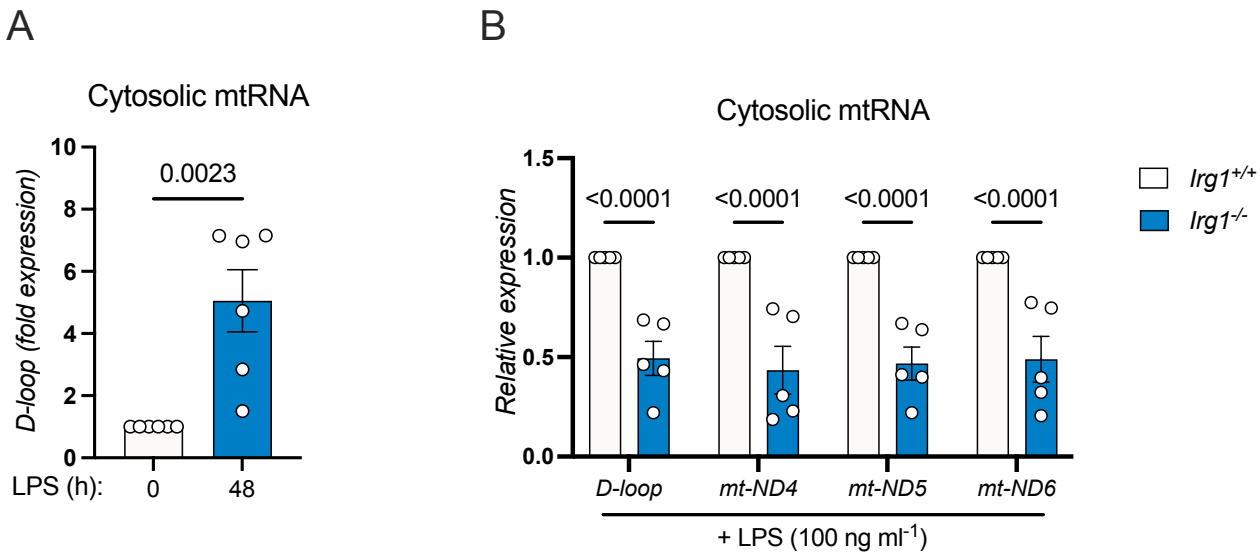
4.1.34 LPS-induced cytosolic mtRNA release is dependent on IRG1

Finally, to test the role of itaconate in cytosolic mtRNA release I tested IRG1-deficient BMDMs. LPS alone increased the cytosolic mtRNA *D-loop* (**Figure 4.1.24 a).** Results showed that *Irg1*$^{-/-}$ BMDMs expressed less cytosolic mtRNA genes *D-loop, mt-Nd4, mt-Nd5*,and *mt-Nd6* (**Figure 4.1.34 b).**



4.1. 33 SDH inhibition increases mitochondrial membrane potential

Immunofluorescence images of BMDMs ($0.5x10^6$ cells) pre-treated with DMSO or TTFA (0.5 mM) for 3 hours followed by LPS (100 ng/mL) for 4 hours. Cells underwent DAPI and TMRM (1.25 nM) staining. Images representative of 2 independent experiments.



4.1 34 LPS-induced cytosolic mtRNA release is dependent on ACOD1

D-loop expression **(a)** relative to *Rps18* in the cytosolic fraction of LPS (100 ng/mL) challenged BMDMs ($0.5x10^6$ cells) for 48 hours from. Mitochondrial gene expression from the cytosolic fraction of LPS (100 ng/mL) challenged *Irg1*$^{+/+}$ and *Irg1*$^{-/-}$ BMDMs ($0.5x10^6$ cells) for 24 hours. Data are mean ± SEM. For n=6 from 3 independent experiments (a), and n=5 from 3 independent experiments (b). P values are calculated using unpaired two-tailed Student's *t*-test for paired comparison and two-way ANOVA with Sidak's multiple comparisons

4.2 Discussion

4.5.1 Rationale

The rationale for investigating the mechanism by which itaconate boosts type I interferon responses originates from the findings described by two important publications, Mills *et al.,* 2018 and Swain *et al.,* 2020 (140, 155). Mills *et al.,* first described the link between the IRG1-itaconate axis and type I interferons. Mills *et al.,* demonstrated that IRG1 expression is reduced in IFNAR$^{-/-}$ BMDMs, determining IRG1 to be an ISG as shown by others (181, 182). Furthermore, they show that 4-OI suppresses IFNβ and *Isg15* in BMDMs, indicating that a negative feedback loop might exist whereby, in response to LPS, itaconate is generated, which blocks type I interferons and other inflammatory markers to block LPS-induced inflammation in BMDMs. However, these claims assumed that 4-OI was a tool compound for underivatized itaconate, which was subsequently demonstrated not to be the case for type I interferon production.

Next, Swain *et al.,* published a study comparing the similarities and differences between itaconate and 4-OI regarding key inflammatory markers in BMDMs. In this study, they demonstrated, using *Irg1*$^{-/-}$ BMDMs and exogenous itaconate, that un-derivatised itaconate boosts LPS-induced type I interferon responses while 4-OI was indeed inhibitory.

A difference between itaconate and 4-OI evident in Swain *et al.,* was their inability to inhibit SDH. Whereby only itaconate could. This result was a clear rationale to investigate how SDH inhibition by itaconate regulates type I interferon responses. At this time works from our lab and others had demonstrated that FH inhibition, via pharmacological inhibition or genetic ablation, caused increased membrane potential and the release of mtRNA and mtDNA which induced type I IFNs (3, 4). This demonstrates that TCA cycle enzyme inhibition drives nucleic acid release and might be the same for SDH inhibition by itaconate.

4.5.2 Itaconate boosts type I interferon production

In my study, I investigated the boost in type I IFN in response to itaconate. Furthermore, using IREA, IFNβ was shown to be an active cytokine in the transcriptional response in itaconate-treated BMDMs. As there are so many ISGs (183), it could be proposed that

even though *Ifnb1* was significantly yet modestly upregulated in itaconate-treated BMDMs, it mediates the transcription of a large number of ISGs.

Furthermore, I demonstrated the *Irg1*$^{-/-}$ BMDMs produce less IFNβ and *Isg15,* again supporting work performed by Swain et al. My study also extended the Swain findings to human macrophages. Utilising a pharmacological approach, via exogenous itaconate, and a genetic approach, by ablation of ACOD1 in both murine and human macrophages, I provided strong evidence for the role of itaconate in boosting LPS-induced type I interferon responses. Moreover, I showed that itaconate boosted IFNβ production in combination with multiple other PRR agonists including LPS (TLR4), Poly (I:C) (TLR3), R848 (TLR7/8), and CPG-ODN 2088 (TLR9). It appears that itaconate did boost poly (I:C)-induced IFNβ but not ISGs to the same degree as the other agonists. A main difference between TLR3 versus TLR4, TLR7/8 and TLR9 signalling is that TLR3 signalling pathways is primarily TRIF-induced while TLR4, TLR7/8, and TLR9 signalling pathways converge primarily via MYD88 signalling. Interestingly, Qin *et al.,* conducted a screen implementing a bioorthogonal probe, itaconate-alkyne, termed iTalk to discover proteins modified by itaconate (157). In their screen they see proteins on the TLR4-MYD88 pathway modified by itaconate and none on the TRIF signalling pathway such as MYD88,. It could be hypothesised therefore, that itaconate could also modify proteins on this pathway, leading to its activation and downstream signalling which might explain the discrepancies in MYD88 vs TRIF-dependent pathways.

4.5.3 Itaconate blocks SDH

I hypothesised that itaconate boosts LPS-induced type I interferon via SDH inhibition it was I demonstrated that itaconate can block SDH in our model testing both exogenous itaconate and *Irg1*$^{-/-}$ BMDMs. I implemented a (3-(4,5-Dimethylthiazol 2-yl)-2,5-diphenyltetrazolium bromide) (MTT) assay as an SDH activity assay as SDHA is the primary enzyme needed for this reaction (184). It has been well-documented, in multiple models, that itaconate is a competitive and reversible SDH inhibitor (92, 126-128, 140, 144, 155). SDH inhibition by itaconate is an important phenotype of macrophage polarisation (105).

A limitation of this work so far is that the effect of 4-OI on SDH activity is yet to be investigated here. Theoretically, 4-OI can be converted to itaconate and thus this should also block SDH activity. However, as I show in this thesis, 4-OI blocks interferon responses which is opposite to the findings shown here. I propose a hypothesis for these discrepancies. I hypothesise that a significant quantity of itaconate is needed for SDH inhibition. According to works by Lampropoulou *et al.,* the Michaelis constant (K_m) for succinate is 0.29 mM, and the K_i for itaconate is 0.22 mM (126), and physiological intracellular succinate levels is approximately 1 mM, which would make itaconate IC_{50} and IC_{100} approximately 1 mM and 10 mM respectively, values found after LPS stimulation by a number of groups (127, 128). Indeed, Hooftman *et al*., 2020 demonstrate that $^{13}C_5$-labelled 4-OI is converted into $^{13}C_5$-labelled itaconate by macrophages while some 4-OI remains as the derivative in the same samples (142). However, the maximum 4-OI concentration tolerised by murine macrophages is 250 μM, so it may be hypothesised that the small amount of itaconate formed from 4-OI is insufficient to outcompete succinate for the active site of SDH. Furthermore, 4-OI is much more thiol-reactive and reacts with many cysteines in the proteome. This includes inhibiting IRF3, and STING activity to block interferons (167, 168).

4.5.4 SDH inhibition boosts type I interferon responses

As it has been demonstrated here that itaconate boosts type I interferon and blocks SDH, it was hypothesised that itaconate boosts LPS-induced type I interferon via SDH inhibition. To investigate this, both pharmacological and genetic approaches were implemented to test this hypothesis. TTFA and AA5 are classical pharmacological SDH inhibitors which function by blocking ubiquinone binding sites, inhibiting succinate-ubiquinone reductase (SQR) activity of SDH, therefore blocking electron transfer from succinate to ubiquinone with minimal effect on complex I and complex III (177, 178). These were easily accessible tool compounds available to show proof of concept of SDH inhibition boosting LPS-induced IFNβ. Pre-treatment with these inhibitors boosted LPS-induced IFNβ and ISGs in murine and human monocyte-derived macrophages. As tool compounds have their limitations regarding unwanted off-target effects, both the $SDHA^{-/-}$ RAW264.7 macrophage cell line and a newly generated $SDHB^{cre/ert2}$ mouse model were used. These also showed that SDH knockout boosts LPS-induced type I interferon and, as a control, blocked *Il1b* expression. These results complement each other and support

data indicating that pharmacological SDH inhibition with DMM blocks *Il1b* expression (126). I was then interested in whether a disease model of SDH inhibition could recapitulate this phenotype. SDH inhibition leads to the accumulation of the oncometabolite succinate to inhibit succinate-sensitive 2-OGDD and can lead to cancers such as SDH-deficient paragangliomas (185, 186). To source paraganglioma samples, I collaborated with Prof. Maureen O'Sullivan, who is a medical consultant and paediatric pathologist who focuses on paediatric solid tumours from Our Lady's Children's Hospital, Dublin, Ireland. We sourced SDH-deficient paragangliomas from site, age, and gender-matched controls. Due to the rarity of these tumours, we attained five samples per group and showed that SDH-deficient tissues had elevated *IFNB* with no difference in *IL1B*. Both itaconate and SDH inhibition are pro-tumour via inhibition of $CD8^+$ T cells and inhibition of TET2 2-OGDDs (187). Both of these lead to succinate accumulation which is an oncometabolite and is known to be immunosuppressive in the TME via $CD8^+$ T cell inhibition. It could be hypothesised that the oncogenic effect of itaconate may be via SDH inhibition and accumulation of the oncometabolite succinate. The pathogenic mutations which lead to paragangliomas include SDH, FH, MDH, and IDH2. Interestingly, FH and IDH2 also regulate mitochondrial nucleic acid release and type I interferon responses. Furthermore, FH-deficient renal cancer cells also have increased mt-nucleic acids and type I interferon responses (3, 4). Type I interferons play a complex role in cancer where, in some cases, both cells in the TME and tumour cells produce chronic interferons which is immunosuppressive and leads to tumour progression and aids in cancer resistance to therapies such as ionizing radiation-induced DNA damage via induction of PD-L1(188). It is not fully understood yet, however, what the role is for type I interferon in SDH-deficient paragangliomas or whether this interferon response is from the cancer cells themselves or the macrophages within the TME, which are SDH-competent. It may be interesting to understand whether the pro-tumour effect of itaconate is predominantly through SDH inhibition.

Anti-inflammatory properties of IFNβ have been shown via IFNβ-induced induction of IL10 and, in turn, suppresses pro-IL1β and pro-IL1α and IFNβ-induced inhibition of NRLP1 and NLRP3 inflammasome (189). It could be hypothesised, therefore, that SDH-dependent inhibition of IL1β may be IFNβ-induced. This could also explain the susceptibility of individuals to secondary bacterial infection after a viral infection, as

IFNβ blocks IL1β needed for the antibacterial response. It might also explains the reduced IL1β in patients with multiple sclerosis or in my paraganglioma model (189).

4.5.5 SDH-inhibition by itaconate leads to mtRNA release

No work to date have linked SDH inhibition and the release of mitochondrial nucleic acids. However, FH inhibition via pharmacological or genetic approaches has been shown to drive mtDNA and mtRNA release (3, 4, 176). Specifically, Hooftman *et al*. demonstrated that FH inhibition in murine macrophages leads to mtRNA release, which is sensed by RIG-I and MDA5 to drive type I interferon responses. Complimentary to Hooftman *et al.,* Zecchini *et al*. showed that FH inhibition caused mtDNA release via mitochondrial-derived vesicles (MDVs) which is sensed by cGAS-STING signalling pathways and also leads to the induction of type I interferon responses. Given the endosymbiotic relationship between mitochondria and eukaryotes, it was hypothesised that unfavourable cellular conditions for mitochondria may lead to a loss of endosymbiosis, contributing to inflammatory disease (190). It could be hypothesised that, like FH inhibition, SDH inhibition may lead to mitochondrial dysfunction and the release of mitochondrial nucleic acids.

The data shown here provides evidence in support of our hypothesis that SDH-inhibition, by itaconate, leads to mtRNA release. The first indication that mtRNA was involved in SDH-dependent induction of type I interferon was after downstream GSEA analysis from RNA-seq suggested that RIG-I and MDA5-dependent genes were significantly upregulated after SDH inhibition. As this was just a transcriptional readout, more was needed to more conclusively implicate mtRNA in SDH-induced type I interferon induction. As ethidium bromide localises to the mitochondria and intercalates DNA, it was used as a tool compound to investigate the role of mitochondrial nucleic acids in the induction of *Ifnb1* after SDH inhibition. EtBr blocked *Ifnb1* and total mitochondria RNA copy number. This indeed suggests the role of mtRNA in the induction of *Ifnb1*. However, EtBr cannot be used to delineate the respective roles of mtRNA and mtDNA in this experiment. To solve this, different nucleic acid sensors were knocked down using siRNA to determine if mitochondrial nucleic acids were being released and what type of nucleic acids were being released. Indeed, RIG-I and MDA5, which sense short dsRNA and long dsRNA, respectively (>1kb) (191), were implicated in the induction of type I

interferon seen with SDH inhibition. TTFA-induced type I interferon was shown to be independent of DNA sensors cGas and Tlr9. However, itaconate-induced induction of IFNβ was shown to be dependent on TLR9. This seems to be unique to itaconate and not pharmacological SDH inhibition with TTFA. This could be hypothesised as an SDH-independent mechanism of IFNβ induction, potentially mediated by cysteine alkylation. It was then shown that pharmacological SDH inhibitors itaconate, TTFA, and DMM all increase the cytosolic release of mtRNA via digitonin fractionation. Furthermore, the results presented show that LPS alone leads to both the induction and release of several mitochondrial RNA species, a previously described phenotype (192). Moreover, This release of mtRNA-release was dependent on endogenous itaconate production as revealed Irg1$^{-/-}$ BMDMs.

4.5.6 SDH inhibition leads to mitochondrial dysfunction

I have shown that SDH inhibition, utilising itaconate or SDH inhibitors, causes mtdsRNA release and the induction of IFNβ. Mitochondrial membrane potential (MMP) is generated by proton pumping across the inner mitochondrial membrane via complex I, III, and IV and is an important factor in macrophage innate immunity, including the generation of mtROS and the transport of factors, including proteins, ions and metabolites (193-195). I found that SDH inhibition boosts MMP, which might lead to mtdsRNA release. This result is consistent with previous literature. Mills *et al*,. have previously shown that LPS-stimulated BMDMs boost MMP. This indicates aerobic glycolysis and an interruption in OXPHOS as the mitochondrial ATPase no longer converts the proton gradient into ATP. This, along with SDH inhibition, is important in mtROS generation and the metabolic reprogramming of macrophages (105). Interestingly, reduced MMP with Carbonyl cyanide m-chlorophenylhydrazone (CCCP), a well-known OXPHOS uncoupler, blocks poly(I:C)-induced RIG-I signalling and subsequent IFNβ production, reducing the antiviral response (196). Hooftman *et al*. show that changes to MMP, whether increased or decreased MMP, can lead to the induction of IFNβ via mtdsRNA release. Oligomycin, which increases MMP via ATPase inhibition, and valinomycin A, the K^+ ionophore, both lead to mtdsRNA release into the cytosol upon fumarate hydratase inhibition in BMDMs. I can conclude, therefore that SDH inhibition leads to changes in membrane polarisation which might lead to the mtdsRNA release.

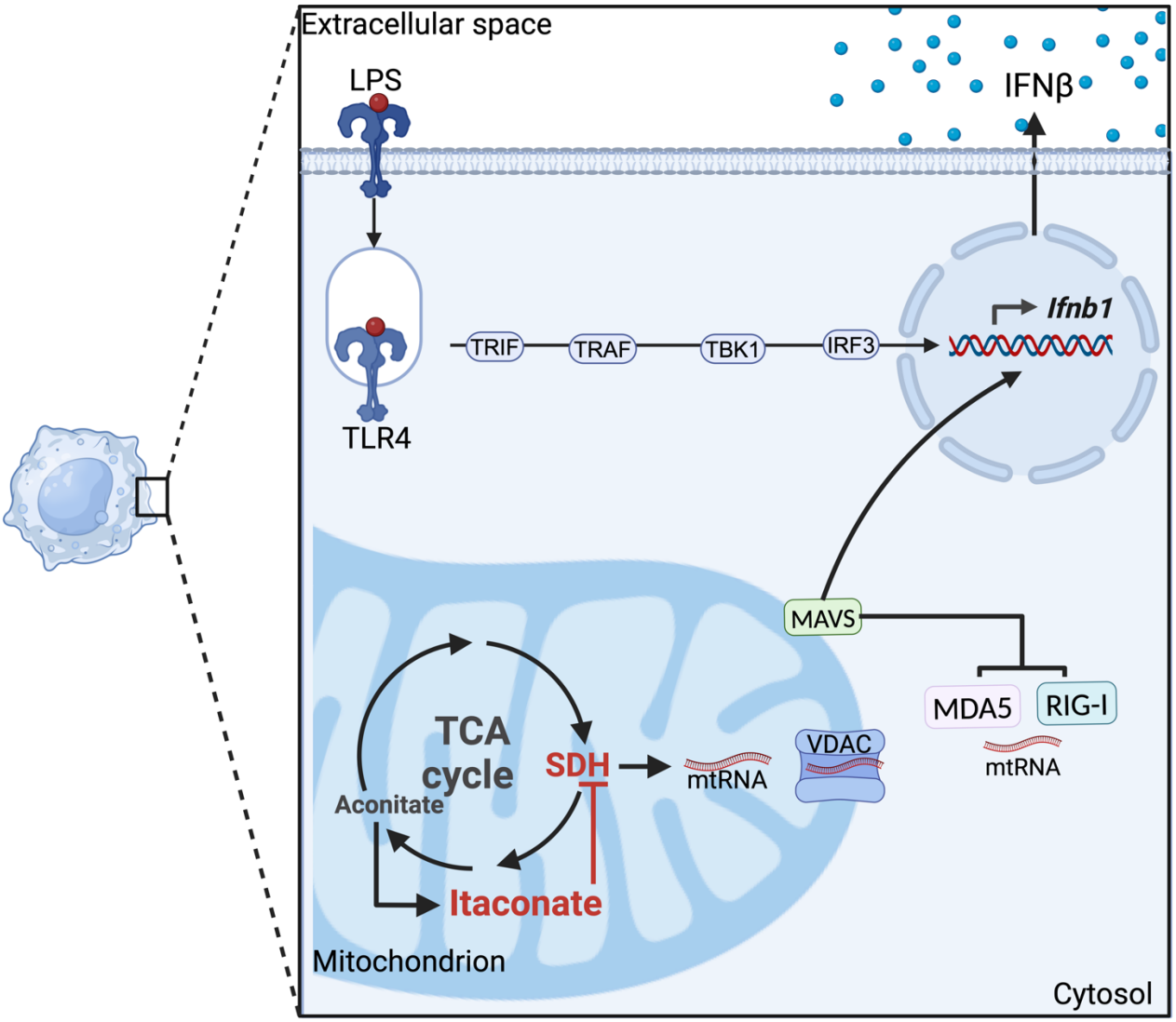
4.5.7 SDH-induced mtRNA release is VDAC dependant

The literature on mitochondrial nucleic acid release mechanisms is well-established. BAX/BAK, VDAC1, mPTP, and SNX9 are all implicated in mitochondrial nucleic acid release (64). Therefore, it was decided to investigate whether these nucleic acid transporters are responsible for the release of mtRNA upon SDH inhibition. A pharmacological inhibitor of voltage-dependent anion channel (VDAC) oligomerisation, VBIT4, blocked type I interferon mediated by SDH inhibition (197). This was also supported by *Vdac1* knockdown which lead to decreased VDAC1 and reduced interferon production. This suggested that the induction of IFNβ was VDAC-dependent. However, this result does not directly link VDAC1 to the release of mtdsRNA. This was the rationale for the next experiment, where we showed that VDAC1 inhibition blocked the itaconate-induced mitochondrial mtdsRNA release.

Much of the current literature regarding VDAC-dependant nucleic acid transport has focussed on mtDNA (64). Therefore, there is limited literature on its ability to transport mtRNA species. These results therefore are a novel mechanism of mitochondrial nucleic acid transport by VDAC1 in inflammatory macrophages. Other mechanisms for mitochondrial nucleic acid release were ruled out such as Bax/Bak and SNX9 as their knockdown had no effect on *Ifnb1* production. As only mtRNA sensors were shown to be involved in SDH-induced IFNβ, it can be concluded that the nucleic acid species is more likely to be long mtdsRNA. A clear unanswered question would be how VDAC oligomerisation preferentially transport mtRNA over DNA.

4.6 Conclusion

Overall, therefore these results further uncover mechanisms of itaconate biology which bring us closer to itaconate derivatives as potential future therapeutics (**Figure 4.6.1)**. Further work should be done to understand the immunological outcome of the itaconate-induced increase in interferons in the context of diseases such as cancer, autoimmune disease, or viral infection. Furthermore, just as targeting FH is gathering interest in immunity, SDH targeting compounds should also be investigated for immune mediated disease



4.6. 1 Graphical abstract; Itaconate drives mtdsRNA release via SDH-inhibition

During metabolic reprogramming, such as after challenge with LPS, itaconate is the most abundant metabolites. Itaconate is anti-inflammatory and has several functions. Itaconate has been shown to block SDH inhibition. SDH inhibition by itaconate leads to mitochondrial dysfunction, and the release of mtdsRNA via the mitochondrial transporter VDAC1. Once mtdsRNA is released into the cytosol, it is sensed by RIG-I and MDA5 which leads to MAVS aggregation, activation and the induction of type I interferon responses, namely IFNβ. Image created with Biorender.com

Chapter 5 Overall discussion and future perspectives

5.1 Itaconate versus 4-OI

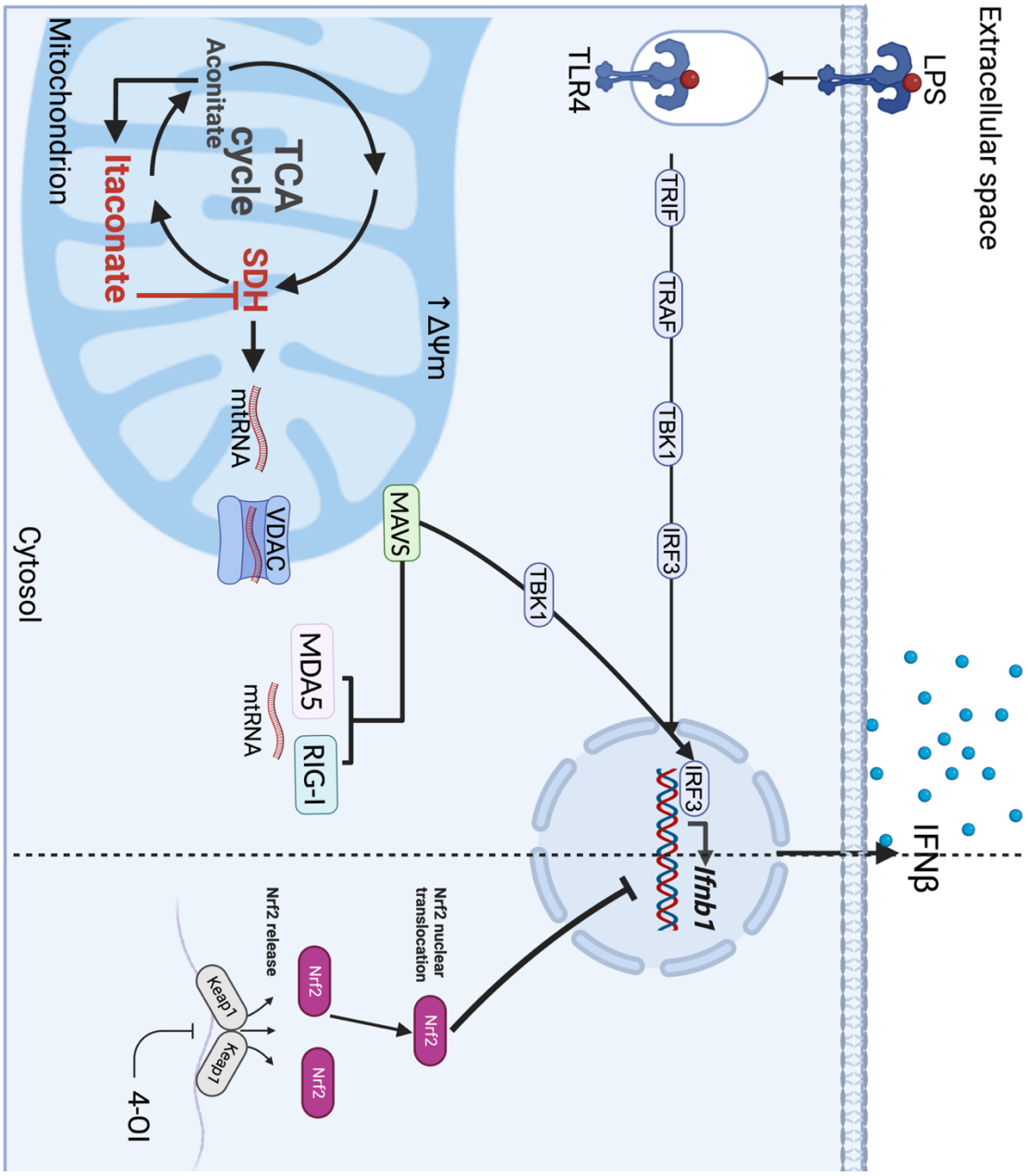
Swain *et al.,* were first to show the initial opposing phenotypes of itaconate and 4-OI, in regulating type I interferon responses in LPS-challenged BMDMs. Understanding how, and then why, these differences occur is very important to itaconate biology and the development of itaconate derivatives or ACOD1 modulators as therapies. With this thesis, I aimed to uncover the mechanisms by which itaconate and 4-OI differentially regulate IFNβ.

It was shown that 4-OI is a potent suppressor of type I interferon responses. Mechanistically, I have demonstrated the role for NRF2 into the negative regulation of type I interferon responses, which was verified by other works published in parallel to mine (165, 166, 168). Again, I have expanded the role of 4-OI in the negative regulation of type I interferons stimulated by multiple PRR agonists, concluding that a common mechanism, NRF2 liberation, must be involved.

In stark contrast, it was demonstrated that underivatised itaconate is a clear SDH inhibitor, and with that, causes increased mitochondrial membrane potential to cause mtdsRNA release into the cytosol through VDAC which is sensed by RIG-I and MDA5 to drive IFNβ **(Figure 5.1).** A clear sequential mechanism by which this occurs has been demonstrated. Furthermore, this inhibition of SDH was also demonstrated in a disease model, SDH-deficient tumours.

SDH inhibition is an important mechanism by how itaconate regulates the inflammatory response and, now, type I interferon responses. Itaconate inhibition of SDH is likely unique to itaconate and not 4-OI. Even though it has been shown that 4-OI can be converted into itaconate, the amount produced is likely to be unable to outcompete succinate levels. This is a clear difference between the two compounds and demonstrates how they differentially regulate interferons.

The results indicating the role for VDAC in itaconate-mediated interferon production is novel. It suggest that mitochondrial RNA, rather than DNA, may be a key driver of interferon responses under conditions of metabolic stress such as seen with SDH inhibition by itaconate. Most of the literature focuses on mtDNA in nucleic acid sensing pathways and opens new avenues for understanding how mitochondrial signaling contributes to inflammation. Future research should aim to understand how VDAC1's selectively transports mtRNA over DNA.. Furthermore, the involvement of VDAC1 in other inflammatory contexts and its potential as a therapeutic target should be explored. In particular, whether VDAC inhibitors could be employed in contexts where mitochondrial nucleic acid release drives type I interferons of dysregulated inflammatory response such as SLE and MS.



5. 1 Itaconate and 4-OI differentially regulate type I interferon responses

LPS activated macrophages upregulate itaconate which inhibits SDH. SDH inhibition increases MMP which leads to the release of mitochondrial dsRNA via VDAC1 into the cytosol which is sensed by RIG-I and MDA5 to drive IFNβ. 4-OI alkylates KEAP1 which liberates NRF2 to block IFNβ. Image created with Biorender.com

Another key difference between itaconate and 4-OI is their relative electrophilicity. 4-OI is a much stronger electrophile than underivatised itaconate. This is due to their structural differences. The addition of the octyl tail to the distal end of C=C chain esterifies the compound, increases cysteine reactivity. It is likely that 4-OI alkylates more of the proteome, causing different immunological phenotypes. Such an example may be KEAP1 itself. It is clear that 4-OI alkylates KEAP1, leading to the liberation of NRF2 and the inhibition of type I interferon signalling (140). However, whether underivatised itaconate can activate NRF2 in this precise same mechanism or to the same extent is still unclear. Data from my thesis suggests that itaconate does drive NRF2-dependent genes, but whether this is via alkylation of KEAP1 is unclear. SDH inhibition causes reverse electron transport (RET) and succinate accumulation via the reduction of fumarate which leads to mtROS production via mitochondrial complex I (198), which is known to activate NRF2, this could be a mechanism of NRF2 activation by underivatized itaconate. It could be possible that the inhibition of SDH, by itaconate, could cause succinate accumulation, and induce NRF2, which is already well established to block interferons, while on the other hand, itaconate causes increased mitochondrial membrane potential, which is known to drive mitochondrial nucleic acid-mediated IFNβ. It could be hypothesised that the minor induction of NRF2 is insufficient to block the induction of IFNβ by itaconate-mediated nucleic acid release and lead to the phenotype we see.

Another difference between the two is their ability to bind OXGR1. Itaconate has been shown to undergo receptor binding via OXGR1 which is important in its antimicrobial functions (123). However, the full immunological outcome of OXGR1 activation by itaconate has not been fully elucidated. Furthermore, it is still unclear whether 4-OI or other derivatives can bind and activate this receptor. If not, this could unveil further differences between itaconate and 4-OI which should be considered.

Itaconate and its derivative, 4-OI, are similar in many aspects. They are both electrophilic, while 4-OI being more electrophilic. 4-OI is cleaved into biologically active itaconate by esterases. Both 4-OI and itaconate activate NRF2, although 4-OI activates NRF2 to a greater extent. They are both antiviral, blocking IAV titres. Moreover, 4-OI and itaconate both block IL1β. Although these compounds have commonalities, this thesis focuses on an important difference. It suggests that claims made with derivatised itaconate should be verified with underivatised itaconate, whether

pharmacologically or by genetic approaches. As itaconate is now known to be taken up by macrophages (155), it may no longer be needed as a tool compound, but could be utilised in its own right.

One major limitation of the experimental models used in my PhD thesis lies in the reliance on in vitro systems, particularly bone marrow-derived macrophages (BMDMs). While BMDMs provide a controlled environment to investigate cellular responses, they fail to fully replicate the complexity of in vivo conditions or patient-specific variability. For example, lipopolysaccharide (LPS) stimulation models an acute inflammatory response, whereas many diseases, including autoimmune disorders, involve chronic inflammation. Additionally, the high activity of ACOD1 (IRG1) in mice compared to humans represents a translational challenge, as human macrophages may not produce itaconate to the same extent. We attempted to address this by incorporating human-derived THP1 macrophages; however, this still does not capture the full metabolic and cellular diversity seen in vivo. Another limitation is the use of superphysiological levels of itaconate (10 mM), exceeding the approximately 5 mM reported as maximal in BMDMs, which could exaggerate effects. The gold standard experiment would involve demonstrating the effects of itaconate in Acod1 knockout (KO) models, ideally rescuing the phenotype by reintroducing itaconate. However, emerging evidence of itaconate-independent roles of the ACOD1 protein itself complicates this approach. Future studies should incorporate ACOD1 catalytic inhibitors or enzymatic-dead mutants alongside omics screens to disentangle the specific contributions of itaconate from ACOD1's broader functions. Expanding the use of in vivo models and patient-derived samples will be critical for translating these findings into clinically relevant contexts.

5.2 Future perspectives

5.2.1 Therapeutic potential

Dimethyl fumarate (DMF), a methyl ester derivative of the TCA cycle intermediate fumarate, is a clinically approved treatment for multiple sclerosis (MS) and psoriasis, marketed under the name Tecfidera. Generating over $4 billion annually for Biogen Pharmaceuticals, Tecfidera exemplifies the therapeutic potential of metabolite derivatives, paving the way for compounds like itaconate derivatives, which are currently in clinical trials. Despite its clinical success, the precise mechanism of action of DMF remains unclear. Interestingly, DMF shares several properties with itaconate and its derivatives, including the ability to modify cysteine residues such as Cys-151 on KEAP1 to activate NRF2 (199) and blocks glycolysis via alkylation of GAPDH (200). DMF, like itaconate, blocks T cell proliferation, activation and cytokine production (201). Similar to 4-OI, DMF is antiviral and anti-inflammatory during viral infection (168) and type I interferon responses (164). Furthermore, both DMF and 4-OI improve oncolytic virotherapy via their anti-inflammatory properties (202, 203). These shared characteristics highlight the potential for itaconate derivatives to follow DMF's path as promising therapeutic agents.

Itaconate derivatives are of interest to the pharmaceutical industry given the dominancy of Tecfidera in the treatment of MS and psoriasis. Tecfidera has some unwanted side effects including face flushing, rashes, and gastrointestinal issues. If itaconate derivatives could be developed without these side effects, they may be an interesting alternative. However, the nonspecific nature of these compounds raises regulatory hurdles, as drugs with unclear mechanisms might face greater scrutiny today than when Tecfidera was first approved. Itaconate derivatives could address this challenge by leveraging their "multi-pronged mechanisms" or polypharmacology, a feature that may contribute to DMF’s effectiveness. For instance, 4-OI blocks viral nuclear export via CRM1 inhibition, blocks type I interferon, and inflammatory markers to blocks the virus, and the associated immunopathology (204, 205). Nonetheless, the lack of specificity and the absence of biomarkers for clinical trials remain significant barriers. Understanding the mechanism of how itaconate functions in disease is critical to developing appropriate biomarkers to demonstrate efficacy and gain regulatory approval.

There is still much to uncover in itaconate biology, particularly utilising catalytic deficient ACOD1 models to delineate the roles of itaconate ACOD1. Moreover, it would be interesting to fully understand the role of itaconate as an oncometabolite and the role of Acod1 inhibitors in cancer. It would be interesting to establish whether any diseases are prevalent in individuals who carry ACOD1 variants, such as the African variant which leads to increased itaconate production (206). Might these individuals be more resistant to bacterial infection but have increased incidence of tumour-progression?

Additionally, the modulation of TCA cycle enzymes, such as FH and SDH, in disease is gathering interest as a therapeutic in metabolic and inflammatory disease. Investigating modulators of these enzymes alongside itaconate biology should be investigated further and could uncover new therapeutic approaches for inflammatory disorders, infections, and cancer.

6 References

1. O'Neill LA, Kishton RJ, Rathmell J. A guide to immunometabolism for immunologists. Nat Rev Immunol. 2016;16(9):553-65.

2. Tannahill GM, Curtis AM, Adamik J, Palsson-McDermott EM, McGettrick AF, Goel G, et al. Succinate is an inflammatory signal that induces IL-1β through HIF-1α. Nature. 2013;496(7444):238-42.

3. Hooftman A, Peace CG, Ryan DG, Day EA, Yang M, McGettrick AF, et al. Macrophage fumarate hydratase restrains mtRNA-mediated interferon production. Nature. 2023;615(7952):490-8.

4. Zecchini V, Paupe V, Herranz-Montoya I, Janssen J, Wortel IMN, Morris JL, et al. Fumarate induces vesicular release of mtDNA to drive innate immunity. Nature. 2023;615(7952):499-506.

5. Medzhitov R, Janeway C. Innate immunity. N Engl J Med. 2000;343(5):338-44.

6. Iwasaki A, Medzhitov R. Control of adaptive immunity by the innate immune system. Nat Immunol. 2015;16(4):343-53.

7. Stremmel C, Schuchert R, Wagner F, Thaler R, Weinberger T, Pick R, et al. Yolk sac macrophage progenitors traffic to the embryo during defined stages of development. Nat Commun. 2018;9(1):75.

8. Wynn TA, Chawla A, Pollard JW. Macrophage biology in development, homeostasis and disease. Nature. 2013;496(7446):445-55.

9. Gordon S. Phagocytosis: An Immunobiologic Process. Immunity. 2016;44(3):463-75.

10. Roche PA, Furuta K. The ins and outs of MHC class II-mediated antigen processing and presentation. Nat Rev Immunol. 2015;15(4):203-16.

11. Mosser DM, Edwards JP. Exploring the full spectrum of macrophage activation. Nat Rev Immunol. 2008;8(12):958-69.

12. Dalton DK, Pitts-Meek S, Keshav S, Figari IS, Bradley A, Stewart TA. Multiple defects of immune cell function in mice with disrupted interferon-gamma genes. Science. 1993;259(5102):1739-42.

13. Yunna C, Mengru H, Lei W, Weidong C. Macrophage M1/M2 polarization. Eur J Pharmacol. 2020;877:173090.

14. Chen S, Saeed AFUH, Liu Q, Jiang Q, Xu H, Xiao GG, et al. Macrophages in immunoregulation and therapeutics. Signal Transduct Target Ther. 2023;8(1):207.

15. Gordon S. Alternative activation of macrophages. Nat Rev Immunol. 2003;3(1):23-35.

16. Li D, Wu M. Pattern recognition receptors in health and diseases. Signal Transduct Target Ther. 2021;6(1):291.

17. Yu B, Wright SD. Catalytic properties of lipopolysaccharide (LPS) binding protein. Transfer of LPS to soluble CD14. J Biol Chem. 1996;271(8):4100-5.

18. Fitzgerald KA, Palsson-McDermott EM, Bowie AG, Jefferies CA, Mansell AS, Brady G, et al. Mal (MyD88-adapter-like) is required for Toll-like receptor-4 signal transduction. Nature. 2001;413(6851):78-83.

19. Lin SC, Lo YC, Wu H. Helical assembly in the MyD88-IRAK4-IRAK2 complex in TLR/IL-1R signalling. Nature. 2010;465(7300):885-90.

20. Marongiu L, Gornati L, Artuso I, Zanoni I, Granucci F. Below the surface: The inner lives of TLR4 and TLR9. J Leukoc Biol. 2019;106(1):147-60.

21. Kawai T, Takeuchi O, Fujita T, Inoue J, Mühlradt PF, Sato S, et al. Lipopolysaccharide stimulates the MyD88-independent pathway and results in activation of IFN-regulatory factor 3 and the expression of a subset of lipopolysaccharide-inducible genes. J Immunol. 2001;167(10):5887-94.

22. Ciesielska A, Matyjek M, Kwiatkowska K. TLR4 and CD14 trafficking and its influence on LPS-induced pro-inflammatory signaling. Cell Mol Life Sci. 2021;78(4):1233-61.

23. ISAACS A, LINDENMANN J. Virus interference. I. The interferon. Proc R Soc Lond B Biol Sci. 1957;147(927):258-67.

24. Ivashkiv LB, Donlin LT. Regulation of type I interferon responses. Nat Rev Immunol. 2014;14(1):36-49.

25. Pestka S, Krause CD, Walter MR. Interferons, interferon-like cytokines, and their receptors. Immunol Rev. 2004;202:8-32.

26. Gibbert K, Schlaak JF, Yang D, Dittmer U. IFN-α subtypes: distinct biological activities in anti-viral therapy. Br J Pharmacol. 2013;168(5):1048-58.

27. Hardy MP, Owczarek CM, Jermiin LS, Ejdebäck M, Hertzog PJ. Characterization of the type I interferon locus and identification of novel genes. Genomics. 2004;84(2):331-45.

28. Rehwinkel J, Gack MU. RIG-I-like receptors: their regulation and roles in RNA sensing. Nat Rev Immunol. 2020;20(9):537-51.

29. Kawai T, Akira S. Innate immune recognition of viral infection. Nat Immunol. 2006;7(2):131-7.

30. Kawasaki T, Kawai T. Toll-like receptor signaling pathways. Front Immunol. 2014;5:461.

31. McNab F, Mayer-Barber K, Sher A, Wack A, O'Garra A. Type I interferons in infectious disease. Nat Rev Immunol. 2015;15(2):87-103.

32. Honda K, Takaoka A, Taniguchi T. Type I interferon [corrected] gene induction by the interferon regulatory factor family of transcription factors. Immunity. 2006;25(3):349-60.

33. Peace CG, Hooftman A, Ryan DG. Inflammatory mitochondrial nucleic acids as drivers of pathophysiology. Clin Transl Med. 2023;13(9):e1403.

34. Boxx GM, Cheng G. The Roles of Type I Interferon in Bacterial Infection. Cell Host Microbe. 2016;19(6):760-9.

35. Gao JJ, Filla MB, Fultz MJ, Vogel SN, Russell SW, Murphy WJ. Autocrine/paracrine IFN-alphabeta mediates the lipopolysaccharide-induced activation of transcription factor Stat1alpha in mouse macrophages: pivotal role of Stat1alpha in induction of the inducible nitric oxide synthase gene. J Immunol. 1998;161(9):4803-10.

36. Olson GS, Murray TA, Jahn AN, Mai D, Diercks AH, Gold ES, et al. Type I interferon decreases macrophage energy metabolism during mycobacterial infection. Cell Rep. 2021;35(9):109195.

37. Carlin JM, Borden EC, Byrne GI. Interferon-induced indoleamine 2,3-dioxygenase activity inhibits Chlamydia psittaci replication in human macrophages. J Interferon Res. 1989;9(3):329-37.

38. Niesel DW, Hess CB, Cho YJ, Klimpel KD, Klimpel GR. Natural and recombinant interferons inhibit epithelial cell invasion by Shigella spp. Infect Immun. 1986;52(3):828-33.

39. Freudenberg MA, Merlin T, Kalis C, Chvatchko Y, Stübig H, Galanos C. Cutting edge: a murine, IL-12-independent pathway of IFN-gamma induction by gram-negative bacteria based on STAT4 activation by Type I IFN and IL-18 signaling. J Immunol. 2002;169(4):1665-8.

40. Coclet-Ninin J, Dayer JM, Burger D. Interferon-beta not only inhibits interleukin-1beta and tumor necrosis factor-alpha but stimulates interleukin-1 receptor antagonist production in human peripheral blood mononuclear cells. Eur Cytokine Netw. 1997;8(4):345-9.

41. Huang Y, Blatt LM, Taylor MW. Type 1 interferon as an antiinflammatory agent: inhibition of lipopolysaccharide-induced interleukin-1 beta and induction of interleukin-1 receptor antagonist. J Interferon Cytokine Res. 1995;15(4):317-21.

42. Mayer-Barber KD, Yan B. Clash of the Cytokine Titans: counter-regulation of interleukin-1 and type I interferon-mediated inflammatory responses. Cell Mol Immunol. 2017;14(1):22-35.

43. Perkins DJ, Rajaiah R, Tennant SM, Ramachandran G, Higginson EE, Dyson TN, et al. Salmonella Typhimurium Co-Opts the Host Type I IFN System To Restrict Macrophage Innate Immune Transcriptional Responses Selectively. J Immunol. 2015;195(5):2461-71.

44. Mayer-Barber KD, Andrade BB, Oland SD, Amaral EP, Barber DL, Gonzales J, et al. Host-directed therapy of tuberculosis based on interleukin-1 and type I interferon crosstalk. Nature. 2014;511(7507):99-103.

45. Rönnblom LE, Alm GV, Oberg KE. Possible induction of systemic lupus erythematosus by interferon-alpha treatment in a patient with a malignant carcinoid tumour. J Intern Med. 1990;227(3):207-10.

46. Aicardi J, Goutières F. A progressive familial encephalopathy in infancy with calcifications of the basal ganglia and chronic cerebrospinal fluid lymphocytosis. Ann Neurol. 1984;15(1):49-54.

47. Crow YJ, Manel N. Aicardi-Goutières syndrome and the type I interferonopathies. Nat Rev Immunol. 2015;15(7):429-40.

48. Crow YJ, Stetson DB. The type I interferonopathies: 10 years on. Nat Rev Immunol. 2022;22(8):471-83.

49. Becker Y, Marcoux G, Allaeys I, Julien AS, Loignon RC, Benk-Fortin H, et al. Autoantibodies in Systemic Lupus Erythematosus Target Mitochondrial RNA. Front Immunol. 2019;10:1026.

50. Paludan SR, Pradeu T, Masters SL, Mogensen TH. Constitutive immune mechanisms: mediators of host defence and immune regulation. Nat Rev Immunol. 2021;21(3):137-50.

51. Dalskov L, Gad HH, Hartmann R. Viral recognition and the antiviral interferon response. EMBO J. 2023;42(14):e112907.

52. Suomalainen A, Nunnari J. Mitochondria at the crossroads of health and disease. Cell. 2024;187(11):2601-27.

53. Lane N, Martin W. The energetics of genome complexity. Nature. 2010;467(7318):929-34.

54. Pfanner N, Warscheid B, Wiedemann N. Mitochondrial proteins: from biogenesis to functional networks. Nat Rev Mol Cell Biol. 2019;20(5):267-84.

55. Fernandez-Vizarra E, Zeviani M. Mitochondrial disorders of the OXPHOS system. FEBS Lett. 2021;595(8):1062-106.

56. Nunnari J, Suomalainen A. Mitochondria: in sickness and in health. Cell. 2012;148(6):1145-59.

57. Rahman S, Blok RB, Dahl HH, Danks DM, Kirby DM, Chow CW, et al. Leigh syndrome: clinical features and biochemical and DNA abnormalities. Ann Neurol. 1996;39(3):343-51.

58. Schubert Baldo M, Vilarinho L. Molecular basis of Leigh syndrome: a current look. Orphanet J Rare Dis. 2020;15(1):31.

59. Neumann HPH, Young WF, Eng C. Pheochromocytoma and Paraganglioma. N Engl J Med. 2019;381(6):552-65.

60. Uher O, Hadrava Vanova K, Taïeb D, Calsina B, Robledo M, Clifton-Bligh R, et al. The Immune Landscape of Pheochromocytoma and Paraganglioma: Current Advances and Perspectives. Endocr Rev. 2024;45(4):521-52.

61. Aldera AP, Govender D. Gene of the month: SDH. J Clin Pathol. 2018;71(2):95-7.

62. Wu JY, Huang TW, Hsieh YT, Wang YF, Yen CC, Lee GL, et al. Cancer-Derived Succinate Promotes Macrophage Polarization and Cancer Metastasis via Succinate Receptor. Mol Cell. 2020;77(2):213-27.e5.

63. Dhir A, Dhir S, Borowski LS, Jimenez L, Teitell M, Rötig A, et al. Mitochondrial double-stranded RNA triggers antiviral signalling in humans. Nature. 2018;560(7717):238-42.

64. Yoon J, Kim S, Lee M, Kim Y. Mitochondrial nucleic acids in innate immunity and beyond. Exp Mol Med. 2023;55(12):2508-18.

65. Caielli S, Athale S, Domic B, Murat E, Chandra M, Banchereau R, et al. Oxidized mitochondrial nucleoids released by neutrophils drive type I interferon production in human lupus. J Exp Med. 2016;213(5):697-713.

66. McArthur K, Whitehead LW, Heddleston JM, Li L, Padman BS, Oorschot V, et al. BAK/BAX macropores facilitate mitochondrial herniation and mtDNA efflux during apoptosis. Science. 2018;359(6378).

67. Xian H, Watari K, Sanchez-Lopez E, Offenberger J, Onyuru J, Sampath H, et al. Oxidized DNA fragments exit mitochondria via mPTP- and VDAC-dependent channels to activate NLRP3 inflammasome and interferon signaling. Immunity. 2022;55(8):1370-85.e8.

68. López-López L, Nieves-Plaza M, Castro MeR, Font YM, Torres-Ramos CA, Vilá LM, et al. Mitochondrial DNA damage is associated with damage accrual and disease duration in patients with systemic lupus erythematosus. Lupus. 2014;23(11):1133-41.

69. Kim J, Gupta R, Blanco LP, Yang S, Shteinfer-Kuzmine A, Wang K, et al. VDAC oligomers form mitochondrial pores to release mtDNA fragments and promote lupus-like disease. Science. 2019;366(6472):1531-6.

70. Zhong Z, Liang S, Sanchez-Lopez E, He F, Shalapour S, Lin XJ, et al. New mitochondrial DNA synthesis enables NLRP3 inflammasome activation. Nature. 2018;560(7717):198-203.

71. Lee JH, Shim YR, Seo W, Kim MH, Choi WM, Kim HH, et al. Mitochondrial Double-Stranded RNA in Exosome Promotes Interleukin-17 Production Through Toll-Like Receptor 3 in Alcohol-associated Liver Injury. Hepatology. 2020;72(2):609-25.

72. Maekawa H, Inoue T, Ouchi H, Jao TM, Inoue R, Nishi H, et al. Mitochondrial Damage Causes Inflammation via cGAS-STING Signaling in Acute Kidney Injury. Cell Rep. 2019;29(5):1261-73.e6.

73. Lee H, Fenster RJ, Pineda SS, Gibbs WS, Mohammadi S, Davila-Velderrain J, et al. Cell Type-Specific Transcriptomics Reveals that Mutant Huntingtin Leads to Mitochondrial RNA Release and Neuronal Innate Immune Activation. Neuron. 2020;107(5):891-908.e8.

74. Kim S, Lee K, Choi YS, Ku J, Kim H, Kharbash R, et al. Mitochondrial double-stranded RNAs govern the stress response in chondrocytes to promote osteoarthritis development. Cell Rep. 2022;40(6):111178.

75. Yoneyama M, Kikuchi M, Natsukawa T, Shinobu N, Imaizumi T, Miyagishi M, et al. The RNA helicase RIG-I has an essential function in double-stranded RNA-induced innate antiviral responses. Nat Immunol. 2004;5(7):730-7.

76. Kang DC, Gopalkrishnan RV, Wu Q, Jankowsky E, Pyle AM, Fisher PB. mda-5: An interferon-inducible putative RNA helicase with double-stranded RNA-dependent ATPase activity and melanoma growth-suppressive properties. Proc Natl Acad Sci U S A. 2002;99(2):637-42.

77. Wu B, Peisley A, Richards C, Yao H, Zeng X, Lin C, et al. Structural basis for dsRNA recognition, filament formation, and antiviral signal activation by MDA5. Cell. 2013;152(1-2):276-89.

78. Tigano M, Vargas DC, Tremblay-Belzile S, Fu Y, Sfeir A. Nuclear sensing of breaks in mitochondrial DNA enhances immune surveillance. Nature. 2021;591(7850):477-81.

79. Tan X, Sun L, Chen J, Chen ZJ. Detection of Microbial Infections Through Innate Immune Sensing of Nucleic Acids. Annu Rev Microbiol. 2018;72:447-78.

80. Ryan DG, O'Neill LAJ. Krebs Cycle Reborn in Macrophage Immunometabolism. Annu Rev Immunol. 2020;38:289-313.

81. Pålsson-McDermott EM, O'Neill LAJ. Targeting immunometabolism as an anti-inflammatory strategy. Cell Res. 2020;30(4):300-14.

82. Galván-Peña S, Carroll RG, Newman C, Hinchy EC, Palsson-McDermott E, Robinson EK, et al. Malonylation of GAPDH is an inflammatory signal in macrophages. Nat Commun. 2019;10(1):338.

83. Li Y, Li YC, Liu XT, Zhang L, Chen YH, Zhao Q, et al. Blockage of citrate export prevents TCA cycle fragmentation via Irg1 inactivation. Cell Rep. 2022;38(7):110391.

84. Zhang W, Xiao D, Mao Q, Xia H. Role of neuroinflammation in neurodegeneration development. Signal Transduct Target Ther. 2023;8(1):267.

85. Duan L, Rao X, Sigdel KR. Regulation of Inflammation in Autoimmune Disease. J Immunol Res. 2019;2019:7403796.

86. Coussens LM, Werb Z. Inflammation and cancer. Nature. 2002;420(6917):860-7.

87. Diskin C, Ryan TAJ, O'Neill LAJ. Modification of Proteins by Metabolites in Immunity. Immunity. 2021;54(1):19-31.

88. Weyand CM, Goronzy JJ. Immunometabolism in early and late stages of rheumatoid arthritis. Nat Rev Rheumatol. 2017;13(5):291-301.

89. Baup. Ueber eine neue Brenzcitronensäure. Physik und Chemie. 1837.

90. Crasso G. Untersuchungen über das Verhalten der Citronsäure in höherer Temperatur und die daraus hervorgehenden Produkte. Justus Liebigs Annalen der Chemie. 1840;34(1):53-81.

91. Kinoshita K. Uber eine neue Aspergillus Art, A. itaconicus. *Bot Mag Tokyo*. 1931:45-50.

92. ACKERMANN WW, POTTER VR. Enzyme inhibition in relation to chemotherapy. Proc Soc Exp Biol Med. 1949;72(1):1-9.

93. Okabe M, Lies D, Kanamasa S, Park EY. Biotechnological production of itaconic acid and its biosynthesis in Aspergillus terreus. Appl Microbiol Biotechnol. 2009;84(4):597-606.

94. Lee CG, Jenkins NA, Gilbert DJ, Copeland NG, O'Brien WE. Cloning and analysis of gene regulation of a novel LPS-inducible cDNA. Immunogenetics. 1995;41(5):263-70.

95. Strelko CL, Lu W, Dufort FJ, Seyfried TN, Chiles TC, Rabinowitz JD, et al. Itaconic acid is a mammalian metabolite induced during macrophage activation. J Am Chem Soc. 2011;133(41):16386-9.

96. Michelucci A, Cordes T, Ghelfi J, Pailot A, Reiling N, Goldmann O, et al. Immune-responsive gene 1 protein links metabolism to immunity by catalyzing itaconic acid production. Proc Natl Acad Sci U S A. 2013;110(19):7820-5.

97. Heinz A, Nonnenmacher Y, Henne A, Khalil MA, Bejkollari K, Dostert C, et al. Itaconate controls its own synthesis via feedback-inhibition of reverse TCA cycle activity at IDH2. Biochim Biophys Acta Mol Basis Dis. 2022;1868(12):166530.

98. Lin J, Ren J, Gao DS, Dai Y, Yu L. The Emerging Application of Itaconate: Promising Molecular Targets and Therapeutic Opportunities. Front Chem. 2021;9:669308.

99. National Center for Biotechnology Information. PubChem Compound Summary for CID 811, Itaconic acid. 2022 [Available from: https://pubchem.ncbi.nlm.nih.gov/compound/Itaconic-acid.

100. Chen C, Zhang Z, Liu C, Sun P, Liu P, Li X. ABCG2 is an itaconate exporter that limits antibacterial innate immunity by alleviating TFEB-dependent lysosomal biogenesis. Cell Metab. 2024.

101. Chen C, Liu C, Sun P, Zhang Z, Wang Z, Liu P, et al. Itaconate uptake via SLC13A3 improves hepatic antibacterial innate immunity. Dev Cell. 2024.

102. ADLER J, WANG SF, LARDY HA. The metabolism of itaconic acid by liver mitochondria. J Biol Chem. 1957;229(2):865-79.

103. Cooper RA, Kornberg HL. The utilization of itaconate by Pseudomonas sp. Biochem J. 1964;91(1):82-91.

104. Shi X, Zhou H, Wei J, Mo W, Li Q, Lv X. The signaling pathways and therapeutic potential of itaconate to alleviate inflammation and oxidative stress in inflammatory diseases. Redox Biol. 2022;58:102553.

105. Mills EL, Kelly B, Logan A, Costa ASH, Varma M, Bryant CE, et al. Succinate Dehydrogenase Supports Metabolic Repurposing of Mitochondria to Drive Inflammatory Macrophages. Cell. 2016;167(2):457-70.e13.

106. Kwai BXC, Collins AJ, Middleditch MJ, Sperry J, Bashiri G, Leung IKH. Itaconate is a covalent inhibitor of the *Mycobacterium tuberculosis* isocitrate lyase. RSC Med Chem. 2021;12(1):57-61.

107. Rittenhouse JW, McFadden BA. Inhibition of isocitrate lyase from Pseudomonas indigofera by itaconate. Arch Biochem Biophys. 1974;163(1):79-86.

108. Sasikaran J, Ziemski M, Zadora PK, Fleig A, Berg IA. Bacterial itaconate degradation promotes pathogenicity. Nat Chem Biol. 2014;10(5):371-7.

109. Daniels BP, Kofman SB, Smith JR, Norris GT, Snyder AG, Kolb JP, et al. The Nucleotide Sensor ZBP1 and Kinase RIPK3 Induce the Enzyme IRG1 to Promote an Antiviral Metabolic State in Neurons. Immunity. 2019;50(1):64-76.e4.

110. Aso K, Kono M, Kanda M, Kudo Y, Sakiyama K, Hisada R, et al. Itaconate ameliorates autoimmunity by modulating T cell imbalance via metabolic and epigenetic reprogramming. Nat Commun. 2023;14(1):984.

111. Ogger PP, Albers GJ, Hewitt RJ, O'Sullivan BJ, Powell JE, Calamita E, et al. Itaconate controls the severity of pulmonary fibrosis. Sci Immunol. 2020;5(52).

112. Tada M, Kudo Y, Kono M, Kanda M, Takeyama S, Sakiyama K, et al. Itaconate reduces proliferation and migration of fibroblast-like synoviocytes and ameliorates arthritis models. Clin Immunol. 2024;264:110255.

113. Zhu D, Zhao Y, Luo Y, Qian X, Zhang Z, Jiang G, et al. Irg1-itaconate axis protects against acute kidney injury via activation of Nrf2. Am J Transl Res. 2021;13(3):1155-69.

114. Cordes T, Lucas A, Divakaruni AS, Murphy AN, Cabrales P, Metallo CM. Itaconate modulates tricarboxylic acid and redox metabolism to mitigate reperfusion injury. Mol Metab. 2020;32:122-35.

115. Zhang Y, Qin W, Liu D, Liu Y, Wang C. Chemoproteomic profiling of itaconations in Salmonella. Chem Sci. 2021;12(17):6059-63.

116. Ruetz M, Campanello GC, Purchal M, Shen H, McDevitt L, Gouda H, et al. Itaconyl-CoA forms a stable biradical in methylmalonyl-CoA mutase and derails its activity and repair. Science. 2019;366(6465):589-93.

117. Chen M, Sun H, Boot M, Shao L, Chang SJ, Wang W, et al. Itaconate is an effector of a Rab GTPase cell-autonomous host defense pathway against Salmonella. Science. 2020;369(6502):450-5.

118. Schuster EM, Epple MW, Glaser KM, Mihlan M, Lucht K, Zimmermann JA, et al. TFEB induces mitochondrial itaconate synthesis to suppress bacterial growth in macrophages. Nat Metab. 2022;4(7):856-66.

119. Tomlinson KL, Lung TWF, Dach F, Annavajhala MK, Gabryszewski SJ, Groves RA, et al. Staphylococcus aureus induces an itaconate-dominated immunometabolic response that drives biofilm formation. Nat Commun. 2021;12(1):1399.

120. Tomlinson KL, Riquelme SA, Baskota SU, Drikic M, Monk IR, Stinear TP, et al. Staphylococcus aureus stimulates neutrophil itaconate production that suppresses the oxidative burst. Cell Rep. 2023;42(2):112064.

121. O'Carroll SM, O'Neill LAJ. Targeting immunometabolism to treat COVID-19. Immunother Adv. 2021;1(1):ltab013.

122. Sohail A, Iqbal AA, Sahini N, Chen F, Tantawy M, Waqas SFH, et al. Itaconate and derivatives reduce interferon responses and inflammation in influenza A virus infection. PLoS Pathog. 2022;18(1):e1010219.

123. Zeng YR, Song JB, Wang D, Huang ZX, Zhang C, Sun YP, et al. The immunometabolite itaconate stimulates OXGR1 to promote mucociliary clearance during the pulmonary innate immune response. J Clin Invest. 2023;133(6).

124. Newsholme P, Curi R, Gordon S, Newsholme EA. Metabolism of glucose, glutamine, long-chain fatty acids and ketone bodies by murine macrophages. Biochem J. 1986;239(1):121-5.

125. Qin W, Qin K, Zhang Y, Jia W, Chen Y, Cheng B, et al. S-glycosylation-based cysteine profiling reveals regulation of glycolysis by itaconate. Nat Chem Biol. 2019;15(10):983-91.

126. Lampropoulou V, Sergushichev A, Bambouskova M, Nair S, Vincent EE, Loginicheva E, et al. Itaconate Links Inhibition of Succinate Dehydrogenase with Macrophage Metabolic Remodeling and Regulation of Inflammation. Cell Metab. 2016;24(1):158-66.

127. Cordes T, Metallo CM. Itaconate Alters Succinate and Coenzyme A Metabolism via Inhibition of Mitochondrial Complex II and Methylmalonyl-CoA Mutase. Metabolites. 2021;11(2).

128. Cordes T, Wallace M, Michelucci A, Divakaruni AS, Sapcariu SC, Sousa C, et al. Immunoresponsive Gene 1 and Itaconate Inhibit Succinate Dehydrogenase to Modulate Intracellular Succinate Levels. J Biol Chem. 2016;291(27):14274-84.

129. Lio CJ, Rao A. TET Enzymes and 5hmC in Adaptive and Innate Immune Systems. Front Immunol. 2019;10:210.

130. Chen LL, Morcelle C, Cheng ZL, Chen X, Xu Y, Gao Y, et al. Itaconate inhibits TET DNA dioxygenases to dampen inflammatory responses. Nat Cell Biol. 2022;24(3):353-63.

131. Human Protein Atlas 2024 [Available from: https://www.proteinatlas.org/ENSG00000165621-OXGR1/single+cell+type.

132. Bak DW, Bechtel TJ, Falco JA, Weerapana E. Cysteine reactivity across the subcellular universe. Curr Opin Chem Biol. 2019;48:96-105.

133. Groeger AL, Freeman BA. Signaling actions of electrophiles: anti-inflammatory therapeutic candidates. Mol Interv. 2010;10(1):39-50.

134. Kobayashi EH, Suzuki T, Funayama R, Nagashima T, Hayashi M, Sekine H, et al. Nrf2 suppresses macrophage inflammatory response by blocking proinflammatory cytokine transcription. Nat Commun. 2016;7:11624.

135. Itoh K, Wakabayashi N, Katoh Y, Ishii T, Igarashi K, Engel JD, et al. Keap1 represses nuclear activation of antioxidant responsive elements by Nrf2 through binding to the amino-terminal Neh2 domain. Genes Dev. 1999;13(1):76-86.

136. Kovac S, Angelova PR, Holmström KM, Zhang Y, Dinkova-Kostova AT, Abramov AY. Nrf2 regulates ROS production by mitochondria and NADPH oxidase. Biochim Biophys Acta. 2015;1850(4):794-801.

137. Thimmulappa RK, Lee H, Rangasamy T, Reddy SP, Yamamoto M, Kensler TW, et al. Nrf2 is a critical regulator of the innate immune response and survival during experimental sepsis. J Clin Invest. 2006;116(4):984-95.

138. Bambouskova M, Gorvel L, Lampropoulou V, Sergushichev A, Loginicheva E, Johnson K, et al. Electrophilic properties of itaconate and derivatives regulate the IκBζ-ATF3 inflammatory axis. Nature. 2018;556(7702):501-4.

139. Cifani P, Li Z, Luo D, Grivainis M, Intlekofer AM, Fenyö D, et al. Discovery of Protein Modifications Using Differential Tandem Mass Spectrometry Proteomics. J Proteome Res. 2021;20(4):1835-48.

140. Mills EL, Ryan DG, Prag HA, Dikovskaya D, Menon D, Zaslona Z, et al. Itaconate is an anti-inflammatory metabolite that activates Nrf2 via alkylation of KEAP1. Nature. 2018;556(7699):113-7.

141. Jo EK, Kim JK, Shin DM, Sasakawa C. Molecular mechanisms regulating NLRP3 inflammasome activation. Cell Mol Immunol. 2016;13(2):148-59.

142. Hooftman A, Angiari S, Hester S, Corcoran SE, Runtsch MC, Ling C, et al. The Immunomodulatory Metabolite Itaconate Modifies NLRP3 and Inhibits Inflammasome Activation. Cell Metab. 2020;32(3):468-78.e7.

143. Liu D, Xiao W, Li H, Zhang Y, Yuan S, Li C, et al. Discovery of Itaconate-Mediated Lysine Acylation. J Am Chem Soc. 2023;145(23):12673-81.

144. He W, Henne A, Lauterbach M, Geißmar E, Nikolka F, Kho C, et al. Mesaconate is synthesized from itaconate and exerts immunomodulatory effects in macrophages. Nat Metab. 2022;4(5):524-33.

145. Chen F, Elgaher WAM, Winterhoff M, Büssow K, Waqas FH, Graner E, et al. Citraconate inhibits ACOD1 (IRG1) catalysis, reduces interferon responses and oxidative stress, and modulates inflammation and cell metabolism. Nat Metab. 2022;4(5):534-46.

146. Zhao N, Yi M, Zhang LJ, Zhang QX, Yang L. 4-Octyl Itaconate Attenuates Neuroinflammation in Experimental Autoimmune Encephalomyelitis Via Regulating Microglia. Inflammation. 2024.

147. Jiang S. Tet2 at the interface between cancer and immunity. Commun Biol. 2020;3(1):667.

148. An J, González-Avalos E, Chawla A, Jeong M, López-Moyado IF, Li W, et al. Acute loss of TET function results in aggressive myeloid cancer in mice. Nat Commun. 2015;6:10071.

149. Feng Y, Li X, Cassady K, Zou Z, Zhang X. TET2 Function in Hematopoietic Malignancies, Immune Regulation, and DNA Repair. Front Oncol. 2019;9:210.

150. Zhao H, Teng D, Yang L, Xu X, Chen J, Jiang T, et al. Myeloid-derived itaconate suppresses cytotoxic CD8+ T cells and promotes tumour growth. Nat Metab. 2022;4(12):1660-73.

151. Chen YJ, Li GN, Li XJ, Wei LX, Fu MJ, Cheng ZL, et al. Targeting IRG1 reverses the immunosuppressive function of tumor-associated macrophages and enhances cancer immunotherapy. Sci Adv. 2023;9(17):eadg0654.

152. Gu X, Wei H, Suo C, Shen S, Zhu C, Chen L, et al. Itaconate promotes hepatocellular carcinoma progression by epigenetic induction of CD8 + T-cell exhaustion. Nat Commun. 2023;14(1):8154.

153. Schofield JH, Longo J, Sheldon RD, Albano E, Ellis AE, Hawk MA, et al. Acod1 expression in cancer cells promotes immune evasion through the generation of inhibitory peptides. Cell Rep. 2024;43(4):113984.

154. Waqas FH, Chen C, Pessler F. Aconitate decarboxylase (ACOD1) has found a disease. Trends Endocrinol Metab. 2024;35(7):561-2.

155. Swain A, Bambouskova M, Kim H, Andhey PS, Duncan D, Auclair K, et al. Comparative evaluation of itaconate and its derivatives reveals divergent inflammasome and type I interferon regulation in macrophages. Nat Metab. 2020;2(7):594-602.

156. Wang D, Zou L, Jin Q, Hou J, Ge G, Yang L. Human carboxylesterases: a comprehensive review. Acta Pharm Sin B. 2018;8(5):699-712.

157. Qin W, Zhang Y, Tang H, Liu D, Chen Y, Liu Y, et al. Chemoproteomic Profiling of Itaconation by Bioorthogonal Probes in Inflammatory Macrophages. J Am Chem Soc. 2020;142(25):10894-8.

158. Bourner LA, Chung LA, Long H, McGettrick AF, Xiao J, Roth K, et al. Endogenously produced itaconate negatively regulates innate-driven cytokine production and drives global ubiquitination in human macrophages. Cell Rep. 2024;43(8):114570.

159. Jiang H, Shi H, Sun M, Wang Y, Meng Q, Guo P, et al. PFKFB3-Driven Macrophage Glycolytic Metabolism Is a Crucial Component of Innate Antiviral Defense. J Immunol. 2016;197(7):2880-90.

160. Wang Q, Fang P, He R, Li M, Yu H, Zhou L, et al. O -GlcNAc transferase promotes influenza A virus–induced cytokine storm by targeting interferon regulatory factor–5. Sci Adv. 2020;6(16):eaaz7086.

161. Li T, Li X, Attri KS, Liu C, Li L, Herring LE, et al. O-GlcNAc Transferase Links Glucose Metabolism to MAVS-Mediated Antiviral Innate Immunity. Cell Host Microbe. 2018;24(6):791-803.e6.

162. Zhang W, Wang G, Xu ZG, Tu H, Hu F, Dai J, et al. Lactate Is a Natural Suppressor of RLR Signaling by Targeting MAVS. Cell. 2019;178(1):176-89.e15.

163. O'Carroll SM, Henkel FDR, O'Neill LAJ. Metabolic regulation of type I interferon production. Immunol Rev. 2024.

164. Ryan TAJ, Hooftman A, Rehill AM, Johansen MD, Brien ECO, Toller-Kawahisa JE, et al. Dimethyl fumarate and 4-octyl itaconate are anticoagulants that suppress Tissue Factor in macrophages via inhibition of Type I Interferon. Nat Commun. 2023;14(1):3513.

165. Ryan DG, Knatko EV, Casey AM, Hukelmann JL, Dayalan Naidu S, Brenes AJ, et al. Nrf2 activation reprograms macrophage intermediary metabolism and suppresses the type I interferon response. iScience. 2022;25(2):103827.

166. Yue YX, Jia BB, Wang JR, Weng YZ, Mao GX, Lu Y, et al. 4-Octyl itaconate inhibits poly(I:C)-induced interferon-β secretion in mouse bone marrow-derived macrophages partially by activating Nrf2. Heliyon. 2023;9(12):e23001.

167. Olagnier D, Brandtoft AM, Gunderstofte C, Villadsen NL, Krapp C, Thielke AL, et al. Nrf2 negatively regulates STING indicating a link between antiviral sensing and metabolic reprogramming. Nat Commun. 2018;9(1):3506.

168. Olagnier D, Farahani E, Thyrsted J, Blay-Cadanet J, Herengt A, Idorn M, et al. SARS-CoV2-mediated suppression of NRF2-signaling reveals potent antiviral and anti-inflammatory activity of 4-octyl-itaconate and dimethyl fumarate. Nat Commun. 2020;11(1):4938.

169. Waqas FH, Shehata M, Elgaher WAM, Lacour A, Kurmasheva N, Begnini F, et al. NRF2 activators inhibit influenza A virus replication by interfering with nucleo-cytoplasmic export of viral RNPs in an NRF2-independent manner. PLoS Pathog. 2023;19(7):e1011506.

170. Li W, Li Y, Kang J, Jiang H, Gong W, Chen L, et al. 4-octyl itaconate as a metabolite derivative inhibits inflammation via alkylation of STING. Cell Rep. 2023;42(3):112145.

171. Runtsch MC, Angiari S, Hooftman A, Wadhwa R, Zhang Y, Zheng Y, et al. Itaconate and itaconate derivatives target JAK1 to suppress alternative activation of macrophages. Cell Metab. 2022;34(3):487-501.e8.

172. Gobelli D, Serrano-Lorenzo P, Esteban-Amo MJ, Serna J, Pérez-García MT, Orduña A, et al. The mitochondrial succinate dehydrogenase complex controls the STAT3-IL-10 pathway in inflammatory macrophages. iScience. 2023;26(8):107473.

173. Cui A, Huang T, Li S, Ma A, Pérez JL, Sander C, et al. Dictionary of immune responses to cytokines at single-cell resolution. Nature. 2023.

174. Sin WX, Yeong JP, Lim TJF, Su IH, Connolly JE, Chin KC. IRF-7 Mediates Type I IFN Responses in Endotoxin-Challenged Mice. Front Immunol. 2020;11:640.

175. Gunderstofte C, Iversen MB, Peri S, Thielke A, Balachandran S, Holm CK, et al. Nrf2 Negatively Regulates Type I Interferon Responses and Increases Susceptibility to Herpes Genital Infection in Mice. Front Immunol. 2019;10:2101.

176. Peace CG, O'Carroll SM, O'Neill LAJ. Fumarate hydratase as a metabolic regulator of immunity. Trends Cell Biol. 2023.

177. Miyadera H, Shiomi K, Ui H, Yamaguchi Y, Masuma R, Tomoda H, et al. Atpenins, potent and specific inhibitors of mitochondrial complex II (succinate-ubiquinone oxidoreductase). Proc Natl Acad Sci U S A. 2003;100(2):473-7.

178. Sun F, Huo X, Zhai Y, Wang A, Xu J, Su D, et al. Crystal structure of mitochondrial respiratory membrane protein complex II. Cell. 2005;121(7):1043-57.

179. Herzner AM, Hagmann CA, Goldeck M, Wolter S, Kübler K, Wittmann S, et al. Sequence-specific activation of the DNA sensor cGAS by Y-form DNA structures as found in primary HIV-1 cDNA. Nat Immunol. 2015;16(10):1025-33.

180. Zylber E, Vesco C, Penman S. Selective inhibition of the synthesis of mitochondria-associated RNA by ethidium bromide. J Mol Biol. 1969;44(1):195-204.

181. Tallam A, Perumal TM, Antony PM, Jäger C, Fritz JV, Vallar L, et al. Gene Regulatory Network Inference of Immunoresponsive Gene 1 (IRG1) Identifies Interferon Regulatory Factor 1 (IRF1) as Its Transcriptional Regulator in Mammalian Macrophages. PLoS One. 2016;11(2):e0149050.

182. Naujoks J, Tabeling C, Dill BD, Hoffmann C, Brown AS, Kunze M, et al. IFNs Modify the Proteome of Legionella-Containing Vacuoles and Restrict Infection Via IRG1-Derived Itaconic Acid. PLoS Pathog. 2016;12(2):e1005408.

183. Schoggins JW, Wilson SJ, Panis M, Murphy MY, Jones CT, Bieniasz P, et al. A diverse range of gene products are effectors of the type I interferon antiviral response. Nature. 2011;472(7344):481-5.

184. Rai Y, Pathak R, Kumari N, Sah DK, Pandey S, Kalra N, et al. Mitochondrial biogenesis and metabolic hyperactivation limits the application of MTT assay in the estimation of radiation induced growth inhibition. Sci Rep. 2018;8(1):1531.

185. Losman JA, Koivunen P, Kaelin WG. 2-Oxoglutarate-dependent dioxygenases in cancer. Nat Rev Cancer. 2020;20(12):710-26.

186. Gill AJ. Succinate dehydrogenase (SDH)-deficient neoplasia. Histopathology. 2018;72(1):106-16.

187. Gudgeon N, Munford H, Bishop EL, Hill J, Fulton-Ward T, Bending D, et al. Succinate uptake by T cells suppresses their effector function via inhibition of mitochondrial glucose oxidation. Cell Rep. 2022;40(7):111193.

188. Cheon H, Holvey-Bates EG, McGrail DJ, Stark GR. PD-L1 sustains chronic, cancer cell-intrinsic responses to type I interferon, enhancing resistance to DNA damage. Proc Natl Acad Sci U S A. 2021;118(47).

189. Guarda G, Braun M, Staehli F, Tardivel A, Mattmann C, Förster I, et al. Type I interferon inhibits interleukin-1 production and inflammasome activation. Immunity. 2011;34(2):213-23.

190. Murphy MP, O'Neill LAJ. A break in mitochondrial endosymbiosis as a basis for inflammatory diseases. Nature. 2024;626(7998):271-9.

191. Kong LZ, Kim SM, Wang C, Lee SY, Oh SC, Lee S, et al. Understanding nucleic acid sensing and its therapeutic applications. Exp Mol Med. 2023;55(11):2320-31.

192. Zhan X, Cui R, Geng X, Li J, Zhou Y, He L, et al. LPS-induced mitochondrial DNA synthesis and release facilitate RAD50-dependent acute lung injury. Signal Transduct Target Ther. 2021;6(1):103.

193. Casey AM, Murphy MP. Uncovering the source of mitochondrial superoxide in pro-inflammatory macrophages: Insights from immunometabolism. Biochim Biophys Acta Mol Basis Dis. 2022;1868(10):166481.

194. Zorova LD, Popkov VA, Plotnikov EY, Silachev DN, Pevzner IB, Jankauskas SS, et al. Mitochondrial membrane potential. Anal Biochem. 2018;552:50-9.

195. Marques E, Kramer R, Ryan DG. Multifaceted mitochondria in innate immunity. NPJ Metab Health Dis. 2024;2(1):6.

196. Koshiba T, Yasukawa K, Yanagi Y, Kawabata S. Mitochondrial membrane potential is required for MAVS-mediated antiviral signaling. Sci Signal. 2011;4(158):ra7.

197. Ben-Hail D, Begas-Shvartz R, Shalev M, Shteinfer-Kuzmine A, Gruzman A, Reina S, et al. Novel Compounds Targeting the Mitochondrial Protein VDAC1 Inhibit Apoptosis and Protect against Mitochondrial Dysfunction. J Biol Chem. 2016;291(48):24986-5003.

198. Chouchani ET, Pell VR, Gaude E, Aksentijević D, Sundier SY, Robb EL, et al. Ischaemic accumulation of succinate controls reperfusion injury through mitochondrial ROS. Nature. 2014;515(7527):431-5.

199. Brennan MS, Matos MF, Li B, Hronowski X, Gao B, Juhasz P, et al. Dimethyl fumarate and monoethyl fumarate exhibit differential effects on KEAP1, NRF2 activation, and glutathione depletion in vitro. PLoS One. 2015;10(3):e0120254.

200. Kornberg MD, Bhargava P, Kim PM, Putluri V, Snowman AM, Putluri N, et al. Dimethyl fumarate targets GAPDH and aerobic glycolysis to modulate immunity. Science. 2018;360(6387):449-53.

201. Wu Q, Wang Q, Mao G, Dowling CA, Lundy SK, Mao-Draayer Y. Dimethyl Fumarate Selectively Reduces Memory T Cells and Shifts the Balance between Th1/Th17 and Th2 in Multiple Sclerosis Patients. J Immunol. 2017;198(8):3069-80.

202. Selman M, Ou P, Rousso C, Bergeron A, Krishnan R, Pikor L, et al. Dimethyl fumarate potentiates oncolytic virotherapy through NF-κB inhibition. Sci Transl Med. 2018;10(425).

203. Kurmasheva N, Said A, Wong B, Kinderman P, Han X, Rahimic AHF, et al. Octyl itaconate enhances VSVΔ51 oncolytic virotherapy by multitarget inhibition of antiviral and inflammatory pathways. Nat Commun. 2024;15(1):4096.

204. Ribó-Molina P, Weiss HJ, Susma B, van Nieuwkoop S, Persoons L, Zheng Y, et al. 4-Octyl itaconate reduces influenza A replication by targeting the nuclear export protein CRM1. J Virol. 2023;97(10):e0132523.

205. Liao ST, Han C, Xu DQ, Fu XW, Wang JS, Kong LY. 4-Octyl itaconate inhibits aerobic glycolysis by targeting GAPDH to exert anti-inflammatory effects. Nat Commun. 2019;10(1):5091.

206. Chen F, Lukat P, Iqbal AA, Saile K, Kaever V, van den Heuvel J, et al. Crystal structure of *cis*-aconitate decarboxylase reveals the impact of naturally occurring human mutations on itaconate synthesis. Proc Natl Acad Sci U S A. 2019;116(41):20644-54.

Publications

nature metabolism

Letter

https://doi.org/10.1038/s42255-024-01145-1

Itaconate drives mtRNA-mediated type I interferon production through inhibition of succinate dehydrogenase

Received: 11 April 2024

Accepted: 19 September 2024

Published online: 15 October 2024

Check for updates

Shane M. O'Carroll[1,7], Christian G. Peace[1,7], Juliana E. Toller-Kawahisa[1], Yukun Min[1], Alexander Hooftman[1], Sara Charki[1], Louise Kehoe[2], Maureen J. O'Sullivan[2,3], Aline Zoller[1], Anne F. Mcgettrick[1], Alessia Zotta[1], Emily A. Day[1], Maria Simarro[4,5], Neali Armstrong[6], Justin P. Annes[6] & Luke A. J. O'Neill[1] ✉

Itaconate is one of the most highly upregulated metabolites in inflammatory macrophages and has been shown to have immunomodulatory properties. Here, we show that itaconate promotes type I interferon production through inhibition of succinate dehydrogenase (SDH). Using pharmacological and genetic approaches, we show that SDH inhibition by endogenous or exogenous itaconate leads to double-stranded mitochondrial RNA (mtRNA) release, which is dependent on the mitochondrial pore formed by VDAC1. In addition, the double-stranded RNA sensors MDA5 and RIG-I are required for IFNβ production in response to SDH inhibition by itaconate. Collectively, our data indicate that inhibition of SDH by itaconate links TCA cycle modulation to type I interferon production through mtRNA release.

Itaconate is one of the most upregulated metabolites in inflammatory macrophages[1]. Itaconate is synthesized through the decarboxylation of the tricarboxylic acid (TCA) cycle intermediate *cis*-aconitate by the enzyme aconitate decarboxylase 1 (ACOD1). ACOD1 is encoded by immune-responsive gene 1 (*Irg1*), expression of which is induced by several inflammatory stimuli[2]. Although many studies have identified mechanisms by which itaconate regulates macrophage function[3], how it exerts its immunomodulatory effects remains to be fully elucidated.

Two such mechanisms of action of itaconate in cells include the inhibition of mitochondrial complex II, also known as succinate dehydrogenase (SDH)[1,4–7], and the post-translational modification of cysteine thiols through a process termed 2,3-dicarboxypropylation. Itaconate has been found to regulate processes such as Nrf2 activation[1], inflammasome activation[8], aerobic glycolysis[9,10], alternative macrophage activation[11] and lysosomal biogenesis[12]. Because it had been unclear whether macrophages could take up extracellular itaconate, esterified derivatives with increased membrane permeability were synthesized to elucidate the intracellular mechanisms of action of itaconate. These derivatives include dimethyl-itaconate (DI) and 4-octyl-itaconate (4-OI), which are more electrophilic than underivatized itaconate. It has since been demonstrated that itaconate can exit macrophages through the ATP-binding cassette transporter G2 (ABCG2)[13] and can subsequently be taken up by macrophages[5].

Itaconate competitively inhibits succinate dehydrogenase (SDH), preventing oxidation of succinate to fumarate[4]. In previous work, inhibition of SDH by itaconate has led to succinate accumulation and, importantly, the inhibition of *Il1b* transcription[5,8]. Mechanistically, inhibiting SDH activity prevents reverse electron transport (RET) and reduces production of reactive oxygen species (ROS)[14], thereby decreasing hypoxia-inducible factor 1-α (HIF1α)-mediated

[1]School of Biochemistry and Immunology, Trinity Biomedical Sciences Institute, Trinity College Dublin, Dublin, Ireland. [2]Histology Lab, Children's Health Ireland at Crumlin, Dublin, Ireland. [3]Departments of Histopathology and Paediatrics, Trinity College Dublin, Dublin, Ireland. [4]Department of Cell Biology, Genetics, Histology and Pharmacology, Faculty of Medicine, University of Valladolid, Valladolid, Spain. [5]Unit of Excellence Institute of Biomedicine and Molecular Genetics (IBGM), University of Valladolid and Spanish National Research Council (CSIC), Valladolid, Spain. [6]Department of Medicine, Division of Endocrinology, Stanford School of Medicine, Stanford, CA, USA. [7]These authors contributed equally: Shane M. O'Carroll, Christian G. Peace.
✉e-mail: laoneill@tcd.ie

https://doi.org/10.1038/s42255-024-01145-1

Il1b transcription[15]. However, the full consequences of SDH inhibition by itaconate are yet to be explored. Here, we provide evidence that SDH inhibition by itaconate is required for type I interferon (type I IFN) production in macrophages in response to lipopolysaccharide (LPS), a product of Gram-negative bacteria. We show that this is due to mtRNA release through VDAC1 pores on the mitochondrial membrane, which signals through RIG-I and MDA5, to upregulate type I IFN production. Our work establishes a link from the TCA cycle to IFNs through SDH inhibition by itaconate.

Results

Itaconate boosts LPS-driven IFNβ production

We first aimed to uncover the main pathways regulated by itaconate in inflammatory macrophages by treating LPS-stimulated murine bone-marrow-derived macrophages (BMDMs) with underivatized itaconate, followed by RNA sequencing (RNA-seq). Using the recently developed bioinformatic tool Immune Response Enrichment Analysis (IREA)[16], which has been refined for studying immune processes, we employed RNA sequencing to determine which cytokine signaling pathways are regulated by itaconate in BMDMs. We found that IFNα and IFNβ were among the most actively signaling cytokines in itaconate-treated macrophages (Fig. 1a). We also observed widespread transcriptomic effects, demonstrating that itaconate has multifaceted roles as an immunometabolite (Extended Data Fig. 1a,b). Consistent with previous literature[1], we found that itaconate suppressed transcription of inflammatory genes (Extended Data Fig. 1c); we also found an upregulation of Nrf2-dependent genes (Extended Data Fig. 1d), illustrating the immunoregulatory properties of itaconate.

Additionally, itaconate treatment boosted LPS-induced IFNβ release (Fig. 1b) and transcription (Fig. 1c), consistent with previous observations by Swain et al.[5]. This effect was conserved in human macrophages, which also produced higher levels of *IFNB* in response to itaconate (Fig. 1d). The effect of itaconate contrasts with the more electrophilic compound 4-octyl itaconate (4-OI) which, as we have shown previously, inhibits the production of IFNβ[1,5] (Extended Data Fig. 2a,b) in a similar manner to the Nrf2 activators diethyl maleate (DEM) (Extended Data Fig. 2c) and dimethyl fumarate (DMF) (Extended Data Fig. 2d). Any effect of 4-OI, or 4-OI-derived itaconate, on SDH is likely to be overcome by 4-OI being more reactive to cysteines, for example those in JAK1; 4-OI and itaconate might also block IFNs through activation of Nrf2 (ref. 11). Furthermore, *Irg1*$^{-/-}$ BMDMs, which lack itaconate, produced less IFNβ than did *Irg1*$^{+/+}$ BMDMs in response to LPS (Fig. 1e and Extended Data Fig. 1e). Genetic ablation of *IRG1* in human peripheral blood mononuclear cells (PBMCs) also caused a reduction in IFNβ production in response to a combination of LPS and IFNγ (Fig. 1f and Extended Data Fig. 1f).

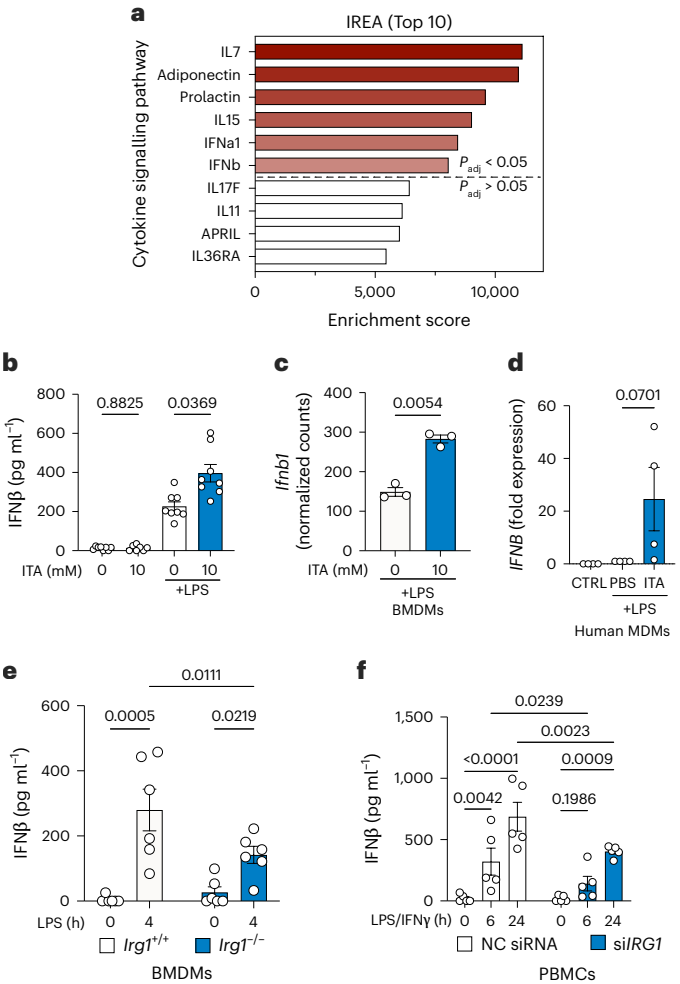


Fig. 1 | Itaconate boosts LPS-mediated IFNβ expression in macrophages. **a**, IREA plot of RNA-seq data of significantly (adjusted P (P_{adj}) < 0.05) differentially expressed genes in BMDMs pretreated with PBS or itaconate (10 mM, 3 h) (n = 3 mice; LPS 4 h). Data are from three independent experiments. **b**, IFNβ release from BMDMs pretreated with PBS itaconate (n = 8; LPS 16 h). Data are from three independent experiments. **c**, *Ifnb1* expression, determined through RNA-seq, in BMDMs pretreated with PBS or itaconate (n = 3 mice, LPS 4 h). Data are from three independent experiments. **d**, *IFNB* expression, assessed by quantitative PCR (qPCR), in human monocyte-derived macrophages (MDMs) pretreated with PBS or itaconate (ITA) (10 mM, 3 h) (n = 4 donors; LPS 4 h). Data are from two independent experiments **e**, IFNβ release from *Irg1*$^{+/+}$ versus *Irg1*$^{-/-}$ BMDMs (n = 6 mice; LPS 4 h). Data are from three independent experiments. **f**, IFNβ release (P = 0.0023) from human PBMCs with *IRG1* knockdown (n = 5 donors; LPS/IFNγ 24 h). NC siRNA, negative control siRNA. Data are from three independent experiments. In the graphs, data are shown as mean ± s.e.m. P values were calculated using one- or two-way analysis of variance (ANOVA).

SDH activity regulates production of type I interferon

Because itaconate is a well-characterized SDH inhibitor, we hypothesized that it could underlie its regulation of type I IFN through SDH inhibition; we have previously observed that inhibition of fumarate hydratase (FH) had this effect[17,18]. We first examined SDH activity in inflammatory macrophages. We found that LPS suppressed SDH activity in *Irg1*$^{+/+}$ BMDMs, but not in *Irg1*$^{-/-}$BMDMs (Fig. 2a), confirming the inhibition of SDH by endogenous itaconate. Furthermore, succinate failed to accumulate in *Irg1*$^{-/-}$ BMDMs, and levels of metabolites directly downstream of SDH were increased (Fig. 2b).

We then used 2-theoyltrifluoroacetone (TTFA) and Atpenin A5 (AA5), two specific and well-characterized pharmacological SDH inhibitors[19,20], to explore whether SDH inhibition could drive IFNβ expression. Both compounds enhanced *Ifnb1* transcription in LPS-activated macrophages (Fig. 2c,d). TTFA also increased IFNβ mRNA levels in human macrophages (Fig. 2e). Using a RAW.264 *Sdha*$^{-/-}$ macrophage cell line, we observed a major enhancement in IFNβ production over the course of LPS stimulation (Fig. 2f). Additionally, we generated a mouse model of tamoxifen-inducible *Sdhb* loss, and we generated BMDMs from these animals (Extended Data Fig. 3a). We found that BMDMs lacking *Sdhb* had decreased levels of *Il1b* expression, as expected (Extended Data Fig. 3b), as well as augmented levels of IFNβ release and transcription (Fig. 2g,h). To further characterize this phenotype, we performed RNA-seq using TTFA-treated BMDMs, in which we found profound transcriptomic changes (Extended Data Fig. 1a). We compared itaconate and TTFA-treated BMDM transcriptomic data and found many commonly upregulated IFN-dependent genes (Fig. 2i), further indicating that SDH inhibition by itaconate was responsible for the induction of type I IFN. TTFA also increased IFNβ levels in *Irg1*$^{-/-}$ BMDMs, further supporting a role for this pathway in a model of increased SDH activity (Extended Data Fig. 3c). Considering that mesaconate is a derivative of itaconate,

https://doi.org/10.1038/s42255-024-01145-1

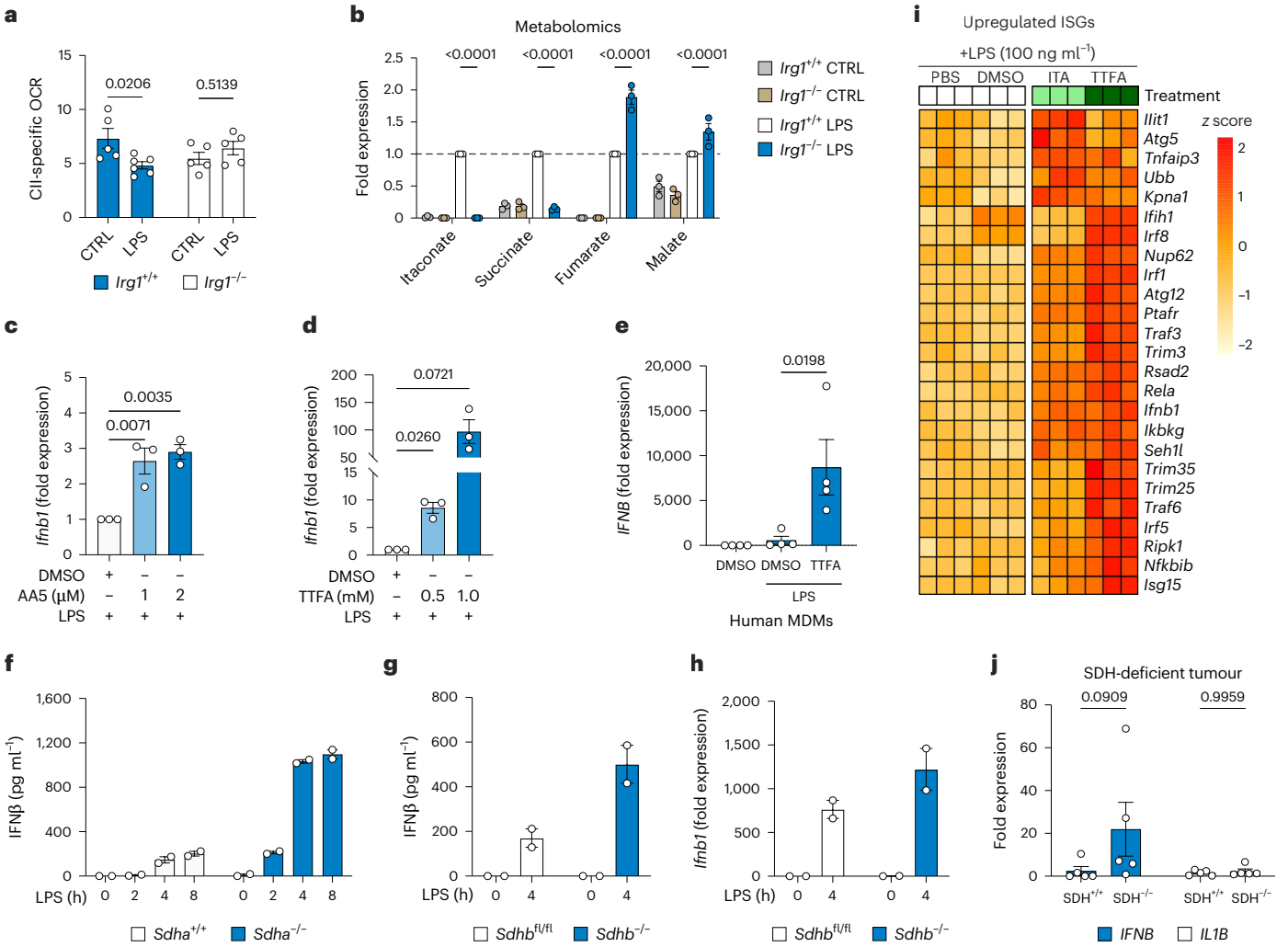


Fig. 2 | SDH inhibition boosts LPS-mediated IFNβ production in macrophages. a, Measurement of the complex II (CII)-specific oxygen consumption rate (OCR), assessed through a Seahorse assay, of *Irg1*$^{+/+}$ and *Irg1*$^{-/-}$ BMDMs ($n = 5$ technical replicates; LPS 24 h). Data are from one experiment. **b**, Metabolomics data showing relative expression of itaconate ($P = 4.15 \times 10^{-15}$), succinate ($P = 2.854.15 \times 10^{-13}$), fumarate ($P = 1.00 \times 10^{-13}$) and malate ($P = 3.38 \times 10^{-5}$) in *Irg1*$^{+/+}$ and *Irg1*$^{-/-}$ BMDMs. Data are from a publicly available dataset[17] ($n = 3$ mice; LPS 24 h). **c**,**d**, qPCR data on *Ifnb1* from BMDMs pretreated with AA5 (**c**), TTFA (**d**) or DMSO (3 h) ($n = 3$ mice, LPS 4 h). Data are from three independent experiments. **e**, *IFNB* expression, assessed by qPCR, in human MDMs pretreated with DMSO or TTFA (0.5 mM; 3 h) ($n = 4$ donors; LPS 4 h). Data are from two independent experiments **f**, IFNβ release in *Sdha*$^{+/+}$ and *Sdha*$^{-/-}$ RAW.264.7 macrophages ($n = 2$ mice; LPS). Data are from one experiment. **g**,**h**, IFNβ release (**g**) and *Ifnb1* expression (**h**) in BMDMs from *Sdhb*$^{fl/fl}$ and *Sdhb*$^{-/-}$ cells ($n = 2$ mice, LPS 4 h). Data are from one experiment. **i**, Heatmap showing relative expression (*z* score) of interferon-stimulated genes (ISGs) commonly upregulated in BMDMs following TTFA and itaconate treatment ($P_{adj} < 0.05$). ($n = 3$ mice, LPS 4 h). Data are from three independent experiments. **j**, *IFNB* and *IL1B* expression in SDH-deficient ($n = 5$ patients) and SDH-competent ($n = 5$ patients) tumor samples. In all graphs, data are presented as mean ± s.e.m. *P* values were calculated using a one- or two-way ANOVA.

we ruled out any potential effects of mesaconate itself, because it does not affect IFNβ expression (Extended Data Fig. 3d). Last, we examined SDH-deficient tumors versus site- and age-matched SDH-competent tumors. We found in these SDH-deficient samples an increase in *IFNB* expression but no change in *IL1B* expression, indicating that a specific IFN response was upregulated (Fig. 2j).

SDH inhibition activates cytosolic-RNA-sensing pathways

Next, we aimed to investigate how SDH inhibition by itaconate increases type I IFN responses. We performed pathway enrichment analysis of the commonly upregulated differentially expressed genes in itaconate- and TTFA-treated macrophages (Fig. 3a). Our results show, within the REACTOME analysis, that the 'DDX58/IFIH1-mediated Induction of IFN-α/β' stood out as a possible candidate pathway that could account for the upregulation of type I IFN (Fig. 3b). Additionally, Kyoto Encyclopedia of Genes and Genomes (KEGG) pathway enrichment analysis revealed a notable upregulation of the 'RIG-I-like receptor signalling pathway' (Fig. 3c), suggesting that RIG-I and MDA5 were possibly involved.

siRNAs targeting *Ddx58* (Extended Data Fig. 4a) and *Ifih1* (Extended Data Fig. 4b) led to inhibition of the TTFA-dependent increase of LPS-induced IFNβ production (Fig. 3d,e). We found that knockdown of cGAS (encoded by *Mb21d1*) (Extended Data Fig. 4c) or TLR9 (Extended Data Fig. 4d) did not affect IFNβ production, indicating that DNA sensing is unlikely to be involved in this process (Fig. 3d,e). Similarly, we showed that itaconate-mediated IFNβ release was also dependent on MDA5 and RIG-I and independent of cGAS (Fig. 3f and Extended Data Fig. 4e–g). We then confirmed that our siRNA approach successfully impaired the ability of the classical stimuli—cGAS, MDA5 and RIG-I—to induce IFN production, validating our method (Extended Data Fig. 4h–j). Further ruling out the role of DNA sensing in the system, we also found that knockdown of STING (encoded by *Tmem173*) had no effect on TTFA-induced IFNβ production (Extended Data Fig. 4k,l).

https://doi.org/10.1038/s42255-024-01145-1

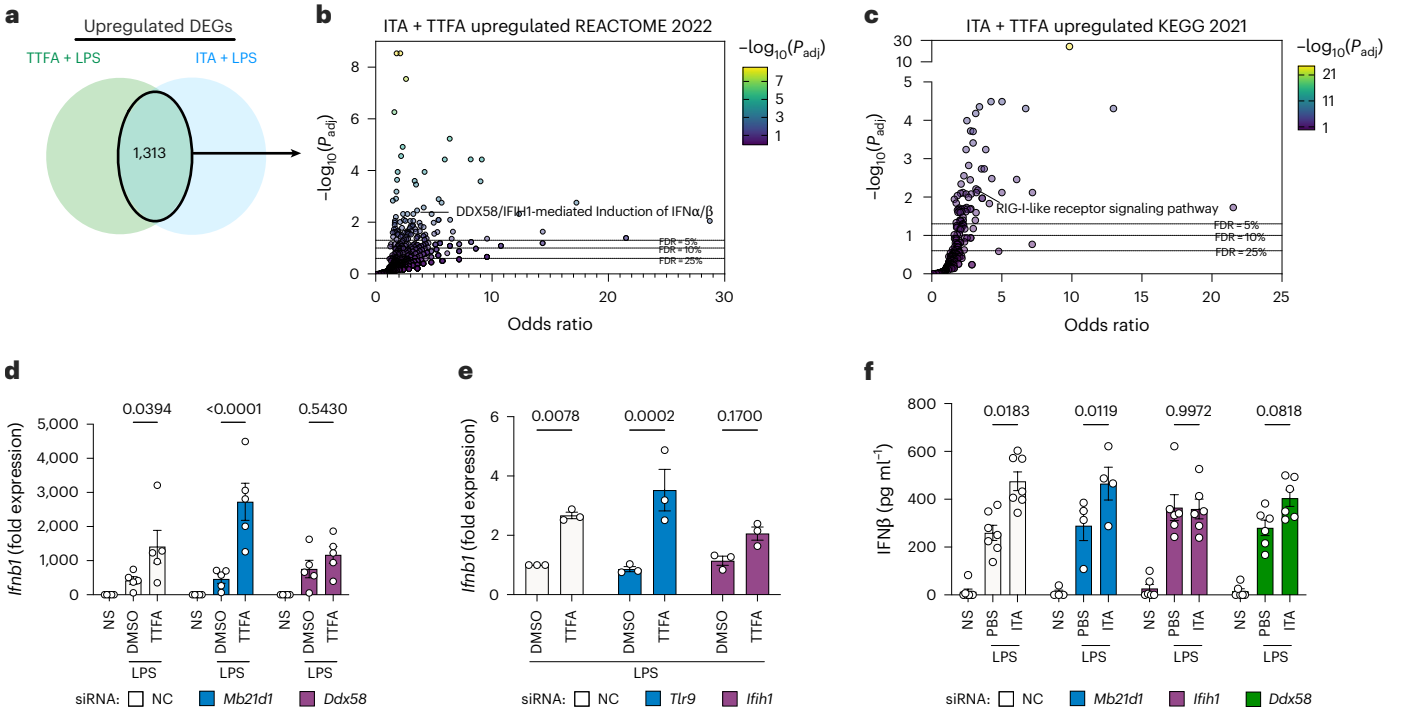


Fig. 3 | SDH inhibition increases IFNβ production through RIG-I- and MDA5-dependent signaling. a, Venn diagram showing the number of shared upregulated differentially expressed genes, determined by RNA-seq, between TTFA- and itaconate-treated BMDMs ($n = 3$ mice; LPS 4 h, $P_{adj} < 0.05$). **b**,**c**, REACTOME pathway enrichment analysis (**b**) and KEGG pathway enrichment analysis (**c**) of commonly upregulated differentially expressed genes between TTFA- and itaconate-treated BMDMs ($n = 3$ mice; LPS 4 h). Data are from three independent experiments. FDR, false discovery rate. **d**, *Ifnb1* expression after siRNA knockdown of *Mb21d1* ($P = 8.42 \times 10^{-10}$) and *Ddx58* in BMDMs pretreated with DMSO or TTFA ($n = 5$ mice; LPS 4 h). Data are from two independent experiments. **e**, *Ifnb1* expression after siRNA knockdown of *Tlr9* and *Ifih1* in BMDMs pretreated with DMSO or TTFA ($n = 3$ mice; LPS 4 h). Data are from three independent experiments. **f**, IFNβ release after treatment with NC siRNA (n = 7 mice) or siRNA targeting *Mb21d1* ($n = 4$ mice), *Ifih1* ($n = 6$) or *Ddx58* ($n = 6$ mice) in BMDMs pretreated with PBS or ITA (LPS 4 h). Data are from three independent experiments. In all graphs, data are presented as mean ± s.e.m. *P* values were calculated using two-way ANOVA.

SDH inhibition drives mtRNA release in a VDAC1-dependent manner

Recent research has shown that mitochondrial nucleic acids regulate type I IFN production by activating both RNA- and DNA-sensing pathways[21–23]. To confirm that mitochondrial nucleic acids are required for the increased IFNβ production with SDH inhibition, we used ethidium bromide to deplete mtRNA levels (Extended Data Fig. 5a). We found that, in the presence of ethidium bromide, the increase in IFNβ production due to TTFA was reduced (Fig. 4a), suggesting that mitochondrial nucleic acids are involved in the increase in type I IFN signaling with SDH inhibition. We then treated cells with IMT1, an inhibitor of the mitochondrial transcription factor POLRMT, which led to reduced expression of mtDNA-encoded genes (Extended Data Fig. 5b). In the presence of IMT1, itaconate could not increase *Ifnb1* levels (Fig. 4b), showing that the effect of itaconate on type I IFN requires mtRNA.

Considering that the increase in IFNβ expression in response to TTFA and itaconate seems to be dependent on cytosolic double-stranded RNA (dsRNA) sensors, we next investigated how these sensors were activated. Using digitonin to isolate the cytosolic from the organellar fraction within BMDMs (Extended Data Fig. 5c), we found that both itaconate and the SDH inhibitors TTFA and dimethyl malonate (DMM) enriched cytosolic mtRNA levels derived from the heavy (ND4 and ND5) and light (ND6) chains (Fig. 4c–e). Strikingly, we found an overall increase in the transcriptional levels of mtDNA-encoded RNAs in inflammatory macrophages, which could serve as a priming signal required to release mtRNA upon SDH inhibition (Fig. 4f).

We then examined how mtRNA is released from mitochondria into the cytosol. We first knocked down *Bax* and *Bak1* expression and found that TTFA could still increase IFNβ levels (Extended Data Fig. 5d). We also found that TTFA could increase IFNβ production after *Snx9* knockdown, whereas *Vdac1* knockdown abrogated the increase in IFNβ production (Fig. 4g and Extended Data Fig. 5e,f). This suggests that VDAC1 pores mediate mtRNA release upon SDH inhibition. To further examine this pathway, we used a well-characterized inhibitor of VDAC1 oligomerization, VBIT-4 (ref. 24), which also reduced IFNβ production in the presence of TTFA (Fig. 4h,i) and itaconate (Fig. 4j). Interestingly, we also found that SDH inhibition strongly increases mitochondrial membrane potential (MMP), as assessed by TMRM staining in immunofluorescence (Extended Data Fig. 5g). This process might be responsible for mtRNA release and VDAC1 oligomerization, given that previous reports have found that other methods of increasing MMP levels, such as FH inhibition and ATP synthase inhibition, resulted in mtRNA release and type I IFN production[17]. This also demonstrates that VDAC1 is directly required for the release of mtRNA into the cytosol by itaconate, as VBIT-4 impaired the accumulation of cytosolic mtRNAs in response to itaconate (Fig. 4k). We next examined whether the release of mtRNA was regulated by endogenously produced itaconate. Treatment of BMDMs with LPS for 48 h induced the release of mtRNA into the cytosol (Fig. 4l). We also found that cytosolic mtRNA levels were reduced in LPS-activated *Irg1*$^{-/-}$ BMDMs (Fig. 4m), suggesting that endogenously produced itaconate is sufficient to activate this pathway and regulate IFN production. Overall, we found that inhibition of SDH by itaconate promotes mtRNA release through VDAC1 to drive type I IFN through RIG-I and MDA5, as represented in Figure 4n.

Discussion

It is now widely understood that TCA cycle metabolites can act as immunomodulatory signals that regulate cytokine production, reclassifying

https://doi.org/10.1038/s42255-024-01145-1

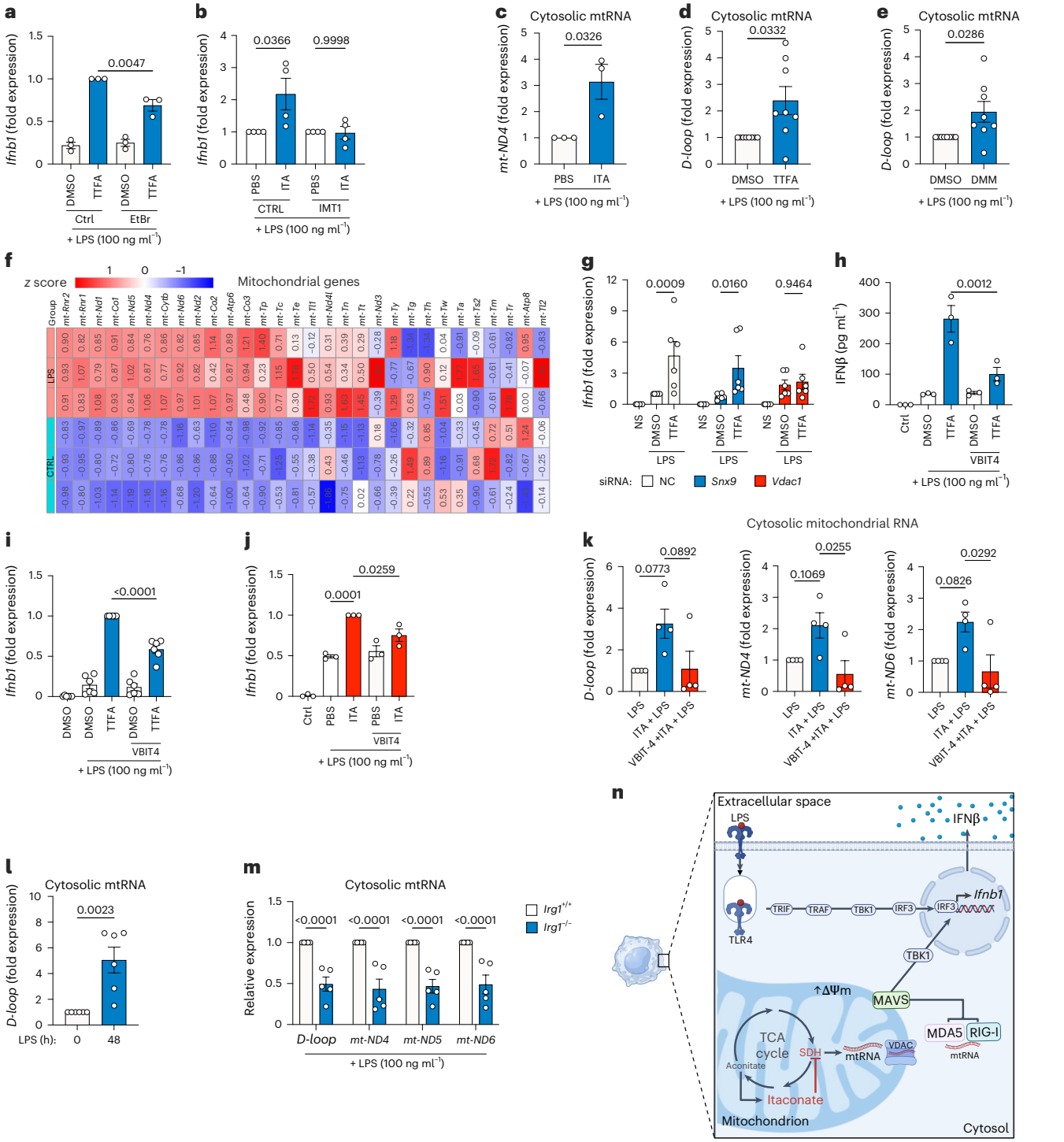


Fig. 4 | SDH inhibition drives mtRNA release in a VDAC1-dependent manner. **a**, *Ifnb1* expression in BMDMs in control or ethidium bromide (EtBr)-containing medium pretreated with DMSO or TTFA (n = 3 mice; LPS 4 h). Data are from three independent experiments. **b**, *Ifnb1* expression in BMDMs pretreated with DMSO, IMT1, PBS or ITA ($n = 4$ mice; LPS 4 h). Data are from two independent experiments. **c**, *mt-ND4* expression in the isolated cytosolic fraction of BMDMs pretreated with PBS or ITA ($n = 3$ mice; LPS 4 h). Data are from three independent experiments. **d**,**e**, Expression of the *D-loop* region of mtDNA in the isolated cytosolic fraction of BMDMs pretreated with DMSO, TTFA (**d**) or DMM (**e**) ($n = 8$ mice; LPS 4 h). Data are from three independent experiments. **f**, Heatmap of RNA-seq data for mitochondrial genes in BMDMs pretreated with ITA or TTFA ($n = 3$ mice; LPS 4 h). Data are from three independent experiments. **g**, *Ifnb1* expression in the presence of NC siRNA or siRNA targeting *Snx9* or *Vdac1* in BMDMs pretreated with DMSO ($n = 6$ mice; LPS 4 h). Data are from three independent experiments. **h**,**i**, IFNβ release (**h**) and *Ifnb1* expression ($P = 2.13 \times 10^{-11}$) (**i**) in BMDMs pretreated with VBIT-4 (16 h), DMSO or TTFA. **h**, ($n = 3$ mice; LPS 4 h); **i**, ($n = 6$ mice; LPS 4 h). Data are from three independent experiments. **j**, *Ifnb1* expression in BMDMs pretreated with DMSO or VBIT-4 (16 h) followed by PBS or ITA pretreatment ($n = 3$ mice; LPS 4 h). **k**, *D-loop*, *mt-ND4* and *mt-ND6* expression in the isolated cytosolic fraction of BMDMs pretreated with DMSO or VBIT-4 (16 h) followed by PBS or ITA pretreatment ($n = 4$; LPS 4 h). Data are from three independent experiments. **l**, D-loop expression in the cytosolic fraction of BMDMs (n = 6; LPS 48 h). Data are from three independent experiments. **m**, Expression of D-loop ($P = 2.32 \times 10^{-5}$), *mt-Nd4* ($P = 4.22 \times 10^{-6}$), *mt-Nd5* ($P = 1.10 \times 10^{-5}$) and *mt-ND6* ($P = 2.03 \times 10^{-5}$) in the cytosolic fraction of $Irg1^{+/+}$ and $Irg1^{-/-}$ BMDMs ($n = 5$ mice; LPS 24 h). Data are from three independent experiments. **n**, Schematic of the mechanism underlying how SDH impairment leads to increased IFNβ production. The figure was created with BioRender.com. Data in graphs are presented as mean ± s.e.m. *P* values were calculated using one or two-way ANOVA for multiple comparisons or two-tailed Student's *t*-test for pairwise comparisons.

them as 'immunometabolites.' Specifically, several reports have explored the TCA cycle and the regulation of IFN production[25].

Focusing on further understanding the role of itaconate in macrophage biology, we provide evidence that itaconate is an endogenous regulator of mtRNA release and type I IFN production. In our unbiased approach, production of type I IFN stood out as a pathway regulated by itaconate. Itaconate boosted LPS-mediated IFNβ expression in murine and human macrophages. Additionally, genetic ablation of the IRG1–itaconate pathway abrogated type I IFN production in LPS-stimulated macrophages and PBMCs. Pharmacological and genetic approaches targeting SDH indicated that SDH inhibition by itaconate is responsible for this effect.

Mitochondria are currently being repositioned as more than just organelles involved in bioenergetics, but as dynamic and multifaceted organelles of endosymbiotic origin with multiple behaviors, functions and activities[26,27]. Mitochondrial release of nucleic acids has been shown to occur in numerous contexts, including apoptosis, inflammatory diseases, mtDNA stress through TFAM deficiency, inflammasome activation and infection[28]. They consist of mtRNA and mtDNA. mtdsDNA can activate AIM2, NLRP3, cGAS and TLR9 DNA sensors, whereas mtRNA can activate RNA sensors, such as RIG-I and MDA-5, to boost IFNβ and cytokine production[29].

Dysregulation of mitochondrial metabolic enzymes, such as FH, has also been shown to cause the release of mtRNA into the cytosol to boost IFNβ production[17,30]. This led us to examine whether SDH inhibition by itaconate drives mtRNA release, which could be responsible for increased levels of IFNβ.

Initially, data suggested that itaconate was a negative regulator of type I IFN production[1,31]. However, this was based on evidence from derivatized itaconate (4-OI and DI), which is more electrophilic and cysteine-reactive than endogenous itaconate[1,5]. Although 4-OI can be directly converted to itaconate once inside macrophages[8], a large proportion of 4-OI likely remains esterified, given that many mass-spectrometry studies have identified modification of cysteine residues by 4-OI itself[1,8]. Furthermore, 4-OI is used in the µM range in vitro, which is insufficient to outcompete physiological levels of succinate[6]. Mechanistically, the suppression of type I IFN production by derivatives is not fully understood, although evidence suggests the activation of Nrf2 is involved[32]. Notably, at concentrations typically used, a crucial discrepancy between underivatized itaconate and 4-OI and DI is that the derivatives failed to increase intracellular levels of succinate and inhibit SDH[5]. Our observation in *Irg1*$^{-/-}$ BMDMs, consistent with data presented in Swain et al.[5], shows decreased IFNβ levels in cells lacking endogenous itaconate. Therefore, inhibition of SDH by itaconate, a property first described more than six decades ago[33], regulates production of type I IFN.

Mechanistically, we suggest that SDH inhibition by itaconate increases production of type I IFN through the activation of cytosolic dsRNA-sensing pathways, which were revealed by Gene Set Enrichment Analysis to be activated by TTFA and itaconate treatment. Furthermore, genetic ablation of RIG-I and MDA5 blocked the ability of TTFA and itaconate to upregulate type I IFN production, whereas DNA-sensing pathways were dispensable. As we see more of a dependency on MDA5 signaling, this suggests the role for longer strand dsRNA in response to itaconate. We found increased mtRNA present in the cytosol when SDH was impaired. Strikingly, *Irg1*$^{-/-}$ BMDMs show a decrease in cytosolic mtRNA levels, indicating that this is an endogenous process mediated by itaconate. To investigate how mtRNA is released, genetic knockdown of the mitochondrial transporter VDAC1, as well as pharmacological inhibition of VDAC pore formation with VBIT-4, blocked the release of mtRNA and the induction of IFNβ expression driven by SDH inhibition and itaconate. This demonstrates that itaconate induces the release of mtRNA by triggering the formation of VDAC1 pores.

Our work therefore adds to the understanding of itaconate as an immunomodulatory metabolite (Fig. 4n). Inhibition of SDH by itaconate is an endogenous process that is essential for metabolic reprogramming in inflammatory macrophages, leading to type I IFN production. This process could play a role in infection or inflammatory diseases, whereby itaconate and type I IFNs are dysregulated. Indeed, previous work has shown that itaconate is an anti-viral metabolite and that this process might involve SDH inhibition[34–36]. Our work also extends to other disease contexts in which SDH is inhibited, such as cancer, and could reveal a new therapeutic target for SDH-deficient tumors. Although our study uncovers a new pathway by which itaconate regulates type I IFN production, further studies are required to investigate the potential impacts of this pathway in the context of infection or inflammation wherein itaconate is highly upregulated.

Methods

Animal details

Wild-type (WT) mice for most in vitro experiments were on a C57BL/6JOlaHsd background. WT mice were bred in house or purchased from Harlan laboratories. *Irg1*$^{-/-}$ mice (named C57BL/6N-Acod1$^{em1(IMPC)J}$/J) were generated through CRISPR-targeted deletion of exon 4 of *Acod1*. These mice were purchased from The Jackson Laboratory. The *Sdhb*$^{fl/fl}$ mice were donated by N. Armstrong, and *R26-Cre-ERT2* mice were purchased from The Jackson Laboratory. Experimental mice were homozygous for the conditional LoxP *Sdhb* allele and expressed the Cre recombinase–ERT2 fusion under control of the *Rosa26* promoter (*Sdhb*$^{fl/fl}$*; R26 CreERT2/CreERT2*). In vitro experiments, which were performed on BMDMs, were done in 6- to 18-week-old female mice.

Generation of BMDMs

Mice (6–18 weeks old) were euthanized using CO_2, and cervical dislocation was used to confirm death; immediately afterwards, bone marrow was flushed from the tibia, femur and ilium, and collected cells were differentiated in DMEM medium containing L929 supernatant (20%), fetal calf serum (FCS) (10%) and antibiotics (penicillin–streptomycin) (1%) for 6 days. The differentiated BMDMs were then counted and plated at 0.5×10^6 cells ml^{-1}, unless stated otherwise. BMDMs were plated in 12- or 6-well cell culture plates and left to adhere for at least 12 hours before experiments. After replating BMDMs from *Sdhb*$^{fl/fl}$*; R26 CreERT2/CreERT2* mice, cells were cultured in DMEM containing 4-hydroxytamoxifen (100 uM) for 72 h before LPS stimulation.

Generation of human PBMCs and macrophages

Blood samples from healthy donors were collected and processed at the School of Biochemistry and Immunology at the Trinity Biomedical Sciences Institute (TCD). Blood was donated and obtained anonymously. Written informed consent for the use of blood for research purposes was given from the donors. Procedures for experiments using human blood were approved by the School of Biochemistry and Immunology Research Ethics Committee (TCD). All experiments were conducted according to the TCD guide on good research practice, which follows the guidelines detailed in the National Institutes of Health Belmont Report (1978) and the Declaration of Helsinki. Whole blood (30 ml) was layered on 20 ml Lymphoprep (Axis-Shield) and centrifuged for 20 min at 400*g* without the brake on. The upper plasma layer was then discarded, and the white layer of PBMCs at the plasma-density-gradient medium interface was retained, and 20 ml PBS was subsequently added. Cells were centrifuged for 8 min at 300*g*, after which the supernatant was discarded. The pelleted PBMCs were then resuspended in RPMII, counted using an automated cell counter and plated at 1×10^6 cells ml^{-1} in RPMI supplemented with FCS (10%) and antibiotics (penicillin–streptomycin) (1%).

Once PBMCs were obtained, CD14$^+$ monocytes were isolated using a MagniSort Human CD14 Positive Selection kit (Thermo Fisher), according to the manufacturer's protocol. Human monocytes were then differentiated in T175 flasks in RPMI containing FCS (10%), antibiotics (penicillin–streptomycin) (1%) and recombinant human macrophage

colony-stimulating factor (1:1,000). After 6 days of differentiation, the supernatant was removed, and remaining monocyte-derived macrophages were scraped and counted, and human monocyte-derived macrophages were plated in 12-well plates at 1×10^6 cells ml^{-1} in RPMI containing FCS (10%) and antibiotics (penicillin– streptomycin) (1%).

SDH-deficient tumor samples

Tissue excess to diagnostic requirements, from SDH-deficient ($n = 5$) and sex-, age- and anatomical-site-matched SDH-competent ($n = 5$) tumors, were used with consent or assent from the donor or their guardian. Consent or assent was obtained following approval of the study by the Medical and Research Ethics Committee at Children's Health Ireland. RNA was extracted in the diagnostic Histology Laboratory at Children's Health Ireland from these tumors for use in qPCR, as described. SDHB immunohistochemistry was performed on the diagnostic tissue, prompting confirmatory germline genetic testing and review by the clinical geneticist, where the tumor immunoreactivity for SDHB was lost.

Cell-line details

Generation of macrophages from THP1 cell lines. THP1 cell lines were donated by F. Dorsay at Eli Lilly and Company. Cells were maintained at a concentration range between 5×10^5 and 1.0×10^6 cells ml^{-1} in RPMI–glutamax medium with 10% FCS, 1% penicillin–streptomycin and 55 µM β-mercaptoethanol. Cells were plated at 0.5×10^6 cells ml^{-1} and treated with 100 ng ml^{-1} PMA for 48 h for macrophage differentiation. Cells were then treated.

SDHA RAW 264.7 cells. Cell lines were donated by M. Simarro, as described in ref. 37. SDHA RAW 264.7 cell lines were maintained in DMEM, 10% FCS and 1% penicillin–streptomycin. Cells were scraped in PBS and centrifuged at 500*g* for 5 min, and were then resuspended and counted. Cells were plated at 0.5×10^6 cells ml^{-1} and left overnight. Cells were then treated.

Reagents. LPS was obtained from *Escherichia coli* serotype EH100 (ALX-581-010-L001), which was acquired from Enzo Life Sciences. High-molecular-weight (HMW) poly(I:C) (tlrl-pic), G3-YSDctrl (tlrl-ydnac), G3-YSD (tlrl-ydna), 5′ppp-dsRNA-control (tlrl-3prnac) and 5′ppp-dsRNA (tlrl-3prna) were purchased from Invivogen. DMSO (D8418), itaconate (I29204-100G), DMM (136441-250g) and DEM (D97703-100G) were all purchased from Sigma-Aldrich. DMF (HY-17363), TTFA (HY-D0190), IMT1 (HY-134539), VBIT-4 (HY-129122) and AA5 (HY-126653) were purchased from MedChemExpress. IFN was purchased from ImmunoTools (11343536).

Compound treatments. All compounds used DMSO as a vehicle, unless otherwise stated. DMM was diluted in ethanol, and itaconate was prepared in PBS. LPS was used at a concentration of 100 ng ml^{-1}, unless otherwise specified, for the indicated time points (in figure legends). HMW Poly(I:C), 5′-PPP-ctrl, 5′-PPP-dsRNA, G3-YSD-ctrl and G3-YSD were transfected at the indicated concentrations using lipofectamine RNAiMax for 6 h. TTFA (500 µM), IMT1 (10 µM), DMM (5 mM), DEM (100 uM), ITA (1-10 mM), 4-OI (62.5–250 µM), DMF (25 µM) and AA5 (1 and 2 µM) pretreatments were performed for 3 h before the addition of LPS. VBIT-4 (10 uM) was used for 16 h before treatment with other compounds.

RT–qPCR. RNA extraction from cells was performed using the Purelink RNA kit (Invitrogen), according to the manufacturer's instructions. BMDMs were treated as required and immediately lysed in 350 µl of RNA lysis buffer. Isolated RNA was quantified using a NanoDrop 2000 spectrophotometer, and the RNA concentration was normalized to the lowest concentration across all samples using RNase-free water. If needed, samples were treated with DNase I (Thermo Fisher) after quantification, following the manufacturer's guidelines. Isolated RNA was then normalized and converted into cDNA using the High-Capacity cDNA Reverse Transcription kit (Thermo Fisher), as directed. Next, 10 µl of RNA (maximum concentration of 100 ng µl^{-1}) was mixed with 10 µl of reverse transcription master mix to complete the reaction. Real-time qPCR (RT–qPCR) was conducted on the resulting cDNA using primers designed in-house and ordered from Eurofins Genomics, as detailed in Supplementary Table 1. The reaction was performed in a 96-well qPCR plate using the 7500 Fast Real-Time PCR machine (Thermo Fisher). Relative expression ($2^{-\Delta\Delta CT}$) was calculated from the CT values for each sample and gene of interest.

RNA interference in BMDMs. Pre-designed silencer select siRNAs were used, targeting *Cgas* (s103166), *Tmem173* (s91058), *Tlr9* (s96268), *Ddx58* (s106376), *Ifih1* (s89787), *Vdac1* (s75920), *Snx9* (s83576), *Bak1* (s62859) or *Bax* (s62874); and NC siRNA (4390843) was also used. These were ordered from Thermo Fisher. BMDMs were transfected with 50 nM siRNA using 5 µl Lipofectamine RNAiMAX, according to the manufacturer's instructions (Thermo Fisher). BMDMs were transfected in DMEM without serum and antibiotics, which was replaced with a complete medium after 8 h. BMDMs were then left for at least a further 12 h before experiments.

RNA interference in PBMCs. Anonymized untransfused blood samples were obtained from the Irish Blood Transfusion Board. The School of Biochemistry and Immunology Research Ethics Committee (TCD) approved all the procedures involving experiments on human samples, which were conducted according to the TCD guide on good research practice. Thirty milliliters of whole blood was layered on 20 ml Lymphoprep (Axis-Shield), followed by centrifugation for 20 min at 400*g* with the brake off, after which the upper plasma layer was removed and discarded. The mononuclear layer at the plasma-density gradient medium interface was retained, and 20 ml PBS was added. Cells were centrifuged for 8 min at 300*g*, and the resulting supernatant was removed and discarded. The remaining pellet of mononuclear cells was resuspended and counted, and 1×10^6 cells per point were used for siRNA transfection. The cells were resuspended in nucleofector buffer along with five pmol siRNA (*IRG1* (s60727)) and pulsed using the Y-010 program on the AMAXA nucleofector machine. The cells were plated in 1 ml of RPMI supplemented with FCS (10%) and placed in a CO_2 incubator for 48 h.

Ethidium bromide treatment. Cells were replated in the presence or absence of ultrapure ethidium bromide (100 ng ml^{-1}) and incubated in the medium for 6 days before treatment to generate mtDNA-depleted cells. Depletion of mtRNA was determined by RT–qPCR of mtDNA-encoded genes (*mt-ND4*, *mt-ND5*, *mt-ND6*).

Digitonin fractionation. BMDMs were plated at 0.5×10^6 cells per well prior to treatment. Following treatment, cells were washed once with room-temperature PBS, scraped on ice into ice-cold PBS and pelleted at 500*g* for 5 min at 4 °C. The supernatant was discarded, and the pellet was resuspended in 400 µl of extraction buffer (150 mM NaCl, 50 mM HEPES pH 7.4, and 25 µg ml^{-1} digitonin). Samples were rotated at 4 °C for 10 min before being centrifuged at 2,000*g* at 4 °C for 5 min. The resulting supernatant constituted the cytosolic fraction, from which RNA and DNA were isolated using the All Prep DNA/RNA Mini kit (Qiagen). Alternatively, the cytosolic fraction was concentrated with Strataclean resin (Agilent) and analyzed by western blot. The pellet, containing membrane-bound organelles, was lysed in RNA lysis buffer for RNA isolation or in western blot lysis buffer for analysis by western blotting. To detect mtRNA and mtDNA in the cytosol, qPCR was performed using primers specific for the mitochondrial D-loop on cDNA reverse-transcribed from cytosolic RNA (mtRNA) and on DNA isolated from the cytosolic fraction (mtDNA).

RNA-seq. BMDMs from three mice were treated as indicated by TTFA and ITA, and RNA was extracted as detailed above using the Purelink RNA extraction kit. The mRNA was isolated from total RNA using poly-T-oligo-attached magnetic beads. After fragmentation, the first strand of complementary DNA was synthesized using random hexamer primers, followed by a second strand of cDNA synthesis. The final library was then checked with Qubit and real-time PCR for quantification, and a bioanalyzer was used to determine the size distribution. The quantified libraries were then pooled and sequenced using a NovaSeq 6000 S4 (Illumina).

Differential expression analysis of the conditions per group was then performed using normalized read counts and the DESeq2 R package. Gene set and pathway enrichment analyses were performed as described below in the 'Quantification and statistical analysis' section.

Seahorse XF complex II. BMDMs were plated at 100,000 cells per well in 100 µl of DMEM and left overnight to adhere. The protocol was carried out as previously described[38]. In brief, BMDMs were treated as indicated, and the medium was then replaced with a mitochondrial assay solution (MAS) and the manufacturer's plasma membrane permeabilizer (Agilent). BMDMs were then kept in a CO_2-free incubator for 40 min. The cell plate was then transferred to the Seahorse XFe/XF96 Analyzer, and the experiment was performed. After the experiment, Seahorse Wave software (Agilent) was used for analysis.

Western blotting. After treatment, the cell supernatant was then removed. Cell lysates were then collected in 30 µl Laemmli buffer (0.125 M Tris pH 6.8, 10% glycerol, 0.02% SDS and 5% DTT) and they were subsequently heated to 95 °C for 5 min to denature proteins. SDS–PAGE was then used to resolve proteins according to their molecular weight. The samples were also heated at 95 °C for 5 min before loading into a 5% stacking gel. The percentage resolving gel used depended on the molecular weight of the given protein of interest and was typically between 10% and 15%. The Bio-Rad gel running system was used to separate proteins, and the Bio-Rad wet transfer system was used to perform the electrophoretic transfer of proteins on PVDF membrane. The membrane was then incubated in powdered milk (5% in TBST) for 1 h and subsequently incubated in primary antibody (IRG1 (Cell Signalling Technologies, 17805), Lamin b1 (Cell Signalling Technologies, 12586), alpha-tublin (Cell Signalling Technologies, 2144) or β-actin (Sigma-Aldrich (A5316)), rolling overnight at 4 °C. The membrane was then washed three times for 5 min each, and incubated for 1 h with a horseradish-peroxidase-conjugated secondary antibody (diluted in 5% milk powder) at room temperature. Before development, the PVDF membrane was sprayed with Western Bright ECL Spray (Advansta). Protein visualization was performed using a ChemiDoc MPTM imaging system (Bio-Rad), and both chemiluminescent and white light images were taken. Images were analyzed using Image Lab 6.0.1 (Bio-Rad).

ELISA. DuoSet ELISA kits for IFN-β were purchased from R&D Systems and were carried out according to the manufacturer's instructions with appropriately diluted cell supernatants added to each plate either in technical duplicates or triplicates.

Absorbance at 450 nm was quantified using a FLUOstar Optima plate reader. Corrected absorbance values were calculated by subtracting the background absorbance, and cytokine concentrations were subsequently obtained by extrapolation from a standard curve plotted using GraphPad Prism 9.2.0.

Immunofluorescence imaging. BMDMs were plated in 35 mm dishes at 0.5×10^6 (cells ml^{-1}) in 2 ml DMEM. After treatments, TMRM (25 nm) and HOESCHT blue (0.5 µg ml^{-1}) were added to the culture medium for 30 min at 37 °C. Cells were then washed three times with warm PBS, and fresh DMEM (10% FCS) containing TMRM (1.25 nM) was added. Slides were imaged using a Leica SP8x scanning confocal microscope with a ×100.0 objective.

Images were analyzed using the LAS X Life Science Microscope Software Platform (Leica). The same microscope instrument settings were used for all samples, and all images were analyzed using the same settings.

Quantification and statistical analyses. Details of all statistical analyses are provided in the figure legends. Representative western blots are shown, and uncropped images are provided as source data. One-way ANOVA corrected for multiple comparisons using the Tukey statistical test was used, and $P_{adj} < 0.05$ was set as the significance cut-off. The Bioconductor package limma was used for analysis using an R-based online tool. Data were visualized using a heatmap with autoscaled features (genes). IREA was used to uncover important cytokines in itaconate-treated cells, as displayed in Figure 1a. Enrichr was used to analyze TTFA- and itaconate-regulated gene sets, as displayed in Figure 3a–c. GraphPad Prism v.9.2.0 was used to calculate statistics in bar charts using the appropriate statistical tests depending on the data described in the figure legends, including one-way ANOVA and two-tailed unpaired *t*-test. P_{adj} values were assessed using appropriate correction methods, such as Tukey, Kruskal–Wallis and Holm–Sidak tests. Sample sizes were determined on the basis of those in previous experiments using similar methodologies. Unless stated otherwise, all depicted data points are biological replicates taken from distinct samples. Each figure consists of at least three independent experiments from multiple biological replicates, unless stated otherwise.

Reporting summary

Further information on research design is available in the Nature Portfolio Reporting Summary linked to this article.

Data availability

The RNA-seq data in this manuscript have been deposited at Dryad (https://doi.org/10.5061/dryad.vhhmgqp36). The IREA data in this manuscript can be found in Supplementary Table 1. Source data are provided with this paper.

References

1. Mills, E. L. et al. Itaconate is an anti-inflammatory metabolite that activates Nrf2 via alkylation of KEAP1. *Nature* **556**, 113–117 (2018).
2. Michelucci, A. et al. Immune-responsive gene 1 protein links metabolism to immunity by catalyzing itaconic acid production. *Proc. Natl Acad. Sci. USA* **110**, 7820–7825 (2013).
3. Peace, C. G. & O'Neill, L. A. The role of itaconate in host defense and inflammation. *J. Clin. Invest.* **132**, e148548 (2022).
4. Cordes, T. et al. Immunoresponsive gene 1 and itaconate inhibit succinate dehydrogenase to modulate intracellular succinate levels. *J. Biol. Chem.* **291**, 14274–14284 (2016).
5. Swain, A. et al. Comparative evaluation of itaconate and its derivatives reveals divergent inflammasome and type I interferon regulation in macrophages. *Nat. Metab.* **2**, 594–602 (2020).
6. Lampropoulou, V. et al. Itaconate links inhibition of succinate dehydrogenase with macrophage metabolic remodeling and regulation of inflammation. *Cell Metab.* **24**, 158–166 (2016).
7. He, W. et al. Mesaconate is synthesized from itaconate and exerts immunomodulatory effects in macrophages. *Nat. Metab.* **4**, 524–533 (2022).
8. Hooftman, A. et al. The immunomodulatory metabolite itaconate modifies NLRP3 and inhibits inflammasome activation. *Cell Metab.* **32**, 468–478 (2020).
9. Liao, S. T. et al. 4-Octyl itaconate inhibits aerobic glycolysis by targeting GAPDH to exert anti-inflammatory effects. *Nat. Commun.* **10**, 5091 (2019).

10. Qin, W. et al. S-glycosylation-based cysteine profiling reveals regulation of glycolysis by itaconate. *Nat. Chem. Biol.* **15**, 983–991 (2019).
11. Runtsch, M. C. et al. Itaconate and itaconate derivatives target JAK1 to suppress alternative activation of macrophages. *Cell Metab.* **34**, 487–501 (2022).
12. Zhang, Z. et al. Itaconate is a lysosomal inducer that promotes antibacterial innate immunity. *Mol. Cell* **82**, 2844–2857 (2022).
13. Chen, C. et al. ABCG2 is an itaconate exporter that limits antibacterial innate immunity by alleviating TFEB-dependent lysosomal biogenesis. *Cell Metab.* https://doi.org/10.1016/j.cmet.2023.12.015 (2024).
14. Chouchani, E. T. et al. Ischaemic accumulation of succinate controls reperfusion injury through mitochondrial ROS. *Nature* **515**, 431–435 (2014).
15. Tannahill, G. M. et al. Succinate is an inflammatory signal that induces IL-1β through HIF-1α. *Nature* **496**, 238–242 (2013).
16. Cui, A. et al. Dictionary of immune responses to cytokines at single-cell resolution. *Nature* **625**, 377–384 (2023).
17. Hooftman, A. et al. Macrophage fumarate hydratase restrains mtRNA-mediated interferon production. *Nature* **615**, 490–498 (2023).
18. Peace, C. G., O'Carroll, S. M. & O'Neill, L. A. J. Fumarate hydratase as a metabolic regulator of immunity. *Trends Cell Biol.* **34**, 442–450 (2023).
19. Miyadera, H. et al. Atpenins, potent and specific inhibitors of mitochondrial complex II (succinate–ubiquinone oxidoreductase). *Proc. Natl Acad. Sci. USA* **100**, 473–477 (2003).
20. Sun, F. et al. Crystal structure of mitochondrial respiratory membrane protein complex II. *Cell* **121**, 1043–1057 (2005).
21. Tigano, M., Vargas, D. C., Tremblay-Belzile, S., Fu, Y. & Sfeir, A. Nuclear sensing of breaks in mitochondrial DNA enhances immune surveillance. *Nature* **591**, 477–481 (2021).
22. Dhir, A. et al. Mitochondrial double-stranded RNA trigger antiviral signalling in humans. *Nature* **560**, 238–242 (2018).
23. Zhong, Z. et al. New mitochondrial DNA synthesis enables NLRP3 inflammasome activation. *Nature* **560**, 198–203 (2018).
24. Kim, J. et al. VDAC oligomers form mitochondrial pores to release mtDNA fragments and promote lupus-like disease. *Science* **366**, 1531–1536 (2019).
25. O'Carroll, S. M., Henkel, F. D. R. & O'Neill, L. A. J. Metabolic regulation of type I interferon production. *Immunol. Rev.* **323**, 276–287 (2024).
26. Monzel, A. S., Enríquez, J. A. & Picard, M. Multifaceted mitochondria: moving mitochondrial science beyond function and dysfunction. *Nat. Metab.* **5**, 546–562 (2023).
27. Murphy, M. P. & O'Neill, L. A. J. A break in mitochondrial endosymbiosis as a basis for inflammatory diseases. *Nature* **626**, 271–279 (2024).
28. Yoon, J., Kim, S., Lee, M. & Kim, Y. Mitochondrial nucleic acids in innate immunity and beyond. *Exp. Mol. Med.* **55**, 2508–2518 (2023).
29. Peace, C. G., Hooftman, A. & Ryan, D. G. Inflammatory mitochondrial nucleic acids as drivers of pathophysiology. *Clin. Transl. Med.* **13**, e1403 (2023).
30. Zecchini, V. et al. Fumarate induces vesicular release of mtDNA to drive innate immunity. *Nature* **615**, 499–506 (2023).
31. Ryan, T. A. J. et al. Dimethyl fumarate and 4-octyl itaconate are anticoagulants that suppress tissue factor in macrophages via inhibition of type I interferon. *Nat. Commun.* **14**, 3513 (2023).
32. Ryan, D. G. et al. Nrf2 activation reprograms macrophage intermediary metabolism and suppresses the type I interferon response. *iScience* **25**, 103827 (2022).
33. Ackermann, W. W. & Potter, V. R. Enzyme inhibition in relation to chemotherapy. *Proc. Soc. Exp. Biol. Med.* **72**, 1–9 (1949).
34. Daniels, B. P. et al. The nucleotide sensor ZBP1 and kinase RIPK3 induce the enzyme IRG1 to promote an antiviral metabolic state in neurons. *Immunity* **50**, 64–76 (2019).
35. Cho, H. et al. Differential innate immune response programs in neuronal subtypes determine susceptibility to infection in the brain by positive-stranded RNA viruses. *Nat. Med.* **19**, 458–464 (2013).
36. O'Carroll, S. M. & O'Neill, L. A. J. Targeting immunometabolism to treat COVID-19. *Immunother. Adv.* **1**, ltab013 (2021).
37. Gobelli, D. et al. The mitochondrial succinate dehydrogenase complex controls the STAT3–IL-10 pathway in inflammatory macrophages. *iScience* **26**, 107473 (2023).
38. Salabei, J. K., Gibb, A. A. & Hill, B. G. Comprehensive measurement of respiratory activity in permeabilized cells using extracellular flux analysis. *Nat. Protoc.* **9**, 421–438 (2014).

Acknowledgements

We acknowledge the Irish Blood Transfusion Service for supporting our research by approving us to use anonymized untransfused blood components in our research. L.A.J.O. was funded by the European Research Council (Metabinnate 834370) and the Science Foundation Ireland (20/SPP/3685). The Simarro lab is funded by (1) Agencia Estatal de Investigación, Grant Number PID2020-118517RB-I00, and (2) Programa Estratégico Instituto de Biomedicina y Genética Molecular (IBGM), Junta de Castilla y León, Award Number CCVC8485. We thank all members of the O'Neill laboratory for helpful discussions.

Author contributions

S.M.O., C.G.P. and L.A.J.O. conceptualized the project. S.M.O. and C.G.P. were experimentalists, provided intellectual input, designed all experiments, analyzed and visualized the data and co-wrote the paper with input from all authors. J.E.T.-K., Y.M., A.H., S.C., A.Z., A.F.M., E.A.D., A.Z. and L.K. performed in vitro experiments. M.J.O., M.S., N.A. and J.P.A. assisted with genetic models and provided intellectual input. L.A.J.O. obtained funding, provided intellectual input and oversaw the research program.

Competing interests

L.A.J.O. is a paid consultant for Sityx Therapeutics, Sail Biomedicines and Montai Health. The other authors declare no competing interests.

Additional information

Extended data is available for this paper at https://doi.org/10.1038/s42255-024-01145-1.

Supplementary information The online version contains supplementary material available at https://doi.org/10.1038/s42255-024-01145-1.

Correspondence and requests for materials should be addressed to Luke A. J. O'Neill.

Peer review information *Nature Metabolism* thanks Ricardo Gazzinelli, Karsten Hiller and the other, anonymous, reviewer(s) for their contribution to the peer review of this work. Primary Handling Editor: Christoph Schmitt, in collaboration with the *Nature Metabolism* editorial team.

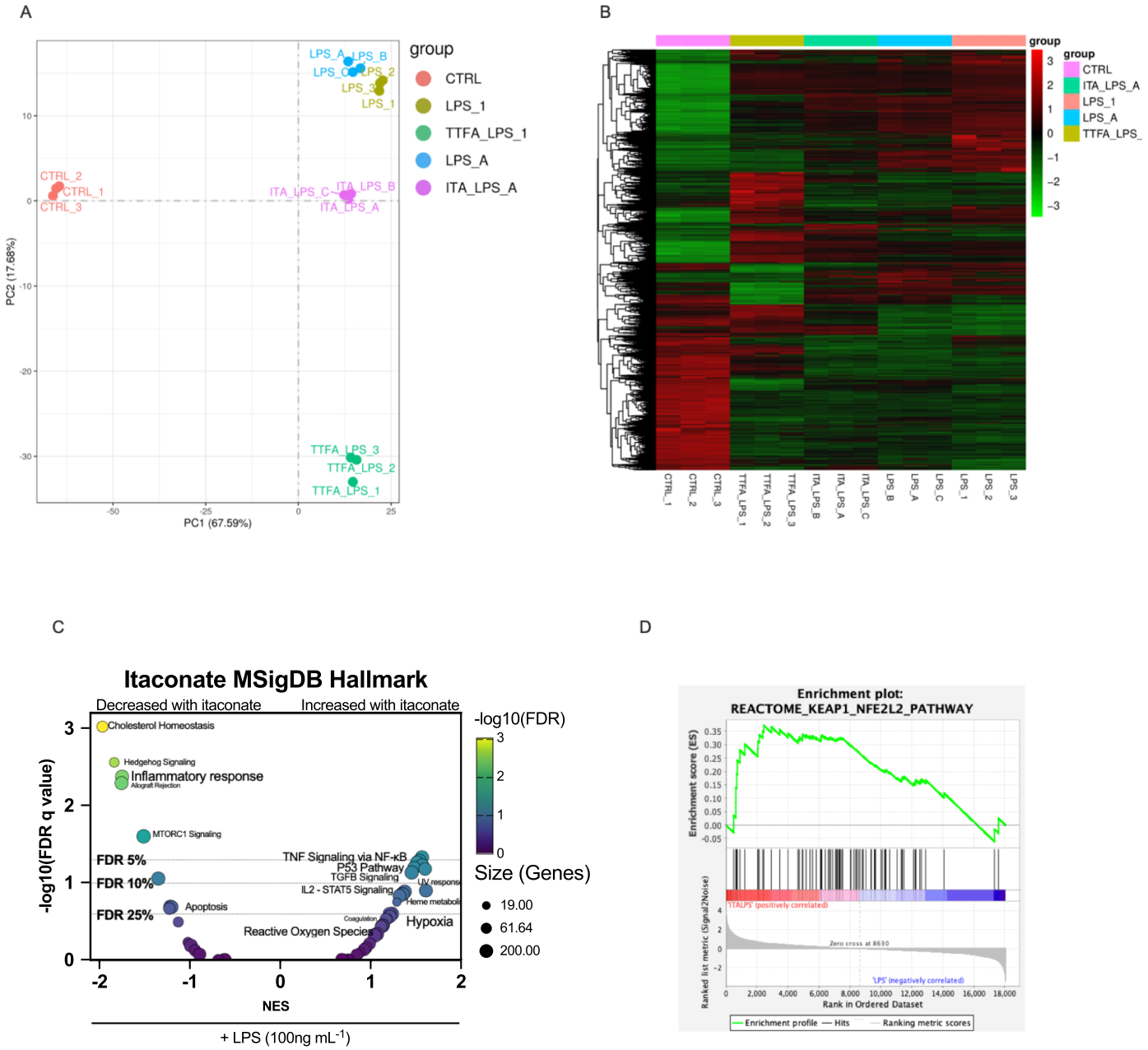
Reprints and permissions information is available at www.nature.com/reprints.

Publisher's note Springer Nature remains neutral with regard to jurisdictional claims in published maps and institutional affiliations.

Springer Nature or its licensor (e.g. a society or other partner) holds exclusive rights to this article under a publishing agreement with the author(s) or other rightsholder(s); author self-archiving of the accepted manuscript version of this article is solely governed by the terms of such publishing agreement and applicable law.

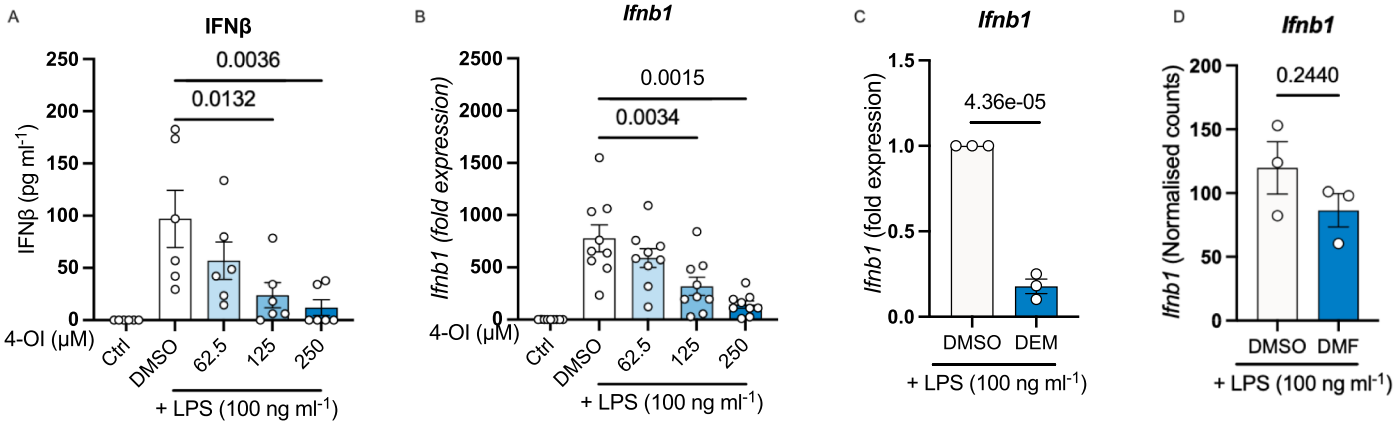
© The Author(s), under exclusive licence to Springer Nature Limited 2024, corrected publication 2024

https://doi.org/10.1038/s42255-024-01145-1



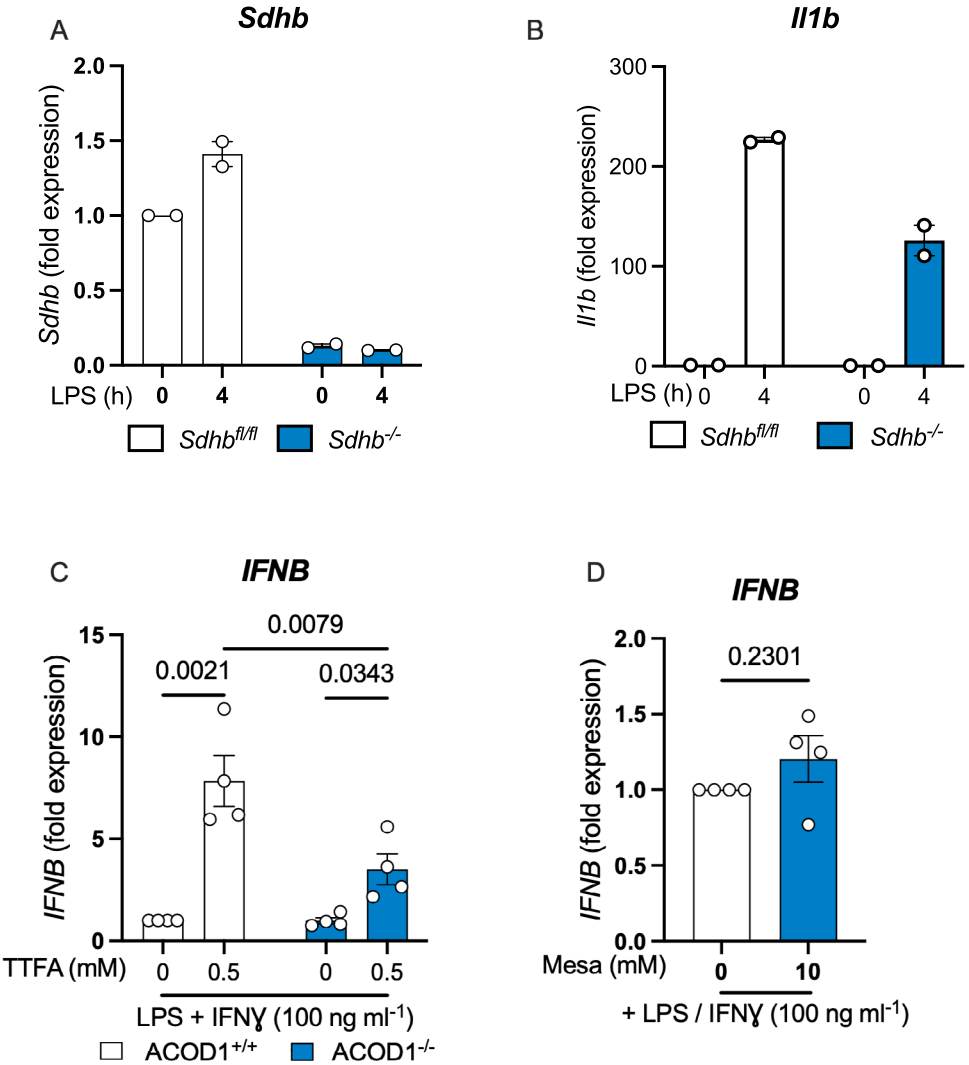
Extended Data Fig. 1 | Immunoregulatory effects of itaconate. a, PCA plot of RNA-Seq analysis. **b**, Differential expression gene clustering heatmap with Z-score. **c**, MsigDB Hallmark pathway enrichment analysis of differentially expressed genes from itaconate pretreated BMDMs followed by 3 h LPS treatment. **d**, NRF2 pathway enrichment plot of itaconate-treated BMDMs. **e)** Western blot of IRG1 in $Irg1^{+/+}$ and $Irg1^{-/-}$ BMDMs treated with LPS for 24 h and 48 h. **f**, qPCR of *IRG1* (p = 1.017e-11) in human PBMCs that were harvested in the presence of *Irg1* siRNA (n=3 donors; LPS 24 h). Data are presented as mean ± SEM. P values were calculated using two-way ANOVA for multiple comparisons.

https://doi.org/10.1038/s42255-024-01145-1



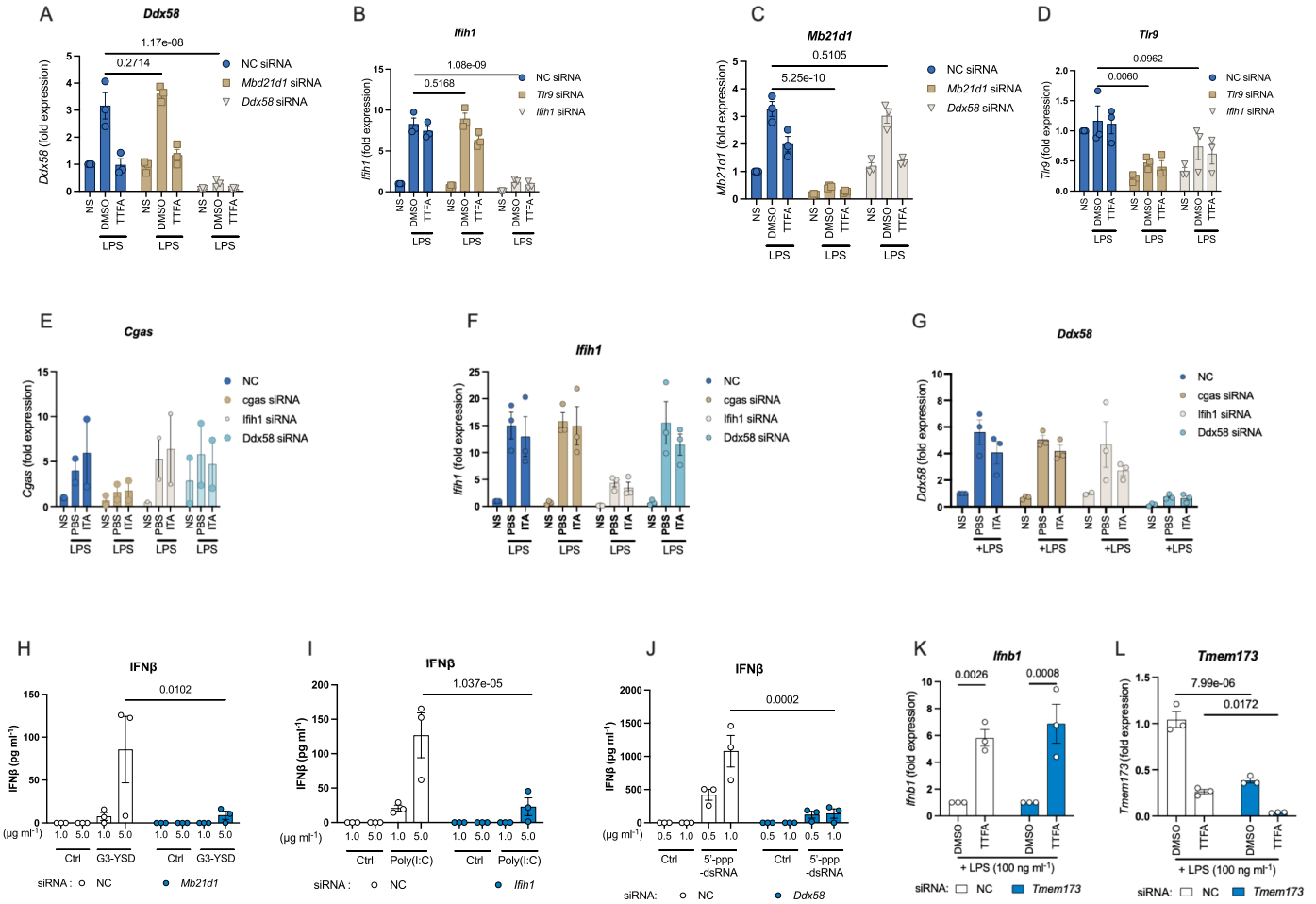
Extended Data Fig. 2 | Effect of electrophilic compounds on IFNβ. a, IFNβ release and **b**, *Ifnb1* expression in BMDMs pretreated with DMSO or 4-OI **a** (n=6 mice; LPS 4 h) **b**, (n=9; LPS 4 h). **c**, *Ifnb1* expression of BMDMs pretreated with DMSO or DEM (n=3 mice; LPS 4 h) from 3 independent experiments. **d**, Normalised counts from RNA-seq data in BMDMs pretreated with DMSO or DMF (n=3 mice; LPS 4 h) from 3 independent experiments Data are presented as mean ± SEM. P values were calculated using one-way ANOVA for multiple comparisons or two-tailed student's t-test for pairwise comparisons.

https://doi.org/10.1038/s42255-024-01145-1



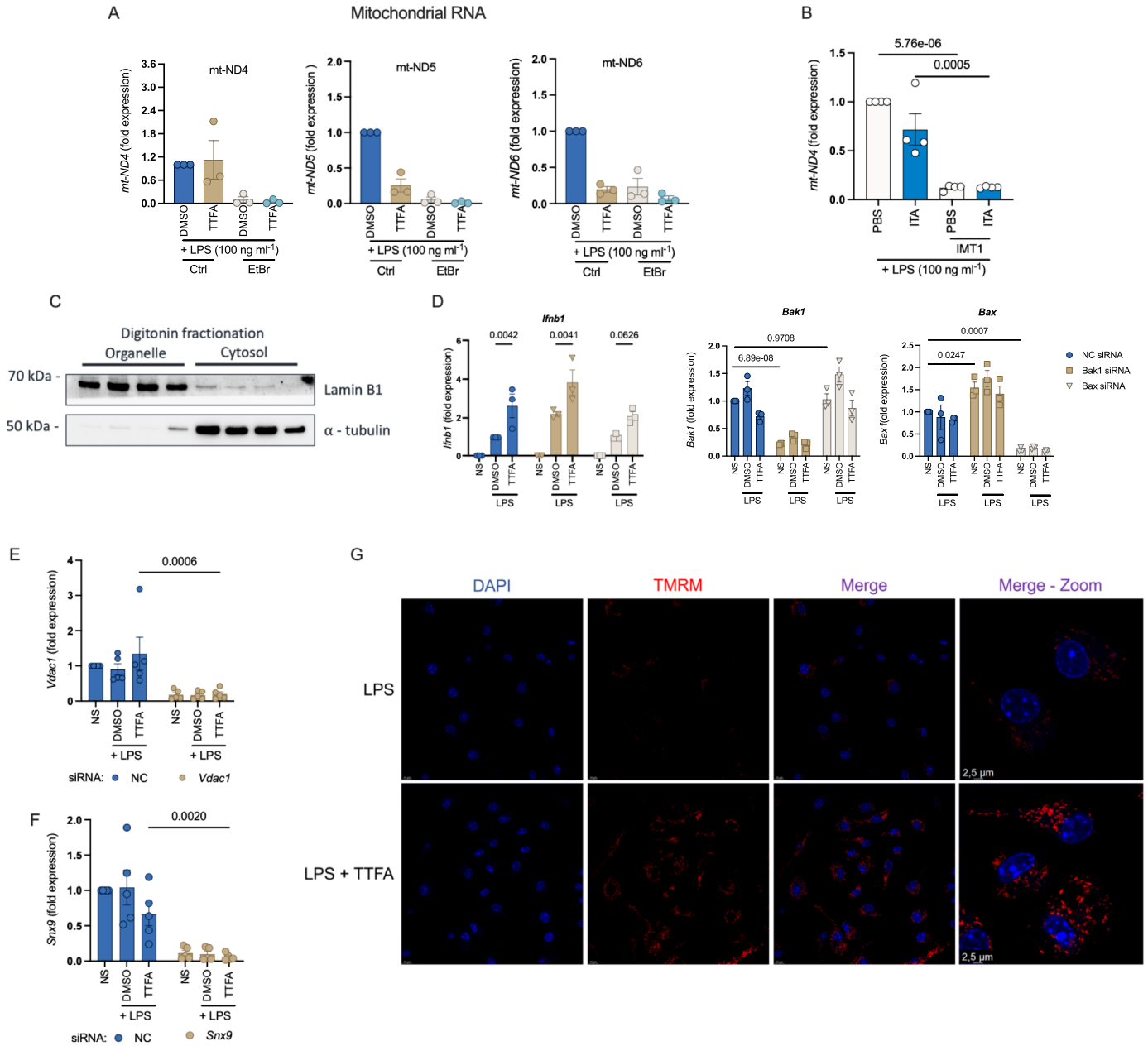
Extended Data Fig. 3 | SDH-deficiency is involved in the itaconate-interferon phenotype. a, *Sdhb* and **b**, *Il1b* expression in *Sdhb*$^{fl/fl}$ and *Sdhb*$^{-/-}$ BMDMs (n=2 mice; LPS 4 h) from 2 independent experiments. **c**, *IFNB* expression in *IRG1*$^{+/+}$ and *IRG1*$^{-/-}$ THP-1 cell lines pretreated with DMSO or TTFA (n=4 replicates; LPS/IFNγ 4 h) from 2 independent experiments **d**, *IFNB* expression in THP-1 derived macrophages pretreated with PBS or Mesaconate (n=4 replicates; LPS/IFNγ 4 h) from 2 independent experiments. Data are presented as mean ± SEM. P values were calculated using two-way ANOVA for multiple comparisons or two-tailed student's t-test for pairwise comparisons.

https://doi.org/10.1038/s42255-024-01145-1



Extended Data Fig. 4 | Knockdown of nucleic acid sensors in BMDMs. **a-d**, Expression of a, *Ddx58*, b, *Ifih1*, c, *Mb21d1*, and d, *Tlr9* in BMDMs in the presence of a,c, *Mb21d1*, *Ddx58*, b,d, *Tlr9* and *Ifih1* siRNA pretreated with DMSO or TTFA (n=3 mice; LPS 4 h) from 3 independent experiments. **e-g**, Expression of e, *Mb21d1* f, *Ifih1*, and g, *Ddx58* in the presence of *Mb21d1*, *Ifih1*, and *Ddx58* siRNA in BMDMs pretreated with PBS or ITA (n=2-3 mice; LPS 4 h) from 2 or 3 independent experiments. **h-j** IFNβ release in BMDMs transfected with h, G3-YSD, i, Poly(I:C), or j, 5′PPP-dsRNA in the presence of h, *Mb21d1*, i, *Ifih1*, or j, *Ddx58* siRNA (n=3 mice; 4 h) from 3 independent experiments. **k**, *Ifnb1* and **l**, *Tmem173* expression in BMDMs pretreated with DMSO or TTFA in the presence of Tmem173 siRNA (n=3 mice; LPS 4 h). Data are presented as mean ± SEM. P values were calculated using two-way ANOVA for multiple comparisons.

https://doi.org/10.1038/s42255-024-01145-1



Extended Data Fig. 5 | mtRNA is released in a VDAC1-dependent manner. **a**, qPCR of mitochondrial DNA-encoded genes in BMDMs after mtDNA depletion with EtBr (6 days) followed by TTFA pretreatment (0.5 mM, 3 h) and LPS stimulation (n = 3 mice, 4 h) from 3 independent experiments. **b**, qPCR of mitochondrial DNA-encoded gene in BMDMs after POLRMT inhibition with IMT1 followed by itaconate pretreatment (3 h) and LPS stimulation (n = 3 mice, 4 h) from 3 independent experiments. **c**, Western blot of organellar and cytosolic fractions of BMDMs after subcellular digitonin fractionation (n=2 mice); Images representative of two independent experiments. **d**, qPCR of *Ifnb1*, *Bak1*, and *Bax*, after *Bak1* or *Bax* siRNA knockdown followed by TTFA pretreatment (3 h) and LPS stimulation (n = 3 mice, 4 h) from 3 independent experiments. qPCR data of **e**, *Vdac1* or **f**, *Snx9* in BMDMs after *Vdac1* or *Snx9* siRNA knockdown followed by pretreated with TTFA (0.5 mM, 3 h) followed by LPS stimulation (n = 5 mice, 4 h) from 3 independent experiments. **g**, Immunofluorescence images of BMDMs pretreated with DMSO or TTFA (0.5 mM, 3 h) followed by LPS (n = 2 mice, 4 h). Images representative of 2 independent experiments. Data are presented as mean ± SEM. P values were calculated using two-way ANOVA for multiple comparisons.

nature portfolio

Corresponding author(s): Luke O'Neill

Last updated by author(s): 22/08/2024

Reporting Summary

Nature Portfolio wishes to improve the reproducibility of the work that we publish. This form provides structure for consistency and transparency in reporting. For further information on Nature Portfolio policies, see our Editorial Policies and the Editorial Policy Checklist.

Statistics

For all statistical analyses, confirm that the following items are present in the figure legend, table legend, main text, or Methods section.

n/a	Confirmed	
☐	☒	The exact sample size (*n*) for each experimental group/condition, given as a discrete number and unit of measurement
☐	☒	A statement on whether measurements were taken from distinct samples or whether the same sample was measured repeatedly
☐	☒	The statistical test(s) used AND whether they are one- or two-sided *Only common tests should be described solely by name; describe more complex techniques in the Methods section.*
☒	☐	A description of all covariates tested
☐	☒	A description of any assumptions or corrections, such as tests of normality and adjustment for multiple comparisons
☐	☒	A full description of the statistical parameters including central tendency (e.g. means) or other basic estimates (e.g. regression coefficient) AND variation (e.g. standard deviation) or associated estimates of uncertainty (e.g. confidence intervals)
☐	☒	For null hypothesis testing, the test statistic (e.g. *F*, *t*, *r*) with confidence intervals, effect sizes, degrees of freedom and *P* value noted *Give P values as exact values whenever suitable.*
☒	☐	For Bayesian analysis, information on the choice of priors and Markov chain Monte Carlo settings
☒	☐	For hierarchical and complex designs, identification of the appropriate level for tests and full reporting of outcomes
☒	☐	Estimates of effect sizes (e.g. Cohen's *d*, Pearson's *r*), indicating how they were calculated

Our web collection on statistics for biologists contains articles on many of the points above.

Software and code

Policy information about availability of computer code

Data collection	Agilent Seahorse Wave (2.4.3), Image Lab (6.0.1)
Data analysis	DESeq2 R Package (1.44.0), Agilent Seahorse Wave (2.4.3), Enrichr, Graphpad Prism (10.1.0), Image Lab 6.0.1

For manuscripts utilizing custom algorithms or software that are central to the research but not yet described in published literature, software must be made available to editors and reviewers. We strongly encourage code deposition in a community repository (e.g. GitHub). See the Nature Portfolio guidelines for submitting code & software for further information.

Data

Policy information about availability of data

All manuscripts must include a data availability statement. This statement should provide the following information, where applicable:

- Accession codes, unique identifiers, or web links for publicly available datasets
- A description of any restrictions on data availability
- For clinical datasets or third party data, please ensure that the statement adheres to our policy

RNAseq data is publicly available and deposited on Dryad (https://doi.org/10.5061/dryad.vhhmgqp36). Metabolomics data was attained from publicly availible dataset (https://doi.org/10.5061/dryad.6wwpzgn28)

Research involving human participants, their data, or biological material

Policy information about studies with human participants or human data. See also policy information about sex, gender (identity/presentation), and sexual orientation and race, ethnicity and racism.

Reporting on sex and gender	Sex and gender were not considered in the experimental design for this study
Reporting on race, ethnicity, or other socially relevant groupings	There were no socially constructed categorization variables used in this study.
Population characteristics	For patients with ctrl and SDH-deficient tumours, age and sex are undisclosed to retain anonymity of patients and was required for ethical approval. There were no significant co-variates between groups.
Recruitment	Blood samples were obtained anonymously, and writtent informed consent for the use of blood for research purposes was obtained by all donors. All the procedures involving experiments on human samples were approved by the School of Biochemistry and Immunology Research Ethics Committee (TCD). Experiments were conducted according to the TCD guide on good research practice, which follows the guidelines detailed in the National Institutes of Health Belmont Report (1978) and the declaration of Helsinki. For experiments with SDH-deficient tumour samples, patients with age- and sex- matched tumours deficient in SDH were obtained from Crumlin Children's Hospital after ethical approval and patient consent. No selection bias was noted.
Ethics oversight	School of Biochemistry and Immunology Research Ethics committee (TCD), Children's Health Ireland Research Ethics committe (Crumlin Children's Hospital)

Note that full information on the approval of the study protocol must also be provided in the manuscript.

Field-specific reporting

Please select the one below that is the best fit for your research. If you are not sure, read the appropriate sections before making your selection.

☒ Life sciences ☐ Behavioural & social sciences ☐ Ecological, evolutionary & environmental sciences

For a reference copy of the document with all sections, see nature.com/documents/nr-reporting-summary-flat.pdf

Life sciences study design

All studies must disclose on these points even when the disclosure is negative.

Sample size	We have used at least 1 biological replicate for each individual experiment, which was performed on 3 independent occasions unless otherwise stated. Although we did not use statistical methods to calculate sample size, we decided to use a minimum of 3 biological replicates per experiment to account for biological variability, taking into account the 3 Rs principle and the fact that the majority of experiments were performed in primary mouse macrophages from inbred mice or from donated blood. See statistical analyses section for full details. For this study, we used the maximum number of SDH-deficient tumour samples that we had access to (5 patients) due to variability within human data.
Data exclusions	No data were excluded in this study.
Replication	The in vitro results were highly reproducible. Each was repeated on at least 3 separate occasions unless otherwise stated.
Randomization	In transcriptomics experiments, experimental conditions and the samples were processed in random order. All in vitro treatment groups were also randomly assigned.
Blinding	In vitro experiments were not blinded due to lack of available experimenters with required expertise. In RNAseq experiments, all experimenters were blinded to experimental conditions.

Reporting for specific materials, systems and methods

We require information from authors about some types of materials, experimental systems and methods used in many studies. Here, indicate whether each material, system or method listed is relevant to your study. If you are not sure if a list item applies to your research, read the appropriate section before selecting a response.

Materials & experimental systems

n/a	Involved in the study
☐	☒ Antibodies
☐	☒ Eukaryotic cell lines
☒	☐ Palaeontology and archaeology
☐	☒ Animals and other organisms
☒	☐ Clinical data
☒	☐ Dual use research of concern
☒	☐ Plants

Methods

n/a	Involved in the study
☒	☐ ChIP-seq
☒	☐ Flow cytometry
☒	☐ MRI-based neuroimaging

Antibodies

Antibodies used

anti-mouse/human β-actin (clone: AC-74, catalogue number: A5316) was purchased from Sigma Aldrich. anti-human IRG1 (clone: D6H2Y, catalogue number: 77510S), Lamin B1 (clone: D4Q4Z, catalogue number: 12586S), and alpha-tubulin (clone: DM1A, catalogue number: 3873) were purchased from Cell Signaling technologies. Primary antibodies were used at a concentration of 1:1000. Secondary antibodies used were the polyclonal HRP-conjugated anti-mouse (catalogue number: 115-035-003) and anti-rabbit (catalogue number: 111-035-003) IgG antibodies which were both used at a concentration of 1:2000.

Validation

All primary antibodies were used according to manufacturer's instructions. Antibody validation on the manufacturer's website is as follows:
β-actin (AC-74): by western blot analysis in multipe human and murine cell lysates. The expected band appeared at the expected molecular weight.
IRG1 (D6H2Y): by western blot analysis in the human THP-1 cell line treated with TPA (24 h) followed by LPS (6 h) which resulted in a band appearing at the expected molecular weight.
Lamin B1 (D4Q4Z): by western blot analysis in HeLa cell lysates which were WT and LaminB1-knockout demonstartimng the presence and absence of a band at the expected molecular weight. Additionally, the antibody was used on numerous human and murine cell lysates.
Alpha-tubulin (DM1A): by western blot analysis in the murine CAD cell line expressing recombinant a recombinant GST-alpha-tubulin or GST-beta-tubulin fusion protein and this antibody was shown to only react with the alpha-tubulin fusion protein at the expected molecular weight. Additionally, histology and immunofluorescence demonstrated colocalisation in the cystosol with other cytoskeletal filaments as expected.

Eukaryotic cell lines

Policy information about cell lines and Sex and Gender in Research

Cell line source(s)

SDHA-/- RAW264.7 macrophages were kindly generated and provided by Dr Maria Simarro and IRG1-/- THP-1 cells were kindly generated and provided by Dr Frank Dorsey

Authentication

Cell lines were authenticated as previously described in PMID:37575201 (SDHA-/-) and PMID:39093697 (IRG1-/-). SDHA-/- clones were identified through target site sequencing and western blotting confirmed loss of protein expression. IRG1-/- THP-1 clones were identified by RNA sequencing and western blot was performed to confirm loss of protein expression.

Mycoplasma contamination

Cell lines tested negative for mycoplasma contamination prior to use.

Commonly misidentified lines
(See ICLAC register)

No commonly misidentified cell lines were used in this study.

Animals and other research organisms

Policy information about studies involving animals; ARRIVE guidelines recommended for reporting animal research, and Sex and Gender in Research

Laboratory animals

In vitro experiments were performed with BMDMs isolated from 6-18- week old female and male mice. All mice were on a C57BL/6JOlaHsd bacground unless stated below. Wild-type (WT) mice were bred in-house or ordered from Harlan. . Irg1-/- mice were on a C57BL6/NJ background. SDHBfl/fl mice were generated as previously described (PMID:35235785) and maintained on a 129/Sv-C57BL/6 mixed background. SDHB loss was confirmed by qPCR in tamoxifen-treated BMDMs. These mice were crossed with Rosa26-Cre-Ert2 mice purchased from Jackson (strain: 008463) which are on a C57BL/6. Mice were kept in 12 hour light/dark cycles, and the facility was maintained at 20-24 degrees (celcius) and 45-65% humidity.

Wild animals

Thsi study did not involve wild animals.

Reporting on sex

Sex was not considered in the study design.

Field-collected samples

The study did not involve field-collected animals

Ethics oversight

Animals were maintained under specific pathogen-free conditions in line with Irish and European Union regulations. All animal

Ethics oversight	procedures were ethically approved by the Trinity College Dublin Animal Research Ethics Committee prior to experiementation and conformed with the Directive 2010/63/EU of the European Parliament.

Note that full information on the approval of the study protocol must also be provided in the manuscript.

Plants

Seed stocks	N/A
Novel plant genotypes	N/A
Authentication	N/A

Check for updates

DOI: 10.1111/imr.13318

INVITED REVIEW

Immunological Reviews WILEY

Metabolic regulation of type I interferon production

Shane M. O'Carroll[1] | Fiona D. R. Henkel[1,2] | Luke A. J. O'Neill[1]

[1]School of Biochemistry and Immunology, Trinity Biomedical Sciences Institute, Trinity College Dublin, Dublin 2, Ireland

[2]Max Planck Institute of Biochemistry, Martinsried, Germany

Correspondence
Shane M. O'Carroll, School of Biochemistry and Immunology, Trinity Biomedical Sciences Institute, Trinity College Dublin, Dublin 2, Ireland.
Email: shocarro@tcd.ie

Funding information
Science Foundation Ireland; European Research Council

Summary

Over the past decade, there has been a surge in discoveries of how metabolic pathways regulate immune cell function in health and disease, establishing the field of immunometabolism. Specifically, pathways such as glycolysis, the tricarboxylic acid (TCA) cycle, and those involving lipid metabolism have been implicated in regulating immune cell function. Viral infections cause immunometabolic changes which lead to antiviral immunity, but little is known about how metabolic changes regulate interferon responses. Interferons are critical cytokines in host defense, rapidly induced upon pathogen recognition, but are also involved in autoimmune diseases. This review summarizes how metabolic change impacts interferon production. We describe how glycolysis, lipid metabolism (specifically involving eicosanoids and cholesterol), and the TCA cycle-linked intermediates itaconate and fumarate impact type I interferons. Targeting these metabolic changes presents new therapeutic possibilities to modulate type I interferons during host defense or autoimmune disorders.

KEYWORDS
Immunometabolism, interferons, macrophage, metabolism

1 | INTRODUCTION

1.1 | Innate immune defense mechanisms

Innate immune cells constitute, along with the epithelial barriers, one of the first lines of defense against viral or bacterial infections. Recognition of pathogen-associated molecular patterns (PAMPs) and danger-associated molecular patterns (DAMPS) by pattern recognition receptors (PRRs) leads to the induction of an inflammatory response. Interferons (IFNs) form part of the innate defense mechanism against infections. IFNs are separated into families based on receptor binding, structure, and biological activity. The type I family comprises IFN-α, IFN-β, and multiple other less well-characterized IFNs. All type I IFNs bind to the heterodimeric IFNAR1/ IFNAR2 receptor complex,[1] leading to the recruitment of the Janus kinases (JAK) JAK1 and tyrosine kinase 2 (TYK2) to receptor intracellular domains resulting in their phosphorylation. Canonical signaling directs phosphorylation of signal transducer and activator of transcription (STAT) 1 and STAT2 inducing expression of a large number of genes which are termed interferon stimulated genes (ISGs).[2–5]

A surge in discoveries in recent years regarding how PRR activation causes metabolic changes which regulate the effector function of immune cells such as myeloid and lymphoid cells has established the field of immunometabolism. In particular, when macrophages are challenged with lipopolysaccharide (LPS), a component of gram-negative bacteria which is sensed by TLR4, aerobic glycolysis is increased to meet the energetic demands of M1 macrophage effector function leading to cytokine production, phagocytosis, and antigen presentation. This response is similar to the increased demand for glucose and glycolysis observed by Otto

This article is part of a series of reviews covering Innate Memory (NK cells, macrophages) appearing in Volume 323 of *Immunological Reviews*.

Shane M. O'Carroll and Fiona D. R. Henkel are co-first authors and contributed equally.

This is an open access article under the terms of the Creative Commons Attribution License, which permits use, distribution and reproduction in any medium, provided the original work is properly cited.
© 2024 The Authors. *Immunological Reviews* published by John Wiley & Sons Ltd.

Warburg in tumors.[6] LPS challenge in macrophages also causes breakpoints in the TCA cycle, leading to changes in levels of metabolites such as succinate, citrate, itaconate, and fumarate which regulate macrophage function. For example, succinate directly blocks prolyl hydroxylases (PHDs), leading to HIF-1α stabilization and subsequent IL-1β production.

Metabolic reprogramming has mostly been studied in the context of immune cells challenged with bacteria or bacterial components. But it is now known that viral infection also causes immunometabolic changes. Viruses such as influenza A virus (IAV) manipulate host cellular metabolism by upregulating glucose uptake, glycolysis, as well as lactate efflux. Increased glycolysis promotes the production of nucleotide biosynthesis via the pentose phosphate pathway (PPP) for viral replication.[7–10] In this review, we discuss recent findings on how metabolic pathways regulate type I interferon responses. New therapeutic possibilities are emerging from these findings which could prove useful for antiviral immunity or in the context of autoimmunity.

1.2 | Glycolysis and interferon responses

Inflammatory activation of dendritic cells (DCs) or macrophages with purified bacterial components results in increased glycolysis and activation of the PPP, albeit metabolic changes during live pathogen infection are more complex.[11,12] Activation of glycolysis is important for the induction of an antiviral response.[13] While infection with live *Mycobacterium tuberculosis* (Mtb) decreases oxygen consumption rate (a measure of oxidative phosphorylation), and glycolysis, heat inactivated Mtb infection increases glycolysis without impacting oxygen consumption rate.[14] Further the authors showed that exogenous type I IFNs induced a similar profile in bone marrow-derived macrophages (BMDM) compared to live Mtb infection, stating that induction of type I IFNs might explain the decreased glycolytic flux and reduced mitochondrial respiration.[14] Indeed, infection of $IFNAR^{-/-}$ BMDMs did not result in reduced glycolysis during live Mtb infection and resulted in elevated glycolytic capacity in alveolar macrophages and monocyte-derived macrophages during in vivo infection of $IFNAR^{-/-}$ mice compared to wild type mice. Additionally, IFN-β can restrain the LPS-induced shift towards aerobic glycolysis in BMDMs.

The hexosamine biosynthesis pathway (HBP) branches off glycolysis synthesizing uridine-5′-di-phospho-N-acetylglucosamine (UDP-GlcNAc) used for protein glycosylation which has been shown to regulate the key interferon regulator IRF5. The enzyme O-GlcNAc transferase (OGT) then catalyzes transfer to target proteins, resulting in protein O-GlcNAcylation. Viral RNA is recognized by retinoic-acid-inducible gene I (RIG-I)-like receptors (RLRs) which further recruit mitochondrial antiviral-signaling protein (MAVS) and induce downstream type I IFN production.[15] Viral infection promotes aerobic glycolysis.[16] Activation of glucose metabolic pathways upon viral infection induces OGT-mediated O-GlcNAcylation of IRF5 and further inflammatory cytokine production, including IFN-β as shown in Figure 1.[13,17] Also, IAV infected individuals had increased blood glucose levels and O-GlcNAcylation of IRF5 in PBMCs.[17] Activation of RLRs by RNA viruses shifts glucose flux from glycolysis to the PPP and the HBP. Activation of those two pathways is necessary for an antiviral immune response and IFN production upon vesicular stomatitis virus (VSV) infection in mice. O-GlcNAcylation of MAVS itself has been shown to induce antiviral immunity, including induction of ISGs and IFN-β production.[18] Another study identified MAVS subcellular localisation as important for the induction of a specific IFN response. Translocation of MAVS to peroxisomes induces type III IFN production via the PPP and IRF1 activation, while MAVS translocation to mitochondria-associated ER membranes induces the HPB and production of type I IFNs as shown in Figure 1. Infection with VSV induces production of type I and III IFNs, while inhibition of either the PPP or the HPB reduced survival upon VSV infection. This shows that the regulation of glucose metabolism and MAVS are coregulated and important for antiviral immune responses.[18,19]

Glucose levels impact on RLR activation by poly(I:C), with low glucose levels leading to stronger induction of IFN-β.[20] This effect was transferrable to mice as fasted mice supplemented with low glucose also showed higher IFN-β production after VSV infection compared to animals that were supplemented with high glucose. Low glucose supplemented animals also had lower viral replication, suggesting that downregulated glucose metabolism promoted the type I IFN response and antiviral response. Recognition of viral particles by RLRs, leads to dissociation of MAVS from hexokinase resulting in hexokinase inactivation and association of MAVS with RIG-I to induce type I IFNs. Therefore, downstream products of hexokinase are reduced during RLR activation, while TBK1 and IRF3 are activated. Downregulation of glucose metabolism has also been shown to lead to an antiviral response, as lactate derived from anaerobic glycolysis binds to MAVS, inhibits its mitochondrial localization and further interaction with RIG-I that are essential for induction of downstream IFN-β production as shown in Figure 1. In line with this, increased type I IFN production during VSV infection of fasted mice supplemented with low glucose was reversed by additional supplementation of lactate, as was the effect in lactate dehydrogenase A-deficient mice.[20]

This shows that modulation of glucose metabolism during viral infections is an important aspect of antiviral responses including induction of type I IFNs. Metabolic flux to lactate inhibits antiviral responses by targeting MAVS, while induction of the PPP or the HBP promotes MAVS-dependent antiviral responses.

1.3 | Cholesterol metabolism and IFNs

Early work demonstrated the importance of the cholesterol pathway in the regulation of host defense and induction of IFNs.[21–23] Infection with cytomegalovirus (CMV) or administration of type I IFNs blocks sterol regulatory element binding protein 2 (SREBP2) and thereby sterol biosynthesis.[21] SREBP2 inhibition, as well as statins, which are inhibitors of HMG-CoA reductase, can constrain viral replication.[24,25]

16000656, 2024, 1, Downloaded from https://onlinelibrary.wiley.com/doi/10.1111/imr.13318 by HEALTH RESEARCH BOARD, Wiley Online Library on [02/10/2024]. See the Terms and Conditions (https://onlinelibrary.wiley.com/terms-and-conditions) on Wiley Online Library for rules of use; OA articles are governed by the applicable Creative Commons License

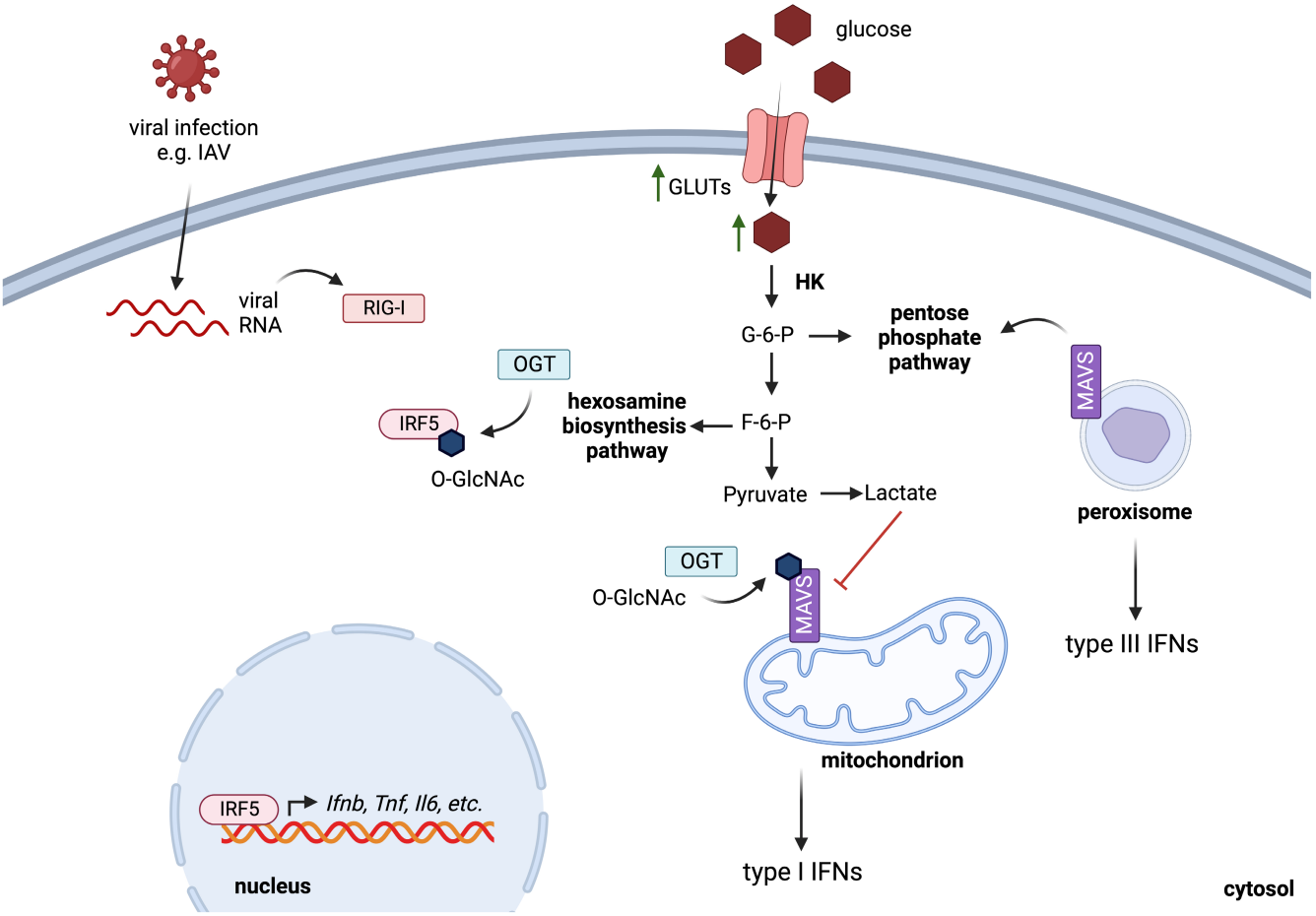


FIGURE 1 Viral infections induce increased glucose metabolism after recognition of viral RNA by RIG-I and MAVS activation. Activation of the hexosamine biosynthesis pathway and OGT (O-GlcNAc transferase) lead to O-GlcNAcylation of IRF5 and increased expression of IFNs, as well as inflammatory cytokines. MAVS is also subjected to O-GlcNAcylation and induction of an antiviral response. Additionally, MAVS subcellular localization impacts on induction of a different IFN response. Peroxisomal MAVS induces the PPP and leads to type III IFN production, while translocation to mitochondria-associated ER membranes induces the HPB and production of type I IFNs. Lactate inhibits MAVS activation and therefore induction of an antiviral response. F-6-P, fructose-6-phosphate; G-6-P, glucose-6-phosphate; GLUT, glucose transporter; HK, hexokinase.

Reduced cholesterol biosynthesis therefore was antiviral. More recently there has been a focus on 25-hydroxycholesterol (25-HC) as shown in Figure 2.

The endoplasmic-reticulum-associated enzyme cholesterol-25-hydroxylase (*CH25H*) catalyzes the oxidation of cholesterol to 25-HC. 25-HC serves as a corepressor of cholesterol biosynthesis through inhibition of SREBP processing.[26] In macrophages and DCs *CH25H* expression is increased by various TLR agonists, as well as IFN-α and IFN-β, making it an ISG[27] (Figure 2A). 25-HC induction by type I IFNs was completely dependent on IFNAR1 signaling in murine macrophages, with exogenous IFN-γ also boosting 25-HC levels.[28] Treatment of BMDM with 25-HC blocked replication of different enveloped DNA and RNA viruses, while this was not the case for non-enveloped viruses.[28,29] IFN-β and IFN-γ treated macrophages exhibited antiviral effects via 25-HC secretion. Transfer of supernatant from those stimulated macrophage could inhibit viral replication in target cells, indicating antiviral activity can also work in a paracrine manner. In vitro treatment with 25-HC also inhibited human immunodeficiency virus (HIV) entry via cell membrane remodeling.[29] Furthermore, in vivo administration of 25-HC reduced HIV infection in humanized mice. In Zika virus (ZIKV) infection 25-HC was protective by inhibiting viral entry independent of IFNAR1 signaling. 25-HC administration reduced mortality in mice in vivo, in wild type and in IFNAR deficient mice, while also reducing viremia in rhesus monkeys. Thus, the type I IFN inducible gene *CH25H* through its product 25-HC acts as an antiviral agent[28–31] (Figure 2A). Overall, 25-HC blocks viral entry by altering membrane composition and thereby impairs viral fusion,[29] while also blocking postentry viral growth.[28] Also, 25-HC and 27-HC lead to the accumulation of cholesterol in late endosomes, encapsulating viral particles and thus inhibiting their replication.[32] Furthermore, 25-HC induces the accumulation of oxysterol binding protein 1 at the Golgi-ER interface, thus leading to endosomal accumulation of cholesterol and blocking replication of human rhinoviruses.[33] Therefore, 25-HC changes the accessibility of cholesterol in the cell membrane via different mechanisms which reduce viral entry and replication.

16000656, 2024, 1, Downloaded from https://onlinelibrary.wiley.com/doi/10.1111/imr.13318 by HEALTH RESEARCH BOARD, Wiley Online Library on [02/10/2024]. See the Terms and Conditions (https://onlinelibrary.wiley.com/terms-and-conditions) on Wiley Online Library for rules of use; OA articles are governed by the applicable Creative Commons License

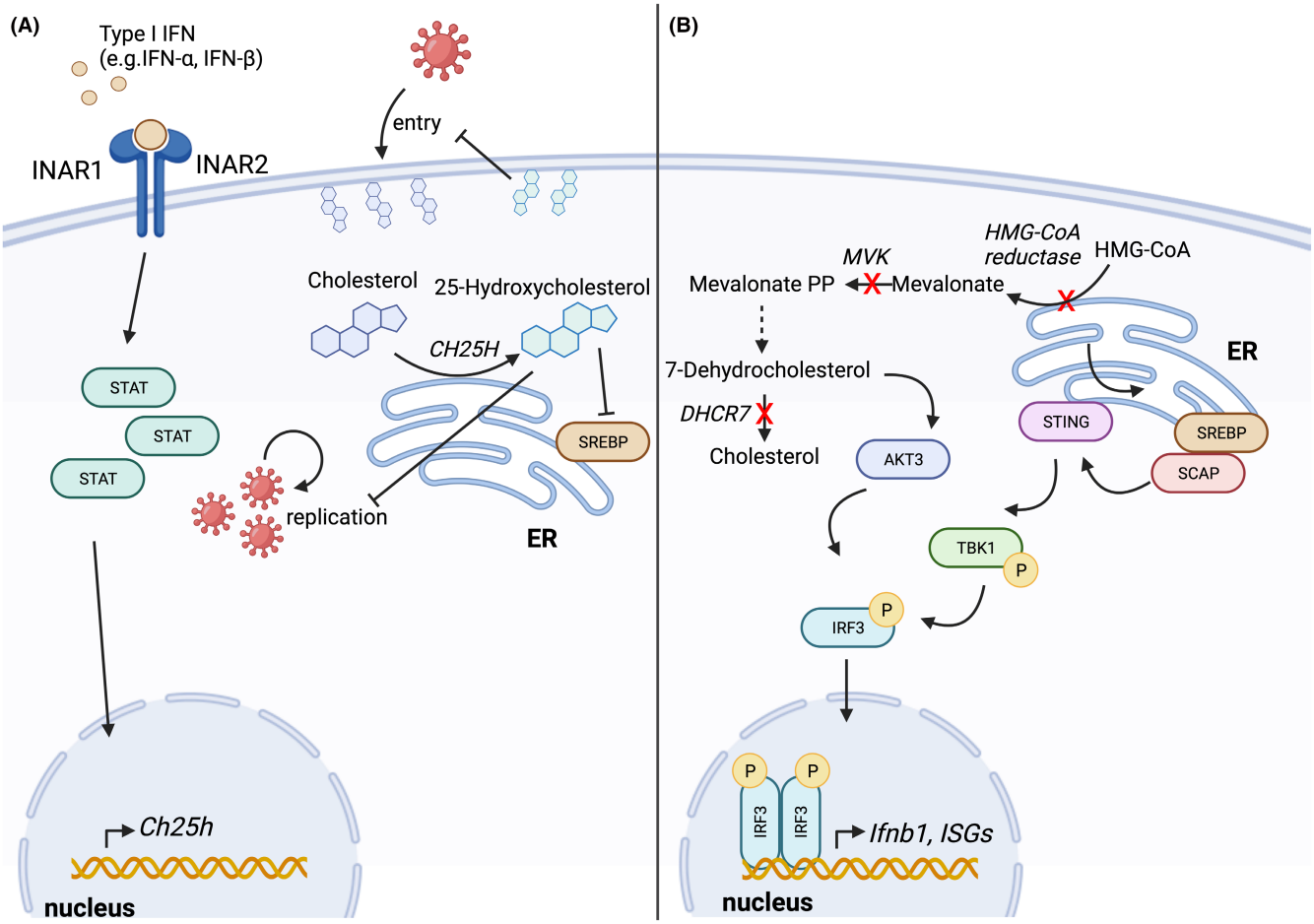


FIGURE 2 Influence of cholesterol on IFN response. (A) Membrane cholesterol facilitates viral entry. Type I IFNs modulate cholesterol metabolism from de novo synthesis to increased import. This is conferred through the induction of CH25H and its product 25-hydroxycholesterol (25-HC), suppressing SREBP processing and thereby cholesterol biosynthesis. 25-HC has been shown to limit viral entry and replication. (B) Alterations in cholesterol metabolism induce type I IFN response and expression of ISGs. Genetic perturbations in the mevalonate pathway leading to reduced ER cholesterol levels activate STING, which further phosphorylates TBK1 and IRF3, and induce the expression of *Ifnb1* and ISGs. Accumulation of 7-Dehydrocholesterol (e.g., though inhibition of 7-dehydrocholesterol reductase (DHCR7)) induces AKT3 and IRF3 phosphorylation and further ISG expression.

Apart from viral infections, LPS induces CH25H in an IFNAR-dependent manner.[30] In vivo lethal LPS administration led to increased IL-1β production in *Ch25h*$^{-/-}$ mice and earlier death. Infecting mice with the bacterium *Listeria monocytogenes* induced *Ch25h* via type I IFNs, while in this case *Ch25h*$^{-/-}$ mice displayed reduced susceptibility to infection. 25-HC therefore participates in a negative feedback loop, downregulating *IL1β* expression, inhibiting caspase-1 activity, and further IL-1β processing, thereby reducing inflammasome activation.[30] This was shown for different NLRP3 inflammasome activators, including ATP, nigericin and alum, as well as the NLRC4-inflammasome flagellin and AIM2-inflammasomes. Increased IL-1β production in *Ch25h* deficient mice relied on ASC-dependent inflammasome activation and involved the DNA sensor AIM2. Treatment of BMDMs with methyl-beta cyclodextrin cholesterol, used to deliver cholesterol to membranes, increased mitochondrial ROS production, suggesting that increased cholesterol levels induced mitochondrial dysfunction. Additionally, the authors describe how *Ch25h*$^{-/-}$ BMDMs showed impaired mitochondrial respiration and accumulated mitochondrial DNA (mtDNA) in the cytosol after LPS stimulation. This links increased mitochondrial, or total, cholesterol levels to mtDNA release and AIM2 activation.

Pathogens can also target membrane cholesterol via cholesterol-dependent cytolysins (CDCs), toxins produced by gram-positive bacteria, inducing pore formation and loss of membrane integrity further leading to cell death. Several repair mechanisms exist, including membrane internalization and releasing or shedding damaged membranes as microvesicles.[34–36] Type I and II IFNs can alter availability of the membrane cholesterol pool and thereby provide resistance to CDCs in macrophages and neutrophils.[37] The effect was conferred by increased production of 25-HC that further reduced de novo cholesterol synthesis. In vivo administration of 25-HC also reduced CDC-mediated tissue damage.[37]

Type I IFNs can shift lipid metabolism from fatty acid and cholesterol de novo synthesis to their import, through changes in gene expression and altered metabolic flux.[28,29,37–39] However, alterations

1600065x, 2024, 1, Downloaded from https://onlinelibrary.wiley.com/doi/10.1111/imr.13318 by HEALTH RESEARCH BOARD, Wiley Online Library on [02/10/2024]. See the Terms and Conditions (https://onlinelibrary.wiley.com/terms-and-conditions) on Wiley Online Library for rules of use; OA articles are governed by the applicable Creative Commons License

in cholesterol and fatty acid metabolism impact IFN production. BMDMs deficient for SREBP cleavage-activating protein (SCAP), an important regulator of SREBP processing, show reduced lipid biosynthesis without affecting the total lipid pool. Additionally, genetic deletion of *Scap* or *Srebp2* in BMDMs resulted in induction of a type I IFN response characterized by increased transcription of *Ifnb1* and several ISGs (e.g., *Mx2*, *Irf7*, *Ccl2*, and *Cxcl10*) and subsequent protection from viral infections.[38] Further characterizing the mechanism, the authors showed that deletion of mevalonate kinase (MVK) or HMG-CoA reductase are sufficient to induce type I IFNs, while cholesterol replenishment reduced the expression of ISGs (Figure 2B). Also, Blanc et al., showed, that the mevalonate pathway was important for 25-HC antiviral functions, suggesting that a decreased flux through the mevalonate pathway prompts type I IFN-mediated inflammation.[28,38] Stimulator of interferon genes (STING) has been shown to facilitate IRF3 phosphorylation and nuclear translocation, as well as *Ifnb1* transcription in response to cytosolic double-stranded DNA or RNA,[40] as well as through binding of ligands generated by cyclic GMP-AMP synthase (cGAS).[41,42] Srebp2 deficient cells showed high basal cGAS expression, and STING activity, leading to increased TANK-binding kinase 1 (TBK1) and IRF3 phosphorylation.[38] Addition of cholesterol to Scap-deficient BMDM reduced their increased phospho-TBK1 levels and *Ifnb1* expression, showing that low cholesterol directly influences STING activation. As cGAMP levels (a STING ligand) were similar between Srebp2-deficient and control cells, low levels of ER membrane cholesterol might facilitate interactions between STING and TBK1. Inhibiting the mevalonate pathway reduced type I IFN production after poly(I:C) or LPS stimulation of BMDM through diminished PI(3)K activation.[43] All these data indicate that perturbations in cholesterol and mevalonate metabolism directly affect STING function, thereby regulating type I IFN production as shown in Figure 2.

In line with the impact of MVK or HMG-CoA reductase on IFN response, alterations of 7-dehydrocholesterol reductase (DHCR7) all affect the type I IFN response.[44] DHCR7 is the enzyme converting 7-dehydrocholesterol (7-DHC) to cholesterol. IFN-β reduced the expression of DHCR7, while siRNA knockdown of DHCR7 enhanced *Ifnb* expression upon poly(I:C) or viral treatment. Accumulation or administration of 7-DHC augmented *Ifnb* production, and ISGs, in an IRF3 dependent manner, also promoting viral clearance.[44] In this setting AKT3 was involved in IRF3 Ser-385 phosphorylation, facilitating IRF3 Ser-386 phosphorylation by TBK1 and thus promoting IRF3 dimerization. IRF3 nuclear translocation resulted in an enhanced antiviral response through IFN-β production and ISG induction (Figure 2B).

Reduced de novo cholesterol biosynthesis and limiting the availability of cholesterol induces antiviral activity. This is either conferred by decreasing flux through the mevalonate pathway or by reducing DHCR7, as well as increasing expression of CH25H. The product 25-HC then reduces SREBP processing as well as proteasomal degradation of HMG-CoA and therefore feeds back to reducing cholesterol synthesis.[26,45] Apart from the effect on cholesterol metabolism, 25-HC mediated antiviral functions via inhibition of pathogen entry or viral replication, while also limiting inflammasome activation. It might seem counterintuitive that limiting cholesterol biosynthesis as well as increasing 25-HC production both show antiviral effects and indeed some studies describe antiviral effects of exogenously supplemented 25-HC (which is not affected by reduced cholesterol synthesis). However, limiting cholesterol synthesis did not affect the total cholesterol pool, while shifting reduced synthesis to increased import. Also, utilising CH25H knockout mice clearly established the antiviral role of 25-HC during virus infections.[38]

1.4 | Impact of eicosanoids on type I interferons

Eicosanoids are another class of lipid mediators implicated in the regulation of type I IFNs as shown in Figure 3. They are bioactive molecules derived from the polyunsaturated fatty acids arachidonic acid through different pathways including the cyclooxygenase (COX) pathway for the formation of prostanoids or the lipoxygenase (LOX) pathway. 5-LOX synthesizes leukotrienes (LTs), while 12/15-LOX forms 12−/15-HETE, as well as a range of specialized pro-resolving mediators such as lipoxin A4.

1.5 | Leukotrienes

Previously, leukotriene (LT) production has been mostly attributed to myeloid cells, while recent studies established specialized epithelial cells, tuft cells, as LT producers.[46,47]

LTB_4 is a proinflammatory chemotactic metabolite signaling through the high-affinity B leukotriene receptor 1 (BLT1) and the lower-affinity receptor BLT2.[48] IAV infection leads to increased production of LTB_4 in the broncho-alveolar lavage (BAL) fluid, lungs, and serum of infected mice as shown in Figure 3A.[49] LTB_4 administration during IAV infection resulted in a reduction in viral load and increased survival,[50,51] suggesting LTB_4 as part of the antiviral immune response. Pernet et al. showed that LTB_4 via BLT1 could induce IFN-α production by pulmonary interstitial macrophages, which reduced inflammatory monocyte-derived macrophage proliferation and thereby limited IAV immunopathology and mortality, see Figure 3B.[49] Another study showed that additional LTB_4 administration during IAV infection could increase survival and viral clearance via IFN-β production, as depicted in Figure 3B. The authors propose that this effect was conferred through potentiating NOD2 signaling through TAK1, IRF3 and NF-κB/MAPK.[51] Several viruses increase host LT production (including LTB_4)[49,52,53] and might thereby contribute to a protective innate immune response through regulation of the IFN response.

IFNs also regulate LT production. Peritoneal macrophages pre-stimulated with IFN-α increased the production of LTB_4 after zymosan stimulation.[54] In a sepsis model, macrophage IFN-β production resulted in reduced production of LTB_4 by recruited neutrophils. Furthermore, IFNAR1 deficiency limited LTB_4 production, as well as inflammation and survival during sepsis.[55]

16000656, 2024, 1, Downloaded from https://onlinelibrary.wiley.com/doi/10.1111/imr.13318 by HEALTH RESEARCH BOARD, Wiley Online Library on [02/10/2024]. See the Terms and Conditions (https://onlinelibrary.wiley.com/terms-and-conditions) on Wiley Online Library for rules of use; OA articles are governed by the applicable Creative Commons License

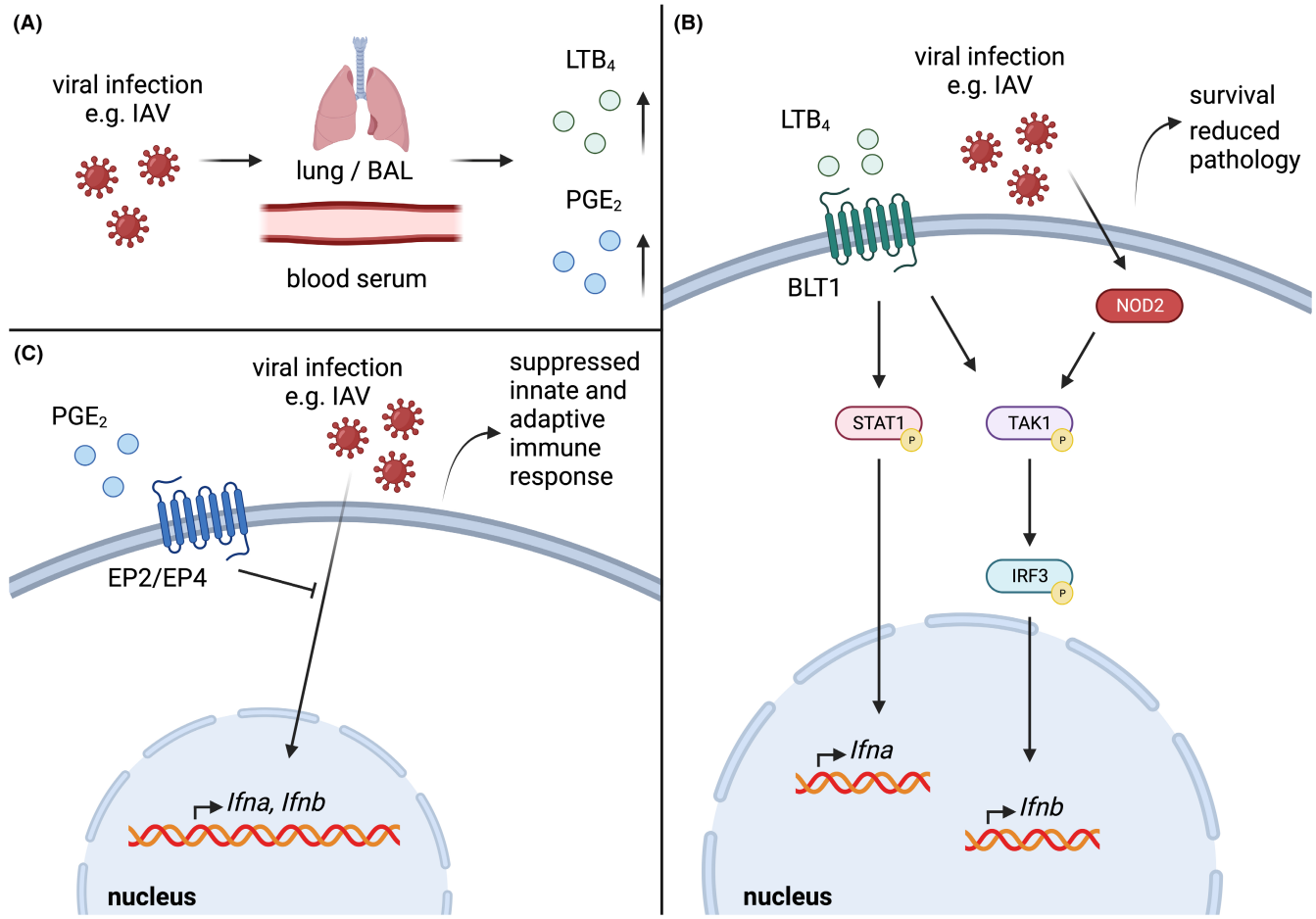


FIGURE 3 Eicosanoids effect on viral defense mechanisms. (A) During viral infections like IAV (influenza A virus) LTB_4 and PGE_2 are increased in the lungs, BAL fluid, as well as serum. (B) During viral infections LTB_4 signaling via BLT1 induces STAT1 phosphorylation and can lead to increased transcription of *Ifna*. Additionally, LTB_4–BLT1 signaling can lead to TAK1 phosphorylation, which further promotes IRF3 activation and *Ifnb* transcription. NOD2 signaling can potentiate this effect. LTB_4 thus increases survival and reduces pathology during viral infections. (C) PGE_2 ligation to the EP2/EP4 receptor can reduce viral induced *Ifna* and *Ifnb* transcription and production in macrophages and thereby suppress antiviral macrophage activity and delay the adaptive immune response.

Additionally, LTB_4 can upregulate TLR2 and TLR9 expression in human polymorphonuclear neutrophils (PMNs)[50,56] and activate STAT1 phosphorylation in murine macrophages.[57] Most studies did not investigate the impact of LTs on IFNs or ISGs, leaving the interplay between LTs and IFNs open for further investigations.

1.6 | Prostaglandins

PGE_2, a COX derived metabolite, exerts its effect through G protein-coupled E prostanoid (EP) receptors 1–4. Depending on the cell type and activated receptor, it can be pro- or anti-inflammatory.[58] PGE_2 impairs the host response to IAV infection by inhibiting type I IFN production, while prostaglandin E synthase deficient ($Ptges^{-/-}$) mice exhibited enhanced protection[59] (Figure 3C). Another study investigated IAV infection in aged mice, since the elderly human population is more at risk of developing complications and succumbing to viral infections.[60,61] The authors found that in aged mice senescent type II alveolar epithelial cells contribute to increased PGE_2 production in the lungs before and during IAV infection that limit alveolar macrophage proliferation. Blocking of the EP2 receptor increased IFN-β production and could improve survival in aged (but not young) mice.[62] This suggested an age-dependent difference, which might be targeted therapeutically. Also other pathways may contribute to the disparity in developing complications to viral infections between different age groups. Deficiency of 15-lipoxygenase (Alox15, 15-LOX), catalyzing the formation of 15-HETE and several anti-inflammatory metabolites termed specialized pro-resolving lipid mediators, promoted senescence in alveolar macrophages via enhanced PGE_2 production.[63] In line with Coulombe et al.[59] the enhanced production of PGE_2 in $Alox15^{-/-}$ mice resulted in delayed IFN-β production after IAV infection and increased viral load.[63]

More work is therefore needed on the interplay between eicosanoids and IFNs. Especially as the most used drugs for milder viral infections (e.g., common cold, flu) are non-steroidal anti-inflammatory drugs, like aspirin or ibuprofen which inhibit COX enzymes. This provides pain and fever relief but might have additional beneficial

1600065x, 2024, 1, Downloaded from https://onlinelibrary.wiley.com/doi/10.1111/imr.13318 by HEALTH RESEARCH BOARD, Wiley Online Library on [02/10/2024]. See the Terms and Conditions (https://onlinelibrary.wiley.com/terms-and-conditions) on Wiley Online Library for rules of use; OA articles are governed by the applicable Creative Commons License

effects by preventing PGE_2 production in infected tissues and boosting type I IFN production.

2 | TCA CYCLE-DERIVED METABOLITES MODULATE INTERFERONS

2.1 | Itaconate

Recently a role for TCA cycle derived metabolites in the regulation of IFNs has emerged, specifically in regard to itaconate and fumarate.

Itaconate is the most abundantly produced metabolite in LPS challenged macrophages, produced from the TCA cycle intermediate aconitate via aconitate decarboxylase 1 (ACOD1), encoded by the gene *immunoresponsive gene 1 (Irg1)* as shown in Figure 4. Due to its α, β-unsaturated dicarboxylic acid structure containing two double bonds and two carboxyl groups, it can covalently modify cysteines on target proteins in a Michael addition reaction. This covalent modification of proteins alters protein function.[64] Itaconate has demonstrated antibacterial, antiviral, and anti-inflammatory properties.[65,66] Itaconate boosts IFNs as $Irg1^{-/-}$ BMDMs have significantly reduced IFN-β and reduced type I interferon signature which is restored upon itaconate treatment.[67] A mechanism whereby itaconate might regulate type I interferon could include succinate dehydrogenase (SDH) inhibition. As itaconate is structurally similar to succinate, itaconate competitively inhibits the active site of SDH. It has been demonstrated that SDHA and SDHB (two subunits of SDH) knockout in RAW 264.7 macrophage cell lines increases IFN-β production.[68] Furthermore, pharmacological irreversible inhibition of SDH by 3-nitropropionic acid (3-NPA) and dimethyl malonate (DMM) also boost the IFN signature in YUMM1.7 male mouse melanoma cell line and BMDMs, respectively.[69,70] SDH, therefore, impacts on IFN production, but the mechanism by which this occurs is still unknown.

2.2 | Itaconate derivatives

Itaconate can be further metabolized into isomers citraconate and mesaconate as reported in the mouse RAW264.7 macrophage cell line as shown in Figure 4. Mesaconate differs only in the location of a double bond and is synthesized via both itaconate and glutamine metabolism. Between itaconate, citraconate, and mesaconate, citraconate is the most electrophilic of the three, fails to block SDH, and is the most potent nuclear factor erythroid 2–related factor 2 (NRF2) activator. Citraconate treatment blocks IFN responses in THP1 human monocyte cell line and A549 human airway epithelial in the context of IAV infection.[71]

Mesaconate is endogenously synthesized from itaconate in macrophages including the RAW264.7 cell line. Mesaconate is a weaker SDH inhibitor than itaconate. It is the least electrophilic of the three itaconate related metabolites. Pretreatment of RAW264.7 murine macrophage cell line with mesaconate for 4 h followed by 3-h LPS challenge significantly boosted IFNB1 levels compared to LPS alone.[71]

Itaconate derivatives have been created to increase cell permeability. These include derivatives such as 4-octyl itaconate (4-OI) and dimethyl itaconate (DI). Although itaconate derivatives and the endogenous metabolite overlap in many contexts, there are also unique properties to each of these derivatives in their immunomodulatory effects. A comparative study has illustrated the differences between itaconate and its derivatives in the content of multiple immune pathways in murine macrophages. In the context of IFNs, they show that itaconate boosts IFNs whereas 4-OI is a potent suppressor of IFNs as shown in Figure 4.[67] Mechanistically, 4-OI inhibits STING phosphorylation by alkylating STING on cysteine 91 and 147 and prevents palmitoylation of STING and its activation.[72,73] 4-OI also alkylates JAK1 on Cys-816 located on the pseudokinase domain, necessary for JAK1 phosphorylation and signaling.[74]

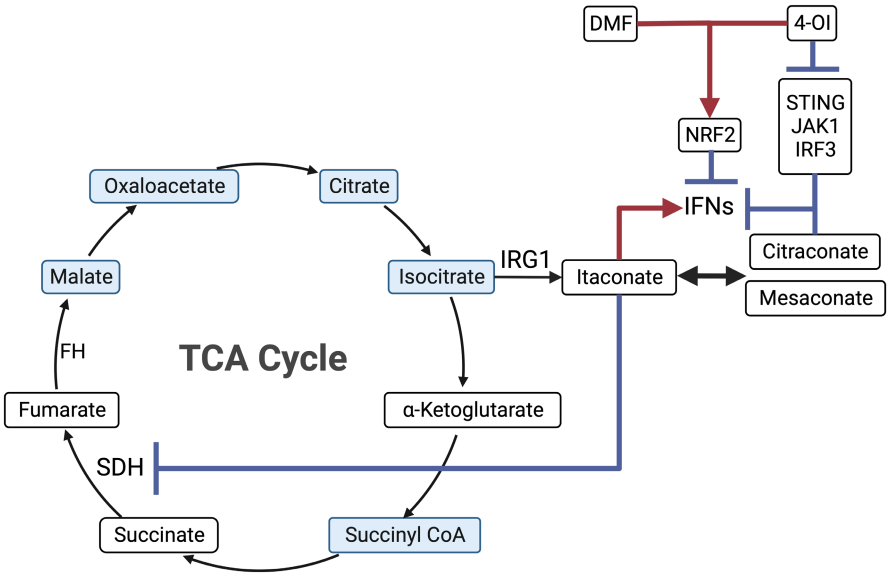


FIGURE 4 The effect of TCA cycle metabolites and derivatives on interferons. Itaconate is the most upregulated metabolite in LPS challenged macrophages. Itaconate blocks SDH essential for macrophage effector function. Both itaconate accumulation and SDH inhibition boost IFN. Itaconate isomers citraconate and mesaconate are more electrophilic and fail to block SDH and induce IFN production. Itaconate derivative 4-OI blocks IFN via alkylation of STING, JAK1, and IRF3.

1600065x, 2024, 1, Downloaded from https://onlinelibrary.wiley.com/doi/10.1111/imr.13318 by HEALTH RESEARCH BOARD, Wiley Online Library on [02/10/2024]. See the Terms and Conditions (https://onlinelibrary.wiley.com/terms-and-conditions) on Wiley Online Library for rules of use; OA articles are governed by the applicable Creative Commons License

4-OI can also regulate IFNs via NRF2. Under homeostatic conditions, NRF2 undergoes constant polyubiquitination and proteasomal degradation regulated by Kelch-like ECH-associated protein 1 (KEAP1). 4-OI alkylates KEAP1 at Cys-151, leading to the liberation of NRF2 where it translocates to the nucleus and, along with musculoaponeurotic fibrosarcoma proteins (MAF), acts as both a transcription factor, binding to the antioxidant response element (ARE) and induction of anti-inflammatory and cytoprotective genes, and the direct inhibition of inflammatory gene transcription including IL-6 and IL-1β by blocking RNA-pol II recruitment.[75,76] NRF2 negatively regulates *Ifnb1*.[77] Furthermore, 4-OI blocks IRF3 dimerization in an NRF2-dependent manner in HaCaT cells and A549 cells.[78] 4-OI has been shown to be beneficial in a mouse model of COVID-19. COVID-19 is a coagulopathy mediated by tissue factor (TF) production and thrombin generation which leads to elevated fibrinogen, collagen deposition, lung inflammation and subsequent thrombo-inflammation. A severe acute respiratory syndrome coronavirus 2 (SARS-CoV-2) infection mouse model had elevated TF levels. TF is an ISG which can be blocked by the itaconate derivative 4-OI. In vivo 4-OI reduced the clinical score, lung inflammation, inflammatory cell infiltration to the lungs, viral loads, and ACE2 expression in SARS-CoV-2 infected mice.[79]

2.3 | Fumarate

Dimethyl fumarate (DMF) is a derivative of fumarate which is clinically approved under the name Tecfidera for the treatment of relapsing remitting multiple sclerosis and psoriasis. DMF, like 4-OI, is electrophilic and cysteine reactive. Like 4-OI, DMF has been shown to inhibit SARS-CoV-2 replication and suppress the inflammatory response, including *IFNB1* and subsequent TF expression.[78]

Fumarate hydratase (FH, encoded by *Fh1* in mice) catalyzes the reversible hydration of fumarate to malate, either in the mitochondria as part of the TCA cycle or in the cytosol. Prolonged LPS challenge in macrophages causes a downregulation of FH.[80] RNAseq analysis revealed that FH inhibition in combination with LPS stimulation resulted in increased expression of *Ifnb1* and ISGs including *Irf1*, *Ifih1*, *Rsad2*, *and Ifit2* compared to LPS alone. Both mitochondrial RNA (mtRNA) and mtDNA were released into the cytosol, increasing IFN-β production. The effect of mtRNA was mediated via MDA5 and TLR7. MtRNA release likely depended on changes in mitochondrial membrane potential, as the ATP synthase inhibitor oligomycin, K^+ ionophore valinomycin A and the uncoupler CCCP could all induce mtRNA release into the cytosol. In mice, in vivo administration of the FH inhibitor before LPS injection increased serum IFN-β levels. Finally, PBMCs from systemic lupus erythematosus (SLE) patients which have elevated type I interferons showed reduced FH expression compared to healthy controls and IFN-β could suppress FH expression.[80] Overall, FH suppression leads to mtRNA release and in turn IFN-β production as displayed in Figure 5. This may be important in the pathogenesis of diseases such as SLE or other interferonopathies.

FH and fumarate have also been shown to drive type I and type II IFN responses in cancer.[81] In rare forms of cancer such as hereditary leiomyomatosis and renal cell cancer (HLRCC), FH deficiency occurs, leading to fumarate accumulation which acts as an oncometabolite.[82] Transcriptomic analysis of mouse kidneys from tamoxifen-inducible $Fh1^{-/-}$ mice revealed induction of an innate inflammatory response, including an increase in cytokines, chemokines, and ISGs. Cytosolic accumulation of mtDNA activated a STING–TBK1–IRF3 cascade and further upregulated ISG expression as shown in Figure 5. cGAS and the RNA sensor RIG-I were necessary to induce TBK1 and IRF3 phosphorylation. The mtDNA was released in a selective way through mitochondrial-derived vesicles (MDVs),[83] dependent on the protein Sorting nexin-9 (SNX9), that had been shown to coordinate intracellular trafficking.[84] Human FH-deficient tumors also displayed different cell composition, as well as cytokine responses, that might link mitochondrial perturbations to cancer immunopathology.[81]

These studies expand the role of FH, from a metabolic enzyme to its role in oncological and inflammatory diseases via effects on type I IFNs as shown in Figure 5.

It has been shown previously that mtDNA can induce an inflammatory response via TLR7 or the cGAS-STING pathway.[85,86] Also, release of mtRNA has been linked to mitochondrial stress and senescence, potentially connected to the disease pathogenesis of primary osteoarthritis.[87] So far, many different sensors have been shown to recognize mitochondrial nucleic acids in the cytosol leading to ISG induction. Mitochondrial nucleic acids are additionally released into the extracellular space,[87] that might drive an IFN response in target cells and thereby promote inflammation in the surrounding cells and tissues.[88]

3 | THERAPEUTIC POSSIBILITIES

Might the targeting of metabolic pathways be useful clinically to promote antiviral immunity or limit autoimmunity via modulation of type I IFNs? Statins, which are targeting cholesterol metabolism significantly reduced risk of viral infection, including SARS-CoV-2[89,90] while data on mortality are unclear.[91] However, studies comparing the efficacy in humans are mostly retrospective, therefore comparing patients already using statins with cohorts without statin treatment.[89,92–94] So, the effect of statins on an active viral infection are unclear. While murine models showed benefits of inhibiting cholesterol metabolism or supplementation of 25-HC during viral infection,[21,28,29] the effect in humans still needs to be investigated. Therefore, targeting CH25H, and its product 25-HC, or otherwise reducing cholesterol in cell membranes in humans might provide further drug targets. Targeting prostaglandins or leukotrienes might also prove effective in regulating the production of type I IFNs in viral infection.

DMF has also been shown to inhibit viral replication, as well as suppressing the anti-inflammatory response and could be a

16000656, 2024, 1, Downloaded from https://onlinelibrary.wiley.com/doi/10.1111/imr.13318 by HEALTH RESEARCH BOARD, Wiley Online Library on [02/10/2024]. See the Terms and Conditions (https://onlinelibrary.wiley.com/terms-and-conditions) on Wiley Online Library for rules of use; OA articles are governed by the applicable Creative Commons License

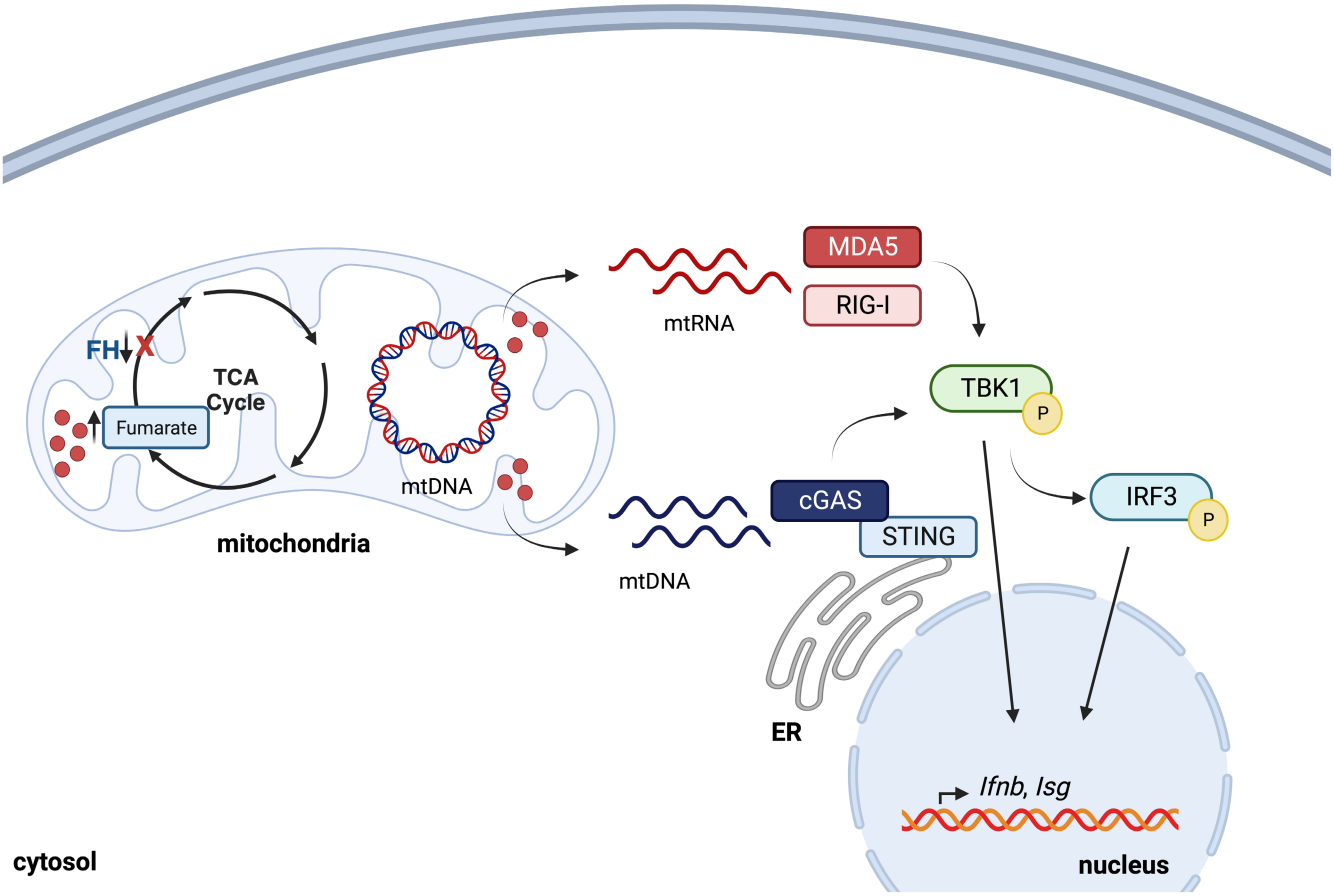


FIGURE 5 Effect of fumarate on IFN response. Inhibition or genetic ablation of fumarate hydratase (FH) leads to accumulation of fumarate, followed by release of mtDNA or mtRNA (depending on the setting and cell type). Those are either recognized by MDA5 and RIG-I or by cGAS-STING and induce TBK1 and IRF3 phosphorylation, as well as expression of type I IFNs and ISGs.

useful adjuvant to antiviral therapies. Itaconate and itaconate-derivatives have been shown to be effective in promoting host defense against bacterial and viral infections (recently reviewed here[64,65,95]). Among others itaconate reduced viral replication and disease pathology in ZIKV infection and rescued increased viral burden in ACOD1 deficient mice,[96] and controlled inflammation.[97] Endogenous itaconate levels could be modulated by specific ACOD1 targeting compounds, or generation of new itaconate derivatives that mimic certain mechanisms of itaconate biology. 4-OI functions as a three in one, an anticoagulant, antiviral, and anti-inflammatory compound. 4-OI blocks IFNs and downstream interferon-mediated coagulopathy. Furthermore, 4-OI can block IAV replication cycle by alkylating chromosomal maintenance 1 protein (CRM1), also known as exportin 1 (XPO1) on Cys-528, thus retaining IAV nucleoprotein in the nucleus which might also apply to other CRM1-dependent viruses.[98] 4-OI and further derivatives based on it should be investigated further for their therapeutic potential in interferon-related diseases such as coagulopathies and viral infection.

Macrophage fumarate hydratase restrains mtRNA-mediated interferon production. In diseases like multiple sclerosis and SLE, a reduced expression of FH might be linked to disease onset or severity so therefore targeting FH could have therapeutic potential.

4 | CONCLUSION

A complex and dynamic relationship between metabolism and IFNs has therefore recently emerged. Further understanding the metabolic regulation of IFNs by cholesterol, eicosanoids, and TCA cycle-linked metabolites will hopefully deepen our appreciation of host-pathogen interactions and provide therapeutic opportunities for the treatment of diseases where the modulation of IFNs might be beneficial.

FUNDING INFORMATION

This work was funded by Science Foundation Ireland and European Research Council.

CONFLICT OF INTEREST STATEMENT

The authors have no conflicts of interest to declare.

DATA AVAILABILITY STATEMENT

There are no data related to this publication.

ORCID

Shane M. O'Carroll https://orcid.org/0000-0002-3485-6128
Fiona D. R. Henkel https://orcid.org/0000-0003-3198-2046
Luke A. J. O'Neill https://orcid.org/0000-0002-4333-2748

16000065x, 2024, 1, Downloaded from https://onlinelibrary.wiley.com/doi/10.1111/imr.13318 by HEALTH RESEARCH BOARD, Wiley Online Library on [02/10/2024]. See the Terms and Conditions (https://onlinelibrary.wiley.com/terms-and-conditions) on Wiley Online Library for rules of use; OA articles are governed by the applicable Creative Commons License

REFERENCES

1. Platanias LC. Mechanisms of type-I- and type-II-interferon-mediated signalling. *Nat Rev Immunol*. 2005;5(5):375-386. doi:10.1038/nri1604
2. Novick D, Cohen B, Rubinstein M. The human interferon alpha/beta receptor: characterization and molecular cloning. *Cell*. 1994;77(3):391-400. doi:10.1016/0092-8674(94)90154-6
3. Schindler C, Shuai K, Prezioso VR, Darnell JE. Interferon-dependent tyrosine phosphorylation of a latent cytoplasmic transcription factor. *Science*. 1992;257(5071):809-813. doi:10.1126/science.1496401
4. Silvennoinen O, Ihle JN, Schlessinger J, Levy DE. Interferon-induced nuclear signalling by Jak protein tyrosine kinases. *Nature*. 1993;366(6455):583-585. doi:10.1038/366583a0
5. de Weerd NA, Samarajiwa SA, Hertzog PJ. Type I interferon receptors: biochemistry and biological functions. *J Biol Chem*. 2007;282(28):20053-20057. doi:10.1074/jbc.R700006200
6. Warburg O, Wind F, Negelein E. The metabolism of tumors in the body. *J Gen Physiol*. 1927;8(6):519-530. doi:10.1085/jgp.8.6.519
7. Passalacqua KD, Lu J, Goodfellow I, et al. Glycolysis is an intrinsic factor for optimal replication of a norovirus. *MBio*. 2019;10(2):e02175-18. doi:10.1128/mBio.02175-18
8. Ritter JB, Wahl AS, Freund S, Genzel Y, Reichl U. Metabolic effects of influenza virus infection in cultured animal cells: intra- and extracellular metabolite profiling. *BMC Syst Biol*. 2010;4:61. doi:10.1186/1752-0509-4-61
9. Abrantes JL, Alves CM, Costa J, et al. Herpes simplex type 1 activates glycolysis through engagement of the enzyme 6-phosphofructo-1-kinase (PFK-1). *Biochim Biophys Acta*. 2012;1822(8):1198-1206. doi:10.1016/j.bbadis.2012.04.011
10. El-Bacha T, Menezes MM, Azevedo Silva MC, Sola-Penna M, Da Poian AT. Mayaro virus infection alters glucose metabolism in cultured cells through activation of the enzyme 6-phosphofructo 1-kinase. *Mol Cell Biochem*. 2004;266(1–2):191-198. doi:10.1023/b:mcbi.0000049154.17866.00
11. Tannahill GM, Curtis AM, Adamik J, et al. Succinate is an inflammatory signal that induces IL-1β through HIF-1α. *Nature*. 2013;496(7444):238-242. doi:10.1038/nature11986
12. Krawczyk CM, Holowka T, Sun J, et al. Toll-like receptor-induced changes in glycolytic metabolism regulate dendritic cell activation. *Blood*. 2010;115(23):4742-4749. doi:10.1182/blood-2009-10-249540
13. Bajwa G, DeBerardinis RJ, Shao B, Hall B, Farrar JD, Gill MA. Cutting edge: critical role of glycolysis in human plasmacytoid dendritic cell antiviral responses. *J Immunol*. 2016;196(5):2004-2009. doi:10.4049/jimmunol.1501557
14. Olson GS, Murray TA, Jahn AN, et al. Type I interferon decreases macrophage energy metabolism during mycobacterial infection. *Cell Rep*. 2021;35(9):109195. doi:10.1016/j.celrep.2021.109195
15. Seth RB, Sun L, Ea CK, Chen ZJ. Identification and characterization of MAVS, a mitochondrial antiviral signaling protein that activates NF-kappaB and IRF 3. *Cell*. 2005;122(5):669-682. doi:10.1016/j.cell.2005.08.012
16. Jiang H, Shi H, Sun M, et al. PFKFB3-driven macrophage glycolytic metabolism is a crucial component of innate antiviral defense. *J Immunol*. 2016;197(7):2880-2890. doi:10.4049/jimmunol.1600474
17. Wang Q, Fang P, He R, et al. O -GlcNAc transferase promotes influenza A virus–induced cytokine storm by targeting interferon regulatory factor–5. *Sci Adv*. 2020;6(16):eaaz7086. doi:10.1126/sciadv.aaz7086
18. Li T, Li X, Attri KS, et al. O-GlcNAc transferase links glucose metabolism to MAVS-mediated antiviral innate immunity. *Cell Host Microbe*. 2018;24(6):791-803.e6. doi:10.1016/j.chom.2018.11.001
19. He QQ, Huang Y, Nie L, et al. MAVS integrates glucose metabolism and RIG-I-like receptor signaling. *Nat Commun*. 2023;14(1):5343. doi:10.1038/s41467-023-41028-9
20. Zhang W, Wang G, Xu ZG, et al. Lactate is a natural suppressor of RLR signaling by targeting MAVS. *Cell*. 2019;178(1):176-189.e15. doi:10.1016/j.cell.2019.05.003
21. Blanc M, Hsieh WY, Robertson KA, et al. Host defense against viral infection involves interferon mediated down-regulation of sterol biosynthesis. *PLoS Biol*. 2011;9(3):e1000598. doi:10.1371/journal.pbio.1000598
22. Mackenzie JM, Khromykh AA, Parton RG. Cholesterol manipulation by West Nile virus perturbs the cellular immune response. *Cell Host Microbe*. 2007;2(4):229-239. doi:10.1016/j.chom.2007.09.003
23. Petersen J, Drake MJ, Bruce EA, et al. The major cellular sterol regulatory pathway is required for Andes virus infection. *PLoS Pathog*. 2014;10(2):e1003911. doi:10.1371/journal.ppat.1003911
24. Bourdon M, Manet C, Montagutelli X. Host genetic susceptibility to viral infections: the role of type I interferon induction. *Genes Immun*. 2020;21(6-8):365-379. doi:10.1038/s41435-020-00116-2
25. Branche E, Wang YT, Viramontes KM, et al. SREBP2-dependent lipid gene transcription enhances the infection of human dendritic cells by Zika virus. *Nat Commun*. 2022;13(1):5341. doi:10.1038/s41467-022-33041-1
26. Radhakrishnan A, Ikeda Y, Kwon HJ, Brown MS, Goldstein JL. Sterol-regulated transport of SREBPs from endoplasmic reticulum to Golgi: oxysterols block transport by binding to Insig. *Proc Natl Acad Sci USA*. 2007;104(16):6511-6518. doi:10.1073/pnas.0700899104
27. Park K, Scott AL. Cholesterol 25-hydroxylase production by dendritic cells and macrophages is regulated by type I interferons. *J Leukoc Biol*. 2010;88(6):1081-1087. doi:10.1189/jlb.0610318
28. Blanc M, Hsieh WY, Robertson KA, et al. The transcription factor STAT-1 couples macrophage synthesis of 25-hydroxycholesterol to the interferon antiviral response. *Immunity*. 2013;38(1):106-118. doi:10.1016/j.immuni.2012.11.004
29. Liu SY, Aliyari R, Chikere K, et al. Interferon-inducible cholesterol-25-hydroxylase broadly inhibits viral entry by production of 25-hydroxycholesterol. *Immunity*. 2013;38(1):92-105. doi:10.1016/j.immuni.2012.11.005
30. Reboldi A, Dang EV, McDonald JG, Liang G, Russell DW, Cyster JG. Inflammation. 25-hydroxycholesterol suppresses interleukin-1-driven inflammation downstream of type I interferon. *Science*. 2014;345(6197):679-684. doi:10.1126/science.1254790
31. Li C, Deng YQ, Wang S, et al. 25-hydroxycholesterol protects host against Zika virus infection and its associated microcephaly in a mouse model. *Immunity*. 2017;46(3):446-456. doi:10.1016/j.immuni.2017.02.012
32. Civra A, Francese R, Gamba P, et al. 25-hydroxycholesterol and 27-hydroxycholesterol inhibit human rotavirus infection by sequestering viral particles into late endosomes. *Redox Biol*. 2018;19:318-330. doi:10.1016/j.redox.2018.09.003
33. Roulin PS, Lötzerich M, Torta F, et al. Rhinovirus uses a phosphatidylinositol 4-phosphate/cholesterol counter-current for the formation of replication compartments at the ER-Golgi interface. *Cell Host Microbe*. 2014;16(5):677-690. doi:10.1016/j.chom.2014.10.003
34. Corrotte M, Fernandes MC, Tam C, Andrews NW. Toxin pores endocytosed during plasma membrane repair traffic into the lumen of MVBs for degradation. *Traffic*. 2012;13(3):483-494. doi:10.1111/j.1600-0854.2011.01323.x
35. McNeil PL, Kirchhausen T. An emergency response team for membrane repair. *Nat Rev Mol Cell Biol*. 2005;6(6):499-505. doi:10.1038/nrm1665
36. Romero M, Keyel M, Shi G, et al. Intrinsic repair protects cells from pore-forming toxins by microvesicle shedding. *Cell Death Differ*. 2017;24(5):798-808. doi:10.1038/cdd.2017.11

1600065x, 2024, 1, Downloaded from https://onlinelibrary.wiley.com/doi/10.1111/imr.13318 by HEALTH RESEARCH BOARD, Wiley Online Library on [02/10/2024]. See the Terms and Conditions (https://onlinelibrary.wiley.com/terms-and-conditions) on Wiley Online Library for rules of use; OA articles are governed by the applicable Creative Commons License

37. Zhou QD, Chi X, Lee MS, et al. Interferon-mediated reprogramming of membrane cholesterol to evade bacterial toxins. *Nat Immunol*. 2020;21(7):746-755. doi:10.1038/s41590-020-0695-4
38. York AG, Williams KJ, Argus JP, et al. Limiting cholesterol biosynthetic flux spontaneously engages type I IFN signaling. *Cell*. 2015;163(7):1716-1729. doi:10.1016/j.cell.2015.11.045
39. Fritsch SD, Weichhart T. Effects of interferons and viruses on metabolism. *Front Immunol*. 2016;7:630. doi:10.3389/fimmu.2016.00630
40. Tanaka Y, Chen ZJ. STING specifies IRF3 phosphorylation by TBK1 in the cytosolic DNA signaling pathway. *Sci Signal*. 2012;5(214):ra20. doi:10.1126/scisignal.2002521
41. Diner EJ, Burdette DL, Wilson SC, et al. The innate immune DNA sensor cGAS produces a noncanonical cyclic dinucleotide that activates human STING. *Cell Rep*. 2013;3(5):1355-1361. doi:10.1016/j.celrep.2013.05.009
42. Ablasser A, Goldeck M, Cavlar T, et al. cGAS produces a 2′-5′-linked cyclic dinucleotide second messenger that activates STING. *Nature*. 2013;498(7454):380-384. doi:10.1038/nature12306
43. Akula MK, Shi M, Jiang Z, et al. Control of the innate immune response by the mevalonate pathway. *Nat Immunol*. 2016;17(8):922-929. doi:10.1038/ni.3487
44. Xiao J, Li W, Zheng X, et al. Targeting 7-dehydrocholesterol reductase integrates cholesterol metabolism and IRF3 activation to eliminate infection. *Immunity*. 2020;52(1):109-122.e6. doi:10.1016/j.immuni.2019.11.015
45. Lu H, Talbot S, Robertson KA, et al. Rapid proteasomal elimination of 3-hydroxy-3-methylglutaryl-CoA reductase by interferon-γ in primary macrophages requires endogenous 25-hydroxycholesterol synthesis. *Steroids*. 2015;99(Pt B):219-229. doi:10.1016/j.steroids.2015.02.022
46. Ualiyeva S, Lemire E, Aviles EC, et al. Tuft cell-produced cysteinyl leukotrienes and IL-25 synergistically initiate lung type 2 inflammation. *Sci Immunol*. 2021;6(66):eabj0474. doi:10.1126/sciimmunol.abj0474
47. McGinty JW, Ting HA, Billipp TE, et al. Tuft-cell-derived leukotrienes drive rapid anti-helminth immunity in the small intestine but are dispensable for anti-protist immunity. *Immunity*. 2020;52(3):528-541.e7. doi:10.1016/j.immuni.2020.02.005
48. Peters-Golden M, Henderson WR. Leukotrienes. *N Engl J Med*. 2007;357(18):1841-1854. doi:10.1056/NEJMra071371
49. Pernet E, Downey J, Vinh DC, Powell WS, Divangahi M. Leukotriene B4–type I interferon axis regulates macrophage-mediated disease tolerance to influenza infection. *Nat Microbiol*. 2019;4(8):1389-1400. doi:10.1038/s41564-019-0444-3
50. Gaudreault É, Paquet-Bouchard C, Fiola S, et al. TAK1 contributes to the enhanced responsiveness of LTB(4)-treated neutrophils to toll-like receptor ligands. *Int Immunol*. 2012;24(11):693-704. doi:10.1093/intimm/dxs074
51. Le Bel M, Gosselin J. Leukotriene B4 enhances NOD2-dependent innate response against influenza virus infection. *PLoS ONE*. 2015;10(10):e0139856. doi:10.1371/journal.pone.0139856
52. Bohnacker S, Hartung F, Henkel F, et al. Mild COVID-19 imprints a long-term inflammatory eicosanoid- and chemokine memory in monocyte-derived macrophages. *Mucosal Immunol*. 2022;15(3):515-524. doi:10.1038/s41385-021-00482-8
53. Shirey KA, Lai W, Pletneva LM, et al. Role of the lipoxygenase pathway in RSV-induced alternatively activated macrophages leading to resolution of lung pathology. *Mucosal Immunol*. 2014;7(3):549-557. doi:10.1038/mi.2013.71
54. Ito M, Ishida E, Tanabe F, Shigeta S, Watanabe Y, Kawade Y. Interferon-alpha enhances the production of leukotriene B4 in murine peritoneal macrophages stimulated by opsonized zymosan. *Immunology*. 1987;60(4):617-619.
55. Weighardt H, Kaiser-Moore S, Schlautkötter S, et al. Type I IFN modulates host defense and late hyperinflammation in septic peritonitis. *J Immunol*. 2006;177(8):5623-5630. doi:10.4049/jimmunol.177.8.5623
56. Gaudreault E, Gosselin J. Leukotriene B4 potentiates CpG signaling for enhanced cytokine secretion by human leukocytes. *J Immunol*. 2009;183(4):2650-2658. doi:10.4049/jimmunol.0804135
57. Serezani CH, Lewis C, Jancar S, Peters-Golden M. Leukotriene B4 amplifies NF-κB activation in mouse macrophages by reducing SOCS1 inhibition of MyD88 expression. *J Clin Invest*. 2011;121(2):671-682. doi:10.1172/JCI43302
58. Esser-von BJ. Immune-regulation and -functions of eicosanoid lipid mediators. *Biol Chem*. 2017;398(11):1177-1191. doi:10.1515/hsz-2017-0146
59. Coulombe F, Jaworska J, Verway M, et al. Targeted prostaglandin E2 inhibition enhances antiviral immunity through induction of type I interferon and apoptosis in macrophages. *Immunity*. 2014;40(4):554-568. doi:10.1016/j.immuni.2014.02.013
60. Thompson WW, Shay DK, Weintraub E, et al. Mortality associated with influenza and respiratory syncytial virus in the United States. *JAMA*. 2003;289(2):179-186. doi:10.1001/jama.289.2.179
61. McElhaney JE, Verschoor CP, Andrew MK, Haynes L, Kuchel GA, Pawelec G. The immune response to influenza in older humans: beyond immune senescence. *Immun Ageing*. 2020;17:10. doi:10.1186/s12979-020-00181-1
62. Chen J, Deng JC, Zemans RL, et al. Age-induced prostaglandin E2 impairs mitochondrial fitness and increases mortality to influenza infection. *Nat Commun*. 2022;13(1):6759. doi:10.1038/s41467-022-34593-y
63. Pernet E, Sun S, Sarden N, et al. Neonatal imprinting of alveolar macrophages via neutrophil-derived 12-HETE. *Nature*. 2023;614(7948):530-538. doi:10.1038/s41586-022-05660-7
64. Day EA, O'Neill LAJ. Protein targeting by the itaconate family in immunity and inflammation. *Biochem J*. 2022;479(24):2499-2510. doi:10.1042/BCJ20220364
65. O'Carroll SM, O'Neill LAJ. Targeting immunometabolism to treat COVID-19. *Immunother Adv*. 2021;1(1):ltab013. doi:10.1093/immadv/ltab013
66. Peace CG, O'Neill LA. The role of itaconate in host defense and inflammation. *J Clin Invest*. 2022;132(2):e148548. doi:10.1172/JCI148548
67. Swain A, Bambouskova M, Kim H, et al. Comparative evaluation of itaconate and its derivatives reveals divergent inflammasome and type I interferon regulation in macrophages. *Nat Metab*. 2020;2(7):594-602. doi:10.1038/s42255-020-0210-0
68. Gobelli D, Serrano-Lorenzo P, Esteban-Amo MJ, et al. The mitochondrial succinate dehydrogenase complex controls the STAT3-IL-10 pathway in inflammatory macrophages. *iScience*. 2023;26(8):107473. doi:10.1016/j.isci.2023.107473
69. Mills EL, Kelly B, Logan A, et al. Succinate dehydrogenase supports metabolic repurposing of mitochondria to drive inflammatory macrophages. *Cell*. 2016;167(2):457-470.e13. doi:10.1016/j.cell.2016.08.064
70. Li Y, Li YC, Liu XT, et al. Blockage of citrate export prevents TCA cycle fragmentation via Irg1 inactivation. *Cell Rep*. 2022;38(7):110391. doi:10.1016/j.celrep.2022.110391
71. Chen F, Elgaher WAM, Winterhoff M, et al. Citraconate inhibits ACOD1 (IRG1) catalysis, reduces interferon responses and oxidative stress, and modulates inflammation and cell metabolism. *Nat Metab*. 2022;4(5):534-546. doi:10.1038/s42255-022-00577-x
72. Li W, Li Y, Kang J, et al. 4-octyl itaconate as a metabolite derivative inhibits inflammation via alkylation of STING. *Cell Rep*. 2023;42(3):112145. doi:10.1016/j.celrep.2023.112145
73. Olagnier D, Brandtoft AM, Gunderstofte C, et al. Nrf2 negatively regulates STING indicating a link between antiviral sensing and metabolic reprogramming. *Nat Commun*. 2018;9(1):3506. doi:10.1038/s41467-018-05861-7

1600065x, 2024, 1, Downloaded from https://onlinelibrary.wiley.com/doi/10.1111/imr.13318 by HEALTH RESEARCH BOARD, Wiley Online Library on [02/10/2024]. See the Terms and Conditions (https://onlinelibrary.wiley.com/terms-and-conditions) on Wiley Online Library for rules of use; OA articles are governed by the applicable Creative Commons License

74. Runtsch MC, Angiari S, Hooftman A, et al. Itaconate and itaconate derivatives target JAK1 to suppress alternative activation of macrophages. *Cell Metab*. 2022;34(3):487-501.e8. doi:10.1016/j.cmet.2022.02.002
75. Kobayashi EH, Suzuki T, Funayama R, et al. Nrf2 suppresses macrophage inflammatory response by blocking proinflammatory cytokine transcription. *Nat Commun*. 2016;7:11624. doi:10.1038/ncomms11624
76. Mills EL, Ryan DG, Prag HA, et al. Itaconate is an anti-inflammatory metabolite that activates Nrf2 via alkylation of KEAP1. *Nature*. 2018;556(7699):113-117. doi:10.1038/nature25986
77. Ryan DG, Knatko EV, Casey AM, et al. Nrf2 activation reprograms macrophage intermediary metabolism and suppresses the type I interferon response. *iScience*. 2022;25(2):103827. doi:10.1016/j.isci.2022.103827
78. Olagnier D, Farahani E, Thyrsted J, et al. SARS-CoV2-mediated suppression of NRF2-signaling reveals potent antiviral and anti-inflammatory activity of 4-octyl-itaconate and dimethyl fumarate. *Nat Commun*. 2020;11(1):4938. doi:10.1038/s41467-020-18764-3
79. Ryan TAJ, Hooftman A, Rehill AM, et al. Dimethyl fumarate and 4-octyl itaconate are anticoagulants that suppress tissue factor in macrophages via inhibition of type I interferon. *Nat Commun*. 2023;14(1):3513. doi:10.1038/s41467-023-39174-1
80. Hooftman A, Peace CG, Ryan DG, et al. Macrophage fumarate hydratase restrains mtRNA-mediated interferon production. *Nature*. 2023;615(7952):490-498. doi:10.1038/s41586-023-05720-6
81. Zecchini V, Paupe V, Herranz-Montoya I, et al. Fumarate induces vesicular release of mtDNA to drive innate immunity. *Nature*. 2023;615(7952):499-506. doi:10.1038/s41586-023-05770-w
82. Valcarcel-Jimenez L, Frezza C. Fumarate hydratase (FH) and cancer: a paradigm of oncometabolism. *Br J Cancer*. 2023;129:1546-1557. doi:10.1038/s41416-023-02412-w
83. Sugiura A, McLelland GL, Fon EA, McBride HM. A new pathway for mitochondrial quality control: mitochondrial-derived vesicles. *EMBO J*. 2014;33(19):2142-2156. doi:10.15252/embj.201488104
84. Bendris N, Schmid SL. Endocytosis, metastasis and beyond: multiple facets of SNX9. *Trends Cell Biol*. 2017;27(3):189-200. doi:10.1016/j.tcb.2016.11.001
85. Kim J, Gupta R, Blanco LP, et al. VDAC oligomers form mitochondrial pores to release mtDNA fragments and promote lupus-like disease. *Science*. 2019;366(6472):1531-1536. doi:10.1126/science.aav4011
86. Oka T, Hikoso S, Yamaguchi O, et al. Mitochondrial DNA that escapes from autophagy causes inflammation and heart failure. *Nature*. 2012;485(7397):251-255. doi:10.1038/nature10992
87. Kim S, Lee K, Choi YS, et al. Mitochondrial double-stranded RNAs govern the stress response in chondrocytes to promote osteoarthritis development. *Cell Rep*. 2022;40(6):111178. doi:10.1016/j.celrep.2022.111178
88. Peace CG, O'Carroll SM, O'Neill LAJ. Fumarate hydratase as a metabolic regulator of immunity. *Trends Cell Biol*. 2023. doi:10.1016/j.tcb.2023.10.005
89. Oh TK, Song IA, Jeon YT. Statin therapy and the risk of COVID-19: a cohort study of the national health insurance service in South Korea. *J Pers Med*. 2021;11(2):116. doi:10.3390/jpm11020116
90. Wu BR, Chen DH, Liao WC, et al. Statin therapy and the risk of viral infection: a retrospective population-based cohort study. *J Clin Med*. 2022;11(19):5626. doi:10.3390/jcm11195626
91. Chen P, Wu M, He Y, Jiang B, He ML. Metabolic alterations upon SARS-CoV-2 infection and potential therapeutic targets against coronavirus infection. *Signal Transduct Target Ther*. 2023;8(1):237. doi:10.1038/s41392-023-01510-8
92. Kow CS, Hasan SS. Meta-analysis of effect of statins in patients with COVID-19. *Am J Cardiol*. 2020;134:153-155. doi:10.1016/j.amjcard.2020.08.004
93. Permana H, Huang I, Purwiga A, et al. In-hospital use of statins is associated with a reduced risk of mortality in coronavirus-2019 (COVID-19): systematic review and meta-analysis. *Pharmacol Rep*. 2021;73(3):769-780. doi:10.1007/s43440-021-00233-3
94. Santosa A, Franzén S, Nåtman J, Wettermark B, Parmryd I, Nyberg F. Protective effects of statins on COVID-19 risk, severity and fatal outcome: a nationwide Swedish cohort study. *Sci Rep*. 2022;12(1):12047. doi:10.1038/s41598-022-16357-2
95. McGettrick AF, O'Neill LA. Two for the price of one: itaconate and its derivatives as an anti-infective and anti-inflammatory immunometabolite. *Curr Opin Immunol*. 2023;80:102268. doi:10.1016/j.coi.2022.102268
96. Daniels BP, Kofman SB, Smith JR, et al. The nucleotide sensor ZBP1 and kinase RIPK3 induce the enzyme IRG1 to promote an antiviral metabolic state in neurons. *Immunity*. 2019;50(1):64-76.e4. doi:10.1016/j.immuni.2018.11.017
97. Sohail A, Iqbal AA, Sahini N, et al. Itaconate and derivatives reduce interferon responses and inflammation in influenza A virus infection. *PLoS Pathog*. 2022;18(1):e1010219. doi:10.1371/journal.ppat.1010219
98. Ribó-Molina P, Weiss HJ, Susma B, et al. 4-Octyl itaconate reduces influenza a replication by targeting the nuclear export protein CRM1. *J Virol*. 2023;97(10):e0132523. doi:10.1128/jvi.01325-23

How to cite this article: O'Carroll SM, Henkel FDR, O'Neill LAJ. Metabolic regulation of type I interferon production. *Immunol Rev*. 2024;323:276-287. doi:10.1111/imr.13318

1600065x, 2024, 1, Downloaded from https://onlinelibrary.wiley.com/doi/10.1111/imr.13318 by HEALTH RESEARCH BOARD, Wiley Online Library on [02/10/2024]. See the Terms and Conditions (https://onlinelibrary.wiley.com/terms-and-conditions) on Wiley Online Library for rules of use; OA articles are governed by the applicable Creative Commons License

Immunotherapy ADVANCES

Immunotherapy Advances, 2021, Vol. 1, No. 1, 1–10
doi:10.1093/immadv/ltab013
Advance Access Publication Date: 2 June 2021
Review

OXFORD

Review

Targeting immunometabolism to treat COVID-19

Shane M. O'Carroll*,[®] and Luke A. J. O'Neill

School of Biochemistry and immunology, Trinity Biomedical Sciences Institute, Trinity College Dublin, Dublin, Ireland

*Correspondence: Shane M. O'Carroll, School of Biochemistry and immunology, Trinity Biomedical Sciences Institute, Trinity College Dublin, Dublin, Ireland. Email: shocarro@tcd.ie

Received 15 March 2021; Revised 7 May 2021; Accepted 31 May 2021

Summary

The COVID-19 crisis has emphasised the need for antiviral therapies to combat current and future viral zoonoses. Recent studies have shown that immune cells such as macrophages are the main contributors to the inflammatory response seen in the later inflammatory phase of COVID-19. Immune cells in the context of a viral infection such as SARS-CoV-2 undergo metabolic reprogramming to elicit these pro-inflammatory effector functions. The evidence of metabolic reprogramming in COVID-19 offers opportunities for metabolites with immunomodulatory properties to be investigated as potential therapies to combat this hyper-inflammatory response. Recent research indicates that the metabolite itaconate, previously known to be broadly antibacterial, may have both antiviral and immunomodulatory potential. Furthermore, low itaconate levels have shown to correlate with COVID-19 disease severity, potentially implicating its importance in the disease. The antiviral potential of itaconate has encouraged researchers to synthesise itaconate derivatives for antiviral screening, with some encouraging results. This review summarises the antiviral and immunomodulatory potential of immunometabolic modulators including metformin, peroxisome proliferator-activated receptor agonists and TEPP-46 as well as itaconate, and its derivatives and their potential use as broad spectrum anti-viral agents.

Abbreviations: ACE2: Angiotensin-converting enzyme 2; ACOD1: Aconitate decarboxylase 1; CCL5: C-C Motif Chemokine Ligand 5; CXCL-10: C-X-C motif chemokine ligand 10; DMF: Dimethyl fumarate; GLUT-1: Glucose transporter 1; HCV: Hepatitis C; HIF1α: Hypoxia-inducible factor 1-alpha; HMOX1: Heme Oxygenase 1; HSV1: Simplex Virus-1; HSV2: Herpes Simplex Virus-2; IFNβ: Interferon beta; IL: Interleukin; IRF-3: Interferon regulatory factor 3; IRG1: Immune responsive gene 1; ISG15: Interferon stimulated gene 15; 4-OI: 4-Octyl itaconate; LDH-A: Lactate dehydrogenase A; LPS: Lipopolysaccharides; Mtb: *Mycobacterium tuberculosis*; mTOR: Mechanistic target of rapamycin; mtROS: Mitochondrial ROS; NETs: Neutrophil extracellular traps; NF-κB: Nuclear factor kappa B; NLRP3: NOD-, LRR- and pyrin domain-containing protein 3; NLRs: NOD-like receptors; NqO1: NAD(P)H Quinone Dehydrogenase 1; NRF2: Nuclear factor-erythroid factor 2-related factor 2; NS5A: Non-Structural Protein 5A; OAS2: 2′-5′-Oligoadenylate Synthetase 2; PBMCs: Peripheral blood mononuclear cells; PFKFB3, 6-Phosphofructo-2-Kinase/Fructose-2,6-Biphosphatase 3; PKM2: Pyruvate kinase M2; PPAR: Peroxisome proliferator activated receptor; PPP: Pentose phosphate pathway; PRR: Pathogen recognition receptor; RAS: Rennin-angiotensin system; RET: Reverse electron transport; RIPK1: Receptor-interacting protein kinase-1; RIPK2: Receptor-interacting protein kinase-2; RSV: Respiratory syncytial virus; T2DM: Type 2 diabetes mellitus; TCA: Tricarboxylic acid cycle; TMPRSS2: Transmembrane protease serine 2; TNF: Tumour necrosis factor; VACV: Vaccinia virus; WNV: West Nile Virus; ZBP1: Z-form nucleic acid sensor; ZIKV: Zika virus.

© The Author(s) 2021. Published by Oxford University Press on behalf of the British Society for Immunology.
This is an Open Access article distributed under the terms of the Creative Commons Attribution License (http://creativecommons.org/licenses/by/4.0/), which permits unrestricted reuse, distribution, and reproduction in any medium, provided the original work is properly cited.

Downloaded from https://academic.oup.com/immunotherapyadv/article/1/1/ltab013/6291349 by guest on 02 October 2024

Keywords: COVID-19, SARS-CoV-2, macrophage, immunometabolism, innate immune reprogramming

Introduction

The innate immune system is our immune system's first line of defence against viruses, such as SARS-CoV-2. It consists of a set of germline-encoded pathogen recognition receptors (PRRs) that function to recognise pathogen-associated molecular patterns. For viral recognition, these PRRs consist of toll-like receptors, RIG-I-like receptors, NOD-like receptors (NLRs), and DNA sensors. Each sense conserved molecular structures in viruses (largely nucleic acid-based) and induce intracellular signalling cascades that converge on transcription factor activation and subsequent transcription of genes encoding pro-inflammatory cytokines, chemokines, and type I interferons to regulate the immune response, induce inflammation and limit viral replication [1].

Apart from the well-known innate immune signalling triggered by a viral infection, metabolic change also occurs downstream of some of these sensors. This was first discovered in response to LPS from Gram-negative bacteria. LPS activation of toll-like receptor 4 pathway upregulates aerobic glycolysis and fatty acid synthesis with a concomitant reduction in mitochondrial respiration and β-oxidation in macrophages. Breakpoints occur in the tricarboxylic acid cycle (TCA) cycle after succinate and citrate, causing these metabolites to accumulate. The accumulation of citrate drives mitochondrial ROS (mtROS), nitric oxide accumulation, itaconate production and contributes to the pro-inflammatory phenotype of M1-like macrophages [2]. Citrate accumulation also causes acetyl-CoA to build up and contributes to epigenetic changes such as histone acetylation, facilitating transcription of inflammatory genes [3].

Accumulation of succinate drives Warburg-like metabolism and acts by inhibiting prolyl hydroxylases, thus increasing hypoxia-inducible factor 1-alpha (HIF1α) stabilisation. This drives glycolysis and also increases transcription of the pro-inflammatory cytokine interleukin-1β (IL-1β). Succinate accumulation also causes reverse electron transport (RET) causing mtROS production and the stabilisation of HIF1α [4, 5].

During viral infection the host undergoes two phases of response, the first phase is a pro-inflammatory viral limiting response and the second phase is the resolution and anti-inflammatory phase. Both phases are important to effective viral clearance and host recovery from infection, and mal-adaptive responses in either phase can result in pathologies not directly related to viral load or viral effects, but the immunopathology caused by cells of the immune system [6].

Given the importance of macrophages in both phases of the immune response and the demonstrated metabolic flexibility modulating macrophage phenotype this review focuses on the metabolic reprogramming and immunological response to metabolic modulation and metabolites as a potential therapeutic avenue to the treatment of the pathogenic inflammation associated with COVID-19.

Metabolic reprogramming during viral infection

Much of the understanding of metabolic reprogramming in innate immunity stems from challenge with bacterial derived LPS in macrophages. However, there is an increasing appreciation for metabolic change in response to viral sensing. Metabolic reprogramming in host cells in response to viral infection facilitates an effective antiviral innate immune response. Many viruses, however, 'hijack' host cell metabolism in an immune evasion strategy. This is done by causing metabolic dysfunction, increasing flux through the pentose phosphate pathway (PPP) to increase nucleotide biosynthesis and diverting amino acid metabolism for virion replication, maturation, and viral dissemination [7]. Many viruses upregulate PPP by increasing aerobic glycolysis. Such experiments include influenza A infection of mammalian cell-lines, hepatitis C (HCV) infection of hepatocyte cell-lines, adenovirus, Kaposi's sarcoma-associated herpesvirus infection of lymphatic endothelial cells, and Epstein-Barr virus infection of neural progenitor cells [7]. Viruses often upregulate glycolysis via viral proteins which interact with and regulate key enzymes. In hepatocyte cell-lines, Non-Structural Protein 5A (NS5A) from HCV binds and activates hexokinase, a rate-limiting glycolytic enzyme, to increase glycolytic rate [8]. Creating this Warburg-like metabolism also contributes to the production of type I interferons and inflammatory cytokines which aid in the anti-viral immune response [9].

Viral infection often activates HIF1α which contributes to anti-viral innate immunity by producing inflammatory mediators. However, HIF1α also upregulates glycolytic genes needed for virion replication and therefore benefits the virus [10]. Many viruses also modulate other metabolic pathways such as downregulating mitochondrial β-oxidation and upregulating fatty acid synthesis to aid virus envelopment for the release of the virus [11].

Downloaded from https://academic.oup.com/immunotherapyadv/article/1/1/ltab013/6291349 by guest on 02 October 2024

Metabolic reprogramming in COVID19 contributes to the antiviral immune response

The progression from SARS-CoV-2 infection to severe COVID-19 is caused by a mal-adaptive immune response which is defined by failure to elicit a timely and robust type-I interferon innate immune response. This leads to increased viral load, followed by a hyperinflammatory immune response, such as acute phase reactants and inflammatory markers such as interleukin-6 (IL-6), tumour necrosis factor (TNF), IL1β, and interleukin-18 (IL-18) [12]. This bi-phasic nature of COVID-19 progression to severe disease, the early viral phase followed by the inflammatory phase, suggests that anti-inflammatory therapies would be suited to those who present later in the infection and have persistently increased inflammatory markers.

Monocytes and macrophages are the most abundant immune cell-types in SARS-CoV-2-infected lungs and contribute to hyper-inflammatory cytokine production evident in severe COVID-19 [13]. SARS-CoV-2 infects many cell types including airway epithelial cells and macrophages. Infection of macrophages causes metabolic reprogramming, similar to that created by LPS, causing an increase in aerobic glycolysis, reduction of the TCA cycle and RET (See Figure 1) [14]. This metabolic reprogramming

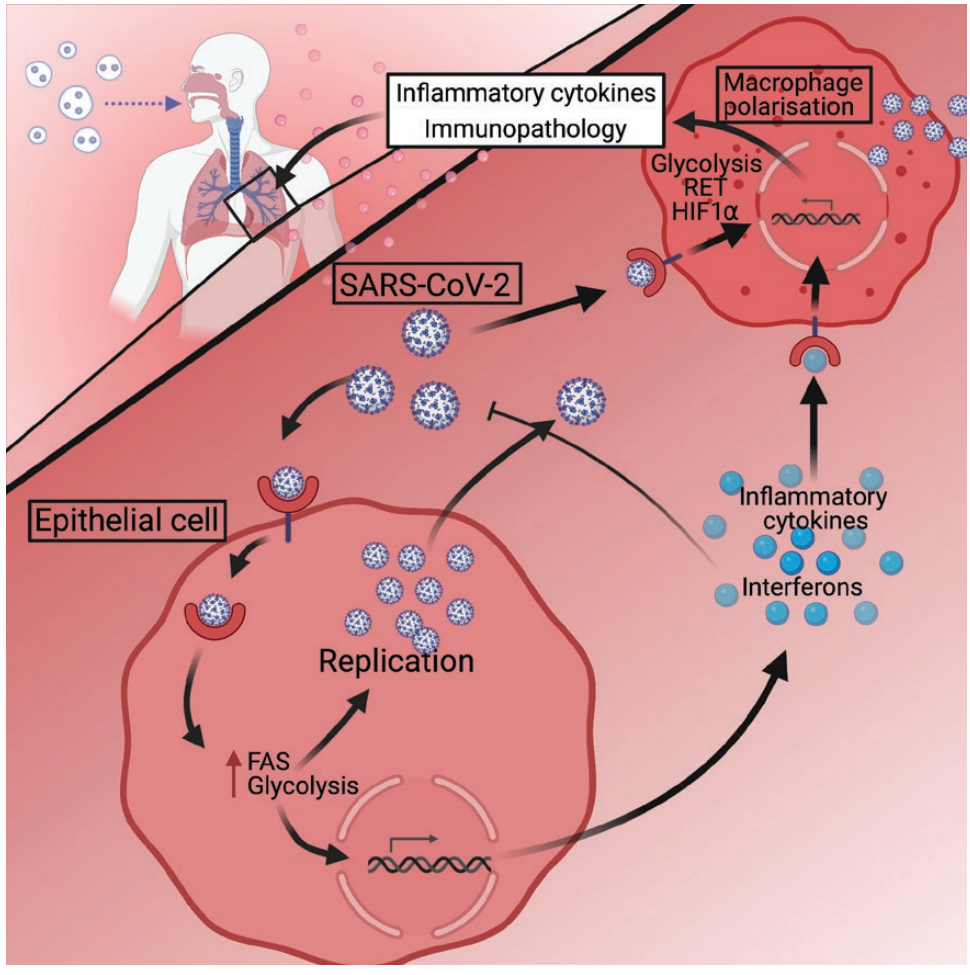


Figure 1. Schematic of SARS-CoV-2 infection in the lung. SARS-CoV-2 infection of airway epithelial cells and macrophages causes an upregulation of glycolysis and fatty acid synthesis (FAS), to enable viral replication and release of SARS-CoV-2. Viral sensing by PRRs causes interferon production, while increased glycolysis and FAS induces inflammatory cytokine production. Macrophages can be infected by SARS-CoV-2 in the same mechanism or can be polarised by inflammatory cytokines produced by airway epithelial cells. M1-like polarisation of macrophages causes the production of inflammatory cytokines that contribute to the immunopathology seen in COVID-19. Created with Biorender.com.

Downloaded from https://academic.oup.com/immunotherapyadv/article/1/1/ltab013/6291349 by guest on 02 October 2024

is mediated by the production of mtROS, stabilisation of HIF1α and HIF1α-mediated transcription of core glycolytic genes involved in glucose import and glycolysis including Glucose transporter 1 (GLUT-1), Pyruvate kinase M2 (PKM2), Lactate dehydrogenase A (LDH-A), and 6-Phosphofructo-2-Kinase/Fructose-2,6-Biphosphatase 3 (PFKFB3). It has also been shown that lactate dehydrogenase, an important enzyme in Warburg metabolism in M1-like macrophages, is a prognostic marker of disease severity in COVID-19 and further highlights the role of glycolysis in COVID-19 [15]. *Ex-vivo* experiments using human monocytes from SARS-CoV-2-infected patients showed that HIF1α protein was significantly increased when compared to uninfected patients. *In-vitro* experiments with SARS-CoV-2-infected human monocytes elegantly demonstrate that elevated glucose levels and glycolysis facilitate SARS-CoV-2 replication, as blocking glycolysis inhibits viral replication. Furthermore, the increased glycolysis also increases the production of IL-1β which contributes to the hyperinflammatory response of COVID-19. These *in-vitro* experiments directly implicate HIF1α in viral replication and inflammatory cytokine production as HIF1α inhibition was shown to inhibit SARS-CoV-2 replication and HIF1α activation increased viral replication. Furthermore, HIF1α inhibition also blocked transcription of inflammatory cytokines associated with severe COVID19 including IL1β, TNF, IL6, interferon alpha (IFNα), interferon beta (IFNβ), and Angiotensin-converting enzyme 2 (ACE2) [14]. This makes compelling evidence for targeting mtROS-HIFα-metabolic reprogramming as a potential treatment of severe COVID-19 by inhibiting viral replication and the inflammatory cytokines seen in COVID-19 pathology (see Figure 2) [14].

Itaconate and COVID-19

Given these metabolic features, and the discovery that low plasma itaconate levels correlate with COVID-19 disease severity, it seems likely that itaconate might play a role in COVID-19 [16]. Itaconate is a metabolite produced by the decarboxylation of the TCA cycle intermediate cis-aconitate, a reaction catalysed by aconitate decarboxylase 1 (ACOD1), also referred to as immune responsive gene 1 (IRG1) [17, 18]. IRG1 and itaconate have been closely associated with the metabolic reprogramming of macrophages *in-vitro* into an M1-like phenotype as IRG1 is one of the most upregulated genes in classically activated macrophages [19]. The main role of itaconate in macrophages is to act in a negative feedback fashion, limiting inflammation [20]. Notably, itaconate is also antibacterial against many pathogens including *Salmonella enterica* and *Mycobacterium tuberculosis* (Mtb). These bacteria use carbon sources produced by the glyoxylate shunt to survive during human infection. Itaconate inhibits this glyoxylate shunt via blocking a key enzyme isocitrate lyase. Itaconate also stops Mtb from using carbon sources from cholesterol degradation by inhibiting Mtb mediated detoxification of propionic acid [21].

As well as being anti-bacterial, itaconate is also immunomodulatory. Biochemically, itaconate has been shown to alkylate cystine residues, resulting in changes to protein structure and binding. *In-vitro* experiments have shown that exogenous itaconate treatment of bone-marrow-derived macrophages upregulates IFN-β in a yet undetermined mechanism [22]. Also, itaconate and its derivative 4-Octyl itaconate, (4-OI), inhibits NOD-, LRR-, and pyrin domain-containing protein 3 (NLRP3) inflammasome activation, preventing the secretion of IL-1β [23] which is implicated in COVID-19 immunopathology [24]. Furthermore, itaconate reduces other inflammatory cytokines such as IL-6 and interleukin-10 (IL-10) [22, 25].

Not only has itaconate potential immunomodulatory effects, but itaconate has previously been shown to be antiviral against Zika virus (ZIKV) in murine models (see Table 1). ZIKV infection of murine neurons is sensed by the Z-form nucleic acid sensor (ZBP1). ZBP1 causes necroptotic-independent signalling via receptor-interacting protein kinase-1 (RIPK1) and receptor-interacting protein kinase-2 (RIPK2) leading to Interferon Regulatory Factor 1(IRF1)-dependant upregulation of IRG1 and concomitant itaconate synthesis. In this case, itaconate inhibits succinate dehydrogenase, causing succinate accumulation and driving an antiviral metabolic state in neurons via reduced TCA cycle metabolism and reduced oxygen consumption rate [26]. This effect was emphasised by demonstrating that IRG1 knock-out mice have higher levels of ZIKV replication [26]. Furthermore, IRG1 mediates an antiviral state in primary cortical neurons against West Nile Virus (WNV), and subsequent knockdown of IRG1 enhanced WNV infection [27]. This suggests that itaconate could have antiviral properties against ZIKV, WNV and possibly SARS-CoV-2 as they are all positive-strand RNA viruses (see Table 1).

An interesting link from itaconate to SARS-CoV-2 was recently reported. 4-OI, a derivative of itaconate, has been shown to activate nuclear factor-erythroid factor 2-related factor 2 (NRF2) via the alkylation of Kelch Like ECH Associated Protein 1 (KEAP1) [28]. Furthermore,

Downloaded from https://academic.oup.com/immunotherapyadv/article/1/1/ltab013/6291349 by guest on 02 October 2024

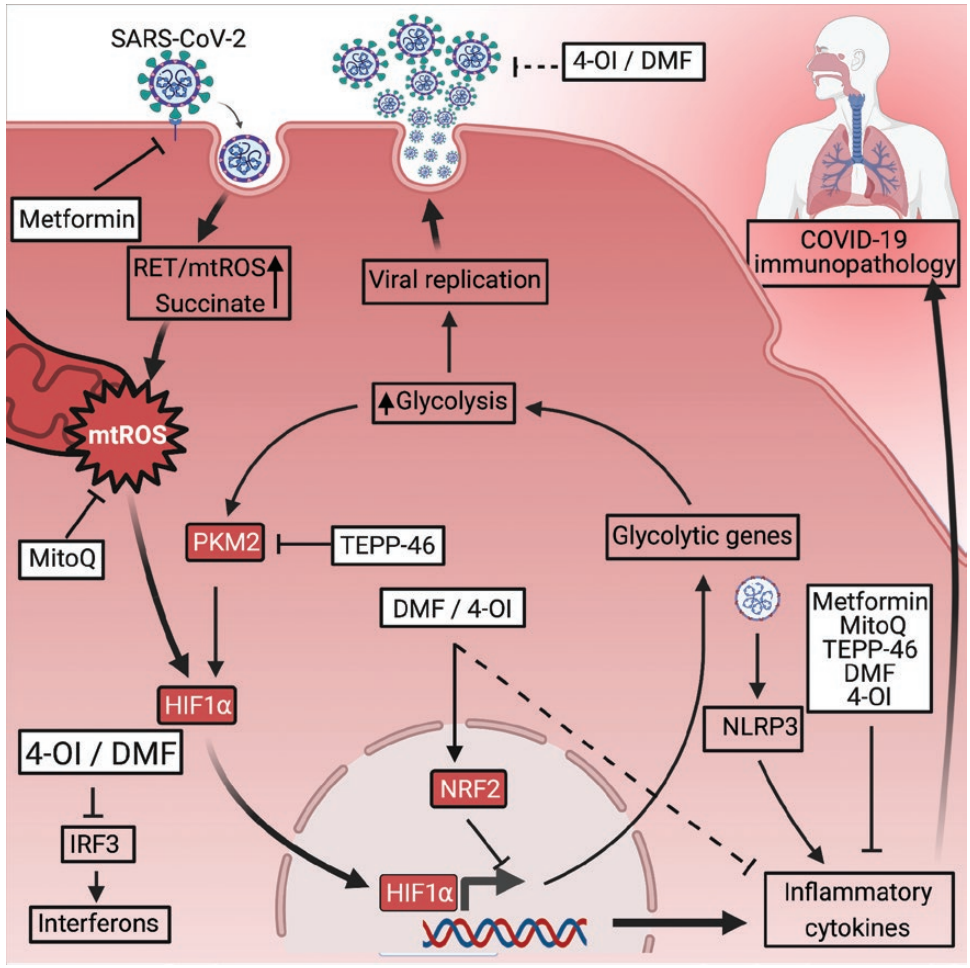


Figure 2. Metabolic modulators to treat COVID-19. 4-OI and DMF activate NRF2 which inhibit inflammatory cytokines. NRF2 activation prevents IRF-3 signalling, inhibiting interferon responses. 4-OI and DMF prevent TMPRSS2 expression which may prevent SARS-CoV-2 cell entry. MitoQ blocks SARS-CoV-2 replication. MitoQ increases autophagy and reduces mtROS to reduce inflammatory cytokines expression. TEPP-46 maintains PKM2 in an inactive conformation, preventing activation of HIF1α and associated inflammatory cytokines. Metformin phosphorylates ACE2 Ser680 which might prevent viral entry. Metformin upregulates ACE2, preventing RAS-mediated inflammation. Metformin inhibits inflammatory cytokine IL1β and upregulates anti-inflammatory cytokine IL-10. Created with Biorender.com.

Table 1. Antiviral immunomodulators

	SARS-CoV-2	WNV	ZIKV	HSV1/2	VACV	Influenza A
Itaconate	ND	(-)	(-)	ND	ND	(-)
4-OI	(-)	ND	(-)	(-)	(-)	ND
DMF	(-)	ND	(-)	(-)	(-)	ND
Metformin	(-)	ND	(-)	ND	ND	(-)

Viral inhibition is annotated with '(-)', not determined is annotated with 'ND'.

NRF2 activation is impaired in IRG-1-deficient macrophages treated with LPS. Of note, itaconate can restore LPS-induced NRF2 activation in IRG-1-deficient macrophages [29, 30]. This is interesting as NRF2 functions as a transcription factor that binds to the promoter region of pro-inflammatory genes, preventing RNA

Downloaded from https://academic.oup.com/immunotherapyadv/article/1/1/ltab013/6291349 by guest on 02 October 2024

Polymerase II binding and also inhibits the transcription of pro-inflammatory cytokines IL6 and IL1β in macrophages [31]. NRF2 also drives antioxidant genes which reduce mtROS and HIF1α-mediated inflammation. Transcriptome analysis of severe COVID-19 patients has shown that NRF2 dependant genes are suppressed including Heme Oxygenase 1 (HMOX1) and NAD(P)H Quinone Dehydrogenase 1 (NqO1) [32]. This suggests that these NRF2 activators could be used as therapies for COVID-19.

Both 4-OI and dimethyl fumarate (DMF) are both NRF2 activators and inhibit SARS-Cov-2 replication in human airway epithelial cells. This antiviral effect also extends to Zika virus, Herpes Simplex Virus-1 (HSV1), Herpes Simplex Virus-2 (HSV2), and Vaccinia virus (VACV) (see Table 1). Furthermore, 4-OI and DMF inhibit the pathogenic interferon response in an NRF2-dependant mechanism by blocking interferon regulatory factor 3 (IRF-3) dimerisation. This was shown by demonstrating that silencing NRF2 rescues IRF-3 signalling. Additionally, NRF2 also reduces interferon responses by reducing stimulator of interferon genes (STING) expression [33]. Interestingly, 4-OI and DMF also inhibit SARS-CoV-2 replication in epithelial cells and human peripheral blood mononuclear cells (PBMCs) in a yet undetermined NRF2-independent mechanism.

Importantly, it was also shown that 4-OI and DMF blocked the expression of inflammatory factors including IFNβ1, C-X-C motif chemokine ligand 10 (CXCL-10), TNF, IL-1β, and C-C Motif Chemokine Ligand 5 (CCL5) induced by SARS-CoV-2 infection. Furthermore, pretreatment with 4-OI or DMF upregulate anti-inflammatory markers such as HMOX1, indicating an increase in the anti-inflammatory responses. This anti-inflammatory effect was also seen in *ex vivo* PBMC samples of severe COVID-19 patients treated with 4-OI. These results show that 4-OI and DMF inhibit SARS-CoV-2 replication in human airway epithelial cells, while also suppressing the macrophage-mediated pathogenic interferon and inflammatory responses seen in the later inflammatory phase of COVID-19 (see Figure 2) [32].

Other Itaconate derivatives are directly antiviral against Influenza A Virus by binding to the viral nucleoprotein and blocking ribonucleoprotein export from the nucleus to the cytosol and preventing the replication cycle of the virus [34].

Other metabolic targets in SARS-CoV-2 infection

Mitochondrial dysfunction and the production of mtROS are common features of SARS-CoV-2 infection in human macrophages *ex-vivo* and *in vivo* and causes the stabilisation of HIF1α and the subsequent production of pro-inflammatory cytokines [14]. This mechanism has also been seen in SARS-CoV-1 studies demonstrating that nucleocapsid protein N disrupts mitochondrial membrane potential and increases mtROS *in vitro* [35]. Furthermore, SARS-CoV-2 infection of bronchial epithelial cells reduces mitochondrial gene expression, leading to mitochondrial dysfunction and increasing mtROS *in vitro* [36]. Proteins involved in mitochondrial fission are also suppressed, increasing mitochondrial fusion and which impairs antiviral interferon responses [37].

With this in mind, MitoQ is a mitochondria-specific antioxidant that increases autophagy and reduces mtROS *in vitro* and in murine models [38]. Additionaly, studies demonstrate that MitoQ has antiviral potential. *In vivo* mouse models have shown that MitoQ reduce dextran sulfate sodium-induced colitis by reducing inflammatory cytokines IL-1β, TNF, and mtROS [39, 40]. Furthermore, *in-vitro* models of Respiratory syncytial virus (RSV) infection of vero and HEK293T-cells have shown that MitoQ suppresses RSV viral infection by blocking mitochondrial dysfunction and mtROS production [39, 41]. Importantly, an *in-vitro* study using SARS-CoV-2 infection of human monocytes shows that MitoQ blocks SARS-CoV-2 replication, and reduces HIF1α stabilisation and inflammatory cytokine IL-1β and ACE2 (see Figure 2) [14]

Increased glycolysis is also associated with SARS-CoV-2 replication. PKM2 is an enzyme that catalyses the final step of glycolysis and also has important roles in immune cell reprogramming and inflammation. However, PKM2 activity depends on its oligomerisation state. PKM2 tetramers are inactive, whereas phosphorylation of PKM2 forms a dimer that enters the nucleus, binds HIF1α, and causes the expression of proinflammatory and glycolytic genes [42]. In the context of COVID-19, both PKM2 levels and phosphorylated PKM2 levels increase with COVID-19 severity. This indicates that PKM2 is important in COVID-19 severity via activation of HIF1α and the expression of inflammatory cytokines [43]. This metabolic reprogramming causes cytosolic succinate accumulation which activates HIF1α. This is supported by *ex-vivo* COVID-19 studies show that succinate levels and nuclear translocation of both HIF1α and PKM2 positively correlate with COVID-19 disease severity [43]. Maintaining PKM2 as a tetramer could therefore be a potential therapy for COVID-19. Compounds such as TEPP-46 maintain PKM2 in a tetramer, inhibiting Warburg-like metabolism, succinate accumulation, inflammatory cytokine IL-1β and inhibits HIF1α dependant transcription of glycolytic genes needed for SARS-CoV-2 (see Figure 2) [44].

Downloaded from https://academic.oup.com/immunotherapyadv/article/1/1/ltab013/6291349 by guest on 02 October 2024

Other potential immunomodulators being proposed for the treatment of COVID-19 include peroxisome proliferator activated receptor (PPAR) agonists. PPARs are a group of transcription factors which regulate glucose and lipid metabolism as well as macrophage polarisation [45]. These transcription factor agonists may be a therapy to dampen the late inflammatory phase of COVID-19 as PPAR-γ agonists such as rosiglitazone can block nuclear factor kappa B (NF-κB)-mediated inflammatory cytokine production in lung epithelial cells [46, 47]. In the case of COVID-19, lung biopsies of COVID-19 patients show PPAR-γ is suppressed in M1-like macrophages, similar to that of PPAR-γ knockout macrophages. Furthermore SUMO1, a protein in the PPAR-γ complex was shown to be repressed in severe COVID-19 and shown to interact with a SARS nucleoprotein [48]. This suggests that SARS-CoV-2 may interact with SUMO1, repress PPAR-γ activity, leading to the hyperinflammatory response seen in severe COVID-19. PPAR-γ agonists could, in theory, be suggested as a therapy to dampen the excessive inflammation seen in the lungs of COVID-19 patients.

Metformin and DMF in COVID-19

Metformin is a safe, widely used glucose lowering agent used to treat type 2 diabetes mellitus (T2DM). The antiviral potential of metformin was first discovered in the 1940s when it showed significant anti-influenza properties [49]. Metformin has been shown to block ZIKA virus replication, increase innate immune signalling via interferon-stimulated genes such as interferon stimulated gene 15 (ISG15), 2′-5′-Oligoadenylate Synthetase 2 (OAS2) and blocks TNF and CCL5 production *in vitro* and *in vivo* (see Table 1) [50].

Metformin significantly reduced hospital mortality in diabetic patients with COVID-19, suggesting therapeutic potential [51]. Metformin's anti-viral effect could be attributed to several potential mechanisms. SARS-CoV-2 entry into cells causes the downregulation of ACE2. ACE2 downregulation dysregulates the rennin-angiotensin system (RAS) which may contribute to increased inflammation. Metformin induces ACE2 expression in Human umbilical vein endothelial cells, potentially preventing RAS dysregulation and reducing inflammation [52]. Furthermore, in human endothelial cells, metformin causes increased phosphorylation of ACE2 Ser680 via AMPK. This might suggest that ACE2 phosphorylation might block spike-ACE2 interaction or binding and therefore reduce SARS-CoV-2 cell entry (see Figure 2) [53]. Metformin also blocks IL1β production and increases the anti-inflammatory cytokine IL-10 and inhibits complex 1 in mitochondria, indicating its anti-inflammatory potential for COVID-19 [40]. Furthermore, neutrophil extracellular traps (NETs) contribute to the immunopathology seen in COVID-19 [54]. Metformin inhibits NETs in diabetic patients [55]. Metformin has also been shown to block mechanistic target of rapamycin (mTOR). Sirolimus, another mTOR inhibitor has been shown to block MERS-CoV infection *in vitro* and significantly improve ICU patient outcome [56, 57]. Clinical trials investigating mTOR inhibitors against COVID-19 are currently recruiting participants. Metformin might have potential as a therapy for COVID-19.

Dimethyl fumarate (DMF) is a common therapy for adult patients with relapsing-remitting multiple sclerosis [58, 59]. Studies suggest that DMF might have a similar mechanism of action as itaconate by activating NRF2 and target enzymes in glycolysis [60]. DMF inhibits SARS-CoV-2 replication and replication of other viruses such as VACV, Zika virus, HSV1/2 in an interferon independent mechanism (see Table 1) [32]. DMF also suppresses inflammatory responses seen in severe COVID-19 by both liberating NRF2 and inhibiting the NF-κB signalling pathway by preventing p65 nuclear translocation. This has been shown to inhibit the transcription of inflammatory cytokines IFNB1, CXCL10, and CCL5 gene expression and upregulation of anti-inflammatory genes HMOX1 (see Figure 2) [32, 61]. Furthermore, activating NRF2 also blocks transmembrane protease serine 2 (TMPRSS2) expression, which is needed for ACE2-mediated cell penetration of SARS-CoV-2 via the spike protein [62, 63]. Given that DMF is an approved medication further research on whether it reduces severity of COVID19 is warranted.

Conclusion

Studies into how SARS-CoV-2 affects intracellular metabolism during infection reveals interesting biochemical features, including increased glycolysis and dysregulated oxidative phosphorylation in innate immune cells. Preventing these metabolic changes in immune cells such as macrophages might yield new anti-viral and anti-inflammatory therapies. Itaconate might have potential antiviral and anti-inflammatory potential. The mounting of a robust innate immune response in the early phase of SARS-CoV-2 infection is important to reduce viral load. However, the ability to limit the viral-mediated metabolic reprogramming in host immune cells and other infected cells to reduce the excessive inflammatory response seen in the later phase of SARS-CoV-2 infection is an interesting prospect for the treatment of individuals who progress to severe COVID-19. The anti-viral and immunomodulatory properties of itaconate derivatives and DMF may give

Downloaded from https://academic.oup.com/immunotherapyadv/article/1/1/ltab013/6291349 by guest on 02 October 2024

us two for the price of one; inhibition of viral replication and suppression of inflammation. Given these features, further studies with these metabolic modulators are well justified.

Acknowledgements

The Editor-in-Chief, Tim Elliott, and handling editor, Marianne Boes, would like to thank the following reviewers, Pedro Moraes Vieira and Bart Everts, for their contribution to the publication of this article.

Author contributions

S.O'C and L.A.J.O'N. wrote the manuscript.

Funding

The O'Neill laboratory acknowledges the following grant support: European Research Council Metabinate (834370), Science Foundation Ireland (12/IA/ 1531), and The Wellcome Trust (205455).

Conflict of interest

The authors declare no competing interests.

Data availability

Not applicable.

References

1. Bourdon M, Manet C, Montagutelli X. Host genetic susceptibility to viral infections: the role of type I interferon induction. *Genes Immun* 2020;**21**(6-8):365–79. https://doi.org/10.1038/s41435-020-00116-2
2. O'Neill LA, Kishton RJ, Rathmell J. A guide to immunometabolism for immunologists. *Nat Rev Immunol* 2016;**16**(9):553–65. https://doi.org/10.1038/nri.2016.70
3. Lauterbach MA, Hanke JE, Serefidou M *et al*. Toll-like receptor signaling rewires macrophage metabolism and promotes histone acetylation via ATP-Citrate Lyase. *Immunity* 2019;**51**(6):997–1011.e7. https://doi.org/10.1016/j.immuni.2019.11.009
4. Selak MA, Armour SM, MacKenzie ED *et al*. Succinate links TCA cycle dysfunction to oncogenesis by inhibiting HIF-alpha prolyl hydroxylase. *Cancer Cell* 2005;**7**(1):77–85. https://doi.org/10.1016/j.ccr.2004.11.022
5. Mills EL, Kelly B, Logan A *et al*. Succinate dehydrogenase supports metabolic repurposing of mitochondria to drive inflammatory macrophages. *Cell* 2016;**167**(2):457–470.e13. https://doi.org/10.1016/j.cell.2016.08.064
6. Rouse BT, Sehrawat S. Immunity and immunopathology to viruses: what decides the outcome? *Nat Rev Immunol* 2010;**10**(7):514–26. https://doi.org/10.1038/nri2802
7. Goodwin CM, Xu S, Munger J. Stealing the keys to the kitchen: Viral manipulation of the host cell metabolic network. *Trends Microbiol* 2015;**23**(12):789–98. https://doi.org/10.1016/j.tim.2015.08.007
8. Ramière C, Rodriguez J, Enache LS *et al*. Activity of hexokinase is increased by its interaction with hepatitis C virus protein NS5A. *J Virol* 2014;**88**(6):3246–54. https://doi.org/10.1128/JVI.02862-13
9. Bajwa G, DeBerardinis RJ, Shao B *et al*. Cutting Edge: Critical role of glycolysis in human plasmacytoid dendritic cell antiviral responses. *J Immunol* 2016;**196**(5):2004–9.
10. Reyes A, Corrales N, Gálvez NMS *et al*. Contribution of hypoxia inducible factor-1 during viral infections. *Virulence* 2020;**11**(1):1482–500. https://doi.org/10.4049/jimmunol.1501557
11. Keshavarz M, Solaymani-Mohammadi F, Namdari H *et al*. Metabolic host response and therapeutic approaches to influenza infection. *Cell Mol Biol Lett* 2020;**25**:15. https://doi.org/10.1186/s11658-020-00211-2
12. Hadjadj J, Yatim N, Barnabei L *et al*. Impaired type I interferon activity and inflammatory responses in severe COVID-19 patients. *Science* 2020;**369**(6504):718–24. https://doi.org/10.1126/science.abc6027
13. Merad M, Martin JC. Pathological inflammation in patients with COVID-19: a key role for monocytes and macrophages. *Nat Rev Immunol* 2020;**20**(6):355–62. https://doi.org/10.1038/s41577-020-0331-4
14. Codo AC, Davanzo GG, Monteiro LB *et al*. Elevated glucose levels favor SARS-CoV-2 infection and monocyte response through a HIF-1α/Glycolysis-dependent axis. *Cell Metab* 2020;**32**(3):437–46.e5. https://doi.org/10.1016/j.cmet.2020.07.007
15. Zhou F, Yu T, Du R *et al*. Clinical course and risk factors for mortality of adult inpatients with COVID-19 in Wuhan, China: a retrospective cohort study. *Lancet* 2020;**395**(10229):1054–62. https://doi.org/10.1016/S0140-6736(20)30566-3
16. Song JW, Lam SM, Fan X *et al*. Omics-Driven systems interrogation of metabolic dysregulation in COVID-19 pathogenesis. *Cell Metab* 2020;**32**(2):188–202.e5. https://doi.org/10.1016/j.cmet.2020.06.016
17. Strelko CL, Lu W, Dufort FJ *et al*. Itaconic acid is a mammalian metabolite induced during macrophage activation. *J Am Chem Soc* 2011;**133**(41):16386–9. https://doi.org/10.1021/ja2070889
18. Michelucci A, Cordes T, Ghelfi J *et al*. Immune-responsive gene 1 protein links metabolism to immunity by catalyzing itaconic acid production. *Proc Natl Acad Sci USA* 2013;**110**(19):7820–5. https://doi.org/10.1073/pnas.1218599110
19. Lampropoulou V, Sergushichev A, Bambouskova M *et al*. Itaconate links inhibition of succinate dehydrogenase with macrophage metabolic remodeling and regulation of inflammation. *Cell Metab* 2016;**24**(1):158–66. https://doi.org/10.1016/j.cmet.2016.06.004
20. Yu XH, Zhang DW, Zheng XL *et al*. Itaconate: an emerging determinant of inflammation in activated macrophages.

Downloaded from https://academic.oup.com/immunotherapyadv/article/1/1/ltab013/6291349 by guest on 02 October 2024

Immunol Cell Biol 2019;**97**(2):134–41. https://doi.org/10.1111/imcb.12218
21. Cordes T, Michelucci A, Hiller K. Itaconic Acid: the surprising role of an industrial compound as a mammalian antimicrobial metabolite. *Annu Rev Nutr* 2015;**35**:451–73. https://doi.org/10.1146/annurev-nutr-071714-034243
22. Swain A, Bambouskova M, Kim H *et al*. Comparative evaluation of itaconate and its derivatives reveals divergent inflammasome and type I interferon regulation in macrophages. *Nat Metab* 2020;**2**(7):594–602. https://doi.org/10.1038/s42255-020-0210-0
23. Hooftman A, Angiari S, Hester S *et al*. The immunomodulatory metabolite itaconate modifies NLRP3 and inhibits inflammasome activation. *Cell Metab* 2020;**32**(3):468–478.e7. https://doi.org/10.1016/j.cmet.2020.07.016
24. Rodrigues TS, de Sá KSG, Ishimoto AY *et al*. Inflammasomes are activated in response to SARS-CoV-2 infection and are associated with COVID-19 severity in patients. *J Exp Med* 2021;**218**(3). https://doi.org/10.1084/jem.20201707
25. Gurung P, Malireddi RK, Anand PK *et al*. Toll or interleukin-1 receptor (TIR) domain-containing adaptor inducing interferon-β (TRIF)-mediated caspase-11 protease production integrates Toll-like receptor 4 (TLR4) protein- and Nlrp3 inflammasome-mediated host defense against enteropathogens. *J Biol Chem* 2012;**287**(41):34474–83. https://doi.org/10.1074/jbc.M112.401406
26. Daniels BP, Kofman SB, Smith JR *et al*. The nucleotide sensor ZBP1 and kinase RIPK3 induce the enzyme IRG1 to promote an antiviral metabolic state in neurons. *Immunity* 2019;**50**(1):64–76.e4. https://doi.org/10.1016/j.immuni.2018.11.017
27. Cho H, Proll SC, Szretter KJ *et al*. Differential innate immune response programs in neuronal subtypes determine susceptibility to infection in the brain by positive-stranded RNA viruses. *Nat Med* 2013;**19**(4):458–64. https://doi.org/10.1038/nm.3108
28. Mills EL, Ryan DG, Prag HA *et al*. Itaconate is an anti-inflammatory metabolite that activates Nrf2 via alkylation of KEAP1. *Nature* 2018;**556**(7699):113–7. https://doi.org/10.1038/nature25986
29. Bambouskova M, Gorvel L, Lampropoulou V *et al*. Electrophilic properties of itaconate and derivatives regulate the IκBζ-ATF3 inflammatory axis. *Nature* 2018;**556**(7702):501–4. https://doi.org/10.1038/s41586-018-0052-z
30. Bambouskova M, Potuckova L, Paulenda T *et al*. Itaconate confers tolerance to late NLRP3 inflammasome activation. *Cell Rep* 2021;**34**(10):108756. https://doi.org/10.1016/j.celrep.2021.108756
31. Kobayashi EH, Suzuki T, Funayama R *et al*. Nrf2 suppresses macrophage inflammatory response by blocking proinflammatory cytokine transcription. *Nat Commun* 2016;**7**:11624. https://doi.org/10.1038/ncomms11624
32. Olagnier D, Farahani E, Thyrsted J *et al*. SARS-CoV2-mediated suppression of NRF2-signaling reveals potent antiviral and anti-inflammatory activity of 4-octyl-itaconate and dimethyl fumarate. *Nat Commun* 2020;**11**(1):4938. https://doi.org/10.1038/s41467-020-18764-3
33. Olagnier D, Brandtoft AM, Gunderstofte C *et al*. Nrf2 negatively regulates STING indicating a link between antiviral sensing and metabolic reprogramming. *Nat Commun* 2018;**9**(1):3506. https://doi.org/10.1038/s41467-018-05861-7
34. Sethy B, Hsieh CF, Lin TJ *et al*. Design, synthesis, and biological evaluation of itaconic acid derivatives as potential anti-influenza agents. *J Med Chem* 2019;**62**(5):2390–403. https://doi.org/10.1021/acs.jmedchem.8b01683
35. Zhang L, Wei L, Jiang D *et al*. SARS-CoV nucleocapsid protein induced apoptosis of COS-1 mediated by the mitochondrial pathway. *Artif Cells Blood Substit Immobil Biotechnol* 2007;**35**(2):237–53. https://doi.org/10.1080/10731190601188422
36. Guzzi PH, Mercatelli D, Ceraolo C *et al*. Master regulator analysis of the SARS-CoV-2/Human interactome. *J Clin Med* 2020;**9**(4). https://doi.org/10.3390/jcm9040982
37. Singh K, Chen YC, Judy JT *et al*. Network analysis and transcriptome profiling identify autophagic and mitochondrial dysfunctions in SARS-CoV-2 Infection. *BioRxiv* 2020. https://doi.org/10.1101/2020.05.13.092536
38. Murphy MP, Smith RA. Targeting antioxidants to mitochondria by conjugation to lipophilic cations. *Annu Rev Pharmacol Toxicol* 2007;**47**:629–56. https://doi.org/10.1146/annurev.pharmtox.47.120505.105110
39. Dashdorj A, Jyothi KR, Lim S *et al*. Mitochondria-targeted antioxidant MitoQ ameliorates experimental mouse colitis by suppressing NLRP3 inflammasome-mediated inflammatory cytokines. *BMC Med* 2013;**11**:178. https://doi.org/10.1186/1741-7015-11-178
40. Kelly B, Tannahill GM, Murphy MP *et al*. Metformin inhibits the production of reactive oxygen species from NADH: Ubiquinone Oxidoreductase to limit induction of Interleukin-1β (IL-1β) and boosts Interleukin-10 (IL-10) in Lipopolysaccharide (LPS)-activated Macrophages. *J Biol Chem* 2015;**290**(33):20348–59. https://doi.org/10.1074/jbc.M115.662114
41. Hu M, Bogoyevitch MA, Jans DA. Subversion of host cell mitochondria by RSV to favor virus production is dependent on inhibition of mitochondrial Complex I and ROS generation. *Cells* 2019;**8**(11). https://doi.org/10.3390/cells8111417
42. Corcoran SE, O'Neill LA. HIF1α and metabolic reprogramming in inflammation. *J Clin Invest* 2016;**126**(10):3699–707. https://doi.org/10.1172/JCI84431
43. McElvaney OJ, McEvoy NL, McElvaney OF *et al*. Characterization of the inflammatory response to severe COVID-19 illness. *Am J Respir Crit Care Med* 2020;**202**(6):812–21. https://doi.org/10.1164/rccm.202005-1583OC
44. Palsson-McDermott EM, Curtis AM, Goel G *et al*. Pyruvate kinase M2 regulates Hif-1α activity and IL-1β induction and is a critical determinant of the warburg effect in LPS-activated macrophages. *Cell Metab* 2015;**21**(1):65–80. https://doi.org/10.1016/j.cmet.2014.12.005
45. Bouhlel MA, Derudas B, Rigamonti E *et al*. PPARgamma activation primes human monocytes into alternative

Downloaded from https://academic.oup.com/immunotherapyadv/article/1/1/ltab013/6291349 by guest on 02 October 2024

M2 macrophages with anti-inflammatory properties. *Cell Metab* 2007;**6**(2):137–43. https://doi.org/10.1016/j.cmet.2007.06.010

46. Neri T, Armani C, Pegoli A *et al*. Role of NF-kappaB and PPAR-gamma in lung inflammation induced by monocyte-derived microparticles. *Eur Respir J* 2011;**37**(6):1494–502. https://doi.org/10.1183/09031936.00023310
47. Ghaffari S, Roshanravan N, Tutunchi H *et al*. Oleoylethanolamide, a bioactive lipid amide, as a promising treatment strategy for Coronavirus/COVID-19. *Arch Med Res* 2020;**51**(5):464–7. https://doi.org/10.1016/j.arcmed.2020.04.006
48. Desterke C, Turhan AG, Bennaceur-Griscelli A *et al*. PPARγ cistrome repression during activation of lung monocyte-macrophages in severe COVID-19. *Iscience* 2020;**23**(10):101611. https://doi.org/10.1016/j.isci.2020.101611
49. Bailey CJ. Metformin: historical overview. *Diabetologia* 2017;**60**(9):1566–76. https://doi.org/10.1007/s00125-017-4318-z
50. Singh S, Singh PK, Suhail H *et al*. AMP-Activated protein kinase restricts zika virus replication in endothelial cells by potentiating innate antiviral responses and inhibiting glycolysis. *J Immunol* 2020;**204**(7):1810–24. https://doi.org/10.4049/jimmunol.1901310
51. Luo P, Qiu L, Liu Y *et al*. Metformin treatment was associated with decreased mortality in COVID-19 patients with diabetes in a retrospective analysis. *Am J Trop Med Hyg* 2020;**103**(1):69–72. https://doi.org/10.4269/ajtmh.20-0375
52. Iwasaki M, Saito J, Zhao H *et al*. Inflammation triggered by SARS-CoV-2 and ACE2 augment drives multiple organ failure of severe COVID-19: molecular mechanisms and implications. *Inflammation* 2021;**44**(1):13–34. https://doi.org/10.1007/s10753-020-01337-3
53. Liu J, Li X, Lu Q *et al*. AMPK: a balancer of the renin-angiotensin system. *Biosci Rep* 2019;**39**(9). https://doi.org/10.1042/BSR20181994
54. Barnes BJ, Adrover JM, Baxter-Stoltzfus A *et al*. Targeting potential drivers of COVID-19: neutrophil extracellular traps. *J Exp Med*. 2020;**217**(6). https://doi.org/10.1084/jem.20200652
55. Carestia A, Frechtel G, Cerrone G *et al*. NETosis before and after hyperglycemic control in Type 2 diabetes mellitus patients. *PLoS One* 2016;**11**(12):e0168647. https://doi.org/10.1371/journal.pone.0168647
56. Kindrachuk J, Ork B, Hart BJ *et al*. Antiviral potential of ERK/MAPK and PI3K/AKT/mTOR signaling modulation for Middle East respiratory syndrome coronavirus infection as identified by temporal kinome analysis. *Antimicrob Agents Chemother* 2015;**59**(2):1088–99. https://doi.org/10.1128/AAC.03659-14
57. Wang CH, Chung FT, Lin SM *et al*. Adjuvant treatment with a mammalian target of rapamycin inhibitor, sirolimus, and steroids improves outcomes in patients with severe H1N1 pneumonia and acute respiratory failure. *Crit Care Med* 2014;**42**(2):313–21. https://doi.org/10.1097/CCM.0b013e3182a2727d
58. Fox RJ, Kita M, Cohan SL *et al*. BG-12 (dimethyl fumarate): a review of mechanism of action, efficacy, and safety. *Curr Med Res Opin* 2014;**30**(2):251–62. https://doi.org/10.1185/03007995.2013.849236
59. Gold R, Kappos L, Arnold DL *et al*.; DEFINE Study Investigators. Placebo-controlled phase 3 study of oral BG-12 for relapsing multiple sclerosis. *N Engl J Med* 2012;**367**(12):1098–107. https://doi.org/10.1056/NEJMoa1114287
60. Kornberg MD, Bhargava P, Kim PM *et al*. Dimethyl fumarate targets GAPDH and aerobic glycolysis to modulate immunity. *Science* 2018;**360**(6387):449–53. https://doi.org/10.1126/science.aan4665
61. Kastrati I, Siklos MI, Calderon-Gierszal EL *et al*. Dimethyl Fumarate inhibits the nuclear factor κB pathway in breast cancer cells by covalent modification of p65 Protein. *J Biol Chem* 2016;**291**(7):3639–47. https://doi.org/10.1074/jbc.M115.679704
62. Schultz MA, Hagan SS, Datta A *et al*. Nrf1 and Nrf2 transcription factors regulate androgen receptor transactivation in prostate cancer cells. *PLoS One* 2014;**9**(1):e87204. https://doi.org/10.1371/journal.pone.0087204
63. Hoffmann M, Kleine-Weber H, Schroeder S *et al*. SARS-CoV-2 cell entry depends on ACE2 and TMPRSS2 and is blocked by a clinically proven protease inhibitor. *Cell* 2020;**181**(2):271–280.e8. https://doi.org/10.1016/j.cell.2020.02.052

Downloaded from https://academic.oup.com/immunotherapyadv/article/1/1/ltab013/6291349 by guest on 02 October 2024

CellPress

Trends in Cell Biology

Opinion

Fumarate hydratase as a metabolic regulator of immunity

Christian G. Peace [1,*], Shane M. O'Carroll [1], and Luke A.J. O'Neill [1]

Tricarboxylic acid (TCA) cycle metabolites have been implicated in modulating signalling pathways in immune cells. Notable examples include succinate and itaconate, which have pro- and anti-inflammatory roles, respectively. Recently, fumarate has emerged as having specific roles in macrophage activation, regulating the production of such cytokines as interleukin (IL)-10 and type I interferons (IFNs). Fumarate hydratase (FH) has been identified as a control point. Notably, FH loss in different models and cell types has been found to lead to DNA and RNA release from mitochondria which are sensed by cytosolic nucleic acid sensors including retinoic acid-inducible gene (RIG)-I, melanoma differentiation-associated protein (MDA)5, and cyclic GMP-AMP synthase (cGAS) to upregulate IFN-β production. These findings may have relevance in the pathogenesis and treatment of diseases associated with decreased FH levels such as systemic lupus erythematosus (SLE) or FH-deficient kidney cancer.

Highlights

Metabolism is a key regulator of immune cell function.

Tricarboxylic acid cycle rewiring and metabolites have immunoregulatory roles.

Fumarate hydratase (FH) and fumarate are now known to regulate cytokine production.

Recent findings suggest FH loss leads to mitochondrial nucleic acid release, leading to type I interferon production.

Introduction

Metabolic pathways determine how the nutrients taken up by cells are utilised to support cellular function. Depending on cell type and requirements, diverse pathways can be used to provide sufficient energy and the biosynthetic precursors required for the production of carbohydrates, nucleic acids, lipids, and proteins [1].

Mitochondria are central metabolic hubs, in which a variety of carbon sources such as glucose, glutamine, or lactate can be metabolized into fuels for the TCA cycle (also known as the Krebs or citric acid cycle). This leads to the generation of substrates that are used in the electron transport chain (ETC), ultimately transferring electrons to oxygen (O_2) to generate ATP, the main bioenergetic intermediate used by most processes in eukaryotic cells.

Although mitochondrial function has traditionally been considered a consequence of cellular demands, recently the concept of mitochondria generating signals which determine cellular function through communicating with the cell in numerous ways has been explored [2,3]. Examples of this include how mitochondria regulate the epigenome via metabolites such as succinate and α-ketoglutarate, and the release of nucleic acids which act as danger-associated molecular patterns (DAMPs) to stimulate innate immune responses. As such, these roles have brought mitochondria and metabolism into the spotlight in recent years in the context of cancer and immunity [4].

The importance of metabolism in innate immunity

Our understanding of how metabolic rewiring in macrophages orchestrates immunity is continuing to grow. Macrophages exposed to M1-polarising stimuli such as lipopolysaccharide (LPS) have vastly different metabolic requirements relative to resting macrophages. These inflammatory

[1]School of Biochemistry and Immunology, Trinity Biomedical Sciences Institute, Trinity College Dublin, Dublin, Ireland

*Correspondence: peacec@tcd.ie (C.G. Peace).

© 2023 Elsevier Ltd. All rights reserved.

macrophages upregulate metabolic programs that facilitate effector functions including cytokine production, antigen presentation, and phagocytosis. Hallmarks of rewiring involves an upregulation of glycolysis, decreased oxidative phosphorylation and oxygen consumption, increased glutamine metabolism, increased production of necessary biosynthetic precursors, as well as the accumulation of signalling metabolites.

The identification of metabolites as signalling molecules has altered traditional views regarding the function of many metabolites, which have been viewed merely as intermediates or byproducts required by cells to meet energetic or biosynthetic demands [5]. Strikingly, certain TCA cycle metabolites naturally accumulate in response to stimuli and dictate cell fate and function and particularly cytokine production.

Importantly, unbiased metabolomics and tracing experiments have identified the pathways which are upregulated and the metabolites which accumulate abundantly in macrophages [6]. A notable early studied example of an immunometabolite is the TCA cycle intermediate succinate [7]. Succinate has been identified as a proinflammatory signal that upregulates transcription of IL-1β through stabilisation of hypoxia inducible factor (HIF)-1α. Product inhibition of prolyl-hydroxylase (PHD) enzymes by cytosolic succinate causes stabilisation of HIF-1α which binds to the *Il1b* promoter to upregulate transcription. Additionally, oxidation of succinate by succinate dehydrogenase (SDH) (also known as complex II of the ETC) leads to a highly reduced ubiquinone pool which is unable to be efficiently consumed by complex III, resulting in reverse electron transport at complex I and the generation of reactive oxygen species (ROS) which are also able to promote HIF-1α stabilisation and IL-1β production [8]. Additionally, extracellular succinate is able to activate its receptor (GPR91) to exacerbate inflammatory signalling as succinate has been found to upregulate IL-1β in this manner in rheumatoid arthritis [9].

While succinate is considered a proinflammatory signal, itaconate is a metabolite which is produced from the decarboxylation of the TCA cycle intermediate, *cis*-aconitate, by the enzyme *cis*-aconitate decarboxylase 1(ACOD1) transcribed by the gene *Irg1* [10]. It has been found to have numerous anti-inflammatory and immunomodulatory properties. Early reports showed that the inhibition of SDH by itaconate prevents the oxidation of succinate, thereby decreasing ROS production [11]. Additionally, as itaconate contains an α-β unsaturated alkene group, it is mildly electrophilic and is able to alkylate cysteine thiols via Michael addition [12]. The modification of cysteines by itaconate, and its cell-permeable derivatives such as 4-octyl-itaconate, has been found to be responsible for numerous important immunomodulatory effects such as the activation of nuclear factor erythroid 2-related factor 2 (Nrf2), leading to an antioxidant and anti-inflammatory transcriptional response, inhibition of the NLRP3 inflammasome [13,14], inhibition of glycolysis [15], inhibition of Janus kinase 1 (JAK1) signalling [16], and induction of lysosomal biogenesis [17]. More recently, itaconate has been found to regulate DNA methylation through inhibition of the 2-oxoglutarate-dependent dioxygenase (2-OGDD) ten eleven translocase 2 (TET2) which may be responsible for many of the immunomodulatory effects observed for itaconate [18]. Similarly, itaconate has also recently been found to signal and activate the G protein-coupled receptor OXGR1 (also known as GPR99) which senses the similar metabolite α-ketoglutarate [19]. Activation of this GPCR may have important physiological implications in diseases such *as Pseudomonas aeruginosa* infection [19]. These effects underscore the centrality of metabolism in regulating macrophage effector function.

Fumarate as a signalling metabolite

Fumarate is another TCA cycle metabolite that has been well studied in the field of cancer metabolism for decades and is now becoming increasingly relevant to immunology. Cancer

studies have predominantly examined FH-deficient and mutant tumours [20–22]. As FH metabolizes fumarate to malate, loss of FH activity results in high levels of fumarate and a dysregulated TCA cycle. This has been found to activate numerous pathways leading to cancer initiation and progression [22–25]. Two of the main chemical properties of fumarate which allow it to act as an oncometabolite are its structural similarity to α-ketoglutarate, and its α-β unsaturated alkene group which makes it mildly electrophilic, similar to itaconate (Figure 1).

The structural similarity of fumarate to α-ketoglutarate allows it to inhibit the family of 2-OGDDs. The inhibition of PHDs by fumarate has been found to promote HIF-1α [21], inhibition of histone demethylases (KDMs) impairs histone demethylation [26], and inhibition of TETs impairs DNA demethylation [25]. Notably, these have been found to facilitate hypoxic responses as well as an epithelial-to-mesenchymal transition by fumarate, both of which are confer protumour properties.

Additionally, the electrophilicity of fumarate is responsible for modification of reactive thiols in cysteine residues resulting in the post-translational modification termed succination [27]. Over the past several years, there have been efforts made using numerous approaches to characterise succination targets. In both FH-deficient tumours and macrophages, these include redox-sensitive cysteines on KEAP1 which induces activation of the antioxidant transcription factor Nrf2, and a cysteine on GAPDH which suppresses its activity to decrease glycolysis. Other targets identified include Lyn in B cells to prevent its downstream signalling, as well as gasdermin D in macrophages which prevents pyroptotic cell death [28–32]. Similarly, FH-deficient tumours

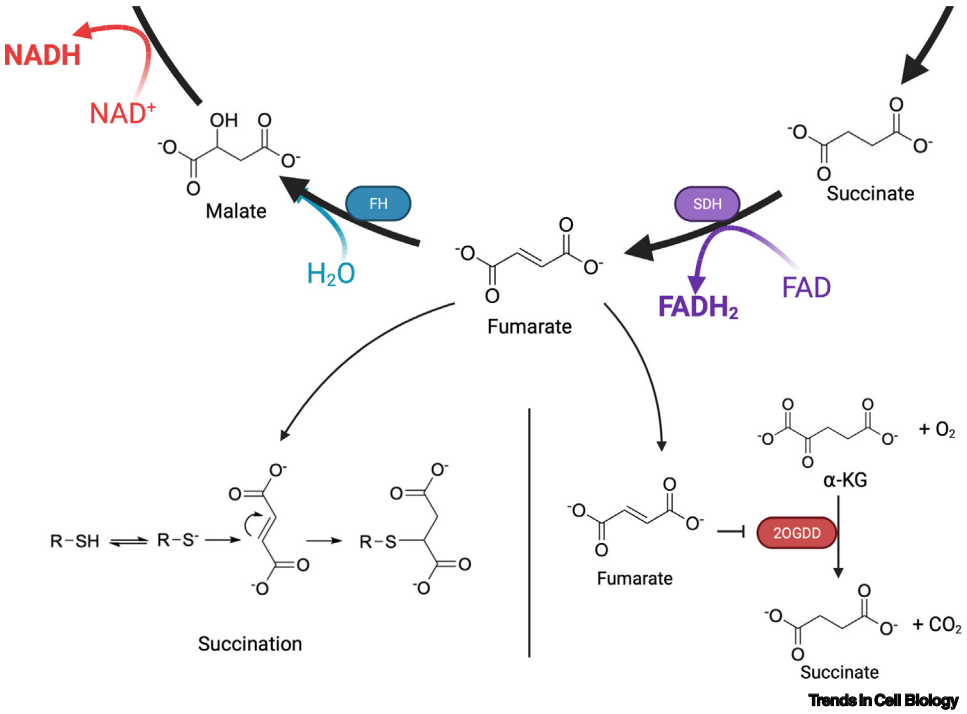


Figure 1. Fumarate as a signalling metabolite. Fumarate is a TCA cycle intermediate which can be converted by FH to malate. It is also able to function as a signalling metabolite with two notable mechanisms of action. Firstly (left) fumarate acts as an electrophilic cysteine modifier in a Michael addition reaction known as succination. Secondly (right) fumarate can inhibit 2-OGDDs to regulate a variety of processes including HIF activation and epigenetic modifications. Abbreviations: α-KG, α-ketoglutarate; FH, fumarate hydratase; 2-OGDD, 2-oxoglutarate-dependent dioxygenase; SDH, succinate dehydrogenase; TCA, tricarboxylic acid.

have recently been shown to suppress CD8+ T cell function through fumarate secretion which enters T cells and succinates ZAP70 to impair T cell receptor signalling [33] (Figure 2).

FH is a novel metabolic regulator of cytokine production

Recently, two studies have added to our understanding of how FH and fumarate regulate cytokine production. These complementary studies were performed in macrophages and kidney epithelial cells and identified similar mechanisms by which FH regulates cytokine production. In macrophages, unbiased metabolomics identified fumarate as a highly upregulated metabolite and FH was found the be downregulated in response to LPS, while the argininosuccinate shunt was increased, which leads to fumarate accumulation in the cytosol [34]. At early time points after LPS stimulation, mitochondrial bioenergetics and FH levels were stable, indicating that the upregulation of argininosuccinate synthase (ASS1) is likely responsible for the accumulation of fumarate. Consistent with this, pharmacological inhibition of this pathway with the GOT2 inhibitor, aminooxyacetic acid, and genetic knockdown of argininosuccinate lyase both prevented the accumulation of fumarate in response to LPS. The downregulation of FH at later time points (24 and 48 h after LPS) may also contribute to fumarate accumulation, but further work is required to elucidate respective roles the regulation of the mitochondrial and cytosolic isoforms of FH and how they regulate fumarate in response to LPS.

Importantly, transcriptomic analysis of pathways potentially regulated by fumarate revealed regulation of IL-10 and tumour necrosis factor (TNF) signalling in activated macrophages. The downregulation of IL-10 by fumarate was found to be through suppressed signalling upstream

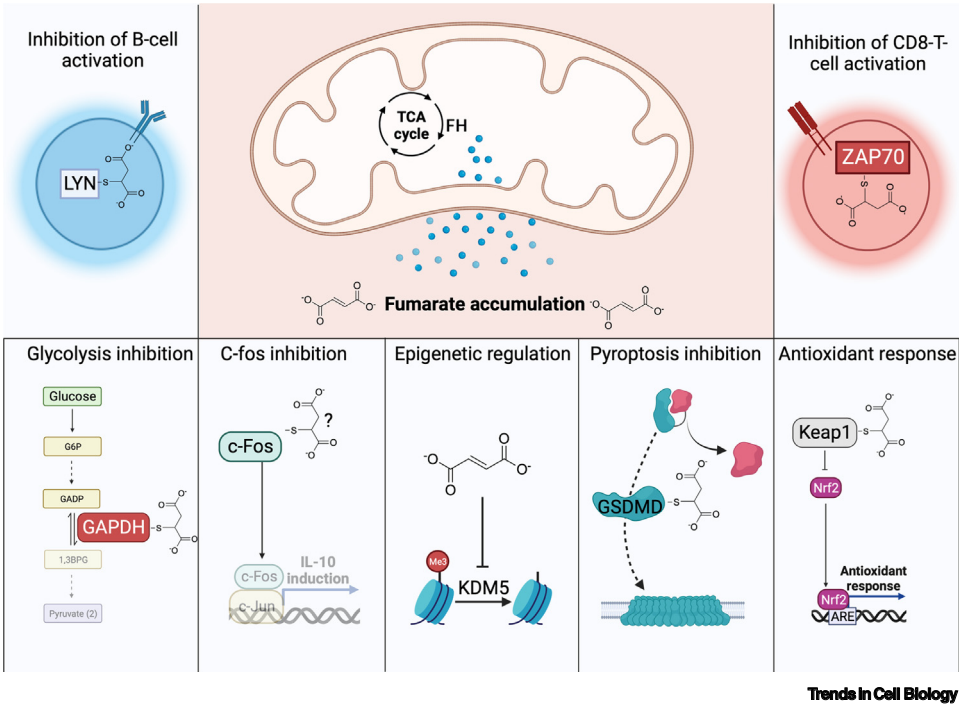


Figure 2. Fumarate in immune cells. With FH impairment or loss, fumarate accumulates in the cytosol and has numerous immunoregulatory effects in immune cells. It is able to modify proteins such as GAPDH, Keap1, GSDMD, LYN, ZAP70, and potentially, c-Fos. Additionally, it is able to impair histone demethylases such as KDM5 to regulate the epigenome and chromatin accessibility. Abbreviations: FH, fumarate hydratase; GSDMD, gasdermin D; IL-10, interleukin-10; KDM5, lysine-specific demethylase 5A; Nrf2, nuclear factor erythroid 2–related factor 2; TCA, tricarboxylic acid.

of its transcription. cFos is transcription factor subunit in the AP-1 family which is important for IL-10 induction [35]. As fumarate was found to decrease c-Fos activity, but had no effect upstream of its activation, this may indicate that fumarate acts directly on c-Fos, potentially through direct modification. The effect on IL-10 was abrogated in the presence of *N*-acetyl cysteine (NAC), which indicates that cysteine modification is the likely mechanism by which fumarate decreases IL-10 production. Importantly, early work on c-Fos found that there are important redox-sensitive cysteines critical for its function, possibly explaining why fumarate accumulation can regulate its activity. Since IL-10 is known to suppress TNF production [35], this provided a potential mechanism by which fumarate may upregulate TNF. Consistently, supplementation with recombinant IL-10 prevented the fumarate-mediated increase in TNF. Therefore, in macrophages, FH was identified as a crucial enzyme required for IL-10 production which prevented aberrant TNF production. FH activity maintains fumarate at a low level, but when it is repressed in response to LPS, fumarate accumulation leads to inhibition of IL-10 most likely via modification and inhibition of c-Fos, which in turn leads to increased TNF production (Figure 3).

Additionally, unbiased proteomics performed in LPS-activated bone marrow-derived macrophages treated with the FH inhibitor, FHIN1, or the fumarate derivative, dimethyl fumarate

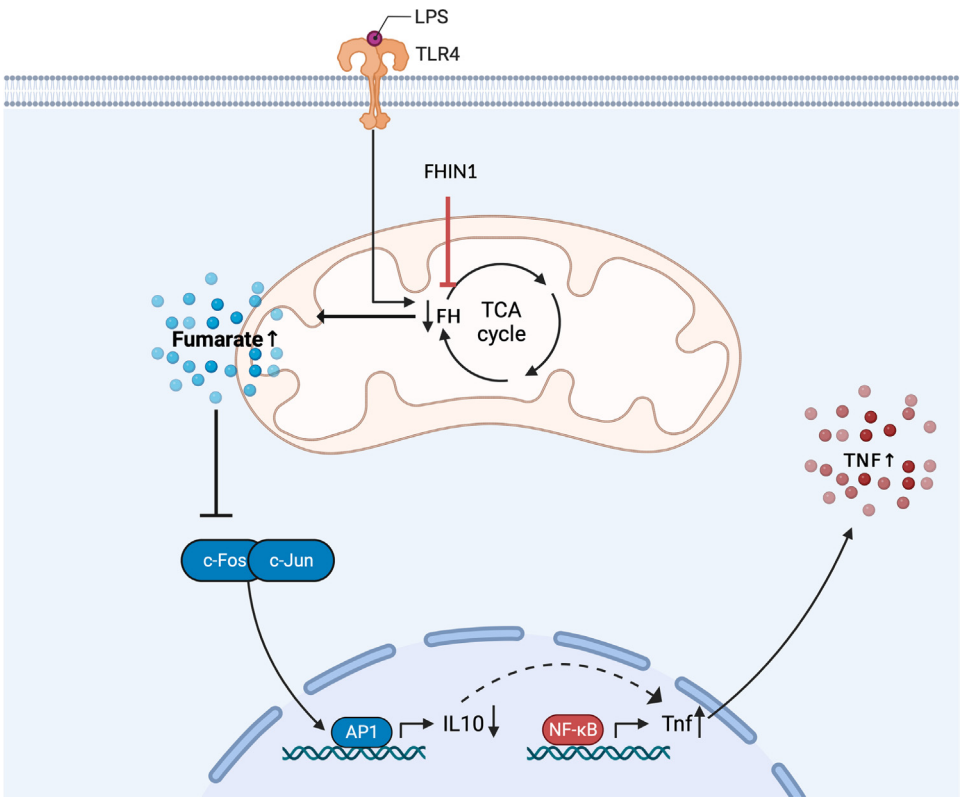


Figure 3. Fumarate decreases IL-10 to increase TNF production. Fumarate accumulation in the context of FH loss results in impaired c-Fos activation and decreased transcription of IL-10, leading to increased aberrant production of the proinflammatory cytokine TNF. Abbreviations: cGAS, cyclic GMP-AMP synthase; FH, fumarate hydratase; IL-10, interleukin-10; IRF3, interferon-regulatory factor 3; MAVS, mitochondrial antiviral-signalling protein; MDA5, melanoma differentiation-associated protein 5; MDV, mitochondria-derived vesicle; RIG-I, retinoic acid-inducible gene I; SNX9, sorting nexin 9; TBK1, TANK-binding kinase 1; TCA, tricarboxylic acid; TLR7, Toll-like receptor 7; TNF, tumour necrosis factor; TRIF, TIR domain-containing adaptor inducing interferon-β.

(DMF), identified growth differentiation factor 15 (GDF15) as one of the most highly upregulated proteins. The transcriptional upregulation of *Gdf15* by FH inhibition was found to be dependent on the transcription factor Nrf2, thereby indicating that succination-mediated Nrf2 activation leads to GDF15 production which may have immunomodulatory consequences, since GDF15 has been shown to have anti-inflammatory properties in macrophages [36,37].

The second study focused primarily on kidney epithelial cells to study the effects of FH loss as this is the cause of hereditary leiomyomatosis and renal cell carcinoma (HRLCC) which causes an aggressive form of kidney cancer [38]. While many effects of fumarate have been identified in the context of FH-deficient kidney cancer, temporal effects resulting from acute loss of FH have not been investigated due to the lack of an appropriate mouse model. Therefore, Zecchini *et al*. developed an inducible model of FH loss where tamoxifen can cause a loss of FH followed by harvesting of the kidney several days later. Transcriptomics in this model identified innate immune signalling processes and particularly a type I IFN response as a highly upregulated pathway within only several days after FH loss in the kidney. The two studies are complementary and overlap in that loss of FH activity was found in both cases to upregulate IFNβ) production.

Mechanistically, FH loss leading to fumarate accumulation in the kidney was found to induce the release of mitochondria-derived vesicles (MDVs) containing mtDNA. This identifies a novel pathway through which mitochondrial nucleic acids can be exported from mitochondria into the cytosol, adding to previous mechanisms such as those involving Bak/Bax, VDAC1 channels, and the mitochondrial permeability transition pore [39,40]. As these effects were recapitulated with the fumarate derivative monomethyl fumarate (MMF), this is likely an effect caused through fumarate accumulation itself in this system. Mechanistically, mtDNA was found to exit mitochondria through vesicle formation dependent on the protein sorting nexin 9 (Snx9). The activation of interferon signalling was subsequently found to be dependent on the cGAS-STING DNA sensing pathway with a partial RIG-I dependency, indicating that dsRNA may also be involved in promoting the interferon response in this model.

In macrophages, FH impairment does not signal through DNA sensing pathways and primarily activates both dsRNA sensing via RIG-I and MDA5 as well as ssRNA sensing via Toll-like receptor 7 (TLR7) (Figure 4). Previous studies have found other contexts where mitochondrial dysfunction leads to mtRNA release and IFN-β production. For example, double-stranded breaks in mtDNA as well as loss of mtRNA degradosome components both induce mtRNA release to activate type I IFN signalling [41,42]. Loss of FH was found to lead to dsRNA accumulation in the cytosol; however, unlike in kidney epithelial cells, this effect was not recapitulated with fumarate derivatives and is therefore likely to be independent of fumarate or protein succination. A recent study in macrophages also found DMF dampened IFN-β production as well [43]. TLR4 activation by LPS at later time points was found to drive dsRNA-dependent IFN-β production, correlating with the downregulation of FH at 24 h of LPS stimulation.

Both findings may have disease relevance for certain cancers and inflammatory diseases. Importantly, Zecchini *et al.* examined patient samples of FH-deficient tumours and demonstrated inflammatory gene expression was increased, along with high IL-6 in tumour tissue. Renal cell carcinomas deficient in FH were also found to exhibit increased infiltration and activation of leukocyte subtypes. These data indicate that FH deficiency may drive tumour initiation and progression through promoting an inflammatory milieu and that targeting the cGAS-STING pathway may be effective as a therapy in this type of cancer.

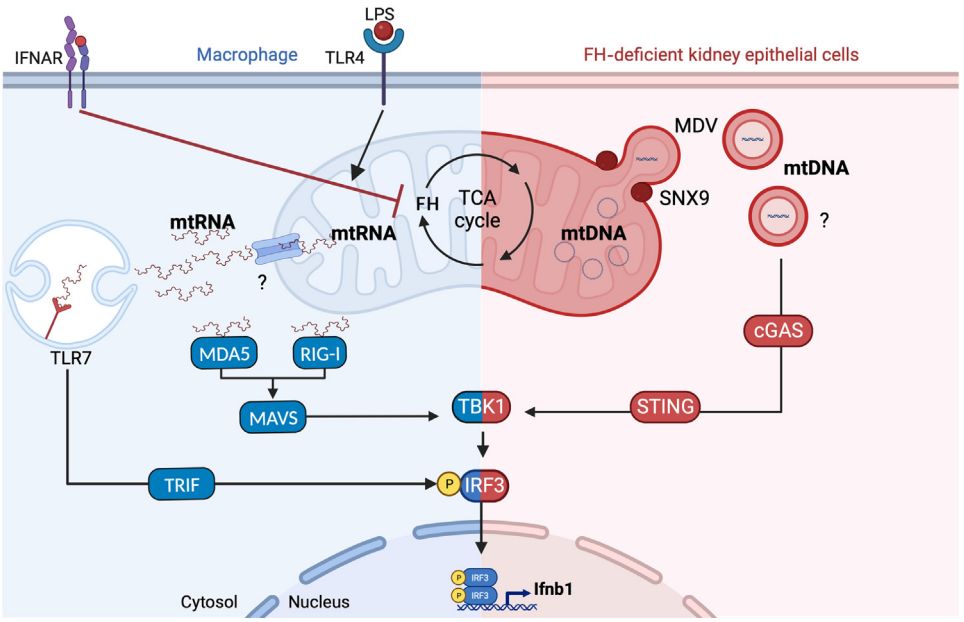


Figure 4. FH loss drives a type I IFN response. FH loss in both macrophages (left) and kidney epithelial cells (right) has been found to drive a type I IFN response through the release of mitochondrial nucleic acids. In macrophages, mtRNA activates cellular RNA sensors while in kidney epithelial cells mtDNA exits mitochondria in vesicles which activates the cGAS-STING pathway. Abbreviations: cGAS, cyclic GMP-AMP synthase; FH, fumarate hydratase; IL-10, interleukin-10; LPS, lipopolysaccharide; NF-κB, nuclear factor-κB; TCA, tricarboxylic acid; TLR4, Toll-like receptor 4; TNF, tumour necrosis factor; TRIF, TIR domain-containing adaptor inducing interferon-β.

Outstanding questions

What succination targets of fumarate have implications for immune cell function?

How does FH loss and fumarate accumulation induce mitochondria-derived vesicle formation?

How does the type I IFN response drive tumour initiation and growth in FH-deficient tumours?

Is FH downregulation pathological in IFN-driven diseases?

Additionally, SLE is an IFN-driven autoimmune disease where antibodies against mtRNA have been identified [44]. Therefore, Hooftman *et al.* examined whole blood of SLE patients and found that FH transcripts are expressed at low levels relative to those in matched healthy controls. Treatment of macrophages with IFN-β also led to downregulation of FH and induction of ASS1, which in turn may promote dsRNA release and induction of IFN-β, in a feedforward loop. This process may therefore be an important contributor to the IFN signature seen in SLE patients.

Concluding remarks and future directions

While the discovery of FH as a regulator of innate immunity strengthens our current understanding of how mitochondria are central signalling organelles in inflammation, these findings may have therapeutic relevance. In the context of patients with HLRCC, a possible intervention in the prevention or treatment of kidney cancer could be the suppression of cGAS-STING with novel inhibitors that have been developed such as H-151 or C-176 [45]. Downregulation of the type I IFN response and the chronic low-grade inflammation observed in these patients may be effective as a strategy as inflammation is considered a hallmark of certain cancers and is able to drive the initiation and progression of cancer at all stages [46].

Additionally, as FH was expressed at low levels in patients with SLE, this could suggest that mitochondrial nucleic acids may be pathological in this autoimmune disease. Therefore, methods preventing these signalling pathways (e.g., by blocking MDA-5) may be useful in treating the disease. Although type I IFN signalling is already a target in SLE, it could be plausible that pharmacological inhibition mitochondrial transcription with the recently developed POLRMT

inhibitor, IMT1, could prevent the induction of type I IFN responses in these patients. Whether this type of approach may be toxic to non-pathological cell types *in vivo* in inflammatory models is still to be determined; however, several studies have reported the efficacy of targeting POLRMT in mouse models [47,48].

Further investigations into the immunomodulatory effects of immunometabolites such as succinate, itaconate, and fumarate and the metabolic pathways they are involved in are warranted. Analysis of the targets for these metabolites might reveal additional processes being regulated. How FH downregulation in macrophages leads to the release of mitochondrial nucleic acids needs to be better elucidated to offer potential therapeutic options in autoimmunity. Finally, targeting fumarate and FH may provide intriguing possibilities for the development of novel effective therapies in oncology and inflammatory diseases (see Outstanding questions).

Acknowledgments

We would like to thank all of the members of the O'Neill laboratory for helpful discussions. This work is supported by the European Research Council (Metabinnate 834370) and the Science Foundation Ireland (20/SPP/3685).

Declaration of interests

The authors declare no competing interests.

References

1. O'Neill, L.A.J. *et al.* (2016) A guide to immunometabolism for immunologists. *Nat. Rev. Immunol.* 16, 553–565
2. Chandel, N.S. (2015) Evolution of mitochondria as signaling organelles. *Cell Metab.* 22, 204–206
3. Mills, E.L. *et al.* (2017) Mitochondria are the powerhouses of immunity. *Nat. Immunol.* 18, 488–498
4. Van den Bossche, J. *et al.* (2017) Macrophage immunometabolism: where are we (going)? *Trends Immunol.* 38, 395–406
5. Zasłona, Z. and O'Neill, L.A.J. (2020) Cytokine-like roles for metabolites in immunity. *Mol. Cell* 78, 814–823
6. Jha, A.K. *et al.* (2015) Network integration of parallel metabolic and transcriptional data reveals metabolic modules that regulate macrophage polarization. *Immunity* 42, 419–430
7. Tannahill, G.M. *et al.* (2013) Succinate is an inflammatory signal that induces IL-1β through HIF-1α. *Nature* 496, 238–242
8. Mills, E.L. *et al.* (2016) Succinate dehydrogenase supports metabolic repurposing of mitochondria to drive inflammatory macrophages. *Cell* 167, 457–470.e13
9. Littlewood-Evans, A. *et al.* (2016) GPR91 senses extracellular succinate released from inflammatory macrophages and exacerbates rheumatoid arthritis. *J. Exp. Med.* 213, 1655–1662
10. Peace, C.G. and O'Neill, L.A. (2022) The role of itaconate in host defense and inflammation. *J. Clin. Invest.* 132, e148548
11. Lampropoulou, V. *et al.* (2016) Itaconate links inhibition of succinate dehydrogenase with macrophage metabolic remodeling and regulation of inflammation. *Cell Metab.* 24, 158–166
12. Mills, E.L. *et al.* (2018) Itaconate is an anti-inflammatory metabolite that activates Nrf2 via alkylation of KEAP1. *Nature* 556, 113–117
13. Hooftman, A. *et al.* (2020) The immunomodulatory metabolite itaconate modifies NLRP3 and inhibits inflammasome activation. *Cell Metab.* 32, 468–478.e7
14. Bambouskova, M. *et al.* (2021) Itaconate confers tolerance to late NLRP3 inflammasome activation. *Cell Rep.* 34, 108756
15. Liao, S.T. *et al.* (2019) 4-Octyl itaconate inhibits aerobic glycolysis by targeting GAPDH to exert anti-inflammatory effects. *Nat. Commun.* 10, 1–11
16. Runtsch, M.C. *et al.* (2022) Itaconate and itaconate derivatives target JAK1 to suppress alternative activation of macrophages. *Cell Metab.* 34, 487–501.e8
17. Zhang, Z. *et al.* (2022) Itaconate is a lysosomal inducer that promotes antibacterial innate immunity. *Mol. Cell* 82, 2844–2857.e10
18. Chen, L.-L. *et al.* (2022) Itaconate inhibits TET DNA dioxygenases to dampen inflammatory responses. *Nat. Cell Biol.* 24, 353–363
19. Zeng, Y.-R. *et al.* (2023) The immunometabolite itaconate stimulates OXGR1 to promote mucociliary clearance during the pulmonary innate immune response. *J. Clin. Invest.* 133, e160463
20. Schmidt, L.S. and Linehan, W.M. (2014) Hereditary leiomyomatosis and renal cell carcinoma. *Int. J. Nephrol. Renovasc. Dis.* 7, 253–260
21. Isaacs, J.S. *et al.* (2005) HIF overexpression correlates with biallelic loss of fumarate hydratase in renal cancer: novel role of fumarate in regulation of HIF stability. *Cancer Cell* 8, 143–153
22. Adam, J. *et al.* (2011) Renal cyst formation in Fh1-deficient mice is independent of the Hif/Phd pathway: roles for fumarate in KEAP1 succination and Nrf2 signaling. *Cancer Cell* 20, 524–537
23. Ge, X. *et al.* (2022) Fumarate inhibits PTEN to promote tumorigenesis and therapeutic resistance of type2 papillary renal cell carcinoma. *Mol. Cell* 82, 1249–1260.e7
24. Kinch, L. *et al.* (2011) Succination of Keap1 and activation of Nrf2-dependent antioxidant pathways in FH-deficient papillary renal cell carcinoma type 2. *Cancer Cell* 20, 418–420
25. Sciacovelli, M. *et al.* (2016) Fumarate is an epigenetic modifier that elicits epithelial-to-mesenchymal transition. *Nature* 537, 544–547
26. Arts, R.J.W. *et al.* (2016) Glutaminolysis and fumarate accumulation integrate immunometabolic and epigenetic programs in trained immunity. *Cell Metab.* 24, 807–819
27. Kulkarni, R.A. *et al.* (2019) A chemoproteomic portrait of the oncometabolite fumarate. *Nat. Chem. Biol.* 15, 391–400
28. Yang, M. *et al.* (2014) The succinated proteome of FH-mutant tumours. *Metabolites* 4, 640–654
29. Blewett, M.M. *et al.* (2016) Chemical proteomic map of dimethyl fumarate–sensitive cysteines in primary human T cells. *Sci. Signal.* 9, rs10
30. Cheng, J. *et al.* (2022) Fumarate suppresses B-cell activation and function through direct inactivation of LYN. *Nat. Chem. Biol.* 18, 954–962
31. Humphries, F. *et al.* (2020) Succination inactivates gasdermin D and blocks pyroptosis. *Science (80-.)* 369, 1633–1637
32. Kornberg, M.D. *et al.* (2018) Dimethyl fumarate targets GAPDH and aerobic glycolysis to modulate immunity. *Science* 360, 449–453
33. Cheng, J. *et al.* (2023) Cancer-cell-derived fumarate suppresses the anti-tumor capacity of $CD8^+$ T cells in the tumor microenvironment. *Cell Metab.* 35, 961–978.e10

34. Hooftman, A. *et al.* (2023) Macrophage fumarate hydratase restrains mtRNA-mediated interferon production. *Nature* 615, 490–498
35. Hu, X. *et al.* (2006) IFN-γ Suppresses IL-10 production and synergizes with TLR2 by regulating GSK3 and CREB/AP-1 proteins. *Immunity* 24, 563–574
36. Weng, J.-H. *et al.* (2021) Colchicine acts selectively in the liver to induce hepatokines that inhibit myeloid cell activation. *Nat. Metab.* 3, 513–522
37. Luan, H.H. *et al.* (2019) GDF15 is an inflammation-induced central mediator of tissue tolerance. *Cell* 178, 1231–1244.e11
38. Zecchini, V. *et al.* (2023) Fumarate induces vesicular release of mtDNA to drive innate immunity. *Nature* 615, 499–506
39. McArthur, K. *et al.* (2018) BAK/BAX macropores facilitate mitochondrial herniation and mtDNA efflux during apoptosis. *Science* 359, eaao6047
40. Xian, H. *et al.* (2022) Oxidized DNA fragments exit mitochondria via mPTP- and VDAC-dependent channels to activate NLRP3 inflammasome and interferon signaling. *Immunity* 55, 1370–1385.e8
41. Tigano, M. *et al.* (2021) Nuclear sensing of breaks in mitochondrial DNA enhances immune surveillance. *Nature* 591, 477–481
42. Dhir, A. *et al.* (2018) Mitochondrial double-stranded RNA triggers antiviral signalling in humans. *Nature* 560, 238–242
43. Ryan, T.A.J. *et al.* (2023) Dimethyl fumarate and 4-octyl itaconate are anticoagulants that suppress tissue factor in macrophages via inhibition of type I interferon. *Nat. Commun.* 14, 3513
44. Becker, Y. *et al.* (2019) Autoantibodies in systemic lupus erythematosus target mitochondrial RNA. *Front. Immunol.* 10, 1026
45. Haag, S.M. *et al.* (2018) Targeting STING with covalent small-molecule inhibitors. *Nature* 559, 269–273
46. Greten, F.R. and Grivennikov, S.I. (2019) Inflammation and cancer: triggers, mechanisms, and consequences. *Immunity* 51, 27–41
47. Li, S. *et al.* (2023) A first-in-class POLRMT specific inhibitor IMT1 suppresses endometrial carcinoma cell growth. *Cell Death Dis.* 14, 152
48. Bonekamp, N.A. *et al.* (2020) Small-molecule inhibitors of human mitochondrial DNA transcription. *Nature* 588, 712–716

Check for updates

IMMUNOLOGY

Mitochondrial respiratory complex III sustains IL-10 production in activated macrophages and promotes tumor-mediated immune evasion

Alessia Zotta[1], Juliana Toller-Kawahisa[1], Eva M. Palsson-McDermott[1], Shane M. O'Carroll[1], Órlaith C. Henry[1], Emily A. Day[1,2], Anne F. McGettrick[1], Ross W. Ward[1], Dylan G. Ryan[3], Mark A. Watson[4], Martin D. Brand[4], Marah C. Runtsch[5], Kathrin Maitz[5], Anna Lueger[5], Julia Kargl[5], Jan L. Miljkovic[3], Ed C. Lavelle[1], Luke A. J. O'Neill[1]*

Copyright © 2025 The Authors, some rights reserved; exclusive licensee American Association for the Advancement of Science. No claim to original U.S. Government Works. Distributed under a Creative Commons Attribution NonCommercial License 4.0 (CC BY-NC).

The cytokine interleukin-10 (IL-10) limits the immune response and promotes resolution of acute inflammation. Because of its immunosuppressive effects, IL-10 up-regulation is a common feature of tumor progression and metastasis. Recently, IL-10 regulation has been shown to depend on mitochondria and redox-sensitive signals. We have found that Suppressor of site III_{Qo} Electron Leak 1.2 (S3QEL 1.2), a specific inhibitor of reactive oxygen species (ROS) production from mitochondrial complex III, and myxothiazol, a complex III inhibitor, decrease IL-10 in lipopolysaccharide (LPS)–activated macrophages. IL-10 down-regulation is likely to be mediated by suppression of c-Fos, which is a subunit of activator protein 1 (AP1), a transcription factor required for *IL-10* gene expression. S3QEL 1.2 impairs IL-10 production in vivo after LPS challenge and promotes the survival of mice bearing B16F10 melanoma by lowering tumor growth. Our data identify a link between complex III–dependent ROS generation and IL-10 production in macrophages, the targeting of which could have potential in boosting antitumor immunity.

INTRODUCTION

Immune cells undergo metabolic reprogramming during activation (*1*), and the intricacies of the metabolic processes occurring are still being unraveled. Macrophages have been a key focus with profound changes in glycolysis and mitochondrial metabolism occurring after stimulation with activators such as lipopolysaccharide (LPS) from Gram-negative bacteria (*2*).

They produce, among many cytokines, the anti-inflammatory cytokine interleukin-10 (IL-10). Initially found as a T helper 2 (T_H2)–specific cytokine (*3*), IL-10 is a soluble mediator whose production is shared by innate and adaptive immune cells such as dendritic cells, monocytes, B cells, and regulatory T cells (T_{regs}) (*4*). IL-10 can elicit immune suppression by limiting antibody production in B cells and costimulatory molecules in T cells (*5*). Considering the further literature on mitochondrial biology, IL-10 has been shown to decrease reactive oxygen species (ROS) production, drive controlled mitophagy, and promote mitochondrial fitness (*6*). IL-10 deficiency leads to dysfunctional mitochondria and impaired oxidative phosphorylation (OXPHOS) with an increase in glycolysis in macrophages (*6*). More recently, the redox protein thioredoxin has been shown to be necessary for the differentiation of $IL\text{-}10^+$ regulatory B cells through a mechanism that includes controlling ROS generation (*7*), providing a link between oxidative stress and IL-10.

Mitochondrial respiratory complex III is part of the electron transport chain (ETC), where it oxidizes coenzyme Q and reduces cytochrome c to generate adenosine triphosphate (ATP) during oxidative phosphorylation. It is also the main source of superoxide anion ($O_2^{\cdot -}$) and subsequent ROS from mitochondria, together with complex I, during forward and reverse electron transport (FET and RET, respectively) (*8*). In humans, mutations in three complex III–specific genes lead to mitochondrial disorders with different onset and clinical manifestations (*9*), making their characterization and treatment a challenge. The contribution of complex III to immune cell function requires further exploration. Complex III has been shown to be essential for hematopoietic stem cell stability by regulating epigenetic changes in histones (*10*) and for the immune suppressive functions of T_{regs} (*11*). Moreover, complex III is required for antigen-specific activation of cytotoxic T cells via ROS (*12*) and for complex I stability and maintenance along the ETC (*13*). The use of complex III–specific inhibitors, such as myxothiazol (MYX), has helped in deciphering the multifaceted nature of complex III. In addition, the small molecule Suppressor of site III_{Qo} Electron Leak (S3QEL) has been developed to stop electron leak from the ETC to oxygen, thus blocking ROS production specifically from complex III (*14*, *15*).

Here, we have examined the role of complex III in macrophages using S3QEL 1.2 and MYX. We have found that inhibition of complex III activity and subsequent ROS generation lead to a decrease in IL-10 production in vitro and in vivo and that the down-regulation of the transcription factor activator protein 1 (AP1) might contribute to this event. Moreover, we show that S3QEL 1.2 treatment decreases melanoma progression and improves the survival of mice in vivo, impairing the production of IL-10 by macrophages in the tumor microenvironment (TME). Our results indicate a role for ROS from complex III in the induction of IL-10 in macrophages, the limiting of which could have utility in the promotion of antitumor immunity.

[1]School of Biochemistry and Immunology, Trinity Biomedical Sciences Institute, Trinity College Dublin, Dublin 2, Ireland. [2]Department of Physiology and Pharmacology, Schulich School of Medicine & Dentistry, University of Western Ontario, London, ON, Canada. [3]Mitochondria Biology Unit, University of Cambridge, Cambridge, UK. [4]Buck Institute for Research on Aging, Novato, CA, USA. [5]Division of Pharmacology, Otto Loewi Research Center, Medical University of Graz, Graz, Austria.
*Corresponding author. Email: laoneill@tcd.ie

RESULTS

S3QEL 1.2 and MYX block ROS production by affecting OXPHOS in macrophages

The previous literature has described S3QEL 1.2 (Fig. 1A), developed by Brand and colleagues (*15*), as a specific inhibitor of complex

Downloaded from https://www.science.org at Trinity College Dublin on January 27, 2025

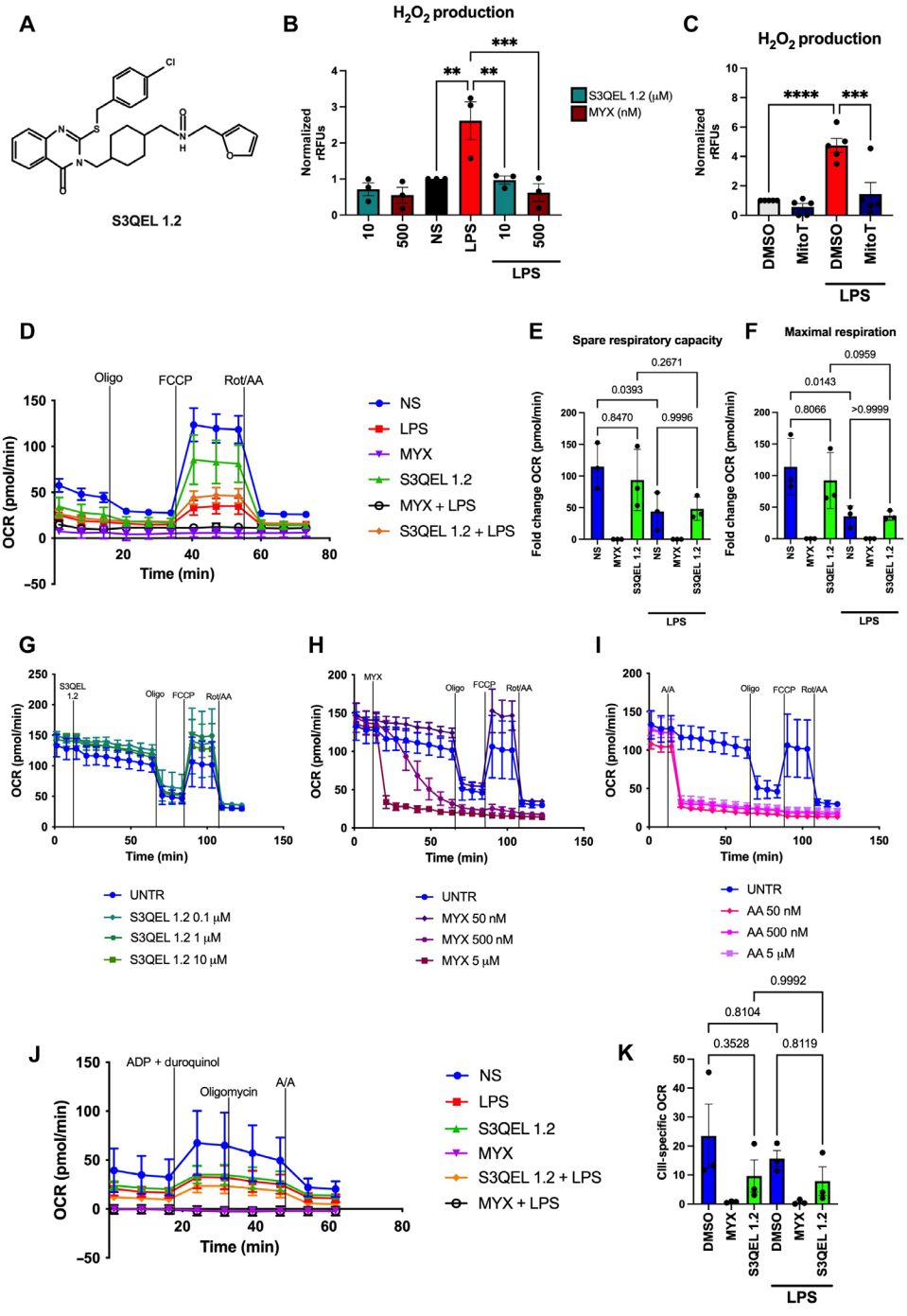


Fig. 1. Characterization of complex III inhibitors in macrophages. (**A**) S3QEL 1.2 chemical structure. (**B** and **C**) Rate of relative resorufin fluorescence units (rRFUs) directly proportional to H_2O_2 production in the presence of DMSO, S3QEL 1.2 (10 μM), and MYX (500 nM) (B) or DMSO, MitoTempo (5 mM), and LPS (100 ng/ml) (C) for 48 hours in BMDMs. NS, not stimulated. (**D** to **F**) BMDMs were pretreated with DMSO, MYX (500 nM), or S3QEL 1.2 (10 μM) for 3 hours followed by LPS (100 ng/ml) for 24 hours. Mito Stress Test showing OCR of cells after addition of oligo, FCCP, and rotenone (Rot)/AA (D). Maximal respiration (E) and spare respiratory capacity (F) calculated from the OCR values. (**G** to **I**) Mito Stress Test showing OCR of cells after treatment with S3QEL 1.2 (0.1, 1, or 10 μM) (G), MYX (50, 500, or 5000 nM) (H), or AA (50, 500, or 5000 nM) (I) and addition of oligo, FCCP, and rotenone/AA. UNTR, untreated. (**J** to **K**) BMDMs were pretreated with DMSO, MYX (500 nM), or S3QEL 1.2 (10 μM) for 3 hours followed by LPS (100 ng/ml) for 24 hours. Metabolic flux analysis showing complex III (CIII)–specific OCR of cells over time after addition of ADP + duroquinol, oligo, and AA. (K) Quantification of complex III–specific OCR. Data in (B) are means ± SEM for $n = 3$ from three independent experiments. Data in (C) are means ± SEM for $n = 5$ from five independent experiments. Data from (D) to (F) are means ± SEM from three independent experiments, with $n = 7$ to 12 technical replicates for each condition. Data from (G) to (I) are means ± SEM from two independent experiments, with $n = 9$ technical replicates for each condition. Data from (J) to (K) are means ± SEM from three independent experiments, with $n = 12$ technical replicates for each condition. *P* values were calculated using one-way ANOVA for multiple comparisons. Differences were statistically significant at $^{**}P < 0.01$, $^{***}P < 0.001$, and $^{****}P < 0.0001$.

Downloaded from https://www.science.org at Trinity College Dublin on January 27, 2025

III–derived ROS production (*15*), but its effect in immune cells has not been established. Here, we sought to investigate the effects of S3QEL 1.2 on activated bone marrow–derived macrophages (BMDMs) and to compare it to MYX, a specific inhibitor for complex III activity. First, we confirmed that LPS increased ROS production in macrophages by measuring H_2O_2 release and demonstrated that S3QEL 1.2 and MYX inhibited this response (Fig. 1B) The same result was obtained with the mitochondria-targeted antioxidant MitoTEMPO at 5 mM, which decreased LPS-induced H_2O_2 production (Fig. 1C). We then performed metabolic flux analysis to assess whether complex III inhibitors were perturbing respiration of macrophages. As shown in Fig. 1 (D to F), S3QEL 1.2 was marginally inhibitory against OXPHOS in macrophages at 10 μM with 500 nM MYX abolishing respiration. LPS inhibited OXPHOS as shown previously (*16*). To confirm this, we performed metabolic flux analysis with different concentrations of S3QEL 1.2, MYX, and AA, another complex III inhibitor, injected into BMDMs in real time. Also here, S3QEL 1.2 did not affect respiration at any concentration used (Fig. 1G), while MYX and AA impaired it (Fig. 1, H and I). Moreover, S3QEL 1.2 did not change the activity of complex III, while MYX completely disrupted it (Fig. 1, J and K), as shown in a previous study (*17*). The two inhibitors were also not toxic to the cells, as shown by 3-(4,5-dimethylthiazol-2-yl)-2,5-diphenyltetrazolium (MTT) assay to examine the viability of cells (fig. S1A), and did not change the protein abundance of the ETC complexes (fig. S1B), analyzed by Western blotting. S3QEL 1.2 and MYX also slightly boosted glycolysis (fig. S1, C and D).

Complex III inhibition provokes specific transcriptional changes in activated macrophages

We then performed RNA sequencing (RNA-seq) analysis on BMDMs treated with S3QEL 1.2 and MYX and activated with LPS to investigate the contribution of complex III to the transcriptomic profile of macrophages. Differential analysis identified 146 genes, which were commonly impaired by both compounds in LPS-treated macrophages (Fig. 2A). Particularly, genes coding for protein that are essential for inflammatory macrophage function, such as cluster of differentiation 14 (*CD14*), the transcription factors *Ets2* and *Fosl2*, the receptors for interferon-α/β *IFNAR1* and *IFNAR2*, the ROS-activated Fgr kinase, NFAT-activating protein with ITAM motif 1 (*Nfam1*), *IL4r*, and suppressor of cytokine signaling 3 (*Socs3*), showed lowered expression, as indicated by arrows (Fig. 2B). Inhibition of complex III by MYX and S3QEL 1.2 boosted certain genes, including that encoding growth differentiation factor 15 (*GDF15*) (fig. S2, A and B). We focused our attention on the cytokine profile of activated macrophages and performed immune-responsive enrichment analysis (IREA) using our RNA-seq dataset. IREA is an approach based on a dictionary of single-cell transcriptomic profiles of 17 immune cell types in response to 86 different cytokines in vivo (publicly available data) (*18*). The analysis revealed that *IL-10* was among the cytokines whose down-regulation by S3QEL 1.2 and MYX after LPS stimulation was prominent (Fig. 2C). In addition, gene set enrichment analysis (GSEA) revealed that genes involved in IL-10 receptor signaling target genes were among the 20 most down-regulated terms (Fig. 1D) and genes contributing to tumor necrosis factor–α (TNF-α) and nuclear factor κB (NF-κB) signaling were among the 20 most up-regulated terms (Fig. 1E). IL-10 is well known to limit TNF-α production (*19*), hence this regulation found in our results.

The inhibition of complex III decreases IL-10 production in activated macrophages

Because of the prominence of IL-10 in our analysis and the reported role of ROS in its regulation, we focused our attention on IL-10. We analyzed *IL-10* transcripts by reverse transcription quantitative polymerase chain reaction (RT-qPCR) and released form by enzyme-linked immunosorbent assay (ELISA), and we found that S3QEL 1.2 decreased LPS-induced IL-10 production in a dose-dependent manner (Fig. 3, A and B) and increased TNF-α (Fig. 3, C and D), as we had observed in the RNA-seq analysis. MYX had the same effects on *IL-10* mRNA and protein expression (Fig. 3, E and F) but curiously did not increase TNF-α (Fig. 3, G and H). We confirmed the redox-sensitive regulation of IL-10 with the pretreatment of macrophages with the mitochondria-targeted antioxidants MitoTEMPO and MitoQ, which, in the case of MitoQ, lowered IL-10 expression in response to LPS (fig. S3, A to D). We also tested the glutathione precursor *N*-acetyl cysteine (NAC), which impaired LPS-induced IL-10 expression especially at 1, 5, and 10 mM (fig. S3, E and F). Moreover, IL-10 regulation appeared to be complex I independent because pretreatment of activated BMDMs with rotenone, an inhibitor of complex I, and S1QEL 1.1, which impairs ROS production from complex I (*20*), did not substantially decrease *IL-10* mRNA or protein production (fig. S3, A, B, G, and H).

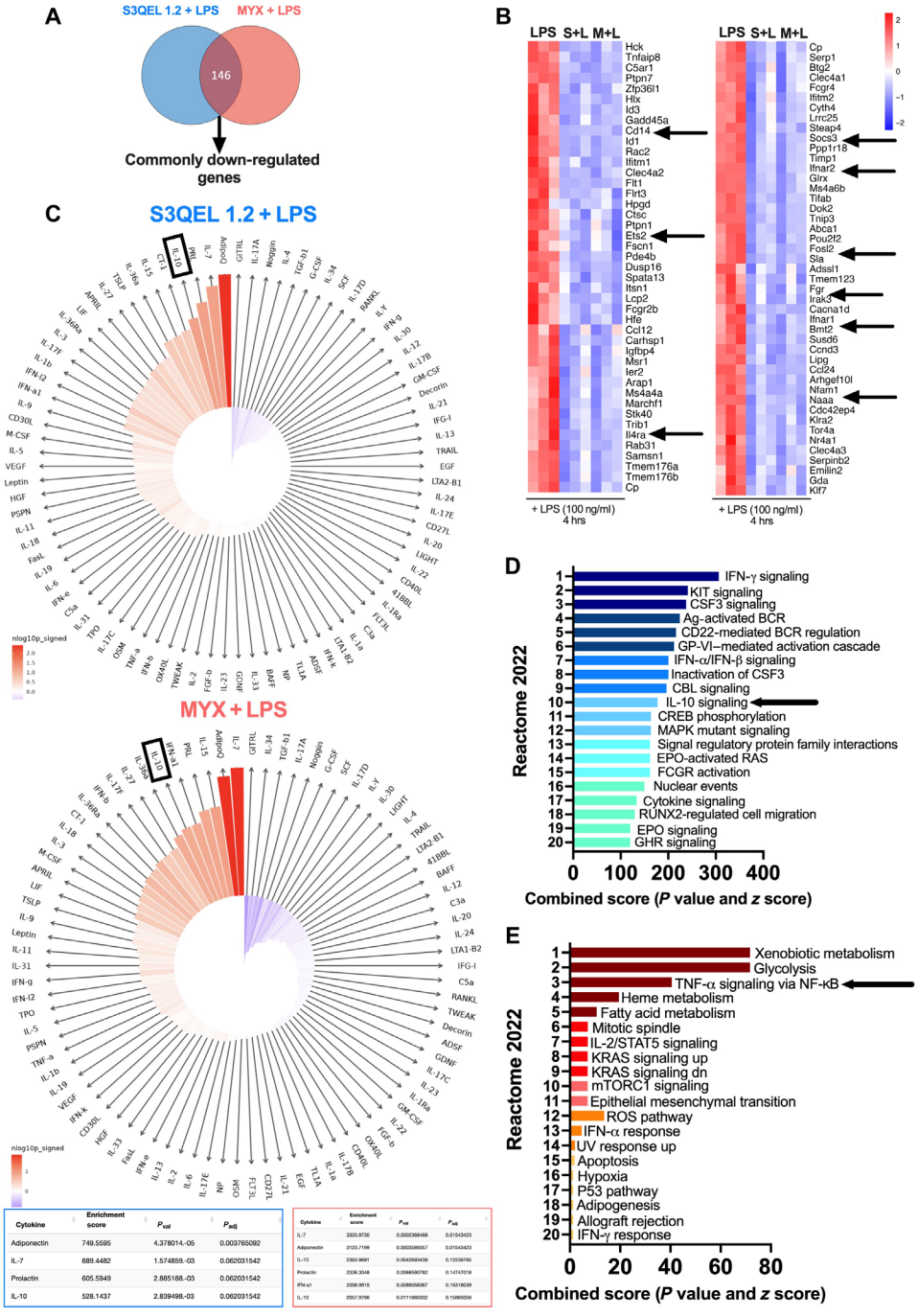
We next tested S3QEL 1.2 in vivo. S3QEL 1.2 has been used in a few studies where it was administered to mice in drinking water (*21*). Here, mice were injected intraperitoneally with S3QEL 1.2 and then injected with LPS after 2 hours (Fig. 3I). LPS-induced IL-10 in the serum was inhibited in the S3QEL 1.2–treated animals (Fig. 3J). Also, TNF-α was increased in serum after LPS injection, but S3QEL 1.2 did not have an inhibitory effect on it (fig. S4A).

We also analyzed S3QEL 1.2 effects on IL-10 produced by T_H1 lymphocytes. S3QEL 1.2 decreased IL-10 release after T_H1 cell polarization (fig. S5, A and B). Furthermore, MYX also suppressed *IL10* expression and release in LPS-stimulated macrophages derived from human peripheral blood mononuclear cells (PBMCs) (fig. S6, A and C). S3QEL 1.2 showed a trend toward a decrease in IL-10 at 0.1 and 0.5 μM (fig. S6, B and D). These results indicate that complex III–regulated IL-10 production is also evident in human cells.

IL-10 suppression depends on inhibition of the AP1 subunit Fos

From the RNA-seq dataset previously analyzed, we performed transcription factor enrichment analysis, which revealed that the expression of *Fosl1* and *Fosl2*, canonical subunits of the transcription factor AP1, was inhibited by S3QEL 1.2 and MYX (Fig. 4A). Furthermore, we found that many of the genes that were down-regulated by S3QEL 1.2 and MYX were Fos-dependent target genes (Fig. 4B). We next analyzed the transcriptional levels of *c-Fos* by RT-qPCR, and we found that S3QEL 1.2 and MYX also diminished *c-Fos* levels after 30 min of LPS stimulation (Fig. 4, C and D). We also analyzed c-Jun, which is another subunit of AP1 and works with c-Fos to form a dimer, moves to the nucleus, and binds to the DNA. *c-Jun* mRNA expression after 30 min of LPS stimulation was decreased upon S3QEL 1.2 (fig. S7A) and MYX (fig. S7B) pretreatment. Subsequent confocal microscopy, performed to assess c-Fos activation and subsequent nuclear translocation, confirmed that the pretreatment with S3QEL 1.2 and MYX diminished the LPS-induced presence of phospho-c-Fos in the nucleus (Fig. 4, E and F). Together,

Downloaded from https://www.science.org at Trinity College Dublin on January 27, 2025



Cytokine	Enrichment score	P_{val}	P_{adj}
Adiponectin	749.5595	4.378014.-05	0.003765092
IL-7	689.4482	1.574859.-03	0.062031542
Prolactin	605.5949	2.885188.-03	0.062031542
IL-10	528.1437	2.839498.-03	0.062031542

Cytokine	Enrichment score	P_{val}	P_{adj}
IL-7	3320.9730	0.000298466	0.01543423
Adiponectin	3120.7199	0.000358057	0.01543423
IL-15	2303.9691	0.004269934338	0.102286785
Prolactin	2336.3048	0.006890782	0.14747018
IFN-a1	2058.9916	0.008959087	0.15518289
IL-10	2057.9798	0.011166032	0.15860056

Fig. 2. Complex III inhibition reveals a specific transcriptional signature in activated macrophages. (**A** to **E**) RNA sequencing of LPS-primed mouse macrophages (BMDMs) and pretreated (3 hours) with DMSO, S3QEL 1.2 (10 μM), and MYX (500 nM). (A) Venn diagram of commonly differentially expressed genes (146) between S3QEL 1.2 + LPS versus LPS and MYX + LPS versus LPS [adjusted *P* (P_{adj}) < 0.1]. (B) Heatmap of the top 100 commonly up-regulated genes by LPS alone (red column) and down-regulated by both MYX and S3QEL 1.2 after LPS priming (second and third columns; in blue). hrs, hours. (C) IREA of differentially down-regulated genes by S3QEL 1.2 (top) and MYX (down) after LPS stimulation [adjusted *P* (P_{adj}) < 0.05]. (D) and (E) GSEA of differentially regulated genes. (D) Overrepresentation analysis of RNA-seq data of BMDMs pretreated with S3QEL 1.2 or MYX (n = 3 from one independent experiment; LPS, 4 hours). Reactome pathway enrichment analysis of differentially down-regulated genes. (E) Overrepresentation analysis of RNA-seq data of BMDMs pretreated with S3QEL 1.2 or MYX (n = 3 from one independent experiment; LPS, 4 hours). Reactome pathway enrichment analysis of differentially up-regulated genes.

Downloaded from https://www.science.org at Trinity College Dublin on January 27, 2025

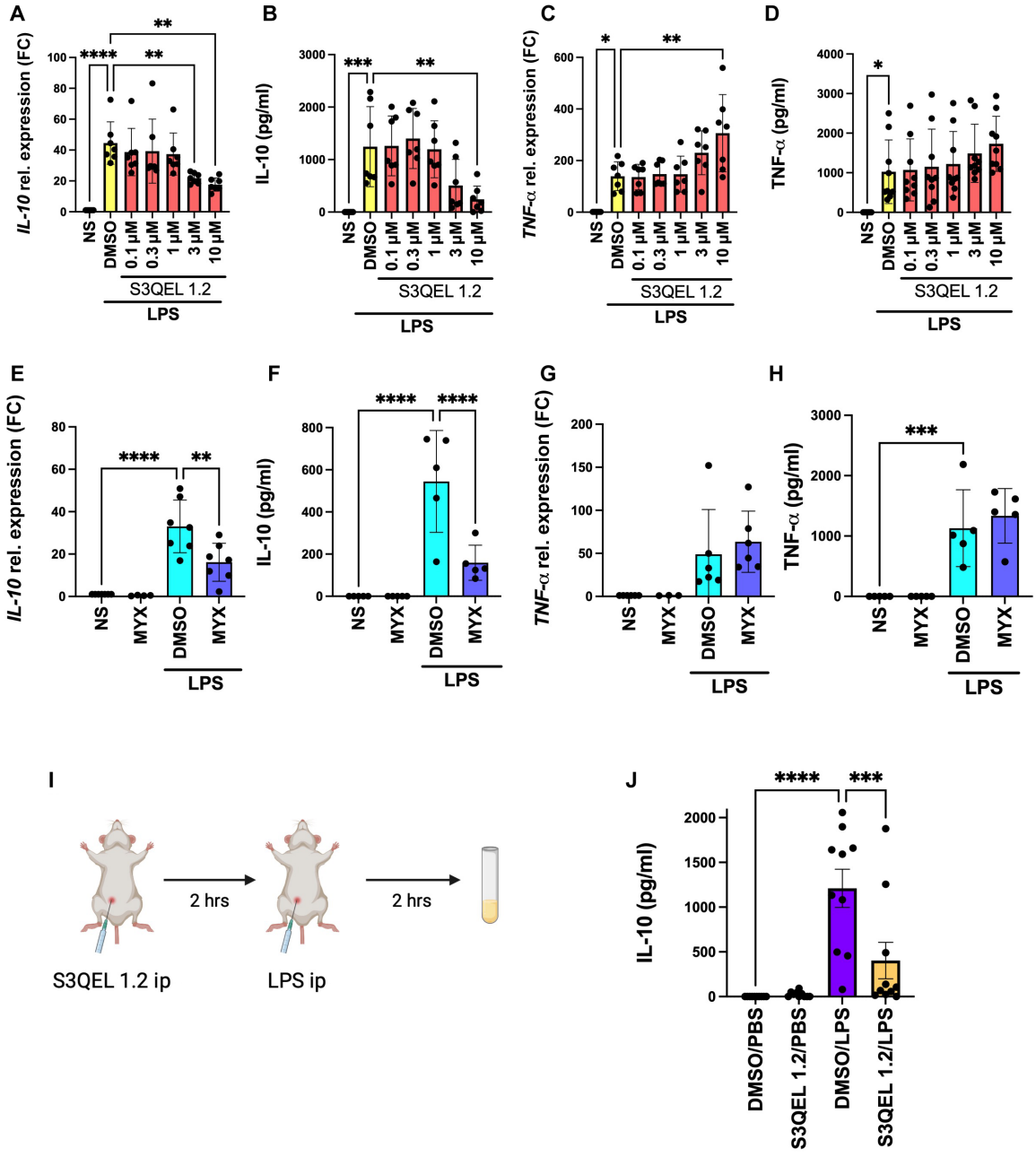


Fig. 3. The inhibition of complex III decreases LPS-induced IL-10 expression in macrophages. (**A** to **D**) BMDMs were pretreated with DMSO or S3QEL 1.2 (0.1 to 10 µM) for 3 hours before LPS (100 ng/ml) stimulation for 4 hours, and cell lysates and supernatants were harvested. (A) and (B) Quantification of *IL-10* mRNA (A) and released protein (B) by RT-qPCR, relative to the *Rps18* housekeeping gene, and ELISA. (C) and (D) Quantification of *TNF*-α mRNA (C) and released protein (D) by RT-qPCR, relative to the *Rps18* housekeeping gene, and ELISA. FC, fold change. (**E** to **H**) BMDMs were pretreated with DMSO and MYX (500 nM) for 3 hours before LPS (100 ng/ml) stimulation for 4 hours, and cell lysates and supernatants were harvested. (E) and (F) Quantification of *IL-10* mRNA (E) and released protein (F) by RT-qPCR, relative to the *Rps18* housekeeping gene, and ELISA. (G) and (H) Quantification of *TNF*-α mRNA (G) and released protein (H) by RT-qPCR, relative to the *Rps18* housekeeping gene, and ELISA. (**I**) Schematic diagram of in vivo procedure and sample collection. Mice were intraperitoneally (ip) injected with PBS or S3QEL 1.2 (1 mg/kg) for 2 hours, followed by LPS (2.5 mg/kg) for 2 hours. Blood (then serum) was collected. hrs, hours. (**J**) Quantification of IL-10 by ELISA in the serum. Data from (A) to (H) are expressed as means ± SEM for $n = 5$ to 9 from three independent experiments. Data from (J) are expressed as means ± SEM ($n = 10$ per group within two independent in vivo experiments). *P* values were calculated using one-way ANOVA for multiple comparisons. Differences were considered statistically significant at $^{*}P < 0.05$, $^{**}P < 0.01$, $^{***}P < 0.001$, and $^{****}P < 0.0001$.

Downloaded from https://www.science.org at Trinity College Dublin on January 27, 2025

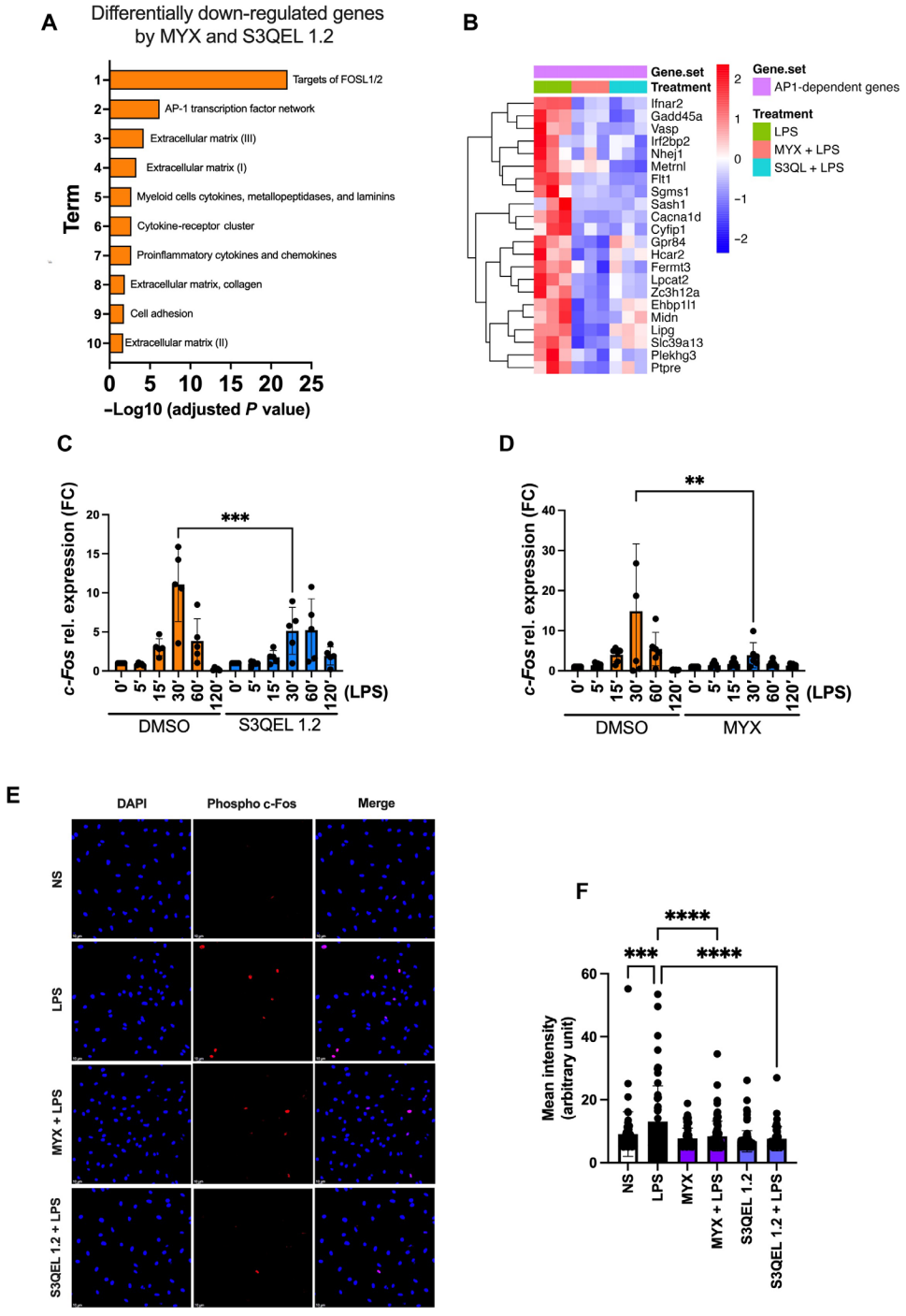


Fig. 4. Complex III–dependent IL-10 regulation is mediated by the c-Fos subunit of the AP1 transcription factor. (**A** and **B**) Overrepresentation analysis of RNA-seq data of BMDMs pretreated with SQ3EL 1.2 or MYX (data are from $n = 3$ from one independent experiment; LPS, 4 hours). (A) EnrichR transcription factor enrichment analysis of differentially down-regulated genes. (B) Heatmap of significantly down-regulated AP1 target genes with adjusted P (P_{adj}) < 0.05. (**C** and **D**) BMDMs were pretreated with DMSO, MYX (500 nM), or S3QEL 1.2 (10 μM) for 1 hour before LPS (100 ng/ml) stimulation for 0 to 120 min, and cell lysates were harvested. Quantification of c-*Fos* mRNA by RT-qPCR, relative to the *Rps18* housekeeping gene, in BMDMs pretreated with S3QEL 1.2 (C) or MYX (D) and stimulated with LPS. (**E** and **F**) Confocal microscopy images (E) and quantification (F) of BMDMs pretreated with DMSO, MYX (500 nM), or S3QEL 1.2 (10 μM) for 1 hour before LPS (100 ng/ml) stimulation for 2 hours. After that, cells were fixed and stained for phospho-c-Fos to assess cellular localization. Merge depicts phospho-c-Fos (red) together with nuclear staining (DAPI). Data in (C) and (D) are means ± SEM for $n = 5$ from three independent experiments. Data in (F) are means ± SD from one of the experiments in (E), showing the activated cells giving a fluorescence signal. Confocal images are representative of two independent experiments. P values were calculated using one-way ANOVA for multiple comparisons. Differences were considered statistically significant at $^{**}P < 0.01$, $^{***}P < 0.001$, and $^{****}P < 0.0001$.

Downloaded from https://www.science.org at Trinity College Dublin on January 27, 2025

these results suggest that the imperfect electron transport–derived ROS perturb AP1, which could likely block IL-10 production by LPS-activated macrophages. Since AP1 is being inhibited by S3QEL 1.2, and since *IL-10* is an AP1-dependent gene, this may be part of the mechanism of IL-10 repression, particularly as AP1 is known to be ROS sensitive (*22*).

S3QEL 1.2 impairs tumor growth and elicit an immune cell response in mice in a B16F10 in vivo model

IL-10 has been shown to be immunosuppressive in several tumor models and promoting tumor survival, notably in the B16F10 melanoma model (*23*). We therefore tested S3QEL 1.2 in this model alone (by intraperitoneal injection) or in combination with the immunostimulatory agent CpG (*24*). We first confirmed that similar to LPS, S3QEL 1.2 would inhibit IL-10 induction by CpG DNA in BMDMs, as shown in Fig. 5A. MYX was also inhibitory (Fig. 5A). The B16F10 model involved treating tumor-bearing mice with CpG DNA intratumorally and repeated intraperitoneal injections of S3QEL 1.2 (Fig. 5B). As shown in Fig. 5C, mice treated with S3QEL 1.2 or CpG alone limited tumor growth but had the most marked effect when given in combination. Similarly, as shown in Fig. 5D, both agents promoted survival with the combination, resulting in the longest survival time. Last, we analyzed by flow cytometry the immune cell subsets infiltrating the tumor [the gating strategy for myeloid cell and non–myeloid cell subsets is shown in fig. S8 (A to D)]. Tumor burden was decreased in the S3QEL 1.2 alone–treated group (Fig. 5E). Cell counts and tumor mass were also lowered (fig. S9, A to C). M1-like macrophages infiltrating the tumor showed increased expression of major histocompatibility complex class II (MHCII) molecules (Fig. 5F), relevant for the presentation of tumor antigens to $CD4^+$ T cells, after S3QEL 1.2 administration while M2-like macrophages presence showed a moderate decrease in the same group (Fig. 5G). IL-10 production by tumor-infiltrating macrophages was impaired by S3QEL 1.2 (Fig. 5H). The number of tumor-infiltrated leukocytes was increased after S3QEL 1.2 administration (fig. S9D), while the number of myeloid cells, neutrophils, and monocyte-macrophages remained the same (fig. S9, E to G). The amounts of dendritic cells were lower in the S3QEL 1.2–treated group (fig. S9H). This last subset of cells did not show any augmented expression of MHCII molecules in mice treated with S3QEL 1.2 (fig. S9I). Last, we also investigated the effect of S3QEL 1.2 on B16F10 melanoma cells in vitro. The highest concentration of S3QEL 1.2 impaired the proliferation of B16F10 cells but did not block OXPHOS and complex III–specific activity, in contrast to MYX, which impaired all these processes (fig. S10, A to F), as assessed by metabolic flux analysis and crystal violet assay. The effect of S3QEL 1.2 on tumor growth may therefore be a combination of a dual effect on tumor cell proliferation and inhibition of IL-10 to promote antitumor immunity.

DISCUSSION

Mitochondrial complex III and its involvement in regulating immune function have only recently begun to be examined. Mice lacking the Rieske iron sulfur protein subunit of complex III showed the diminished suppressive capacity of T_{regs}, together with decreased expression of markers of T_{regs} such as EOS and CTLA-4, without changing their Foxp3 and HELIOS expression (*11*). In another study, complex III knockout mice had lower numbers of $CD4^+$ and $CD8^+$ T cells in the periphery, with less IL-2 expression (*12*).

Here, we have deployed S3QEL 1.2, a highly selective suppressor of complex III–derived ROS, which has been developed by Brand and colleagues (*15*). S3QELs were identified through an Amplex UltraRed–based detection system used to screen 635,000 small molecules against H_2O_2 production caused by electron leak at sites III_{Qo}, I_Q, and II_F in isolated muscle mitochondria. After the elimination of compounds that were unselective for site III_{Qo} or that inhibited energy metabolism, S3QELs were confirmed to potently and selectively suppress site III_{Qo} superoxide production without impairing any bioenergetic function, including mitochondrial membrane potential ($\Delta\Psi_m$) (*15*). S3QEL 1.2 has been shown to prevent the accumulation of ROS produced by complex III and IL-6 production from alveolar macrophages exposed to particulate matter (*25*). In addition, in another study involving BMDMs activated by LPS and extracellular ATP, S3QEL 1.2 did not affect IL-1β production, suggesting a mechanism for NLRP3 inflammasome activation that is independent of complex III–derived ROS (*26*). However, a role for complex III–derived ROS in the production of other key cytokines from macrophages was not investigated. IL-10 appeared to be strongly affected by complex III inhibition in our data, and increasing literature is highlighting its dependency on mitochondrial ETC, although precise details are lacking (*27*–*29*).

Our findings show that complex III sustains IL-10 generation through intact respiration and production of ROS. Inhibition of complex II has been shown to block IL-10 production (*27*), possibly because of electron flow to complex III, preventing it from generating ROS. In addition, our bioinformatics analysis suggests that complex III can regulate the cellular antioxidant response and drive cytokine production via a plethora of pathways. From our findings, it is clear that complex III impairment up-regulates glycolysis as a possible compensatory mechanism to fuel ATP production in the absence of O_2-dependent respiration.

The mechanism that we propose for the decrease in IL-10 expression by complex III impairment is down-regulation of the transcription factor AP1 and, especially, its subunit c-Fos (fig. S11). We hypothesize that ROS produced by complex III would oxidize specific cysteine residues on AP1 or its upstream regulators and subsequently activate them. The redox-sensitive nature of c-Fos has already been described by Wang and colleagues, who showed that the mitochondria-targeted antioxidant mitoTEMPO decreased the oxLDL-mediated abundance of c-Fos and phosphorylated c-Fos in smooth muscle cells (*30*). In another study, mitoTEMPO abolished the binding of AP1 to DNA in endothelial cells activated by lysophosphatidylcholine (*31*). As *c-Fos* and *c-Jun* transcripts are lowered by S3QEL 1.2 and MYX, we do not exclude the possibility of the regulation of proteins that control the stability of mRNAs here (*32*). However, further investigation is necessary to understand the exact mechanism for c-Fos regulation by ROS. Peroxiredoxins, which are antioxidant enzymes responsible for the maintenance of redox balance within the cell, and particularly peroxiredoxin-6, have been detected as interactors of AP1 in mice (*33*).

IL-10 overexpression is a key feature of aggressive and highly proliferative tumors, such as melanoma and colorectal cancer (*34*). Because tumor-associated macrophages (TAMs), together with myeloid-derived suppressor cells (MDSCs) and T_{regs} and B cells, are the main sources of IL-10 in the tumor microenvironment and contribute to the abolishment of the cytotoxic T cell response (*35*), we hypothesized that S3QEL 1.2 could have a beneficial effect through the dampening of tumor-driven immunotolerance mediated by IL-10. We therefore tested

Downloaded from https://www.science.org at Trinity College Dublin on January 27, 2025

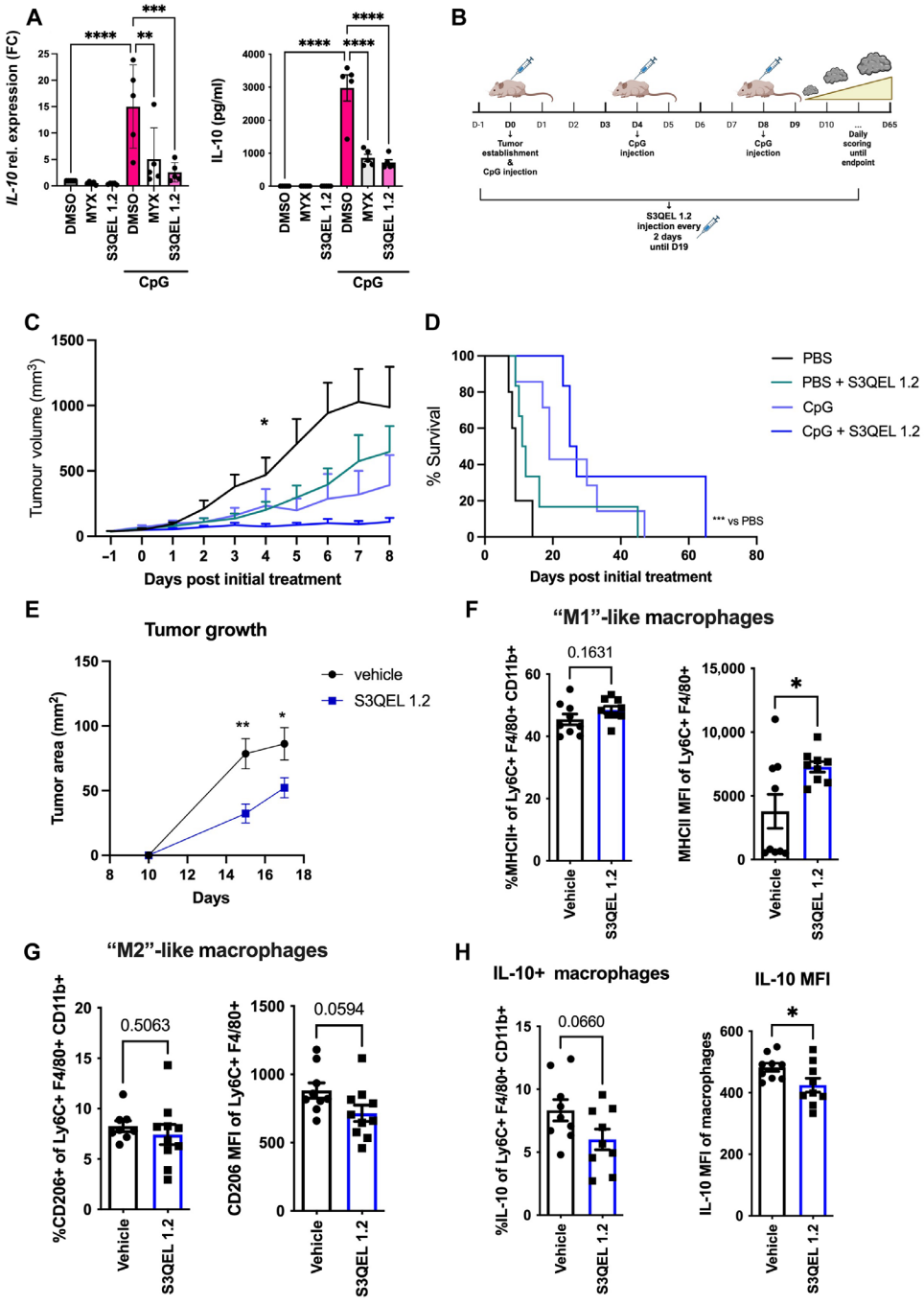


Fig. 5. S3QEL 1.2 administration ameliorates survival and inhibits melanoma progression in mice in vivo. (**A**) BMDMs were pretreated with DMSO, MYX (500 nM), or S3QEL 1.2 (10 μM) for 3 hours, stimulated with CpG (1 μg/ml) for 4 hours, and cell lysates and supernatants were harvested. Quantification of *IL-10* mRNA by RT-qPCR, relative to the *Rps18* housekeeping gene, and of IL-10 levels by ELISA. (**B**) Schematic diagram of the melanoma in vivo model. Mice were challenged with 5×10^6 B16F10 cells subcutaneously and administered with PBS, S3QEL 1.2 (1 mg/kg), and/or CpG (2.5 mg/kg). Tumors were measured daily. D, day. (**C**) Mean initial tumor growth curve relative to tumor volume from day −1 to day 8. (**D**) Kaplan-Meier survival graph up to day 65 (end of experiment). (**E**) Tumor growth rate curve relative to tumor area from day 0 to day 17. (**F** to **H**) Immune cells infiltrating the tumor were analyzed by flow cytometry. Cells expressing the surface markers Ly6C, F4/80, and CD11b showing the percentage of $MHCII^+$ macrophages and mean fluorescence intensity (MFI) of MHCII (F), the percentage of $CD206^+$ macrophages and MFI of CD206 (G), and the percentage of $IL\text{-}10^+$ macrophages and MFI of IL-10 (H). Data from (A) are means ± SEM for $n = 5$ from three independent experiments. Data from (C) and (D) are means ± SEM for $n = 5$ for the PBS group, $n = 6$ for the S3QEL 1.2 group, $n = 7$ for the CpG group, and $n = 6$ for the S3QEL 1.2 + CpG group. Statistical significance for survival analysis was determined by Mantel-Cox test. Statistical significance for tumor growth analysis was determined by two-way ANOVA; asterisks are for $P < 0.05$ in the group's comparison. Data from (E) to (H) are means ± SD for $n = 9$ from one independent in vivo experiment. *P* values were calculated using two-tailed unpaired Student's *t* test. Differences were statistically significant at $*P < 0.05$, $**P < 0.01$, $***P < 0.001$, and $****P < 0.0001$.

Downloaded from https://www.science.org at Trinity College Dublin on January 27, 2025

S3QEL 1.2 in the B16F10 melanoma in vivo model, where neutralization of the IL-10 receptor with an antibody has been shown to boost antitumor immunity, especially in combination with CpG DNA (*36*). The beneficial effect of S3QEL 1.2 here is likely to be via inhibition of IL-10 production by macrophages. However, other pro-inflammatory cytokines and chemokines involved in the cross-talk between tumor and immune cells are differentially regulated after complex III impairment. For example, *CXCL9* is up-regulated by S3QEL 1.2 pretreatment (fig. S2B) and it has been shown to define macrophage polarization, thus an antitumor immune response, in human colorectal cancers (*37*). In addition, *IL-7* and *IL-15* are other two cytokines that are down-regulated after complex III impairment (Fig. 2C). Previous findings have described IL-7 as fundamental for the activation of myeloid cell populations in mice bearing CT26 tumors (*38*) and for tumor invasiveness in prostate cancer (*39*), while IL-15–dependent signaling in tumor-associated macrophages inhibited $CD8^+$ T cell recruitment in breast cancer (*40*). Taking into consideration the complexity of the tumor microenvironment, we cannot rule out possible effects of S3QEL 1.2 on other cell types and we believe that S3QEL 1.2 might also inhibit proliferation of the B16F10 melanoma cells themselves. Therefore, the treatment of macrophages before in vivo injection with tumor cells, as previously deployed (*41*), or the use of IL-10 conditional knockout models may represent other options required to further elucidate the specific mechanism of action and target of S3QEL 1.2.

In conclusion, our work provides evidence for complex III–derived ROS in regulating IL-10 production in macrophages, broadening the existing knowledge about ETC-mediated rewiring of myeloid cells (*42*). Moreover, S3QEL 1.2 could be a useful tool for dissecting immunotolerance in the context of tumor development and progression. Recently, a complex I inhibitor was tested in acute myeloid leukemia and advanced solid tumors but proved to be neurotoxic (*43*). The advantage of S3QEL 1.2 is its limited effect on respiration, and therefore, it may be less toxic in the treatment of cancer.

MATERIALS AND METHODS

Animal details

All mice used for the in vitro experiments were on a C57BL/6JOlaHsd background, unless stated below. Wild-type mice, when needed, were purchased from Envigo. In vivo experiments were performed with 8-week-old female mice bred under specific pathogen–free conditions, under the license and approval of the local animal research ethics committee (Health Products Regulatory Authority) under European Union regulations. The first two in vivo LPS models were performed with 6-to-12-week-old C57BL/6JOlaHsd mice, and littermates were randomly assigned to experimental groups. All animal procedures were ethically approved by the Trinity College Dublin Animal Research Ethics Committee before experimentation and conformed to the directive 2010/63/EU of the European Parliament (authorization AE19136/P148).

The first B16F10 melanoma in vivo model was performed with 6-to-12-week-old C57BL/6J mice, which were randomly assigned to experimental groups. All animal procedures were ethically approved by the Trinity College Dublin Animal Research Ethics Committee before experimentation and conformed to the directive 2010/63/EU of the European Parliament (authorization AE19136/P172).

The second B16F10 melanoma in vivo model was performed in the animal facilities of the Medical University of Graz. Wild-type C57BL/6J mice were purchased from Charles River Laboratories. Ethical approval for animal experimental protocols was granted by the Austrian Federal Ministry of Science and Research (protocol number: 2022-0.748.851/2024-0.783.500).

B16F10 in vivo model

B16F10 cells (American Type Culture Collection) were maintained in Dulbecco's modified Eagle's medium (DMEM) (Gibco) containing 10% fetal bovine serum (FBS) and 1% penicillin-streptomycin at 37°C and 5% CO_2 in a humified incubator. Mice were injected subcutaneously with 3.5×10^5 B16F10 cells on the right flank, which has been previously shaved. Tumor growth was measured daily using a digital caliper, and the tumor volume was calculated as [Length × $(\text{Width})^2$]/2. Upon reaching 30 to 60 mm^3, mice were randomly assigned to experimental treatment groups and received intratumoral injections of phosphate-buffered saline (PBS) or CpG ODN 1826 (2.5 mg/kg each treatment), with treatments repeated 4 days later on day 4 and on day 8 for a total of three intratumoral treatments. In one experiment, two groups of mice received S3QEL 1.2 (1 mg/kg; 5% in PBS) via the intraperitoneal route every 2 days from day one before the first intratumoral treatment until day 19. Mice were culled upon reaching the predetermined humane end point of tumor diameter >15 mm or, in the case of ulceration, with survival analyzed using Kaplan-Meier analysis.

In the second in vivo experiment, B16F10 cells (American Type Culture Collection) were maintained in DMEM (Gibco) containing 10% FBS and 1% penicillin-streptomycin at 37°C and 5% CO_2 in a humified incubator. Mice were injected subcutaneously with 5×10^6 B16F10 cells on the right flank, which has been previously shaved. Tumor growth was measured daily using a digital caliper, and the tumor volume was calculated as [Length × $(\text{Width})^2$]/2. Upon reaching 30 to 60 mm^3, mice were randomly assigned to experimental treatment groups and received S3QEL 1.2 or PBS intraperitoneally. S3QEL 1.2 was dissolved in a vehicle containing dimethyl sulfoxide (DMSO):ethanol:Kolliphor EL (Sigma-Aldrich) at a 1:1:2 ratio and divided into aliquots; a vehicle control containing no drug was also prepared. Before injection, an aliquot of S3QEL 1.2 or vehicle in DMSO/ethanol/Kolliphor was added to pre-prepared 5% (w/v) glucose in water at a 1:6.66667 ratio. Two hundred microliters of this mixture per mouse was injected intraperitoneally every other day to give a final S3QEL 1.2 concentration of 1 mg/kg per mouse.

Flow cytometry of tumor single-cell suspensions

B16F10 tumors were removed, mechanically minced using surgical scissors, and subsequently digested with deoxyribonuclease I (160 U/ml; Worthington) and collagenase (4.5 U/ml; Worthington) for 30 min at 37°C, with vortexing and shaking. Samples were then passed through a 40-μm cell strainer, washed in PBS and 2% FBS, and resuspended in flow staining buffer (PBS containing 2% FBS and 2 mM EDTA). Cells were counted on the EVE automated cell counter (NanoEntek).

A total of 3×10^6 cells per sample in 100 μl of staining buffer were used for flow cytometry staining. Single-cell suspensions were incubated for 20 min in fixable viability dye eFluor 780 (eBioscience) according to the manufacturer's instructions. Fc receptor blocking was then performed using TruStain FcX (BioLegend) according to the manufacturer's instructions. For surface staining, cells were incubated for 30 min at 4°C in the dark in flow staining buffer with the following antibodies (all purchased from BD/BioLegend): CD45-AF700 (clone 30-F11, 560510), CD3-BV421 (clone 17A2, 564008), CD4-BUV496

Downloaded from https://www.science.org at Trinity College Dublin on January 27, 2025

(clone GK1.5, 612952), CD8-PE-Cy7 (clone 53-6.7, 561097), NKp46-BV510 (clone 29A1.4, 563455), CD19-BV711 (clone 1D3, 563157), CD11b-BUV737 (clone M1/70, 612801), Ly6C-APC (clone AL21, 560595), Ly6G-PE/Dazzle594 (clone 1A8, 127648), CD11c-BV605 (clone N418, 117333), F4/80-BUV395 (clone T45-2342, 565614), SiglecF-PE (clone E50-2440, 552126), CD206-FITC (clone C068C2, 141704), and MHCII-PerCP-Cy5.5 (clone M5/114.15.2, 107626). Single stains and fluorescence minus one (FMO) controls were also used. Cells were then washed twice in flow staining buffer, fixed using IC Fixation Buffer (eBioscience) for 10 min, washed again twice, and resuspended in flow staining buffer.

For intracellular staining of IL-10, 3×10^6 cells of each single-cell suspension sample were seeded into a 96-well U-bottom plate with RPMI containing GolgiStop (1.5 μl/ml, BD Biosciences) and incubated for 1 hour in a 37°C cell culture incubator. Fixable viability dye staining, Fc receptor blocking, and surface antibody staining were performed as above. Cells were then permeabilized and fixed using Perm/Fix Buffer (BD Biosciences) for 30 min, followed by subsequent staining for IL-10 using an IL-10-PE antibody (BioLegend) for 30 min. Single stains and FMO controls were also used. Cells were then washed twice in Perm/Fix buffer (prepared according to the manufacturer's instructions; BD Biosciences), and resuspended in flow staining buffer.

Samples were analyzed on a BD LSRFortessa flow cytometer using FACSDiva software (BD Biosciences). Analyses were performed using FlowJo version 10.10 software, and FMO and single stains were used to compensate and define gates.

Flow cytometry of T_H1 lymphocytes

After activation, the cells were then washed and stained for 10 min at room temperature with fixable viability dye (Thermo Fisher Scientific) for dead cell exclusion and fluorochrome-labeled monoclonal antibodies against surface cell markers (CD4-PerCPCy5.5, clone RM4-4, 116011). Afterward, cells were washed and fixed for 15 min at room temperature using the eBioscience Foxp3 Fixation/Permeabilization Kit. After other washing steps, cells were permeabilized using the same kit and stained intracellularly with monoclonal antibodies (IFN-γ-APC, clone XMG1.2, 505810; and IL-10-APCCy7, JES5-16E3, 505035). Data were acquired on FACSCanto II machines (BD Biosciences) and analyzed using FlowJo software (Tree Star), and unstained single-stained controls were used to compensate and define gates.

Generation of murine BMDMs

Mice (6- to 12-week-old) were euthanized in a CO_2 chamber, and death was confirmed by cervical dislocation [procedures previously described in (*44*, *45*)]. Bone marrow was subsequently harvested from the tibia, femur, and ilium. For monocyte/macrophage isolation, cells were differentiated in DMEM containing L929 supernatant (20%), FBS (10%), and penicillin-streptomycin (1%) for 6 days, after which cells were counted and plated at 0.5×10^6 cells/ml in 10% L929 supernatant, unless otherwise stated.

Isolation of human PBMCs

Human blood samples from healthy donors were collected and processed at the School of Biochemistry and Immunology at the Trinity Biomedical Sciences Institute (TCD). Blood samples were obtained anonymously, and written informed consent for the use of blood for research purposes was obtained from the donors. All the procedures involving experiments on human samples were approved by the School of Biochemistry and Immunology Research Ethics Committee (TCD). Experiments were conducted according to the TCD guide on good research practice, which follows the guidelines detailed in the National Institutes of Health Belmont Report (1978) and the Declaration of Helsinki. Whole blood (30 ml) was layered on 20 ml of Lymphoprep (Axis-Shield), followed by centrifugation for 20 min at 400*g* with the brake off, after which the upper plasma layer was removed and discarded. The layer of mononuclear cells at the plasma-density gradient medium interface was retained, and 20 ml of PBS was added. Cells were centrifuged for 8 min at 300*g*, and the resulting supernatant was removed and discarded. The remaining pellet of mononuclear cells was resuspended, counted, and plated at 1×10^6 cells/ml in RPMI supplemented with FBS (10%) and penicillin-streptomycin (1%).

Generation of human macrophages

PBMCs were obtained, and $CD14^+$ monocytes were isolated using a MagniSort Human CD14 Positive Selection kit (Thermo Fisher Scientific) according to the manufacturer's protocol. CD14 monocytes were then differentiated in T-175 flasks in RPMI containing FBS (10%), penicillin-streptomycin (1%), and recombinant human macrophage colony-stimulating factor (1:10,000). After 6 days, the supernatant was discarded, cells were scraped and counted, and human monocyte-derived macrophages were plated in 12-well plates at 1×10^6 cells/ml in RPMI containing FBS (10%) and penicillin-streptomycin (1%).

In vitro T_H1 cell differentiation

Naive $CD4^+CD25^-$ T cells were purified from spleens of wild-type C57BL/6OlaHsd mice with the naïve CD4 T cell isolation kit (Miltenyi Biotec) by using an AutoMACS magnetic cell sorter (Miltenyi Biotec) according to the manufacturer's protocol. Purified cells were activated with anti-CD3ε:CD28 (3 and 2 μg/ml, respectively; BD Biosciences) coated on an F-bottomed plate (10^5 per well). Skewing conditions were rmIL-12 and rmIL-2 (both 20 ng/ml; R&D Systems) for T_H1 cells for 72 hours. When indicated, MYX (50, 500, or 5000 nM) and S3QEL 1.2 (0.1, 1, or 10 μM) were added to the polarization media. Subsequently, T_H1 cells were activated by phorbol 12-myristate 13-acetate/ionomycin stimulation (50 and 500 ng/ml, respectively) in the presence of StopGolgi solution (1.5 μl/ml, BD Biosciences) at 37°C in a humidified 5% CO_2 chamber for 3 hours.

Reagents

MYX was dissolved in DMSO, both purchased from Sigma-Aldrich. S3QEL 1.2 and S1QEL 1.1 were provided by M. D. Brand (Buck Institute for Research on Aging, Novato, CA, US). LPS from *Escherichia coli* (ALX-581-010-L002) was purchased from Enzo Life Sciences for in vitro experiments. NAC and MitoTEMPO were purchased by Sigma-Aldrich. CpG ODN 1826 (130-109-373/374) was purchased from Miltenyi Biotec for in vitro and in vivo experiments. LPS from *E. coli* (L4524) was purchased from Sigma-Aldrich for in vivo experiments. MitoTEMPO was purchased from Sigma-Aldrich (0737), and MitoQ was purchased from Abcam (ab285406) for in vitro experiments. Rotenone (Sigma-Aldrich, 8875) and piericidin A (MedChemExpress, HY-114936) were also used for in vitro experiments. NAC was purchased from Merck (A7250) for in vitro experiments.

RNA isolation and real-time qPCR

Total RNA was isolated using the PureLink RNA Mini Kit (Invitrogen) and quantified using a Nanodrop 2000 UV-visible spectrophotometer. cDNA was prepared using total RNA (20 to 100 ng/μl) by

Downloaded from https://www.science.org at Trinity College Dublin on January 27, 2025

RT-PCR using a high-capacity cDNA reverse transcription kit (Applied Biosystems) according to the manufacturer's instructions. Real-time qPCR was performed with an ABI 7500 Fast real-time PCR system (Applied Biosystems) on cDNA using SYBR Green (Invitrogen). Data were normalized to murine RPS18 as endogenous controls, and the mRNA expression fold change relative to controls was calculated using the $2^{-\Delta\Delta Ct}$ method. All fold changes are expressed normalized to the untreated control. The following murine primers were used: *IL-1*β, 5′-GAGGACATGAGCACCTTCTTT-3′, 3′-GCCTGTAGTGCAGTTGTCTAA-5′; *TNF*-α, 5′-GCCTCTTCTCATTCCTGCTT-3′, 3′-TGGGAACTTCTCATCCCTTTG-5′; *IL-10*, 5′-AGGCGCTGTCATCGATTT-3′, 3′-CACCTTGGTCTTGGAGCTTAT-5′; *IL-6*, 5′-CCACAGTCCTTCAGAGAGATACA-3′, 3′-CCTTCTGTGACTCCAGCTTATC-5′; *c-Fos*, 5′-GGGAATGGTGAAGACCGTGTCA-3′, 3′-GCAGCCATCTTATTCCGTTCCC-5′; *c-Jun*, 5′-CAGTCCAGCAATGGGCACATCA-3′, 3′-GGAAGCGTGTTCTGGCTATGCA-5′; *Act*β, 5′-GCCTTCCTTCTTGGGTATGG-3′, 3′-A GCACTGTGTTGGCATAGAG-5′; *RPS18*, 5′-GCGAGTACTCAACACCAACA-3′, 3′-CCTCAACACCACATGAGCATA-5′. The following human primers were used: *IL-10*, 5′-GTCCTTGCTGGAGGACTTTA-3′, 3′-ATGTCTGGGTCTTGGTTCTC-5′; *RPS13*, 5′-CGAAAGCATCTTGAGAGGAACA-3′, 3′-TCGAGCCAAACGGTGAATC-5′.

RNA sequencing

BMDMs (three independent mice) were treated as indicated, and RNA was extracted as previously detailed. mRNA was extracted from total RNA using poly-T-oligo–attached magnetic beads. After fragmentation, the first-strand cDNA was synthesized using random hexamer primers, followed by second-strand cDNA synthesis using either deoxyuridine triphosphate for directional library or deoxythymidine triphosphate for nondirectional library. The library was checked with Qubit and real-time PCR for quantification and a bioanalyzer for size distribution detection. Quantified libraries were pooled and sequenced on the NovaSeq 6000 S4 (Illumina).

Raw data (raw reads) in fastq format were first processed through in-house (Novogene) perl scripts. In this step, clean data (clean reads) were obtained by removing reads containing an adapter, reads containing ploy-N, and low-quality reads from raw data. At the same time, Q20, Q30, and GC content were calculated. All the downstream analyses were based on the clean data with high quality. The index of the reference genome was built usingHisat2 version 2.0.5, and paired-end clean reads were aligned to the reference genome using Hisat2 version 2.0.5.

FeatureCounts version 1.5.0-p3 was used to count the read numbers mapped to each gene. Then, fragments per kilobase of transcript per million mapped reads of each gene were calculated on the basis of the length of the gene and read counts mapped to this gene.

Differential expression was analyzed using the DESeq2R package (1.20.0). The resulting *P* values were adjusted using Benjamini and Hochberg's approach for controlling the false discovery rate. Genes with an adjusted $P \leq 0.05$ found by DESeq2 were assigned as differentially expressed. All the analyses and heatmaps were performed using custom scripts in R version 4.3.1. GSEA was performed using the online EnrichR tool.

ELISA

A DuoSet ELISA kit for IL-10 and TNF-α (R&D Systems) in the supernatant of BMDMs was purchased and used according to the manufacturer's instructions with appropriately diluted cell supernatants added to each plate in duplicate or triplicate. For in vivo samples, a Quantikine ELISA kit for mouse IL-10 (R&D Systems) was used according to the manufacturer's instructions with appropriately diluted serum added to each plate. Absorbance was read at 450 nm and quantified using a FLUOstar Optima plate reader. Corrected absorbance values were calculated by subtracting the background absorbance, and cytokine concentrations were subsequently obtained by extrapolation from a standard curve plotted on GraphPad Prism 10.1.1.

MTT assay

BMDMs at a concentration of 1×10^5 cells were seeded in each well of a 96-well F-bottom plate in duplicates or triplicates and treated accordingly. MTT was purchased from Sigma-Aldrich and reconstituted in PBS to a concentration of 1 mg/ml. On each plate, three wells had no cells but the medium only to serve as a blank. At the end of the treatment, cells were washed with 100 μl per well and 100 μl of MTT solution was added in each well. The plate was incubated for 2 hours at 37°C wrapped in tin foil. At the end of the incubation, the MTT solution was discarded, and the crystals were dissolved in 100 μl of DMSO solution in each well. The plate was incubated for 20 min at 37°C in the dark and read on a spectrophotometer at 595 nm of wavelength. Data were normalized to untreated and unstimulated cells.

Extracellular flux analysis

A Seahorse XFe-96 extracellular flux analyzer (Seahorse Bioscience, Agilent Technologies) was used to define oxygen consumption rates (OCRs) and extracellular acidification rates. For monitoring OXPHOS, cells were plated at 1×10^5 cells per well in XF DMEM (pH 7.4) supplemented with pyruvate, glutamine, and glucose. Mitochondrial perturbation experiments were carried out by sequential addition of oligomycin (oligo), carbonyl cyanide 4-(trifluoromethoxy) phenylhydrazone (FCCP), antimycin A (AA), and rotenone according to the manufacturer's instructions. For monitoring glycolysis, cells were plated in XF DMEM (pH 7.4) supplemented with glutamine. Glycolysis perturbation experiments were carried out by sequential addition of glucose, oligo, and 2-deoxyglucose according to the manufacturer's instructions. For monitoring the OCR of only intact mitochondria, cells were plated in MAS buffer (70 mM sucrose, 220 mM mannitol, 10 mM KH_2PO_4, 5 mM $MgCl_2$, 2 mM Hepes, and 1 mM EGTA) and then treated with the XF plasma membrane permeabilizer (Seahorse, Agilent Technologies), followed by addition of 0.5 mM duroquinol, 1 mM adenosine 5′-diphosphate (ADP), 15 μM oligo, and 0.02 mM AA for monitoring complex III–driven respiration. In this case, the assay includes a cycle of mixing for 2′, waiting for 2′, and measuring for 3′ (repeated three times); duroquinol and ADP injections, followed by the same cycle repeated two times; then oligomycin injection, followed by the same cycle repeated two times; and AA injection, followed by the same cycle repeated two times. Changes in OCR on substrate addition were calculated relative to the preinjection rate.

Western blotting

The supernatant was removed from cells after stimulation, and lysates were harvested in 30 to 50 μl of lysis buffer [0.125 M Tris (pH 6.8), 10% glycerol, 0.02% SDS, and 5% dithiothreitol]. Lysates were subsequently heated to 95°C for 5 min to denature proteins. SDS–polyacrylamide gel electrophoresis was used to resolve proteins by

Downloaded from https://www.science.org at Trinity College Dublin on January 27, 2025

molecular weight. Samples were boiled at 95°C for 5 min before loading into a 5% stacking gel. The percentage resolving gel (8 to 12%) depended on the molecular weight of the given protein. The Bio-Rad gel running system was used to resolve proteins, and the Bio-Rad wet transfer system was used for the electrophoretic transfer of proteins onto the polyvinylidene difluoride membrane. After transfer, the membrane was incubated in blocking solution [5% milk powder or 5% bovine serum albumin (BSA) in Tris-buffered saline with Tween 20 (TBST)] for 1 hour and subsequently incubated in a primary antibody (5% milk powder or 5% BSA in TBST) rolling overnight at 4°C. The membrane was incubated for 1 hour with a secondary antibody (diluted in 5% milk powder or 5% BSA in TBST) at room temperature. Before visualization, the membrane was immersed in WesternBright ECL Spray (Advansta). Proteins were visualized on a ChemiDoc MPTM Imaging System (Bio-Rad), and both chemiluminescent and white light images were taken.

Quantification of Western blot images was performed using Image Lab Software (Bio-Rad). The adjusted band volume was calculated for each band, and for each experimental condition, this was presented as the target protein/housekeeping protein.

The following antibodies were used: antimouse c-Fos (2250), phospho-c-Fos (5348), c-Jun (9165), phospho-c-Jun (3270), GAPDH (glyceraldehyde-3-phosphate dehydrogenase; 2118), and α-tubulin (2144); they were purchased from Cell Signaling Technology. Total OXPHOS rodent Western blot antibody cocktail was purchased from Abcam (ab110413). Antimouse β-actin (A5316) was purchased from Sigma-Aldrich.

Immunofluorescence and confocal microscopy

Cells (2.5×10^5) were plated on 12-mm coverslips in 24-well plates. Cells were treated as required and washed three times with warm PBS. Cells were subsequently fixed for 10 min with 2% paraformaldehyde in PBS at 37°C. Cells were washed three times with PBS and permeabilized for 1 hour in block solution [1% BSA, glycine (22.52 mg/ml), and 0.1% Tween 20 in PBS]. Anti-phospho-c-Fos antibody (Cell Signaling Technology, 5348) was diluted 1:800 in block solution and incubated with cells overnight at 4°C. Cells were washed three times with PBS for 5 min per wash. A mix containing Alexa 647–conjugated goat antirabbit IgG (H + L) antibody (1:1000) and DAPI (4′,6-diamidino-2-phenylindole; 1:1000, Thermo Fisher Scientific, 62248) was subsequently added to cells for 90 min at room temperature in the dark. Cells were subsequently washed three times with PBS for 5 min per wash. Coverslips were mounted onto microscope slides using 10 to 20 μl of ProLong Gold antifade reagent (Thermo Fisher Scientific, P36930). Slides were imaged using a Leica SP8 scanning confocal microscope with a ×40.0 objective. Images were analyzed using LAS X Life Science Microscope Software Platform (Leica). The same microscope instrument settings were used for all samples, and all images were analyzed using the same settings. Quantification of phospho-c-Fos signal intensity was performed using Imaris software 10.1.1. The mean signal intensity was calculated for individual cells in single-color images and displayed relative to the signal intensity of control cells.

Amplex Red H_2O_2 measurement

BMDMs were seeded in a 96-well plate with black opaque inserts with a concentration of 1×10^5 cells per well in duplicates. Cells were treated accordingly and stimulated with LPS for 48 hours (100 ng/ml) and with MitoTEMPO for 48 hours (5 mM). Cells were treated with S3QEL 1.2 (10 μM) and MYX (500*n*M) on the day of the assay, and media were changed to KRPG Buffer. The H_2O_2 standard was prepared as per the manufacturer's instructions. Fifty microliters of 100 μM Amplex Red and HRP working solution (0.2 U/ml) were added to the wells of the H_2O_2 standard. One hundred microliters of 50 μM Amplex Red and HRP working solution (0.1 U/ml) were added to the wells containing the samples. Fluorescence with excitation between 450 and 490 nm and emission of 590 nm was read at the beginning of the reaction, after 30 min, and then every hour for maximum 3 hours. The fluorescence of the samples was extrapolated from the H_2O_2 standard curve and normalized to the untreated sample.

LPS-induced model of inflammation

C57BL/6OlaHsd mice were pretreated intraperitoneally with S3QEL 1.2 or DMSO vehicle control at the final concentration of 1 mg/kg (1:10 in PBS) for 2 hours and then injected intraperitoneally with LPS or PBS vehicle control at the final concentration of 2.5 mg/kg for 2 hours. After 4 hours, mice were euthanized and blood was collected retro-orbitally. Peritoneal exudate cells were harvested in PBS. Blood was centrifuged at 4°C for 10 min at 5000 rcf, and then the supernatant (serum) was kept at −80°C for further analysis by ELISA. Peritoneal exudate cells were pelleted and lysed in RNA lysis buffer (Invitrogen) for further analysis by qPCR.

Quantification and statistical analysis

Details of all statistical analyses performed can be found in the figure legends. Data were expressed as means ± SEM, unless stated otherwise. *P* values were calculated using two-tailed Student's *t* test for pairwise comparison of variables and one-way analysis of variance (ANOVA) for multiple comparisons of variables. A Sidak's multiple comparisons test was used as a post test when performing an ANOVA. A Mantel-Cox test was used for log-rank analysis of the survival Kaplan-Meier curve. A confidence interval of 95% was used for all statistical tests. For statistical significance, exact *P* values are included within each panel. Sample sizes were determined on the basis of previous experiments using similar methodologies. All depicted data points are biological replicates taken from distinct samples. Each figure consists of a minimum of three independent experiments from multiple biological replicates, unless stated otherwise in the figure legends. *n* refers to the number of animals or the number of independent experiments with cell lines. For in vivo studies, age-matched mice were randomly assigned to treatment groups.

Supplementary Materials

This PDF file includes:

Figs. S1 to S11

REFERENCES AND NOTES

1. B. Kelly, L. A. O'Neill, Metabolic reprogramming in macrophages and dendritic cells in innate immunity. *Cell Res.* **25**, 771–784 (2015).
2. D. G. Russell, L. Huang, B. C. VanderVen, Immunometabolism at the interface between macrophages and pathogens. *Nat. Rev. Immunol.* **19**, 291–304 (2019).
3. D. F. Fiorentino, M. W. Bond, T. R. Mosmann, Two types of mouse T helper cell. IV. Th2 clones secrete a factor that inhibits cytokine production by Th1 clones. *J. Exp. Med.* **170**, 2081–2095 (1989).
4. M. Saraiva, A. O'Garra, The regulation of IL-10 production by immune cells. *Nat. Rev. Immunol.* **10**, 170–181 (2010).
5. A. Taylor, J. Verhagen, K. Blaser, M. Akdis, C. A. Akdis, Mechanisms of immune suppression by interleukin-10 and transforming growth factor-β: The role of T regulatory cells. *Immunology* **117**, 433–442 (2006).

Downloaded from https://www.science.org at Trinity College Dublin on January 27, 2025

6. W. K. E. Ip, N. Hoshi, D. S. Shouval, S. Snapper, R. Medzhitov, Anti-inflammatory effect of IL-10 mediated by metabolic reprogramming of macrophages. *Science* **356**, 513–519 (2017).
7. H. F. Bradford, T. C. R. McDonnell, A. Stewart, A. Skelton, J. Ng, Z. Baig, F. Fraternali, D. Dunn-Walters, D. A. Isenberg, A. R. Khan, C. Mauro, C. Mauri, Thioredoxin is a metabolic rheostat controlling regulatory B cells. *Nat. Immunol.* **25**, 873–885 (2024).
8. M. A. Watson, H. S. Wong, M. D. Brand, Use of S1QELs and S3QELs to link mitochondrial sites of superoxide and hydrogen peroxide generation to physiological and pathological outcomes. *Biochem. Soc. Trans.* **47**, 1461–1469 (2019).
9. P. Benit, S. Lebon, P. Rustin, Respiratory-chain diseases related to complex III deficiency. *Biochim. Biophys. Acta* **1793**, 181–185 (2009).
10. E. Anso, S. E. Weinberg, L. P. Diebold, B. J. Thompson, S. Malinge, P. T. Schumacker, X. Liu, Y. Zhang, Z. Shao, M. Steadman, K. M. Marsh, J. Xu, J. D. Crispino, N. S. Chandel, The mitochondrial respiratory chain is essential for haematopoietic stem cell function. *Nat. Cell Biol.* **19**, 614–625 (2017).
11. S. E. Weinberg, B. D. Singer, E. M. Steinert, C. A. Martinez, M. M. Mehta, I. Martinez-Reyes, P. Gao, K. A. Helmin, H. Abdala-Valencia, L. A. Sena, P. T. Schumacker, L. A. Turka, N. S. Chandel, Mitochondrial complex III is essential for suppressive function of regulatory T cells. *Nature* **565**, 495–499 (2019).
12. L. A. Sena, S. Li, A. Jairaman, M. Prakriya, T. Ezponda, D. A. Hildeman, C. R. Wang, P. T. Schumacker, J. D. Licht, H. Perlman, P. J. Bryce, N. S. Chandel, Mitochondria are required for antigen-specific T cell activation through reactive oxygen species signaling. *Immunity* **38**, 225–236 (2013).
13. R. Acin-Perez, M. P. Bayona-Bafaluy, P. Fernandez-Silva, R. Moreno-Loshuertos, A. Perez-Martos, C. Bruno, C. T. Moraes, J. A. Enriquez, Respiratory complex III is required to maintain complex I in mammalian mitochondria. *Mol. Cell* **13**, 805–815 (2004).
14. M. D. Brand, Riding the tiger – Physiological and pathological effects of superoxide and hydrogen peroxide generated in the mitochondrial matrix. *Crit. Rev. Biochem. Mol. Biol.* **55**, 592–661 (2020).
15. A. L. Orr, L. Vargas, C. N. Turk, J. E. Baaten, J. T. Matzen, V. J. Dardov, S. J. Attle, J. Li, D. C. Quackenbush, R. L. Goncalves, I. V. Perevoshchikova, H. M. Petrassi, S. L. Meeusen, E. K. Ainscow, M. D. Brand, Suppressors of superoxide production from mitochondrial complex III. *Nat. Chem. Biol.* **11**, 834–836 (2015).
16. S. Galvan-Pena, L. A. O'Neill, Metabolic reprograming in macrophage polarization. *Front. Immunol.* **5**, 420 (2014).
17. A. M. Cameron, A. Castoldi, D. E. Sanin, L. J. Flachsmann, C. S. Field, D. J. Puleston, R. L. Kyle, A. E. Patterson, F. Hassler, J. M. Buescher, B. Kelly, E. L. Pearce, E. J. Pearce, Inflammatory macrophage dependence on NAD^+ salvage is a consequence of reactive oxygen species-mediated DNA damage. *Nat. Immunol.* **20**, 420–432 (2019).
18. A. Cui, T. Huang, S. Li, A. Ma, J. L. Perez, C. Sander, D. B. Keskin, C. J. Wu, E. Fraenkel, N. Hacohen, Dictionary of immune responses to cytokines at single-cell resolution. *Nature* **625**, 377–384 (2024).
19. M. Rossato, G. Curtale, N. Tamassia, M. Castellucci, L. Mori, S. Gasperini, B. Mariotti, M. De Luca, M. Mirolo, M. A. Cassatella, M. Locati, F. Bazzoni, IL-10-induced microRNA-187 negatively regulates TNF-α, IL-6, and IL-12p40 production in TLR4-stimulated monocytes. *Proc. Natl. Acad. Sci. U.S.A.* **109**, E3101–E3110 (2012).
20. H. S. Wong, P. A. Monternier, M. D. Brand, S1QELs suppress mitochondrial superoxide/hydrogen peroxide production from site IQ without inhibiting reverse electron flow through Complex I. *Free Radic. Biol. Med.* **143**, 545–559 (2019).
21. M. A. Watson, B. Pattavina, T. A. U. Hilsabeck, J. Lopez-Dominguez, P. Kapahi, M. D. Brand, S3QELs protect against diet-induced intestinal barrier dysfunction. *Aging Cell* **20**, e13476 (2021).
22. M. Ding, X. Shi, Y. Lu, C. Huang, S. Leonard, J. Roberts, J. Antonini, V. Castranova, V. Vallyathan, Induction of activator protein-1 through reactive oxygen species by crystalline silica in JB6 cells. *J. Biol. Chem.* **276**, 9108–9114 (2001).
23. T. Kobayashi, K. Oishi, A. Okamura, S. Maeda, A. Komuro, Y. Hamaguchi, M. Fujimoto, K. Takehara, T. Matsushita, Regulatory B1a cells suppress melanoma tumor immunity via IL-10 production and inhibiting T Helper Type 1 cytokine production in tumor-infiltrating $CD8^+$ T cells. *J. Invest. Dermatol.* **139**, 1535–1544.e1 (2019).
24. G. J. Weiner, The immunobiology and clinical potential of immunostimulatory CpG oligodeoxynucleotides. *J. Leukoc. Biol.* **68**, 455–463 (2000).
25. S. Soberanes, A. V. Misharin, A. Jairaman, L. Morales-Nebreda, A. C. McQuattie-Pimentel, T. Cho, R. B. Hamanaka, A. Y. Meliton, P. A. Reyfman, J. M. Walter, C. I. Chen, M. Chi, S. Chiu, F. J. Gonzalez-Gonzalez, M. Antalek, H. Abdala-Valencia, S. E. Chiarella, K. A. Sun, P. S. Woods, A. J. Ghio, M. Jain, H. Perlman, K. M. Ridge, R. I. Morimoto, J. I. Sznajder, W. E. Balch, S. M. Bhorade, A. Bharat, M. Prakriya, N. S. Chandel, G. M. Mutlu, G. R. S. Budinger, Metformin targets mitochondrial electron transport to reduce air-pollution-induced thrombosis. *Cell Metab.* **29**, 335–347.e5 (2019).
26. L. K. Billingham, J. S. Stoolman, K. Vasan, A. E. Rodriguez, T. A. Poor, M. Szibor, H. T. Jacobs, C. R. Reczek, A. Rashidi, P. Zhang, J. Miska, N. S. Chandel, Mitochondrial electron transport chain is necessary for NLRP3 inflammasome activation. *Nat. Immunol.* **23**, 692–704 (2022).
27. D. Gobelli, P. Serrano-Lorenzo, M. J. Esteban-Amo, J. Serna, M. T. Perez-Garcia, A. Orduna, A. A. Jourdain, M. A. Martin-Casanueva, M. Á. de la Fuente, M. Simarro, The mitochondrial succinate dehydrogenase complex controls the STAT3-IL-10 pathway in inflammatory macrophages. *iScience* **26**, 107473 (2023).
28. B. Kelly, G. M. Tannahill, M. P. Murphy, L. A. O'Neill, Metformin inhibits the production of reactive oxygen species from NADH:Ubiquinone oxidoreductase to limit induction of interleukin-1β (IL-1β) and boosts interleukin-10 (IL-10) in lipopolysaccharide (LPS)-activated macrophages. *J. Biol. Chem.* **290**, 20348–20359 (2015).
29. E. L. Mills, B. Kelly, A. Logan, A. S. H. Costa, M. Varma, C. E. Bryant, P. Tourlomousis, J. H. M. Dabritz, E. Gottlieb, I. Latorre, S. C. Corr, G. McManus, D. Ryan, H. T. Jacobs, M. Szibor, R. J. Xavier, T. Braun, C. Frezza, M. P. Murphy, L. A. O'Neill, Succinate dehydrogenase supports metabolic repurposing of mitochondria to drive inflammatory macrophages. *Cell* **167**, 457–470.e13 (2016).
30. G. Miao, X. Zhao, S. L. Chan, L. Zhang, Y. Li, Y. Zhang, L. Zhang, B. Wang, Vascular smooth muscle cell c-Fos is critical for foam cell formation and atherosclerosis. *Metabolism* **132**, 155213 (2022).
31. X. Li, P. Fang, Y. Li, Y. M. Kuo, A. J. Andrews, G. Nanayakkara, C. Johnson, H. Fu, H. Shan, F. Du, N. E. Hoffman, D. Yu, S. Eguchi, M. Madesh, W. J. Koch, J. Sun, X. Jiang, H. Wang, X. Yang, Mitochondrial reactive oxygen species mediate lysophosphatidylcholine-induced endothelial cell activation. *Arterioscler. Thromb. Vasc. Biol.* **36**, 1090–1100 (2016).
32. Y. Mikhed, A. Gorlach, U. G. Knaus, A. Daiber, Redox regulation of genome stability by effects on gene expression, epigenetic pathways and DNA damage/repair. *Redox Biol.* **5**, 275–289 (2015).
33. H. M. Yun, K. R. Park, H. P. Lee, D. H. Lee, M. Jo, D. H. Shin, D. Y. Yoon, S. B. Han, J. T. Hong, PRDX6 promotes lung tumor progression via its GPx and iPLA2 activities. *Free Radic. Biol. Med.* **69**, 367–376 (2014).
34. E. Itakura, R. R. Huang, D. R. Wen, E. Paul, P. H. Wunsch, A. J. Cochran, IL-10 expression by primary tumor cells correlates with melanoma progression from radial to vertical growth phase and development of metastatic competence. *Mod. Pathol.* **24**, 801–809 (2011).
35. B. Ruffell, D. Chang-Strachan, V. Chan, A. Rosenbusch, C. M. Ho, N. Pryer, D. Daniel, E. S. Hwang, H. S. Rugo, L. M. Coussens, Macrophage IL-10 blocks $CD8^+$ T cell-dependent responses to chemotherapy by suppressing IL-12 expression in intratumoral dendritic cells. *Cancer Cell* **26**, 623–637 (2014).
36. A. P. Vicari, C. Chiodoni, C. Vaure, S. Ait-Yahia, C. Dercamp, F. Matsos, O. Reynard, C. Taverne, P. Merle, M. P. Colombo, A. O'Garra, G. Trinchieri, C. Caux, Reversal of tumor-induced dendritic cell paralysis by CpG immunostimulatory oligonucleotide and anti-interleukin 10 receptor antibody. *J. Exp. Med.* **196**, 541–549 (2002).
37. R. Bill, P. Wirapati, M. Messemaker, W. Roh, B. Zitti, F. Duval, M. Kiss, J. C. Park, T. M. Saal, J. Hoelzl, D. Tarussio, F. Benedetti, S. Tissot, L. Kandalaft, M. Varrone, G. Ciriello, T. A. McKee, Y. Monnier, M. Mermod, E. M. Blaum, I. Gushterova, A. L. K. Gonye, N. Hacohen, G. Getz, T. R. Mempel, A. M. Klein, R. Weissleder, W. C. Faquin, P. M. Sadow, D. Lin, S. I. Pai, M. Sade-Feldman, M. J. Pittet, CXCL9:SPP1 macrophage polarity identifies a network of cellular programs that control human cancers. *Science* **381**, 515–524 (2023).
38. H. H. Eum, D. Jeong, N. Kim, A. Jo, M. Na, H. Kang, Y. Hong, J. S. Kong, G. H. Jeong, S. A. Yoo, H. O. Lee, Single-cell RNA sequencing reveals myeloid and T cell co-stimulation mediated by IL-7 anti-cancer immunotherapy. *Br. J. Cancer* **130**, 1388–1401 (2024).
39. M. A. Seol, J. H. Kim, K. Oh, G. Kim, M. W. Seo, Y. K. Shin, J. H. Sim, H. M. Shin, B. Y. Seo, D. S. Lee, J. L. Ku, I. Han, I. Kang, S. I. Park, H. R. Kim, Interleukin-7 contributes to the invasiveness of prostate cancer cells by promoting epithelial-mesenchymal transition. *Sci. Rep.* **9**, 6917 (2019).
40. W. Zhang, Q. Zhang, N. Yang, Q. Shi, H. Su, T. Lin, Z. He, W. Wang, H. Guo, P. Shen, Crosstalk between IL-15Rα$^+$ tumor-associated macrophages and breast cancer cells reduces $CD8^+$T cell recruitment. *Cancer Commun.* **42**, 536–557 (2022).
41. M. M. Kaneda, K. S. Messer, N. Ralainirina, H. Li, C. J. Leem, S. Gorjestani, G. Woo, A. V. Nguyen, C. C. Figueiredo, P. Foubert, M. C. Schmid, M. Pink, D. G. Winkler, M. Rausch, V. J. Palombella, J. Kutok, K. McGovern, K. A. Frazer, X. Wu, M. Karin, R. Sasik, E. E. Cohen, J. A. Varner, Corrigendum: PI3Kγ is a molecular switch that controls immune suppression. *Nature* **542**, 124 (2017).
42. A. Zotta, L. A. J. O'Neill, M. Yin, Unlocking potential: The role of the electron transport chain in immunometabolism. *Trends Immunol.* **45**, 259–273 (2024).
43. T. A. Yap, N. Daver, M. Mahendra, J. Zhang, C. Kamiya-Matsuoka, F. Meric-Bernstam, H. M. Kantarjian, F. Ravandi, M. E. Collins, M. E. D. Francesco, E. E. Dumbrava, S. Fu, S. Gao, J. P. Gay, S. Gera, J. Han, D. S. Hong, E. J. Jabbour, Z. Ju, D. D. Karp, A. Lodi, J. R. Molina, N. Baran, A. Naing, M. Ohanian, S. Pant, N. Pemmaraju, P. Bose, S. A. Piha-Paul, J. Rodon, C. Salguero, K. Sasaki, A. K. Singh, V. Subbiah, A. M. Tsimberidou, Q. A. Xu, M. Yilmaz, Q. Zhang, Y. Li, C. A. Bristow, M. B. Bhattacharjee, S. Tiziani, T. P. Heffernan, C. P. Vellano, P. Jones, C. J. Heijnen, A. Kavelaars, J. R. Marszalek, M. Konopleva, Complex I inhibitor of oxidative phosphorylation in advanced solid tumors and acute myeloid leukemia: Phase I trials. *Nat. Med.* **29**, 115–126 (2023).
44. A. Hooftman, C. G. Peace, D. G. Ryan, E. A. Day, M. Yang, A. F. McGettrick, M. Yin, E. N. Montano, L. Huo, J. E. Toller-Kawahisa, V. Zecchini, T. A. J. Ryan, A. Bolado-Carrancio,

Downloaded from https://www.science.org at Trinity College Dublin on January 27, 2025

A. M. Casey, H. A. Prag, A. S. H. Costa, G. De Los Santos, M. Ishimori, D. J. Wallace, S. Venuturupalli, E. Nikitopoulou, N. Frizzell, C. Johansson, A. Von Kriegsheim, M. P. Murphy, C. Jefferies, C. Frezza, L. A. J. O'Neill, Macrophage fumarate hydratase restrains mtRNA-mediated interferon production. *Nature* **615**, 490–498 (2023).
45. K. M. Usher, S. Zhu, G. Mavropalias, J. A. Carrino, J. Zhao, J. Xu, Pathological mechanisms and therapeutic outlooks for arthrofibrosis. *Bone Res.* **7**, 9 (2019).

Acknowledgments: We would like to thank the O'Neill laboratory for helpful discussions, in particular K. Banahan for assistance in the laboratory. We also thank M. Brand (Buck Institute for Research on Aging, San Francisco, CA) for the gift of S3QEL 1.2 and the other backbones for S3QEL and S1QEL. **Funding:** This work was supported by the European Research Metabinnate (834370) and has received funding from the European Union's Horizon 2020 research and innovation programme under the Marie Sklodowska-Curie grant agreement INsTRuCT no. 860003. E.C.L. and R.W.W. received support from Science Foundation Ireland Frontiers of the future award 19/FFP/6484. R.W.W. received support from IRC GOIPG/2019/4236. **Authorship contributions:** Conceptualization: A.Z., D.G.R., M.D.B., M.A.W., E.C.L., and L.A.J.O'N. Data curation: S.M.O'C. Formal analysis: A.Z., A.L., M.C.R., and J.K. Funding acquisition: E.M.P.-M., E.C.L., and L.A.J.O'N. Investigation: A.Z., J.E.T.-K., D.G.R., A.L., E.A.D., S.M.O'C., A.F.M., R.W.W., M.C.R., E.M.P.-M., E.C.L., K.M., and L.A.J.O'N. Methodology: A.Z., O.C.H., A.F.M., E.M.P.-M., E.A.D., R.W.W., M.C.R., J.K., E.C.L., J.L.M., and M.A.W. Project administration: A.Z., J.K., and L.A.J.O'N. Resources: M.A.W., M.D.B., J.L.M., J.K., K.M., M.C.R., E.C.L., and L.A.J.O'N. Software: S.M.O'C. Supervision: A.Z., J.K., M.D.B., E.C.L., and L.A.J.O'N. Validation: M.A.W., J.K., O.C.H., A.Z., E.C.L., and M.C.R. Visualization: A.Z., M.C.R., and S.M.O'C. Writing—original draft: A.Z. Writing—review and editing: A.Z., M.D.B., M.A.W., D.G.R., J.K., E.C.L., and L.A.J.O'N. **Competing interest:** M.D.B. is an inventor on a patent application 048674-507P01US held/submitted by Buck Institute for Research on Aging, Abbvie Inc. that covers chemical and materials sciences and organic chemistry. The other authors declare that they have no competing interests. **Data and materials availability:** All data needed to evaluate the conclusions in the paper are present in the paper and/or the Supplementary Materials. We have uploaded the RNA-seq contents to the appropriate community-supported public databases at Dryad (https://doi.org/10.5061/dryad.zkh1893k1). S1QEL and S3QEL can be provided by M.D.B.'s pending scientific review and a completed material transfer agreement. Requests for S1QELs and S3QELs compound should be submitted to mbrand@buckinstitute.org.

Submitted 28 May 2024
Accepted 19 December 2024
Published 22 January 2025
10.1126/sciadv.adq7307

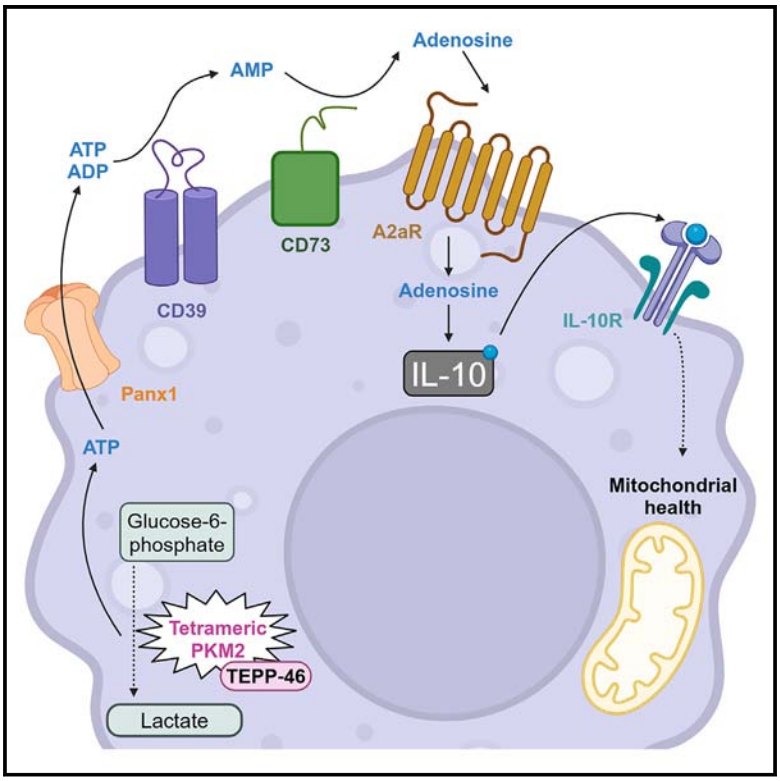
Downloaded from https://www.science.org at Trinity College Dublin on January 27, 2025

Cell Reports

Report

Metabolic reprogramming of macrophages by PKM2 promotes IL-10 production via adenosine

Graphical abstract



Authors

Juliana Escher Toller-Kawahisa, Paula Ramos Viacava, Eva Margareta Palsson-McDermott, ..., Fernando de Queiroz Cunha, Luke Anthony John O'Neill, José Carlos Alves-Filho

Correspondence

laoneill@tcd.ie (L.A.J.O.), jcafilho@usp.br (J.C.A.-F.)

In brief

TEPP-46 activates PKM2 by inducing a tetramer formation, which leads to a metabolic reprogramming in macrophages, resulting in an increase in ATP and IL-10 production. Toller-Kawahisa et al. showed that this increase in IL-10 improves mitochondrial health and is due to a mechanism dependent on the ATP hydrolysis to adenosine.

Highlights

- PKM2 activation increases IL-10 production by LPS-activated macrophages
- PKM2 activation leads to the metabolic reprogramming of ATP production from glycolysis
- Extracellular ATP is converted into adenosine, which enhances IL-10 production
- IL-10 production induced by PKM2 is associated with improved mitochondrial health

Toller-Kawahisa et al., 2025, Cell Reports *44*, 115172
January 28, 2025 © 2025 The Authors. Published by Elsevier Inc.
https://doi.org/10.1016/j.celrep.2024.115172

CellPress

Cell Reports

CellPress
OPEN ACCESS

Report

Metabolic reprogramming of macrophages by PKM2 promotes IL-10 production via adenosine

Juliana Escher Toller-Kawahisa,[1,2,3,6] Paula Ramos Viacava,[1,2,6] Eva Margareta Palsson-McDermott,[3,6] Daniele Carvalho Nascimento,[1,2] Mariana Patricia Cervantes-Silva,[4] Shane Myles O'Carroll,[3] Alessia Zotta,[3] Luis Eduardo Alves Damasceno,[1,2] Gabriel Azevedo Públio,[1,2] Pedro Forti,[1,2] João Paulo Mesquita Luiz,[1,2] Bruno Marcel Silva de Melo,[1,2] Timna Varela Martins,[1,2] Vitor Marcel Faça,[5] Annie Curtis,[4] Thiago Mattar Cunha,[1,2] Fernando de Queiroz Cunha,[1,2] Luke Anthony John O'Neill,[3,*] and José Carlos Alves-Filho[1,2,7,*]

[1]Department of Pharmacology, Ribeirao Preto Medical School, University of Sao Paulo, Ribeirao Preto, Brazil
[2]Center for Research in Inflammatory Diseases, Ribeirao Preto Medical School, University of Sao Paulo, Ribeirao Preto, Brazil
[3]School of Biochemistry and Immunology, Trinity Biomedical Science Institute, Trinity College Dublin, Dublin, Ireland
[4]School of Pharmacy and Biomolecular Sciences and Tissue Engineering Research Group, Royal College of Surgeons in Ireland, Dublin, Ireland
[5]Department of Biochemistry and Immunology, Ribeirao Preto Medical School, University of São Paulo, Ribeirao Preto, Brazil
[6]These authors contributed equally
[7]Lead contact
*Correspondence: laoneill@tcd.ie (L.A.J.O.), jcafilho@usp.br (J.C.A.-F.)
https://doi.org/10.1016/j.celrep.2024.115172

SUMMARY

Macrophages play a crucial role in immune responses and undergo metabolic reprogramming to fulfill their functions. The tetramerization of the glycolytic enzyme pyruvate kinase M2 (PKM2) induces the production of the anti-inflammatory cytokine interleukin (IL)-10 *in vivo*, but the underlying mechanism remains elusive. Here, we report that PKM2 activation with the pharmacological agent TEPP-46 increases IL-10 production in LPS-activated macrophages by metabolic reprogramming, leading to the production and release of ATP from glycolysis. The effect of TEPP-46 is abolished in PKM2-deficient macrophages. Extracellular ATP is converted into adenosine by ectonucleotidases that activate adenosine receptor A2a (A2aR) to enhance IL-10 production. Interestingly, IL-10 production induced by PKM2 activation is associated with improved mitochondrial health. Our results identify adenosine derived from glycolytic ATP as a driver of IL-10 production, highlighting the role of tetrameric PKM2 in regulating glycolysis to promote IL-10 production.

INTRODUCTION

Macrophages are key innate immune cells that constitute a barrier against invading pathogens, contributing to infection resolution and tissue repair. Depending on the stimuli, macrophages can rapidly switch their metabolic profile to fulfill their functions.[1] In fact, pro-inflammatory macrophages rely mainly on glycolysis[2–4] to meet their adenosine triphosphate (ATP) requirements and have low oxidative phosphorylation (OXPHOS) and fatty acid oxidation (FAO) activity.[5–7] In contrast, anti-inflammatory macrophages are less dependent on glycolysis and have higher FAO and OXPHOS activation.[5]

Particularly, pro-inflammatory LPS-activated macrophages highly express pyruvate kinase M2 (PKM2),[8] a key regulator of metabolic changes in many immune cells.[8–11] PKM2 can be expressed in a tetrameric rate-limiting glycolytic enzyme that catalyzes the conversion of phosphoenolpyruvic acid (PEP) to pyruvate[12] or in its enzymatically inactive dimeric/monomeric form that translocates to the nucleus and regulates genes involved in glycolysis and the inflammatory response.[8] PKM2 can be allosterically activated to its tetrameric form by endogenous ligands, including fructose-1,6-bisphosphate (F1,6B) or small synthetic molecules, such as TEPP-46. Of note, activated PKM2 is expressed in the cytoplasm and has a high pyruvate kinase (PK) activity but no nuclear function.[13] Interestingly, PKM2 activation by TEPP-46 in a sepsis model increased the serum concentration of interleukin (IL)-10[8], an important anti-inflammatory cytokine. However, the mechanism by which tetrameric PKM2 modulates IL-10 production is unknown.

Seo and collaborators[14] showed that IL-10 production can be regulated by ATP, produced during glycolysis and through cellular respiration in mitochondria. Despite ATP being mainly intracellular, it can be released from cells under specific conditions and act as a signaling molecule. Once in the extracellular space, ATP and ADP are hydrolyzed to AMP by CD39 (ectonucleotidase triphosphate diphosphohydrolase-1, ENTPD1) and then to adenosine by CD73 (ecto-5′ nucleotidase, E5NT).[15,16] Thus, adenosine can bind to its receptor, A2aR, and modulate several immune processes,[17] including IL-10 production in macrophages.[18]

Here we investigated whether PKM2 modulates IL-10 production in macrophages by an adenosine-dependent mechanism. We have found that allosteric activation of PKM2 by TEPP-46 increases glycolysis and boosts ATP production in LPS-activated

This is an open access article under the CC BY-NC-ND license (http://creativecommons.org/licenses/by-nc-nd/4.0/).

macrophages. ATP is hydrolyzed to adenosine, which binds to its receptor A2aR and promotes IL-10 production. IL-10, in turn, induces mitochondrial fusion and increases OXPHOS, improving mitochondrial health. Altogether, our data suggest a role for PKM2 in metabolic reprogramming of macrophages to regulate adenosine and, consequently, IL-10 production and highlight the importance of PKM2 as a potential therapeutic target in inflammatory diseases.

RESULTS

PKM2 activation boosts IL-10 production

We initially investigated PKM2 expression in LPS-activated macrophages. The gene expression of *Pkm2* but not *Pkm1* increased over time in LPS-activated bone marrow-derived macrophages (BMDMs), and this was not affected after treatment with TEPP-46 (Figures S1A and S1B). Nevertheless, as described before,[8] LPS increased PKM2 expression in BMDMs, and pre-treatment with TEPP-46 boosted the tetrameric form of PKM2 (Figure 1A). The protein expression of PKM1 was not affected by LPS activation or TEPP-46 treatment (Figure 1A), as PKM1 is constitutively expressed in macrophages. Accordingly, while PKM2 migrated to the nucleus in LPS-activated BMDMs, TEPP-46 pre-treatment maintained PKM2 in the cytoplasm (Figure 1B). Palsson-McDermott and collaborators[8] have previously shown that TEPP-46 boosts IL-10 production in serum in an LPS-induced sepsis model. Here, we found that LPS-activated BMDMs increased *Il-10* expression (Figure 1C) and IL-10 production (Figure 1D) over time *in vitro* and that this effect was boosted by PKM2 activation. To address TEPP-46 selectivity for PKM2, BMDMs from control ($Pkm2^{fl/fl}$) or PKM2-deficient ($Pkm2^{\Delta Lyz2}$) mice were pre-treated with TEPP-46 and then activated with LPS. While LPS induced IL-10 production in both control and PKM2-deficient BMDMs, TEPP-46 boosted it only in control BMDMs (Figure 1E). Together, these results indicate that LPS induces IL-10 production by a PKM2-independent mechanism; however, when LPS-induced PKM2 is activated by TEPP-46 in its tetrameric form, there is a boost in IL-10 production. Since PKM2 regulates metabolic reprogramming in different cell types,[8–10] we next analyzed the effect of PKM2 activation on the metabolic status of LPS-activated BMDMs. As expected, LPS increased glycolytic activity (Figure 1F) and lactate production (Figure 1G) while decreasing the oxygen consumption rate (OCR) (Figure 1H). In addition, TEPP-46 boosted glycolysis (Figure 1F) and lactate production (Figure 1G) and restored OXPHOS (Figure 1H). Consistently, PKM2 activation boosted PK activity (Figure 1I) and lactate production (Figure 1J) in control but not in PKM2-deficient BMDMs. Together, these data demonstrate that PKM2 activation modulates both glycolytic and mitochondrial metabolism and boosts IL-10 production in LPS-activated BMDMs.

PKM2 activation regulates mitochondrial dynamics

IL-10 is a potent regulator of both inflammation and mitochondrial dynamics.[19] We next investigated whether the OXPHOS restoration by PKM2 activation was IL-10 dependent. Indeed, inhibition of the IL-10 receptor (IL-10R, CD210)[20] impaired the effect of TEPP-46 on enhancing OXPHOS (Figure 2A). Assessing mitochondrial dynamics revealed that while LPS-activated BMDMs had more mitochondrial fission, LPS-activated BMDMs pre-treated with TEPP-46 had more fused mitochondria. Consistently, this effect was lost when IL-10R was inhibited (Figure 2B). In addition, PKM2 activation increased mitochondrial membrane potential (Figure 2C), indicating an improvement in mitochondrial health. It was recently shown that PKM2 is expressed in the mitochondria, where it regulates mitochondrial dynamics.[20] We found that PKM2 is basally expressed in the mitochondria of BMDMs, which is unchanged by LPS activation. However, treatment with TEPP-46 decreased PKM2 expression in the mitochondria (Figures 2D and 2E), consistent with its effect on maintaining PKM2 in its tetrameric form, mainly expressed in the cytoplasm. Together, these data indicate that PKM2 activation indirectly promotes mitochondrial fusion and health by boosting IL-10 production in BMDMs.

PKM2 activation induces ATP production from glycolysis in BMDMs

It is known that IL-10 production can be regulated by extracellular ATP in LPS-activated microglia.[14] Thus, we next investigated whether PKM2 activation boosts IL-10 production by an ATP-dependent mechanism. TEPP-46 pre-treatment boosted intracellular (Figure 3A) and released ATP (Figure 3B) in LPS-activated BMDMs. Additionally, the increase in intracellular (Figure 3C) and released ATP (Figure 3D) was lost in PKM2-deficient BMDMs, confirming that its effect was PKM2 dependent. It has been shown that LPS-activated BMDMs switch their metabolism from OXPHOS to glycolysis,[21] carrying on ATP production in the cell.[22] To better understand the role of PKM2 activation on ATP production through glycolysis, BMDMs pre-treated with TEPP-46 were activated with LPS in the presence of different glucose concentrations. We found that lactate production triggered by LPS was dependent on glucose concentration and that TEPP-46 efficacy was impaired in lower glucose concentrations (Figure 3E). Intriguingly, lower glucose concentrations had no impact on intracellular (Figure 3F) and released ATP (Figure 3G) in LPS-activated BMDMs but impaired the ability of TEPP-46 to boost ATP levels. In addition, IL-10 production was dependent on glucose concentrations in LPS-activated BMDMs (Figure 3H). To further investigate whether IL-10 production was dependent on the ATP produced during glycolysis, we pre-treated BMDMs with oligomycin (which inhibits ATP synthase) or heptelidic acid (which inhibits glyceraldehyde 3-phosphate dehydrogenase, GAPDH) and found that, while oligomycin did not affect IL-10, inhibition of GAPDH completely inhibited it in response to TEPP-46 (Figure 3I). Together, these data show that PKM2 activation by TEPP-46 boosts ATP and IL-10 production, which depends on glycolysis but not OXPHOS.

Because released ATP can trigger immune responses,[23] we next evaluated whether IL-10 production was dependent on ATP release in BMDMs. To this end, we treated BMDMs with carbenoxolone (CBX), an inhibitor of pannexin-1 ATP-permeable channel (Panx1), or used Panx1-deficient ($Panx1^{-/-}$) BMDMs (Figure 3J). As expected, released but not intracellular ATP was impaired (Figures S2A–S2D, respectively). Also, we found that the inhibition of ATP release impaired IL-10

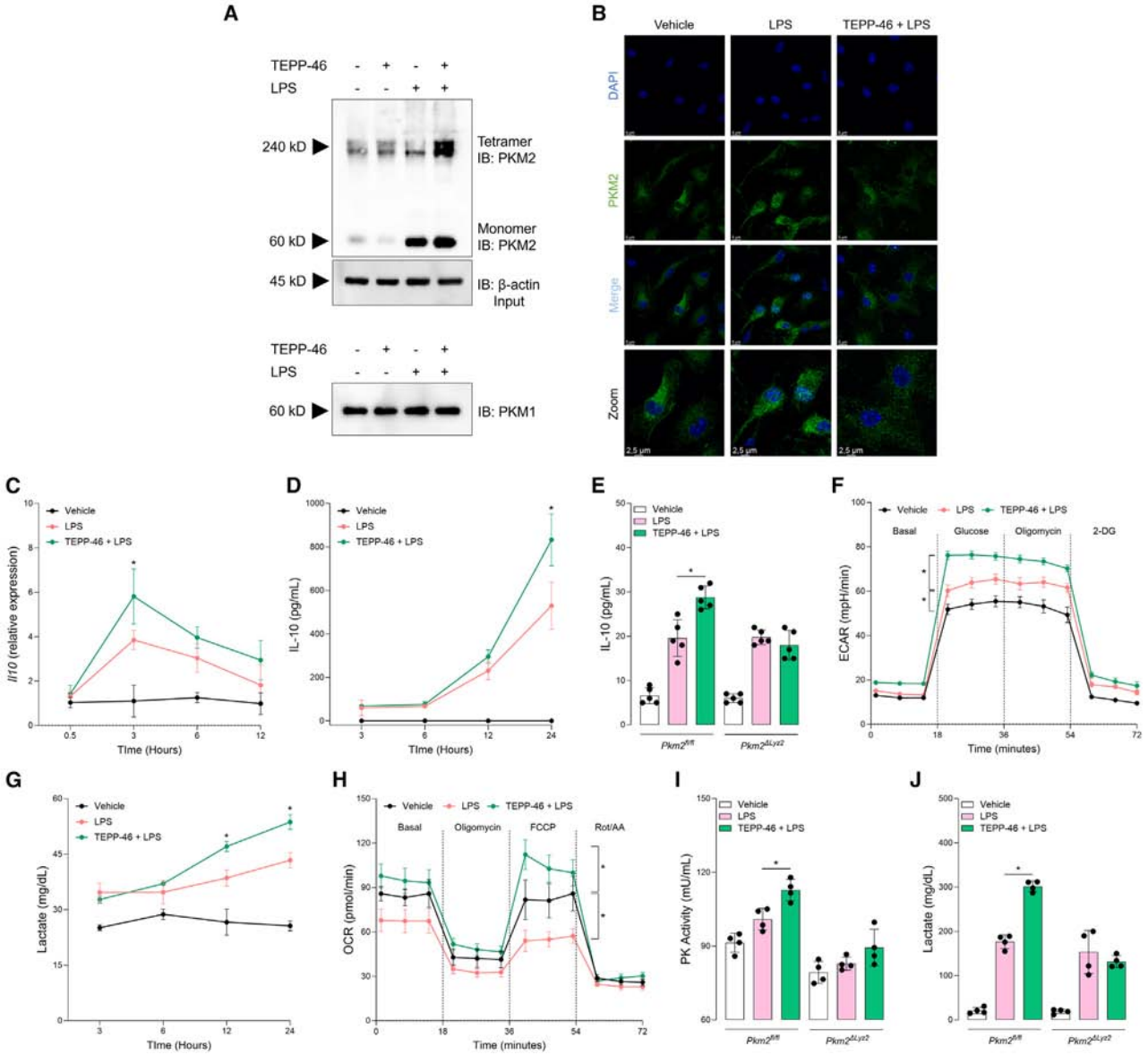


Figure 1. PKM2 activation boosts macrophage metabolism and IL-10 production

(A) Immunoblot analysis of PKM2 conformational states in BMDMs pre-treated with TEPP-46 (30 μM) for 1 h and activated with LPS (100 ng/mL) for 24 h.

(B) Confocal immunofluorescence analysis stained for PKM2 (green) in BMDMs pre-treated with TEPP-46 for 1 h and activated with LPS for 24 h.

(C) *il-10* mRNA expression in BMDMs pre-treated with TEPP-46 for 1 h and activated with LPS for indicated time points. Data were normalized to *Gapdh* (*glyceraldehyde 3-phosphate dehydrogenase*); fold change is relative to unstimulated BMDMs. $n = 3$.

(D) IL-10 production by BMDMs pre-treated with TEPP-46 for 1 h and activated with LPS for indicated time points. $n = 4$.

(E) IL-10 production by control ($Pkm2^{fl/fl}$) and PKM2-deficient ($Pkm2^{\Delta Lyz2}$) BMDMs pre-treated with TEPP-46 for 1 h and activated with LPS for 24 h. $n = 5$.

(F) Kinetic profile of ECAR (extracellular acidification rate) in BMDMs pre-treated with TEPP-46 for 1 h and activated with LPS for 6 h. $n = 6$.

(G) Lactate production by BMDMs pre-treated with TEPP-46 for 1 h and activated with LPS for indicated time points. $n = 4$.

(H) Kinetic profile of OCR in BMDMs pre-treated with TEPP-46 for 1 h and activated with LPS for 4 h. $n = 3$.

(I) Pyruvate kinase activity in control and PKM2-deficient BMDMs pre-treated with TEPP-46 for 1 h and activated with LPS for 24 h. $n = 4$.

(J) Lactate production by control and PKM2-deficient BMDMs pre-treated with TEPP-46 for 1 h and activated with LPS for 24 h. $n = 4$.

Data are represented as mean ± SEM. *, $p < 0.05$. *p value*s were determined by one-way ANOVA followed by Tukey's *post hoc* test. Scale bars: 5 μm.

(Figures 3K and 3L) but not lactate production (Figures 3M and 3N). It is known that the production of IL-10 by activated macrophages is dependent on p38 mitogen-activated protein kinase (MAPK)[24,25] and, in parallel, exogenous adenosine can boost the production of IL-10 in activated macrophages.[26] Since adenosine is being produced by extracellular hydrolysis of ATP, these results suggest that PKM2 activation by TEPP-46 increases ATP production from glycolysis and promotes ATP

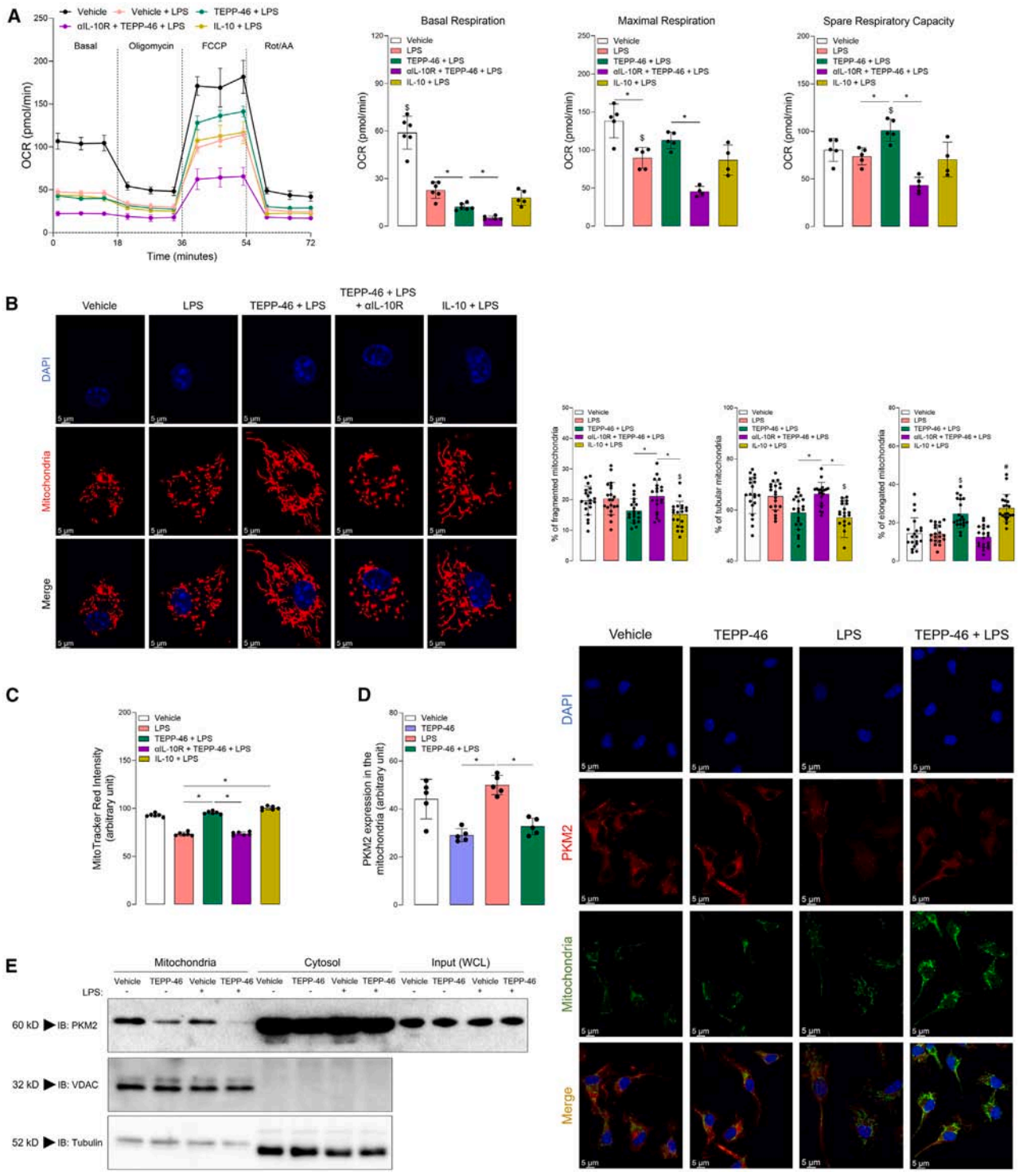


Figure 2. PKM2 activation improves mitochondrial health

(A) Kinetic profile of OCR in BMDMs pre-treated with αIL-10R (20 μg/mL) for 1 h, treated with TEPP-46 (30 μM) or IL-10 (100 ng/mL) for 1 h, and activated with LPS (100 ng/mL) for 24 h. $n = 5$.

(B) Representative confocal immunofluorescence analysis stained with MitoTracker Red (red) and Hoechst (blue) in BMDMs pre-treated with αIL-10R for 1 h, treated with TEPP-46 or IL-10 for 1 h, and activated with LPS for 24 h. Mitochondrial morphology was classified as fragmented (≤1 μm), tubular (1–3 μm), or elongated (≥3 μm).

(legend continued on next page)

release, which in turn increases IL-10 production. LPS alone does not have this effect because it can also act via p38 MAPK.

PKM2 activation boosts IL-10 production by an adenosine-dependent mechanism

In the extracellular space, ATP can be hydrolyzed by CD39 and CD73 enzymes that catalyze the hydrolysis of ATP/ADP to AMP and AMP to adenosine, respectively (Figure 4A). Adenosine then binds to its receptor A2aR[17] and mediates an intracellular signaling pathway that triggers various immunological processes, including the production of anti-inflammatory cytokines, suppression of microbial killing, and an increase in M2 macrophage differentiation.[27] Once we found that PKM2 activation boosts ATP release in LPS-activated BMDMs, we investigated whether ATP was being hydrolyzed to adenosine in these cells. LPS increased, and TEPP-46 treatment boosted adenosine production (Figure 4B). As expected, inhibition of CD39 abrogated adenosine production in BMDMs (Figure 4C). To better understand the role of PKM2 activation on ATP hydrolysis and subsequent IL-10 production, we used A2aR-deficient (*Adora2a*$^{-/-}$) BMDMs and found that IL-10 production was impaired (Figure 4D). Treatment of BMDMs with the A2aR inhibitor also prevented the boost in IL-10 by TEPP-46 (Figure 4E). In addition, ATP treatment increased IL-10 production in LPS-activated BMDMs, and the inhibition of CD39 (Figure 4F) or CD73 (Figure 4G) prevented this effect. Altogether, our results show that PKM2 activation increases ATP production from glycolysis and ATP release. ATP is then hydrolyzed to adenosine, which binds to A2aR and boosts IL-10 production, improving mitochondrial health *in vitro*.

DISCUSSION

PKM2 plays a critical role in metabolic reprogramming and cellular activation in LPS-stimulated macrophages.[8] However, the role of PKM2 in macrophage activation by LPS has mainly been focused on its transcriptional regulatory effects,[8,28,29] which is a moonlighting role for this enzyme. Other enzymes in glycolysis have also been shown to have an additional role, a notable example being GAPDH, which can bind various mRNAs, stabilizing them.[30,31] Palsson-McDermott and collaborators[8] showed that PKM2, in its dimeric form, promotes Hif-1α stabilization by LPS in macrophages, which is important for enhancing its transcriptional activity, including IL-1β production. In addition, PKM2 small-molecule activators attenuated the M1 phenotype of LPS-activated macrophages and increased IL-10 production by inducing PKM2 tetramerization. Therefore, PKM2 activators inducing tetramerization are a potential pharmacological tool to be used in inflammatory diseases, and their mechanism of action needs to be better understood.

In our present work, we have focused mainly on the metabolic role of PKM2 rather than its transcriptional effects, employing a pharmacological modulation of PKM2 function. Long-term effects of LPS require dimeric PKM2 to promote the expression of glycolytic enzymes, which is attenuated by the PKM2 activator TEPP-46. Shorter-term effects on glycolysis are promoted by TEPP-46, which activates PKM2 in its tetrameric form. We showed that PKM2 activation with TEPP-46 in LPS-activated BMDMs boosted the production and the release of ATP, which is hydrolyzed into adenosine. Adenosine signaling via A2aR enhances IL-10 production by LPS-activated BMDMs *in vitro*. It is known that pyruvate is produced from activation of glycolysis, whereby pyruvate enters the tricarboxylic acid (TCA) cycle generating high levels of ATP. However, the activation of macrophages via Toll-like receptor 4 (TLR4) by LPS increases glucose consumption and glycolysis activation, and pyruvate is rather converted to lactate instead of entering the TCA cycle, decreasing OXPHOS.[32,33] Interestingly, we found that PKM2 activation by TEPP-46 restored OXPHOS in LPS-activated macrophages and modulated mitochondrial morphology.

Mitochondrial dynamics is regulated by several factors, including glucose concentration.[34] Baseler and collaborators[35] showed that IL-10 regulates macrophage glycolytic commitment by preserving OXPHOS through its suppression of nitric oxide. Recently, it was shown that IL-10 is critical for mitochondrial fusion in macrophages by a mechanism dependent on arginase-2.[36] Accordingly, here we found that the boost in IL-10 production induced by TEPP-46 was accompanied by a dramatic increase in mitochondrial fusion and membrane potential, indicating an improvement in mitochondrial health. Although previous studies have described a role for PKM2 in mitochondrial function,[20,37] our study indicates that an intact IL-10R signaling pathway is required for the optimal effect of TEPP-46 on mitochondrial dynamics. Rather than mitochondrial fusion regulating IL-10 production, our data indicate that IL-10 is targeting mitochondria with the effect of TEPP-46 on mitochondria requiring IL-10.

IL-10 is a potent anti-inflammatory cytokine produced by LPS-activated macrophages as an essential autoregulatory mechanism to limit tumor necrosis factor alpha (TNF-α) and IL-1β production, contributing to inflammation modulation and resolution.[38,39] IL-10 production can be triggered by several mechanisms, including p38 MAPK activation,[24,25] and the activation of the adenosine signaling pathway.[40–42] In fact, Nascimento and collaborators[43] showed that adenosine is an essential mediator that triggers IL-10 production by macrophages. Here we showed that PKM2 activation boosts IL-10 production in LPS-activated macrophages by a mechanism dependent on adenosine production and glycolysis, as treatment with the GAPDH inhibitor, heptelidic acid, impaired IL-10 production. Accordingly, treatment with oligomycin had no effect on IL-10 production. It is important to emphasize that PKM2-deficient LPS-activated BMDMs produced the same amount of IL-10, lactate, and ATP compared to control BMDMs. In this way, our results indicate

(C) Fluorescence intensity of mitochondrial membrane potential determined with MitoTracker Red in BMDMs pre-treated with TEPP-46 for 1 h and activated with LPS for 24 h determined by confocal. $n = 6$.

(D) Representative confocal immunofluorescence analysis stained for PKM2 (red), mitochondria (MitoTracker Red), and nucleus (blue). Bar graph represents the quantification of PKM2 expression in the mitochondria.

(E) Immunoprecipitation of PKM2 in BMDMs pre-treated with TEPP-46 for 1 h and activated with LPS for 24 h.

Data are represented as mean ± SEM. *, $p < 0.05$. *p value*s were determined by one-way ANOVA followed by Tukey's *post hoc* test. Scale bars: 5 μm.

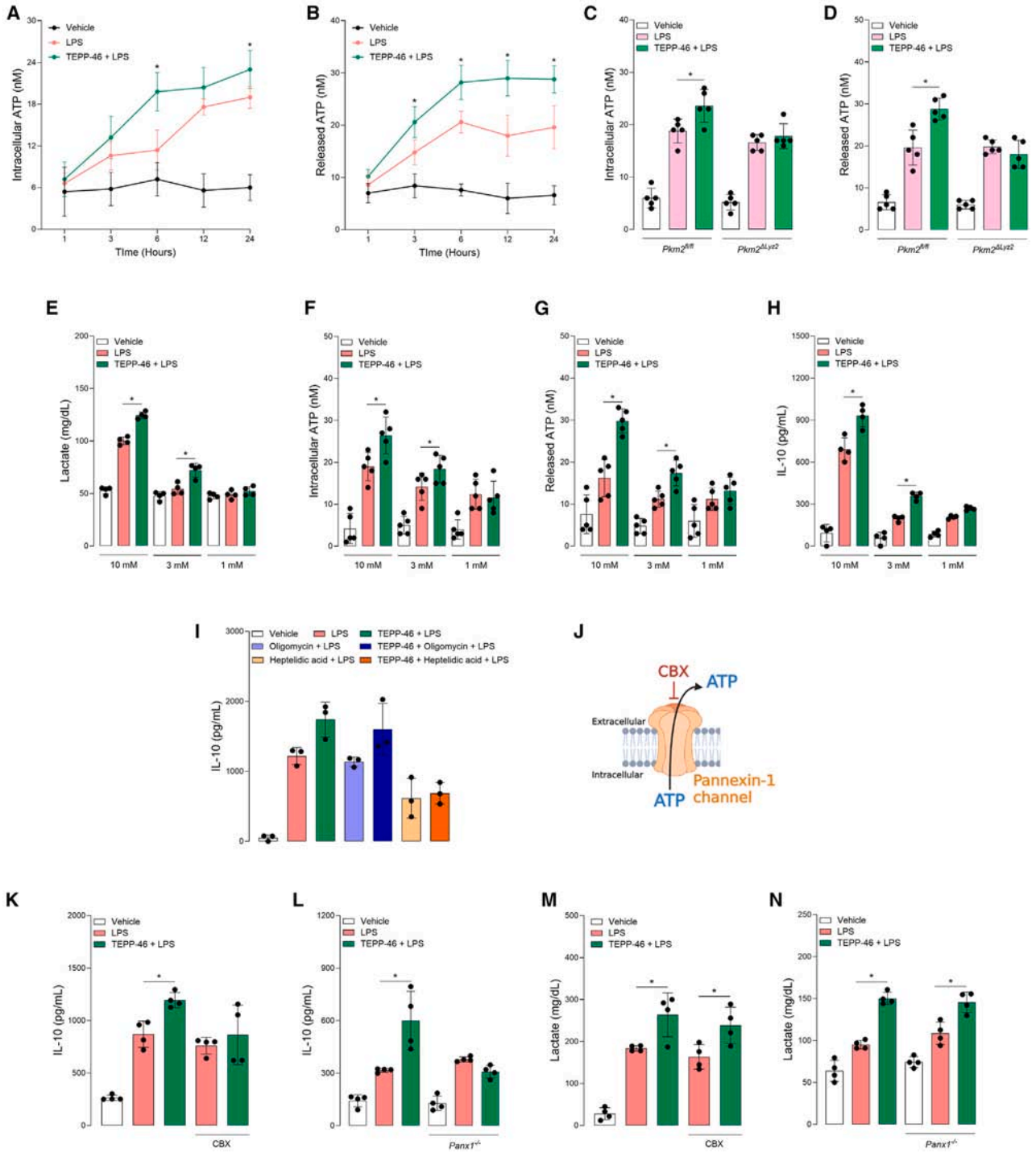


Figure 3. IL-10 production by PKM2 activation requires ATP release in LPS-activated BMDMs

(A and B) (A) Intracellular and (B) released ATP in BMDMs pre-treated with TEPP-46 (100 μM) for 1 h and activated with LPS (100 ng/mL) for indicated time points. $n = 5$.

(C and D) (C) Intracellular and (D) released ATP production by control and PKM2-deficient BMDMs pre-treated with TEPP-46 for 1 h and activated with LPS for 24 h. $n = 5$.

(E) Lactate production by BMDMs pre-treated with TEPP-46 for 1 h and activated with LPS for 24 h in the presence of different glucose concentrations. $n = 4$.

(F and G) (F) Intracellular and (G) released ATP in BMDMs pre-treated with TEPP-46 for 1 h and then activated with LPS for 24 h in the presence of different glucose concentrations. $n = 5$.

(legend continued on next page)

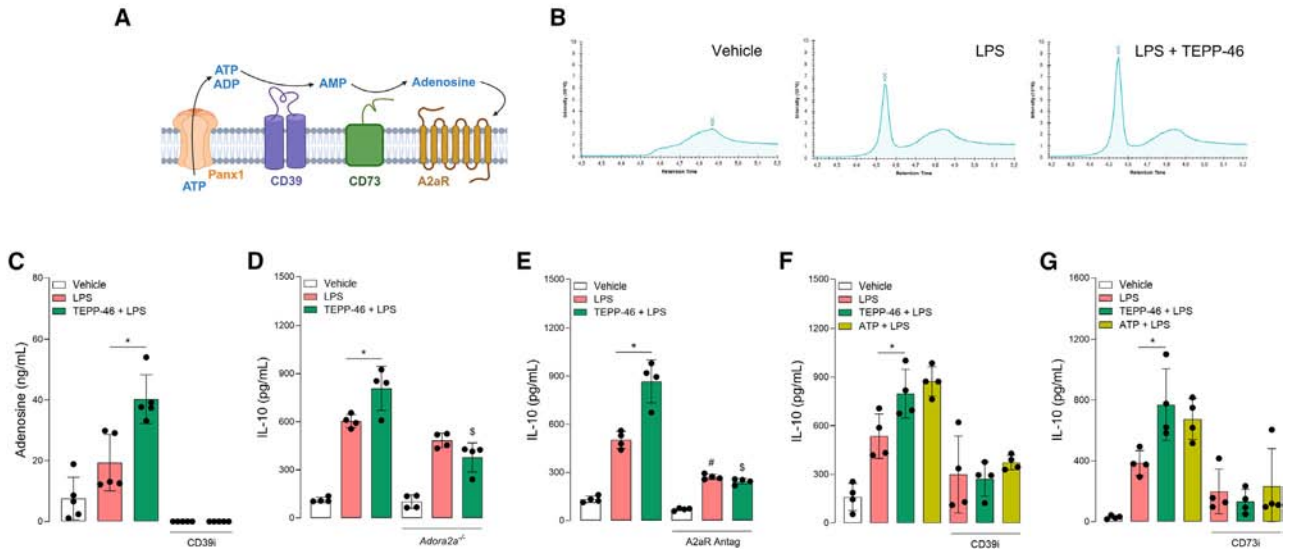


Figure 4. PKM2 activation boosts IL-10 production by an adenosine-dependent mechanism

(A) Illustration showing adenosine production through ATP hydrolysis by CD39 and CD73.

(B and C) (B) Representative liquid chromatography-tandem mass spectrometry (LC-MS/MS) chromatograms and (C) adenosine concentration in the supernatant of BMDMs pre-treated with TEPP-46 (100 μM) for 6 h and activated with LPS (100 ng/mL) for 3 h. $n = 5$.

(D) IL-10 production by control and A2aR-deficient (*Adora2a*$^{-/-}$) BMDMs pre-treated with TEPP-46 for 1 h and activated with LPS for 24 h. $n = 4$.

(E) IL-10 production by BMDMs pre-treated with TEPP-46 for 1 h and activated with LPS for 24 h in the presence of A2aR antagonist (100 μM). $n = 4$.

(F) IL-10 production by BMDMs pre-treated with TEPP-46 for 1 h and activated with LPS for 24 h in the presence of CD39 inhibitor (ARL 67156 trisodium salt, 200 μM). ATP (100 μM) was used as positive control. $n = 4$.

(G) IL-10 production by BMDMs pre-treated with TEPP-46 for 1 h and activated with LPS for 24 h in the presence of CD73 inhibitor (Adenosine 5'-(α,β-methylene) diphosphate sodium salt, 100 μM). ATP was used as positive control. $n = 4$.

Data are represented as mean ± SEM. *, $p < 0.05$. *p values* were determined by one-way ANOVA followed by Tukey's *post hoc* test.

that TEPP-46 boosts IL-10 production through a mechanism distinct from LPS.

In conclusion, our results reveal a role for tetrameric PKM2 in regulating IL-10 production in an adenosine-dependent manner, which improves mitochondrial health in LPS-activated BMDMs. These findings fill a gap in the current knowledge of the importance of the glycolytic pathway for IL-10 production and elucidate the mechanism underlying the regulation of IL-10 production by TEPP-46. Our work also further emphasizes the role of adenosine in regulating the key anti-inflammatory cytokine IL-10, with mitochondrial fusion likely to be a key aspect of IL-10 function in macrophages. Therefore, targeting PKM2 with tetramerization-inducing activators represents a potential pharmacological strategy for inflammatory disorders.

Limitations of the study

We demonstrated that the metabolic reprogramming in LPS-activated macrophages treated with TEPP-46 increases IL-10 production by enhancing ATP production and its hydrolysis to adenosine, which increases mitochondrial health. However, future studies are needed to determine the full impact of IL-10 on mitochondrial health. We were not able to measure mitochondrial reactive oxygen species (ROS) as no reliable probe is available commercially. It is worth noting that, in this paper, we used different time points and different doses of TEPP-46 depending on the experiment performed. The reason for this was that, in some experiments, it was important to get the maximum PKM2 activation with TEPP-46 to show that, regardless of the dose, these cells were unresponsive to TEPP-46. In other experiments, we used lower doses of TEPP-46 to avoid off-target effects or non-specific inhibitory effects and to observe the subtle differences induced by TEPP-46 in macrophage metabolism.

RESOURCE AVAILABILITY

Lead contact

Further information and requests for resources and reagents should be directed to and will be fulfilled by the lead contact, José Carlos Alves-Filho (jcafilho@usp.br).

(H) IL-10 production by BMDMs pre-treated with TEPP-46 for 1 h and activated with LPS for 24 h in the presence of different glucose concentrations. $n = 5$.

(I) IL-10 production by BMDMs pre-treated with TEPP-46, oligomycin (1.5 μM), and/or heptelidic acid (5 μM) for 1 h and activated with LPS for 4 h. $n = 3$.

(J) Illustration showing CBX blocking the pannexin-1 channel and the subsequent ATP release.

(K) IL-10 production by BMDMs pre-treated with TEPP-46 for 1 h and then activated with LPS for 24 h in the presence of CBX (100 μM). $n = 4$.

(L) IL-10 production by control and Panx1-deficient (*Panx1*$^{-/-}$) BMDMs pre-treated with TEPP-46 for 1 h and activated with LPS for 24 h. $n = 5$.

(M) Lactate production by BMDMs pre-treated with TEPP-46 for 1 h and activated with LPS for 24 h in the presence of CBX. $n = 4$.

(N) Lactate production by control and Panx1-deficient BMDMs pre-treated with TEPP-46 for 1 h and activated with LPS for 24 h. $n = 4$.

Data are represented as mean ± SEM. *, $p < 0.05$. *p values* were determined by one-way ANOVA followed by Tukey's *post hoc* test.

Materials availability

This study did not generate new unique reagents.

Data and code availability

- The datasets generated and analyzed related to this paper are available from the lead contact on reasonable request.
- This paper does not report original code.
- Any additional information required to reanalyze the data reported in this paper is available from the lead contact upon request.

ACKNOWLEDGMENTS

We thank Ieda Schivo, Sergio Rosa, Ana Katia Santos, Marcella Daruge Grando, Juliana Trench Abumansur, Denise Ferraz, Cait Donoghue, Kathy Banahan, and Gavin Mc Manus for technical assistance. This work was supported by Brazilian research funding from São Paulo Research Foundation (FAPESP) (2013/08216-2 to the Center for Research in Inflammatory Diseases), FAPESP fellowships (2017/01714-8 and 2019/25298-9 to J.E.T.-K.), European Research Council (Metabinnate 834370), and Science Foundation Ireland (20/SPP/3685). J.C.A.-F. is a research fellow from the National Council for Scientific and Technological Development (CNPq, no. 315880/2021-0).

AUTHOR CONTRIBUTIONS

J.E.T.-K., P.R.V., and E.M.P.-M. designed and performed experiments, analyzed data, and wrote the manuscript. L.A.J.O. and J.C.A.-F. supervised the project, designed experiments, and acquired fundings. V.M.F., A.C., T.M.C., and F.d.Q.C. planned and analyzed experiments. D.C.N., M.P.C.-S., S.M.O., A.Z., L.E.A.D., G.A.P., P.F., J.P.M.L., B.M.S.d.M., and T.V.M. performed and analyzed experiments.

DECLARATION OF INTERESTS

The authors declare no competing interests.

STAR★METHODS

Detailed methods are provided in the online version of this paper and include the following:

- KEY RESOURCES TABLE
- EXPERIMENTAL MODEL AND STUDY PARTICIPANT DETAILS
  - Mice
  - Cell culture
- METHOD DETAILS
  - ELISA
  - qPCR
  - Biochemical parameters
  - ATP assay
  - Seahorse XF test
  - Adenosine quantification
  - Confocal microscopy
  - Mitochondria isolation
  - Western Blot
- QUANTIFICATION AND STATISTICAL ANALYSIS

SUPPLEMENTAL INFORMATION

Supplemental information can be found online at https://doi.org/10.1016/j.celrep.2024.115172.

Received: September 1, 2023
Revised: September 24, 2024
Accepted: December 17, 2024

REFERENCES

1. Viola, A., Munari, F., Sánchez-Rodríguez, R., Scolaro, T., and Castegna, A. (2019). The Metabolic Signature of Macrophage Responses. Front. Immunol. *10*, 1462. https://doi.org/10.3389/fimmu.2019.01462.
2. Freemerman, A.J., Johnson, A.R., Sacks, G.N., Milner, J.J., Kirk, E.L., Troester, M.A., Macintyre, A.N., Goraksha-Hicks, P., Rathmell, J.C., and Makowski, L. (2014). Metabolic reprogramming of macrophages: glucose transporter 1 (GLUT1)-mediated glucose metabolism drives a proinflammatory phenotype. J. Biol. Chem. *289*, 7884–7896. https://doi.org/10.1074/jbc.M113.522037.
3. Fukuzumi, M., Shinomiya, H., Shimizu, Y., Ohishi, K., and Utsumi, S. (1996). Endotoxin-induced enhancement of glucose influx into murine peritoneal macrophages via GLUT1. Infect. Immun. *64*, 108–112. https://doi.org/10.1128/iai.64.1.108-112.1996.
4. Tannahill, G.M., Curtis, A.M., Adamik, J., Palsson-McDermott, E.M., McGettrick, A.F., Goel, G., Frezza, C., Bernard, N.J., Kelly, B., Foley, N.H., et al. (2013). Succinate is an inflammatory signal that induces IL-1β through HIF-1α. Nature *496*, 238–242. https://doi.org/10.1038/nature11986.
5. Jha, A.K., Huang, S.C.C., Sergushichev, A., Lampropoulou, V., Ivanova, Y., Loginicheva, E., Chmielewski, K., Stewart, K.M., Ashall, J., Everts, B., et al. (2015). Network integration of parallel metabolic and transcriptional data reveals metabolic modules that regulate macrophage polarization. Immunity *42*, 419–430. https://doi.org/10.1016/j.immuni.2015.02.005.
6. Funk, J.L., Feingold, K.R., Moser, A.H., and Grunfeld, C. (1993). Lipopolysaccharide stimulation of RAW 264.7 macrophages induces lipid accumulation and foam cell formation. Atherosclerosis *98*, 67–82. https://doi.org/10.1016/0021-9150(93)90224-i.
7. Feingold, K.R., Shigenaga, J.K., Kazemi, M.R., McDonald, C.M., Patzek, S.M., Cross, A.S., Moser, A., and Grunfeld, C. (2012). Mechanisms of triglyceride accumulation in activated macrophages. J. Leukoc. Biol. *92*, 829–839. https://doi.org/10.1189/jlb.1111537.
8. Palsson-McDermott, E.M., Curtis, A.M., Goel, G., Lauterbach, M.A.R., Sheedy, F.J., Gleeson, L.E., van den Bosch, M.W.M., Quinn, S.R., Domingo-Fernandez, R., Johnston, D.G.W., et al. (2015). Pyruvate Kinase M2 Regulates Hif-1α Activity and IL-1β Induction and Is a Critical Determinant of the Warburg Effect in LPS-Activated Macrophages. Cell Metabol. *21*, 347. https://doi.org/10.1016/j.cmet.2015.01.017.
9. Damasceno, L.E.A., Prado, D.S., Veras, F.P., Fonseca, M.M., Toller-Kawahisa, J.E., Rosa, M.H., Públio, G.A., Martins, T.V., Ramalho, F.S., Waisman, A., et al. (2020). PKM2 promotes Th17 cell differentiation and autoimmune inflammation by fine-tuning STAT3 activation. J. Exp. Med. *217*, e20190613. https://doi.org/10.1084/jem.20190613.
10. Angiari, S., Runtsch, M.C., Sutton, C.E., Palsson-McDermott, E.M., Kelly, B., Rana, N., Kane, H., Papadopoulou, G., Pearce, E.L., Mills, K.H.G., and O'Neill, L.A.J. (2020). Pharmacological activation of pyruvate kinase M2 inhibits CD4+ T cell pathogenicity and suppresses autoimmunity. Cell Metabol. *31*, 391–405.e8. https://doi.org/10.1016/j.cmet.2019.10.015.
11. Toller-Kawahisa, J.E., Hiroki, C.H., Silva, C.M.d.S., Nascimento, D.C., Públio, G.A., Martins, T.V., Damasceno, L.E.A., Veras, F.P., Viacava, P.R., Sukesada, F.Y., et al. (2023). The metabolic function of pyruvate kinase M2 regulates reactive oxygen species production and microbial killing by neutrophils. Nat. Commun. *14*, 4280. https://doi.org/10.1038/s41467-023-40021-6.
12. Yang, W., and Lu, Z. (2015). Pyruvate kinase M2 at a glance. J. Cell Sci. *128*, 1655–1660. https://doi.org/10.1242/jcs.166629.
13. Alves-Filho, J.C., and Pålsson-McDermott, E.M. (2016). Pyruvate Kinase M2: A Potential Target for Regulating Inflammation. Front. Immunol. *7*, 145. https://doi.org/10.3389/fimmu.2016.00145.
14. Seo, D.R., Kim, K.Y., and Lee, Y.B. (2004). Interleukin-10 expression in lipopolysaccharide-activated microglia is mediated by extracellular ATP

in an autocrine fashion. Neuroreport *15*, 1157–1161. https://doi.org/10.1097/00001756-200405190-00015.

15. Colgan, S.P., Eltzschig, H.K., Eckle, T., and Thompson, L.F. (2006). Physiological roles for ecto-5'-nucleotidase (CD73). Purinergic Signal. *2*, 351–360. https://doi.org/10.1007/s11302-005-5302-5.
16. Dwyer, K.M., Deaglio, S., Gao, W., Friedman, D., Strom, T.B., and Robson, S.C. (2007). CD39 and control of cellular immune responses. Purinergic Signal. *3*, 171–180. https://doi.org/10.1007/s11302-006-9050-y.
17. Haskó, G., Linden, J., Cronstein, B., and Pacher, P. (2008). Adenosine receptors: therapeutic aspects for inflammatory and immune diseases. Nat. Rev. Drug Discov. *7*, 759–770. https://doi.org/10.1038/nrd2638.
18. Csóka, B., Németh, Z.H., Virág, L., Gergely, P., Leibovich, S.J., Pacher, P., Sun, C.X., Blackburn, M.R., Vizi, E.S., Deitch, E.A., and Haskó, G. (2007). A2A adenosine receptors and C/EBPbeta are crucially required for IL-10 production by macrophages exposed to Escherichia coli. Blood *110*, 2685–2695. https://doi.org/10.1182/blood-2007-01-065870.
19. Ip, W.K.E., Hoshi, N., Shouval, D.S., Snapper, S., and Medzhitov, R. (2017). Anti-inflammatory effect of IL-10 mediated by metabolic reprogramming of macrophages. Science (Washington, D.C.) *356*, 513–519. https://doi.org/10.1126/science.aal3535.
20. Li, T., Han, J., Jia, L., Hu, X., Chen, L., and Wang, Y. (2019). PKM2 coordinates glycolysis with mitochondrial fusion and oxidative phosphorylation. Protein Cell *10*, 583–594. https://doi.org/10.1007/s13238-019-0618-z.
21. Van den Bossche, J., Baardman, J., and de Winther, M.P.J. (2015). Metabolic Characterization of Polarized M1 and M2 Bone Marrow-derived Macrophages Using Real-time Extracellular Flux Analysis. J. Vis. Exp. *105*, 53424. https://doi.org/10.3791/53424.
22. Garedew, A., Henderson, S.O., and Moncada, S. (2010). Activated macrophages utilize glycolytic ATP to maintain mitochondrial membrane potential and prevent apoptotic cell death. Cell Death Differ. *17*, 1540–1550. https://doi.org/10.1038/cdd.2010.27.
23. Haag, F., Adriouch, S., Braß, A., Jung, C., Möller, S., Scheuplein, F., Bannas, P., Seman, M., and Koch-Nolte, F. (2007). Extracellular NAD and ATP: Partners in immune cell modulation. Purinergic Signal. *3*, 71–81. https://doi.org/10.1007/s11302-006-9038-7.
24. Ma, W., Lim, W., Gee, K., Aucoin, S., Nandan, D., Kozlowski, M., Diaz-Mitoma, F., and Kumar, A. (2001). The p38 mitogen-activated kinase pathway regulates the human interleukin-10 promoter via the activation of Sp1 transcription factor in lipopolysaccharide-stimulated human macrophages. J. Biol. Chem. *276*, 13664–13674. https://doi.org/10.1074/jbc.M011157200.
25. Foey, A.D., Parry, S.L., Williams, L.M., Feldmann, M., Foxwell, B.M., and Brennan, F.M. (1998). Regulation of monocyte IL-10 synthesis by endogenous IL-1 and TNF-alpha: role of the p38 and p42/44 mitogen-activated protein kinases. J. Immunol. *160*, 920–928.
26. Csóka, B., Németh, Z.H., Virág, L., Gergely, P., Leibovich, S.J., Pacher, P., Sun, C.X., Blackburn, M.R., Vizi, E.S., Deitch, E.A., and Haskó, G. (2007). A2A adenosine receptors and C/EBPbeta are crucially required for IL-10 production by macrophages exposed to Escherichia coli. Blood *110*, 2685–2695. https://doi.org/10.1182/blood-2007-01-065870.
27. Haskó, G., and Cronstein, B. (2013). Regulation of inflammation by adenosine. Front. Immunol. *4*, 85. https://doi.org/10.3389/fimmu.2013.00085.
28. Shirai, T., Nazarewicz, R.R., Wallis, B.B., Yanes, R.E., Watanabe, R., Hilhorst, M., Tian, L., Harrison, D.G., Giacomini, J.C., Assimes, T.L., et al. (2016). The glycolytic enzyme PKM2 bridges metabolic and inflammatory dysfunction in coronary artery disease. J. Exp. Med. *213*, 337–354. https://doi.org/10.1084/jem.20150900.
29. Li, L., Tang, L., Yang, X., Chen, R., Zhang, Z., Leng, Y., and Chen, A.F. (2020). Gene Regulatory Effect of Pyruvate Kinase M2 is Involved in Renal Inflammation in Type 2 Diabetic Nephropathy. Exp. Clin. Endocrinol. Diabetes *128*, 599–606. https://doi.org/10.1055/a-1069-7290.
30. Galván-Peña, S., Carroll, R.G., Newman, C., Hinchy, E.C., Palsson-McDermott, E., Robinson, E.K., Covarrubias, S., Nadin, A., James, A.M., Haneklaus, M., et al. (2019). Malonylation of GAPDH is an inflammatory signal in macrophages. Nat. Commun. *10*, 338. https://doi.org/10.1038/s41467-018-08187-6.
31. Millet, P., Vachharajani, V., McPhail, L., Yoza, B., and McCall, C.E. (2016). GAPDH Binding to TNF-α mRNA Contributes to Posttranscriptional Repression in Monocytes: A Novel Mechanism of Communication between Inflammation and Metabolism. J. Immunol. *196*, 2541–2551. https://doi.org/10.4049/jimmunol.1501345.
32. El Kasmi, K.C., and Stenmark, K.R. (2015). Contribution of metabolic reprogramming to macrophage plasticity and function. Semin. Immunol. *27*, 267–275. https://doi.org/10.1016/j.smim.2015.09.001.
33. Rodríguez-Prados, J.C., Través, P.G., Cuenca, J., Rico, D., Aragonés, J., Martín-Sanz, P., Cascante, M., and Boscá, L. (2010). Substrate fate in activated macrophages: a comparison between innate, classic, and alternative activation. J. Immunol. *185*, 605–614. https://doi.org/10.4049/jimmunol.0901698.
34. Oliva-Ramírez, J., Moreno-Altamirano, M.M.B., Pineda-Olvera, B., Cauich-Sánchez, P., and Sánchez-García, F.J. (2014). Crosstalk between circadian rhythmicity, mitochondrial dynamics and macrophage bactericidal activity. Immunology *143*, 490–497. https://doi.org/10.1111/imm.12329.
35. Baseler, W.A., Davies, L.C., Quigley, L., Ridnour, L.A., Weiss, J.M., Hussain, S.P., Wink, D.A., and McVicar, D.W. (2016). Autocrine IL-10 functions as a rheostat for M1 macrophage glycolytic commitment by tuning nitric oxide production. Redox Biol. *10*, 12–23. https://doi.org/10.1016/j.redox.2016.09.005.
36. Dowling, J.K., Afzal, R., Gearing, L.J., Cervantes-Silva, M.P., Annett, S., Davis, G.M., De Santi, C., Assmann, N., Dettmer, K., Gough, D.J., et al. (2021). Mitochondrial arginase-2 is essential for IL-10 metabolic reprogramming of inflammatory macrophages. Nat. Commun. *12*, 1460. https://doi.org/10.1038/s41467-021-21617-2.
37. Yi, Z., Wu, Y., Zhang, W., Wang, T., Gong, J., Cheng, Y., and Miao, C. (2020). Activator-Mediated Pyruvate Kinase M2 Activation Contributes to Endotoxin Tolerance by Promoting Mitochondrial Biogenesis. Front. Immunol. *11*, 595316. https://doi.org/10.3389/fimmu.2020.595316.
38. Moore, K.W., de Waal Malefyt, R., Coffman, R.L., and O'Garra, A. (2001). Interleukin-10 and the interleukin-10 receptor. Annu. Rev. Immunol. *19*, 683–765. https://doi.org/10.1146/annurev.immunol.19.1.683.
39. Gilroy, D.W., Lawrence, T., Perretti, M., and Rossi, A.G. (2004). Inflammatory resolution: new opportunities for drug discovery. Nat. Rev. Drug Discov. *3*, 401–416. https://doi.org/10.1038/nrd1383.
40. Link, A.A., Kino, T., Worth, J.A., McGuire, J.L., Crane, M.L., Chrousos, G.P., Wilder, R.L., and Elenkov, I.J. (2000). Ligand-activation of the adenosine A2a receptors inhibits IL-12 production by human monocytes. J. Immunol. *164*, 436–442. https://doi.org/10.4049/jimmunol.164.1.436.
41. Khoa, N.D., Montesinos, M.C., Reiss, A.B., Delano, D., Awadallah, N., and Cronstein, B.N. (2001). Inflammatory cytokines regulate function and expression of adenosine A(2A) receptors in human monocytic THP-1 cells. J. Immunol. *167*, 4026–4032. https://doi.org/10.4049/jimmunol.167.7.4026.
42. Németh, Z.H., Lutz, C.S., Csóka, B., Deitch, E.A., Leibovich, S.J., Gause, W.C., Tone, M., Pacher, P., Vizi, E.S., and Haskó, G. (2005). Adenosine augments IL-10 production by macrophages through an A2B receptor-mediated posttranscriptional mechanism. J. Immunol. *175*, 8260–8270. https://doi.org/10.4049/jimmunol.175.12.8260.
43. Nascimento, D.C., Viacava, P.R., Ferreira, R.G., Damaceno, M.A., Piñeros, A.R., Melo, P.H., Donate, P.B., Toller-Kawahisa, J.E., Zoppi, D., Veras, F.P., et al. (2021). Sepsis expands a CD39+ plasmablast population that promotes immunosuppression via adenosine-mediated inhibition of macrophage antimicrobial activity. Immunity *54*, 2024–2041.e8. https://doi.org/10.1016/j.immuni.2021.08.005.

44. Israelsen, W.J., Dayton, T.L., Davidson, S.M., Fiske, B.P., Hosios, A.M., Bellinger, G., Li, J., Yu, Y., Sasaki, M., Horner, J.W., et al. (2013). PKM2 isoform-specific deletion reveals a differential requirement for pyruvate kinase in tumor cells. Cell *155*, 397–409. https://doi.org/10.1016/j.cell.2013.09.025.

45. Luiz, J.P.M., Toller-Kawahisa, J.E., Viacava, P.R., Nascimento, D.C., Pereira, P.T., Saraiva, A.L., Prado, D.S., LeBert, M., Giurisato, E., Tournier, C., et al. (2020). MEK5/ERK5 signaling mediates IL-4-induced M2 macrophage differentiation through regulation of c-Myc expression. J. Leukoc. Biol. *108*, 1215–1223. https://doi.org/10.1002/JLB.1MA0520-016R.

46. Cervantes-Silva, M.P., Carroll, R.G., Wilk, M.M., Moreira, D., Payet, C.A., O'Siorain, J.R., Cox, S.L., Fagan, L.E., Klavina, P.A., He, Y., et al. (2022). The circadian clock influences T cell responses to vaccination by regulating dendritic cell antigen processing. Nat. Commun. *13*, 7217. https://doi.org/10.1038/s41467-022-34897-z.

STAR★METHODS

KEY RESOURCES TABLE

REAGENT or RESOURCE	SOURCE	IDENTIFIER
Antibodies		
Anti-mouse PKM2 (Clone D78A4)	Cell signaling	Cat# 4053P; RRID: AB_1904096
Anti-PKM1 (Clone D30G6)	Cell signaling	Cat# 7067S; RRID: AB_2715534
Anti-β-actin (Clone 8H10D10)	Cell signaling	Cat# 3700S; RRID: AB_2242334
Anti-tubulin	Cell signaling	Cat# 2144S; RRID: AB_2210548
Anti-VDAC1	Thermo Fisher Scientific	Cat# SA93-03; RRID: AB_2898842
Goat anti-Rabbit IgG (H + L) Cross-Adsorbed Secondary Antibody, Alexa Fluor™ 647	Invitrogen	Cat# A21244; RRID: AB_2535812
Ultra-LEAF Purified anti-mouse CD210 (IL-10R) Clone:1B1.3A Isotype:Rat IgG1,x	Biolegend	Cat# 112710; RRID: AB_11149684
Chemicals, peptides, and recombinant proteins		
ProLong ® Gold antifade reagent	Thermo Fisher Scientific	Cat# P36930
Mitotracker Red	Thermo Fisher Scientific	Cat# M7512
Hoechst blue	Invitrogen	Cat# H3570
DAPI solution	Thermo Fisher Scientific	Cat# 62248
Laemmli Sample Buffer	Biorad	Cat#161-0737
ECL prime reagent	GE Healthcare	Cat# RPN2236
ARL 67156 trisodium salt	Tocris	Cat# 1283
Adenosine 5'-(α,β-methylene)diphosphate sodium salt	Sigma	Cat# M8386
Heptelidic acid	Abcam	Cat# ab144269
Oligomycin A	Sigma-Aldrich	Cat# 75351
Recombinant mouse IL-10 protein	Bio-techne	Cat# 417-ML-005/CF
Disuccinimidyl suberate	Sigma-Aldrich	Cat# S1885
Pentostatin	Tocris	Cat# 2033
TEPP-46	Calbiochem	Cat# 505487
LPS from E.Coli serotype EH1	Enzo life Sciences	Cat# ALX-581-010-L001
Adenosine 5′-triphosphate disodium salt hydrate (ATP)	Sigma-Aldrich	Cat# A26209
RPMI1640 with phenol red	Corning	Cat# 15-040-CV
HEPES	Corning	Cat# 25-060-CI
1X RBC Lysis Buffer	Thermo Fisher Scientific	Cat# 00-4333-57
Penicillin and streptomycin	Sigma-Aldrich	Cat# P4333
HyClone Research Grade Fetal Bovine Serum, South American Origin	GE Life Sciences	Cat# SV30160.03
Amphotericin B (Fungisone)	Gibco	Cat# 15-290-018
L-glutamine	Sigma-Aldrich	Cat# G7513
DPBS, 1X	Corning	Cat# 21-031-CV
EDTA	Synth	Cat# E2005.01.AH
NaHCO3	Synth	Cat# B2007.01.AH
D-(+)-Glucose	Sigma-Aldrich	Cat# G8270
Carbenoxolone disodium salt	Sigma-Aldrich	Cat# C4790
Bovine Serum Albumin	Sigma-Aldrich	Cat# A7906
Tween 20	Sigma-Aldrich	Cat# P2287
Rneasy Mini Kit	Qiagen	Cat# 74106
High-Capacity cDNA Reverse Transcription Kit	Thermo Fisher Scientific	Cat# 4368814
SYBR™ Green PCR Master Mix	Thermo Fisher Scientific	Cat# 4364346

(*Continued on next page*)

Continued		
REAGENT or RESOURCE	SOURCE	IDENTIFIER
Adenosine	Sigma-Aldrich	Cat# A4036
Ketamine	Agener União, br	Cat# 1724751
Xylazine	Agener União, br	Cat# 1906587
Critical commercial assays		
Mouse IL-10 DuoSet ELISA	R&D Systems	Cat# DY417
ATPlite Luminescence ATP Detection Assay	PerkinElmer	Cat# 6016941
Lactate Kit	Labtest, br	Cat# 138
Glucose Kit	Bioclin, br	Cat# K082
Pyruvate Kinase Activity Colorimetric/Fluorometric Assay Kit	BioVision	Cat# K709
XF Glycosis Stress test Kit	Agilent Technologies	Cat# 103020-100
Seahorse XF Cell Mito Stress Test Kit	Agilent Technologies	Cat# 103015-100
Mitochondria Isolation Kit for Cultured cells	Thermo Fisher Scientific	Cat# 89874
Experimental models: Organisms/strains		
Adora2a$^{-/-}$ mice	The Jackson Laboratory	Cat# 010685
Lyz2^{Cre} mice	The Jackson Laboratory	Cat# 004781
Pkm2^{flox} mice	The Jackson Laboratory	Israelsen et al.[44]
Panx1$^{-/-}$ mice	The Jackson Laboratory	Cat# 026021
C57BL/6 wild-type mice	Charles River	ND
BALB/c wild-type mice	Charles River	ND
Oligonucleotides		
Il10 – Forward: TGGACAACATACTGCT Reverse: GGATCATTTCCGATAAGGCT	Sigma-Aldrich	ND
Pkm2 – Forward: TCGCATGCAGVACCTGATT Reverse: CCTCGAATAGCTGCAAGTGGTA	Sigma-Aldrich	ND
Pkm1 – Forward: GCTGTTTGAAGAGCTTGTGC Reverse: TTATAAGAGGCCTCCACGCT	Sigma-Aldrich	ND
Gapdh – Forward: GGGTGTGAACCACGAGAAAT Reverse: CCTTCCACAATGCCAAAGTT	Sigma-Aldrich	ND
Software and algorithms		
Fiji/ImageJ	ImageJ	https://imagej.nih.gov/ij/
Prism 9.2.0	GraphPad	https://www.graphpad.com/scientificsoftware/prism/
FlowJo	TreeStar	ND
MassLynx software	Micromass	ND

EXPERIMENTAL MODEL AND STUDY PARTICIPANT DETAILS

Mice

BALB/c and C57BL/6 were purchased from Charles River. *Adora2a*$^{-/-}$ (010685), *Lyz2*^{Cre} (004781), *Panx1*$^{-/-}$ (026021) and *Pkm2*^{flox} (129S-Pkmtm1.1Mgvh/J) mice were purchased from the Jackson Laboratory. *Lyz2*^{Cre}, *Panx1*$^{-/-}$ and *Pkm2*^{flox} mice were on a C57BL/6 background and *Adora2a*$^{-/-}$ mice were on a BALB/c background. Myeloid cell-(*Pkm2*$^{\Delta Lyz2}$) specific–Pkm2-deficient mice were generated by crossing the *Pkm2*$^{flox/flox}$ mice with *Lyz2*^{Cre} mice. Experiments were carried out with 6-week-old male or female mice according to the guidelines of the Animal Welfare Committee of the Ribeirao Preto Medical School, University of São Paulo (protocol number: 113/2015 and 0145/2019). All mice were kept under controlled environmental conditions with water and food *ad libitum* and bred and maintained under specific pathogen-free conditions at the Animal Facility of the Ribeirao Preto Medical School, University of São Paulo.

Cell culture

Bone-marrow-derived macrophages (BMDMs) were obtained as described previously.[45] Briefly, both mice femurs were collected and flushed with RPMI-1640. After centrifugation, cells were resuspended in RPMI-1640 supplemented with 20% L929 cell-conditioned medium, 10% of inactivated fetal bovine serum (FBS), L-glutamine (2 mM), penicillin (100 U/mL) and fungizone (2.5 μg/mL). Cells were seeded in four untreated Petri dishes and incubated at 37°C, 5% CO2, for 3 days. After this period, 10 mL of supplemented RPMI-1640 were added to each plate, and cells were incubated for 4 days. BMDMs were harvested and plated in tissue culture dishes for subsequent experiments. BMDMs were pre-treated with TEPP-46 (30 μM or 100 μM) for 1 h before being stimulated with LPS (100 ng/mL) for different time points.

METHOD DETAILS

ELISA

IL-10 concentration in the culture supernatant, serum, peritoneal lavage, and lung tissue was determined by the ELISA method according to the manufacturer's instructions.

qPCR

Total RNA from BMDMs was extracted using a RNeasy Mini Kit, according to the manufacturer's directions. First-strand cDNA was synthesized from 1 μg of RNA using the high-capacity cDNA Reverse Transcription Kit. Quantitative real-time PCR was performed using Power Syber Green PCR Master Mix (Applied Biosystems) in the Viia7 Real-Time PCR system. The data were normalized to *Gapdh* values, and the fold change was analyzed using the DDCt method. The relative gene expression was expressed in arbitrary units based on the untreated group, which was assigned a value of 1. Primers were purchased from Sigma-Aldrich.

Biochemical parameters

Lactate and glucose concentrations were measured in culture supernatants using commercial kits according to the manufacturer's instructions. Pyruvate Kinase activity was determined using Pyruvate Colorimetric/Fluorometric Assay Kit, according to the manufacturer's instructions.

ATP assay

ATP was detected as described by Nascimento and collaborators.[43] Briefly, to access the intracellular ATP concentration, BMDMs were treated with TEPP-46 (100 μM) and stimulated with LPS (100 ng/mL) at 37°C, 5% CO_2, in the presence of a pannexin-1 channel inhibitor (carbenoxolone disodium salt (CBX), 100 μM). BMDMs were lysed to measure intracellular ATP levels at indicated time points. For the detection of extracellular ATP, BMDMs were treated with TEPP-46 (100 μM) and stimulated with LPS (100 ng/mL) at 37°C, 5% CO_2, in the presence of the CD39 inhibitor (ARL 67156 trisodium salt, 200 μM). Culture supernatants were collected to measure extracellular ATP levels at indicated time points. Intracellular or extracellular ATP was detected using the ATPlite Luminescence ATP Detection Assay, according to the manufacturer's protocol.

Seahorse XF test

Extracellular acidification rate and oxygen consumption rate were measured using the Seahorse XF96 Analyzer (Agilent Technologies) according to the manufacturer's guidelines (Agilent Seahorse XF24). Briefly, BMDMs were treated with TEPP-46 (30 μM) for 1 h and stimulated with LPS (100 ng/mL) for 4 h. Before analysis, cells were washed with XF media (non-buffered RPMI-1640 containing 2 mM L-glutamine and 1 mM sodium pyruvate) and incubated for 45 min without CO_2. ECAR was measured under basal conditions and after adding the following drugs: 10 mM glucose, 1 μM oligomycin, 50 mM 2DG (XF Glycolysis Stress test Kit). OCR was measured under basal conditions and after adding the following drugs: 10 μM oligomycin, 5 μM FCCP, 5 μM Rot/AA (XF Cell Mito Stress Test Kit).

Adenosine quantification

BMDMs were treated with TEPP-46 (100 μM) for 1 h and stimulated with LPS (100 ng/mL) for 3 h. The supernatants were precipitated with a solution of 66% acetonitrile in water (v/v) (J. T. Baker) to denature and precipitate proteins and to stabilize adenosine, and then further diluted with water to final concentration of 33% acetonitrile for adenosine LC-MS/MS analysis. Different concentrations of adenosine were prepared in methanol to construct a standard curve. LC-MS/MS equipment and conditions: For adenosine detection in the supernatant, samples or standards were injected in a Xevo TQ-S system coupled to a Waters Acquity UPLC-Class H and equipped with a C18 Acquity UPLC HSS column (1,0 × 150 mm) The liquid chromatography separation was carried out at 40°C and the solvent system consisted of 0.1% acetic acid in water (v/v) (solvent A) and 0.1% acetic acid in methanol (v/v) (solvent B). The flow rate was set to 500 μL/min and 5 μL of samples were injected for separation in a 4.5 min isocratic gradient of 50:50 solvent A and B. The detection was performed in multiple reaction monitoring mode for a positive precursor ion of m/z 268 and fragment ion of m/z 136. The analytical data was processed by MassLynx software (Micromass, Manchester, UK) to obtain calibrated peak areas.

Confocal microscopy

BMDMs were treated with TEPP-46 (30 μM) for 1 h and then activated with LPS (100 ng/mL) for 24 h. Samples were fixed and stained with anti-PKM2. The samples were washed and incubated with a secondary antibody. Coverslips were washed in PBS and mounted onto microscope slides using a DAPI-containing mounting medium. For live BMDMs, cells were treated with TEPP-46 for 1 h and then activated with LPS for 4 h. Mitotracker Red (50nM) and Hoechst blue (0.5 μg/mL) were added to the culture media for 30 min. BMDMs were washed with warm PBS, and fresh DMEM, 10% FCS, was added.[46] Images were acquired by Leica SP8 X confocal microscope with a 100× objective. Images were analyzed using the Fiji/ImageJ software. For mitochondrial morphology analysis, 25 cells per condition showing at least 50 mitochondria were analyzed using Fiji/ImageJ software.

Mitochondria isolation

Mitochondrial fractions were prepared from BMDMs (10^7) using the Mitochondria Isolation Kit for Cultured cells according to manufacturer's recommendations; 20 μl of each fraction prepared was separated by SDS-PAGE prior to western blotting.

Western Blot

BMDMs were cultured in RPMI-1640 medium with 10% FBS in 12-well plates, treated with TEPP-46 (30 μM) for 1 h and then stimulated with LPS (100 ng/mL) for 24 h. For standard western blot protocols, cells were harvested in boiling Laemmli Sample Buffer, followed by heating at 95°C for 5 min. For crosslink assay, BMDMs were incubated with 500 μM disuccinimidyl suberate for 30 min, and then cell lysates were prepared as described above. Protein samples were resolved on SDS-PAGE gels and transferred onto a nitrocellulose membrane (GE Healthcare). Membranes were blocked with 5% (wt/vol) nonfat milk (Cell Signaling) in Tris-buffered saline with 0.1% Tween 20 (TBST) for 1 h at room temperature and then incubated overnight at 4°C with 1:1000 dilutions of primary antibodies against PKM2, PKM1, β-actin, VDAC1, and tubulin. Membranes were repeatedly washed with TBST and incubated for 2 h with the appropriate HRP-conjugated secondary antibody (1:5000 dilution; Sigma-Aldrich). Immunoreactivity was detected using the ECL prime reagent (GE Healthcare, RPN2236), and then the chemiluminescence signal was recorded on the ChemiDoc XRS Imager (Bio-Rad Laboratories). Data were analyzed with Image Lab software (Bio-Rad Laboratories). Total β-actin levels were used as a loading control.

QUANTIFICATION AND STATISTICAL ANALYSIS

All data are presented as the mean ± SEM (standard error of the mean). Statistical significance was estimated by unpaired Student's t-test for comparison between the two groups. For comparison among multiple groups, 1-way or two-way ANOVA was used, followed by Tukey's posthoc test. All statistical analyses were conducted using GraphPad Prism 9.0 (GraphPad software, San Diego, CA, USA). *p-value* of less than 0.05 was considered to be statistically significant and was indicated in the graphs by an *. The specific statistical details can be found in Figures legends, including the number of mice, cells or mitochondria (n) used for the analysis.